Tylkowski, Wieszczycka, Jastrzab (Eds.)

Polymer Engineering

Also of interest

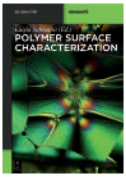

Polymer Surface Characterization
Sabbatini (Ed.), 2014
ISBN 978-3-11-027508-7, e-ISBN 978-3-11-028811-7

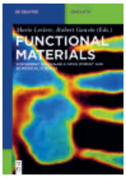

Functional Materials.
For Energy, Sustainable Development and Biomedical Sciences
Leclerc, Gauvin (Eds.), 2014
ISBN 978-3-11-030781-8, e-ISBN 978-3-11-030782-5

Microencapsulation.
Innovative Applications
Giamberini, Fernandez Prieto, Tylkowski (Eds.), 2015
ISBN 978-3-11-033187-5, e-ISBN 978-3-11-033199-8

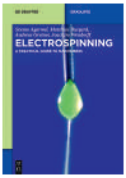

Electrospinning.
A Practical Guide to Nanofibers
Agarwal, Burgard, Greiner, Wendorff, 2016
ISBN 978-3-11-033180-6, e-ISBN 978-3-11-033351-0

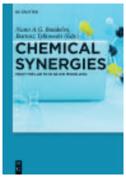

Chemical Synergies.
From the Lab to In Silico Modelling
Bandeira, Tylkowski (Eds.), 2018
ISBN 978-3-11-048135-8, e-ISBN 978-3-11-048206-5

Physical Sciences Reviews.
e-ISSN 2365-659X

Polymer Engineering

Edited by
Bartosz Tylkowski, Karolina Wieszczycka, Renata Jastrzab

DE GRUYTER

Editors
Dr. hab. Karolina Wieszczycka
Poznan University of Technology
Institute of Chemical Technology & Engineering
Berdychowo 4
60-965 Poznan
Poland
karolina.wieszczycka@put.poznan.pl

Prof. UAM Renata Jastrzab
Adam Mickiewicz University
Faculty of Chemistry
Umultowska 89b
61-614 Poznan
Poland
renatad@amu.edu.pl

Dr. Bartosz Tylkowski
Chemistry Technology Centre of Catalonia (CTQC),
C/Marcel·lí Domingo,
43007 Tarragona, S
Spain
bartosz.tylkowski@ctqc.org

The Open Access of this publication was supported by the State Digitization Program for Science and Culture of the Free State of Saxony (cf. https://sachsen.digital/das-programm/).

ISBN 978-3-11-046828-1
e-ISBN (PDF) 978-3-11-046974-5
e-ISBN (EPUB) 978-3-11-046834-2
Set-ISBN 978-3-11-046975-2

The articles in this book have been previously published in the journal Physical Sciences Reviews (ISSN 2365-659X).

Library of Congress Cataloging-in-Publication Data
A CIP catalog record for this book has been applied for at the Library of Congress.

Bibliographic information published by the Deutsche Nationalbibliothek
The Deutsche Nationalbibliothek lists this publication in the Deutsche Nationalbibliografie; detailed bibliographic data are available on the Internet at http://dnb.dnb.de.

Typesetting: Integra Software Services Pvt. Ltd.
Printing and binding: CPI books GmbH, Leck
Cover image: RGAP/iStock/Thinkstock
♾ Printed on acid-free paper
Printed in Germany

www.degruyter.com

Preface

Polymer is a term used since 1866 by Berthelot who, in a publication released in the Bulletin of the Chemical Society of France, noted that "*styrolene* (styrene), *heated at 200°C during a few hours, transforms itself into a resinous polymer*". It was the first recognized synthetic polymer. However, Hermann Staudinger was the first one who in 1920 proposed the concept of polymers in the sense that we use today. The universality of polymers is now well established. They are present in all fields of industrial production as an additive or structural materials and are impossible to avoid. The improvement of their properties gradually removed their bad reputation and, nowadays one can say "*There are no bad polymers, only bad applications of them*".

The book aims to review the art of polymers and to provide the readers with a comprehensive and in-depth understanding of recent developments in polymers science, technologies and engineering. Chapter 1 explains an improvement of modified epoxy thermosets by using different hyperbranched poly(ethyleneimine) derivatives. Chapter 2 provides an overview on developments in the use of rare earth metals complexes as efficient catalysts for ring-opening polymerization of cyclic esters used in biomedical applications. Chapters 3 and 4 emphasize knowledge and recent advances in bioartificial polymers and based nanovectores. The topics detailed in Chapters 5–7 provide current developments in capsules technologies, polymer additives and polymers application in consumer goods products. Chapters 8-10 describe polymers application in membrane technologies, while Chapter 11 provides modeling and simulation understanding membrane process. Nanomaterials often show unique and considerably changed physical, chemical and biological properties compared to their macro scaled counterparts. Utilization of nanoparticles often requires the construction of integrated chemical systems. Most popular of these are polymer-supported nanoparticles, which are highlighted in Chapter 12. Spectroscopic properties of polymer composites are given in Chapter 13. Chapter 14 underlines catalytical and biological processes used to transform cellulose into high value-added products.

We would like to express our gratitude to the contributing authors in making this project a success, and to Dr. Ria Fritz and Ms. Jana Habermann of DeGruyter Publisher, Germany for their assistance and encouragement in this venture. Moreover, we would like to gratefully acknowledge a financial support from European Community's Seventh Framework Programme (FP/2007–2013) under REA grant agreement no. 600388 (TECNIOspring programme), and from the Agency for Business Competitiveness of the Government of Catalonia, ACCIÓ, under which Dr. Tylkowski co-edits this book as a part of outreaching activity of his Individual Incoming TECNIOspring Marie Curie Grant.

Bartosz Tylkowski
Karolina Wieszczycka
Renata Jastrzab

https://doi.org/10.1515/9783110469745-202

Contents

Monissa Paderes, Deepak Ahirwal and Susana Fernández Prieto

Karolina Wieszczycka and Katarzyna Staszak

Bartosz Tylkowski and Irene Tsibranska

List of contributing authors

Cristina Acebo
Universitat Rovira i Virgili
Department of Analytical and Organic Chemistry
Carrer de Marcel·lí Domingo, 1
43007 Tarragona
Spain
cristina.acebo@urv.cat

Deepak Ahirwal
Procter & Gamble Co.
Temselaan 100
1853 Strombeek-Bever
Belgium

Veronica Ambrogi
University of Naples
Department of Chemical, Materials and Production Engineering
Piazzale Tecchio 80
80125 Naples
Italy
ambrogi@unina.it

Pierfrancesco Cerruti
Institute for Polymers, Composites and Biomaterials (IPCB-CNR)
Via Campi Flegrei 34
80078 Pozzuoli
Italy
cerruti@unina.it

Magda Constantí
Universitat Rovira i Virgili
Department of Chemical Engineering
Av. Països Catalans 26
43007 Tarragona
Spain
magda.constanti@urv.cat

Raffaele Conte
Institute for Polymers, Composites and Biomaterials (IPCB-CNR)
Via Campi Flegrei 34
80078 Pozzuoli
Italy
raffaele.conte@ibbr.cnr.it

Iuliana Cota
Universidade Federal da Bahia
Escola Politécnica
40210-630 Salvador
Brazil
iuliana.cota2010@gmail.com

Ilenia De Luca
Institute of Bioscience and BioResources (CNR)
Pietro Castellino 111
80131 Naples
Italy
ilenia.deluca@ibbr.cnr.it

Anna Di Salle
Institute of Bioscience and BioResources (CNR)
Pietro Castellino 111
80131 Naples
Italy
anna.disalle@ibbr.cnr.it

Susana Fernandez Prieto
Procter & Gamble Co.
Temselaan 100
1853 Strombeek-Bever
Belgium
fernandezprieto.s@pg.com

Ricard Garcia-Valls
Universitat Rovira i Virgili
Department of Chemical Engineering
Av. Països Catalans 26
43007 Tarragona
Spain
ricard.garcia@urv.cat

Llorenç Gavilà
Universitat Rovira i Virgili
Department of Chemical Engineering
Av. Països Catalans 26
43007 Tarragona
Spain
lloren.gavila@urv.cat

Marta Giamberini
Universitat Rovira i Virgili
Department of Chemical Engineering
Av. Països Catalans 26
43007 Tarragona
Spain
marta.giamberini@urv.cat

Edgar Güell
Universitat Rovira i Virgili
Department of Chemical Engineering
Av. Països Catalans 26
43007 Tarragona
Spain
edgarbiotec8@gmail.com

Tania Gumi
Universitat Rovira i Virgili
Department of Chemical Engineering
Av. Països Catalans 26
43007 Tarragona
Spain
tania.gumi@urv.net

Henryk Koroniak
Adam Mickiewicz University
Faculty of Chemistry
Umultowska 89b
61-614 Poznan
Poland
koroniak@amu.edu.pl

Lukasz Marciniak
Adam Mickiewicz University
Faculty of Chemistry
Umultowska 89b
61-614 Poznan
Poland
lukaszluke13@gmail.com

Valentina Marturano
Institute for Polymers, Composites and Biomaterials (IPCB-CNR)
Via Campi Flegrei 34
80078 Pozzuoli
Italy
valentina.marturano@unina.it

Biniam Maru
Universitat Rovira i Virgili
Department of Chemical Engineering
Av. Països Catalans 26
43007 Tarragona
Spain
biniammaru@gmail.com

Francesc Medina
Universitat Rovira i Virgili
Department of Chemical Engineering
Av. Països Catalans 26
43007 Tarragona
Spain
francesc.medina@urv.cat

Adrianna Nogalska
Universitat Rovira i Virgili
Department of Chemical Engineering
Av. Països Catalans 26
43007 Tarragona
Spain
adrianna.nogalska@gmail.com

Martyna Nowak
Adam Mickiewicz University
Faculty of Chemistry
Umultowska 89b
61-614 Poznan
Poland
martynan@amu.edu.pl

Monissa Paderes
University of Leuven
Department of Chemistry
Celestijnenlaan 200F bus 2404
3001 Heverlee
Belgium
monissa.Paderes@chem.kuleuven.be

Gianfranco Peluso
Institute of Bioscience and BioResources (CNR)
Pietro Castellino 111
80131 Naples
Italy
gianfranco.peluso@ibbr.cnr.it

Xavier Ramis
Universitat Politècnica de Catalunya
Thermodynamics Laboratory (ETSEIB)
Avinguda Diagonal 647
08028 Barcelona
Spain
xavier.fernandez@mmt.upc.edu

Tomasz Runka
Poznan University of Technology
Ul. Piotrowo 3
60-905 Poznan
Poland
tomasz.runka@put.poznan.pl

Angels Serra
Rovira i Virgili University
Department of Analytical and Organic Chemistry
Carrer de Marcel·lí Domingo, 1
43007 Tarragona
Spain
angels.serra@urv.cat

Maciej Staszak
Poznan University of Technology
Instute of Chemical Techology and Engineering
Berdychowo 4
60-965 Poznan
Poland
Maciej.Staszak@put.poznan.pl

Kamila Szalata
Universitat Rovira i Virgili
Department of Chemical Engineering
Av. Països Catalans 26
43007 Tarragona
Spain
kamilamaria.szalata@urv.cat

Anna Trojanowska
Universitat Rovira i Virgili
Department of Chemical Engineering
Av. Països Catalans 26
43007 Tarragona
Spain
anna.trojanowska@ctqc.org

Irene Tsibranka
Bulgarian Academy of Sciences
Institute of Chemical Engineering
u. Akad. G. Bonchev
1113 Sofia
tsibranska@yahoo.com

Anna Valentino
Institute of Bioscience and BioResources (CNR)
Pietro Castellino 111
80131 Naples
Italy
anna.valentino@ibbr.cnr.it

Justyna Walkowiak-Kulikowska
Adam Mickiewicz University
Faculty of Chemistry
Umultowska 89b
61-614 Poznan
Poland
Justyna.A.Walkowiak@amu.edu.pl

Joanna Wolska
Adam Mickiewicz University
Faculty of Chemistry
Umultowska 89b
61-614 Poznan
Poland
j.wolska@amu.edu.pl

Cristina Acebo, Xavier Ramis and Angels Serra

1 Improved epoxy thermosets by the use of poly(ethyleneimine) derivatives

Abstract: Epoxy resins are commonly used as thermosetting materials due to their excellent mechanical properties, high adhesion to many substrates and good heat and chemical resistances. This type of thermosets is intensively used in a wide range of fields, where they act as fiber-reinforced materials, general-purpose adhesives, high-performance coatings and encapsulating materials. These materials are formed by the chemical reaction of multifunctional epoxy monomers forming a polymer network produced through an irreversible way. In this article the improvement of the characteristics of epoxy thermosets using different hyperbranched poly(ethyleneimine) (PEI) derivatives will be explained.

Keywords: adhesives, epoxy, dendrimers

1.1 General introduction

Epoxy resins are commonly used as thermosetting materials due to their excellent mechanical properties, high adhesion to many substrates and good heat and chemical resistances. This type of thermosets is intensively used in a wide range of fields, where they act as fiber-reinforced materials, general-purpose adhesives, high-performance coatings and encapsulating materials. These materials are formed by the chemical reaction of multifunctional epoxy monomers forming a polymer network produced through an irreversible way [1]. In this article the improvement of the characteristics of epoxy thermosets using different hyperbranched poly(ethyleneimine) (PEI) derivatives will be explained.

1.2 General concepts of epoxy thermosets

The term epoxy or epoxide refers to compounds characterized by the presence of an oxirane or epoxy ring, a three-member ring containing an oxygen atom that is bonded with two carbon atoms as shown in Figure 1.1.

From the structural point of view of chemistry, epoxy resins are monomers or oligomers containing two or more epoxy groups in their structure. P. Castan [2] developed the first system based on the well-known diglycidyl ether of bisphenol A (DGEBA). The commercialization of this resin dates back to 1940 [3]. It is obtained by the reaction of bisphenol A with epichlorohydrin in the presence of a strong base

https://doi.org/10.1515/9783110469745-001

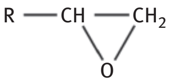

Figure 1.1: Chemical structure of epoxy ring.

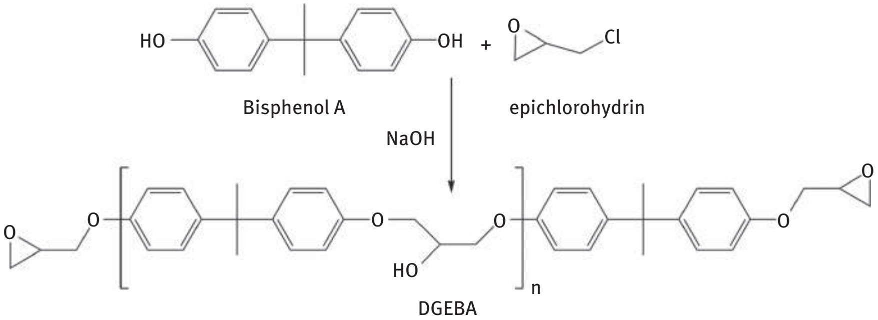

Figure 1.2: Synthetic scheme for the preparation of Bisphenol A epoxy resins.

such as NaOH. Depending on the ratio between reactants, the resulting molecular weight can be tuned in order to have different resins being possible to obtain liquid, waxy or solid DGEBA resins [4]. The reaction, still used nowadays, is depicted in Figure 1.2.

There are other types of resins with different structures that lead to materials with different characteristics. Some of the most typical resins are collected in Figure 1.3. The non-epoxy part of the molecule can have an aliphatic, cycloaliphatic or aromatic structure and the functionality, related to the number of epoxide groups, can also be varied.

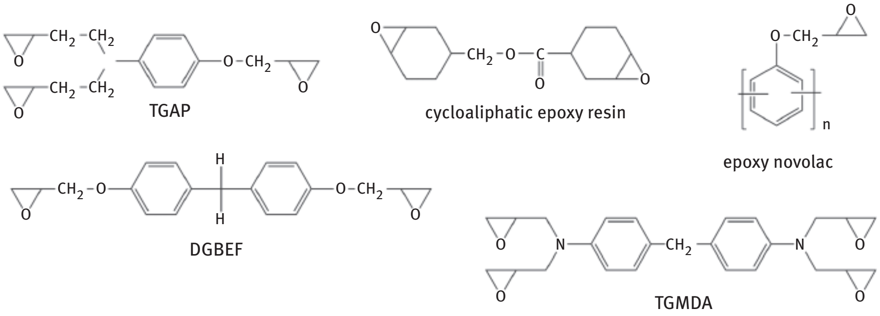

Figure 1.3: Structures of several commercially available epoxy resins.

Epoxy resins are capable of reacting with different active compounds known as curing agents (with or without catalyst) or with themselves (via an initiator) to form solid, crosslinked materials. This transformation is generally referred to as curing.

From a fundamental point of view, thermosetting epoxy polymers may be defined as polymer networks obtained by a chemical reaction of monomers, which contain two or more epoxy groups per molecule (a functionality equal to or higher than 2) [5]. The functionality of an epoxy monomer is defined by the number of arms (bonding sites) that participates in the formation of the polymer network. The functionality of the epoxy monomers depends on the curing system used and will be discussed below, but a necessary condition for the formation of a network is that at least one of the monomers involved in the reaction has a functionality higher than two, since the global functionality of the system to reach a network structure is a minimum of 4.

1.3 Curing agents

Crosslinked epoxy polymers are obtained by the reaction of epoxy monomers with curing agents (co-monomers or initiators). Epoxy polymers can be produced by step or chain growth polymerizations or, eventually, by a combination of both mechanisms [5].

Step growth polymerization (polycondensation) proceeds via a step-by-step succession of elementary reactions between reactive sites. Each independent step causes the disappearance of two co-reacting sites and creates a new covalent bond between a pair of functional groups. In this case curing agents like amines, alcohols, anhydrides, isocyanates or acids have been used in stoichiometric ratio [6].

Chain growth polymerization (ring opening) is characterized by the occurrence of initiation, propagation, chain transfer and termination steps. In the case of epoxides, the initiation step produces an ion (either an anion or a cation) that is called the active center of the polymerization. The ion may be generated by thermal treatment or by an adequate source of irradiation. Once active centers are generated, they produce primary chains by the consecutive addition of monomers through the propagation step of the reaction.

Polycondensation curing mechanisms require an accurate knowledge of the stoichiometry of the system. Among them, the most used curing agents for epoxy resins are primary and secondary amines. In this system, DGEBA is bifunctional and a requirement for the amines is that they must be multifunctional (more than two reacting groups). Considering that primary amines account for a functionality of two and secondary for a functionality of one, usually primary diamines are used. The reaction of epoxy with amines is depicted in Figure 1.4[6].

Primary and secondary aliphatic amines react rapidly with epoxy groups at low temperature to form three-dimensional crosslinked structures. However, they can

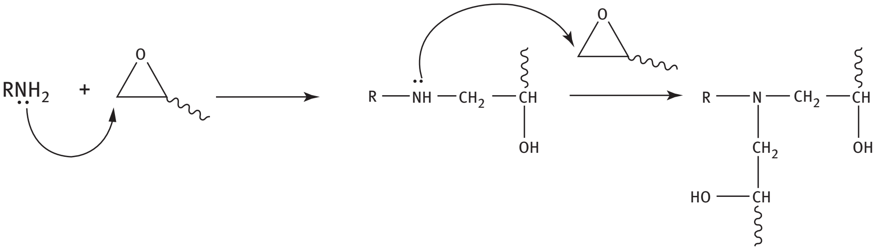

Figure 1.4: Reaction of a primary amine with epoxides.

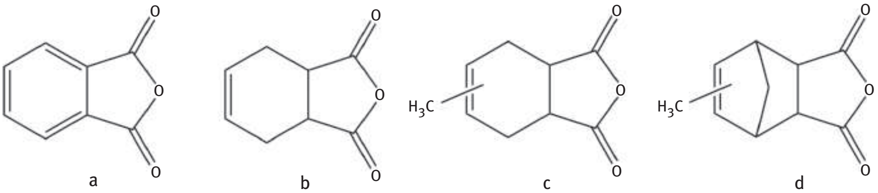

Figure 1.5: Chemical structure of anhydrides used as curing agents of epoxy resins.

also be cured at higher temperatures to provide a more densely crosslinked structure with better mechanical properties, elevated-temperature performance and chemical resistance. Other amines, such as aromatic or cycloaliphatic, are less reactive and generally require higher curing temperatures.

After amines, acid anhydrides are the second most used group of curing agents. Among the most common anhydrides, phthalic anhydride (PA, a), tetrahydrophthalic anhydride (THPA, b), methyl tetrahydrophthalic anhydride (MTHPA, c) and nadic methyl anhydride (NMA, d) can be mentioned (Figure 1.5).

The reaction of anhydrides with epoxy groups has been extensively studied and follows a complex mechanism, with several competitive reactions capable of taking place [7, 8]. The limitation of the use of anhydrides as curing agents is the low reactivity and, therefore, curing has to be carried out at high temperatures to obtain optimal properties [9]. The presence of catalysts such as tertiary amines, metallic salts and imidazoles can accelerate the curing and overcome this drawback [10].

The main reaction that takes place on curing epoxide/anhydride mixtures without amine is illustrated in Figure 1.6. The first reaction is the opening of the anhydride ring by reaction of a hydroxyl group to form the monoester (**1**) and subsequently the nascent carboxylic group reacts with the epoxy to provide an ester linkage (**2**). The reaction proceeds by the presence of existing hydroxyl groups (**3**).

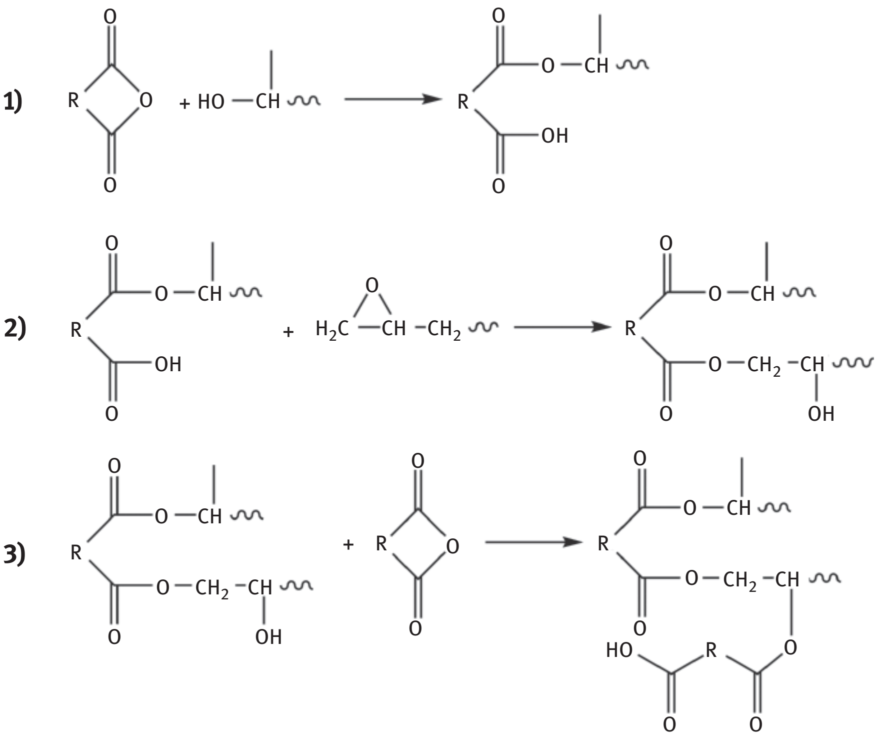

Figure 1.6: Uncatalyzed curing mechanism of epoxides with anhydrides.

In the presence of tertiary amine a different mechanism occurs (Figure 1.7). It is proposed that the tertiary amine reacts with the epoxy monomer and forms a zwitterion that contains a quaternary nitrogen atom and an alkoxide (**1**). The alkoxide rapidly reacts further with an anhydride group, leading to a carboxylate anion (**2**). Propagation occurs through the reaction of the generated carboxylate with an epoxy group and the formation of a new alkoxide anion (**3**). There is still no definite validation regarding the termination step and whether the initiator remains chemically attached during the whole course of the reaction. Some authors describe an irreversible bonding of the initiator [11], but there is disagreement on this point [12, 13].

The other main group of curing agents used is the one of initiators. Commonly used initiators include Lewis bases such as tertiary amines or imidazoles for anionic chain polymerization, and Lewis acids such as boron trifluoride complexes or other metal salts. These initiators are used in catalytic amounts and promote the homopolymerization of epoxides via the ring-opening polymerization (ROP) [14]. This ring-opening mechanism is similar in terms of the kinetics to poly-addition since it presents an initiation step, a propagation and finally a termination, but

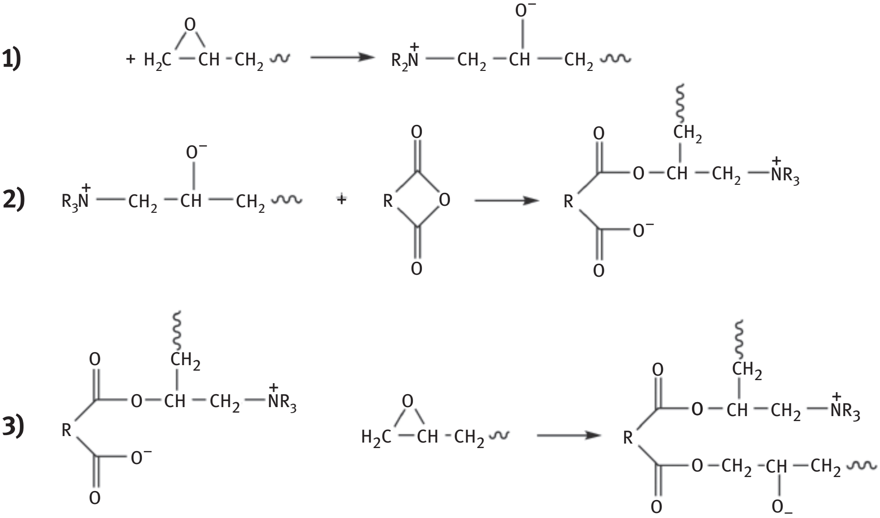

Figure 1.7: Curing mechanism of epoxides with anhydrides in the presence of tertiary amines.

mechanistically it is more complex and leads to the introduction of heteroatoms in the network structure.

In these initiated curing systems, the functionality of the epoxide group is two and therefore the global functionality of a diepoxy resin is four. Thus, from a diepoxide, crosslinked structures can be obtained by the use of the adequate initiator and conditions.

Anionic polymerization can be promoted by several initiators with high nucleophilic character or strong basic characteristics, but in the field of epoxy thermosets the most extended anionic initiators are tertiary amines [1], such as 1-methyl imidazole (1-MI) [15] or 4-(N,N-dimethylamino)pyridine (DMAP) [16] (Figure 1.8).

The curing mechanism initiated by tertiary amines is depicted in Figure 1.9. As can be seen, the opening of the epoxide by the nucleophilic attack of the amine forming an

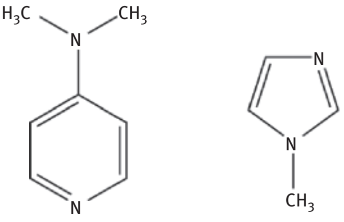

Figure 1.8: Chemical structures of tertiary amines used as anionic initiators.

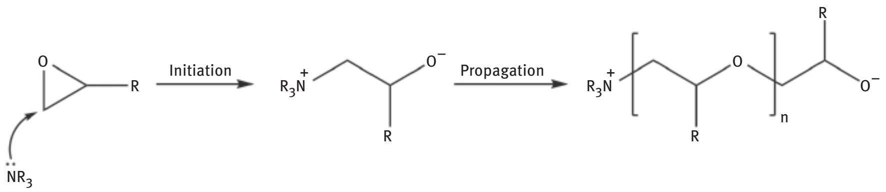

Figure 1.9: Anionic ring-opening homopolymerization of epoxides initiated by a tertiary amine.

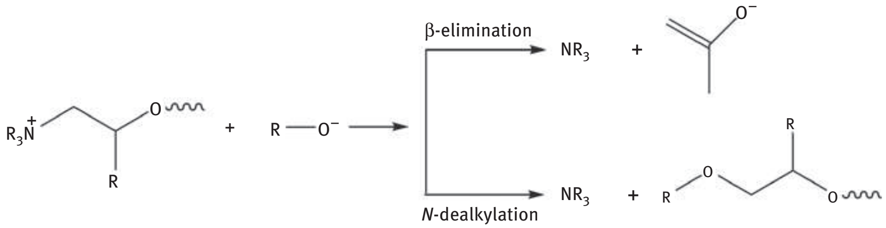

Figure 1.10: Possible pathways of tertiary amines regeneration.

alkoxide is the first step. Initiation and propagation proceed by nucleophilic substitution (S_N2) and as a consequence nucleophilic attack occurs in the less-substituted carbon.

Ooi *et al.* [17] observed by differential scanning calorimetric (DSC) studies two exothermic peaks during the curing process of N-alkyl substituted imidazole-DGEBA formulations. These results indicated that the curing mechanism represented in Figure 1.9 was more complex. The cause of the additional peak was associated with imidazole regeneration by β-elimination or *N*-dealkylation process, which then reinitiates the polymerization, as discussed in Figure 1.10.

Moreover, in previous studies it could be demonstrated that the presence of species that can coordinate with epoxides (such as hydroxyl groups) promotes the initiation step, speeding up the reaction due to the interaction between the hydroxyl group and the oxygen in the oxirane ring, which helps increase the positive charge in the oxirane ring methylene carbons (Figure 1.11). The imidazole regeneration can be also favored by the presence of hydroxyl groups [18, 19].

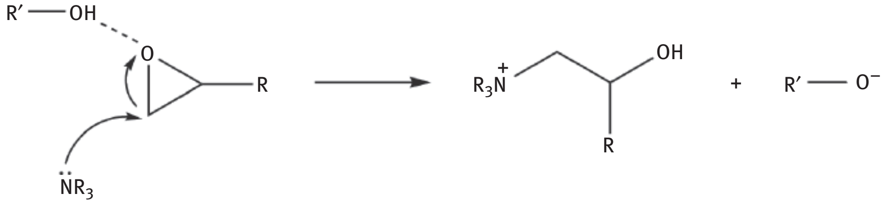

Figure 1.11: Nucleophilic opening of the epoxide group favoured by coordination with hydroxyl groups.

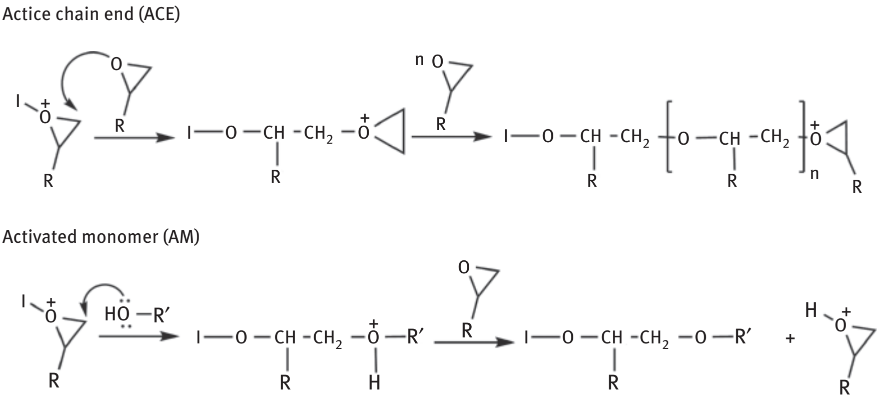

Actice chain end (ACE)

Activated monomer (AM)

Figure 1.12: Active chain end (ACE) and activated monomer (AM) propagation mechanisms for the cationic polymerization of epoxides.

If the initiation step is catalyzed by Brönsted or Lewis acids, the propagation takes place via a cationic mechanism. $TiCl_4$, $AlCl_3$, $ZnCl_2$, BCl_3, $SiCl_4$, $FeCl_3$, $MgCl_2$ and $SbCl_5$ are Lewis acids used as catalysts, but the most extended one is the BF_3/amine complex [20]. In recent years also lanthanide and rare earth metal triflates have demonstrated to be good cationic initiators [21–24].

Figure 1.12 shows the mechanism of propagation for the cationic polymerization of epoxides. In this case, there are two propagation mechanisms that coexist: active chain end (ACE) and activated monomer (AM) [25]. Both mechanisms start by the coordination of the initiator with the epoxide to promote the ring opening. The ACE mechanism consists in the reaction between an activated epoxide and a nonactivated one. In that way, the activated epoxide is always linked to the growing chain forming a cyclic oxonium cation. On the contrary, the AM mechanism requires a hydroxyl group to first open an activated epoxide. Then, there is an intermolecular interchange of protons with an epoxide that now becomes activated. Thus, the monomer is always the activated epoxide.

All these systems described constitute a two-component system in which the monomer and curing agents are stored separately and they are mixed in the correct quantity just prior to use. However, one-component systems in which the mixture of epoxy resin and curing agent is commercially supplied, also called one-pot resins, have considerable advantages over the others, since they are easier to use. One-pot epoxy resins require a latent curing agent, which does not react at room temperature, but reacts with epoxy resins under external stimulation, heat or irradiation [26]. Thermal latent curing agents can act mainly by two different mechanisms: the first one is based on their low compatibility in the epoxy resin because of their crystalline character or by encapsulation of the active species [27]. The second mechanism is based on the use of a precursor compound, inactive at room temperature, but which under triggering by heat transforms into an active curing agent [28]. Photoirradiation can also lead to the formation of active species, which originate homopolymerization by cationic or anionic processes [29]. Although photoirradiation is a more convenient way of triggering, from the point of view of energy savings, it presents some disadvantages, such as the curing of thick samples or with a complex geometry [30]. The initiation by heat is easier from the experimental point of view and can be applied to thicker samples or to hidden parts of surfaces.

The selection of the curing agent is the key point in the application, workability of the curing mixture, characteristics of the final thermosets and other factors.

1.4 Characteristics of epoxy thermosets

The degree of crosslinking and the nature of the bonds in the cured epoxies give them many desirable characteristics that have placed these thermosets as the standard option for a variety of applications such as adhesives, coatings, composites for structural applications, and so on.

Some of the most important characteristics of these materials are the absence of volatile matter on curing and the capacity to adhere to most substrates due to the presence of polar groups like hydroxyl or ether [10]. In addition, epoxy resins are resistant to thermal degradation and are stable to the attack by corrosive chemicals. These properties are related to the covalent bonds present in the network, which define their stability. The presence of groups that can be removed by chemical reactions using weak alkalis, strong acids and organic solvents reduce the chemical resistance [31, 32]. Moreover, the addition of cleavable linkages in the network structure allows thermosetting materials to be removed under thermal controlled conditions [33–35].

Epoxy thermosets are amorphous and highly crosslinked materials. The crosslinking density is a key parameter in determining the mechanical properties of an epoxy resin after cure. The higher crosslinked density allows these thermosetting materials to have high glass transition temperatures and useful properties like high values of hardness, tensile strength, shear strength or Young’s modulus.

However, in terms of structural applications, they have some disadvantages that limit their range of applications. Epoxy resins are in general brittle due to their high crosslinked character, which confers low impact strength and poor resistance to crack propagation [2]. The fracture resistance decreased with increasing crosslinking density [35]. Moreover, the tight structure implies a shrinkage that is undergone during the curing process, which finally leads to the apparition of stresses and defects in the material. The crosslinked nature enhances the thermal resistance, so they cannot be removed from a substrate without damaging it. In coatings technology, the resistance to scratch is another interesting issue to be improved. Thus, new strategies to overcome these drawbacks are needed, but these strategies should not compromise other properties.

1.4.1 Toughness

Toughness of a specimen refers to the total energy required to cause failure, i.e. the total area under the stress–strain curve or the energy absorbed in an impact test. Toughening of the epoxy resins by the addition of toughening agents or modifiers helps improve the amount energy absorption capacity. As a result, tremendous effort has been focused on improving the toughness of such materials during the past decades and many reviews in this area are available [36–38].

There are many approaches for improving toughness in epoxy resins, which include: a) chemical modification of the network structure to make it more flexible, b) increasing the molecular weight of the epoxy resin to improve the molecular weight between crosslinks, c) lowering the crosslink density of the matrix by adjusting the ratio of epoxy resin/crosslinking agent, d) adding reactive diluents, e) adding toughness modifiers in the formulation or f) incorporating inorganic fillers/reinforcements into the neat resin [36].

The most promising strategy for increasing the toughness of epoxy thermosets is the incorporation of plasticizers, like thermoplastic or rubbers, which increase the flexibility of the final network by the incorporation of a second dispersed phase [39, 40]. However, the addition of these modifiers usually compromises the modulus and thermomechanical characteristics of the thermosets, leading to a reduction of Young modulus and T_g, and worsening the processability of the formulation by increasing its viscosity [36].

Another method of preventing the crack from freely developing after impact is the addition of a modifier that induces the formation of particles that absorb the impact energy and deflect the crack. The formation of micro/nanostructures in multicomponent thermosets can further optimize the interactions between the thermosetting matrix and the modifiers and thus the mechanical properties of materials can be significantly improved. This is known as “toughening by micro/nanostructures” and can be achieved, among other procedures, following the chemical-induced phase separation methodology (CIPS) [41, 42]. It starts from an initial homogeneous mixture composed of the resin, curing agent and modifiers. On curing, a blend of epoxy matrix filled with rubber or thermoplastic microspheres is formed, with a final size of these particles controlled by the viscosity of the reacting mixture during curing [43].

Alternatively, new strategies as the incorporation of hyperbranched polymers (HBPs) [44, 45] or multiarm star polymers (SPs) [42] have been applied with good results in improving toughness without affecting the other properties of the resin [46]. The improvement in toughness in the case of HBPs is attributed either to the flexibilizing effect induced by the homogeneous incorporation of the HBP [47] or to

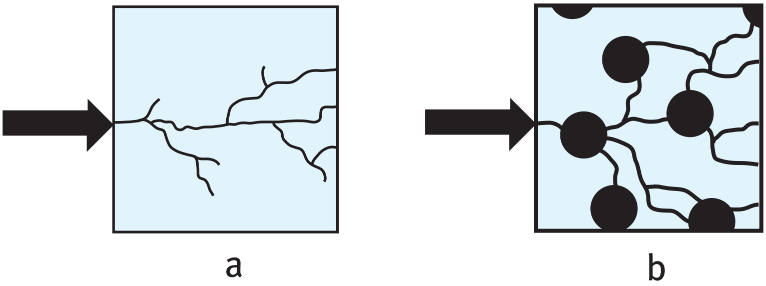

Figure 1.13: Crack propagation in materials: a) without particles and b) with dispersed particles.

the local inhomogeneities created in the crosslinked network by the formation of phase-separated nanoparticles with good interfacial adhesion between phases [48]. The particles hinder the propagation of a certain crack in the material as seen in Figure 1.13. Since the interaction between phases plays a key role in this toughness reinforcement mechanism, the structure of the HBP must be carefully selected in order to obtain the desired properties.

1.4.2 Shrinkage

When any type of monomers undergoes polymerization and crosslinking, shrinkage occurs throughout the cure process. Shrinkage is the reduction in volume brought about by increase in density. The curing process of epoxy resins entails shrinkage, which is a critical point in the field of coatings since it can lead to the appearance of internal stresses and consequently to defects in the materials, such as microvoids, microcracks or warping [49]. For this reason, the reduction of stresses is an important goal since the protection capability is reduced when thermosets are used as coatings.

One should distinguish between thermal and chemical shrinkage. Thermal shrinkage occurs in thermal curing because after curing the thermosets obtained at high temperature should be cooled down until room temperature and therefore the contraction is difficult to avoid. On the other hand, chemical shrinkage occurs because of the formation of new covalent bonding in the reactions taking place during the curing process. In general, as the monomer polymerizes, its density changes as a direct result of the bond changes being affected during polymer formation. Usually, the new bonds formed are shorter in the polymer than the distances between monomers [50]. This shrinkage is caused by the chemical reactions taking place during curing and it is described that the shrinkage during ROP is lower than chain growth and step growth polymerizations [50]. This is due to the fact that per each Van der Waals distance that becomes a covalent bond, there is one covalent bond going to a nearly Van der Waals distance (Figure 1.14). Thus, the use of ROP is a good strategy to produce the minimally shrinking epoxy thermosets.

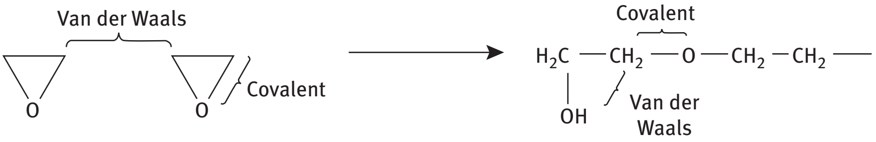

Figure 1.14: Changes of distances before and after ring opening polymerization.

Many approaches have been developed to solve the shrinkage issue related to the chemical reactions occurring during the curing process like the addition of inorganic inert charges (silica, quartz or mica) or polymeric charges (polyurethane foams, PVC or polystyrene). Unfortunately, the main problem of this strategy is that the T_g of the resulting thermosets decreases dramatically, reduces toughness, increases the viscosity and worsens the material properties, thereby limiting their range of applications [2].

New strategies such as the addition of HBPs as modifiers in epoxy thermosets can reduce the shrinkage during curing by reducing the internal stresses [51]. The incorporation of HBPs in the network decreases the coefficients of thermal expansion (CTEs) due to the higher degree of crosslinking coming from the high number of reactive groups in the HBP and does not reduce the T_g of the final materials [52]. Moreover, it has been reported that the increase in the amount of HBP added to the formulation reduces not only the global shrinkage but also the shrinkage after gelation, which is the true responsible of the apparition of stresses. [51]. It is worth noting that after the gelation, the material loses its mobility and therefore the shrinkage produced after gelation produces tensile, compressive and shear forces within the resin.

1.4.3 Reworkability

The concept of reworkability in thermosets is related to the ability of the material to break down under controlled conditions in order to be removed from a given substrate (Figure 1.15), but it does not mean that the polymeric material can be reused or recycled [34].

The decomposition of the degradable linkages upon heating is expected to lead to a decrease in crosslinking density and modulus of the adhesive or coating,

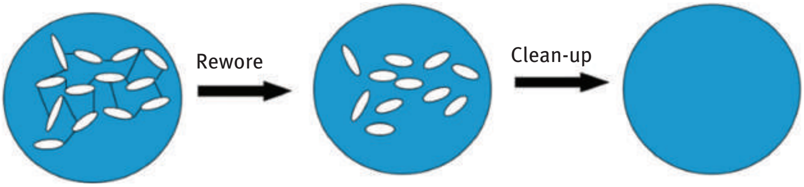

Figure 1.15: Scheme of the process of the elimination of a reworkable coating.

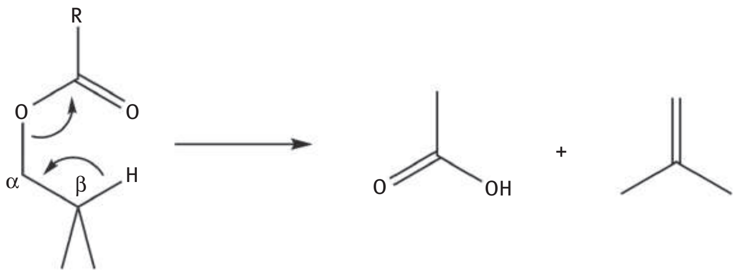

Figure 1.16: Mechanism of pyrolytic β-elimination of esters.

allowing its removal and replacement. The optimal temperature range for safe rework operation is desired to be within 200–250 °C [33, 53].

In order to obtain thermally reworkable epoxy thermosets, one of the first approaches was the introduction of disulfur linkages in the amine curing agent, which allows the fragmentation of the thermoset with temperature [54]. Other authors proposed the introduction of thermally labile groups in the structure of the resin [55, 56]. The introduction of ester groups improves the reworkability since they can be broken by a *β*-elimination process (Figure 1.16) at a temperature of about 235 °C [33].

Alternatively, there also exists the possibility of introducing groups that can be eliminated by chemical reactions. This is the so-called “chemical reworkability”. There are many strategies based on this principle. For instance, the introduction of olefinic unsaturation in the structure of the resins allows the cleavage of the network by oxidation of the double bonds with permanganate. If the groups introduced are carbamates, the cleavage is carried out by strong acid treatment [57].

Other examples are the use of epoxy resins with ketal groups in their structure, which can be hydrolyzed after acid treatment [58] or the copolymerization of epoxy resins with spirocyclic γ-bislactone obtaining thermosets that can be completely solubilized in 1 M ethanolic KOH solutions [59].

1.4.4 Scratch resistance

In many coating systems, the uppermost layer is a thin coating, which not only protects the underlying layers or substrate from chemical and UV degradation, but also provides protection from mechanical damage that can result in surface blemishes/scratches [60]. Excellent scratch-resistance coatings are characterized by large plastic deformation, small cracks and high elastic recovery [61].

There are two main ways of improving the scratch resistance of organic coatings: one is to optimize the polymer lacquer components and the other is to reinforce the coating by embedding fillers into them [62]. The addition of nanosized silica and alumina particles having diameters of 10–50 nm represents an attractive alternative to conventional fillers. Because of their nanometer size and their large active surface, it can be expected that polymeric nanocomposites exhibit markedly improved properties as compared to pure polymers or conventional composites. Thus, different inorganic and organic nanopowders, such as SiO_2, Al_2O_3 or ZrO_2, have been employed, yielding considerable mechanical reinforcement [63].

Hybrid organic–inorganic nanocomposites have drawn considerable attention, in recent years, because they combine the advantages of an organic polymer (flexibility, light weight, good impact resistance and good processability) and inorganic materials (high mechanical strength, good chemical resistance, thermal stability and optical properties) [64]. The formation of inorganic domains generated in situ for enhanced surface scratch resistance seems to be a very promising approach toward new, multifunctional technical coatings [65]. The generation of nanostructures in the polymer matrix by sol–gel processes leads to a fine dispersion of the inorganic phase into the epoxy matrix, which could be advantageous in comparison to the addition of performed inorganic nanoparticles, improving scratch characteristics.

Nowadays, the combined use of HBPs and sol–gel reactions in the preparation of nanocomposites seems to be advantageous as they can allow better interaction of the organic phase with the inorganic particles [66, 67]. The multifunctional HBP structure allows to prepare silica hybrid coatings with a strong increase in surface hardness and scratch resistance.

1.5 Dendritic polymers

In the 1980s, a kind of highly branched three-dimensional macromolecules, also named dendritic polymers, was born and gradually became one of the most interesting areas of polymer science and engineering [68]. Dendritic architecture is recognized as the main fourth class of polymer architecture after traditional types of linear, crosslinked and chain-branched polymers that have been widely studied and industrially used [69].

Dendritic molecules are composed of repeating units emanating from a central core. When the structure of the molecule is perfectly symmetric around the core and adopts a spherical three-dimensional morphology, a dendrimer is formed. In contrast, the presence of some imperfections results in a hyperbranched polymer (HBP). A schematic representation of dendrimers and HBPs is represented in Figure 1.17.

In a perfectly branched dendrimer, only one type of repeating unit can be distinguished, apart from the terminal units. However, HBPs present three different types of repeating units, named D, L and T, as illustrated in Figure 1.18.

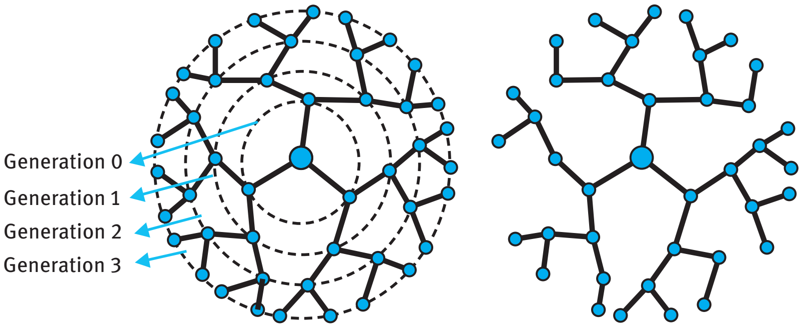

Figure 1.17: Schematic representation of a dendrimer and a hyperbranched polymer.

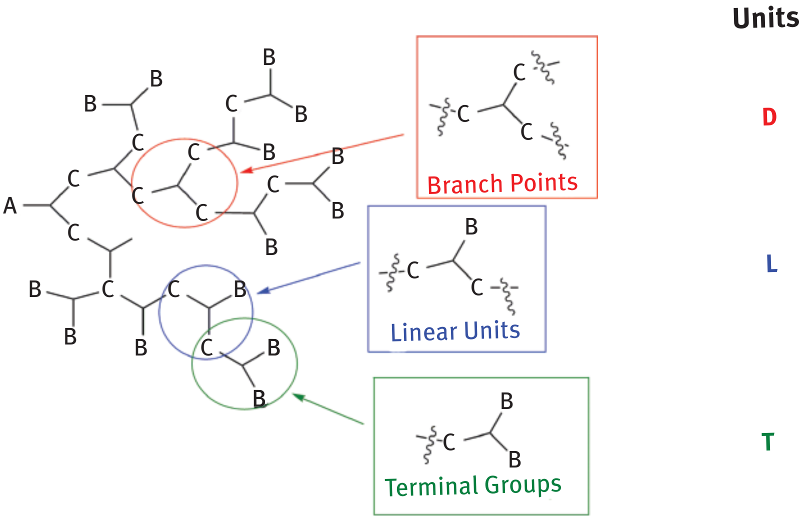

Figure 1.18: Different units present in a HBP obtained from the polymerization of an AB_2 monomer.

The degree of branching (DB) is a structural parameter used to characterize the topology of dendritic polymers and is one of the most important because it has a close relationship with polymer properties such as free volume, chain entanglement, mean-square radius of gyration, glass transition temperature (T_g), degree of crystallization (DC), capability of encapsulation, mechanical strength, melting/solution viscosity, biocompatibility and self-assembly behaviors [70, 71]. Fréchet and coworkers [72] defined the DB as the ratio of the molar fraction of branched and terminal units relative to that of the total possible branching sites.

$$DB = \frac{D + T}{D + T + L} \tag{1.1}$$

where D is the number of fully branched units and L is the number of partially reacted units. The value of the DB varies from 0 for linear polymers to 1 for dendrimers or fully branched HBPs (see **Figure 1.4**).

Dendritic polymers are characterized by special features that make them promising candidates for a number of applications. One of the most interesting physical properties is their lower viscosity in comparison with their linear analogues, which is a consequence of the architecture of the molecules [73]. The relationship between molecular weight and viscosity for various polymer topologies is represented in Figure 1.20. Dendrimers in solution reach a maximum of intrinsic viscosity as a function of molecular weight as their shape changes from an extended to a more compact globular structure, especially at high molecular weights [74, 75].

Well-defined structures require a stepwise synthesis and dendrimers are usually prepared by an iterative synthesis, with the purification of intermediate stages or generations while hyperbranched molecules can be synthesized in one step. This characteristic and their good properties such as low viscosity, good solubility and good chemical reactivity make HBPs suitable products for a larger application scale in typical technological fields like coatings and adhesives [76].

1.5.1 Hyperbranched polymers

HBPs are highly branched three-dimensional macromolecules with a large number of end groups (Figure 1.19) [77]. They have special properties, which are key to their industrial applications. As mentioned before, one of them is low viscosity compared with their linear analogues.

Besides, HBPs have high chemical reactivity and enhanced solubility when compared to their linear analogues. They also exhibit enhanced compatibility with other polymers as has been demonstrated by blending studies [73]. Hyperbranched

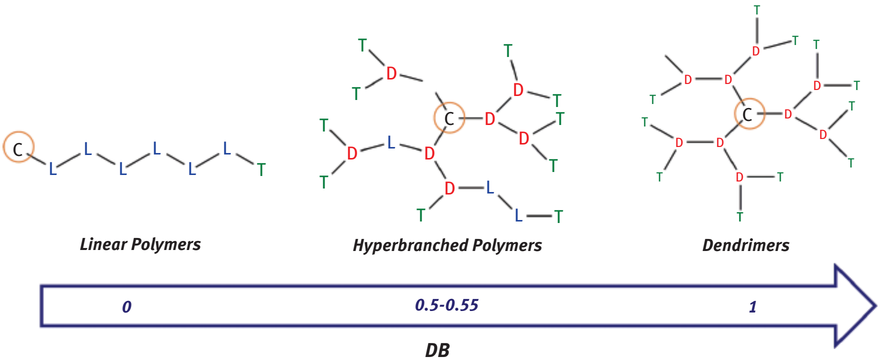

Figure 1.19: Values of the DB of linear polymers, HBPs and dendrimers.

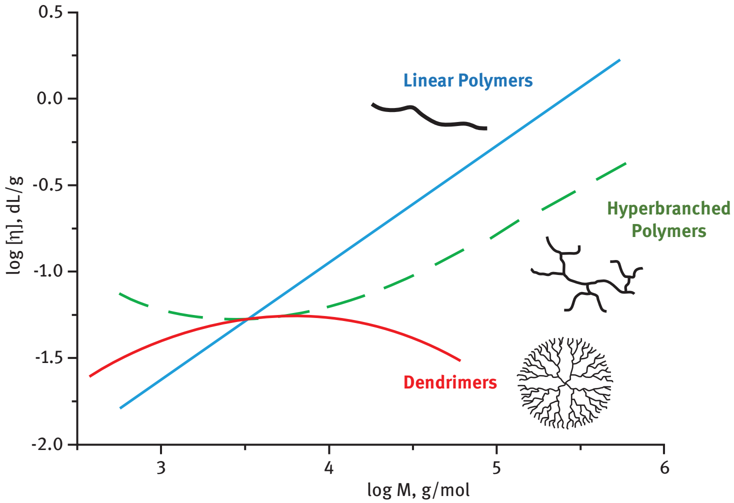

Figure 1.20: Relationship between intrinsic viscosity (η) and molecular weight (M).

materials also have outstanding mechanical properties such as modulus, tensile strength and compressive moduli, which reflect the compact highly branched structures [73]. Owing to those special properties, HBPs have been used as rheology modifiers or blend components [44, 78], tougheners for thermosets [43, 45] and crosslinking or adhesive agents [79]. Also, HBPs have been used as the base for various coating resins [80], including powder coatings [81], flame-retardant coatings [82] and barrier coatings for flexible packaging [83].

1.5.2 Star polymers

Dendritic polymers with a single branch point and all arms exhibiting low degrees of compositional heterogeneity with respect to composition, molecular weight and molecular weight distribution are named star polymers (SPs) [84]. Basically, SPs consist of linear polymeric chains radiating from one single branched point, called “core” or central nodule, and which can itself be polymeric. If the arms are identical, the SP is said to be regular. If the adjacent arms are composed of different repeating subunits, the SP is said to be miktoarm. The copolymeric nature of the arms leads to the so-called copolymeric stars (Figure 1.21). For the preparation of multiarm SPs, a multifunctional core is needed. The lower cost of HBPs, the presence of reactive final groups and their easy synthesis from commercially available monomers make them adequate cores for their preparation.

SPs resemble more closely the hard sphere model, especially when the numbers of arms in the SP are high. The hard sphere character of SP is directly correlated to entanglement. If the number of arms is high, the entanglement decreases and it is

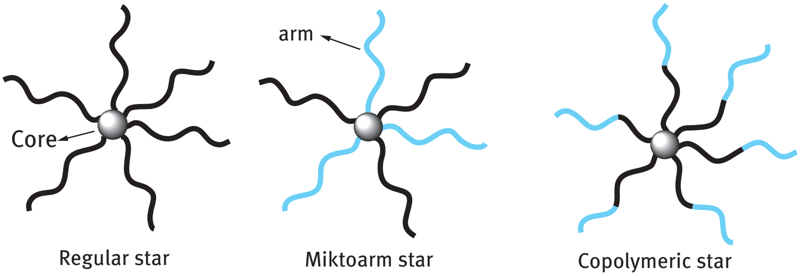

Figure 1.21: Schematic representation of star polymer structures.

lower than in linear polymers, causing lower intrinsic viscosity of these materials as compared to linear polymers of the same molecular weight, which is one of the main features of SPs [75, 85, 86].

Owing to their compact structures and high segment density, SPs have gained increasing interest. Nowadays, the incorporation of biocompatible segments on the star copolymer structures is of particular interest for biomedical applications [87]. Moreover, SPs have potential applications as components of different types of complexes, hydrogels, networks, ultrathin coatings, thermoset modifiers, etc. [88]-[90].

1.6 Modified epoxy thermosets by using HBPs and other highly branched topologies

Over the past few years, HBPs have received much attention as modifiers of epoxy systems to improve the mechanical properties, reduce the shrinkage on curing [51] and increase the reworkability [31], if the structures are conveniently selected [45, 91].

One of the first HBPs used as modifier for epoxy resins was an aliphatic hyperbranched polyester based on 2,2-bis(hydroxymethyl)propionic acid (BHMPA) [92]. This polymer was produced and commercialized by Perstorp as Boltorn HX (where X can be 20, 30 or 40 related with the degree of polymerization). There are several published papers on the use of Boltorn as a modifier in different epoxy thermosetting systems. Ratna *et al.* [93] used Boltorn H30 as a modifier in epoxy/amine thermosets. The final materials showed globular HBP particles dispersed in the epoxy matrix and the result was a significant improvement of the impact strength, approximately twice the value of the neat material, when a high concentration of HBP was used. However, Yang *et al.* [94] obtained homogeneous materials in epoxy/anhydride systems and the improvement in impact strength was around 25 % over the pure epoxy/anhydride matrix by the addition of HBP as a modifier. This could be explained by the formation of particles in the first case and a homogeneous material in the second due to the different chemistry implied in the curing process.

Different modifications of Boltorn-like polymers have been described in the field of thermosets. Varley and Tian [95] reported the use of an epoxidized Boltorn as a modifier of epoxy/anhydride systems. The addition of HBP had a minimal effect on the viscosity of the mixture. Furthermore, the modified materials showed excellent improvements in toughness. A 100 % increase in fracture toughness was achieved by the presence of a 20%wt of HBP in the epoxy network.

The effect of DB of HBP in the improvement of epoxy materials cured by the cationic initiator was studied [96]. In these systems, the viscosity of the formulation was lower on increasing the DB of the modifier, which confirms the advantages in the rheological behavior of HBP-modified formulations. On increasing the DB, the T_g was increased and the storage moduli in the rubbery state followed the same trend. The addition of HBP to the formulation led to a reduction of the global shrinkage on the curing process, which increased with the proportion of modifier and DB. Because of the aromatic poly(ester) nature of these HBPs, the thermal stability increased, but the chemical reworkability in the basic solution improved. The high thermal stability is due to the fact that aromatic ester groups cannot be broken by β-elimination processes because of the absence of hydrogen in the β-position [31]. This study put in evidence the validity of the dendritic characteristics in the improvement of epoxy thermosets.

Boltorn polyesters have also been used to control the shrinkage in the cationic polymerization of DGEBA using hydroxyl-terminated HBPs [51]. The reduction in contraction during curing was observed because intermolecular and intramolecular H-bond interactions decreased and the free volume increased when HBP reacts and gets incorporated into the network.

The large number of reactive sites present in the HBPs structure allows the possibility of changing their solubility in the epoxy matrix by the attachment of polar or nonpolar units to the end groups [97]. As a result, optimal shell chemistry design of the HBP could be achieved, which permits one to obtain homogeneous or nano- and microstructured thermosetting materials [91]. Moreover, by tailoring their chemistry, it is possible to reach suitable mechanical properties for inducing the most efficient toughening mechanism [98]. Flores *et al.* [99, 100] reported the use of partially modified Boltorn-type polyesters and hyperbranched poly(glycidol) with 10-undecenoyl moieties as modifiers in DGEBA thermosets. The materials obtained resulted in a significant increase in impact strength, since the use of partially modified HBP led to phase-separated materials with particle sizes on the nanometric or micrometric scale with good interaction between particles and matrix because of partial covalent bonding. Both structural facts led to a cavitation mechanism of toughness enhancement. This enhancement was possible without affecting the thermal stability, thermomechanical characteristics or processability of the formulations.

Other HBPs as poly(ester-amide) and poly(amino-ester) have been used as modifiers for epoxy resins, leading to improvements in shrinkage, degradability or mechanical properties [52, 101]-[103]. The effect of molecular weight of different hyperbranched poly(ester-amide)s before shrinkage was investigated and a progressive decrease of global shrinkage was observed on increasing the proportion of HBP and in the higher molecular weight [101].

In addition to HBPs, multiarm SPs can also be considered as a new class of modifiers for epoxy resins. Meng *et al.* [42] obtained nanostructured diglycidylether of bisphenol A thermosets using core-crosslinked stars based on poly(styrene) core with poly(ethyleneoxide) or poly(styrene)-*b*-poly(ethyleneoxide) arms. T_gs values of the epoxy thermosets containing the modifiers were clearly improved. The mechanical properties (Young's modulus, impact strength and microhardness) showed a maximum value when 10%wt of the modifier was added to the formulation.

It has been reported that multiarm stars with poly(ε-caprolactone) (PCL) arms and different cores were used as epoxy thermoset modifiers [90, 102, 104]. The addition of these polymers led to homogeneous materials with a more tough fracture while reducing the shrinkage on curing without compromising the thermomechanical properties. Multiarm SPs with poly(styrene) and poly(methyl methacrylate) arms were also used as modifiers in epoxy systems obtaining phase-separated materials or nanograined morphologies [105, 106]. The impact strength was improved in the material with the highest content of modifier. Chemically reworkable epoxy coatings by the addition of these star topologies were also prepared [32]. An important characteristic of these modifiers is the low viscosity of the formulation. It could be demonstrated that on increasing the number of arms and shortening them, the viscosity was lower [107].

Miktoarm SPs were also synthesized with a hyperbranched polyester core and poly(ethylene glycol) arms or poly(ethylene glycol)/PCL arms [108]. The resulting materials, due to the amphiphilic character of the multiarm star, showed phase-separated morphologies with nanosized particles and a significant improvement on impact strength. The best improvement was obtained by using the miktoarm containing poly(ethylene glycol)/PCL arms. Due to the hydrophilic/hydrophobic character, this modifier demonstrated a high self-assembly tendency, responsible for the improvement.

1.7 HBPs and multiarm SPs from PEI

The common terminal groups of HBPs are hydroxyl moieties. Through them, numerous functional components can be introduced into the HBP structure. However, amine-terminated HBPs are also interesting and have been scarcely explored. Hyperbranched PEI presents a high content of amino groups and is very attractive for several industrial applications [109]. One of the most important features of PEI macromolecules is their availability at industrial scale and low cost.

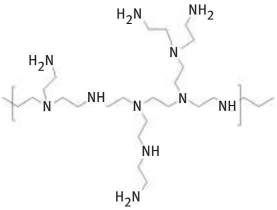

Figure 1.22: Chemical structure of hyperbranched poly(ethyleneimine).

Nowadays, there are many companies selling HBPs, which are used in many industrial applications. Among them, BASF commercializes a family of HBPs with the name of Lupasol® that consists of hyperbranched poly(ethylenimine) (PEI) [110]. It should be said that firstly PEI was commercialized under the name Polymin [111]. PEI, also called poly(aziridine), is a polymer with a repeating unit composed of an amino group and an ethylene spacer (Figure 1.22).

The industrial production of ethyleneimine and PEI began in Germany about 1938, when I.G. Farbenindustrie (founded as a merger of BASF, Bayer, Agfa, Hoechst, Chemische Fabrik Griesheim-Elektron and Chemische Fabrik) built and operated a plant in Ludwigshafen. In 1951, the company was split into its original constituent companies. The four largest companies (BASF, Bayer, Agfa and Hoechst) quickly bought the smaller ones.

Hyperbranched PEIs are produced in a large scale by self-condensing ROP. In this methodology, a heterocyclic monomer is used and a cationic or anionic mechanism is applied. Lupasol products are obtained through cationic polymerization of the ethyleneimine monomer (aziridine) by a wide variety of acidic reagents and quaternizing agents [112]. The polymerization is terminated by reaction with water. Under these conditions, branched-chain structures are formed as is shown in Figure 1.23. The DB is dependent upon reaction conditions such as catalyst and ethyleneimine concentration. PEI dendrimers were also prepared [113].

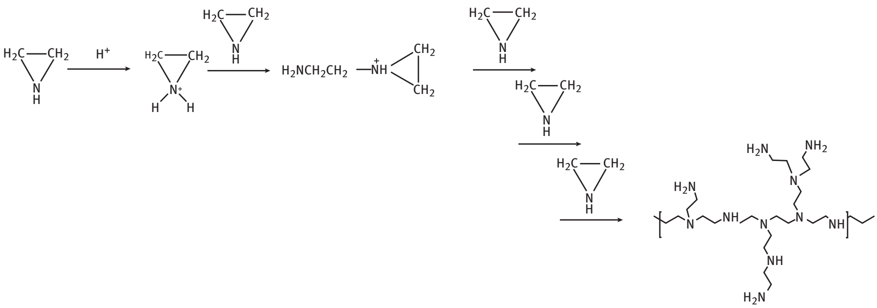

Figure 1.23: Synthesis of poly(ethyleneimine) from aziridine monomer.

The Lupasol product range is extensive. Water-free products and aqueous solutions are commercially available and applied to a huge variety of materials providing advantages and new properties. PEI was first described as an agent for producing wet-strength papers, being usable in neutral or alkaline systems, a significant departure from the acid-requiring urea-formaldehyde resins that were extensively used. However, the use as additive in this field has been diminished, with the exception of certain special papers, by the arrival of new wet-strength agents that can perform this function more advantageously [114]. In addition, PEI has been used for the preparation of cationically active papers from chromatography and electrophoresis [115].

In the textile industry, PEI improves the dye fixation [116], hydrophilicity [117] and flame-proofing of cotton [118], among others. Moreover, the unique properties of PEI make it useful in many applications (plastics, metals, etc.) [119] and can be used as flocculating agents, disinfectants, etc. [120]. In coating technology, the addition of PEI makes coatings and adhesives stick better to porous and nonporous surfaces [121]. In the biomedical field, PEI has attracted an increasing interest because of its potential application in gene delivery [122].

By modification of PEI, the application range can be further expanded. Amidation with acids, alkoxylation, alkylation and carboxylation has been performed, leading to PEI-modified structures used as CO_2 cells [123, 124], detectors with specific recognition elements [125, 126], drug delivery [127] or nano-carriers [128], among others.

Recently, Appelhans *et al.* introduced mono- and oligosaccharide units on the PEI surface by reductive amidation or N-carboxyanhydride polymerization [129, 130]. These defined novel oligosaccharide architectures on dendritic polymer surfaces have been studied as nano-sized carrier systems for gene delivery [131, 132] or metal nanoparticles [133, 134].

PEI shows high potential for the preparation of core-shell-type SPs and it has been used as a macroinitiator since amine groups can react easily with many of the reactive groups. Bauman *et al.* [135] grafted linear polyamide-12 into PEI by two different pathways, through transamidation of linear PA12 in the presence of PEI core or by ROP of laurolactam.

Starting from PEI as the core, SPs have been synthesized polymerizing ε-caprolactone (CL) [136]. These polymers were used as unimolecular micellar nanocapsules for accommodating guest molecules [122, 137]. Following the same methodology, SPs containing a PEI core and poly(lactide) arms were prepared and used as nano-carriers [138].

Unmodified PEI has also been used as a curing agent of the epoxy-amine system. The HBP can be incorporated into the network structure of the thermosets to improve the shape-memory behavior with an enhancement of the thermal-mechanical properties [139, 140].

The reactivity of amino groups in the PEI structure toward acids, isocyanates, acrylates and epoxides allowed one to prepare a series of new structures that can be used in the improvement of epoxy thermosets. The incorporation of different reactive end groups in PEI has opened the possibility of obtaining thermosetting materials by different methodologies. Hybrid organic–inorganic epoxy materials could be prepared by the sol–gel approach from trialkoxysilylated PEI [141, 142] and by using "click chemistry" different thiol click reactions could be performed on conveniently modified PEI, forming copolymeric materials with epoxy networks [143, 144]. The possibility of growing polyester arms from PEI cores by ROP has also been applied to prepare a family of multiarm stars that have been further used in the epoxy thermosets modification [145]-[148].

1.8 Modification of hyperbranched PEI with long alkyl chains and its use as modifier in epoxy thermosets

The toughness of epoxy thermosets is an important characteristic in many applications and many efforts have been made to date in order to improve it. The addition of conventional toughening modifiers such as rubbers and high-performance thermoplastics is the main strategy that has been followed by several authors [149, 150]. However, these additives compromise the modulus and the thermomechanical characteristics of the thermosets, which restrict their range of application. In order to overcome these limitations, HBPs have been proposed as reactive modifiers, leading to a significant improvement of this property without negatively affecting the thermomechanical characteristics [151].

The modification of different epoxy systems using commercially available HBPs has been reported [52, 103, 152, 153]. An increase in impact strength was achieved without sacrificing the thermal and thermomechanical properties. The enhancement of toughness could be explained by the flexible structures from the HBPs, which increase the capability of the epoxy matrix to undergo plastic deformation. The high density of hydroxylic groups that can react with some curing agents allows the covalent linkage of the HBP to the epoxy matrix, resulting in homogenous materials.

PEI could be considered as an alternative to hyperbranched polyesters for the modification of DGEBA since the presence of a high content of amines can increase the compatibility between the HBP and the epoxy matrix. Santiago *et al.* reported the use of hyperbranched PEIs as curing agent and studied in detail the curing kinetics in comparison with a linear aliphatic triamine [139]. Moreover, as epoxy modifier, the effect of the molecular weight of the PEI on the thermal, dynamomechanical and mechanical properties of 1-MI/epoxy-based materials was examined [154]. Recently, taking into account the results obtained using the PEI as a crosslinking agent, the shape-memory behavior has been studied [140]. High values of shape-recovery rate were achieved depending on the crosslinking density. However, amines are very reactive at room temperature with epoxy resins, leading to a short pot-life. Therefore, the reduction of the amino reactive groups in the structure is sometimes needed. The easy modification of the amino reactive groups allows one to obtain PEI-modified polymers with many different groups in order to make them suitable for different applications.

It is known that impact resistance is determined by the morphology formed during the curing process. The addition of a modifier that can undergo phase separation during curing is an alternative approach for toughening thermoset polymers [155]. An important method to produce phase-separated thermosets is CIPS. CIPS generally proceeds from an initially homogeneous solution via liquid–liquid phase separation to yield a regular phase-separated morphology in the course of reaction. The increase in the molecular weight of the polymer with the curing reaction results in a decrease in the entropy of the system. To date, there are several reviews on the preparation of micro/nanostructured thermosetting polymers by means of the CIPS methodology [41, 156].

HBPs offer the potential for tailoring their compatibility with epoxy resins through the conversion of their end-groups. The introduction of nonpolar moieties reduces the polarity of HBPs with a consequent decrease in their miscibility with epoxies leading to phase-separated materials by the CIPS methodology. On this base, the modification of HBPs using long aliphatic chains has been reported [157]. Flores *et al.* prepared a series of partially modified Boltorn H30 by the acylation process with 10-undecenoyl chloride [99]. Their addition to epoxy/anhydride formulations led to a great increase in the impact strength (more than 400 %) compared with the neat material. Following the same approach, different modifications of hyperbranched poly(glycidol) were performed and the epoxy thermosets prepared showed a significant increase in impact strength (greater than 200 %) with respect to the unmodified material [100]. In both cases, the enhancement in impact strength was achieved by the formation of microphase-separated particles by CIPS with a good interaction with the epoxy matrix due to the covalent linkage of the remaining OH groups of HBPs with the curing agent.

The preparation and characterization of PEI derivatives by the amidation process have been followed by several authors [158]-[161]. For example, amidation with fatty acids leads to pigment dispersants for nonpolar solvents [162] due to the decrease in the polar character by the reduction of the amine content. PEIs modified with alkanoic acids with different alkyl chains were used as macromolecular antioxidants [163].

The reactive amines present in the PEI structure can be modified by the amidation procedure, since amines can react with acyl chlorides and acids. To form amide bonds by using acyl chlorides, an additional base is usually required to trap the formed HCl and to avoid the conversion of the amine into its unreactive HCl salt and normally 4-(N,N-dimethylamino)pyridine is added [164]. Taking this into account, the modification of PEI by this procedure is limited by the presence of a high quantity of amines, which can be protonated, which makes the purification process difficult. As an alternative, N,N-carbonyldiimidazole (CDI) and dicyclohexyl carbodiimide

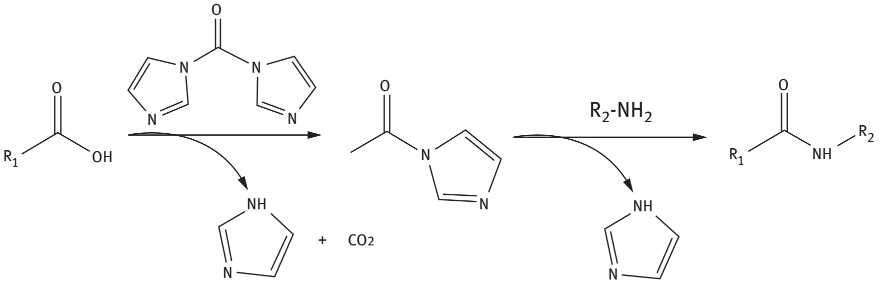

Figure 1.24: Synthetic procedure of CDI mediated amide formation.

(DCC) are frequently used for amide bond formation since they do not need an additional base [164]. CDI is the most commonly used reagent for the synthesis of amides from carboxylic acids and amines through the acyl imidazole intermediate (Figure 1.24) due to the mild conditions under which it can be used, its low cost and the formation of innocuous by-products (CO_2 and imidazoles).

The synthetic process is carried out in one pot and two steps: first, the activation of 10-undecenoic acid by reaction with CDI and then the nucleophilic substitution of imidazole group in the CDI derivative by amines of the PEI structure. On changing the proportion of CDI and 10-undecenoic acid to NH reactive groups, different modification percentages could be obtained [165].

1.9 Synthesis of multiarm SPs by ROP and their use as modifiers in epoxy thermosets

SPs are characterized as the simplest case of branched species where all chains of a given macromolecule are connected to a core. The preparation methods and properties of star-branched polymers were examined in detail several years back [84].

Commonly, SPs have been widely used as well-defined nanoparticles for applications in nanomedicine, catalysis, drug and gene delivery, among others [166, 167]. Different functional cores can be used to synthesize multiarm SPs [168, 169] and the arms can be obtained using different synthetic methods [170, 171]. The possibility of modifying the structure by the conjugation of different segments to their end functional groups is an advantage to determine the good host–guest properties. Moreover, star-like topologies have attracted considerable interest as toughness modifiers of thermally cured epoxy thermosets because of their unusual physical and rheological properties [42]. The properties of the final materials are related to the SPs structure, the amount of end groups and the molecular weight and length of the arms.

The use of SPs as modifiers in epoxy resins has been explored. Different multiarm SPs were synthesized using poly(glycidol) [104] and poly(styrene) [90] as a

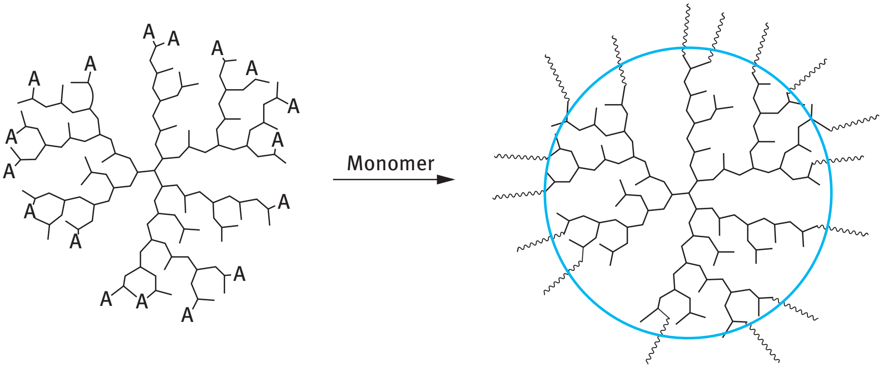

Figure 1.25: Synthesis of a muktiarm star polymer by the core-first methodology.

macroinitiator and PCL arms and the use of these star-like structures has been demonstrated to be suitable to modify epoxy resins due to their potential as toughening agents. They also showed the capacity to improve other characteristics, without negatively affecting the curing and processability as well as the final thermomechanical properties of the materials.

Generally, SPs can be prepared by “core-first” and “arm-first” methodologies. In the first method, the polymerization of the monomer for the growth of arms is conducted from either a well-defined initiator with a known number of initiating groups or a less-defined multifunctional macromolecule or HBP (Figure 1.25) [172].

In the arm-first synthesis (Figure 1.26), two different approaches are possible: one is where a linear polymer, previously synthesized, with a reactive chain end is directly attached to a multifunctional core (**A**). The other is the direct copolymerization of a macromonomer with a di- or multifunctional monomer in the presence of an initiator (**B**) [84].

In the core-first methodology, the arm length can be tailored by the ratio of active sites to the amount of added monomer obtaining well-defined SPs with a known number of arms. High yields are achieved with only simple purification methods compared with the arm-first method in which the purification processes are much more complex since the impurities consist of polymers that have not been attached to the star structure. Moreover, the number of arms in “arm-first” methodology is not always well-controlled. Despite the approach used, obtaining SP with a high number of arms is a tough task since a macroinitiator is needed (i. e. HBP) and the molecular weight of the arms can be only determined by indirect methods. In most of the core-first syntheses, HBPs like polyesters, polyethers or PEI have been used as macroinitiator [173]-[175].

To date, well-defined stars have been prepared through the ROP of lactide (LA) and CL using polyhydroxyl compounds as co-initiators [174, 176]. ROP processes, which take place by a living polymerization, provide sufficient polymerization

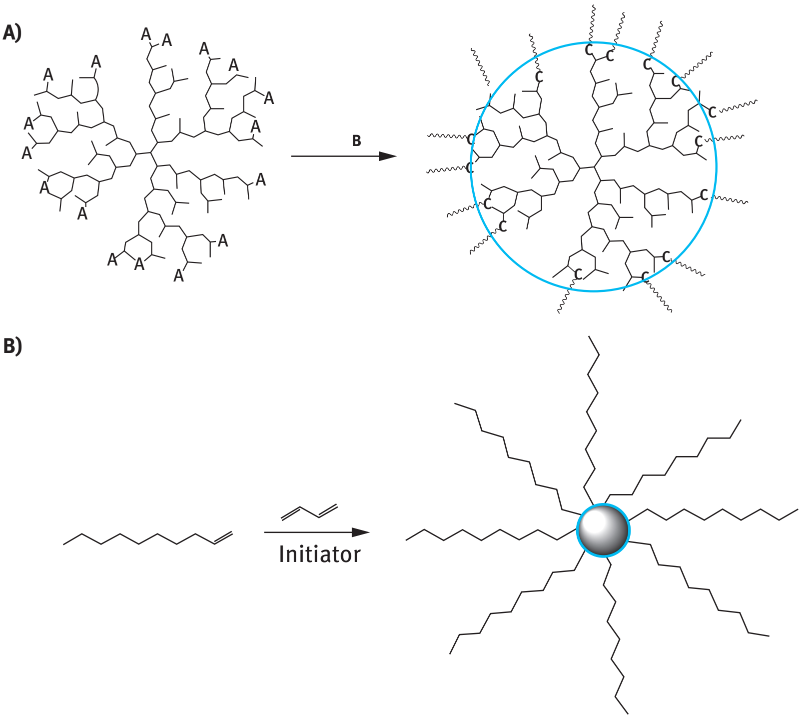

Figure 1.26: Synthesis of multiarm star polymers by arm-first methodology.

control, producing polymers of the expected molar masses and leading to the desired end-groups [177]. The mechanism allows preparing defined arms in the SPs structures. It has been shown that LA and CL can be polymerized in a controlled manner using Sn-based catalysts in combination with initiating hydroxyl or amine groups. However, references devoted to SPs prepared through the PEI-initiated ROP of LA and CL were scarce [136, 138].

The polymerization mechanism of CL and LA co-initiated with amines involves several steps to obtain the desired products [178]. The reaction of PEI with CL is preceded by the carboxylate-imine groups exchange at the tin atom in $Sn(Oct)_2$, accompanied by the octanoic acid (OctH) release (Figure 1.27).

Figure 1.27: Activation of the macroinititor (PEI) using $Sn(Oct)_2$.

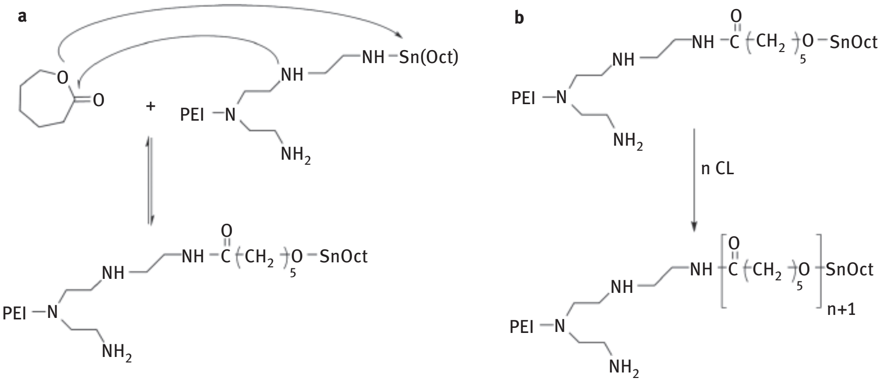

Figure 1.28: Initiation (a) and propagation (b) of the polymerization reaction.

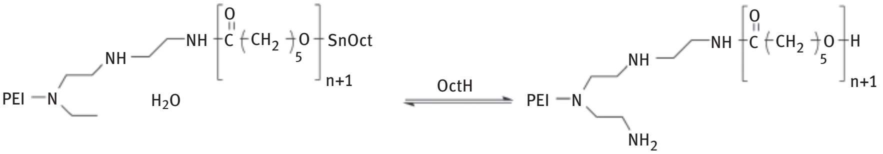

Figure 1.29: Termination step.

The polymerization is followed by CL monomer insertion, forming a new tin(II)-alkoxide specie (Figure 1.28.a) initiating the propagation step (Figure 1.28.b).

Finally, the exchange reaction with OctH results in the final product and the $Sn(Oct)_2$ is recovered again (Figure 1.29).

By this mechanism, different degrees of polymerization in the arms can be achieved taking into account the ratio of CL and LA to the reactive amine groups. The different structures of repetitive units in the arms can tailor the characteristics of the SPs modifiers [145, 146].

PCL is a hydrophobic, semicrystalline polyester with a high chain flexibility, which is miscible in most epoxy systems [179]. The use of PCL to modify epoxy resins appears to be a good choice due to the presence of OH groups as chain end that could be covalently linked to the epoxy network if the proper curing agent is used. Its flexible structure is capable of promoting crazing and shear yielding, leading to a toughened material [180]. Moreover, the presence of aliphatic esters, which can undergo thermal degradation by a pyrolytic elimination process, allows the reworkability of the modified coating.

In the same manner, the incorporation of poly(lactide) (PLA) in SPs can enhance the final mechanical properties of the thermosetting materials and a higher thermal reworkability is expected by the lower thermal stability of the secondary ester groups of PLA compared to esters of the primary alkyl groups of PCL [181].

It is known that the formation of micro- or nanostructures improves the overall properties of thermosetting materials [182]. One strategy to reduce the compatibility of SPs and to form well-dispersed SPs microparticles in the final materials is the modification of hydroxyl groups by acetylation to obtain end-capped multiarm SPs [147, 148]. Following this strategy, impact resistance could be enhanced by 300 % compared to neat DGEBA/anhydride formulations.

1.10 Ethoxysilylation of hyperbranched PEI and the use in the preparation of hybrid thermosets

Demands for epoxy resins are extremely strong because of their wide applications as adhesives, coatings and as advanced composites in aerospace and electronic industries [10]. However, epoxy thermosets have several limitations mainly related to their low mechanical properties and high thermal expansion coefficient (CTE) compared with inorganic materials. Thus, when applied as protective coatings on metal substrates, they are quite fragile and the variation in the temperature leads to a mismatch between the substrate and the coating, leading to the loss of adhesion and to the apparition of cracks. These limitations can be overcome by using inorganic/epoxy materials [183]. Inorganic fillers are the most common additives used in epoxy formulations to improve mechanical properties, such as modulus, strength and scratch resistance [184].

These materials can be obtained by different routes: (a) by the addition of preformed nanoparticles or nanoclusters [185] or (b) by the in situ generation of an inorganic phase through a conventional sol–gel process [186]. The in situ sol–gel polymerization of metal precursors in a polymeric (or monomeric) matrix is a better approach before the addition of silica fillers since this makes possible a very fine dispersion of the inorganic phase in the polymeric matrix.

The sol–gel process consists of two different reactions on metal oxide precursors: hydrolysis and condensation, which occur in aqueous solutions, or in the liquid state, or in organic solutions in a highly humid atmosphere, producing polymeric inorganic metal oxide particles. As inorganic precursors, Si derivatives, Al, Ti, Zr, Sn and V salts can be used [187]. However, Si derivatives are the most used. The formation of silica structures is represented in Figure 1.30.

Hydrolysis is a reversible process in which there is the possibility that alcohol attacks the silanol, leading to the formation of an alkoxide. This process is known as re-esterification and is favored at high content of alcohol as the solvent or in the presence of other hydroxylic species [188].

Another reaction that can occur during a sol–gel process is transesterification, which is the reaction of an alcohol with a silylalkoxide with the corresponding formation of a different silylalkoxide (Figure 1.31).

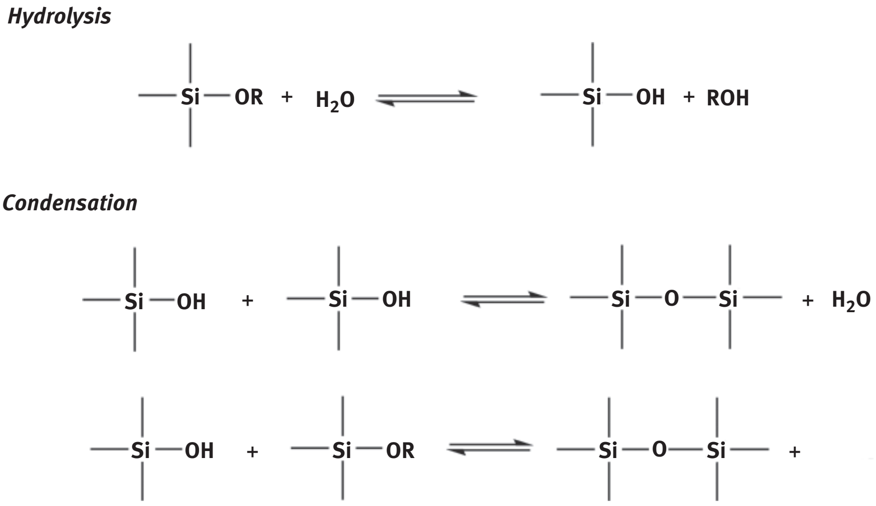

Figure 1.30: Sol-gel reaction of silicon inorganic precursors.

Figure 1.31: Transesterification reaction.

This reaction occurs when the alcohol used as the solvent is different from that formed in the hydrolysis reaction but can also be used to link poly(hydroxylic) compounds to silica structures or to functionalize hydroxylated surfaces.

The sol–gel process is acid or base catalyzed and the silica structure is determined mainly by the catalytic conditions. Thus, acid catalysis favors a faster hydrolysis of the precursor, finally leading to an open weakly branched polymer-like structure. On the contrary, in a basic medium the hydrolysis occurs slower but the polycondensation is faster, producing compact colloidal particles [189, 190]. In Figure 1.32 the effect of the catalyst in the morphology of the network is depicted.

The formation of the inorganic silica network depends on the condensation reaction of the previously formed silanol structures that leads to new Si–O–Si bonds. Generally, the precursors have three (trialkoxysilane, T_n) or four (tetraalkoxysilane, Q_n) hydrolyzable groups. The subscript n indicates the number of silanol groups condensed to siloxane bonds. In Figure 1.33 the chemical structures of silanols and the possible structures produced in the condensation are represented.

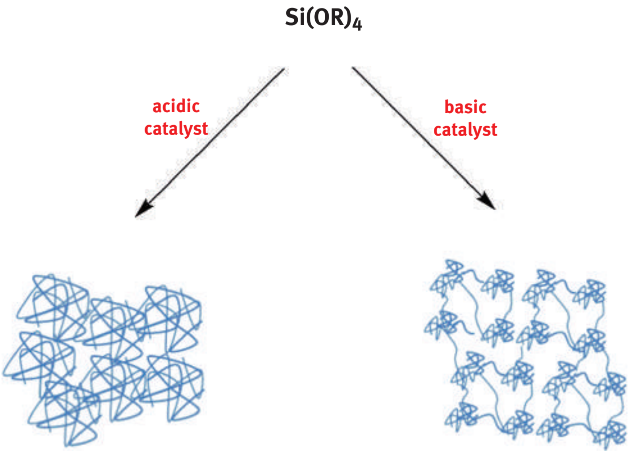

Figure 1.32: Catalyst influence in the formation of the inorganic network by sol-gel.

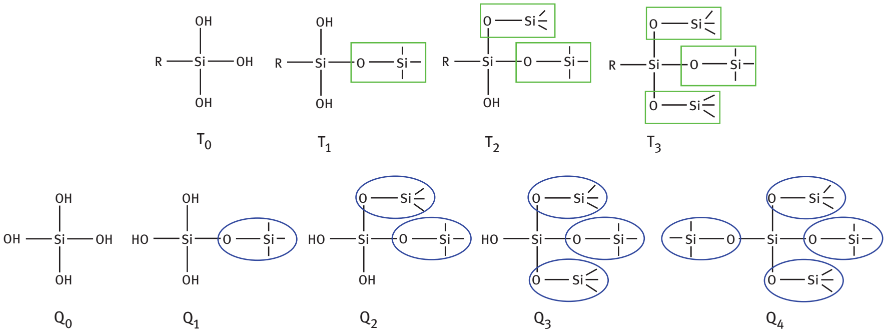

Figure 1.33: Structure of the possible condensed forms during the sol-gel process.

From [29] Si NMR experiments, it is possible to determine the structural details on the degree of hydrolysis and polycondensation.

The formation of the inorganic silica structure in epoxy hybrids can take place before or after the curing process. Many sol–gel hybrid materials have been prepared by different curing methodologies [191]. In order to obtain good mechanical properties, the compatibility of organic and inorganic structures by the formation of covalent bonding is an essential condition, and for this reason, the use of coupling agents is needed [192, 193]. Usually, commercially available trialkoxysilyl compounds with organic reactive groups are applied as coupling agents in epoxy hybrids, with (3-glycidyloxypropyl)trimethoxysilane (GPTMS) being the most widely used [194, 195]. Moreover, the addition of tetraethyl orthosilicate (TEOS) to the formulation containing organoalkoxysilane precursors usually aims to increase the SiO_2 content and the

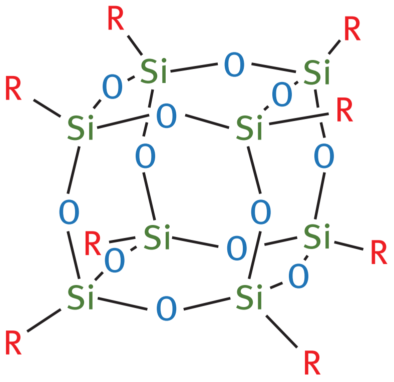

Figure 1.34: Chemical structure of octameric cage (POSS).

size of the particles formed. The organic–inorganic networks can be tailored by combining the addition of TEOS and the type of coupling agent [196], and the size of particles formed is related to the mechanical properties of the final material [197].

The cyclization of alkoxysilanes by intramolecular polycondensation allows one to form polyhedral functional silsesquioxanes (POSS) with random, ladder cage or semi-cage structures. Octasililsesquioxane T_8 (Figure 1.34) has been observed in sol–gel processes starting from trialkoxysilanes under some particular synthetic conditions [198].

The cage-like structures of POSS can allow the construction of materials with precise control of the nanoarchitecture. For this reason, POSS reagents, monomers and polymers are emerging as a new chemical technology for the nanoreinforced organic–inorganic hybrids and the polymers incorporating POSS are becoming the focus of many studies due to the simplicity in processing and the excellent comprehensive properties of this class of hybrid materials [199, 200].

As has been mentioned before, HBPs are advantageous modifiers to enhance the properties of epoxy thermosets. Taking all of this into account, some authors combined the strategy of the generation of silica particles by the sol–gel procedure with the use of hyperbranched structures to improve some characteristics of thermosetting materials [66, 201, 202].

Since the use of coupling agents is highly advisable, the preparation of multifunctional coupling agents by silylation of the final groups of HBPs can be greatly advantageous to improve epoxy resins by the generation of silica particles by the sol–gel process from the alkoxysilanes at the end groups of the hyperbranched structures [67]. As an alternative, the use of epoxy-terminated HBP as an epoxy component has also been proposed [203].

Taking into account that amino groups are reactive toward isocyanates, the complete modification of PEI with (3-isocyanatopropyl) triethoxysilane was achieved

[141, 142]. Triethoxysilylated hyperbranched PEI (PEI-Si) was used to prepare different hybrid organic–inorganic materials with different silica contents and different inorganic structures. An advantage of the amino groups in the PEI structure is that the amines cannot react with silanol groups in contrast with the hydroxyl groups, avoiding the gelation process during the preparation of the modifier or during storage, which is an undesired side-reaction in OH-terminated hyperbranch. The hybrid materials obtained by the sol–gel process of mixtures of DGEBA and PEI-Si in different proportions showed improved scratch resistance and even self-repairing behavior was observed with the highest proportion of PEI-Si. The mechanical characteristics were studied in depth using the depth-sensing indentation methods, which showed the special viscoelastic behavior explaining the self-repairing characteristics [204].

1.11 Use of modified hyperbranched PEI as a macromonomer in the preparation of thermosets by a two-stage click-chemistry process

"Click Chemistry" is a term that was introduced by K. B. Sharpless and coworkers in 2001 to describe reactions that are high yielding, wide in scope, stereospecific, simple to perform and can be conducted in easily removable or benign solvents [205]. Sharpless defined click chemistry early on as the generation of complex substances by bringing together smaller units via heteroatoms. This chemistry is not limited to a specific type of reaction and the most commonly used click reactions that have been adapted to fulfill the above criteria are: a) pericyclic reactions commonly the Huisgen type [3+2] cycloadditions and Diels–Alder reaction [206, 207], b) ring-opening of strained molecules such as epoxides, aziridines and aziridiniumions [208], c) non-aldol carbonyl chemistry (involving amines, oximes and hydrazones) [209], d) addition reactions especially thiol-ene/yne chemistry, and Michael additions (Figure 1.35) [210]. Nowadays, the characteristics of click reactions include a) high yields, b) regiospecificity and stereospecificity, c) insensitivity to oxygen or water, d) mild, solventless (or aqueous) reaction conditions, e) orthogonality with other common organic synthesis reactions and f) amenability to a wide variety of readily available starting compounds [211, 212].

Since the foundation of click chemistry, there has been an explosive growth in publications of this practical and sensible chemical approach, and over the years, the developments in the area of click chemistry have been considerable. As a consequence of its simplicity, this chemistry has a significant impact in applications such as bioconjugation [213], materials science [214] and drug delivery systems [215].

Click chemistry provides powerful and versatile tools for materials synthesis owing to its simplicity, selectivity, efficiency and tolerance of various functional groups. Consequently, a wide range of controlled-architecture materials have been

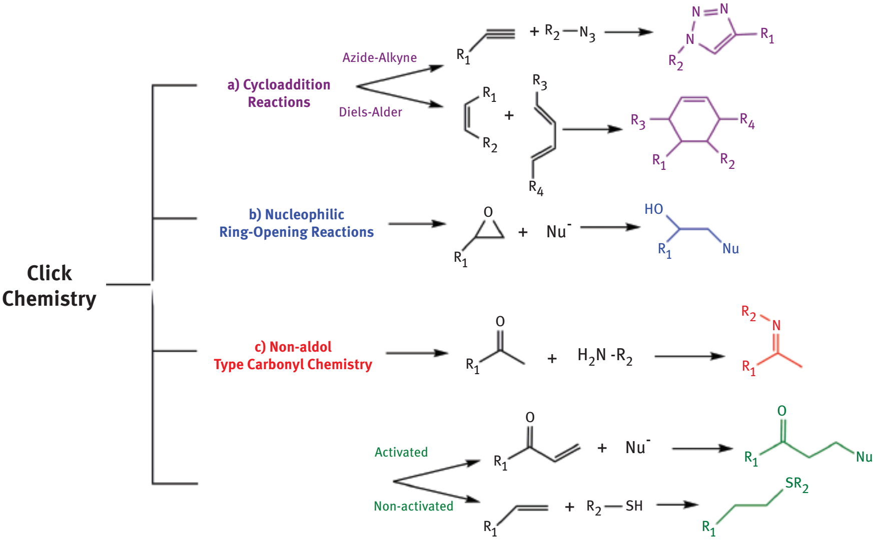

Figure 1.35: Selection of click reactions.

synthesized through various click reactions, including block copolymers, micelles, dendrimers, gels and networks [216, 217].

In material science, the aim is to achieve performance and a set of desired characteristics in the final material and/or device in as simple and effective manner as possible. These performances include specifications on mechanical and physical behavior as well as chemical characteristics. This is related to the goal of click chemistry wherein it argues that the focus of chemical process selection should be directed toward the identification, optimization and simplification of an overall process [205]. For this reason, click chemistry is used in materials development as an effective tool to modify polymers or materials with a variety of functional components and to prepare polymer networks [218]-[220]. Moreover, by different click methodologies stimuli-responsive materials have been synthesized [221] and nanoscale materials have been prepared due to their efficiency and selectivity [222].

Among all the click reactions, thiol chemistry has attracted a great deal of attention due to its efficiency and versatility with numerous thiol reactions [223]. The reactivity of the thiol gives rise to an advantage of the thiol-click reactions in that they proceed, under appropriate conditions, more rapidly than many other click processes in some cases, with the reaction times necessary to achieve high conversions being less than 1–10 s.

Thiol chemistry can be divided into two categories: the base-catalyzed nucleophilic reactions associated with the thiol–epoxy, thiol–isocyanate and thiol Michael addition reactions and radical-mediated reactions related to the thiol–ene and thiol–yne reactions (Figure 1.36) [210].

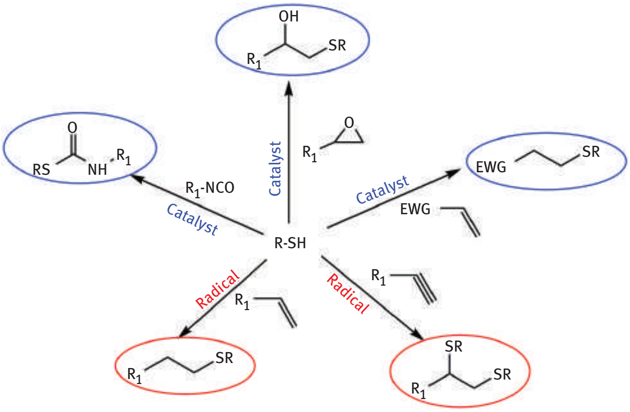

Figure 1.36: Different thiol-click reactions.

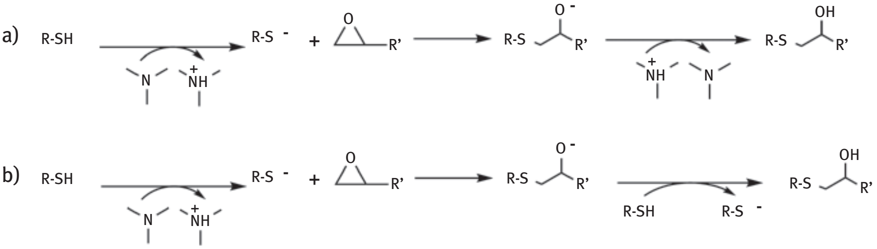

Figure 1.37: Catalyzed thiol-epoxy ring opening polymerization.

The thiol–epoxide reaction has been implemented in many important biosynthetic and biomedical applications [224]. In addition, the ring-opening reaction involving thiols and epoxides is industrially important and involved in the formation of adhesives, high-performance coatings and composites [225].

The basic thiol–epoxy reaction mechanism is a simple nucleophilic ring-opening reaction by the thiolate anion followed by protonation of the alkoxide anion via the quaternary ammonium (Figure 1.37a) originally formed via reaction of the base catalyst and thiol to generate the initial thiolate or by proton exchange between the formed alkoxide and another thiol (Figure 1.25). This mechanism was proposed to describe the curing of thiol–epoxy systems catalyzed by bases [226].

However, the low basicity of some tertiary amines that can be used as catalyst for the thiol–epoxy reaction makes the proton exchange leading to the formation of a thiolate anion highly unlikely. An alternative reaction mechanism was recently proposed to model successfully the thiol–epoxy curing catalyzed by a moderately basic tertiary amine [227]. First of all, there is a nucleophilic attack of the tertiary amine on the epoxy ring, with the assistance of a proton donor such as an alcohol to

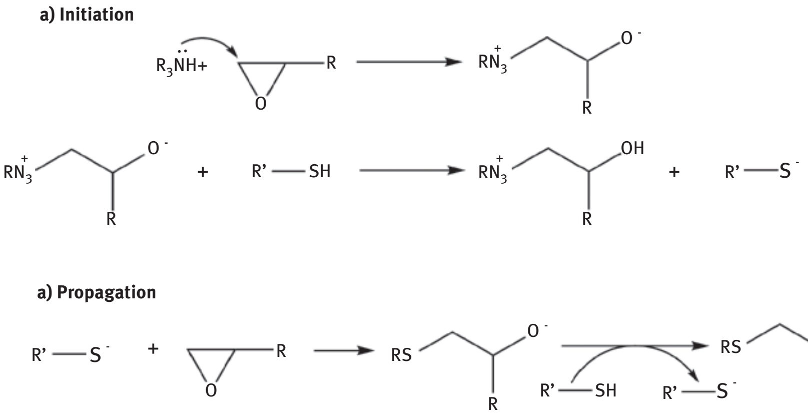

Figure 1.38: Proposed curing mechanism of thiol-epoxy condensation catalyzed by tertiary amine.

facilitate ring-opening (Figure 1.37), followed by proton exchange between the thiol and the alkoxide to produce the thiolate anion and a hydroxyl ammonium compound. The thiolate anion propagates the reaction by nucleophilic attack on the epoxy ring and the regeneration of the thiolate anion by proton exchange of the formed alkoxide with another thiol (Figure 1.37). Usually, this reaction occurs under thermal conditions and the reaction kinetics and the mechanism of the curing process are determined by the base used (Figure 1.38).

Thiol-ene and thiol-yne processes take place by the stoichiometric reaction of alkynes with thiols via a radical step growth mechanism that can be initiated by light, peroxides, thermal initiators or any systems whereby radicals are generated [228]. However, these reactions are commonly initiated photochemically [229]. It should be said that one of the distinct features between thiol-ene and thiol-yne is that in thiol-ene each ene functional group reacts only once with a thiol group whereas in thiol-yne each yne group reacts twice. The use of these thiol reactions ranges from high-performance protective polymer networks to processes that are important in the optical, biomedical, sensing and bioorganic modification fields [230].

Both reactions are efficient tools for the post-polymerization modification of well-defined reactive precursor (co)polymers [231] and for the construction of complex (macro)molecules, such as poly(thioether) dendrimers (Figure 1.39) [232]. Due to their fast reaction kinetics and high yield, thiol-ene and thiol-yne reactions are highly used for the bioconjugation of polymers, for tissue engineering applications, for the production of degradable polymers and for the preparation of high-quality soft imprint lithographic stamps, among others [230].

In the thermosetting field, thiol-ene and thiol-yne step growth processes are widely used since they allow one to obtain uniform networks with low shrinkage

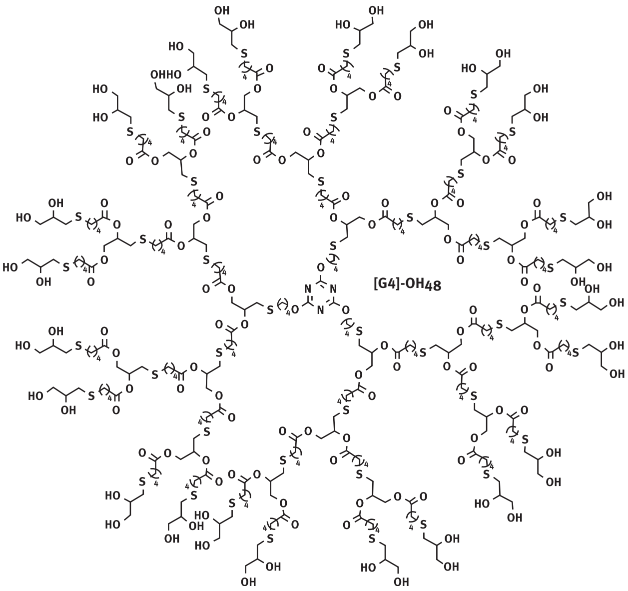

Figure 1.39: Dendrimer synthesized via radical thiol-ene reaction.

and stress. Moreover, the incorporation of tioether networks permits a higher refractive index than comparable organic networks [233, 234].

Using thiol-ene and thiol-yne methodologies, polysulfide networks have been prepared [235, 236]. However, the materials obtained are limited by their poor mechanical and physical properties due to the flexibility of the thiol monomers. To overcome this disadvantage, several authors combine thiol-ene systems with a network structure derived from thiol-acrylate or thiol-epoxy reaction [237]-[239]. As an alternative, the use of a multifunctional monomer to increase the functionality of the reactive mixture to enhance the thermomechanical characteristics of the final materials has been reported [240].

Taking into account this new alternative, the preparation of allyl and propargyl terminated-hyperbranched PEI as multifunctional macromonomers for thiol-ene and thiol-yne polymerizations was carried out [143, 144]. The nucleophylic attack of amine groups in the PEI structure to the oxirane of allyl or propargyl glycidylethers allow one to reach a quite high degree of modification in mild conditions.

Dual curing is a processing methodology based on the combination of two different and compatible polymerization reactions taking place simultaneously or sequentially, in a well-controlled way. Sequential dual-curing processing makes possible to obtain stable materials after the first curing stage that maintain the ability, upon application of a second stimulus, to activate the second curing stage and complete the processing, leading to a fully cured material with the desired final properties [241].

One goal of click chemistry is the potential of combining multiple click reactions, either performed simultaneously or in tandem, to synthesize complex structures and materials. In recognition of this task, several recent examples of sequential processes involving two thiol reactions, or even more interestingly, thiol-click and alkyne–azide click reactions, are considered. An advantage coming from the first combination is that the thiol component can participate in both processes and therefore the networks arising from thiol-ene and thiol-epoxy reactions are covalently interconnected. Another advantage comes from the fact that both thiol-ene and thiol-epoxy reactions are step-wise so that relevant network buildup parameters during both curing stages such as gel point conversion, gel fraction or crosslinking density can be easily calculated using well-established methods [242]. Thus, it is possible to tailor the curing process and the material properties in the intermediate stage and at the end of it in order to fit different processes and material requirements in a flexible way.

Recently, sequential dual curing systems have been reported using different methodologies. Thermosets by two-stage sequential aza-Michael addition and free-radical polymerization of amine-acrylate systems have been prepared. Furthermore, the strategy of combining two thiol-click reactions has been studied [227, 243]. Thermosetting materials were obtained by combining sequential thiol-ene/thiol-epoxy reactions in which the first stage is a radical thiol-ene reaction initiated by a photoinitiator and the second one is a base-catalyzed thiol-epoxy reaction initiated by a tertiary amine [243]. Since the first process is activated by UV-light and the second one is thermal, the aim of this methodology was to reach a dual-curing system with a controlled curing sequence, with no overlapping between both curing reactions, and with sufficient stability in the intermediate stage.

The use of allyl and propargyl-terminated PEIs as macromonomers in thiol-ene and thiol-yne reactions has been studied [143, 144]. The formation of hybrid networks from the combination of thiol-ene or thiol-yne and thiol-epoxy process allows one to increase the crosslinking density in the final materials obtaining higher T_g values compared with polysulfides. Moreover, the use of these macromonomers as modifiers in epoxy thermosetting materials improves the plastic character of the fracture which must enhance the toughness of the materials.

References

[1] May CA. Chemistry and technology, 2nd New York: Marcel Dekker, 1988.

[2] Lee H, Neville K. Handbook of epoxy resins. New York: McGraw-Hill, 1967.

[3] Castan P. Swiss Pat. 211,116, 1940.

[4] Ellis B. Chemistry and technology of epoxy resins. London: Blackie Academic & Professional, 1993.

[5] Pascault JP, Williams RJJ. Epoxy polymers. Weinheim: Wiley VCH. Chapter 1 2010.

[6] Pascault JP, Sautereau H, Verdu J, Williams RJJ. Thermosetting polymers. New York: Marcel Dekker. Chapter 2 2002.

[7] Fisch, W.; Hofmann, W.; Koskikallio, J. The curing mechanism of epoxy resins. J Appl Chem 1956, 6, 429–441.

[8] O'Neill LA, Col CP. Chemical and spectroscopic studies of epoxy resin reactions in the surface coating field. J Appl Chem 1956;6:356–364.

[9] Montserrat S, Flaqué C, Calafell M, Andreu G, Málek J. Influence of the accelerator concentration on the curing reaction of an epoxy–anhydride system. Thermochim Acta. 1995;269:213–229.

[10] Petrie EM. Epoxy adhesive formulations. New York: McGraw-Hill, 2006.

[11] Leukel J, Burchard W, Krüguer RP, Much H, Schulz G. Mechanism of the anionic copolymerization of anhydride–cured epoxies – analyzed by matrix–assisted laser desorption ionization time–of–flight mass spectrometry (MALDI–TOF–MS). Macromol Rapid Commun. 1996;17:359–366.

[12] Fedtke M, Domaratius F. Curing of epoxide resins by anhydrides of dicarboxylic acids: model reactions. Polymer Bull. 1986;15:13–19.

[13] Fernández-Francos X, Rybak A, Sekula R, Ramis X, Serra A. Modification of epoxy–anhydride thermosets using a hyperbranched poly (ester-amide): I. Kinetic study. Polym Int. 2012;61: 1710–1725.

[14] Brunelle DJ. Ring-opening polymerization: Mechanism, catalysts, structure and utility. Munich: Hanser Publishers, 1993.

[15] Ricciardi F, Romanchick WA, Joullié MM. J Mechanism of imidazole catalysis in the curing of epoxy resins. Polym Sci: Polym Chem Ed. 1983;21:1475–1490.

[16] Galià M, Serra A, Mantecón A, Cádiz V. Synthesis of diglicydilesters with alicyclic imide structure and their thermal and tertiary amine catalyzed curing. J Appl Polym Sci. 1995;56: 193–200.

[17] Ooi SK, Cook WD, Simon GP, DSC studies of the curing mechanisms and kinetics of DGEBA using imidazole curing agents. Such CH. Polymer. 2000;41:3639–3649.

[18] Rozenberg BA. Kinetics, thermodynamics and mechanism of reactions of epoxy oligomers with amines. Adv Polym Sci. 1986;75:113–165.

[19] Fernández-Francos X, Cook WD, Serra A, Ramis X, Liang GG, Salla JM. Crosslinking of mixtures of DGEBA with 1,6–dioxaspiro[4,4]nonan–2,7–dione initiated by tertiary amines. Part IV. Effect of hydroxyl groups on initiation and curing kinetics. Polymer. 2010;51:26–34.

[20] Ghaemy M, Khandani MH. Kinetics of curing reaction of DGEBA with BF3-amin complexes using isothermal DSC technique. Eur Polym J. 1998;34:477–486.

[21] Castell P, Galià M, Serra A, Salla JM, Ramis X. Study of lanthanide triflates as new curing initiators for DGEBA. Polymer. 2000;41:8465–8474.

[22] Mas C, Serra A, Mantecón A, Salla JM, Ramis X. Study of lanthanide triflates as new curing initiators for cycloaliphatic epoxy resins. Macromol Chem Phys. 2001;202:2554–2564.

[23] García SJ, Ramis X, Serra A, Suay J. Addition effect of Erbium (III) trifluoromethanesulfonate in the homopolymerization kinetics of a DGEBA resin. Thermochim Acta. 2006;441:45–52.

[24] García SJ, Ramis X, Serra A, Suay J. Cationic crosslinking of solid dgeba resins with ytterbium (III) trifluoromethanesulfonate as initiator. J Therm Anal Calorim. 2006;83:429–438.

[25] Kubisa P, Penczek S. Cationic activated monomer polymerization of heterocyclic monomers. Prog Polym Sci. 1999;24:1409–1437.

[26] Endo T, Sanda F. Design of latent catalysts and their application to polymer synthesis. Macromol Symp. 1996;107:237–242.

[27] Tomuta AM, Ramis X, Ferrando F, Serra A. The use of dihydrazides as latent curing agents in diglycidyl ether of bisphenol A coatings. Prog Org Coat. 2011;74:59–66.

[28] Hua CZ, Wan SJ, Wang L, Liu XD, Endo T. Carbonyldiimidazole–accelerated efficient cure of epoxidized soybean oil with dicyandiamide. J Polym Sci, Part A: Polym Chem. 2014;52: 375–382.

[29] Crivello JV, Sangermano M. Visible and long–wavelength photoinitiated cationic polymerization. J Polym Sci, Part A: Polym Chem. 2001;39:343–356.

[30] He D, Susanto H, Modification and stimulation of polymeric membranes. Ulbricht M. Prog Polym Sci. 2009;34:62–98.

[31] Foix D, Erber M, Voit B, Ramis X, Mantecón A, Serra A. New hyperbranched polyester modified DGEBA thermosets with improved chemical reworkability. Polym Degrad Stab. 2010;95: 445–452.

[32] Tomuta A, Ramis X, Fernández-Francos X, Ferrando F, Serra A. New chemically reworkable epoxy coatings obtained by the addition of polyesters with star topologies to diglycidyl ether of bisphenol A resins. Prog Org Coat. 2013;76:1616–1624.

[33] Chen JS, Ober CK, Poliks MD. Characterization of thermally reworkable thermosets: Materials for environmentally friendly processing and reuse. Polymer. 2002;43:131–139.

[34] Chen JS, Ober CK, Poliks MD, Zhang Y, Wiesner U, Cohen C. Controlled degradation of epoxy networks: Analysis of crosslink density and glass transition temperature changes in thermally reworkable thermosets. Polymer. 2004;45:1939–1950.

[35] Levitas G, De Petris S, Marchetti A, Lazzeri A. Crosslink density and fracture toughness of epoxy resins. J Mater Sci. 1991;26:2348–2352.

[36] Bagheri R, Marouf BT, Pearson RA. Rubber-toughened epoxies: a critical review. Polymer Rev. 2009;49:201–225.

[37] Arends CB. Polymer toughening. New York: Marcel Dekker, 1996.

[38] Unnikrishnan KP, Thachil ET. Toughening of epoxy resins. Des Monomers Polym. 2006;9: 129–152.

[39] Manzione LT, Gillham JK, McPherson CA. Rubber–modified epoxies, I. Transitions and morphology. J Appl Polym Sci. 1981;26:889–905.

[40] Garg AC, Mai YW. Failure mechanisms in toughened epoxy resins—a review. Compos Sci Technol. 1988;31:179–223.

[41] Ruiz-Pérez L, Royston GJ, Fairclough JPA, Ryan AJ. Toughening by nanostructure. Polymer. 2008;49:4475–4488.

[42] Meng Y, Zhang X-H, Du B-Y, Zhou B-X, Zhou X, Qi G-R. Thermosets with core–shell nanodomain by incorporation of core crosslinked star polymer into epoxy resin. Polymer. 2011;52:391–399.

[43] Mezzenga R, Plummer CJG, Boogh L, Manson JAE. Morphology build–up in dendritic hyperbranched polymer modified epoxy resins: modelling and characterization. Polymer. 2001;42:305–317.

[44] Ratna D, Varley R, Simon GP. Toughening of trifunctional epoxy using an epoxy–functionalized hyperbranched polymer. J Appl Polym Sci. 2003;89:2339–2345.

[45] Boogh L, Pettersson B, Månson J-AE. Dendritic hyperbranched polymers as tougheners for epoxy resins. Polymer. 1999;40:2249–2261.

[46] Fu J-F, Shi L-Y, Yuan S, Zhong Q-D, Zhang D-S, Chen Y, et al. Morphology, toughness mechanism, and thermal properties of hyperbranched epoxy modified diglycidyl ether of bisphenol A (DGEBA) interpenetrating polymer networks. Polym Adv Technol. 2008;19: 1597–1607.

[47] Zahng D, Chen Y, Jia D. Toughness and reinforcement of diglycidylether of bisphenol A by hyperbranched poly(trimellitic anhydride–butanediol glycol) ester epoxy resin. Polym Compos. 2009;30:918–925.

[48] Mital V. Optimization of polymer nanocomposite properties. Weinheim: Wiley VCH. Chapter 2 2010.

[49] Chekanov YA, Korotkov VN, Rozenberg BA, Dhzavadyan EA, Bogdanova LM. Cure shrinkage defects in epoxy resins. Polymer 1995; 36 2013–2017.

[50] Sadhir RK, Luck MR. Expanding monomers. Synthesis, characterization and applications. Boca Raton: CRC Press, 1992.

[51] Fernández-Francos X, Salla JM, Cadenato A, Morancho JM, Serra A, Mantecón A. A new strategy for controlling shrinkage of DGEBA resins cured by cationic copolymerization with hydroxyl–terminated hyperbranched polymers and ytterbium triflate as an initiator. J Appl Polym Sci. 2009;111:2822–2929.

[52] Morell M, Ramis X, Ferrando F, Yu Y, Serra A. New improved thermosets obtained from DGEBA and a hyperbranched poly(esteramide). Polymer. 2009;50:5374–5383.

[53] Khosravi E, Musa OM. Thermally degradable thermosetting materials. Eur Polym J. 2011;47: 465–473.

[54] Tesoro GC, Sastri VR. Reversible crosslinking in epoxy resins. II. New approaches. J Appl Polym Sci. 1990;39:1439–1457.

[55] Yang S, Chen JS, Körner H, Breiner T, Ober CK, Poliks MD. Reworkable epoxies: thermosets with thermally cleavable groups for controlled network breakdown. Chem Mater. 1998;10: 1475–1482.

[56] Wang L, Li H, Wong CP. Syntheses and characterizations of thermally reworkable epoxy resins. Part 1. J Polym Sci, Part A: Polym Chem. 1999;37:2991–3001.

[57] Griffith JR. Epoxy resin chemistry. Washington DC: ACS, 1979.

[58] Buchwalter SL, Kosbar LL. Cleavable epoxy resins: design for disassembly of a thermoset. J Polym Sci, Part A: Polym Chem. 1996;34:249–260.

[59] Fernández-Francos X, Salla JM, Mantecón A, Serra A, Ramis X. Crosslinking of mixtures of DGEBA with 1,6–dioxaspiro[4.4]nonan–2,7–dione initiated by tertiary amines, Part II: Thermomechanical properties and reworkability. Polym Degrad Stab. 2008;93:760–769.

[60] Seubert C, Nietering K, Nichols M, Wykoff R, Bollin S. An overview of the scratch resistance of automotive coatings: exterior clearcoats and polycarbonate hardcoats. Coatings. 2012;2: 221–234.

[61] Mittal V. Polymer nanocomposite coatings. Boca Raton: CRC Press, 2014.

[62] Sangermano M, Messori M. Scratch resistance enhancement of polymer coatings. Macromol Mater Eng. 2010;295:603–612.

[63] Bauer F, Ernst H, Decker U, Findeisen M, Gläsel H-J, Langguth H, et al. Preparation of scratch and abrasion resistant polymeric nanocomposites by monomer grafting onto nanoparticles, 1 FTIR and multi-nuclear NMR spectroscopy to the characterization of methacryl grafting. Macromol Chem Phys. 2000;201:2654–2659.

[64] Mark JE, Lee C, Bianconi PA. Hybrid organic–inorganic composites, vol. 585. Washington, DC: ACS, 1995.

[65] Toselli M, Marini M, Fabbri P, Messori M, Pilati F. J Sol-gel derived hybrid coatings for the improvement of scratch resistance of polyethylene. Sol-Gel Sci Technol. 2007;43:73–83.

[66] Sangermano M, Messori M, Martin Galleco M, Rizza G, Voit B. Scratch-resistant tough nanocomposite epoxy coatings based on hyperbranched polyesters. Polymer. 2009;50: 5647–5652.

[67] Sangermano M, El Sayed H, Voit B. Ethoxysilyl-modified hyperbranched polyesters as mulitfunctional coupling agents for epoxy-silica hybrid coatings. Polymer. 2011;52: 2103–2109.

[68] Fréchet JMJ, Tomalia DA. Dendrimers and other dendritic poymers. Edithvale: John Wiley & Sons, 2001.

[69] Yan D, Gao C, Frey H. Hyperbranched polymers. Synthesis, properties and applications, 1st Hoboken: Wiley Interscience, 2011.

[70] Gong W, Mai Y, Zhou Y, Qi N, Wang B, Yan D. Effect of the degree of branching on atomic-scale free volume in hyperbranched Poly[3–ethyl–3–(hydroxymethyl)oxetane]. A positron study. Macromolecules. 2005;38:9644–9649.

[71] Khalyavina A, Schallausky F, Komber H, Al Samman M, Radke W, Lederer A. Aromatic–aliphatic polyesters with tailored degree of branching based on AB/AB2 and ABB*/AB2 monomers. Macromolecules. 2010;43:3268–3276.

[72] Hawker CJ, Lee R, Fréchet JMJ. One-step synthesis of hyperbranched dendritic polyesters. J Am Chem Soc. 1991;113:4583–4588.

[73] Yates CR, Hayes W. Synthesis and applications of hyperbranched polymers. Eur Polym J. 2004;40:1257–1281.

[74] Lyulin AV, Adolf DB, Davies GR. Computer simulations of hyperbranched polymers in shear flows. Macromolecules. 2001;34:3783–3789.

[75] Voit B, Lederer A. Hyperbranched and highly branched polymer architectures—synthetic strategies and major characterization aspects. Chem Rev. 2009;109:5924–5973.

[76] Voit B. Hyperbranched polymers—all problems solved after 15 years of research? J Polym Sci, Part A: Polym Chem. 2005;43:2679–2699.

[77] Zheng Y, Li S, Weng Z, Gao C. Hyperbranched polymers: advances from synthesis to applications. Chem Soc Rev. 2015;44:4091–4130.

[78] Kim YH, Webster OW. Hyperbranched polyphenylenes. Macromolecules. 1992;25:5561–5572.

[79] Oh JH, Jang J, Lee S-H. Curing behavior of tetrafunctional epoxy resin/hyperbranched polymer system. Polymer. 2001;42:8339–8347.

[80] Gao C, Yan D. Hyperbranched polymers: from synthesis to applications. Prog Polym Sci. 2004;29:183–275.

[81] Johansson M, Malmström E, Jansson A, Hult A. Novel concept for low temperature curing powder coatings based on hyperbranched polyesters. J Coatings Technol. 2000;72:49–54.

[82] Zhu S-W, Shi W-F. Flame retardant mechanism of hyperbranched polyurethane acrylates used for UV curable flame retardant coatings. Polym Degrad Stab. 2002;75:543–547.

[83] Lange J, Stenroos E, Johansson M, Malmström E. Barrier coatings for flexible packaging. Based on hyperbranched resins. Polymer. 2001;42:7403–7410.

[84] Mishra MK, Kobayashi S. Star and hyperbranched polymers. New York: Marcel Dekker, Inc., 1999.

[85] Aert HAM, Genderen MHP, Meijer EW. Star-shaped poly(2,6–dimethyl–1,4–phenylene ether). Polymer Bull. 1996;37:273–280.

[86] Erwin BM, Cloitre M, Gauthier M, Vlassopoulos D. Dynamics and rheology of colloidal star polymers. Soft Matter. 2010;6:2825–2833.

[87] Wu W, Wang W, Li J. Star polymers: advances in biomedical applications. Prog Polym Sci. 2015;46:55–85.

[88] Miao J, Xu G, Zhu L, Tian L, Uhrich KE, Avila-Orta CA, et al. Chain-folding and overall molecular conformation in a novel amphiphilic starlike macromolecule. Macromolecules. 2005;38:7074–7082.

[89] Steege KE, Wang J, Uhrich KE, Castner EW. Local polarity and microviscosity in the hydrophobic cores of amphiphilic star-like and scorpion-like macromolecules. Macromolecules. 2007;40:3739–3748.

[90] Morell M, Foix D, Lederer A, Ramis X, Voit B, Serra A. Synthesis of a new multiarm star polymer based on hyperbranched Poly(styrene) core and Poly(epsilon-Caprolactone) arms and its use as reactive modifier of epoxy thermosets. J Polymer Sci A: Polymer Chem. 2011;49:4639–4649.

[91] Mezzenga R, Boogh L, Månson J-AE. A review of dendritic hyperbranched polymer as modifiers in epoxy composites. Compos Sci Technol. 2001;61:787–795.

[92] Hult A, Johansson M, Malmström E. Hyperbranched polymers. Adv Polymer Sci. 1999;143:1–34.

[93] Ratna D, Simon GP. Thermomechanical properties and morphology of blends of a hydroxy-functionalized hyperbranched polymer and epoxy resin. Polymer. 2001;42:8833–8839.

[94] Yang JP, Chen ZK, Yang G, Fu SY, Ye L. Simultaneous improvements in the cryogenic tensile strength, ductility and impact strength of epoxy resins by a hyperbranched polymer. Polymer. 2008;49:3168–3175.

[95] Varley RJ, Tian W. Toughening of an epoxy anhydride resin system using an epoxidized hyperbranched polymer. Polym Int. 2004;53:69–77.

[96] Foix D, Khalyavina A, Morell M, Voit B, Lederer A, Ramis X, et al. The effect of the degree of branching in hyperbranched polyesters used as reactive modifiers in epoxy thermosets. Macromol Mater Eng. 2012;297:85–94.

[97] Mezzenga R, Boogh L, Månson J-AE. Evaluation of solubility parameters during polymerisation of amine-cured epoxy resins. J Polymer Sci B: Polymer Phys. 2000;38:1883–1892.

[98] Mezzenga R, Boogh L, Pettersson B, Månson J-AE. Chemically induced phase separated morphologies in epoxy resin-hyperbranched polymer blends. Macromol Symp. 2000;149: 17–22.

[99] Flores M, Fernández-Francos X, Ferrando F, Ramis X, Serra A. Efficient impact resistance improvement of epoxy/anhydride thermosets by adding hyperbranched polyesters partially modified with undecenoyl chains. Polymer. 2012;53:5232–5241.

[100] Flores M, Morell M, Fernández-Francos X, Ferrando F, Ramis X, Serra A. Enhancement of the impact strength of cationically cured cycloaliphatic diepoxide by adding hyperbranched poly(glycidol) partially modified with 10–undecenoyl chains. Eur Polym J. 2013;49: 1610–1620.

[101] Morell M, Erber M, Ramis X, Ferrando F, Voit B, Serra A. New epoxy thermosets modified with hyperbranched poly(ester-amide) of different molecular weight. Eur Polym J. 2010;46: 1498–1509.

[102] Tomuta A, Fernández-Francos X, Ferrando F, Serra A, Ramis X. New epoxy-anhydride thermosets modified with multiarm stars with hyperbranched polyester cores and poly(e-caprolactone) arms. Polym Plast Technol Eng. 2014;53:1–10.

[103] Morell M, Fernández-Francos X, Ramis X, Serra A. Synthesis of a new hyperbranched polyaminoester and its use as a reactive modifier in anionic curing of DGEBA thermosets. Macromol Chem Phys. 2010;211:1879–1889.

[104] Morell M, Lederer A, Ramis X, Voit B, Serra A. Multiarm star poly(glycidol)–*block*–poly(e-caprolactone) of different arm lengths and their use as modifiers of diglycidylether of bisphenol A thermosets. J Polym Sci, Part A: Polym Chem. 2011;49:2395–2406.

[105] Morell M, Fernández-Francos X, Gombau J, Ferrando F, Lederer A, Ramis X, et al. Multiarm star poly(glycidol)–*block*–poly(styrene) as modifier of anionically cured diglycidylether of bisphenol A thermosetting coatings. Prog Org Coat. 2012;73:62–69.

[106] Morell M, Ramis X, Ferrando F, Serra A. New improved thermosets obtained from diglycidylether of bisphenol A and a multiarm star copolymer based on hyperbranched poly (glycidol) core and poly(methylmethacrylate) arms. Macromol Chem Phys. 2012;213:335–343.

[107] Morell M, Ramis X, Ferrando F, Serra A. Effect of polymer topology on the curing process and mechanical characteristics of epoxy thermosets modified with linear or multiarm star poly(e-caprolactone). Polymer. 2011;52:4694–4702.

[108] Lagunas C, Fernández-Francos X, Ferrando F, Flores M, Serra A, Morancho JM, et al. New epoxy thermosets modified with amphiphilic multiarm star polymers as toughness enhancer. React Funct Polym. 2014;83:132–143.

[109] Krämer M, Stumbé J-F, Grimm G, Kaufmann B, Krüger U, Weber M, et al. Dendritic polyamines: simple access to new materials with defined treelike structures for application in nonviral gene delivery. ChemBioChem. 2004;5:1081–1087.

[110] Available at: http://worldaccount.basf.com/wa/NAFTA~en_US/Catalog/ChemicalsNAFTA/pi/BASF/Brand/lupasol /brand_top/. Accesed 18 April 2016.

[111] Tomalia DA, Killat GR. Encyclopedia of Polymer Science and Engineering. Edited by Joseph C. Salamone 2nd ed., Vol. 1 New York: John Wiley & Son, 1985:680–739.

[112] Dermer OC, Ham GE. Ethylenimine and other aziridines; chemistry and applications. New York: Academic Press. Chapter 4 1969.

[113] Yemul O, Imae T. Synthesis and characterization of poly(ethyleneimine) dendrimers. Colloid Polym Sci. 2008;286:747–752.

[114] Available at:. Accessed 18 April 2016 http://www.innventia.com/Documents/Rapporter/STFI-Packforsk%20report%2032.pdf.

[115] Morrison A, Murray K. The behaviour of oligodeoxynucleotides on thin-layer chromatography on polyethyleneimine-cellulose and ion-exchange paper electrophoresis. Biochem J. 1974;141:321–330.

[116] Ware D, Soane S, Millward DB, Linford MR. US Patent 6.679.924 (to Nano Tex LLC.), 20 January 2004.

[117] Bayer LS, Fragouli D, Attanasio A, Sorce B, Bertoni G, Bresci R, et al. Water-repellent cellulose fiber networks with multifunctional properties. Appl Mater Interfaces. 2011;3:4024–4031.

[118] Andrew M, Frederic MS. US Patent 2.472.335, 7 June 1949.

[119] Elias H-G, Mülhaupt R. Ullmann's polymer and plastics: Products and processes. Weinheim: Wiley VCH, 2016.

[120] Carmona-Ribeiro AM, Melo LD. Cationic antimicrobial polymers and their assemblies. Int J Moleuclar Sci. 2013;14:9906–9946.

[121] Bacher K, Schmidt K, Gardin G. US Patent 20.080.199.706, 21 August 2008.

[122] Abdallah B, Hassan A, Benoist C, Goula D, Behr J-P, Demeneix BA. gene transfer into the adult mammalian brain: polyethylenimine. Hum Gene Ther. 1996;7:1947–1954.

[123] Ma J, Liu Q, Chen D, Zhou Y, Wen S. Carbon dioxide adsorption using amine-functionalized mesocellular siliceous foams. J Material Sci. 2014;49:7585–7596.

[124] Wang X, Song C, Gaffney AM, Song R. New molecular basket sorbents for CO2 capture based on mesoporous sponge-like TUD-1. Catalysis Today. 2014;238:95–102.

[125] Shi Y, Chen Z, Cheng X, Pan Y, Zhang H, Zhang Z, et al. A novel dual-emission ratiometric fluorescent nanoprobe for sensing and intracellular imaging of Zn^{2+}. Biosens Bioelectron. 2014;61:397–403.

[126] Zheng F, Guo S, Zeng F, Li J, Wu S. Ratiometric fluorescent probe for alkaline phosphatase based on betaine-modified polyethylenimine via excimer/monomer conversion. Anal Chem. 2014;86:9873–9879.

[127] Lin G, Zhu W, Yang L, Wu J, Lin B, Cheng Z, et al. Delivery of siRNA by MRI–visible nanovehicles to overcome drug resistance in MCF–7/ADR human breast cancer cells. Biomaterials. 2014;35: 9495–9507.

[128] Chen Y, Gu H, Zhang Z, Li F, Liu T, Xia W. Highly effective inhibition of lung cancer growth and metastasis by systemic delivery of siRNA via multimodal mesoporous silica-based nanocarrier. Biomaterials. 2014;35:10058–10069.

[129] Appelhans D, Komber H, Quadir MA, Richter S, Schwarz S, Van Der Vlist J, et al. Hyperbranched PEI with various oligosaccharide architectures: synthesis, characterization, ATP complexation, and cellular uptake properties. Biomacromolecules. 2009;10:1114–1124.

[130] Strieglera C, Frankea M, Müller M, Boye S, Oertel U, Janke A, et al. Amino acid modified hyperbranched poly(ethylene imine) with disaccharide decoration as anionic core-shell architecture: Influence of the pH and molecular architecture on solution behaviour. Polymer. 2015;80:188–204.

[131] Rumschöttel J, Kosmella S, Prietzel C, Appelhans D, Koetz J. Change in size, morphology and stability of DNA polyplexes with hyperbranched poly(ethyleneimines) containing bulky maltose units. Colloids Surf, B. 2016;138:78–85.

[132] Bekhradnia S, Naz I, Lund R, Effenberg C, Appelhans D, Sande SA, et al. Characterization of oligosaccharide-functionalized hyperbranched Poly(ethylene Imine) and their complexes With retinol in aqueous solution. J Colloid Interface Sci. 2015;458:178–186.

[133] Hauptmann N, Pion M, Muñoz-Fernández M-Á, Komber H, Werner C, Voit B, et al. Ni(II)-NTA modified Poly(ethylene imine) glycopolymers: physicochemical properties and first in vitro study of polyplexes formed with HIV-derived peptides Macromol Biosci. 2013;13:531–538.

[134] Hauptmann N, Pion M, Wehner R, Muñoz-Fernández M-Á, Schmitz M, Voit B, et al. Potential of Ni(II)-NTA-modified Poly(ethylene imine) glycopolymers as carrier system for future dendritic cell-based immunotherapy. Biomacromolecules. 2014;15:957–967.

[135] Bauman FE, Haeger H, Novikova O, Oenbrink G, Richter R, Finke M. Synthesis and characterization of star-branched PA12 grafted onto PEi core molecule. J Appl Polym Sci. 2004;96:2413–2422.

[136] Cao X, Li Z, Song X, Cui X, Cao P, Liu H, et al. Core-shell type multiarm star poly(ε-caprolactone) with high molecular weight hyperbranched polyethylenimine as core: Synthesis, characterization and encapsulation properties. Eur Polym J. 2008;44:1060–1070.

[137] Liu H, Shen Z, Stiriba S-E, Chen Y, Zhang W, Wei L. Core–shell-type multiarm star polyethylenimine-block-poly(ε-caprolactone): Synthesis and guest encapsulation potentia. J Polym Sci, Part A: Polym Chem. 2006;44:4165–4173.

[138] Adeli M, Haag R. Multiarm star nanocarriers containing a poly(ethylene imine) core and polylactide arms. J Polym Sci, Part A: Polym Chem. 2006;44:5740–5749.

[139] Santiago D, Fernández-Francos X, Ramis X, Salla JM, Sangermano M. Comparative curing kinetics and thermal–mechanical properties of DGEBA thermosets cured with a hyperbranched poly(ethyleneimine) and an aliphatic triamine. Thermochim Acta. 2011;526: 9–21.

[140] Santiago D, Fernández-Francos X, Ferrando F, De La Flor S. Shape-memory effect in hyperbranched poly(ethyleneimine)-modified epoxy thermosets. J Polym Sci, Part B: Polym Phys. 2015;53:924–933.

[141] Acebo C, Fernández-Francos X, Messori M, Ramis X, Serra A. Shape-memory effect in hyperbranched poly(ethyleneimine)-modified epoxy thermosets. Polymer. 2014;55: 5028–5035.

[142] Acebo C, Fernández-Francos X, Santos J-I, Messori M, Ramis X, Serra A. Shape-memory effect in hyperbranched poly(ethyleneimine)-modified epoxy thermosets. Eur Polym J. 2015;70: 18–27.

[143] Acebo C, Fernández-Francos X, Ramis X, Serra A. Multifunctional allyl-terminated hyperbranched poly(ethyleneimine) as component of new thiol–ene/thiol–epoxy materials. React Funct Polym. 2016;99:17–25.

[144] Acebo C, Fernández-Francos X, Ramis X, Serra A. Thiol-yne/thiol-epoxy hybrid crosslinked materials based on propargyl modified hyperbranched poly(ethyleneimine) and diglycidylether of bisphenol A resins. RSC Adv. 2016;6:61576–61584.

[145] Acebo C, Fernández-Francos X, Ferrando F, Serra A, Salla JM, Ramis X. Thiol-yne/thiol-epoxy hybrid crosslinked materials based on propargyl modified hyperbranched poly (ethyleneimine) and diglycidylether of bisphenol a resins. React Funct Polym. 2013;73: 431–441.

[146] Acebo C, Fernández-Francos X, Ferrando F, Serra A, Ramis X. New epoxy thermosets modified with multiarm star poly(lactide) with poly(ethyleneimine) as core of different molecular weight. Eur Polym J. 2013;49:2316–2326.

[147] Acebo C, Picardi A, Fernández-Francos X, De La Flor S, Ramis X, Serra A. Effect of hydroxyl ended and end-capped multiarm star polymers on the curing process and mechanical characteristics of epoxy/anhydride thermosets. Prog Org Coat. 2014;77:1288–1298.

[148] Acebo C, Alorda M, Ferrando F, Fernández-Francos X, Serra A, Morancho JM, et al. Epoxy/anhydride thermosets modified with end-capped star polymers with poly(ethyleneimine) cores of different molecular weight and poly(!–caprolactone) arms. Express Polym Lett. 2015;9:809–823.

[149] Mimura K, Ito H, Fujioka H. Improvement of thermal and mechanical properties by control of morphologies in PES-modified epoxy resins. Polymer. 2000;41:4451–4459.

[150] Chikhi N, Fellahi S, Bakar M. Modification of epoxy resin using reactive liquid (ATBN) rubber. Eur Polym J. 2002;38:251–264.

[151] Däbritz F, Voit B, Naguib M, Sangermano M. Hyperstar poly(ester-methacrylate)s as additives in thermally and photocured epoxy resins. Polymer. 2011;5723–5731.

[152] Foix D, Yu Y, Serra A, Ramis X, Salla JM. Study on the chemical modification of epoxy/anhydride thermosets using a hydroxyl terminated hyperbranched polymer. Eur Polym J. 2009;45:1454–1466.

[153] Foix D, Fernández-Francos X, Salla JM, Serra A, Morancho JM, Ramis X. New thermosets obtained from bisphenol A diglycidyl ether and hydroxyl-ended hyperbranched polymers partially blocked with benzoyl and trimethylsilyl groups. Polym Int. 2011;60:389–397.

[154] Fernández-Francos X, Santiago D, Ferrando F, Ramis X, Salla JM, Serra A, et al. Network structure and thermomechanical properties of hybrid DGEBA networks cured with 1–methylimidazole and hyperbranched poly(ethyleneimine)s. J Polym Sci, Part B: Polym Phys. 2012;50:1489–1503.

[155] Siddhamalli SK, Kyu T. Toughening of thermoset/thermoplastic composites via reaction-induced phase separation: epoxy/phenoxy blends. J Appl Polym Sci. 2000;77:1257–1268.

[156] Inoue T. Reaction-induced phase decomposition in polymer blends. Prog Polym Sci. 1995;20: 119–153.

[157] Fernández-Francos X, Foix D, Serra A, Salla JM, Ramis X. Novel thermosets based on DGEBA and hyperbranched polymers modified with vinyl and epoxy end groups. React Funct Polym. 2010;70:798–806.

[158] Johnson TW, Klotz IM. Preparation and characterization of some derivatives of poly (ethylenimine). Macromolecules. 1974;7:149–153.

[159] Antonietti L, Aymonier C, Schlotterbeck U, Garamus VM, Maksimova T, Richtering W, et al. Core–shell-structured highly branched poly(ethylenimine amide)s: synthesis and structure. Macromolecules. 2005;14:5914–5920.

[160] Liu H, Chen Y, Zhu D, Shen Z, Stiriba S-E. Hyperbranched polyethylenimines as versatile precursors for the preparation of different type of unimolecular micelles. React Funct Polym. 2007;67:383–395.

[161] Qin H, Liu H, Chen Y. Influence of aliphatic amide terminals on the thermoresponsive properties of hyperbranched polyethylenimines. Chin J Polym Sci. 2014;32:1338–1347.

[162] Thetford D, Schofield JD. US Patent 5.700.395, 23 December 1997.

[163] Kasza G, Mosnácková K, Nádor A, Osváth Z, Stumphauser T, Szarka G, et al. Hyperbranched polyethylenimines as versatile precursors for the preparation of different type of unimolecular micelles. Eur Polym J. 2015;68:609–617.

[164] Montalbetti CAGN, Falque V. Amide bond formation and peptide coupling. Tetrahedron. 2015;61:10827–10852.

[165] Acebo C, Fernández-Francos X, De La Flor S, Ramis X, Serra A. New anhydride/epoxy thermosets based on diglycidyl ether of bisphenol A and 10–undecenoyl modified poly (ethyleneimine) with improved impact resistance. Prog Org Coat. 2015;85:52–59.

[166] Liu J, Duong H, Whittaker MR, Davis TP, Boyer C. Synthesis of functional core, star polymers via RAFT polymerization for drug delivery applications. Macromol Rapid Commun. 2012;33: 760–766.

[167] Rodionov V, Gao H, Scroggins S, Unruh DA, Avestro A-J, Fréchet JMJ. Easy access to a family of polymer catalysts from modular star polymers. J Am Chem Soc. 2010;132:2570–2572.

[168] Xia W, Jiang G, Chen W. Synthesis and drug-release properties of hyperbranched polyesters grafted with biocompatible poly(ϵ-caprolactone). J Appl Polym Sci. 2008;109:2089–2094.

[169] Zhang X, Cheng J, Wang Q, Zhong Z, Zhuo R. Miktoarm copolymers bearing one poly(ethylene glycol) chain and several poly(ε-caprolactone) chains on a hyperbranched polyglycerol core. Macromolecules. 2010;43:6671–6677.

[170] Cameron DJA, Shaver MP. Aliphatic polyester polymer stars: synthesis, properties and applications in biomedicine and nanotechnology. Chem Soc Rev. 2011;40:1761–1776.

[171] Duréault A, Taton D, Destarac M, Leising F, Gnanou Y. Synthesis of multifunctional dithioesters using tetraphosphorus decasulfide and their behavior as RAFT agents. Macromolecules. 2004;37:5513–5519.

[172] Maier S, Sunder A, Frey H, Mülhaupt R. Synthesis of poly(glycerol)-block-poly(methyl acrylate) multi-arm star polymers. Macromol Rapid Commun. 2000;21:226–230.

[173] Trollsås M, Hawker CJ, Remenar JF, Hedrick JL, Johanson H, Ihre H, et al. Highly branched radial block copolymers via dendritic initiation of aliphatic polyesters. J Polym Sci, Part A: Polym Chem. 1998;36:2793–2798.

[174] Burgath A, Sunder A, Neuner I, Mülhaupt R, Frey H. Multi-arm star block copolymers based on ε-caprolactone with hyperbranched polyglycerol core. Macromol Chem Phys. 2000;201: 792–797.

[175] Cao PF, Xiang R, Liu XY, Zhang CX, Cheng F, Chen YJ. Modulating the guest encapsulation and release properties of multi-arm star polyethylenimine-block-poly(ε-caprolactone). J Polym Sci, Part A: Polym Chem. 2009;47:5184–5193.

[176] Schömer M, Frey H. Organobase-catalyzed synthesis of multiarm star polylactide with hyperbranched poly(ethylene glycol) as the core. Macromol Chem Phys. 2011;212:2478–2486.

[177] Biela T, Kowalski A, Libiszowski J, Duda A, Penczek S. Progress in polymerization of cyclic esters: mechanisms and synthetic applications. Macromol Symp. 2006;240:47–55.

[178] Kowalski A, Libiszowski J, Biela T, Cypryk M, Duda A, Penczek S. Kinetics and mechanism of cyclic esters polymerization initiated with Tin(II) octoate. Polymerization of ε-Caprolactone and l,l-Lactide co-initiated with primary amines. Macromolecules. 2005;38:8170–8176.

[179] Hameed N, Guo Q, Hanley T, Mai YW. J Polym Sci, Part B: Hydrogen bonding interactions, crystallization, and surface hydrophobicity in nanostructured epoxy/block copolymer blends. Polym Phys. 2010;48:790–800.

[180] Lützen H, Bitomsky P, Rezwan K, Hartwig A. Partially crystalline polyols lead to morphology changes and improved mechanical properties of cationically polymerized epoxy resins. Eur Polym J. 2013;49:167–176.

[181] .Chen JS, Ober CK, Poliks MD. Characterization of thermally reworkable thermosets: materials for environmentally friendly processing and reuse. Polymer. 2002;43:131–139.

[182] Meng F, Xu Z, Zheng S. Microphase separation in thermosetting blends of epoxy resin and poly (ε-caprolactone)-block-polystyrene block copolymers. Macromolecules. 2008;41:1411–1420.

[183] Chruściel JJ, Leśniak E. Modification of epoxy resins with functional silanes, polysiloxanes, silsesquioxanes, silica and silicates. Prog Polym Sci. 2015;41:67–121.

[184] Pierre AC. New types of sol-gel derived materials. In: Pierre AC, editor. Introduction to sol-gel processing. Norwell: Kluver Academic, 1998.

[185] Gröhn F, Kim G, Bauer BJ, Amis EJ. Nanoparticle formation within dendrimer-containing polymer networks: route to new organic–inorganic hybrid materials. Macromolecules. 2001;34:2179–2185.

[186] Matejka L, Dukh O, Kolarik J. Reinforcement of crosslinked rubbery epoxies by in-situ formed silica. Polymer. 2000;41:1449–1459.

[187] Wen J, Wilkes GL. Organic/inorganic hybrid network materials by the sol–gel approach. Chem Mater. 1996;8:1667–1681.

[188] Georgieva N, Bryaskova R, Tzoneva R. New polyvinyl alcohol-based hybrid materials for biomedical application. Material Lett. 2012;88:19–22.

[189] Matějka L, Pleštil J, Dušek K. Structure evolution in epoxy–silica hybrids: sol–gel process. J Non Cryst Solids. 1998;226:114–121.

[190] Silva CR, Airoldi C. Acid and Base Catalysts in the Hybrid Silica Sol–Gel Process. J Colloid Interface Sci. 1997;195:381–387.

[191] Serra A, Ramis X, Fernández-Francos X. Epoxy sol-gel hybrid thermosets. Coatings. 2016;6:8.

[192] Branda F, Tescione F, Ambrogi V, Sannino D, Silvestri B, Luciani G, et al. A new extra situ sol–gel route to silica/epoxy (DGEBA) nanocomposite. A DTA study of imidazole cure kinetic. Polymer Bull. 2011;66:1289–1300.

[193] Beneŝ H, Galy J, Gérard J-F, Pleŝtil J, Valette L. Preparation and characterization of organic/inorganic hybrid epoxy networks from reactive inorganic precursors. J Appl Polym Sci. 2012;125:1000–1011.

[194] Pisticelli F, Lavorgna M, Buonocore GG, Verdolotti L, Galy J, Mascia L. Plasticizing and reinforcing features of siloxane domains in amine-cured epoxy/silica hybrids. Macromol Mater Eng. 2013;298:896–909.

[195] Davis SR, Brough AR, Atkinson A. Formation of silica/epoxy hybrid network polymers. J Non-Cryst Solids. 2003;315:197–205.

[196] Prezzi L, Mascia L. Network density control in epoxy–silica hybrids by selective silane functionalization of precursors. Adv Polymer Technol. 2005;24:91–102.

[197] Palraj S, Selvaraj M, Maruthan K, Rajagopal G. Corrosion and wear resistance behavior of nano-silica epoxy composite coatings. Prog Org Coat. 2015;81:132–139.

[198] Kaneko Y, Shoirikia M, Mizumob T. Preparation of cage-like octa(3–aminopropyl) silsesquioxane trifluoromethanesulfonate in higher yield with a shorter reaction time. J Mater Chem. 2012;22:14475–14478.

[199] Chruściel JJ, Leśniak E. Modification of epoxy resins with functional silanes, polysiloxanes, silsesquioxanes, silica and silicates. Prog Polym Sci. 2015;41:67–121.

[200] Choi J, Harcup J, Yee AF, Zhu Q, Laine RM. Organic/inorganic hybrid composites from cubic silsesquioxanes. J Am Chem Soc. 2001;123:11420–11430.

[201] Houel A, Galy J, Charlot A, Gérard J-F. Synthesis and characterization of hybrid films from hyperbranched polyester using a sol–gel process. J Appl Polym Sci 2014. DOI:10.1002/app.39830.

[202] Geiser V, Letterrier Y, Månson J-AE. Low-stress hyperbranched polymer/silica nanostructures produced by UV curing, sol/gel processing and nanoimprint lithography. Macromol Mater Eng. 2012;297:155–166.

[203] Allauddin S, Chandran MKA, Jena KK, Narayan R, Raju KVSN. Synthesis and characterization of APTMS/melamine cured hyperbranched polyester-epoxy hybrid coatings. Prog Org Coat. 2013;76:1402–1412.

[204] Lorenzo V, Acebo C, Ramis X, Serra A. Synthesis and characterization of APTMS/melamine cured hyperbranched polyester-epoxy hybrid coatings. Prog Org Coat. 2016;92:16–22.

[205] Kolb HC, Finn MG, Sharpless KB. Click chemistry: diverse chemical function from a few good reactions. Ange Chem Int Ed. 2001;40:2004–2021.

[206] Franc G, Kakkar AK. Diels–Alder “Click” chemistry in designing dendritic macromolecules. Chem Eur J. 2009;15:5630–5639.

[207] Voit B. The potential of cycloaddition reactions in the synthesis of dendritic polymers. New J Chem. 2007;31:1139–1151.

[208] Kumaraswamy G, Ankamma K, Pitchaiah A. Tandem epoxide or aziridine ring opening by azide/copper catalyzed [3+2] cycloaddition: efficient synthesis of 1,2,3–triazolo β-hydroxy or β-tosylamino functionality motif. J Org Chem. 2007;72:9822–9825.

[209] Heredia KL, Tolstyka ZP, Maynard HD. Aminooxy end-functionalized polymers synthesized by ATRP for chemoselective conjugation to proteins. Macromolecules. 2007;40:4772–4779.

[210] Hoyle CE, Lowe AB, Bowman CN. Thiol-click chemistry: a multifaceted toolbox for small molecule and polymer synthesis. Chem Soc Rev. 2010;39:1355–1387.

[211] Tasdelena MA, Kiskanb B, Yagci Y. Externally stimulated click reactions for macromolecular syntheses. Prog Polym Sci. 2016;52:19–78.

[212] Wong C-H, Zimmerman SC. Orthogonality in organic, polymer, and supramolecular chemistry: from Merrifield to click chemistry. Chem Commun. 2013;49:1679–1695.

[213] Lutz J-F, Börner HG, Weichenhan K. Combining ATRP and “Click” chemistry: a promising platform toward functional biocompatible polymers and polymer bioconjugates. Macromolecules. 2006;39:6376–6383.

[214] Iha RK, Wooley KL, Nyström AM, Burke DJ, Kade MJ, Hawker CJ. Applications of orthogonal “click” chemistries in the synthesis of functional soft materials. Chem Rev. 2009;109: 5620–5686.

[215] Kolb HC, Sharpless KB. The growing impact of click chemistry on drug discovery. Drug Discov Today. 2003;8:1128–1137.

[216] Xi W, Scott TF, Kloxin CJ, Bowman CN. Click chemistry in materials science. Adv Funct Mater. 2014;24:2572–2590.

[217] Thirumurugan P, Matosiuk D, Jozwiak K. Click chemistry for drug development and diverse chemical–biology applications. Chem Rev. 2013;113:4905–4979.

[218] Chen GJ, Tao L, Mantovani G, Ladmiral V, Burt DP, Macpherson JV, et al. Synthesis of azide/alkyne-terminal polymers and application for surface functionalisation through a [2 + 3] Huisgen cycloaddition process, “click chemistry”. Soft Matter. 2007;3:732–739.

[219] Nischang I, Brueggemann O, Teasdale I. Facile, single-step preparation of versatile, high-surface-area, hierarchically structured hybrid materials. Ange Chem Int Ed. 2011;50: 4592–4596.

[220] De Forest CA, Anseth KS. Cytocompatible click-based hydrogels with dynamically-tunable properties through orthogonal photoconjugation and photocleavage reactions. Nat Chem. 2011;3:925–931.

[221] Zhang Q, Ning ZJ, Yan YL, Qian SX, Tian H. Photochromic spiropyran dendrimers: ‘Click’ syntheses, characterization, and optical properties. Macromol Rapid Commun. 2008;29: 193–201.

[222] Li HM, Cheng FO, Duft AM, Adronov A. Functionalization of single-walled carbon nanotubes with well-defined polystyrene by “Click” coupling. J Am Chem Soc. 2005;127:14518–14524.

[223] Jian Y, He Y, Sun Y, Yang H, Yang W, Nie JJ. Thiol–epoxy/thiol–acrylate hybrid materials synthesized by photopolymerization. Mater Chem C. 2013;1:4481–4489.

[224] De S, Khan A. Efficient synthesis of multifunctional polymersviathiol–epoxy “click” chemistry. Chem Commun. 2012;48:3130–3132.

[225] Yuan YC, Rong MZ, Zhang MQ, Chen J, Yang GC, Li XM. Self-healing polymeric materials using epoxy/mercaptan as the healant. Macromolecules. 2008;41:5197–5202.

[226] Jin K, Heath WH, Torkelson JM. Kinetics of multifunctional thiol-epoxy click reactions studied by differential scanning calorimetry: effects of catalysis and functionality. Polymer. 2015;81: 70–78.

[227] Fernández-Francos X, Konuray A-O, Belmonte A, De La Flor S, Serra A, Ramis X. Sequential curing of off-stoichiometric thiol–epoxythermosets with a custom-tailored structure. Polym Chem. 2016;7:2280–2290.

[228] Hoyle CE, Bowman CN. Thiol–ene click chemistry. Ange Chem Int Ed. 2010;49:1540–1573.

[229] Hoyle CE, Lee TY, Roper T. Thiol–enes: chemistry of the past with promise for the future. J Polym Sci, Part A: Polym Chem. 2004;42:5301–5338.

[230] Lowe AB, Bowman CN. 2013. Thiol-X Chemistries in polymer and material science. Croydon: RSC Publishing.

[231] Sprafke JK, Spruell JM, Mattson KM, Montarnal D, McGrath AJ, Pötzsch R, et al. Revisiting thiol-yne chemistry: selective and efficient monoaddition for block and graft copolymer formation. J Polym Sci, Part A: Polym Chem. 2015;53:319–326.

[232] Killops KL, Campos LM, Hawker CJ. Robust, efficient, and orthogonal synthesis of dendrimers via thiol-ene "click" chemistry. J Am Chem Soc. 2008;130:5062–5064.

[233] Chan JW, Zhou H, Hoyle CE, Lowe AB. Photopolymerization of thiol-alkynes: polysulfide networks. Chem Mater. 2009;21:1579–1585.

[234] Wei Q, Pötzsch R, Liu X, Komber H, Kiriy A, Voit B, et al. Hyperbranched polymers with high transparency and inherent high refractive index for application in organic light-emitting diodes. Adv Funct Mater 2016;26:2545–2553.

[235] Cramer NB, Scott JP, Bowman CN. Photopolymerizations of thiol–ene polymers without photoinitiators. Macromolecules. 2002;35:5361–5365.

[236] Lowe AB. Polymer. Thiol-yne ‘click’/coupling chemistry and recent applications in polymer and materials synthesis and modification. 2014;55:5517–5549.

[237] Sangermano M, Roppolo I, Acosta Ortiz R, Navarro Tovar AG, García Valdez AE, Berlanga Duarte L. Interpenetrated hybrid thiol-ene/epoxy Uv-cured network withenhanced impact resistance. Prog Org Coat. 2015;78:244–248.

[238] Carioscia JA, Stansbury JW, Bowman CN. Evaluation and control of thiol–ene/thiol–epoxy hybrid networks. Polymer. 2007;48:1526–1532.

[239] Jian Y, He Y, Sun Y, Yang H, Yang W, Nie J. J Mater Chem C. Thiol–epoxy/thiol–acrylate hybrid materials synthesized by photopolymerization. 2013;1:4481–4489.

[240] Yoshimura T, Shimasaki T, Teramoto N, Shibata M. Bio-based polymer networks by thiol–ene photopolymerizations of allyl-etherified eugenol derivatives. Eur Polym J. 2015;67:397–408.

[241] Nair DP, Cramer NB, Gaipa JC, McBride MK, Matherly EM, McLeod RR, et al. Two-stage reactive polymer network forming systems. Adv Funct Mater. 2012;22:1502–1510.

[242] Miller DR, Valles EM, Macosko CW. Calculation of molecular parameters for stepwise polyfunctional polymerization. Polymer Eng Sci. 1979;19:272–283.

[243] Guzmán D, Ramis X, Fernández-Francos X, Serra A. Preparation of click thiol-ene/thiol-epoxy thermosets by controlled photo/thermal dual curing sequence. RSC Adv. 2015;5: 101623–101633.

Iuliana Cota

2 Developments in the use of rare earth metal complexes as efficient catalysts for ring-opening polymerization of cyclic esters used in biomedical applications

Abstract: Biodegradable polymers represent a class of particularly useful materials for many biomedical and pharmaceutical applications. Among these types of polyesters, poly(ε-caprolactone) and polylactides are considered very promising for controlled drug delivery devices. These polymers are mainly produced by ring-opening polymerization of their respective cyclic esters, since this method allows a strict control of the molecular parameters (molecular weight and distribution) of the obtained polymers. The most widely used catalysts for ring-opening polymerization of cyclic esters are tin- and aluminium-based organometallic complexes; however since the contamination of the aliphatic polyesters by potentially toxic metallic residues is particularly of concern for biomedical applications, the possibility of replacing organometallic initiators by novel less toxic or more efficient organometallic complexes has been intensively studied. Thus, in the recent years, the use of highly reactive rare earth initiators/catalysts leading to lower polymer contamination has been developed. The use of rare earth complexes is considered a valuable strategy to decrease the polyester contamination by metallic residues and represents an attractive alternative to traditional organometallic complexes.

Keywords: biodegradable polymers, catalysts, polymerization

2.1 Biodegradable polymers

In the last decades, biodegradable polymers have become increasingly important in the development of drug delivery systems (DDS). Most of the polymers used in DDS are based on biodegradable and biocompatible materials, mainly aliphatic polyesters, polyanhydrides, polyethers, polyamides, polyorthoesters and polyurethanes [1].

Biodegradable polymers can be natural or synthetic. The synthetic polymers have many advantages over the natural ones since their structure can be tailored to meet specific requirements such as hydrophobicity, crystallinity, degradability, solubility, glass transition temperature and melting temperature, by changing the

https://doi.org/10.1515/9783110469745-002

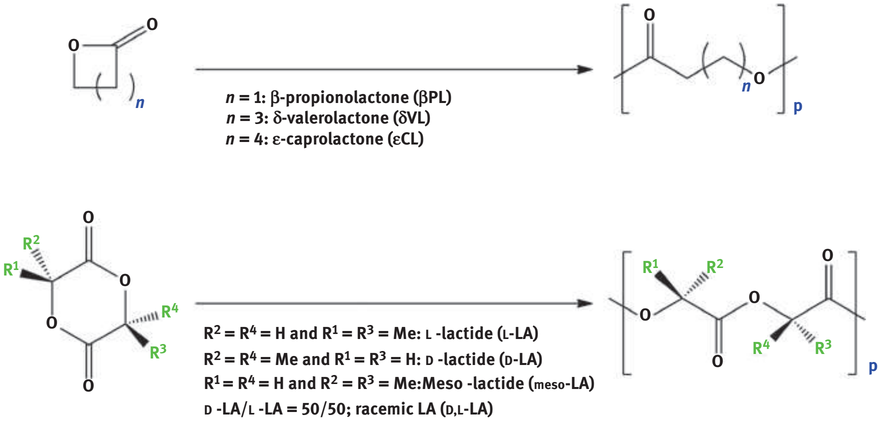

Figure 2.1: Ring-opening polymerization of unsubstituted lactones and lactides.

synthesis protocol. In contrast, natural biodegradable polymers lack versatility since they can only be modified. Among the various families of biodegradable polymers, aliphatic polyesters are of most interest since by their chain cleavage, compounds which are easily metabolized are formed.

Poly(lactides) (PLAs) (Figure 2.1) are the most used among the aliphatic polyesters for drug delivery as a result of their fast and adjustable degradation rate. Due to their versatile physical properties, PLAs are being widely used in medicine as surgical sutures and resorptable prostheses and in pharmaceutics and tissue engineering such as media for the controlled drugs release, scaffolds and delivery of antibodies and genes [2].

2.2 Polymerization mechanisms for polyester synthesis

Polyesters can be synthesized by two types of mechanisms:

– step-growth polymerization or polycondensation (PC);–ring-opening polymerization (ROP) of cyclic esters and related compounds.

The PC technique consists of condensation between hydroxy-acids or mixtures of diacids and diols (Figure 2.2).

The PC method may appear more direct than ROP, but with this technique it is difficult to obtain high-molecular-weight polymers with well-defined structure. Another major drawback of the PC mechanism is that it requires high temperatures and long reaction times, which ultimately favour the side reactions. Moreover, since they are equilibrium reactions, water must be removed from the polymerization medium in order to increase the conversion and the molecular weight of the obtained product.

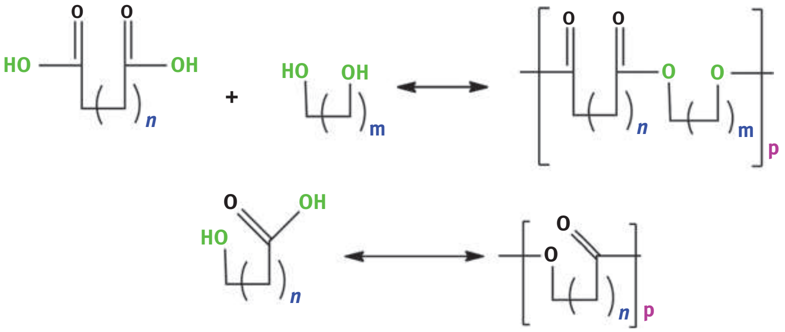

Figure 2.2: Synthesis of aliphatic polyesters by step-growth polycondensation.

On the other hand, the polymerization of lactides and lactones by the ROP process does not present these limitations. ROP mechanism allows a good control of the polymer characteristics; thus high-molecular-weight polyesters can be easily prepared under mild conditions from lactones of different ring size, substituted or not by functional groups [3, 4].

The ROP proceeds mainly via two major polymerization mechanisms depending on the used organometallics. Some of them act as catalysts and activate the monomer by complexation with the carbonyl group (Figure 2.3). Polymerization is then initiated by any nucleophile (water or alcohol) present in the polymerization medium as impurities or as added compound.

In the second mechanism, the organometallic plays the role of initiator and the polymerization proceeds through an "insertion–coordination" mechanism (Figure 2.4).

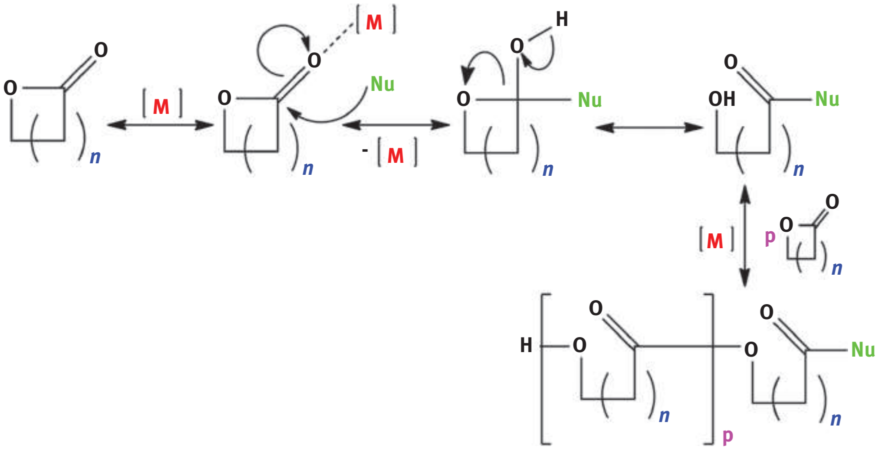

Figure 2.3: ROP of lactones catalyzed by organometallic species [M] in presence of nucleophiles (Nu).

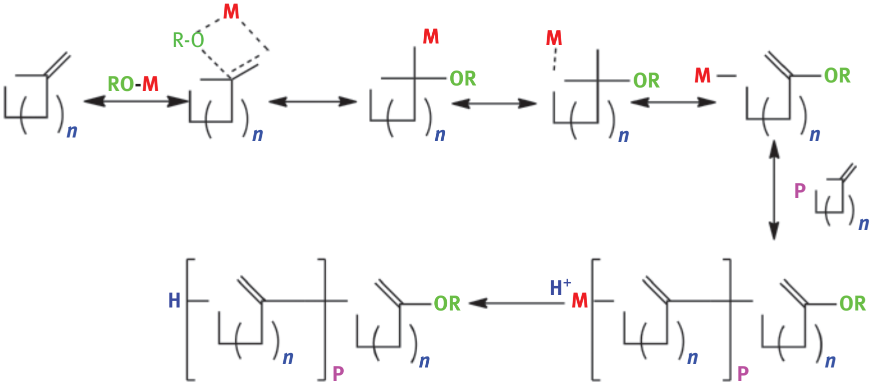

Figure 2.4: ROP of lactones by the “coordination–insertion” mechanism.

The initiator (typically metal alkoxides) first coordinates the carbonyl of the monomer, followed by the cleavage of the acyl–oxygen bond of the monomer and simultaneous insertion into the metal alkoxide bond [1].

Stridsberg et al. explored for the first time the ROP technique for lactones, cyclic anhydrides and carbonates [5]. Since then, this method has been applied to a wide range of monomers with a great variety of initiator and catalyst systems. Table 2.1 lists some of the most commonly used monomers and their related polyester chains obtained by ROP which are currently used as biomaterials as well as ecological materials that preserve the environment.

Table 2.1: Monomer and polymer structures of the most common aliphatic polyesters obtained by ROP [6].

Monomer	**Polymer**
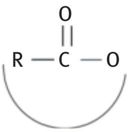 R = -$(CH_2)_2$-βPL, β-propiolactone R = -$(CH_2)_3$-γBL, γ-butyrolactone R = -$(CH_2)_4$-δVL, δ-valerolactone R = -$(CH_2)_5$-εCL, ε-caprolactone R = -$(CH_2)_2$-O-$(CH_2)_2$-DXO, 1,5-dioxepan-2-one R= -$(CH_2{-}CH(CH_3))$–βBL, β-butyrolactone R = -$(C(CH_3)_2{-}CH_2)$-PVL, pivalolactone R = -CH_2-$CH(CO_2C_7H_7)$–βMLABz, benzyl β-malolactonate	Polylactone poly(ω-hydroxy acid) PβPL PγBL PδVL PεCL PDXO PβBL isotactic PβBL atactic PPVL P(R,S)MLABz P(R)MLABz P(S)MLABz Polydilactone

(*continued*)

Table 2.1: (*continued*)

Monomer	Polymer
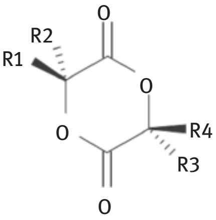 $R_1 = R_2 = R_3 = R_4 = H$ GA, glycolide $R_1 = R_4 = CH_3$, $R_2 = R_3 = H$ L,L-LA, L,L-lactide $R_1 = R_4 = H$, $R_2 = R_3 = CH_3$ D,D-LA, D,D-lactide $R_1 = R_3 = CH_3$, $R_2 = R_4 = H$ meso-LA, meso-lactide D,D-LA/L,L-LA (50-50) D,L-LA, (D,L) racemic lactide	Poly(α-hydroxyacid) PGA PL, L-LA PD, D-LA PmesoLA PDLLA

Nowadays, PLAs of high molecular weight are produced almost exclusively by ROP of the corresponding cyclic monomers.

2.3 Catalysts for ROP of PLAs

A broad range of catalysts have been reported for the ROP; most of them are organometallic derivatives of metals with d-orbitals of a favourable energy, such as Al, Sn, Nd, Y, Yb, Sm, La, Fe, Zn, Zr, Ca, Ti and Mg [7, 8].

Since the contamination of the aliphatic polyesters by potentially toxic metallic residues is particularly of concern for biomedical applications, the possibility to replace organometallic initiators by novel less toxic or more efficient organometallics has been studied. Thus, a large variety of rare earth (RE) derivatives have been used to initiate the ROP of lactones and lactides due to their high reactivity [9]. The use of a catalytic amount of lanthanide complexes is a valuable strategy to decrease the polyester contamination by metallic residues as compared to the previously described tin- and aluminum-based initiators which must be used in stoichiometric amount vs. alcohol to favour the polymerization kinetics [1].

On the other hand, lanthanide complexes have been of considerable interest in the recent years as a result of their implications in the optical imaging of cells, such as luminescent chemosensors for medical diagnostics and contrast reagents for medical magnetic resonance imaging, in bioorganic chemistry [10, 11] and in the manufacture of superconductors [12–15], ceramics [16] and glass for optical, electronic and medical applications [13].

RE metal oxides have also found numerous applications in the field of catalysis [17–20]. Thus, organolanthanide chemistry has registered a growing interest in the past decades; the design and application of organolanthanide complexes as catalysts for polymerization and organic synthesis have occupied an especially important place. Changing the ligand environment of a complex to modify its properties has been an important strategy for the development of more efficient or selective catalysts.

Initially, organolanthanide chemistry has been dominated mainly by metallocene complexes that bear two substituted or unsubstituted cyclopentadienyl ligands. In the following years, the search for new ligand systems to extend the lanthanide chemistry has increased considerably [21].

2.4 Rare earth-based catalysts for synthesis of PLAs

In 1995, Mortreux et al. patented a method for the synthesis of complexes of the type $[(C_5Me_5)_2LnCl_2Li(OEt_2)_2]$ with Ln-Sc, Y and lanthanides as initiators for the preparation of caprolactone–ethylene block copolymers [22]. One year later, Nomura et al. reported the block copolymerization of tetrahydrofuran (THF) with δ-valerolactone by alkylsamarium ($RSmI_2$) complex [23]. Polymerization of δ-valerolactone by butylsamarium gave the corresponding poly(valerolactone) in good yield, while the polymerization of δ-valerolactone with poly-THF led to the block copolymer of THF with δ-valerolactone.

In 1997, Boffa and Novak reported the synthesis of “link-functionalized” poly(ε-caprolactone) (LFP) using bimetallic complexes of the type $(C_5Me_5)_2Sm/R/Sm(C_5Me_5)_2$ [24].

LFPs are of special interest because:

- they may serve as building blocks to other architectures;
- are useful models for the environment experienced by the polymer backbone;
- their functionality may be used to influence the polymerization process itself [25].

Hultzsch et al. investigated the ROP of ε-caprolactone catalysed by the heterobimetallic complexes $Li[Ln(\eta^5{:}\eta^1\text{-}C_5R_4Si\text{-}Me_2NCH_2CH_2X)_2]$ (Ln = Lu, Y) [26]. The product of this polymerization had a high molecular weight and moderate polydispersity. The initial step of the polymerization is a nucleophilic attack by one of the nucleophilic amido-nitrogen atoms at the lactone carbonyl–carbon atom, followed by acyl bond cleavage and formation of an alkoxide (Figure 2.5).

In 1998, Nomura et al. published a novel transformation reaction of living poly(THF) from cationic into anionic propagation species [27]. These species were formed by end-capping of living poly(THF) with potassium iodide (Figure 2.6) followed by the reduction with bis(pentamethyl cyclopentadienyl)samarium ($Cp^*{}_2Sm$).

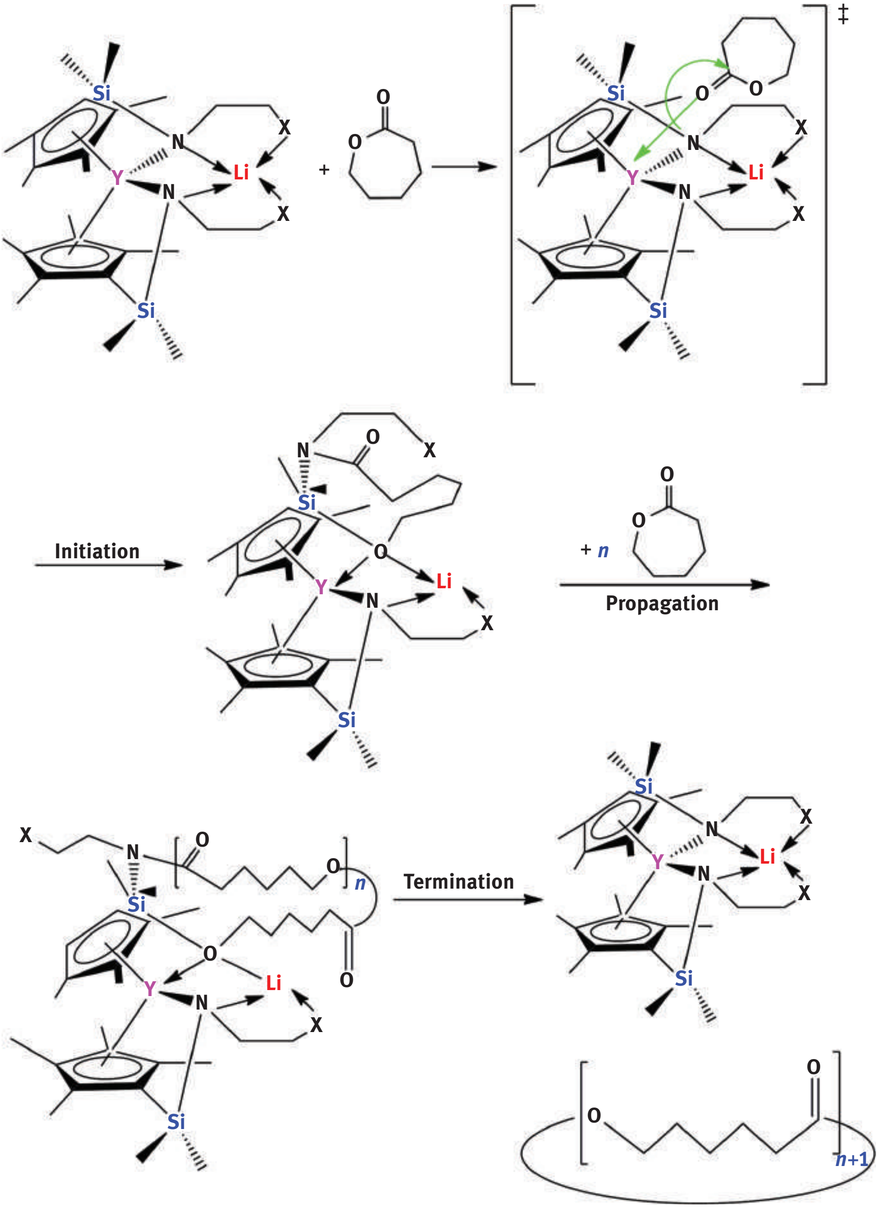

Figure 2.5: ROP of ε-caprolactone catalyzed by the heterobimetallic complexes Li[Ln(η^5:η^1-C_5R_4Si-$Me_2NCH_2CH_2X)_2$].

The formed terminal anionic carbanion was active for the polymerization of ε-caprolatone and δ-valerolactone and leads to the selective formation of unimodal block copolymers.

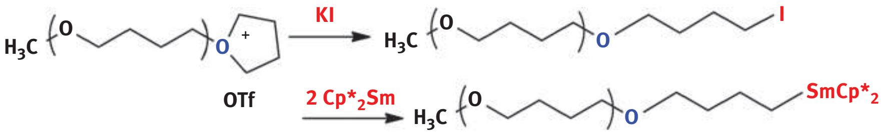

Figure 2.6: Transformation reaction of living poly(THF) with potassium iodide.

ROP of lactones using SmX_2 (X = I, Br, C_5H_5) catalysts was reported by Agarwal et al. [28]. Successful room temperature ROP of ε-caprolactone and δ-valerolactone has been carried out using the SmX_2 catalysts. SmI_2 in the presence of metallic Sm was found to enhance the reactivity at room temperature in ROP processes as compared to pure SmI_2. $SmBr_2$ and $Sm(C_5H_5)_2$ showed increased reactivity compared with the Sm/SmI_2 system owing to their higher reductive power [28].

Among other studies of other samarium (II) aryloxide complexes, Nishiura et al. showed that $[(C_5Me_5)Sm(\mu\text{-}OC_6H_2{}^tBu_2\text{-}2,6\text{-}Me\text{-}4)]_2$ exhibited an extremely high activity for the ROP of ε-caprolactone and δ-valerolactone [29].

In the article of Yuan et al., it was shown that the homopolymerization and copolymerization of ε-caprolactone and lactides can be initiated efficiently by 2-methylphenyl samarium according to the mechanism of “coordination–deprotonation–insertion,” by which the monomer is inserted on the Ln–O bond of RE enolate [30]. When the polymerizations are conducted in bulk, 2-methylphenyl samarium can give high yield and high-molecular-weight products.

Desurmont et al. described the first example of well-controlled block copolymerization of 1-olefins with ε-caprolactone using bridged $Me_2Si(C_5R_4)_2LnH$ (Ln =Y, Sm) type complexes [31]. These initiators are highly active in copolymerization processes without the presence of any cocatalyst (Figure 2.7).

The dimeric structure of the yttrium and samarium hydride complexes is converted into a monomeric structure in the first step of the reaction. Subsequent reactions lead to a chain elongation. The authors reported the preparation of block copolymers of hexene or pentene with ε-caprolactone [31].

In the study of Deng et al., ROP of D,L-lactide was initiated with RE phenyl compound in bulk and solution [32]. These RE phenyl initiators gave high yield and high-molecular-weight poly(D,L-lactide) products. The results showed that reaction conditions have a great influence on the yield and molecular weight of PLA. Thus, a high molecular weight of PLA was obtained in the case of lower M/I molar ratio.

The ROP of cyclic esters (ε-caprolactone and L-lactide) initiated with $LnCp_3$ complexes (Ln = Sm, Er, Pr, Gd and Ce) was reported by Agarwal and Puchner [33]. The size of the metal atom was found to have an effect on the catalytic activity. Thus, the order of reactivity was Er ~ Gd > Sm > Pr > Ce. Although the polymerization system was not living, the growing polymer chains were found to be active for the polymerization of second monomer, thus capable of synthesizing block copolymers.

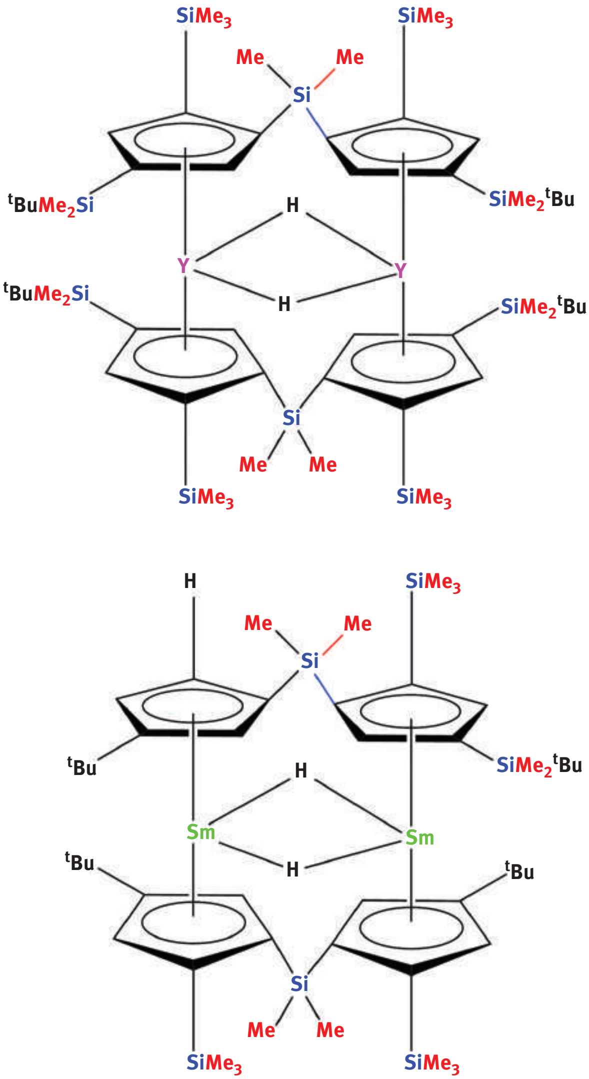

Figure 2.7: Bridged organolanthanide hydrides of yttrium and samarium.

In the work of Cui et al., the substituted indenyl ytterbium (II) complex $(C_9H_6C_5H_9)_2Yb(THF)_2$ showed high activity for ROP of lactones [34]. Scandium dialkyl complexes containing bulky iminophenolato ligands have been found to be efficient catalysts for the ROP of ε-caprolactone [35]. The ROP of cyclic esters (ε-caprolactone and L-lactide) is initiated by Cp_3Ln complexes (Ln = Ce, Pr, Sm, Gd, Er), and it was observed that the size of the metal ion had an effect on the catalytic activity. Other complexes which have been found to exhibit high catalytic activity in the ROP of ε-caprolactone include $Cp_3Dy_2(NPPh_3)_3$ [36].

ROP and block copolymerization of L-lactide has also been achieved with the divalent samarocene complexes $(C_5H_4C_5H_9)_2Sm(THF)_2$ as catalyst [37], while D,L-lactide was effectively polymerized using $Cp^*{}_2SmMe$ (THF) [38].

In their study, Satoh et al. showed that the complexes $[(C_5H_4SiMe_3)_2Sm(\mu\text{-}Me)]_2$ and $[\{C_5H_3(SiMe_3)2\text{-}1,3\}_2Ln(\mu\text{-}Me)]_2$ (Ln = Nd, Sm) performed the block copolymerization of L-lactide with ε-caprolactone with high yields in the absence of any cocatalysts [39]. The guanidinate lanthanide methyl complexes $[(Me_3Si)_2NC(NPr^i)_2]_2Ln(\mu\text{-}Me)_2Li$ (TMEDA) (Ln = Nd, Yb) have been established as effective single-component initiators for ε-caprolactone polymerization [40]. Other organolanthanide complexes reported to catalyse the (co-)polymerization of ε-caprolactone include homoleptic lanthanide guanidinate complexes [41], $Cp^*{}_2Sm(BH_4)(THF)$ [42] and sterically hindered lanthanide allyl complexes [43].

Single-component RE tris(4-tert-butylphenolate)s $[Ln(OTBP)_3]$ (Ln=La, Nd, Gd, Er, Y) were found to be effective initiators for the ROP of ε-caprolactone. Among them, $La(OTBP)_3$ has shown higher activity and gave higher-molecular-weight poly(ε-caprolactone) [44].

In the work of Fan et al., a novel single-component RE phenolate catalyst-lanthanide tris(2,4,6-trimethylphenolate)s $[Ln(OTMP)_3]$ (Ln=La, Nd, Sm, Er, Y) (Figure 2.8) initiated ROP of ε-caprolactone [45]. It was found that the polymerization activity of the compounds had the following order: La ≈ Sm > Nd > Er > Y. Among the studied complexes, $La(OTMP)_3$ exhibited the highest activity and the prepared poly(ε-caprolactone).

Single-component RE 2,6-dimethylaryloxide $[Ln(ODMP)_3]$ (Figure 2.9) was used as catalyst or initiator for the ROP of L-lactide, and it was shown that the catalytic

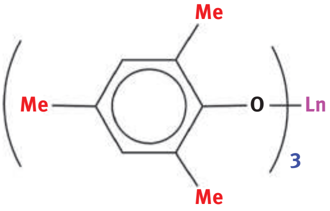

Figure 2.8: Structure of $Ln(OTMP)_3$ (Ln = La, Nd, Sm, Y, Er).

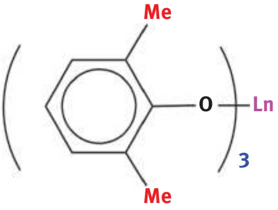

Figure 2.9: Structure of $Ln(ODMP)_3$ (Ln = La, Nd, Sm, Gd, Er, Y).

activity of different RE compounds followed the order: La > Nd > Sm > Gd > Er > Y, which may result from different coordination abilities of these RE elements with the monomer [46].

In the same work, ROP of ε-caprolactone was achieved by a novel RE initiator of scandium tris(2,6-di-tert-butyl-4-methylphenolat) producing poly(ε-caprolactone) under mild conditions [47].

Several tris(allyl) and bis(allyl)(diketiminato)lanthanide complexes have been demonstrated to be highly effective single-component catalysts for the ROP of ε-caprolactone and *rac*-LA. Polymer end-group analysis showed that the polymerization process was initiated by allyl transfer to the monomer [48]. Reactivity studies of amine–bis(phenolate) complexes of the type $[Me_2NCH_2CH_2N\{CH_2(2\text{-}OC_6H_2Bu_2t\text{-}3,5)\}_2]$ LnMe(THF) (Ln = Er, Yb) showed them to be efficient initiators for the ROP of ε-caprolactone [49].

A comparison of organolanthanide complexes $Cp^*{}_2SmMe(THF)$ and $(\mu\text{-}PhC{=}C{=}C{=}CPh)[Cp^*{}_2Sm]_2$, with tin compounds $Bu^n{}_2Sn(OMe)_2$ and $Bu^n{}_2Sn(OCH_2CH_2CH_2O)$ in the preparation of random diblock and triblock copolymers composed of L-lactide and D,L-lactide, has been described by Nakayama et al. [50].

In the same year, Wu et al. reported that lanthanide complexes containing silyl group-functionalized indenyl ligands exhibited high catalytic activities for ε-caprolactone polymerization [51]. Also, the organosamarium thiolate complex $[(MeC_5H_4)_2Sm(\mu\text{-}SPh)(THF)]_2$ has been reported to be an efficient initiator for the homo- and copolymerization of ε-caprolactone [52].

A Lewis acidic yttrium (III) complex of an anionic, metal-tethered carbene ligand (Figure 2.10) was reported to act as bifunctional catalyst for the polymerization of D,L-lactide, using a combination of Lewis acid and base functionalities to initiate the ROP of the cyclic monomer.

The alcohol- and amino-functionalized carbenes from which the complexes derive provide models for the first insertion step and also display metal-free polymerization catalysts to generate polylactic acid [53].

In 2007, several articles dealing with the use of lanthanide complexes as catalysts for the ROP of lactide were published. For example, the lanthanide alkyl complexes bearing *N,O*-multidentate ligands shown in Figure 2.11 were successfully

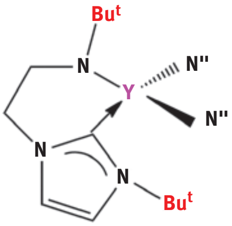

Figure 2.10: Structure of metal-tethered carbene ligand N" = N $(SiMe_3)_2$.

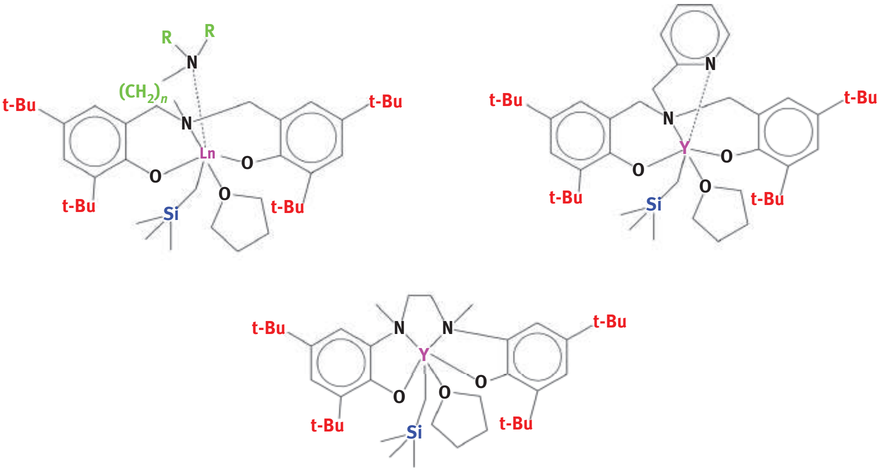

Figure 2.11: Structure of the lanthanide alkyl complexes with N,O-multidentate ligands.

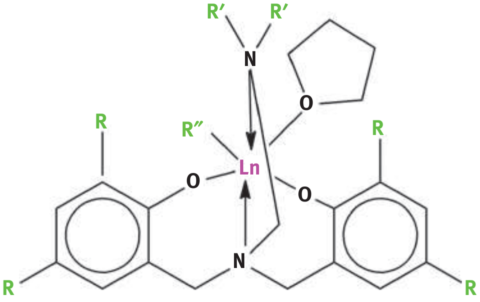

Figure 2.12: Structure of RE complexes (R = H, Me, ^{t}Bu; R' = Me, Et, pyridyl; R" = alkyl, amino, phenoxy; Ln = Sc, Y, Lu).

tested. It was found that the combination of aminoamine-modified bis(phenolate) ligands with lanthanide alkyl units generated unprecedented stereoselective initiators for the ROP of *rac*-LA to give heterotactic poly(lactide) [54].

The RE complexes shown in Figure 2.12 (R = H, Me, ^{t}Bu; R′ = Me, Et, pyridyl; R″ = alkyl, amino, phenoxy; Ln = Sc, Y, Lu) were also found to catalyse the stereoselective ROP of *rac*-LA.

Bulk polymerizations were carried out with THF, dichloromethane or toluene as solvents, obtaining a conversion of 100%. The content of heterotactic polymer in the obtained poly(lactide) reached 0.99, which is higher than the highest value (0.96) previously reported [55].

The aminophenolate-supported lanthanide mono(alkyl) complexes shown in Figure 2.13 were found to be highly active initiators for the ROP of L-lactide to give

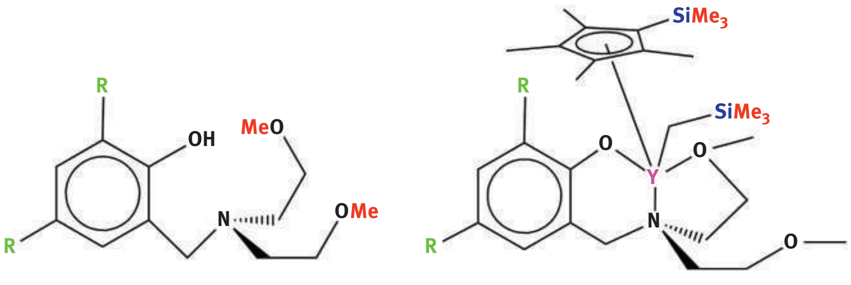

HL^1 : R = Me
HL^2 : R = ^tBu

R = Me
R = ^tBu

Figure 2.13: Structure of aminophenolate-supported lanthanide mono(alkyl) complexes.

isotactic poly(lactide) with high molecular weight and narrow-to-moderate polydispersity [56]. RE metal alkyl complexes stabilized by anilido-phosphinimine and amino-phosphine ligands (Figure 2.14) were reported to initiate the ROP of D,L-lactide with high activity to give atactic PLAs [57].

Atactic PLAs were also obtained from D,L-lactide using as catalysts the pyrrolide–ligated organoyttrium complexes shown in Figure 2.15 [58].

Lanthanide (II) complexes containing tetrahydro-2H-pyranyl functionalized indenyl ligands (Figure 2.16) were reported to exhibit high catalytic activity in the polymerization of ε-caprolactone [59].

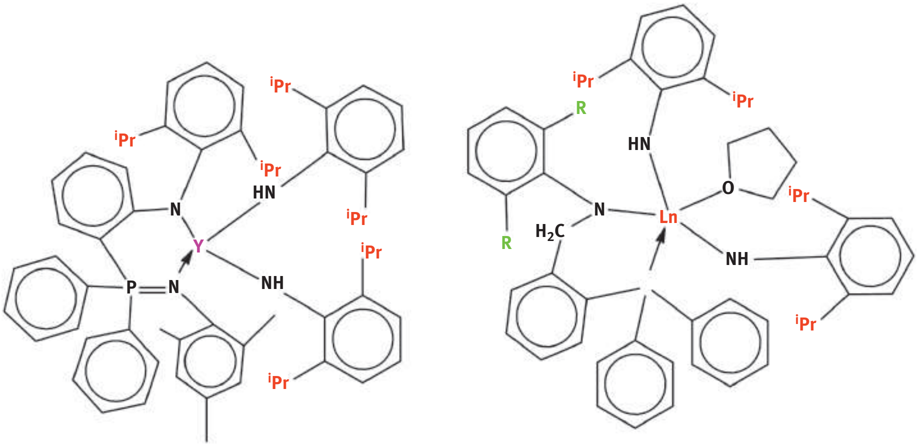

Ln = Y, R = Me
Ln = Y, R = ^iPr

Figure 2.14: Structure of RE metal alkyl complexes stabilized by anilido phosphinimine and amino phosphine ligands.

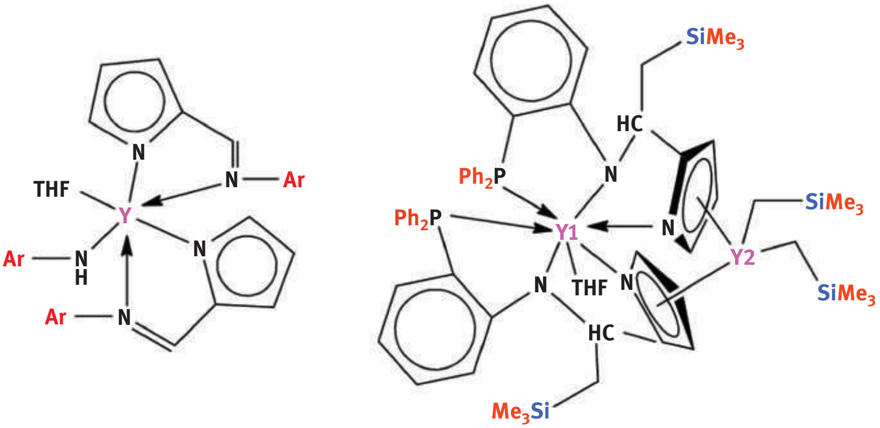

Figure 2.15: Structure of pyrrolide-ligated organoyttrium complexes.

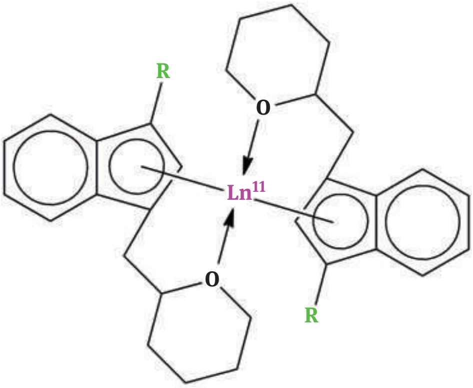

R = H, Ln = Yb, Eu
R = Me$_3$Si, Ln = Yb, Eu

Figure 2.16: Structure of lanthanide (II) complexes containing tetrahydro-2H-pyranyl functionalized indenyl ligands.

ROP of ε-caprolactone was also achieved using [ethylene bis (η^5indenyl)][bis (trimethylsilyl)amido] lanthanide (III) complexes (EBI)LnN(SiMe$_3$)$_2$ (Ln = Y, Sm, Yb) (Figure 2.17) [60].

The polymerization mechanisms of ε-caprolactone initiated by either the RE hydride Cp$_2$Eu(H) or the borohydrides Cp$_2$Eu(BH$_4$) or (N$_2$NN′)Eu(BH$_4$) (N$_2$NN′=(2-C$_5$H$_4$N)CH$_2$(CH$_2$CH$_2$NMe)$_2$) proceed in two steps: hydride transfer from the RE initiator to the carbonyl carbon of the lactone, followed by ring-opening of the monomer. In the last step, a difference was observed between the hydride and borohydride

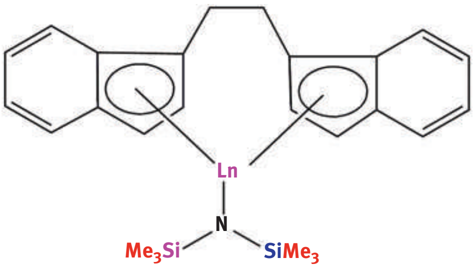

Ln = Y, Sm

Figure 2.17: Structure of [ethylene-bis(η^5- indenyl)][bis(trimethylsilyl)amido]lanthanide(III) complexes (EBI)LnN$(SiMe_3)_2$ (Ln = Y, Sm).

complexes, because for the latter, the ring-opening is induced by an additional B–H bond cleavage leading to a terminal $-CH_2OBH_2$ group. This corresponds to the reduction by BH_3 of the carbonyl group of ε-caprolactone. Upon reaction of $Cp_2Eu(H)$ with ε-caprolactone, the alkoxy–aldehyde complex produced $Cp_2Eu[O(CH_2)_5C(O)H]$ is the first-formed initiating specie. In contrast, for the reaction of ε-caprolactone with the borohydride complexes $(L_x)Eu(BH_4)$ ($L_x = Cp_2$ or N_2NN'), an aliphatic alkoxide with a terminal $-CH_2OBH_2$ group, $(L_x)Eu[O(CH_2)_6OBH_2]$ is formed and subsequently propagates the polymerization [61].

The dialkyllanthanide complexes shown in Figure 2.18 were found to display high activities for the ROP of ε-caprolactone, in which narrow-polydispersity polymers were produced.

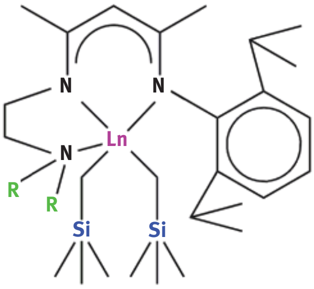

R = Me, Ln = Y
R = Me, Ln = Lu
R = Me, Ln = Sm
R = Me, Ln = Nd
R = Et, Ln = Y
R-R = -$(CH_2)_5$, L = Y

Figure 2.18: Structure of dialkyllanthanide complexes.

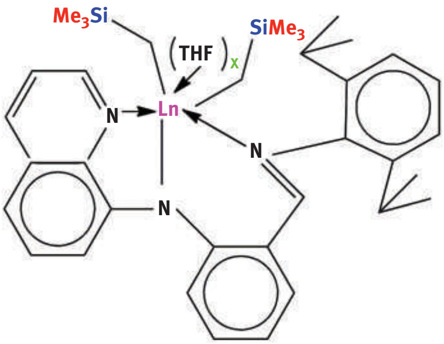

Ln = Sc; X = 0
Ln = Y; X = 1
Ln = Lu, X = 0

Figure 2.19: RE metal bis(alkyls) supported by a quinolinyl anilido-imine.

The size of the pendant arm has a significant effect on the molecular weight of the obtained polymer. In comparison to the Y complex with an $-NMe_2$ group, the Y complexes with NEt_2 and $-N((CH_2CH_2)_2CH_2)$ groups yield much higher-molecular-weight polymers (60,000 vs. 20,000) [62].

RE metal bis(alkyls) supported by a quinolinyl anilido-imine ligand (Figure 2.19) were reported to catalyse the ROP of ε-caprolactone with high activities; the Lu complex was proved to be more active than its Sc and Y analogues [63].

The scandium dimethylbenzyl complex $Sc(fc[NSi(^tBu)Me_2]_2)(CH_2Xy\text{-}3,5)(THF)$ and its adduct with $AlMe_3$ (Figure 2.20) were reported to polymerize L-lactide [64].

RE metal complexes having piperazine-alkyl-bridged bis(aryloxy) ligands have been claimed in a patent as polymerization catalysts for L-lactide [65]. In particular, the complexes $[OArNNArO]Ln(CH_2SiMe_3)(THF)$, wherein Ln = heavy RE metals selected from Gd, Tb, Dy, Ho, Er, Tm, Yb, Lu and Y($[OArNNArO] = C_4H_8N_2[1,4\text{-}(2\text{-}O\text{-}5\text{-}R^1\text{-}3\text{-}R^2\text{-}C_6H_2CH_2)_2]$, $R^{1,2}$ = C1-C4 alkyl) were found to be useful as monocomponent catalysts for the ROP of L-lactide under mild conditions with high catalytic activity, high poly(lactide) molecular weight, narrow poly(lactide) molecular weight distribution and good polymerization controllability [65].

In the work of Mahrova et al., the tertbutoxide and borohydride complexes (DAB) $Y(O^tBu)(THF)(DME)$ and $[Li(DME)_3][(DAB)Y(BH_4)_2]$ shown in Figure 2.21 acted as monoinitiators for the room temperature ROP of *rac*-LA and β-butyrolactone (Figure 2.22). In these reactions, atactic polymers with controlled molecular weights and relatively narrow polydispersities were obtained [66].

The neutral mono(amidinato) RE metal bis(alkyl) complexes shown in Figure 2.23 exhibited activity towards L-lactide polymerization to give high-molecular-weight and narrow-molecular-weight distribution polymers [67]. The neodymium

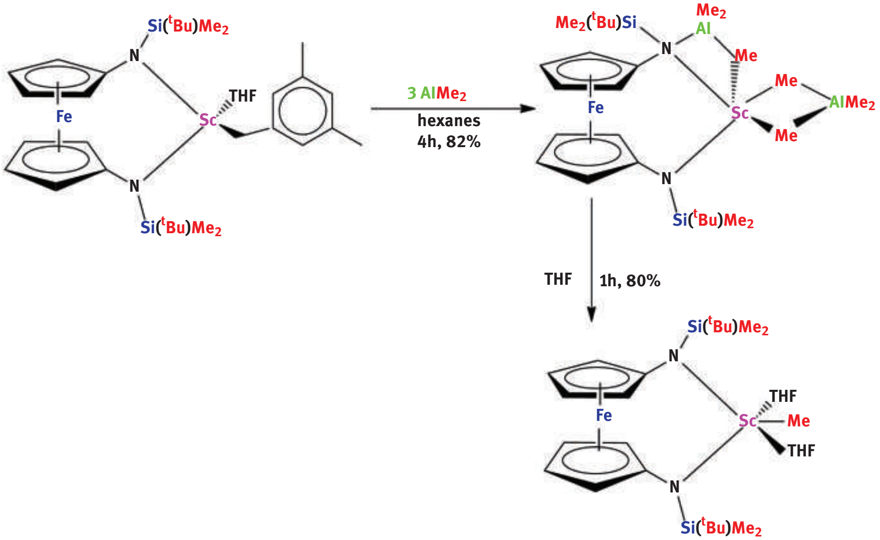

Figure 2.20: Synthesis route for scandium dimethylbenzyl complex Sc(fc[NSi(^{t}Bu)Me$_2$]$_2$)(CH$_2$Xy-3,5)(THF) and its adduct with AlMe$_3$.

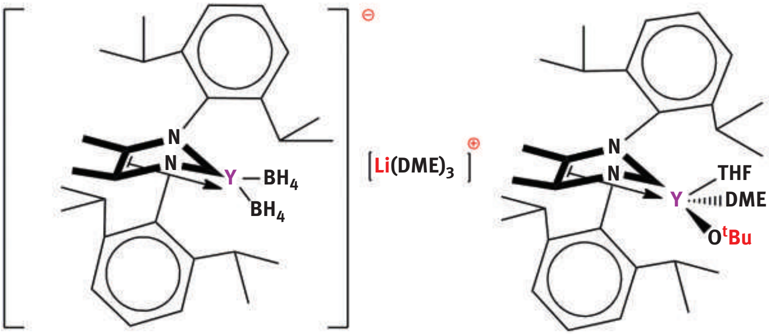

Figure 2.21: Structure of tertbutoxide and borohydride complexes (DAB)Y(O^{t}Bu)(THF)(DME) and [Li(DME)$_3$][(DAB)Y(BH$_4$)$_2$].

heteroscorpionate complex shown in Figure 2.24 acted as an efficient single-site initiator for the controlled ROP of *rac*-LA, which showed a homosteric preference for one of the two enantiomers at low conversions [68].

Preliminary results of Otero et al. showed that heteroscorpionate complexes with acetamide and thioacetamide functionalities (Figure 2.25) can act as single-component living initiators for ROP reactions. Polymerization of ε-caprolactone occurred within minutes to give medium-molecular weight polymers and narrow polydispersities. Polymer end-group analysis showed that the polymerization process is initiated by alkyl transfer to the monomer [69].

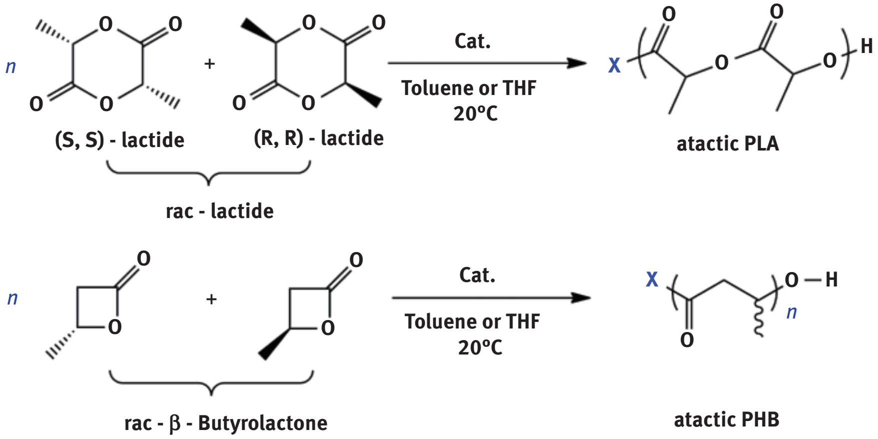

Figure 2.22: ROP of rac-LA and β-butyrolactone catalyzed by tertbutoxide and borohydride complexes (DAB)Y(O^{t}Bu)(THF)(DME) and [Li(DME)$_3$][(DAB)Y(BH$_4$)$_2$].

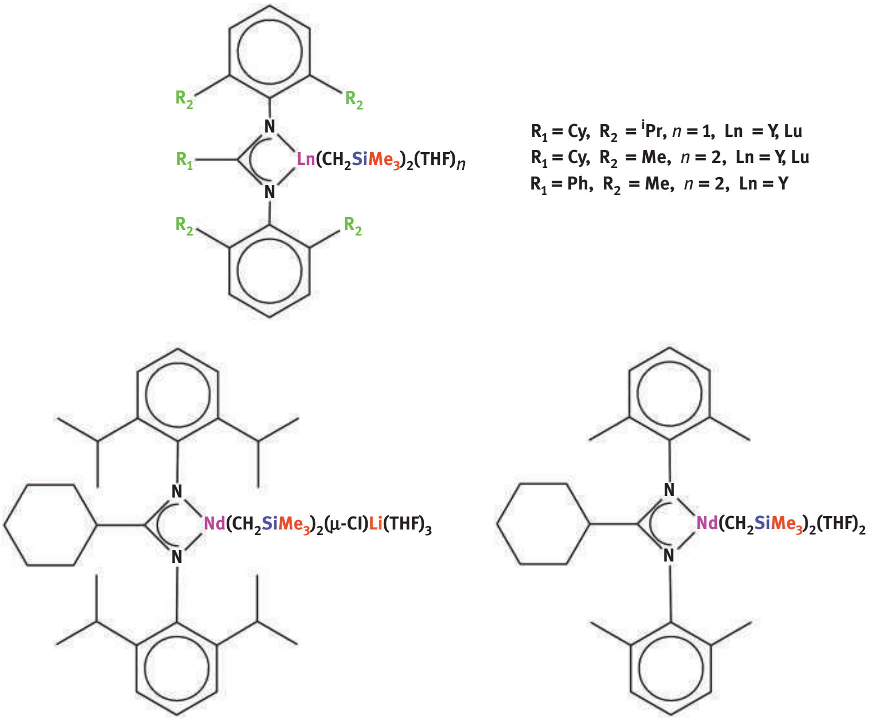

R_1 = Cy, R_2 = ^{i}Pr, n = 1, Ln = Y, Lu
R_1 = Cy, R_2 = Me, n = 2, Ln = Y, Lu
R_1 = Ph, R_2 = Me, n = 2, Ln = Y

Figure 2.23: Structure of mono(amidinato) RE metal bis(alkyl) complexes.

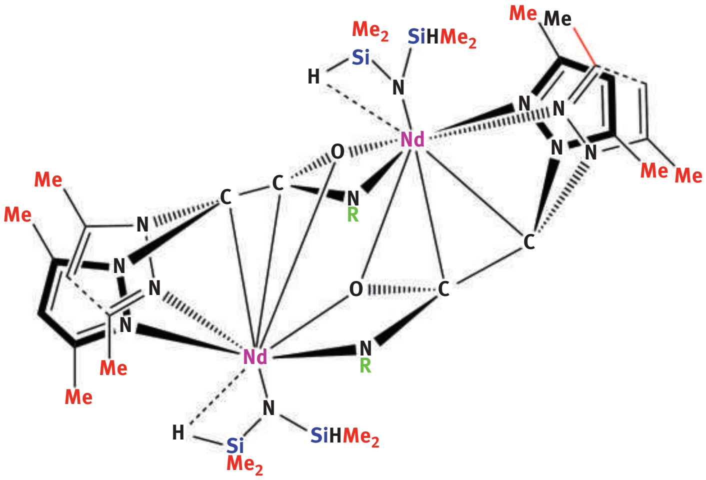

R = (S)-PhMeCH

Figure 2.24: Structure of neodymium heteroscorpionate complex.

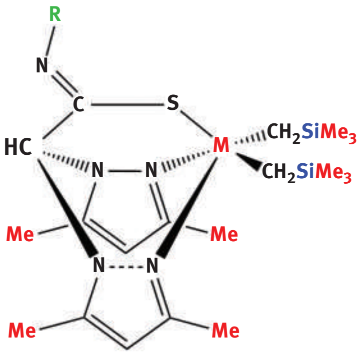

R = Ph, M = Sc, Y
R = ^{t}Bu, M = Sc, Y

Figure 2.25: Structure of heteroscorpionate complexes with acetamide and thioacetamide functionalities.

The catalytic properties of the divalent lanthanide 2-pyridylmethyl-substituted fluorenyl complexes $(\eta^5:\eta^1\text{-}C_5H_4NCH_2C_{13}H_8)_2Ln$ (Ln = Eu, Y) on the ROP of ε-caprolactone have been studied and the temperatures and solvent effects on the catalytic activities of the complexes examined [70]. It was reported that the lanthanide alkyl complexes supported by a piperazidine-bridged bis(phenolato) ligand shown in Figure 2.26 are highly efficient initiators for the controlled ROP of L-lactide, giving polymers with high molecular weights and narrow-molecular-weight distributions.

It was found that the complex [ONNO]Y(CH_2SiMe_3)(THF) (Figure 2.26) can also initiate *rac*-LA polymerization with high activity, but the stereoselectivity was poor. In contrast, the dimeric gadolinium complex depicted in Figure 2.27 exhibited apparently low activity for this polymerization [71].

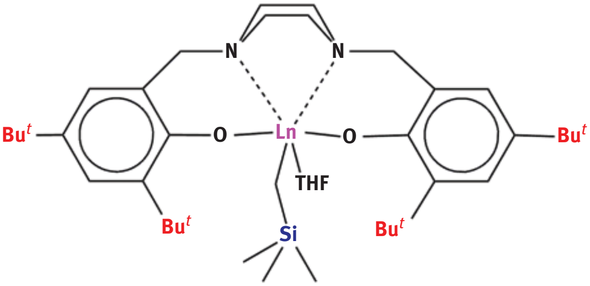

Ln = Y, Gd, Yb, Lu

Figure 2.26: Structure of divalent lanthanide 2-pyridylmethyl substituted fluorenil complexes (η^5:η^1-$C_5H_4NCH_2C_{13}H_8$)$_2$Ln (Ln = Eu, Y).

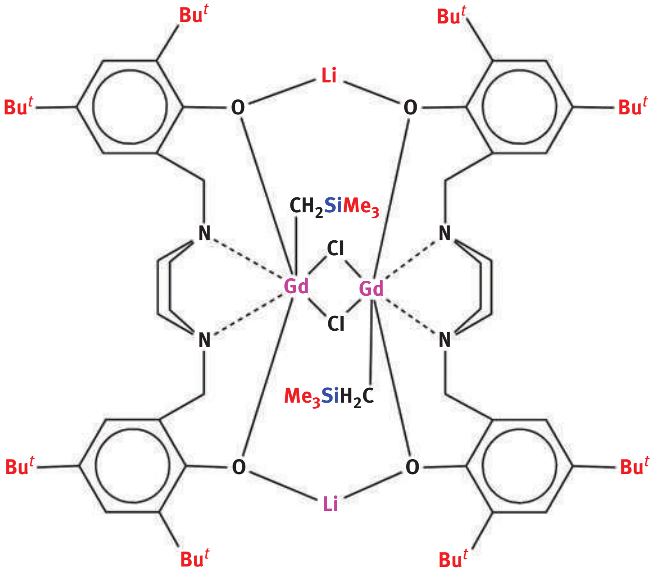

Figure 2.27: Structure of gadolinium alkyl complex, {[ONNO]Gd(CH_2SiMe_3)(μ-Li)(μ-Cl)}$_2$.

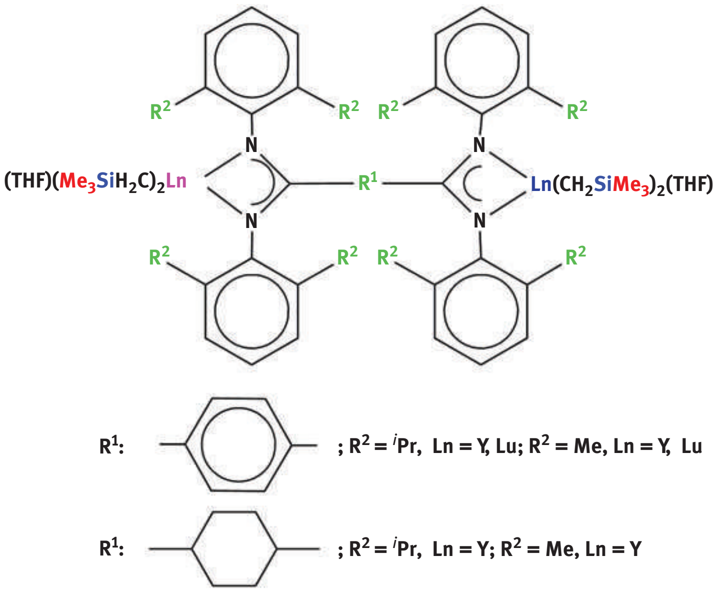

Figure 2.28: Structure of binuclear lanthanide bis(alkyl) derivatives with bridged amidinate ligands.

Several bimetallic lanthanide bis(alkyl)complexes bearing bridged amidinate ligands (Figure 2.28) also showed activity towards L-lactide polymerization in toluene [72].

In another study, the behaviour of the samarium (II) borohydrides $Sm(BH_4)_2(THF)_2$ and $Cp^*Sm(BH_4)(THF)_2$ as initiators in the ROP of ε-caprolactone has been investigated [73]. ROP could be performed rapidly at room temperature with both initiators. The half-sandwich complex $Cp^*Sm(BH_4)(THF)_2$ led to narrow polydispersities and higher activity.

An initiating system comprising a rare neodymium–alkyl–carbene complex $Nd[C(PPh_2N^iPr)_2][CH(PPh_2N^iPr)_2]$ and externally added ^{i}PrOH was also proved to be an efficient catalyst for the ROP of lactide [74].

Dicationic and zwitterionic yttrium compounds, prepared according to Figure 2.29 from the tris(alkyl) precursors Ln, have been reported to act as catalysts for the primary or secondary amine-initiated immortal ROP of *rac*-LA [75]. Amine-terminated, highly heterotactic poly(*rac*-LA) with narrow polydispersities and well-controlled molecular weights have been obtained following this method.

The scandium and yttrium complexes supported by tridentatephosphidodiphosphine ligands shown in Figure 2.30 have been studied as initiators for the ROP of lactide [76].

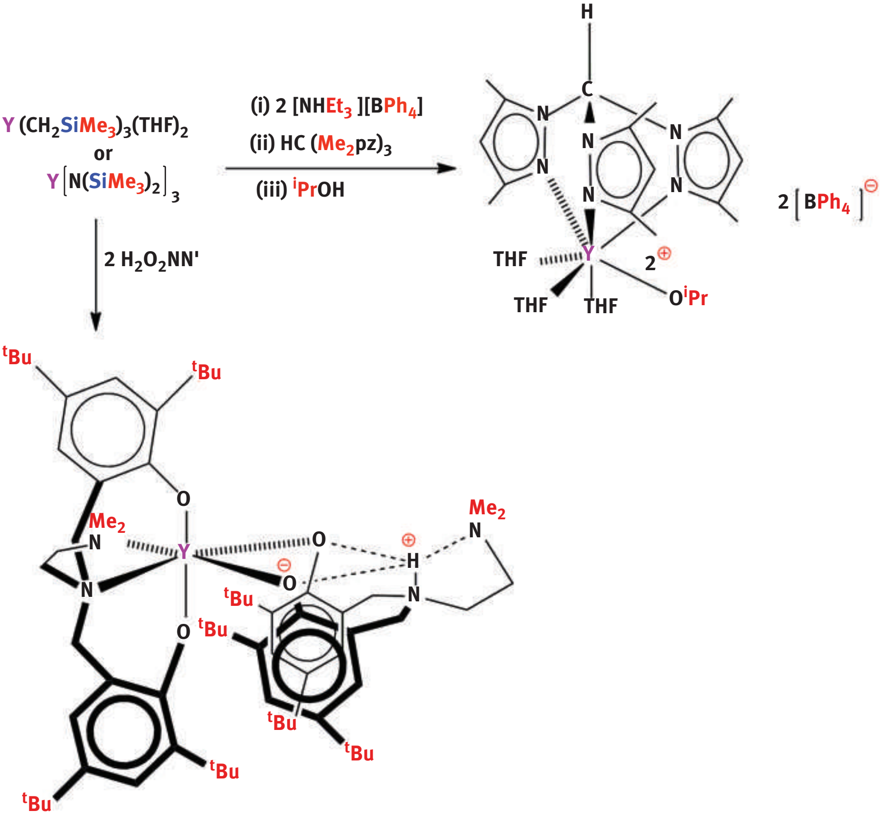

Figure 2.29: Synthesis route for dicationic and zwitterionic yttrium compounds.

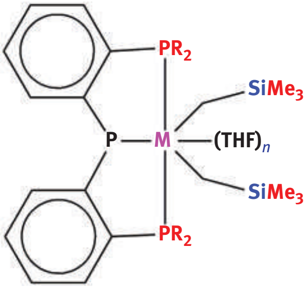

M = Y, R = ^{i}Pr, $n = 1$
M = Y, R = Ph, $n = 1$
M = Sc, R = ^{i}Pr, $n = 1$
M = Sc, R = Ph, $n = 2$

Figure 2.30: Structure of scandium and yttrium complexes of the type LLn$(CH_2SiMe_3)_2(THF)_n$ supported by the related tridentate phosphido-diphosphine pincer ligands (o-$C_6H_4PR_2)_2PH$ (L^1H: R = ^{i}Pr, L^2H: R = Ph).

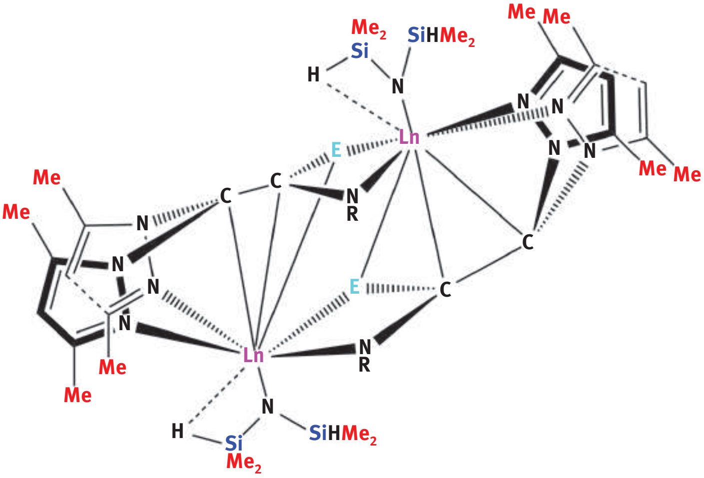

R = (S)-PhMeCH, E = O, Ln = Nd, Sm
R = ^{s}Bu, E = O, Ln = Nd, Sm
R = Ph, E = S, Ln = Nd, Sm
R = ^{t}Bu, E = S, Ln = Nd, Sm

Figure 2.31: Structure of complexes containing dianionic heteroscorpionate pseudoallyl ligands.

The yttrium complexes exhibited high activity and good polymerization control, while the analogous scandium complexes gave a good molar mass control but lower activities.

Neodymium complexes are known to be active initiators for the ROP of lactide and lactones, giving rise to medium–high molar mass polymers under mild conditions and with narrow polydispersities. The heteroscorpionate complexes depicted in Figure 2.31 were found to be well-suited for achieving well-controlled polymerization through an insertion–coordination mechanism.

A chiral and racemic complexes did not affect stereocontrol in the polymerization of *rac*-LA, but the enantiomerically pure complex $[\mathrm{Nd}\{\mathrm{N}(\mathrm{SiHMe}_2)_2\}(\mathrm{NNE})]_2$ was found to exhibit a homosteric preference for one of the two enantiomers of *rac*-LA at low conversions [77].

DAuria et al. reported the ROP of cyclic esters promoted by phosphido-diphosphine pincer Group 3 metal bis(alkyl) complexes [78]. The phosphido-diphosphine complexes $[(o\text{-}\mathrm{C}_6\mathrm{H}_4\mathrm{PR}_2)_2\mathrm{P}]\mathrm{Ln}(\mathrm{CH}_2\mathrm{SiMe}_3)_2$ (Ln = Sc, Y; R = iPr, Ph) have been found to be very efficient catalysts for the ROP of ε-caprolactone, L-lactide and δ-valerolactone under mild polymerization conditions. In the ROP of ε-caprolactone, all four complexes promoted the quantitative conversion of high amounts of monomer with very high turnover frequencies showing a catalytic activity among the highest reported in the literature. In the ROP of δ-valerolactone, the catalysts showed the same activity

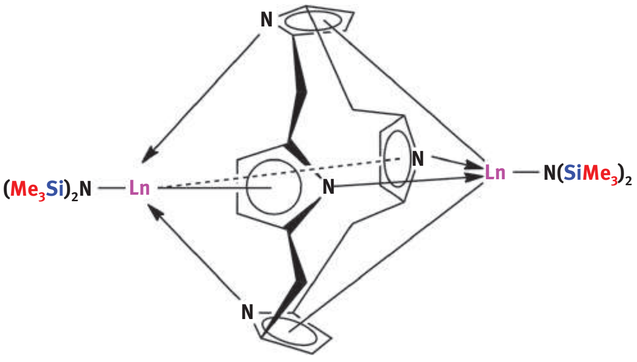

R = Me, Ln = Nd, Sm, Dy
R = { - (CH$_2$)$_5$ - }$_{0.5}$, Ln = Nd, Sm
R groups were omitted for clearity

Figure 2.32: Structure of dinuclear alkali metal-free trivalent lanthanide amido complexes (5:1:5:1-R$_8$-calix[4]-pyrrolyl)[LnN(SiMe$_3$)$_2$]$_2$ (R =Me, Ln = Nd, Sm, Dy; R={ (CH$_2$)$_5$}$_{0.5}$, Ln = Nd, Sm).

observed for lactides (L- and D,L-lactide) producing high-molecular-weight polymers with narrow distribution of molar masses. The complexes also promoted the ROP of *rac*-β-butyrolactone affording at low-molecular-weight poly(hydroxybutyrate) bearing unsaturated end-groups probably generated by elimination reactions [78].

The bent-sandwiched calix[4]-pyrrolyl lanthanide amido complexes displayed in Figure 2.32 were found to exhibit high catalytic activities towards the ROP of L-lactide, using the dinuclear trivalent lanthanide amido complexes bearing a {(CH$_2$)$_5$}4-calix [4]-pyrrolyl ligand [79].

The heterobimetallic oxo-bridged aluminum–RE metal complexes shown in Figure 2.33 have been investigated as lactide polymerization initiators. The heterobimetallic samarium alkoxide derivative (Figure 2.33 right) was found to be highly active, yielding high-molecular-weight PLs with over 91% conversion [80]. Reactions of LAl[C(Ph)CH(Ph)](μ-O)Ln(CH$_2$SiMe$_3$)[NN](THF)$_2$ (Ln = Y, Sm) with 1 equiv. of ^{i}PrOH yielded the corresponding alkoxide complexes (Figure 2.33 left).

A germyl-bridged lanthanocene chloride, [Me$_2$Ge(^{t}BuC$_5$H$_3$)$_2$]NdCl, was prepared and successfully used as single catalyst to initiate the ROP of ε-caprolactone for the first time [81]. It was found that under mild conditions, [Me$_2$Ge(^{t}BuC$_5$H$_3$)$_2$]NdCl efficiently catalysed the polymerization of ε-caprolactone, giving high yield (> 95%) of poly(lactones) with high molecular weight. When the polymerization was carried out in bulk or in petroleum ether solution, it gave poly(lactones) with higher molecular weight and perfect conversion (100%). The higher catalytic activity of this neodymocene chloride could be attributed to the bigger atom (Ge) in the bridged ring ligands. It was also found that some activators, such as NaBPh$_4$, KBH$_4$, AlEt$_3$ and Al(^{i}Bu)$_3$, can promote the polymerization of ε-caprolactone by [Me$_2$Ge(^{t}BuC$_5$H$_3$)$_2$]

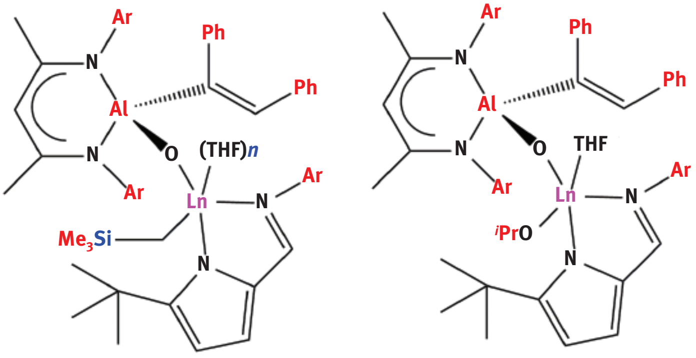

Ln = Y, *n* = 2
Ln = Sm, *n* = 2

Ln = Y
Ln = Sm

Figure 2.33: Structure of LAl[C(Ph)CH(Ph)](μ-O)Ln(CH$_2$SiMe$_3$)[NN](THF)$_2$ (Ln = Y, Sm) (right) and its corresponding alkoxide complexes (left).

NdCl, which leads to an increase both in the polymerization conversion and in the molecular weight of poly(lactones) [81].

Zhao et al. developed a new strategy for the facile synthesis of fluorescent dye-labelled polyesters via immortal ROP of heterocyclic monomers (ε-caprolactone, racemic β-butyrolactone and *rac*-LA, etc.) by using a catalytic amount of metal-based complexes (including a lutetium alkyl derivative) with an excess of hydroxylated dye compounds (Figure 2.34) [82].

This strategy breaks the “one catalyst-one dye-labeled polymer chain” limitation in that a series of “clean” dye-labeled polyesters have been obtained in the form of low metal residue, designed molecular weight, narrow distributions, excellent α-dye labelled and *o*-hydroxyl fidelity and high stereoregularity [82].

Bis(imino)diphenylamido RE metal dialkyl catalysts [o-(2,6-^{i}Pr$_2$C$_6$H$_3$N CC$_6$H$_4$)$_2$N] Ln(CH$_2$SiMe$_3$)$_2$ (Ln = Sc, Y, Lu) have been synthesized according to Figure 2.35 in good yields. They served as highly efficient single-component catalysts for the living ROP of ε-caprolactone, with the activity being dependent on the steric hindrance around the metal centre [83].

The neutral mono-indenyl-ligated RE metal bis(silylamide) complexes (C$_9$H$_6$CMe$_2$CH$_2$C$_5$H$_4$N-α)Ln[N(SiHMe$_2$)$_2$]$_2$ (Ln = La, Sm, Er, Lu) shown in Figure 2.36 have been found to be highly active for the ROP of L-lactide and *rac*-LA (Figure 2.37) [84].

Several dinuclear RE metal bis(o-aminobenzyl) complexes bearing a 1,4-phenylenediamidinate co-ligand (Figure 2.38) have also been reported to show high activity for *rac*-LA and ε-caprolactone polymerization. For *rac*-LA, a synergistic effect between two metal centres was observed [85].

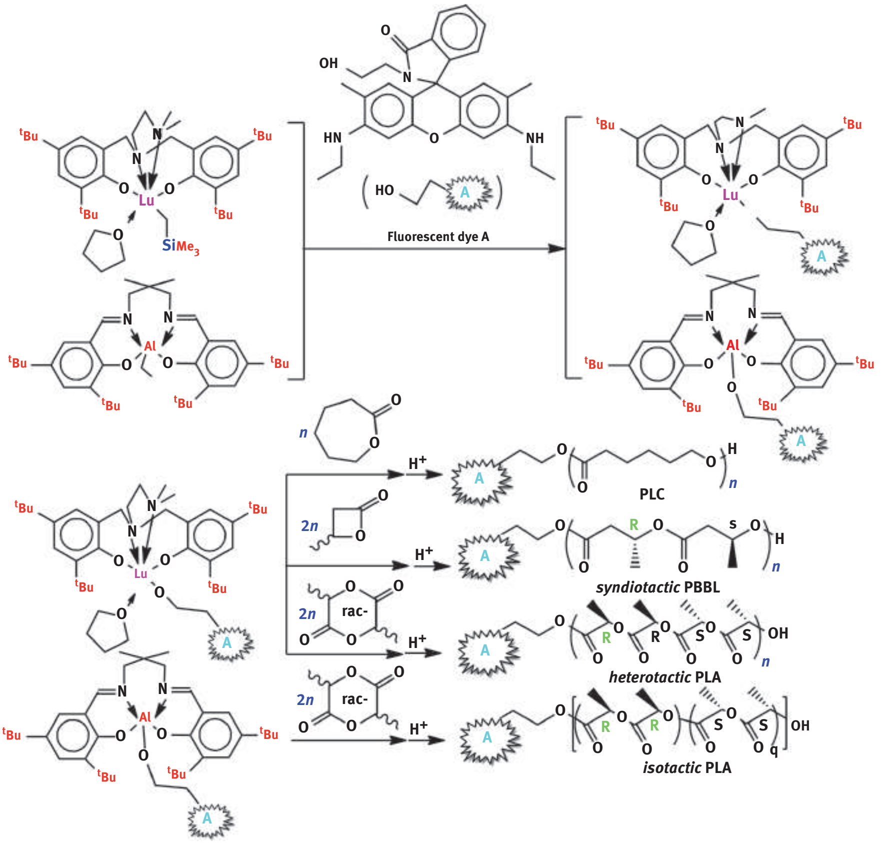

Figure 2.34: Synthesis of fluorescent dye-labeled polyesters via immortal ROP of heterocyclic monomers.

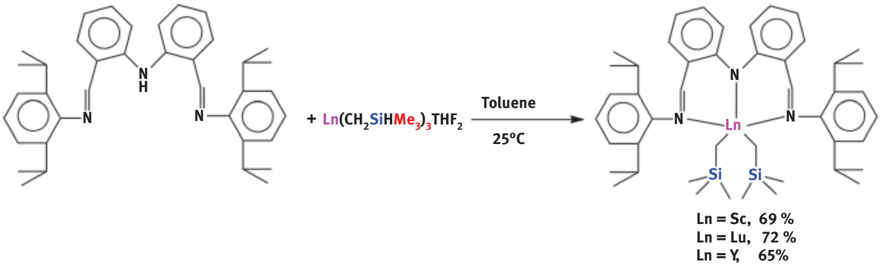

Figure 2.35: Synthesis of bis(imino)diphenylamido RE metal dialkyl catalysts $[o\text{-}(2,6\text{-}^{i}Pr_2C_6H_3N\,CC_6H_4)_2N]Ln(CH_2SiMe_3)_2$ (Ln = Sc, Y, Lu).

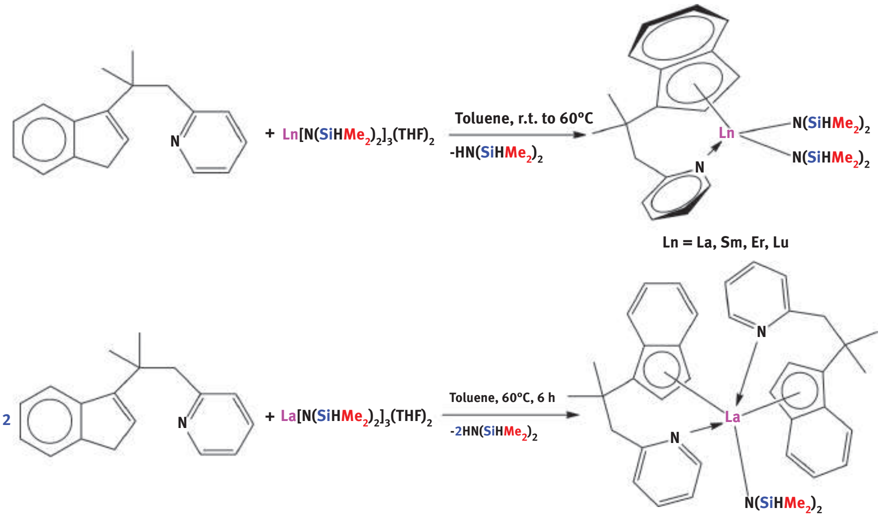

Figure 2.36: Synthesis route for $(C_9H_6CMe_2CH_2C_5H_4N\text{-}\alpha)Ln[N(SiHMe_2)_2]_2$ (Ln = La, Sm, Er, Lu) and $(C_9H_6CMe_2CH_2C_5H_4N\text{-}\alpha)2LaN(SiHMe_2)_2$.

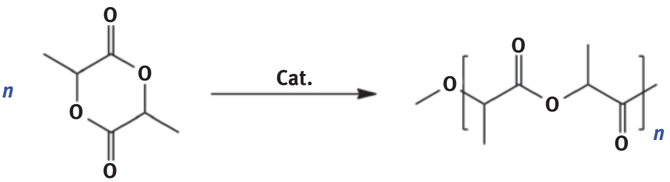

Figure 2.37: ROP of lactide.

The bis(oxazolinylphenyl)amide (BOPA) ligand-supported lanthanide alkyl complexes shown in Figure 2.39 have been successfully employed in the ROP of *rac*-LA [86].

A series of heteroscorpionate yttrium and lutetium zwitterionic initiators (Figure 2.40) all showed similar high activity towards the ROP of *rac*-LA at room temperature, and both the alkyl species participated in initiation, of which the lutetium complexes exhibited slightly higher selectivity than their yttrium analogues [87].

2.5 Conclusions

Biodegradable polymers represent a class of particularly useful materials for many biomedical and pharmaceutical applications. Among these types of polyesters, poly (ε-caprolactone) and polylactides are considered very promising for controlled drug delivery devices. These polymers are mainly produced by ROP of their respective

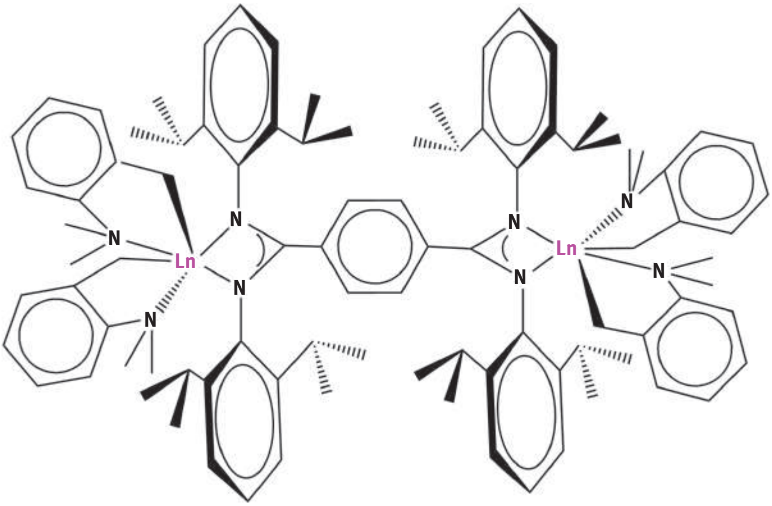

Ln = Sc, Y, Lu

Figure 2.38: Structures of dinuclear RE metal bis(o-aminobenzyl)complexes with 1,4-$C_6H_4[C(NR)_2Ln(o\text{-}CH_2C_6H_4NMe_2)_2]_2$ (R = 2,6-$^iPr_2C_6H_3$, Ln = Sc, Y, Lu) catalysts.

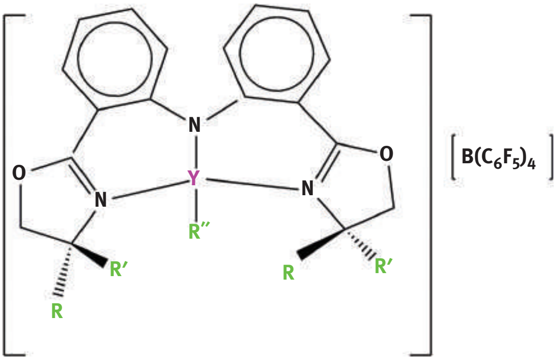

R = H ; R' = ^{i}Pr, Bn
R = Ph ; R' = H
R" = CH_2SiMe_2Ph

Figure 2.39: Bis(oxazolinylphenyl)amide (BOPA)-supported yttrium alkyl complexes.

cyclic esters, since this method allows a strict control of the molecular parameters (molecular weight and distribution) of the obtained polymers. The most widely used catalysts for ROP of cyclic esters are tin- and aluminium-based organometallic complexes; however, since the contamination of the aliphatic polyesters by potentially

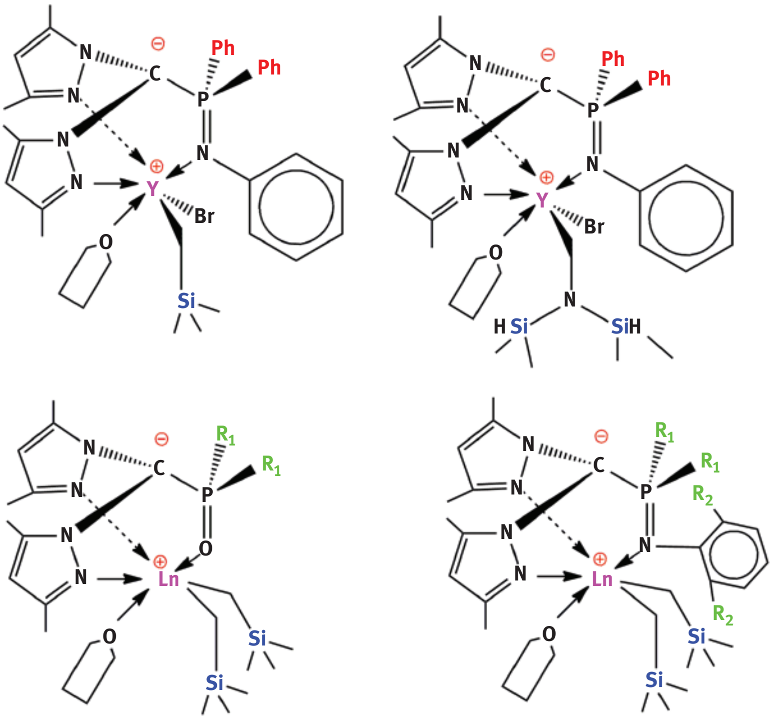

$R_1 = {}^tBu$, Ln = Y, Lu
R_1 = Cy, Ln = Y, Lu

R_1 = Cy, R_2 = H, Ln = Y, Lu
R_1 = Ph, R_2 = H, Ln = Y, Lu
R_1 = Ph, R_2 = Me, Ln = Y, Lu

Figure 2.40: Structures of zwitterionic bis(alkyl) complexes $L^{1-5}Ln(CH_2SiMe_3)_2(THF)$ (Ln = Y, Lu).

toxic metallic residues is particularly of concern for biomedical applications, the possibility of replacing organometallic initiators by novel less toxic or more efficient organometallics has been intensively studied. Thus, in the recent years, the use of highly reactive RE initiator/catalysts leading to lower polymer contamination has been developed. The use of RE complexes is considered a valuable strategy to decrease the polyester contamination by metallic residues and represents an attractive alternative to traditional organometallic complexes.

References

[1] Jérôme C, Lecomte P. Recent advances in the synthesis of aliphatic polyesters by ring-opening polymerization. Adv Drug Deliver Rev. 2008;60:1056.
[2] Edelmann FT. Lanthanides and actinides: Annual survey of their organometallic chemistry covering the year 2007. Coord Chem Rev. 2009;253:2515.

[3] Williams CK. Synthesis of functionalized biodegradable polyesters. Chem Soc Rev. 2007;36:1573.

[4] Lou X, Detrembleur C, Jérôme R. Novel aliphatic polyesters based on functional cyclic (di) esters. Macromol Rapid Commun. 2003a;24:161.

[5] Stridsberg K, Ryner M, Albertsson AC. Controlled ring-opening polymerization: polymers with designed macromolecular architecture. Adv Polym Sci. 2002;157:41.

[6] Coulembier O, Degée P, Hedrick JL, Dubois P. From controlled ring-opening polymerization to biodegradable aliphatic polyester: especially poly (β-malic acid) derivatives. Prog Polym Sci. 2006;31:723.

[7] Penczek S, Cypryk M, Duda A, Kubisa P, Slomkowski S. Living ring-opening polymerizations of heterocyclic monomers. Prog Polym Sci. 2007;32:247.

[8] Lecomte P, Jérôme R. New developments in the synthesis of aliphatic polyesters b ring-opening polymerization. In: Smith R, editors. Biodegradable polymers for polymer industrial applications. Cambridge: Woodhead Publishing Ltd. editor 2005:77–106.

[9] Agarwal S, Mast C, Dehnicke K, Greiner A. Rare earth metal initiated ring-opening polymerization of lactones. Macromol Rapid Commun. 2000;21:195.

[10] Bunzli JC. Benefiting from the unique properties of lanthanide ions. Acc Chem Res. 2006;39:53.

[11] Bunzli JC, Piquet C. Lanthanide-Containing Molecular and Supramolecular Polymetallic Functional Assemblies. Chem Rev. 2002;102:1897.

[12] Berry AD, Holm RT, Fatemi M, Gaskill DK. OMCVD of thin films from metal diketonates and triphenylbismuth. Mater Res. 1990;5:1169.

[13] Matsuzawa H. Novel magnetic applications of high-Tc bulk superconductors: Lenses for electron beams. J Appl Phys. 1994;74(12):111.

[14] Ilott DJ, Saiful Islam M. J Chem Soc Faraday Trans. 1993;89:3833.

[15] Schulte B, Maul M, Becker W, Schlosser EG, Haussler P, Adrain II. Carrier gas-free chemical vapor deposition technique for in situ preparation of high quality $YBa_2Cu_3O_{7-\delta}$ thin films. Appl Phys Lett. 1991;59:869.

[16] Uchikawa F, Mackenzi JD. Superconducting $YBa_2Cu_3O_{7-x}$ fibers from the thermoplastic gel method. J Mater Res. 1989;4:787.

[17] Tanabe K, Mismo K, Ono Y, Hattori H. New solid acids and bases. New York: Kodansha, Tokyo Elsevier, 1989:41–47.

[18] Arakawa H. Technol Jpn. 1988;21(11):32.

[19] Otsuka K, Jinn K, Morikawa A. Active and selective catalysts for the synthesis of C_2H_4 and C_2H_6 via oxidative coupling of methane. J Catal. 1986;100(2):353.

[20] Okabe K, Sayarna K, Kusama H, Arakawa H. Effect of Catalyst Preparation on the Oxidative Coupling of Methane over $SrO–La_2O_3$. Bull Chem Soc Jpn. 1994;67:2894.

[21] Hou Z, Wakatsuki Y. Recent developments in organolanthanide polymerization catalysts. Coord Chem Rev. 2002;231:1.

[22] Pelletier J-F, Bujadoux K, Olonde X, Adisson E, Mortreux A. Eur. Pat. Appl. EP 736,536 (Cl.C07F3:02), 9 Oct. 1996, FR Appl. 95:4,203. 7Apr 1995.

[23] Nomura R, Shibasaki Y, Endo T. Block copolymerization of tetrahydrofuran with δ-valerolactone by the samarium iodide-induced transformation. Polym Bull. 1996;37:597.

[24] Boffa LS, Novak BM. “Link-Functionalized” Polymers: An Unusual Macromolecular Architecture through Bifunctional Initiation. Macromolecules. 1997;30:3494.

[25] Hyeon J-Y, Edelmann FT. Lanthanides and actinides: annual survey of their organometallic chemistry covering the year 1997. Coord Chem Rev. 2003;241:249.

[26] Hultzsch KC, Spaniol TP, Okuda J. Chiral Lanthanocene Derivatives Containing Two Linked Amido– Cyclopentadienyl Ligands: Heterobimetallic Structure and Lactone Polymerization Activity. Organometallics. 1997;16:4845.

[27] Nomura R, Shibasaki Y, Endo T. Transformation of the cationic growing center of poly (tetrahydrofuran) into an anionic one by bis (pentamethylcyclopentadienyl) samarium. J Polym Sci A. 1998;36:2209.

[28] Agarwal S, Brandukova-Szmikowski NE, Greiner A. Reactivity of Sm (II) compounds as ring-opening polymerization initiators for lactones. Macromol Rapid Commun. 1999;20:274.

[29] Nishiura M, Hou Z, Koizumi T-A, Imamoto T, Wakatsuki Y. Ring-opening polymerization and copolymerization of lactones by samarium (II) aryloxide complexes. Macromolecules. 1999;32:8245.

[30] Yuan M, Li X, Xiong C, Deng X. Polymerization of lactides and lactones 5. Ring-opening polymerization of ε-caprolactone and dl-lactide by rare earth 2-methylphenyl samarium. Eur Polym J. 1999;35:2131.

[31] Desurmont G, Tokimitsu T, Yasuda H. First Controlled Block Copolymerizations of Higher 1-Olefins with Polar Monomers Using Metallocene Type Single Component Lanthanide Initiators. Macromolecules. 2000;33:7679.

[32] Deng X, Yuan M, Li X, Xiong C. Polymerization of lactides and lactones: VII. Ring-opening polymerization of lactide by rare earth phenyl compounds. Eur Polym J. 2000;36:1151.

[33] Agarwal S, Puchner M. Ring opening polymerisations of cyclic esters and carbonate by rare-earth LnCp 3. Eur Polym J. 2002;38:2365.

[34] Cui D, Tang T, Cheng J, Hu N, Chen W, Huang B. Synthesis and characterization of $(C_5H_9C_9H_6)_2Yb(THF)_2$(II) (1) and $[(C_5H_9C_5H_4)_2Yb(THF)]_2O_2$ (2), and ring-opening polymerization of lactones with 1. J Organomet Chem. 2002;650:84.

[35] Emslie DJ, Piers WE, Parvez M, McDonalds R. Organometallic complexes of scandium and yttrium supported by a bulky salicylaldimine ligand. Organometallics. 2002;21:4226.

[36] Ravi P, Grob T, Dehnicke D, Greiner A. Ring-Opening Polymerization of ε-Caprolactone by Phosphorane Iminato and Cyclopentadienyl Complexes of Rare Earth Elements. Macromol Chem Phys. 2001;202:2641.

[37] Cui D, Tang T, Bi W, Cheng J, Chen W, Huang B. Ring-opening polymerization and block copolymerization of L-lactide with divalent samarocene complex. J Polym Sci Part A Polym Chem. 2003;41:2667.

[38] Tsutsumi C, Nakagawa K, Shirahama H, Yasuda H. Biodegradations of statistical copolymers composed of D, L-lactide and cyclic carbonates. Polym Int. 2003;52:439.

[39] Satoh Y, Ikitake N, Nakayama Y, Okuno S, Yasuda H. Syntheses of bis- and tetra(trimethylsilyl) substituted lanthanocene methyl complexes and their catalyses for polymerizations of methyl methacrylate, ε-caprolactone and l-lactide. J Organomet Chem. 2003;667:42.

[40] Lou Y, Yao Y, Shen Q, Yu K, Weng L. Synthesis and Characterization of Lanthanide(III) Bis(guanidinate) Derivatives and the Catalytic Activity of Methyllanthanide Bis(guanidinate) Complexes for the Polymerization of ϵ-Caprolactone and Methyl Methacrylate. Eur J Inorg Chem. 2003;2003(2):318.

[41] Chen J-L, Yao Y-M, Luo Y-J, Zhou L-Y, Zhang Y, Shen Q. Synthesis, characterization of homoleptic guanidino lanthanide complexes and their catalytic activity for the ring-opening polymerization of ε-caprolactone. J Organomet Chem. 2004;689:1019.

[42] Palard I, Soum A, Guillaume SM. Unprecedented Polymerization of ε-Caprolactone Initiated by a Single-Site Lanthanide Borohydride Complex, $[Sm(\eta\text{-}C_5Me_5)_2(BH_4)(thf)]$: Mechanistic Insights. Chem Eur J. 2004;10:4054.

[43] Kuehl CJ, Simpson CK, John KD, Sattelberger AP, Carlson CN, Hanusa TP. Monomeric f-element chemistry with sterically encumbered allyl ligands. J Organomet Chem. 2003;683:149.

[44] Yu C, Zhang L, Shen Z. Ring-opening polymerization of ε-caprolactone using rare earth tris (4-tert-butylphenolate) s as a single component initiator. Eur Polym J. 2003;39:2035.

[45] Fan L, Zhang L, Shen Z. Characteristics and kinetics of ring-opening polymerization of ε-caprolactone initiated by lanthanide tris (2, 4, 6-trimethylphenolate) s. Polym J. 2004;36(2):91.

[46] Zhang L, Shen Z, Yu C, Fan L. Characteristics and mechanism of L-lactide polymerization by lanthanide 2, 6-dimethylaryloxide. J Mol Catal A Chem. 2004;214:199.

[47] Zhu W, Ling J, Shen Z. Homopolymerization of ε-caprolactone Initiated by a Scandium Aryloxide. Polym Bull. 2004;52:185.

[48] Sanchez-Barba LF, Hughes DL, Humphrey SM, Bochmann M. New bis (allyl)(diketiminato) and tris (allyl) lanthanide complexes and their reactivity in the polymerization of polar monomers. Organometallics. 2005;24:3792.

[49] Yao Y, Ma M, Xu X, Zhang Y, Shen Q, Wong W-T. Synthesis, reactivity, and characterization of amine bis (phenolate) lanthanide complexes and their application in the polymerization of ε-caprolactone. Organometallics. 2005;24:4014.

[50] Nakayama Y, Yasuda H, Yamamoto K, Tsutsumi C, Jerome R, Lecomte P. Comparison of Sm complexes with Sn compounds for syntheses of copolymers composed of lactide and cyclic carbonates and their biodegradabilities. React Funct Polym. 2005;63:95.

[51] Wu Y, Wang S, Qian C, Sheng W, Xie M, Yang G, et al. Homolysis of the Ln–N bond: Synthesis, characterization and catalytic activity of organolanthanide(II) complexes with furfuryl- and tetrahydrofurfuryl-functionalized indenyl ligands. J Organomet Chem. 2005;690:4139.

[52] Li H, Yao Y, Yao C, Sheng H, Shen Q. You have free access to this contentHomo- and copolymerization of 2,2-dimethyltrimethylene carbonate promoted by samarium thiolate derivatives: Novel and versatile initiators. J Polymer Sci. 2005;43:1312.

[53] Patel D, Liddle ST, Mungur SA, Rodden M, Blake AJ, Arnold PL. Bifunctional yttrium(III) and titanium(IV) NHC catalysts for lactide polymerisation. Chem Commun. 2006;(10):1124.

[54] Liu X, Shang X, Tang T, Hu N, Pei F, Cui D, et al. Achiral lanthanide alkyl complexes bearing N, O multidentate ligands. Synthesis and catalysis of highly heteroselective ring-opening polymerization of rac-lactide. Organomet. 2007a;26:2747.

[55] Miao W, Li S, Cui D, Huang B. Rare earth metal alkyl complexes bearing N,O,P multidentate ligands: Synthesis, characterization and catalysis on the ring-opening polymerization of l-lactide. J Organomet Chem. 2007a;692:3823.

[56] Miao W, Li S, Zhang H, Cui D, Wang Y, Huang B. Synthesis, characterization, and catalytic activity of divalent organolanthanide complexes with new tetrahydro-2H-pyranyl-functionlized indenyl ligands. J Organomet Chem. 2007;692:2099.

[57] Liu B, Cui D, Ma J, Chen X, Jing X. Synthesis and reactivity of rare earth metal alkyl complexes stabilized by anilido phosphinimine and amino phosphine ligands. Chem Eur J. 2007;13:834.

[58] Yang Y, Li S, Cui D, Chen X, Jing X. Pyrrolide-ligated organoyttrium complexes. Synthesis, characterization, and lactide polymerization behavior. Organometallics. 2007;26:671.

[59] Wang S, Wang S, Zhou S, Yang G, Luo W, Hu N, et al. Mixed ligands supported yttrium alkyl complexes:: Synthesis, characterization and catalysis toward lactide polymerization. J Organomet Chem. 2007;692:4828.

[60] Zhou S, Wang S, Yang G, Li Q, Zhang L, Yao Z, et al. Synthesis, Structure, and Diverse Catalytic Activities of [Ethylenebis(indenyl)]lanthanide(III) Amides on N–H and C–H Addition to Carbodiimides and ε-Caprolactone Polymerization. Organometallics. 2007;26:3755.

[61] Barros N, Mountford P, Guillaume SM, Maron L. A DFT Study of the Mechanism of Polymerization of ε-Caprolactone Initiated by Organolanthanide Borohydride Complexes. Chem Eur J. 2008;14:5507.

[62] Xu X, Xu X, Chen Y, Sun J. Dialkyllanthanide complexes containing new tridentate monoanionic ligands with nitrogen donors. Organometallics. 2008;27:758.

[63] Gao W, Cui D. Rare-earth metal bis(alkyl) s supported by a quinolinyl anilido-imine ligand: synthesis and catalysis on living polymerization of ε-caprolactone. Organometallics. 2008;27:5889.

[64] Carver CT, Monreal MJ, Diaconescu PL. Scandium alkyl complexes supported by a ferrocene diamide ligand. Organometallics. 2008;27:363.

[65] Chen Z-W, Dou J. U.S. Pat. Appl. Publ., US 2009315444 A1 20091224 2009.

[66] Mahrova TV, Fukin GK, Cherkasov AV, Trifonov AA, Ajellal N, Carpentier J-F. Yttrium complexes supported by linked bis(amide) ligand: synthesis, structure, and catalytic activity in the ring-opening polymerization of cyclic esters. Inorg Chem. 2009;48:4258.

[67] Luo Y, Wang X, Chen J, Luo C, Zhang Y, Yao Y. Mono(amidinate) rare earth metal bis(alkyl) complexes: Synthesis, structure and their activity for l-lactide polymerization. J Organomet Chem. 2009;694:1289.

[68] Otero A, Fernandez-Baeza J, Lara-Sanchez A, Alonso-Moreno C, Marquez-Segovia I, Sanchez-Barba LF, et al. Ring-Opening Polymerization of Cyclic Esters by an Enantiopure Heteroscorpionate Rare Earth Initiator. Angew Chem. 2009;121:2210.

[69] Otero A, Lara-Sanchez A, Fernandez-Baeza J, Martinez-Caballero E, Marquez-Segovia I, Alonso-Moreno C, et al. New achiral and chiral NNE heteroscorpionate ligands. Synthesis of homoleptic lithium complexes as well as halide and alkyl scandium and yttrium complexes. Dalton T. 2010;39:930.

[70] Miao H, Wang S, Zhou S, Wei Y, Zhou Z, Zhu H, et al. Synthesis, characterization of some organolanthanide complexes containing 2-pyridylmethyl substituted fluorenyl ligand and catalytic activity of organolanthanide(II) complexes. Inorg Chim Acta. 2010;363:1325.

[71] Luo Y, Li W, Lin D, Yao Y, Zhang Y, Shen Q. Lanthanide Alkyl Complexes Supported by a Piperazidine-Bridged Bis(phenolato) Ligand: Synthesis, Structural Characterization, and Catalysis for the Polymerization of l-Lactide and rac-Lactide. Organometallics. 2010;29:3507.

[72] Yang J, Xu P, Luo Y. Bimetallic Rare Earth Alkyl Complexes Bearing Bridged Amidinate Ligands: Synthesis and Activity for L-Lactide Polymerization. Chin J Chem. 2010;28:457.

[73] Jaroschik F, Bonnet F, Le Goff X-F, Ricard L, Nief F, Visseaux M, et al. Synthesis of samarium (ii) borohydrides and their behaviour as initiators in styrene and ε-caprolactone polymerisation. Dalton T. 2010;39:6761.

[74] Buchard A, Platel RH, Auffrant A, Le Goff XF, Le Floch P, Williams CK. Iminophosphorane neodymium (III) complexes as efficient initiators for lactide polymerization. Organometallics. 2010;29:2892.

[75] Clark L, Cushion MG, Dyer HE, Schwarz AD, Duchateau R, Mountford P. Dicationic and zwitterionic catalysts for the amine-initiated, immortal ring-opening polymerisation of rac-lactide: facile synthesis of amine-terminated, highly heterotactic PLA. Chem Commun. 2010;46:273.

[76] Mazzeo M, Lamberti M, DAuria I, Milione S, Peters JC, Pellecchia C. Phosphido-diphosphine pincer group 3 complexes as efficient initiators for lactide polymerization. J Polym Sci A Polym Chem. 2010;48:1374.

[77] Otero A, Lara-Sanchez A, Fernandez-Baeza J, Alonso-Moreno C, Marquez-Segovia I, Sanchez-Barba LF, et al. Heteroscorpionate rare-earth initiators for the controlled ring-opening polymerization of cyclic esters. Dalton T. 2011;40:4687.

[78] DAuria I, Mazzeo M, Pappalardo D, Lamberti M, Pellecchia C. Ring-opening polymerization of cyclic esters promoted by phosphido-diphosphine pincer group 3 complexes. J Polym Sci A Polym Chem. 2011;49:403.

[79] Zhou S, Wu S, Zhu H, Wang S, Zhu X, Zhang L, et al. Synthesis, structure and catalytic activity of alkali metal-free bent-sandwiched lanthanide amido complexes with calix [4]-pyrrolyl ligands. Dalton T. 2011;40:9447.

[80] Hao J, Li J, Cui C, Roesky HW. Synthesis and Characterization of Heterobimetallic Oxo-Bridged Aluminum–Rare Earth Metal Complexes. Inorg Chem. 2011;50:7453.

[81] Hou W, Chen J, Yan X, Shi Z, Sun J. A single active site metal center of neodymocene chloride for the ring-opening polymerization of ε-caprolactone. J Appl Polym Sci. 2012;123:1212.

[82] Zhao W, Wang Y, Liu X, Cui D. Facile synthesis of fluorescent dye labeled biocompatible polymers via immortal ring-opening polymerization. Chem Commun. 2012;48:4483.

[83] Du G, Wei Y, Zhang W, Dong Y, Lin Z, He H, et al. Bis(imino)diphenylamido rare-earth metal dialkyl complexes: synthesis, structure, and catalytic activity in living ring-opening ε-caprolactone polymerization and copolymerization with γ-butyrolactone. Dalton T. 2013;42:1278.

[84] Wang Y, Lei Y, Chi S, Luo Y. Rare earth metal bis(silylamide) complexes bearing pyridyl-functionalized indenyl ligand: Synthesis, structure and performance in the living polymerization of L-lactide and rac-lactide. Dalton T. 2013;42:1862.

[85] Li M, Hong J, Chen Z, Zhou X, Zhang L. Synthesis, structure and reactivity of dinuclear rare earth metal bis (o-aminobenzyl) complexes bearing a 1, 4-phenylenediamidinate co-ligand. Dalton T. 2013;42:8288.

[86] Bennett SD, Core BA, Blake MP, Pope SJA, Mountford P, Ward BD, et al. Chiral lanthanide complexes: coordination chemistry, spectroscopy, and catalysis. Dalton T. 2014;43:5871.

[87] Mou Z, Liu B, Liu X, Xie H, Rong W, Li L, et al. Efficient and Heteroselective Heteroscorpionate Rare-Earth-Metal Zwitterionic Initiators for ROP of rac-Lactide: Role of σ-Ligand. Macromolecules. 2014;47:2233.

Kamila Szałata and Tania Gumi

3 BioArtificial polymers

Abstract: Nowadays, the polymer science has impact in practically all life areas. Countless benefits coming from the usage of materials with high mechanical and chemical resistance, variety of functionalities and potentiality of modification drive to the development of new application fields. Novel approaches of combining these synthetic substances with biomolecules lead to obtain multifunctional hybrid conjugates which merge the bioactivity of natural component with outstanding properties of artificial polymer. Over the decades, an immense progress in bioartificial composites domain allowed to reach a high level of knowledge in terms of natural-like systems engineering, leading to diverse strategies of biomolecule immobilization. Together with different available options, including covalent and noncovalent attachment, come various challenges, related mainly with maintaining the biological activity of fixed molecules. Even though the amount of applications that achieve commercial status is still not substantial, and is expanding continuously in the disciplines like “smart materials,” biosensors, delivery systems, nanoreactors and many others. A huge number of remarkable developments reported in the literature present a potential of bioartificial conjugates as a fabrics with highly controllable structure and multiple functionalities, serving as a powerful nanotechnological tool. This novel approach brings closer biologists, chemists and engineers, who sharing their effort and complementing the knowledge can revolutionize the field of bioartificial polymer science.

Keywords: polymeric biomaterials, biomimetic materials, stimuli-responsive polymers

3.1 Introduction

Imitating the nature by researchers from all the fields of science is a common trend since decades and is continuously developing dynamically. The versatile applications of materials able to work like biological structures have made them a major interdisciplinary research focus. Since the discovery of macromolecules by the German scientist Herman Staudinger (Nobel Prize in 1953), the field of material sciences and technology reached countless life-changing developments, followed up with a drastic growth of plastic–polymer industry. The variety of possibilities offered by compounds chemically and mechanically stable with simultaneous potential of modification and functionalization opened a door for novel approaches that focus on designing materials able to adapt multiple functions, structures and

https://doi.org/10.1515/9783110469745-003

capabilities – also biological like. The evolution of bioinspired polymeric materials leads to obtaining structures that combine the benefits coming from both sources – biological and synthetic ones. They can have advantages over the natural version, like improved mechanical robustness and reproducible chemistry, but at the same time operate according to biological mechanism, with the same or even higher efficiency. Those materials are developed by applying various strategies.

One of them is the synthesis of completely new chemical compounds that are able to adopt the same structure and function like pattern biomolecule. They are named biomimetic materials.

Within this approach, many stimuli-responsive polymers have been designed, like for instance a novel gel system developed by Yoshida from Tokyo University [1]. Over years of improvement, those polymeric gels are able to mimic autonomous oscillation movements present in living systems such as heartbeat or brain waves. This so-called biomimetic actuators convert a chemical oscillation process into a mechanical alteration in gels and can be also controlled by change of some parameters, like temperature or substrate concentration. This development provides a smart material that can generate self-propelled motions, pendulum motions, or directional motions and find variety of applications in biomedical sciences. Another example of the same concept is imitation of enzymes for widely understood sensing applications and biocatalysis [2, 3], which recently improved, overcomes the challenges concerning poor selectivity of synthesized sensors by application of molecular imprinted polymers [4]. It is reported that molecular imprinted polymers-based nitroreductase has been already successfully applied for efficient determination of a drug metronidazole or hexazinone herbicide – pervasive ground water contaminant [5]. A known example of natural polymer replacement by artificial one can be synthetic rubber; which it is used e. g. for car wheels production or artificial hair as a synthetic substitute of keratin [6–9].

Another approach to create polymeric biomaterials is based on a concept of its biocompatibility and, thus, possibility to use them in living organisms. This is a common challenge in terms of application of many synthetic structures – to be safely used in vivo, polymers need to be biodegradable and its decomposition products cannot be toxic at all. Several synthetic polymers have been found to fulfil these requirements and are widely used, for instance polypropylene and polyurethane in breast implants, polyurethane in artificial heart or poly(glycolic acid) as absorbable sutures [10–12].

Besides, a big part of the research concerning the design of biological-like artificial systems is dedicated to the development of hybrid protein-synthetic polymer materials. The first attempts to obtain synthetic polymers containing biomolecule have been reported already in 1964 [13], and since this time the knowledge in this term has evolved significantly. This combination of synthetic and biological parts is a step forward to fabrication of hybrid bioinspired structures with unprecedented properties and applications which are discussed in this chapter.

3.2 Biomolecule immobilization techniques

This chapter is dedicated to specific kind of materials that contain both units – artificial polymer and biomolecule. The goal of this approach is to obtain materials, which would possess advantages of synthetic polymers, like their performing mechanical properties, reproducible chemistry and thus possible large-scale production, and also coming from biomolecule- biocompatibility and functionality of natural system. This establishment correlates to many challenges which depend on the type of protein incorporated into artificial medium and on the desired application of the material. However, the main defiance, present in all kinds of used protein, is maintaining their biological activity, which often is lost due to change in a conformation or incompatibility with polymer [14–16]. Thus, within this particular concept, different methods of protein incorporation can be applied and are usually classified as follows.

3.2.1 Adsorption

The simplest and very commonly used method is physical adsorption on a support material (Figure 3.1). If performed under suitable conditions, this method can efficiently bind biomolecule into a support via hydrophobic or van der Waals interactions. Although this strategy found application in immobilizing enzymes for e. g. medicine purification purposes [17–20], it is usually too weak to cope industrial conditions; thus, in this field, it is preferable to employ other methods.

Adsorption is relatively easy to perform and due to the fact that it is free from chemical modification, it is a very efficient and non-invasive method, which maintains the biological activity of proteins. Also, since it is reversible, it facilitates the purification of used biomolecules and supports. However, the main handicap is requirement of mild working conditions and very careful adaptation of both molecules and carriers.

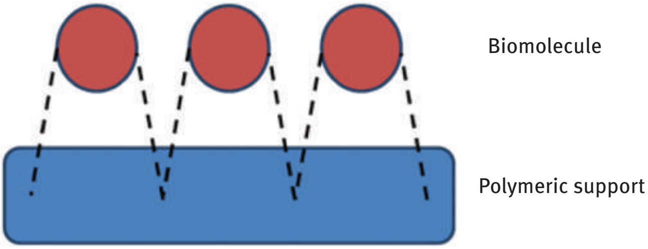

Figure 3.1: Scheme of physical adsorption of biomolecule on the polymeric support.

3.2.2 Covalent binding

This method provides much stronger linkages between polymeric support and biomolecule (Figure 3.2). Normally linkage occurs between functional groups present in the support surface and the groups of protein. Usually reactions used to create new bonds are 1,3-dipolar cycloadditions of terminal alkynes and azides, peptide bond formation, isourea linkage, [21] coupling via tresyl chloride, coupling via cyanogen bromide, coupling via cyanuric chloride or glutaraldehyde coupling [22].

In this case, due to strong interactions, leakage of biomolecule is minimized. However; this is a much more expensive immobilization method in comparison to physical adsorption. Moreover, it is also connected with the use of organic solvents what, unfortunately, is very often related to the loss of biological activity.

3.2.3 Entrapment

Entrapment of biomolecules consists of suspending them within the polymeric gel which delimits the movements and stabilizes the protein/polymer structure (Figure 3.3). In this system, the gel acts also as a biomolecule protector, separating it from environment. As the polymer porosity can be controlled, it is possible to create a gel-net adjusted to the protein size in order to avoid leakage, with simultaneous permission to free moieties and active structure adaptation.

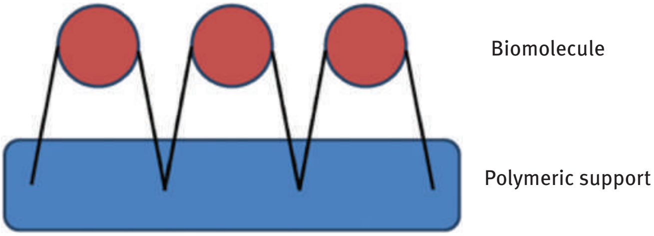

Figure 3.2: Scheme of chemical attachment of biomolecule to the polymeric support.

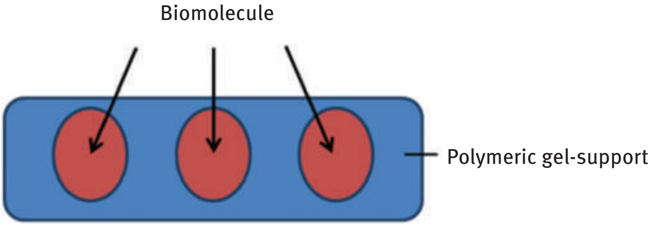

Figure 3.3: Scheme of entrapment of biomolecule in the polymeric gel.

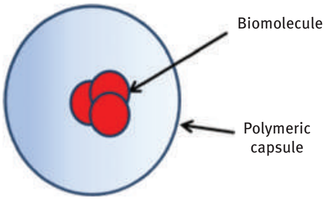

Figure 3.4: Scheme of biomolecule entrapment inside the polymeric capsule.

Although protein loading achieved with this technique can be very high, there is a big disadvantage of this technique related to diffusion limitation through the gel: certain times, the gel does not allow the products of enzymatic reaction to release from it.

3.2.4 Encapsulation

Encapsulation is widely used in drug delivery system as well as in biocatalysis. Biomolecule closed in a polymeric semi-permeable shell has enough free space to freely move, but is isolated from environment (Figure 3.4). Possibility to create pH- or light-sensitive microcapsules allows to release the protein from its core under desirable conditions [23, 24]. Because of the capability to produce capsules in different sizes, it is possible to encapsulate even relatively big biomolecules. The limitations related to this method are similar to the one with gel entrapment and concern diffusion problems. Another important factor is sensitivity of polymer to external factors like temperature or pH. Depending on the biomolecule function, the properties of polymeric capsules needs to be adjusted in order to release it under the adequate condition in the target. The next chapter will discuss in more detail the function of nanospheres and nanocapsules for drug delivery systems.

All these techniques have some disadvantages and the concrete design of the perfect system needs to take into account both types of limitation – from the side of polymeric support and from the site of biomolecule. However, development of new chemical strategies and production process optimization resulted in the immobilization of various biological elements on different polymers and induced many remarkable discoveries. Election of the method depends on the type of immobilized biocompound and application of the final product.

3.3 Polymer/biomolecule conjugates

Researchers from all over the world are struggling to face challenges connected with specificity of particular biomolecules and polymers, trying to overcome obstacles to obtain desirable, perfect, defect-free biomaterials with multiple functions.

Biological/artificial conjugates found plenty of application in industry, technology, biosensing, tissue engineering and pharmacology [25, 26]. Those applications according to the type of used biomolecules and polymers are described in the following section, while application in drug delivery systems will be discussed specifically in the next chapter.

3.3.1 Enzymes

Enzymes are proteins that assist catalytic functions of biochemical processes. Their presence is crucial for living organisms because most of the reactions do not occur spontaneously at normal body temperature. The characteristic work done by enzymes is related to their extremely high specificity coming from its particular geometric configuration, which allows to bind only proper-shaped molecules (key and lock mechanism). The catalytic activity of enzymes can be affected by different factors like temperature, pH or concentration of enzyme or substrate. They are also sensitive to various chemicals which inhibit catalytic reactions in a reversible or irreversible way [27]. Thus, all those features need to be taken into account while designing immobilization conditions and method.

High efficiency and selectivity of enzymatic reactions has always been an inspiration for the development of novel bioreactors and biosensors. Recently, the industrial competence in biocatalysis is achieved due to common use of lipases, esterase or peptidases [18, 20, 28–30]. Polymer/enzyme conjugates are reaching significance also in the field of decontamination. As a trend in green chemistry, organophosphorus (OP) hydrolase was used [24, 25, 31]. This enzyme hydrolyzes OP compounds present in the soil, which are pesticide components. OPs are very toxic and can cause damage to the central nervous system. An example of hydrolase/polymer conjugate is reported in the literature and employs enzyme immobilization in the thermostable triblock copolymer micelles. This strategy overcomes low biomolecule stability under different working and storage conditions [32]. Methyl parathion hydrolase was entrapped, for the same purpose in the poly(gamma-glutamic-acid)/gelatin hydrogel and this even enhanced its catalytic efficiency. An interesting approach, published recently by Xiao-Yu Yan and coworkers [33], was the creation of nanofibrous membrane containing OP hydrolase which managed to fulfil both filtration and degradation functions for biochemical protective applications. In this approach, OP hydrolase is immobilized covalently via glutaraldehyde crosslinking on polyamide nanofibers. This novel design of the material makes it a potential tool for various civilian and military protection equipment and clothier production. Those fabrics would be able to protect human body via double mechanisms: by filtration of toxic products and converting it to nontoxic derivatives. This purpose is schematically demonstrated in Figure 3.5.

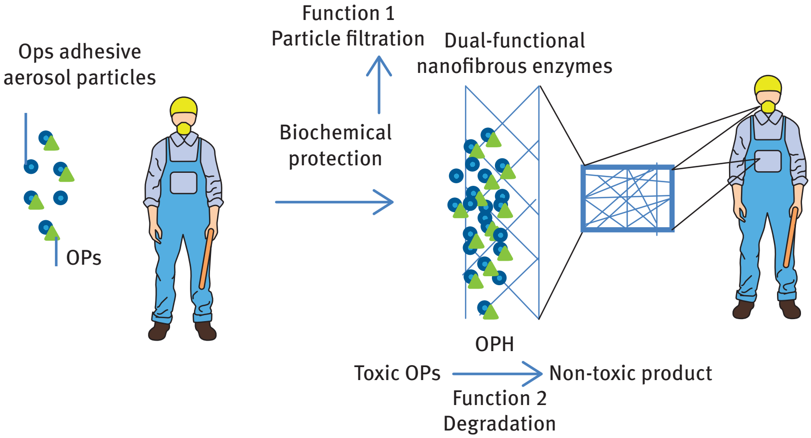

Figure 3.5: Schematic demonstration of double function of OP hydrolase-immobilized nanofibrous polymeric clothing.

Immobilization of OPH via the same technique – glutaraldehyde crosslinking – found also an application in bioremediation. Obtained in this way, OPH-polyester textiles are cheap in production and easy to handle. Immobilized enzyme has enhanced stability, has good activity in un-buffered water and is able to degrade even very low concentrations of organophosphate pesticides. Moreover, its reusability in batch or continuous processes demonstrates that this kind of polymer/enzyme structure has a potential in environmental bioremediation of contaminated water [34].

Noncovalent immobilization strategy was used to design a membrane that was able to immobilize even three enzymes at the same time [35]. This goal was reached by creation of flat sheet polypropylene membrane first coated with cellulose sublayer and application of simple pressure-driven filtration. By controlling of biofouling formation and driving it to form enzyme cake layers, obtained sheets maintain the activity of all three enzymes (formate dehydrogenase, formaldehyde dehydrogenase and alcohol dehydrogenase). This strategy provides a membrane that has an excellent potential application in multienzymatic cascade reactions, in this case bioconversion of carbon dioxide into methanol. The benefit coming from the strategy selected in this study is that there is no need to use organic solvents which very often are toxic and difficult to handle, and thus, may influence enzyme activity. To better understand the concept of performed immobilization, the new method was compared to sequential immobilization technique. Both options are shown in Figure 3.6.

Another interesting point found by authors of this work is considering simultaneously two immobilization mechanisms. At first, enzymes are physically immobilized on a surface by adsorption, but some of the aggregates were also found inside of

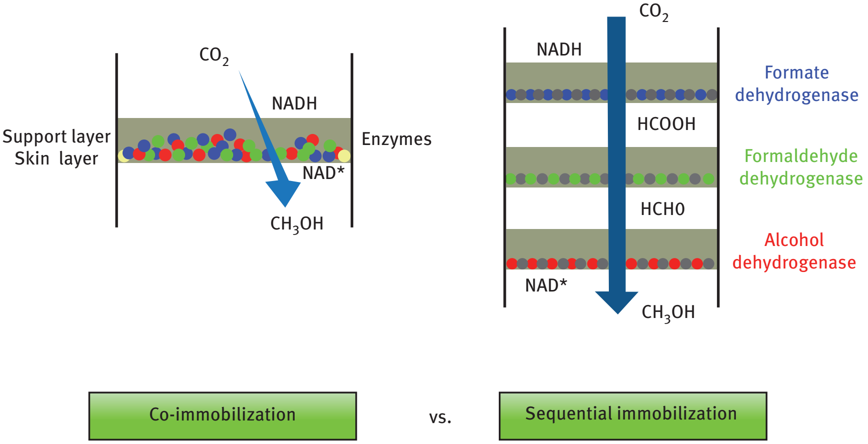

Figure 3.6: Schematic representation of two biomolecule immobilization mechanisms: pressure driven filtration-co-immobilization and sequential immobilization.

the membrane, which suggests also an entrapment of the biomolecules. Nevertheless, because of the fact that any of those techniques is not involved in the creation of new covalent bonds, enzymes are still maintaining their performance. However, results of CO_2 conversion prove that the presented method requires additional modifications and improvements because of poor efficiency of carbon dioxide transformation, which is probably a result of insufficient space between the immobilized enzymes. Interferences coming from this fact cannot ensure proper reaction conditions for the following enzymatic reaction steps.

Most part of the research in this field is dedicated to enzyme immobilization for biosensing application, and the literature reports multiple examples of successful uses of this approach. The initiator of this branch of development was Thompson, who already in 1980 made a first step into novel material science expansion [36]. He used natural lipid bilayer with incorporated bioreceptors, which in living organisms play a role of biosensors. Thompson isolated this primal structure and immobilized on artificial polyamide support. By increasing the support stability, he made this sensitive structure handable and useful in biosensing applications. Since this moment, his idea was applied for immobilizing lipid bilayer on various supports and further modifying with proteins or artificial receptors, enzymes, antibodies, channel formers and carriers which play the role of transducers or analyte detectors. Possible determination of many psychoactive or toxic substances at very low concentration level makes biosensors have almost unlimited applications in our daily life. Very fast development of new bioelectronics makes a huge impact on progressing analytics, diagnostics, biomedicine and in all type of industries like agriculture and other industries. To draw an idea about how large is the application area of enzyme-based bioartificial polymers in biosensor production a few examples will be mentioned below.

As suitable supports for enzyme immobilization are chosen electroconductive polymers which, thanks to its electronic properties, enhance the speed and sensitivity of biosensors [37]. Those kinds of conjugates are based on direct binding of biomolecule (biocatalyst) into the electronic device. Azak et al. and Ekiz [38, 39] e. g. developed a novel conducting polymer matrix electropolymerized onto the graphite electrode, to which glucose oxidase was covalently attached using glutaraldehyde crosslinking. Later, Ayranci used the same method to bond an enzyme to a metalo-polymer, ferrocenyldithiophosphonate [40]. These examples of hybrid materials found application in glucose detection biosensors. One interesting approach uses enzymatic degradation of ethanol by alcohol dehydrogenase, or alcohol oxidase, for the production of detectors for alcohol concentration in breath [41, 42]. In this kind of system, the reactions take place in the three-phase interface; thus, a perfect application in this field found breathable electrodes. To better understand the working principle of those equipment, a device developed by Winther-Jensen can be mentioned [43]. The group from Monash University immobilized alcohol dehydrogenaze [44] on a widely used biocompatible conductive polymer poly(3,4-ethylenedioxythiophene) PEDOT. Immobilization of biomolecule was performed by stuffing method, which is considered to be a gentle and noninvasive technique, potentially applicable for immobilization of biological elements. In the aforementioned method, biomolecule immobilization was enhanced also as an effect of shrinkage of material after additional post-polymerization coating. The schematic reactions occurring in this three-phase interface system and its application in the construction of breathable electrode are shown in Figure 3.7. Alcohol dehydrogenaze-immobilized PEDOT material is placed between two compartments – to the first one is collected the breath air, and the second is filled with a solution containing NADH (redox mediator), Ag/AgCl reference electrode and counter-electrode. As the alcohol vapour concentration in the first compartment increases, ADH in the presence of NADH converts it into the aldehyde and the reaction performance is amplified to a current response detectable by the electrode. Experiments show that enzyme maintained its activity and oxidizes alcohol efficiently.

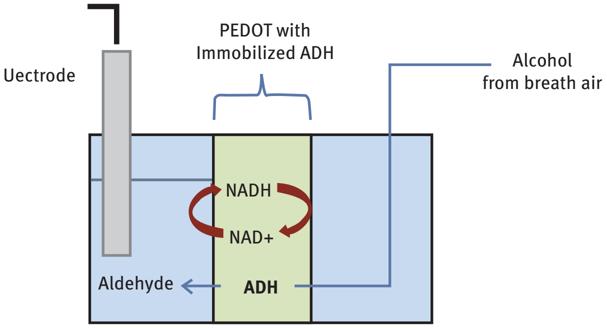

Figure 3.7: Schematic representation of the breathable electrode based alcohol detector device.

Besides this fields, in a food industry alike agriculture and other life areas, gas sensors known as a electronic noses are also of great importance. They are devices that are designed to mimic human olfactory systems. This technology is a novel trend in “smell” sensors for a quick detection of vapour even at very low concentration. Possibility of using it in the determination of toxic gases in conditions that are dangerous for human health and life is an excellent and beneficial approach. An example of detector for formaldehyde (very harmful), widespread in environment volatile organic compound, was presented by Mitsubayashi et al. [45], who designed bio-sniffer stick based on a formaldehyde dehydrogenase enzymatic reaction. Dehydrogenase was mixed with functionalized poly(vinyl alcohol) and then immobilized on polytetrafluoroethylene (PTFE) chip. This chip was then placed on a PTFE/Pt electrode, which provides chemical stability and mechanical strength by maintaining flexibility of the device. Dehydrogenation of formaldehyde is performed at first by oxidized NAD^+, next reduced NADH is oxidized as a result of reaction with PTFE/Pt electrode. Reactions occurring in the system are as follow:

$$HCHO + NAD^+ \xrightarrow[\ ]{\text{Formaldehyde dehydrogenase}} HCOOH + NADH$$

$$NADH \xrightarrow{+700\text{ mV vs Pt}} NAD^+ + H^+ + 2e^-$$

The fabricated biosensor exhibits high selectivity for formaldehyde recognition, and the detection limit is much lower than the human sense of smell; thus it presents a great perspectives for application in environmental monitoring. This is only one of many examples of the human sense reflection in electronic devices. Fast development of biosensor market allowed creating various apparatus like electronic tongue or stimuli-sensitive artificial skin. Fabrication of bioinspired enzyme-based materials is a revolution in nanotechnology and continuously delivers new tools with untold number of applications.

3.3.2 Polysaccharides

Polysaccharides are complex carbohydrates formed from at least two monosaccharides linked by glycosidic bond. In living organisms, they serve as energy storage and building functions. They are widespread and easy to obtain from natural sources. They possess a variety of structural and chemical properties, and they can be long chain or short chain, water soluble or insoluble and exhibit different functionalities. What is also the most important in terms of use it for bioconjugates synthesis, is their non-toxicity and environmental friendliness.

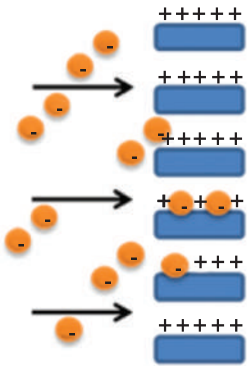

Figure 3.8: Scheme of affinity membrane separation mechanism.

Polysaccharides found application in production of affinity membranes [46, 47]. The filtration mechanism through these kinds of membranes leads to adsorbate capturing (depending on the case; it might be for example viruses, endotoxins, bacteria or heavy metals) onto functionalized material surface, while the feed is passing through it. Rejected substance can be even smaller than the pores present in a membrane, but even though, due to big affinity to the "capturing" area, it will get adsorbed. For example, the pore surface might be functionalized with positively charged active group and within electrostatic interaction adsorb negatively charged ones from the feed [48] (Figure 3.8).

These kind of membranes are characterized by low pressure drop and thus low energy consumption, high efficiency and high fluxes and can be easily regenerated. Various examples of the use of polysaccharide/polymer composite concern chitosan, a natural amino polymer extracted from chitin. As it is positively charged at low pH, it found application in development of materials which exhibit big affinity to removal of negatively charged species, such as heavy metals, across nanofibers or membrane contactors (chitosan//polyvinyl alcohol) reported by Prateek Khare et al. [49] or through membranes (PET/chitosan membrane) described by Li [50]. One of the interesting approaches of implementing this polysaccharide into artificial polymeric matrix is artificial liver development studied among others by Teotia [51]. They designed a system composed of polysulfone/tocopheryl polyethylene glycol succinate (Psf/TPGS) composite hollow fibre membrane, which is coated with chitosan. The coating procedure was performed by introducing first negatively charged groups into the polymer composite (sulfonation), which facilitated electrostatic interaction with amine groups of chitosan. The surface coated with polysaccharide exhibits biocompatibility and supports growth of cells (HepG2 cell line), thus mimicking liver-specific functions. This particular approach perfectly shows advantages of mechanical and chemical stability of synthetic Psf/TPGS membrane and biofunctionality of natural chitosan, which makes this polymer/polysaccharide conjugate a good potential material for artificial liver application.

Tissue engineering is another focus of scientists around the world who keep on looking for new ways to develop materials able to mimic biological bone tissues, facilitating its regeneration and simultaneously maintaining good mechanical stability. In this approach, polysaccharide-based composites are applied in a membrane configuration, like cellulose, alginate and chitosan [44, 52, 53], which supports tissue regeneration and makes permeable platform for new cells growth. Because of its ability to adopt different shapes and well adapt to hydrated environment, hydrogels are a type of polysaccharide composites that have been widely studied recently [54–56]. This group of highly hydrophilic polymeric materials is able to accumulate large amount of water and thus can form flexible, three-dimensional structures[57]. Examples of chitin/PCL and chitin/PCL/nHAp microgel developed by Arun Kumar et al. [58] explore the potentiality of its use in engineering of bone tissue in inaccessible places, like skull. Moreover, hydrogels due to its unique structure can incorporate drugs and other growth factors, which accelerate tissue regeneration and the most important – its degradation products are completely biocompatible. Nevertheless, although the easiness of handling and good rheological properties are remarkable, poor mechanical stability is undoubtedly the main disadvantage of hydrogels. However, this handicap is recently improving by mixing polysaccharides with natural minerals. This is the case of composite of less explored natural polymer which is pullulan. Developed by Amrita et al., hybrid fibres containing poly(β-hydroxybutyrate) (PHB) and hydroxyapatite (naturally occurred mineral), when combined with pullulan, enhance the mechanical stability of hydrogel even 10 times [59].

Chitosan has also shown potential as a flame retardant coating material. Laufer et al. applied its properties in coating polyurethane foams and polylactic acid (PLA) film [60] using layer-by-layer (LbL) assembly method. Positively charged chitosan was used to construct a multilayered film by convertible deposition of negatively charged mineral montmorillonite. The good performance of formed “nanobricks” presents a promising alternative for substituting halogenated flame retardant materials for environmentally friendly eco-coatings.

Another polysaccharide having big industrial importance is cellulose. This material found application not only in food packaging industry or as a biomedical device component but its interesting mechanical and optical properties give light on new potential functions. In the literature, various examples can be found of the use cellulose/synthetic polymer composites for construction of optoelectronic devices such as light diodes, flexible electrodes, biosensors or optical displays [4, 61–64]. Shaukat Khan et al. prepared PEDOT/PPS/cellulose composite membranes by ex situ incorporation of those conductive polymers into bacterial cellulose pellicles. A similar approach has been achieved by Marins et al. who polymerized polyaniline doped with dodecyl benzene sulfonic acid onto bacterial cellulose sheets [65]. One year later, Müller et al. applied the same method by polymerizing polyaniline onto cellulose nanofibers [66]. Those novel conductive materials characterize outstanding stiffness and strength followed by biodegradability and renewability. Those properties make polymer/cellulose conjugates a material to be used for the production of intelligent clothes e. g. for health-monitoring system like heartbeat recording, body temperature control, body odour control, hemostatic materials and plenty of other tremendous possibilities [67–70].

Cellulose is used also to produce other smart - shape memory materials, which deformed to temporary configuration are able to recover their original form as a result of response to some external stimulating factor. In the case of thermo-responsive shape memory materials, this factor is temperature. The original form of material can be first modified by applying external force and temperature above transition temperature and then, if the material is cooled down without releasing external force, a temporary shape will be fixed. To recover the original shape, the only thing needed is again heating up the device above transition temperature. Auad et al. [71] demonstrate reinforcement of thermoplastic polyurethane after confinement of small concentration of cellulose nanofibrils. Those kind of materials have potential application in medical devices; however, very often the temperature needed to induce shape change is not applicable for use in human body. This handicap has been overcome by Bai et al. [72], who applied ethyl cellulose/polycaprolactone (PCL) conjugate in order to adjust transition temperature to human body friendly (around 40 °C). This interesting strategy lies in a design of water-activated rapidly switchable shape memory effect, reported by Zhu et al. [73] in cellulose nano-whiskers/thermoplastic polyurethane. They used the unique properties of a percolation network in nanocellulose which in combination with elasticity of a polymer lead to temporary shape fastening and original form quick recovery when wetted (Figure 3.9).

Later, Liu et al. [74] applied a similar strategy in microcrystalline cellulose/poly (D,L-lactide) composite. This recent enhancement has an unprecedented impact on development of novel smart materials with shape memory functions with innumerable and inestimable potential. Moreover, polysaccharide availability and easiness of

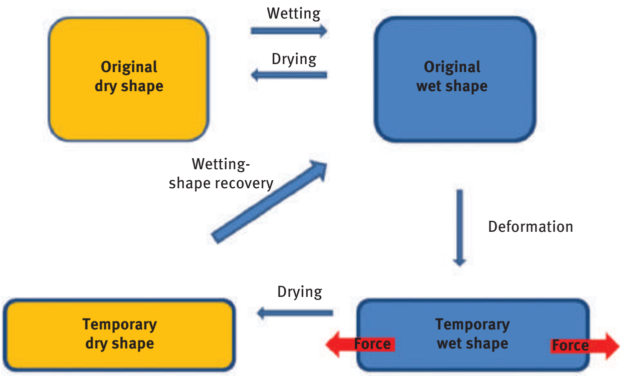

Figure 3.9: Schematic representation of water activated switchable shape memory effect mechanism.

handling and treatment continuously force the researchers to explore new properties of natural polymers and find still new applications.

3.3.3 Channels

Other biomolecules widely used in the field of bioartificial composites are ionic channels. Ion channels are proteins that catalyse the diffusion of ions across the biological membranes and thus are responsible for maintaining electrochemical balance between cell and its surrounding. Since the cell membranes are electrical insulators, ionic channels function as a selective gate which opens for some of the molecules allowing them to pass into the cell and due to conformation change closes to the others [75]. Because of the type of factor which impact its “gating” motions, ion channels can be classified into different groups.

One of the transport mechanisms occurs when the ligand attached to the channel binds the ion and then, because of conformational change, allows it to pass through that formed door, according to the concentration gradient. That type of receptor is called extracellular ligand-gated ion channel and it is present in brain and muscles. Voltage-gated ion channels are activated due to the change in membrane electrical potential. Those proteins are well-known potassium and sodium ion channels and also calcium channel and proton channel. When the signal influencing conformational change in a protein structure comes from the interior of the cell, this channel is called intracellular ligand-gated ion channel, e. g. cystic fibrosis transmembrane conductance regulator which is ATP-gating anionic channel. Understanding completely all of these mechanisms leads to proper design of bioartificial conjugates with very specific functions and destiny. Ion channels are proteins with incredible importance in many biological processes that cause rapid changes in cells, like muscle contraction, selective transport of nutrients and ions or hormone release. They work very specifically and its characteristic selectivity is a result of responsive conformational changes which then regulate the ionic transport [75]. Because of its extraordinary properties, they found a huge interest in developing new polymeric hybrid materials, mainly for biomedical and biosensing applications. Since ion channel functionality is related to transportation, their properties are mostly applied in biomimetic membrane technology.

To incorporate this biomolecule into artificial polymeric matrix with maintaining its proper functionality and without affecting the structure, it is desirable to reflect its natural environment, the most possibly similar to the one in the cell membrane. To cope with this goal, scientists tended to synthetize materials able to mimic those present in living organism lipid bilayer. The most important criterion was obtaining materials which have high thermal and chemical long-term stability and mechanical durability but simultaneously exhibited specific flexibility which would provide a proper free space necessary to perform ionic channel conformational changes. The great alternative to cope with this challenge is synthesis of self-assembly block copolymers which, in combination with bioactive component, offer variety of possibilities to create highly organized supramolecular structures. Because of its dual nature, those synthetic amphiphiles provide large variability of possible architectures. They are built from hydrophobic and hydrophilic blocks which are organizing spontaneously in the solution, similar to the natural lipid bilayers present in cellular membranes. The layer binding occurs through weak noncovalent interactions like van der Waals forces, hydrophobic interactions or hydrogen bonds, and thus they are flexible and can adapt to diverse topologies. As an example, Zhang et al. [76] synthetized an amphiphilic block copolymer (poly(butadiene)52-blockpoly(ethylene oxide)) in which functionally incorporated model membrane channel protein alpha-haemolysin, responsible for transport of little molecules like ions, nutrients or antibiotics. This innovative approach coped with the challenge of incorporating biomolecule in a large area in a stable, supported artificial tethered solid-supported membrane, which provided a novel material with potential applications in drug screening, biosensing or trace analysing. Those kinds of active self-assemblies can be organized in a shape of membrane, micelles, tubes or vesicles. An important factor regulating successful protein ion channel incorporation into artificial surface was discussed by the research group of Meier [77], who studied in detail protein interaction with the support and events which can lead to deactivation or affect a structure. Their work concerning preparation of well-organized hybrid ion channel/artificial polymer structures resulted in the production of supramolecular assemblies. Hydrophobic polymer polydimethylsiloxane (PDMS) plays a role in the plasticity maintenance of structure in contact with solid support, while hydrophilic component – PMOXA – is separating ion channel from the direct contact with the base material. The same group from Basel proposed the modern concept of nano-machines, based on the combination of functionality and adjustability of amphiphilic copolymers and powerful biological activities [78]. Designed by them, nanoreactors connect enzymatic operation with function of ionic channel/polymer conjugate. Enzyme was encapsulated in amphiphilic poly(2-methyloxazoline)-block-poly(dimethylsiloxane)-block-poly(2-methyloxazoline) ($PMOXA_6$–$PDMS_{44}$–$PMOXA_6$) copolymer with incorporated outer membrane protein F (OmpF) ion channel, which additionally modified, acts like a stimuli responsive gate- opening and closing dependently on the pH (Figure 3.10). This strategy is a big step leading to create robust and stable capsules, which can serve as a device to entrap various biological components, and apart from that, the concept of regulating membrane shell permeability by introducing stimuli responsive ion channel is a step forward to optimize nanoreactors in terms of the size of transported species and type of reaction performed.

Ion channels are perfect candidates to be used in applications related to ion exchange membranes and technologies as fuel cells or energy conversion systems. In the literature, we can find various examples of synthetizing polymers and copolymers with incorporated biological channels for this aim [79]. Aquaporins attract great

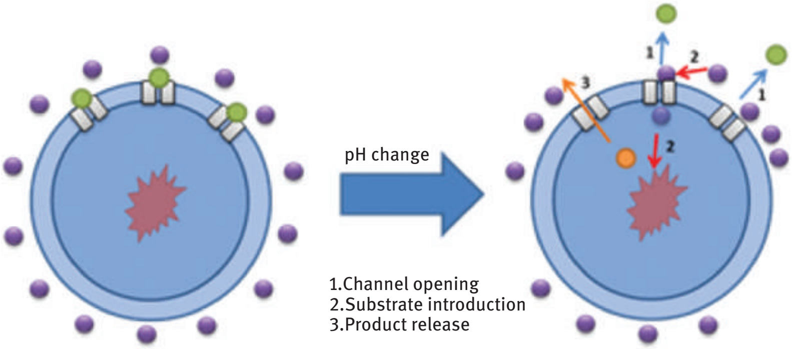

Figure 3.10: Scheme of the nanoreactor working mechanism.

interest in researchers because of its enhancing water flux properties [80]. This membrane water channel is bidirectional, which means that it regulates flow of water entering and going out of the cell. Aquaporins are composed of four monomers assembled in a way that the channel is narrow in the middle and wider at the ends, so allowing the passing of water molecule chain, but rejecting bigger solutes. Moreover, the internal local electrostatic field pushes the water molecules to rotate, which enhances the transport. These unusual properties depict aquaporin molecules as an excellent candidate for potential use for increasing water passage in water treatment membranes. Since aquaporin works in two directions, its orientation in a membrane film is not crucial for the membrane performance. This convenience allowed applying various techniques of its incorporation. In the literature, one can find examples of LbL immobilization [81], active layer formation [82, 83] or covalent bonding to lipid bilayer [84]. Improvements in gradient-driven water diffusion in ion channel containing membrane designs have been discussed wider in recent reviews [85, 86]. Since the incorporation of aquaporin focused mainly on the water flow increase, random organization of channels did not affect significantly the attainment of the goal. However, for selective ion transport, confinement of channels requires the highest possible organization of biomolecule. But still, together with increase of transport properties, it is difficult to maintain the high specificity of incorporated ionic gates, which is often related to the lack of control during the immobilization process. This challenge is continuously a main problem for researchers who face difficulties with assembling ion channels in the desired orientation along the membrane. The study on a well-controlled immobilization of biological channels within confinement in a precisely shaped and sized nanopores of polymers like PC and PET was performed by Balme et al. [87–89]. They studied the controlled incorporation of avidin, streptavidin and amphotericin B in track-etched membranes and also successfully incorporated gramicidin ion channel improving both flux and selectivity of polymers. Gramicidin was also reported as an biomolecule used for reverse osmosis desalination enhancement [90]. This protein, selective for monopositive ions in combination with polymeric membrane, increased water flux ameliorating desalination efficiency. In this approach, the most important factor, which decided the novelty of applying this particular molecule, was high resistance in the presence of big hydraulic pressure, which is standard operation condition during reverse osmosis process.

Apart from overcoming water scarcity problem, biological channel-based biomimetic filters have good potential in recently developing application which is membrane crystallization technique [91]. Crystallization is a widely used separation technique in a chemical industry in which a crucial parameter is the ability to reproduce crystals with the desired, strict characteristics. However, traditional methods assimilate many disadvantages which hamper reaching this goal. Not exact agitation and nonhomogenous solvent–nonsolvent distribution in traditional evaporators results in poor crystal recurrence and thus low efficiency of the process. Furthermore, high energy consumption related to this technology drives for looking for alternatives. Membrane crystallization is definitely a more economic approach, which applies membrane technology to produce well-controlled crystals that grow gradually from unsaturated solution. Aquaporin biomimetic membrane found an application in this technology [92]. Significantly enhanced water passage through the protein channels incorporated in the commercial polymeric membrane (AIM60 FO membrane from Aquaporin Inside^{TM}) constitutes an interesting alternative for use in sodium carbonate crystallization systems in carbon dioxide capturing purpose.

Energy storage and conversion, solutions for energetic crisis and water scarcity, biosensing technology, tissue engineering, drug industry and models of understanding the mechanisms occurring in biological systems are invaluable gains from biomimetic ion channels/polymer materials. Continuous interest and growth of ideas, strategies and methods of functional channel immobilization make those biomimetic materials very special implement in membrane technology and other fields.

3.3.4 Nucleic acids

Nucleic acids, which include DNA and RNA, are composed of a pentose sugar, a phosphate group and a nitrogenous base. They fulfil a function of encoding and transmitting genetic information in all living organisms. Because of extremely specific interactions between nucleic acids in DNA helix (Watson–Crick base pairing AT and GC affinity), those components provide invention of highly programmable materials which are very useful biotechnological and biomedical tool. Development of amphiphilic bioinspired polymers which are able to self-organize in a form of various shapes, as mentioned before, is widely applied to separation of nucleotides, encapsulate biomolecules and drugs. Amphiphilic phenomenon is also used for fabrication micelles and solid lipid nanoparticles which have been broadly reported as efficient drug carriers (see the chapter "Recent advances in Bioartificial Polymeric Materials Based Nanovectors"). Combination of nucleic acids and synthetic elements allows production of materials which possess excellent information storage capability. Unusual properties of artificial matrix is an outset to create constructs with many possible assemblies and related to these functions. DNA can be conjugated with hydrophilic or hydrophobic polymers by covalent attachment. The strategies applied for this purpose is click chemistry coupling, Michael addition, amide bond formation, phosphoramidate linkage and others [93–96]. The challenging factor of this tactics is the difficulty related to common DNA denaturation caused by harsh reaction condition. Even though covalent methods introduce some limitations and various strategies to overcome this fact were applied, many examples of covalently conjugated materials with variety of applications are reported [97, 98].

As described before, amphiphilic properties of synthetized conjugates lead to obtain specific properties which allow the formation of nanoscale components. In case of copolymers being a base to ion channel immobilization, the whole amphiphilic constituent was artificial. However, for DNA, the only artificial element needed to create amphiphile is hydrophobic polymeric tie, while the other part is made by nucleic acid itself. Properties of those designed composites permit engineering structures in various shapes, related to their particular and unique properties. They can be organized in the shape of micelles, when hydrophobic polymeric tie is directed to the interior of the sphere and hydrophilic DNA is turned to the exterior, forming a core. The same single amphiphilic layer can form elongated shape of tubes; however, double layer can be arranged in vesicles. In vesicles, both interior and exterior are hydrophilic, but the middle layer is built from hydrophobic polymeric chain. All of the morphologies are presented in Figure 3.11. Also, possibilities to engineer the structure in a very controlled way allow the design of a variety of architectures, e. g. so-called star polymers [99].

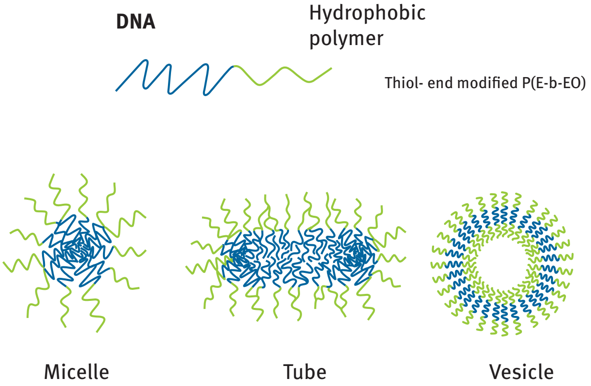

Figure 3.11: Scheme of DNA/hydrophobic polymer conjugates morphologies.

Even though polymers conjugated with DNA have found application mainly in drug delivery systems, a wide range of possibilities offered by those structures found other applications with a great impact on a technology expansion.

Because of the high organization level of nucleic acids, they may be used in the organization of other macromolecular constructions [100–102]. Going along with the capability of DNA/polymer conjugates to bind to other particles, the range of its applicability is widening, e.g. in combination with magnetic nanoparticles they could be used for magnetic resonance imaging [97]. With extremely advanced specificity of binding and the highest level of molecular recognition, they are also perfect tools for diagnostics and analytic assays, because nucleic acid sequence identification in real time allows recognizing genetic mutations or monitoring gene delivery.

DNA-grafted polymeric probe reported by Gaylord et al. has potential as a detector for DNA, proteins and other biological molecules. For this approach, properties of conjugated polymers were studied [103]. Conjugated polymers are the class of compounds, which, due to the presence of delocalized electrons in their structure are fluorescent and able to interact with light. In proposed assay, detection mechanism bases on a Forester energy transfer effect, which occurrs between two chromophores. Schematic representation of those interactions is presented in the Figure 3.12. Conjugated polymer (poly(9,9-bis(6-*N*,*N*,*N*-trimethylammonium)-hexyl)-fluorene phenylene)), called donor chromophore, is placed in a solution with peptide nucleic acid which has exactly determined sequence, called acceptor chromophore- previously labelled with a chromophore dye. When the donor chromophore enters in an excitation state, it transfers the energy to the acceptor chromophore within

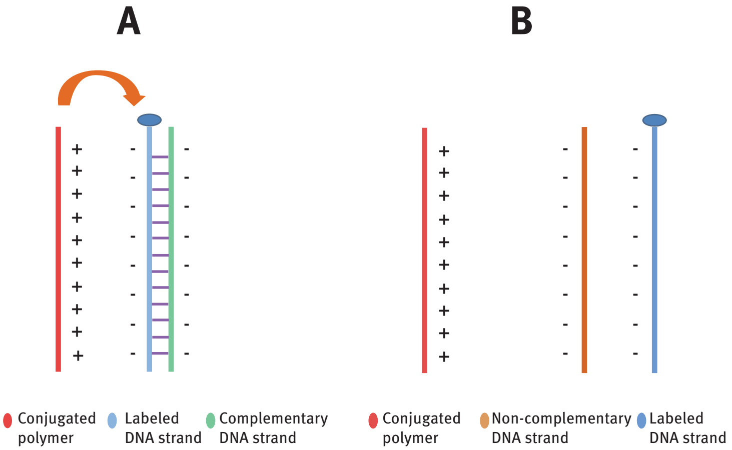

Figure 3.12: Schematic representation of interaction between conjugated polymer and DNA strand in the presence of complementary DNA strand (A) and non-complementary strand (B).

dipole–dipole interaction. Thus, the smallest is the distance between donor and acceptor, the more efficient is energy transfer and thus the optical properties of both polymer and peptide need to be adjusted in a way that they would favour FRET. When conjugated polymer is in the solution with noncomplementary nucleic acid strand, electrostatic interactions are too weak and the distance between strands is too large for efficient FRET effect. When a complementary single-strand DNA appears, occurs hybridization with present peptide nucleic acid and as a result, a donor chromophore gains multiple negative charges. This local higher charge density enables electrostatic interactions with conjugated polymer, which decrease the distance between donor and acceptor activating FRET.

The accessibility of nucleic acid/polymer conjugate allows very high, characteristic specificity and can be used in DNA diagnostics even in very low concentrations. Moreover, recent progress in modification of DNA creates new perspectives for novel composite materials which exhibit biocompatibility, adopt various shapes and morphologies (capsules, vesicles, hydrogels etc.) and are important implement for biorecognition approaches.

3.3.5 Cells

The basic structural unit of an organism is a cell. This macromolecule can reproduce independently, is filled with cytoplasm, contains organelles and genetic material and is surrounded by semi-permeable membrane. Immobilization of cells is a proponent in the creation of so-called “living composites.” Those types of synthetic polymeric materials contain immobilized live microorganisms, and its applications vary from medicine to agriculture or food industry.

Use of free cells in technological spheres is quite widely described [104–106]. However, immobilized microorganisms have a lot of advantages over their nonimmobilized forms. Thanks to attachment to artificial polymers, it is possible to separate them from environment, protect its biological activity and control its release. For encapsulation of microorganisms, polyvinyl alcohol (PVA) is widely used. To better control or even stop release, different blocking strategies have also been studied [107]. There are also many examples of entrapping bacteria for tissue engineering or biosensing approaches in various types of hydrogels [108–110]. Their high water content and elasticity make them perfect candidates as a scaffold matrix for growing cells and entrapment of live or mobile microorganisms and also drugs (look at the chapter “RECENT ADVANCES IN BIOARTIFICIAL POLYMERIC MATERIALS BASED NANOVECTORS”). Those gel crosslinked cells are introduced to degraded tissue and, while growing, they induce polymer fibres to degradation, allowing the growth of new tissues [108] (Figure 3.13).

Synthetic polymers that found application as a tissue engineering biodegradable matrix are, for example PEG or PLGA, used for entrapment of human bone and

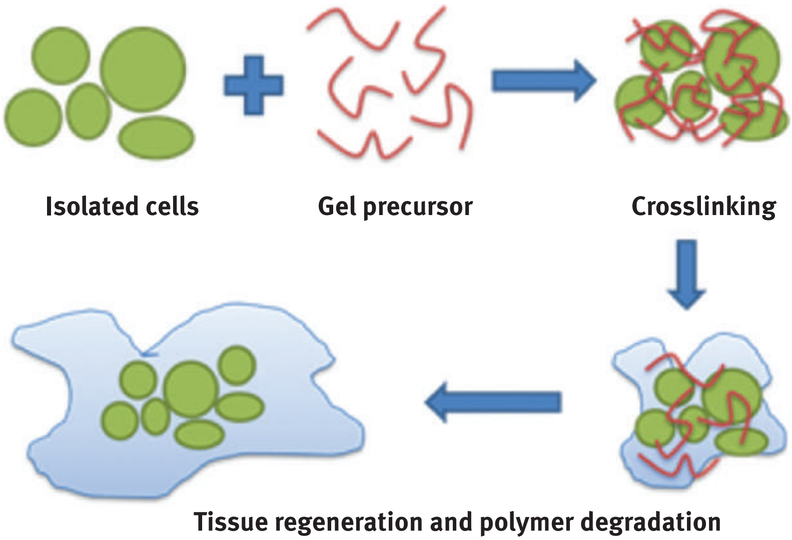

Figure 3.13: Schematic representation of a new tissue cell growth mechanism over the crosslinked gel.

embryonic stem cells [111–113]. However, limited diffusion abilities of hydrogels put some restriction in their application in medicine and thus resulted in developing new research interests which are colloidal carriers called nanoaggregated (see the chapter "RECENT ADVANCES IN BIOARTIFICIAL POLYMERIC MATERIALS BASED NANOVECTORS"). PEG hydrogels are used also in cell biosensors for environmental monitoring, drug screening and diagnostics, as a captor of *E. coli* or murine fibroblasts [114, 115].

Cell immobilization, as in the case of other biomolecules, is related to some limitations, which in this case is construction barrier. Due to cultivation method and conditions, researchers perform usually two-dimensional growth of the culture. Nevertheless, this challenge has been overcome recently, again with the help of polymeric hydrogel. Flexibility of those provide creation of tridimensional cell-entrapping structures which are potential tool for progress in tissue engineering and biotechnology [109].

Immobilization of microbial cells is also considered to be a potential solution in terms of bioremediation and for removal of pollutants in soil and water. PDMS, PVA, latex copolymer, PLA, PU/PC and many other polymers are used as encapsulants for biomolecules. However, some of these materials, although commonly used, are poorly applicable in the bioremediation field because of its water solubility [116] or biomolecule activity limitations. Lately, another way to entrap cell biomaterial is the production of electrospun polymeric fibres [117–119]. In this approach, design of the cell/polymer composite provides significant improvement. In order to last longer, for

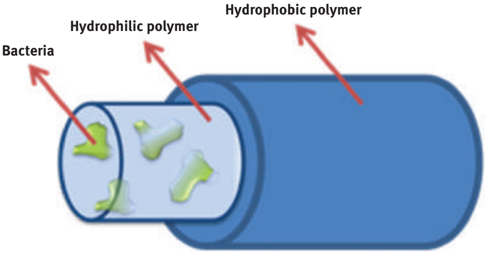

Figure 3.14: Scheme of a composite nanofiber.

a predetermined period of time, biomolecules need to be entrapped in a water-insoluble material which still allows for mobility of the cell. To do it, Klein et al. immobilized cells of *Escherichia coli*, Pseudomonas ADP and *Pseudomonas putida* S12 in an electrospun hollow fibre PCL fibres [119]. From the performance of the composed fibres, it can be seen that design needs to be enhanced even though the study shows that denitrification activity in the fibres is maintained. A similar approach was repeated by Knierim who uses a similar strategy to encapsulate bacteria in PVA and then cover the shell with hydrophobic poly-chloro-p-xylylene (PPX) [116] and letnic, closing yeast cells in PVA and cover it with PVDF [118]. This newly developing method is a potential way to support bioremediation material challenges, and the principle of the idea is presented in Figure 3.14.

Many examples of applying nanofiber technology (especially as blends with chitosan) in drug entrapment for tissue engineering approaches are mentioned in the following chapter. The immobilization of living cells is a challenge, but a variety of applications and benefits which it can bring over the “free cells” use approach drive researchers to find new methods for efficient entrapment with maintaining biological activity. Biodegradable, synthetic polymers with adjusted or modified properties are promising devices to settle numerous problems and inconveniences related to fixing microorganisms, and new methods are continuously developing.

3.4 Summary

Nowadays, the polymer science has an impact in practically all life areas. Countless benefits coming from the usage of materials with high mechanical and chemical resistance, a variety of functionalities and potentiality of modification drive to the development of new application fields. A novel approach of combining these synthetic substances with biomolecules leads to obtaining multifunctional hybrid conjugates which implement bioactivity of natural component with outstanding properties of artificial polymer. Over the decades, an immense progress in bioartificial composites domain allowed to reach a high level of knowledge in terms of natural-like systems engineering, leading to diverse strategies of biomolecule immobilization. Together with different available options, including covalent and noncovalent attachment, come various challenges, related mainly with maintaining the biological activity of fixed molecules. Even though the amount of applications that achieve commercial status is still not substantial, and is expanding continuously in disciplines like “smart materials,” biosensors, delivery systems, nanoreactors and many others. A huge number of remarkable developments reported in the literature present a potential of bioartificial conjugates as a fabrics with highly controllable structure and multiple functionalities, serving as a powerful nanotechnological tool. This novel approach brings closer biologists, chemists and engineers, who sharing their effort and complement the knowledge can revolutionize the field of bioartificial polymer science.

References

[1] Yoshida R. Self-oscillating polymer gels as novel biomimetic materials. In: Ngo TD, editors. Biomimetic technologies: principles and applications Vol. 82. Osaka, Japan: Woodhead Publishing, 2015:181–198.
[2] Breslow R. Artificial enzymes. Wienheim: Wiley-VCH Verlag, 2005.
[3] Qigang Wang ZY, Zhang X, Xiao X, Chang CK, Xu B. A supramolecular-hydrogel-encapsulated hemin as an artificial enzyme to mimic peroxidase. Angew Chem Int Ed. 2007;46(23):4285–4289.
[4] Hu Weili, Shiyan Chen, Zhenhua Yang, Luting Liu, Huaping Wang, et al. Flexible electrically conductive nanocomposite membrane based on bacterial cellulose and polyaniline. J Phys Chem B. 2011;115(26):8453–8457.
[5] Gu Y., et al. Biomimetic sensor based on molecularly imprinted polymer with nitroreductase-like activity for metronidazole detection. Biosens Bioelectron. 2016;77:393–399.
[6] Dudley MF. Process for the preparation of synthetic rubber latex 1966. Google Patents.
[7] Fryling CF. Production of adhesives and adhesive bases from synthetic rubber latex by causing phase inversion with a protective colloid and adding organic solvent 1956. Google Patents.
[8] Mielzynski Felix C, Zbikowski T. Hair darts for implanting in live or artificial media 1961. Google Patents.
[9] Okazaki M, Sone M, Ueyama Y. Synthetic fibers for artificial hair and production thereof 1974. Google Patents.
[10] Rodeheaver GT, Thacker JG, Edlich RF. Mechanical performance of polyglycolic acid and polyglactin 910 synthetic absorbable sutures. Surg Gynecol Obstet. 1981;153(6):835–841.
[11] Mohammad F. Specialty polymers materials and applications. New Delhi: I. K. International Publishing House Pvt. Ltd., 2007.
[12] Yu L.S., et al. New polyurethane valves in new soft artificial hearts. ASAIO Trans. 1989;35(3): 301–304.
[13] Khomyakov KP, Virnik AD, Rogovin ZZ. The prolongation of the action of pharmaceutical preparations by mixing or combining them with polymers. Russ Chem Rev. 1964;33(9):462–647.
[14] Brady Dean JJ. Advances in enzyme immobilization. Biotechnol Lett. 2009;31:1639–1650.
[15] Bowie JU. Solving the membrane protein folding problem. Nature. 2005;438(7068):581–589.
[16] Jungbauer A, Kaar W. Current status of technical protein refolding. J Biotechnol. 2007; 128(3):587–596.
[17] Ying Liu, Fang Wang. Method for preparing S-ibuprofen and S-ibuprofen ester by biological catalysis 2008. Google Patents.

[18] Gekas VC. Artificial membranes as carriers for the immobilization of biocatalysts. Enzyme Microb Technol. 1986;8(8):450–460.

[19] Nabeshima HHS, Fujimoto M, Tsuneyuki Nagase T. Enzyme immobilization with pullan gel. Osaka, Japan: Sumitomo Chemical Company, Limited, 1981.

[20] Sekhon S.S., et al. Immobilization of para-nitrobenzyl esterase-CLEA on electrospun polymer nanofibers for potential use in the synthesis of cephalosporin-derived antibiotics. Mol Cell Toxicol. 2014;10(2):215–221.

[21] Elnashar MMM. The art of immobilization using biopolymers, biomaterials and nanobiotechnology. In: Elnashar PM, editors. Biotechnology of biopolymers. United Kingdom, Germany: InTech Europe, 2011.

[22] Trevan MD. Enzyme immobilization by covalent bonding. In: Walker JM, editors. New protein techniques. Totowa, NJ: Humana Press, 1988:495–510.

[23] Okhamafe A, Amsden B, Chu W, Goosen M. Modulation of protein release from chitosan-alginate microcapsules using the pH-sensitive polymer hydroxypropyl methylcellulose acetate succinate. J Microencapsul. 1996;13(5):497–508.

[24] Gill I, Ballesteros A. Bioencapsulation within synthetic polymers (Part 2): non-sol–gel protein–polymer biocomposites. Trends Biotechnol. 2000;18(11):469–479.

[25] Sassolas A, Prieto-Simón B, Marty J. Biosensors for pesticide detection: new trends. Am J Anal Chem. 2012;3(3):210–232.

[26] Min K, Yoo YJ. Recent progress in nanobiocatalysis for enzyme immobilization and its application. Biotechnol Bioprocess Eng. 2014;19(4):553–567.

[27] Harris TK, Keshwani MM. Chapter 7 measurement of enzyme activity. In: Richard RB, Murray PD, editors. Methods in enzymology. USA: Academic Press, 2009:57–71.

[28] Gitlesen T, Bauer M, Adlercreutz P. Adsorption of lipase on polypropylene powder. Biochimica Et Biophysica Acta (BBA) – Lipids Lipid Metab. 1997;1345(2):188–196.

[29] Singh R., et al. From protein engineering to immobilization: promising strategies for the upgrade of industrial enzymes. Int J Mol Sci. 2013;14(1):1232.

[30] Li S.-F., et al. Immobilization of pseudomonas cepacia lipase onto the electrospun PAN nanofibrous membranes for transesterification reaction. J Mol Catal B Enzym. 2011;73(1–4): 98–103.

[31] Kim M., et al. Enhanced activity and stability of organophosphorus hydrolase via interaction with an amphiphilic polymer. Chem Commun. 2014;50(40):5345–5348.

[32] Suthiwangcharoen N, Nagarajan R. Enhancing enzyme stability by construction of polymer–enzyme conjugate micelles for decontamination of organophosphate agents. Biomacromolecules. 2014;15(4):1142–1152.

[33] Yan XY, et al. Dual-functional OPH-immobilized polyamide nanofibrous membrane for effective organophosphorus toxic agents protection. Biochem Eng J. 2015;98:47–55.

[34] Gao Y., et al. Bioremediation of pesticide contaminated water using an organophosphate degrading enzyme immobilized on nonwoven polyester textiles. Enzyme Microb Technol. 2014;54:38–44.

[35] Luo J., et al. Cascade catalysis in membranes with enzyme immobilization for multi-enzymatic conversion of CO2 to methanol. New Biotechnol. 2015;32(3):319–327.

[36] Thompson M, Krull UJ, Worsfold PJ. The structure and electrochemical properties of a polymer-supported lipid biosensor. Anal Chim Acta. 1980;117:133–145.

[37] Gerard M, Chaubey A, Malhotra BD. Application of conducting polymers to biosensors. Biosens Bioelectron. 2002;17(5):345–359.

[38] Azak H., et al. Synthesis of an amine-functionalized naphthalene-containing conducting polymer as a matrix for biomolecule immobilization. RSC Adv. 2013;3(42):19582.

[39] Ekiz F., et al. Synthesis and application of poly-SNS-anchored carboxylic acid: a novel functional matrix for biomolecule conjugation. J Mater Chem. 2011;21(33):12337.

[40] Ayranci R., et al. Ferrocene-functionalized 4-(2,5-Di(thiophen-2-yl)-1H-pyrrol-1-yl)aniline: a novel design in conducting polymer-based electrochemical biosensors. Sensors. 2015; 15(1):1389–1403.

[41] Park J.-K., et al. Determination of breath alcohol using a differential-type amperometric biosensor based on alcohol dehydrogenase. Anal Chim Acta. 1999;390(1–3):83–91.

[42] Bidan G. Electroconducting conjugated polymers: new sensitive matrices to build up chemical or electrochemical sensors. A review. Sens Actuators, B. 1992;6(1):45–56.

[43] Winther-Jensen O, Kerr R, Winther-Jensen B. Alcohol vapour detection at the three phase interface using enzyme-conducting polymer composites. Biosens Bioelectron. 2014;52:143–146.

[44] Madhumathi K., et al. Preparation and characterization of novel β-chitin–hydroxyapatite composite membranes for tissue engineering applications. Int J Biol Macromol. 2009; 44(1):1–5.

[45] Mitsubayashi K., et al. A bio-sniffer stick with FALDH (formaldehyde dehydrogenase) for convenient analysis of gaseous formaldehyde. Sens Actuators, B. 2008;130(1):32–37.

[46] Webster M., et al. Tunable thermo-responsive poly(N-vinylcaprolactam) cellulose nanofibers: synthesis, characterization, and fabrication. Macromol Mater Eng. 2013;298(4):447–453.

[47] Barroso T., et al. Preparation and characterization of a cellulose affinity membrane for human immunoglobulin G (IgG) purification. J Memb Sci. 2010;348(1–2):224–230.

[48] Angelo Basile CC. Integrated membrane systems and processes. United Kingdom: Wiley, 2016.

[49] Khare P., et al. Microchannel-embedded metal–carbon–polymer nanocomposite as a novel support for chitosan for efficient removal of hexavalent chromium from water under dynamic conditions. Chem Eng J. 2016;293:44–54.

[50] Li L, Li Y, Yang C. Chemical filtration of Cr (VI) with electrospun chitosan nanofiber membranes. Carbohydr Polym. 2016;140:299–307.

[51] Teotia R.S., et al. Bifunctional polysulfone-chitosan composite hollow fiber membrane for bioartificial liver. ACS Biomater Sci Eng. 2015;1(6):372–381.

[52] Huang RYM, Pal R, Moon GY. Pervaporation dehydration of aqueous ethanol and isopropanol mixtures through alginate/chitosan two ply composite membranes supported by poly (vinylidene fluoride) porous membrane. J Memb Sci. 2000;167(2):275–289.

[53] Milella E., et al. Poly(L-lactide)acid/alginate composite membranes for guided tissue regeneration. J Biomed Mater Res. 2001;57(2):248–257.

[54] Kim YB, Kim GH. PCL/alginate composite scaffolds for hard tissue engineering: fabrication, characterization, and cellular activities. ACS Comb Sci. 2015;17(2):87–99.

[55] Croisier F, Jérôme C. Chitosan-based biomaterials for tissue engineering. Eur Polym J. 2013; 49(4):780–792.

[56] Hu J., et al. Visible light crosslinkable chitosan hydrogels for tissue engineering. Acta Biomater. 2012;8(5):1730–1738.

[57] Ahmed EM. Hydrogel: preparation, characterization, and applications: a review. J Adv Res. 2015;6(2):105–121.

[58] Arun Kumar R., et al. Injectable chitin-poly(epsilon-caprolactone)/nanohydroxyapatite composite microgels prepared by simple regeneration technique for bone tissue engineering. ACS Appl Mater Interfaces. 2015;7(18):9399–9409.

[59] Amrita A., Arora A., Sharma P., Katti D.S. Pullulan-based composite scaffolds for bone tissue engineering: improved osteoconductivity by pore wall mineralization. Carbohydr Polym. 2015;123:180–189.

[60] Laufer G., et al. Clay–chitosan nanobrick walls: completely renewable gas barrier and flame-retardant nanocoatings. ACS Appl Mater Interfaces. 2012;4(3):1643–1649.

[61] Nyholm L., et al. Toward flexible polymer and paper-based energy storage devices. Adv Mater. 2011;23(33):3751–3769.

[62] Siró I, Plackett D. Microfibrillated cellulose and new nanocomposite materials: a review. Cellulose. 2010;17(3):459–494.

[63] Chen X, Dong S. Sol-gel-derived titanium oxide/copolymer composite based glucose biosensor. Biosens Bioelectron. 2003;18(8):999–1004.

[64] Mo Zl, et al. Heterogeneous preparation of cellulose–polyaniline conductive composites with cellulose activated by acids and its electrical properties. Carbohydr Polym. 2009;75(4):660–664.

[65] Khan S., et al. Bacterial cellulose–poly(3,4-ethylenedioxythiophene)–poly(styrenesulfonate) composites for optoelectronic applications. Carbohydr Polym. 2015;127:86–93.

[66] Müller D., et al. Electrically conducting nanocomposites: preparation and properties of polyaniline (PAni)-coated bacterial cellulose nanofibers (BC). Cellulose. 2012;19(5):1645–1654.

[67] Rock M. Temperature and moisture responsive smart textile 2008. Google Patents.

[68] Filatov V.N., et al. Hemostatic textile material 2008. Google Patents.

[69] Hartmann M, Worley J, North M. Temperature regulating cellulosic fibers and applications thereof 2007. Google Patents.

[70] McNamara JJ, Ware W, Yu W. Modification of cellulosic substrates to control body odor 2014. Google Patents.

[71] Auad M.L., et al. Polyaniline-modified cellulose nanofibrils as reinforcement of a smart polyurethane. Polym Int. 2011;60(5):743–750.

[72] Bai Y., et al. A novel high mechanical strength shape memory polymer based on ethyl cellulose and polycaprolactone. Carbohydr Polym. 2013;96(2):522–527.

[73] Zhu Y., et al. Rapidly switchable water-sensitive shape-memory cellulose/elastomer nano-composites. Soft Matter. 2012;8(8):2509.

[74] Liu Y., et al. Water-induced shape-memory poly(d,l-lactide)/microcrystalline cellulose composites. Carbohydr Polym. 2014;104:101–108.

[75] Aidley DJ, Stanfield PR. Ion channels: molecules in action. Cambridge: Cambridge University Press, 1996.

[76] Zhang X., et al. Natural channel protein inserts and functions in a completely artificial, solid-supported bilayer membrane. Sci Rep. 2013;3:2196.

[77] Palivan C.G., et al. Bioinspired polymer vesicles and membranes for biological and medical applications. Chem Soc Rev. 2016;45(2):377–411.

[78] Einfalt T., et al. Stimuli-triggered activity of nanoreactors by biomimetic engineering polymer membranes. Nano Lett. 2015;15(11):7596–7603.

[79] Zhang Z., et al. A bioinspired multifunctional heterogeneous membrane with ultrahigh ionic rectification and highly efficient selective ionic gating. Adv Mater. 2016;28(1):144–150.

[80] Agre P, Kozono D. Aquaporin water channels: molecular mechanisms for human diseases. FEBS Lett. 2003;555(1):72–78.

[81] Wang M., et al. Layer-by-layer assembly of aquaporin Z-incorporated biomimetic membranes for water purification. Environ Sci Technol. 2015;49(6):3761–3768.

[82] Wagh P., et al. A new technique to fabricate high-performance biologically inspired membranes for water treatment. Sep Purif Technol. 2015;156:754–765.

[83] Xie W., et al. An aquaporin-based vesicle-embedded polymeric membrane for low energy water filtration. J Mater Chem A. 2013;1(26):7592–7600.

[84] Ding W., et al. Fabrication of an aquaporin-based forward osmosis membrane through covalent bonding of a lipid bilayer to a microporous support. J Mater Chem A. 2015; 3(40):20118–20126.

[85] Tang C.Y., et al. Desalination by biomimetic aquaporin membranes: review of status and prospects. Desalination. 2013;308:34–40.

[86] Habel J., et al. Aquaporin-based biomimetic polymeric membranes: approaches and challenges. Membranes. 2015;5(3):307.

[87] Balme S., et al. Controlling potassium selectivity and proton blocking in a hybrid biological/solid-state polymer nanoporous membrane. Nanoscale. 2013;5(9):3961–3968.

[88] Balme S., et al. New bioinspired membrane made of a biological ion channel confined into the cylindrical nanopore of a solid-state polymer. Nano Lett. 2011;11(2):712–716.

[89] Bonhenry D., et al. Stability of the gramicidin-a channel structure in view of nanofiltration: a computational and experimental study. Soft Matter. 2011;7(22):10651–10659.

[90] Saeki D., et al. Reverse osmosis membranes based on a supported lipid bilayer with gramicidin a water channels. Desalination. 2015;375:48–53.

[91] Drioli E, Di Profio G, Curcio E. Progress in membrane crystallization. Curr Opin Chem Eng. 2012;1 (2):178–182.

[92] Ye W., et al. Enhanced performance of a biomimetic membrane for Na2CO3 crystallization in the scenario of CO2 capture. J Memb Sci. 2016;498:75–85.

[93] Jeong JH, Kim SW, Park TG. Novel intracellular delivery system of antisense oligonucleotide by self-assembled hybrid micelles composed of DNA/PEG conjugate and cationic fusogenic peptide. Bioconjugate Chem. 2003;14(2):473–479.

[94] Li M., et al. Responsive polymer-protein bioconjugates prepared by RAFT polymerization and copper-catalyzed azide-alkyne click chemistry. Macromol Rapid Commun. 2008;29 (12-13):1172–1176.

[95] He P, He L. Synthesis of surface-anchored DNA-polymer bioconjugates using reversible addition-fragmentation chain transfer polymerization. Biomacromolecules. 2009;10(7):1804–1809.

[96] Wilks TR. Synthesis of DNA-polymer conjugates using RAFT polymerisation, in department of chemistry. Coventry: University of Warwick, 2013.

[97] Peterson AM, Heemstra JM. Controlling self-assembly of DNA-polymer conjugates for applications in imaging and drug delivery. Wiley Interdiscip Rev Nanomed Nanobiotechnol. 2015;
7(3):282–297.

[98] Peng L., et al. Engineering and applications of DNA-grafted polymer materials. Chem Sci. 2013;4(5):1928.

[99] Wu W, Wang W, Li J. Star polymers: advances in biomedical applications. Prog Polym Sci. 2015;46:55–85.

[100] Li J., et al. Functional nucleic acid-based hydrogels for bioanalytical and biomedical applications. Chem Soc Rev. 2016;45(5):1410–1431.

[101] Li Z., et al. Reversible and chemically programmable micelle assembly with DNA block-copolymer amphiphiles. Nano Lett. 2004;4(6):1055–1058.

[102] Ding K., et al. Engineering the structural properties of DNA block copolymer micelles by molecular recognition. Angew Chem Int Ed. 2007;46(7):1172–1175.

[103] Gaylord BS, Heeger AJ, Bazan GC. DNA detection using water-soluble conjugated polymers and peptide nucleic acid probes. Proc Natl Acad Sci. 2002;99(17):10954–10957.

[104] Ding WK, Shah NP. Acid, bile, and heat tolerance of free and microencapsulated probiotic bacteria. J Food Sci. 2007;72(9) M446-M450.

[105] Kailasapathy K. Survival of free and encapsulated probiotic bacteria and their effect on the sensory properties of yoghurt. LWT Food Sci Technol. 2006;39(10):1221–1227.

[106] Siripattanakul S, Pochant CJ, Khan E. Nitrate removal from agricultural infiltrate by bioaugmented free and alginate entrapped cells. Water Environ Res. 2010;82(7):617–621.

[107] Knierim C., et al. Blocked bacteria escape by ATRP grafting of a PMMA shell on PVA microparticles. Macromol Biosci. 2014;14(4):537–545.

[108] Nicodemus GD, Bryant SJ. Cell encapsulation in biodegradable hydrogels for tissue engineering applications. Tissue Eng Part B Rev. 2008;14(2):149–165.

[109] Zhou L., et al. Advances in cell-based biosensors using three-dimensional cell-encapsulating hydrogels. Biotechnol J. 2011;6(12):1466–1476.

[110] Orive G., et al. Cell encapsulation: promise and progress. Nat Med. 2003;9(1):104–107.

[111] Khademhosseini A., et al. Molded polyethylene glycol microstructures for capturing cells within microfluidic channels. Lab Chip. 2004;4(5):425–430.

[112] Xin X, Hussain M, Mao JJ. Continuing differentiation of human mesenchymal stem cells and induced chondrogenic and osteogenic lineages in electrospun PLGA nanofiber scaffold. Biomaterials. 2007;28(2):316–325.

[113] Partridge K., et al. Adenoviral BMP-2 gene transfer in mesenchymal stem cells: in vitro and in vivo bone formation on biodegradable polymer scaffolds. Biochem Biophys Res Commun. 2002;292(1):144–152.

[114] Lee K.G., et al. Synthesis and utilization of E. coli-encapsulated PEG-based microdroplet using a microfluidic chip for biological application. Biotechnol Bioeng. 2010;107(4):747–751.

[115] Schulte V.A., et al. Microengineered PEG hydrogels: 3D scaffolds for guided cell growth. Macromol Biosci. 2013;13(5):562–572.

[116] Knierim C., et al. Living composites of bacteria and polymers as biomimetic films for metal sequestration and bioremediation. Macromol Biosci. 2015;15(8):1052–1059.

[117] Homaeigohar S, Elbahri M. Nanocomposite electrospun nanofiber membranes for environmental remediation. Materials. 2014;7(2):1017–1045.

[118] Letnik I., et al. Living composites of electrospun yeast cells for bioremediation and ethanol production. Biomacromolecules. 2015;16(10):3322–3328.

[119] Klein S., et al. Encapsulation of bacterial cells in electrospun microtubes. Biomacromolecules. 2009;10(7):1751–1756.

Raffaele Conte, Ilenia De Luca, Anna Valentino, Anna Di Salle,
Anna Calarco, Francesco Riccitiello and Gianfranco Peluso

4 Recent advances in “bioartificial polymeric materials” based nanovectors

Abstract: This chapter analyzes the advantages of the use of bioartificial polymers as carriers and the main strategies used for their design. Despite the enormous progresses in this field, more studies are required for the fully evaluation of these nanovectors in complex organisms and for the characterization of the pharmacodynamic and pharmacokinetic of the loaded drugs. Moreover, progresses in polymer chemistry are introducing a wide range of functionalities in the bioartificial polymeric material (BPM) nanostructures leading to a second generation of bioartificial polymer therapeutics based on novel and heterogeneous architectures with higher molecular weight and predictable structures, in order to achieve greater multivalency and increased loading capacity. Therefore, research on bioartificial polymeric nanovectors is an “ongoing” field capable of attracting medical interest.

Keywords: chitosan, doxorubicin, nanofibers, poly(ethylene glycol)

4.1 Introduction

4.1.1 Bioartificial polymeric materials

“Bioartificial polymeric materials” (BPMs) are a class of polymeric composites based on the blend between synthetic and natural polymers, designed to produce new materials combining the biocompatibility of the biological components with the physical and mechanical features of the synthetics [1–3]. These materials are engineered for different applications such as biodegradable delivery systems, leak proof membranes, systems of proteins purification, dialysis membranes, wound dressing, artificial skin, cardiovascular devices, nerve guide channels, implantable devices, bone graft substitutes [4–6] and have an enormous repercussion in the human life quality [7]. Table 4.1 summarizes the main applications of these materials (Table 4.1).

4.1.1.1 Natural polymers for BPMs

Natural polymers are macromolecules produced by living organisms (e.g. plants, mammals, crustaceans) with structural or functional purposes. The main classes of natural polymers are polynucleotides, polypeptides and polysaccharides [8]. Polynucleotides act as carriers of the genetic information, polypeptides function as structural materials or catalysts, polysaccharides are components of membranes and

https://doi.org/10.1515/9783110469745-004

Table 4.1: Uses of bioartificial polymeric materials.

Area	Examples
Replacement of damaged parts	Artificial joint
Healing devices	Sutures, bone plates
Assistance of functionality	Cardiac pacemaker, ocular devices
Diagnosis	Probes
Aesthetics	Breast implants
Drug delivery	Nanoparticles, Nanofibers

Table 4.2: Natural polymers used for bioartificial polymeric materials.

Polymer	Structure	Natural derivation
Albumin	NH_2-E-A-H-K-S-E- (N terminal sequence of the protein)	Blood plasma
Chitosan	$(C_6H_{11}NO_4)_n$	Shrimp and other crustacean shells
Collagen	-(-G-Hyp-P-A-Hyp-P-)- (repeated sequence of the glycoprotein)	Animal connective tissues
Fibrin	NH_2-Q-G-V-N-D-N- (N terminal sequence of the protein)	Blood plasma
Fibroin	-(-G-S-G-A-G-A-)- (repeated sequence of the protein)	Silk
Heparin	$C_{12}H_{19}NO_{20}S_3$	Blood plasma
Hyaluronic acid	$(C_{14}H_{21}NO_{11})n$	Animal synovial fluids Microbial production

enhance intracellular communication [9]. Natural polymers are broadly used as advanced materials for the production of fibers, adhesives, coatings, gels, thermoplastics, resins, etc. and most of them have medical applications [9, 10]. (Table 4.2). These polymers possess several inherent advantages such as bioactivity, the ability to present receptor-binding ligands to cells, susceptibility to cell-triggered proteolytic degradation and natural remodeling. However, their immunogenicity, variability in purity across groups, complex structure, strength inadequacies and difficulty in controlling material degradability limit their utilization [11].

4.1.1.2 Synthetic polymers for BPMs

Synthetic polymers are petroleum-based products produced by chemical reactions. These materials are important components of BPMs thanks to their inert nature, high resistance of chemical linkages to hydrolytic and oxidative degradation and ability to tailor mechanical properties. Synthetic polymers contribute to the efficient functioning of devices providing mechanical support to implants such as articulating surfaces and scaffolds (e.g. knee and hip implants), protective coatings to improve blood compatibility, electrically stimulating devices (e.g. pacemakers, heart valves), catheters and

Table 4.3: Synthetic polymers used for bioartificial polymeric materials.

Polymer	Structure	Key properties
Poly(ethylene)	$(C_2H_4)_n$	Excellent chemical resistance Low- and high-density grades Thermoplastics features
Poly(propylene)	$(C_3H_6)_n$	Flexible with good fatigue resistance Thermoplastics features
Poly(methyl methacrylate)	$(C_5O_2H_8)_n$	Good impact strength Lightweight, transparent Poor chemical resistance Thermoplastics features
Poly(dimethyl siloxane)	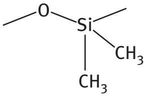	Excellent viscoelastic properties Transparent, elastic, inert, nontoxic
Poly(ether ether ketone)	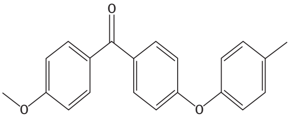	Excellent chemical resistance Excellent mechanic properties Thermoplastics features
Polyurethane	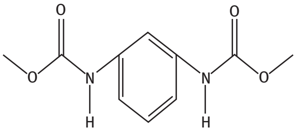	Biodegradable Biostable Thermoplastics features

dialysis tubing, vascular grafts and implantable drug delivery systems (e.g. drug eluting coatings on vascular stents). The main classes of synthetic polymers used in BPMs include poly(olefins), poly(urethanes), poly(carbonates), poly(siloxanes), poly (amides), poly(ethers), poly(sulfones) and poly(esters) [12–15]. Table 4.3 summarizes their chemical structures and general properties (Table 4.3).

4.1.2 Nanotechnology and medicine

Nanotechnology (NT) is the science of manipulating matter at the atomic or molecular scale and holds the promise of providing significant improvements in the technologies intended to enhance human well-being and protect the environment [15]. NT is often regarded as a product of the latter part of the twentieth century but it influenced human evolution from the earliest civilization. Indeed, the ancient Greeks used permanent hair-dying recipes composed of 5 nm lead sulfide crystals and European medieval artists colored stained glass using metal nanoparticles. Modern NT, started in 1959 when physicist Richard Feynman recognized the possibility to build machines able to manufacture objects with atomic precision and explained that, at the nanoscale, surface phenomena dominate the behavior of the objects [16]. The term NT, however, was

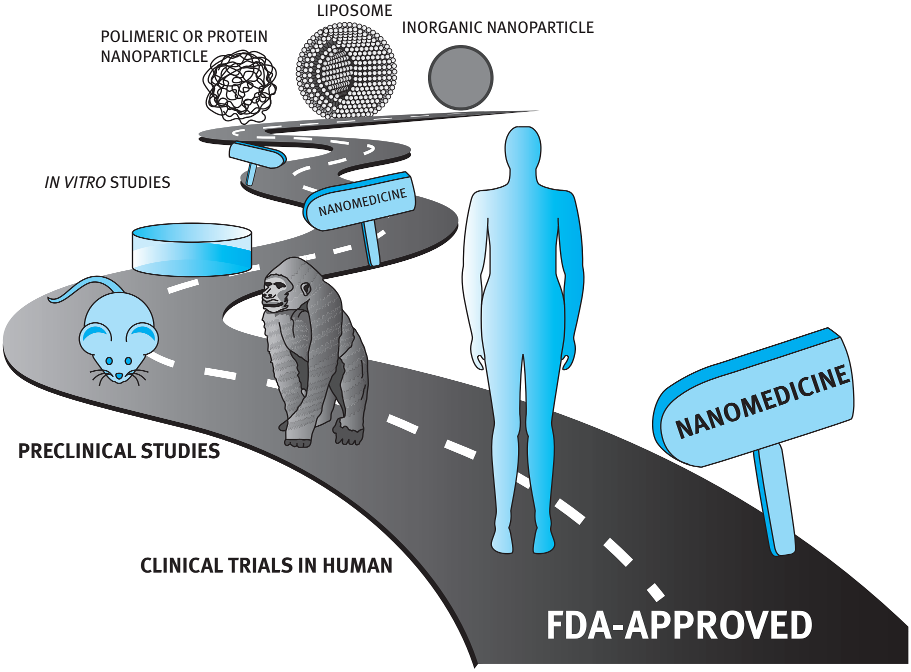

Figure 4.1: Nanovectors direction to the FDA approval.

introduced in 1974 by Norio Taniguchi referring to the “production technology to get the extra-high accuracy and ultra-fine dimensions” [17]. Practical application of NT started with the description of the molecular manufacturing [18] and the invention of the scanning tunneling microscope (STM) that allowed the first direct manipulation of individual atoms [17]. Nowadays, NT is a dynamic field where over 50,000 articles published annually and more than 2,500 patents filed [19].

Nanomedicine, an offshoot of NT, uses nano-sized tools for the diagnosis, prevention and treatment of diseases (Figure 4.1). Applicative examples are biosensors, implantable devices, prostheses components and drug delivery platforms. This chapter focuses on the delivery of therapeutic substances through bioartificial polymeric nanovectors, a novel and interesting aspect of nanomedicine.

4.2 Bioartificial polymeric nanovectors

Drug delivery is the method of administering pharmaceutical compounds to achieve therapeutic effects in humans or animals [20]. The delivery vehicles are films, plasters, gels and polymeric-based nanovectors. Among these, nano-sized delivery systems have a significant role in the alteration of bioavailability, pharmacokinetic and pharmacodynamic properties of drug molecules thanks to their favorable chemical-physical characteristics due to the reduced dimensions, their ability of delivering therapeutic agents directly into the intended site of action and their capability to overcome tight junction membrane barriers (e.g. blood brain barrier and blood-ocular-barrier) [21–24]. Nanovectors are particularly useful to transport drugs that have poor solubility or a short half-life and have numerous biological applications such as cancer therapy, stabilization and protection of molecules, proteins, peptides and DNA, analysis of environmental hazards, protein and gene delivery, action as self-regulated devices bio-recognizable systems and stimuli-controlled vectors [25–27].

BPMs are widely used as nano-sized drug delivery systems due to the synthetically controllable size, surface charge and morphology, solubility, mechanical properties and pharmacokinetic [24, 28–30]. Bioartificial polymeric nanovectors are targeted to the biological substrate using three different mechanisms: active targeting, passive targeting and endocytosis. Active targeting is an internalization method that uses receptors, surface ligands, antigen-antibody combinations or aptamers to enter targeted tissues or cells. Passive targeting takes advantage of nanosystems' physicochemical properties (e.g. small size, surface functionalization, morphology) to accumulate in target tissues. In particular, the nanovehicles are able to enter into the cells through van der Waals forces, electrostatic charges, steric interactions or interfacial tension based on the pathophysiological characteristics of the tissues (e.g. extravasation of nanovectors through the "leaky" endothelium of tumor tissue). Finally, endocytosis, the major route for nanomedicines, allows transport of nanodelivery systems across cell membrane and is generally classified into phagocytosis and pinocytosis [31–34]. The synthesis of BPM nanovectors depends on the polymeric units of the material and follows top down or bottom up approaches. "Top down" approach refers to the reduction of a bulk material to get nano-sized particle, while "bottom up" allows the build of nanoparticles starting from the monomers [35]. The technique used greatly impacts the physical, chemical and biological properties of the produced vehicles and influences their size, shape and surface chemistry [36–38]. However, clinical utilization of BPM-based nanovectors is still at the early stages and the commercialized vehicles are mainly composed of synthetic polymers. Table 4.4 summarizes the marketed polymeric nanovectors for drug delivery applications (Table 4.4).

4.2.1 Nanospheres and Nanocapsules

Nanospheres (NSs) and nanocapsules (NCs) are nano-sized vectors composed of amphiphilic copolymers structured with hydrophobic chains forming the inner part of the particles and hydrophilic portions on the surface. NSs have homogeneous solid matrices [39] while NCs exhibit a core-shell structure in which the drug is confined to a reservoir or within a cavity surrounded by a polymer membrane [40]. Both NSs and NCs allow the fine tuning of their properties through surface functionalization, the use of different shell materials and with the regulation of their size [41–43]. Poly-lactic acid (PLA), poly-glycolic acid (PGA), poly-lactic-co-glycolic acid (PLGA), poly

Table 4.4: Commercialized polymeric nanovectors for drug delivery applications.

Product	Nano-system	Payload	Therapeutic indication
Copaxone®	Polymeric drug	Poly(alanine, lysine, glutamic acid, tyrosine)	multiple sclerosis
Renagel®	Polymeric drug	Poly(allylamine)	end stage renal failure
Emmelle® gel	Polymeric drug	dextrin-2-sulphate	HIV/AIDS - vaginalvirucide
Adagen®	Polymer-protein conjugate	PEG-adenosine deaminase	severe combined immunodeficiency syndrome
Zinostatin Stimalmer®	Polymer-protein conjugate	SMANCS	cancer - hepatocellularcarcinoma
Oncaspar®	Polymer-protein conjugate	PEG-L-asparaginase	acute lymphoblastic leukamia
PEG-intron™	Polymer-protein conjugate	PEG-a-interferon 2b	hepatitis C
PEG-Asys®	Polymer-protein conjugate	PEG-a-interferon 2a	hepatitis C
Pegvisomant®	Polymer-protein conjugate	PEG-human growth hormone	acromegaly
Neulasta™	Polymer-protein conjugate	PEG-GCSF	prevention of neutropeniaassociated with cancerchemotherapy

ε-caprolactone (PCL), chitosan (CS) and polyethylene glycol (PEG) are the main materials used for the synthesis of these systems due to their wide biocompatibility and biodegradability [44–48]. NS drugs are dissolved, entrapped, encapsulated, chemically bound or adsorbed to the constituent polymer matrix [49, 50] while NCs carry the active substance in the core, or on their surfaces or absorbed in the polymeric membrane [51–53]. The use of NSs and NCs is an attractive strategy for the vectorization of a variety of active substances such as antineoplastics, antiinflammatories, immunosuppressants, antigens, hormones, antivirals, antibacterials, antifungals, diuretics, antipneumocystics and vitamins. Moreover, these systems are useful to mask unpleasant tastes, to provide controlled release properties, to protect vulnerable molecules from degradation and to increase the therapeutic efficacy of active molecules [54, 55]. Finally, NSs and NCs have high intracellular uptake and require a low amount of polymer for each particle, resulting in high drug loading [46, 49]. NSs and NCs have common preparation techniques that are classified into two general categories depending on the starting material. The use of monomers requires emulsion polymerization, interfacial polymerization or ionic gelation methods. Differently, for preformed polymers, nanoparticle preparation is achieved through emulsification/solvent evaporation, emulsification/solvent diffusion, salting out, dialysis and nanoprecipitation. The emulsion polymerization method is carried out using organic or aqueous solvents as continuous phase

[46]. Surfactants or protective soluble polymers are used to prevent aggregation in the early stages of the polymerization. The polymerization process starts using an initiator molecule (ion or free radical), or activating the monomer with high-energy radiations. Incorporation of active principles is obtained dissolving the substance in the same phase of the monomers. The interfacial polymerization is a process with a similar mechanism that involves the dissolution of two reactive agents into two phases (i.e., continuous- and dispersed-phase), with the reaction that takes place at the interface of the two liquids [56]. Interfacial polymerization permits to modulate the formation of NSs or NCs using different eluents. In fact, to promote NC formation, aprotic solvents are used, while protic liquids induce the formation of NSs [57]. Incorporation of active principles is obtained dissolving the drug into the dispersed phase. Ionic gelation permits the preparation of polymeric nanoparticles using biodegradable hydrophilic polymers such as CS, gelatin and sodium alginate. This method requires the mixture of two aqueous phases, one containing the hydrophilic polymer and the other a crosslinker (e.g. poly-anion sodium tripolyphosphate). The positive groups of the polymer interact with negative charged crosslinkers to form nano-sized vectors [58]. Drug is added in the same phase of the hydrophilic polymer [58]. Emulsification/solvent evaporation is a method that requires the preparation of the polymer solution in lipophilic volatile solvent with a subsequent formation of an emulsion, adding water and stabilizers. The lipophilic solvent diffuses through the emulsion and its evaporation lead to the formation of a nanoparticle suspension. High-speed homogenization or sonication is utilized to improve the diffusion, while the solvent evaporation is favored by continuous magnetic stirring at room temperature or under reduced pressure. The solidified nanoparticles are collected by centrifugation and washed with distilled water to remove additives [59]. Drug loading is carried dispersing the substance in the volatile solvent. Similarly, in the emulsification/solvent diffusion method, the encapsulating polymer is dissolved in a partially water soluble eluent and saturated with water to ensure the diffusion. Subsequently, the polymer-water saturated solvent phase is emulsified in an aqueous solution containing stabilizers, leading to the solvent diffusion to the external phase and to the formation of nanovectors. Drug loading is achieved dissolving the substance in the polymer phase [46]. Salting out is a modification of the emulsification/solvent diffusion in which polymer and drug are initially solubilized in the volatile solvent which is emulsified into an aqueous gel containing salting-out agents (e.g. electrolytes, such as magnesium chloride, calcium chloride, and magnesium acetate, or non-electrolytes such as sucrose) and colloidal stabilizers (e.g. polyvinylpyrrolidone or hydroxyethylcellulose). This oil/water emulsion is diluted with aqueous solutions to enhance the diffusion. The salting out agents improve the encapsulation efficiency of the drug [46]. In the dialysis methodology, the polymer is dissolved in an organic solvent and placed inside a dialysis tube. Dialysis is performed against a non-solvent miscible with the lipophilic eluent. The progressive aggregation of polymer and the formation of nanoparticles is the consequence of the displacement of the organic solvent inside the membrane [59]. Drug incorporation is obtained adding

the active principle in the same eluent of the polymer. Finally, in the nanoprecipitation method, the polymer is solubilized in a water-miscible solvent and is injected into a stirred aqueous solution containing a surfactant. The stirring causes a fast diffusion of the solvent and the polymer deposition on the interface between the water and the organic eluent, leading to the instantaneous formation of a colloidal suspension [60]. The aqueous solution must be a non-solvent of the polymer [61]. Drug encapsulation is achieved solubilizing the drug into the organic solvent [61]. A schematic representation of the described preparation techniques is available in Figure 4.2. Bioartificial polymers are widely studied as components of NSs and NCs. Such systems are described by Bellotti et al. as composed of butyl methacrylate, poly(ethylene glycol) methyl ether methacrylate, 2-(dimethylamino) ethyl methacrylate crosslinked with trimethylolpropane trimethacrylate and functionalized with folic acid on their surface in order to specific target enclosed anticancer drug to cancer cells [62]. The antitumor activity is the subject of research of several other authors. For example, Cui et al. formed ionically assembled nanoparticles from poly(ionic liquid-co-N-isopropylacrylamide) with deoxycholic acid through electrostatic interactions. These nanoparticles exhibit dual-responsive properties based on pH and thermal environment conditions with practical applications as drug delivery carriers, as shown by the encapsulation of doxorubicin.

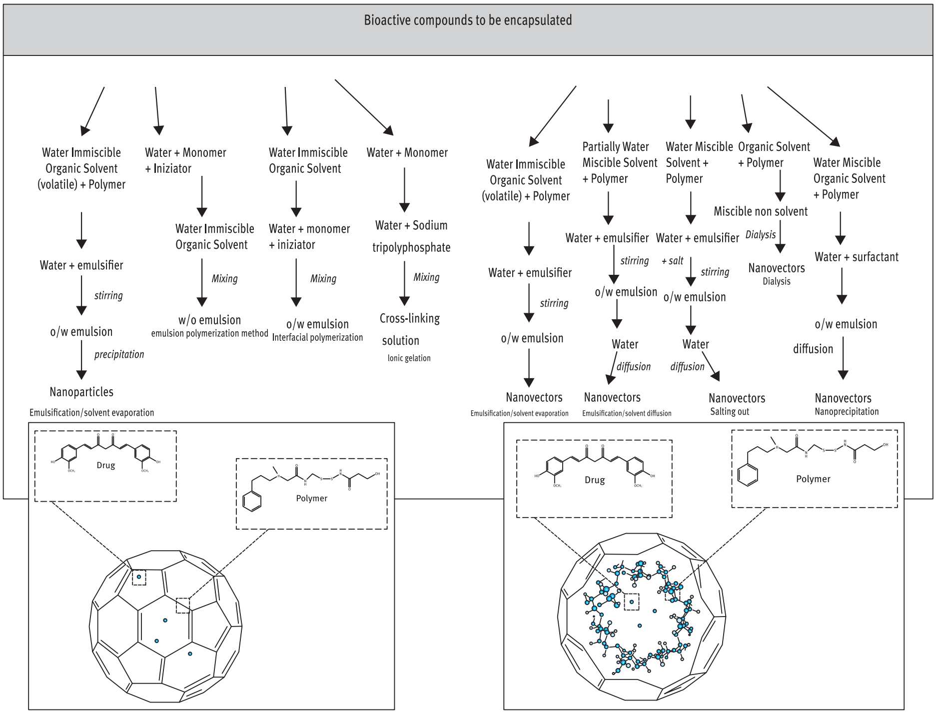

Figure 4.2: Schematic representation and manufacturing methods of nanospheres –left- and nanocapsules –right.

In particular, low pH and high temperature provoke structural collapse of the ionically assembled nanoparticle and the release of doxorubicin. In fact, 80 % of drug molecules are released within 48 h at pH 5.2, 43 °C, but only 30 % of doxorubicin is released within 48 h at 37 °C and pH 7.4 [63]. Bahadur et al. designed nanoparticles formed by poly(2-(pyridin-2-yldisulfanyl)ethyl acrylate) conjugated with PEG and cyclo(Arg-Gly-Asp-d-Phe-Cys) peptide. These nanovectors are loaded with doxorubicin. The size of the vehicle is 50.13 ± 0.5 nm in PBS. Such vectors are stable in physiological condition and release doxorubicin with the trigger of acidic pH and redox potential. Moreover, these acrylate-based nanoparticles show a two-phase release kinetics, providing both loading and maintenance doses for cancer therapy. The conjugation with the peptide enhances the cellular uptake and nuclear localization. In fact, these vectors exhibit significantly higher anticancer efficacy compared to that of free doxorubicin at concentrations higher than 5 µM [64]. Barick et al. synthesized glycine functionalized magnetite (Fe_3O_4) nanoparticles by Michael addition/amidation reaction. These nanocarriers have average size of about 10 nm and are resistant to protein adsorption in physiological medium. Moreover, the terminal amino acids on the shell of the magnetic nanocarriers allow outer functionalization and potential conjugation with drug molecules. The encapsulation of doxorubicin as model drug revealed high loading affinity, sustained release profile, magnetic-field-induced heating and substantial cellular internalization. Moreover, the enhanced toxicity to tumor cells using a local magnetic field suggests their potential for combination therapy involving hyperthermia and chemotherapy [65]. Similarly, Zhao et al. produced arginine–glycine–aspartic acid-modified Fe_3O_4 nanoparticles to control the delivery and release of doxorubicin. The conjugation of these targeted magnetite nanoparticles with the drug is *via* acid-labile imine bond. Such linkage gives magnetic control, specific targeting and pH-responsivity to the nanocarriers. The cell toxicity assays indicate higher anticancer activity of these pH-sensitive magnetic nanocarriers compared to free doxorubicin and increased cytotoxicity consequent to the conjugation with arginine–glycine–aspartic acid peptides [66]. Cheng et al. developed nanoparticles of carboxy-terminated poly(d,L-lactide-co-glycolide)-block-poly(ethylene glycol) conjugated with A10 RNA aptamers, able to bind the prostate specific membrane antigens. Such nanoparticles deliver docetaxel and paclitaxel to tumor cells. These nanovectors are evaluated in a xenograft mouse model of prostate cancer. The surface functionalization with A10 aptamers significantly enhances the delivery to tumors [67]. Patil et al. synthesized copolymer PLA–PEG nanoparticles functionalized with biotin or folic acid and incorporating paclitaxel, by solvent polymerization technique. The addiction of the ligands significantly enhances nanoparticles accumulation in tumor cells *in vitro* and results in improved efficacy of in a mouse xenograft tumor model [68]. Farokhzad et al. synthesized a bioconjugate composed of PLA-block-PEG copolymer and aptamers for targeted delivery to prostate cancer cells. These nanovectors encapsulate the model drug rhodamine labeled with dextran. Such nanoparticles present carboxylic acid groups on the particle surface, useful for functionalization and for covalent conjugation with amine-modified aptamers. Moreover, the coating of PEG enhances circulating half-life and decreases the uptake into non-targeted cells. The bioconjugation with RNA aptamers permits the targeting on prostate LNCaP epithelial cells [69]. Schiffelers et al. produced self-assembling nanoparticles with siRNA and polyethyleneimine PEGylated with an Arg-Gly-Asp (RGD) peptide ligand attached at the distal end of the PEG. These nanovectors deliver siRNA inhibiting vascular endothelial growth factor receptor-2 expression into tumor neovasculature expressing integrins. Intravenous administration of this system into tumor-bearing mice results in selective tumor uptake, siRNA sequence-specific inhibition of protein expression within the tumor and reduction of both tumor angiogenesis and growth rate [70]. Cho et al. synthesized retinoic acid loaded poly(L-lactic acid) nanoparticles coated with galactose-carrying polymer for hepatocyte-specific targeting using galactose ligands as recognition signals to asialoglycoprotein receptors. The authors study the effects of released retinoic acid on morphology and DNA synthesis of hepatocytes. Such drugs modify *in vitro* shapes of hepatocytes. Moreover, fluorescence and confocal laser microscopic studies confirm the positive influence of galactose-carrying polymers coating on nanoparticles internalization [71] Soppimath et al. synthesized core-shell nanoparticles, self-assembled from the amphiphilic tercopolymer poly(N-isopropylacrylamide-co-N,N-dimethylacrylamide-co-10-undecenoic acid) in which 10-undecenoic acid is employed as hydrophobic and pH-sensitive segment. The temperature responsiveness of the core-shell nanoparticles is triggered by a change in the environmental pH. The shell of these nanoparticles is composed of amine groups able to conjugate biological signals for specific affinities to certain cell types. Such nanoparticles, loaded with doxorubicin, are stable in PBS at 37 °C but precipitate in acidic environment, triggering the release of the enclosed drug molecules [72]. Shu et al. produced crosslinked hollow polyelectrolyte NCs composed of cysteamine conjugated CS and dextran sulfate by adsorption on β-cyclodextrin functionalized silica spheres. These NCs have enhanced physical stability against acidic pH conditions and decrease the loss of protein caused by the gastric cavity and the release of drugs in the intracellular environment after glutathione reduction. Bovine serum albumin (BSA) used as model drug exhibits spherical morphology, dimension of 120 nm, with a good polydispersion index and sustained release without the initial burst [73]. The cited vehicles are summarized in Table 4.5.

4.2.2 Nanohydrogels and nanoaggregates

Nanohydrogels (NHYs) are nano-sized networks of polymer chains able to incorporate H_2O in their structure. Usually, NHYs are macromolecular hydrocolloids with numerous hydrophilic functional groups [74]. Their composition ranges from linear water-soluble polymers to water insoluble molecules that act as swellable networks stabilized by crosslinking agents. In general, these substances have high molecular weight (5000–10000 Da) and cannot cross-biological membranes. Further, they include cellulosic components like sodium carboxymethyl cellulose or polyanion bioadhesives

Table 4.5: Bioartificial polymeric nanospheres and nanocapsules.

Nanovectors	Composition	Encapsulated drug	Reference
Nanospheres	Butyl methacrylate, poly(ethylene glycol) methyl ether methacrylate, 2-(dimethylamino) ethyl methacrylate crosslinked with trimethylolpropane trimethacrylate and functionalized with folic acid	Anti-cancer drugs	[62]
	Ionically assembled nanoparticles from poly(ionic liquid-co-N-isopropylacrylamide) with deoxycholic acid	Doxorubicin	[63]
	Poly(2-(pyridin-2-yldisulfanyl)ethyl acrylate) conjugated with polyethylene glycol and cyclo(Arg-Gly-Asp-d-Phe-Cys) peptide	Doxorubicin	[64]
	Glycine functionalized Fe_3O_4 magnetic nanoparticles	Doxorubicin	[65]
	Arginine–glycine–aspartic acid (RGD)-modified Fe_3O_4 nanoparticles	Doxorubicin	[66]
	Poly(d,L-lactide-co-glycolide)-block-poly(ethylene glycol) conjugated with A10 RNA aptamers	Docetaxel and paclitaxel	[67]
	Polylactide–polyethylene glycol nanoparticles functionalized with biotin or folic acid	Paclitaxel	[68]
	Bioconjugate composed of poly(lactic acid)-block-polyethylene glycol copolymer and aptamers	Rhodamine-labeled dextran	[69]
	Polyethyleneimine PEGylated with an Arg-Gly-Asp peptide ligand attached at the distal end of the polyethylene glycol	siRNA	[70]
	Poly(L-lactic acid) nanoparticles coated with galactose-carrying polymer	Retinoic acid	[71]
Nanocapsules	Butyl methacrylate, poly(ethylene glycol) methyl ether methacrylate, 2-(dimethylamino) ethyl methacrylate crosslinked with trimethylolpropane trimethacrylate and functionalized with folic acid	Anti-cancer drugs	[62]
	Poly(N-isopropylacrylamide-co-N,N-dimethylacrylamide- co-10-undecenoic acid)	Doxorubicin	[72]
	Cysteamine conjugated chitosan and dextran sulfate	Bovine serum albumin	[73]

like polyacrylic acid. These nanovectors are classified on the basis of the presence or absence of electrical charge located on the crosslinked chains. In fact, they are grouped as nonionic, anionic, cationic, amphoteric electrolytes or zwitterions. The surface charge regulates the adhesivity. For example NHYs, due to their capability of forming strong non-covalent bonds with the mucin, have prolonged ocular residence time and reduced dosing frequency [75]. Production of hydrogels requires the simple preparation of polymer solutions in low or intermediate concentrations and the formation of crosslinks for the prevention of the dissolution. Many crosslinking methods are currently available for hydrogel synthesis. Generally, physically crosslinked gels are those whereas physical interactions exist between polymer chains (e.g. hydrogen bonds, amphiphilic graft) while chemically crosslinked hydrogels are synthesized with covalent bonds (e.g. crosslink with aldehydes, free radical polymerization). The nanodimensions are usually obtained with sonication [76]. The medical application of nano-sized hydrogels is limited by the difficult administration of an accurate dose of active principle due to the variable release of gelified systems [75]. Nanoaggregates (NAGs) are colloidal carriers formed from amphiphilic block copolymers. In some cases, further molecules act as crosslinker agents. NAGs possess inherent properties such as high loading efficiency and *in vivo* stability. These vehicles are able to provide site-specific drug delivery via either a passive or active targeting mechanisms. NAGs are suitable for encapsulation of poorly water-soluble drugs by covalent conjugation as well as physical encapsulation. Active transport is achieved by conjugating a drug with vectors or ligands that bind specific receptors [77]. The synthesis of NHYs and NAGs is summarized in Figure 4.3. The use of bioartificial materials for the preparation of NHYs and NAGs is a novel research interest. Despite of this, a number of papers are available in literature. For example, CS-poly (acrylamide-co-methacrylic acid) hydrogels were synthesized by Ullah et al. They use different coupling agents (3-dimethylaminopropyl)-3-ethylcarbodimide hydrochloride and 3-aminopropyltriethoxysilane) and the functionalization with phenylboronic acid, a glucose sensing moiety, to design multifunctional NHYs with enhanced glucose sensitivity, stability, drug loading and release profile. Moreover, the authors study the glucose-induced volume phase transition and release profile at physiological conditions of the model drug Alizarin Red (a compound

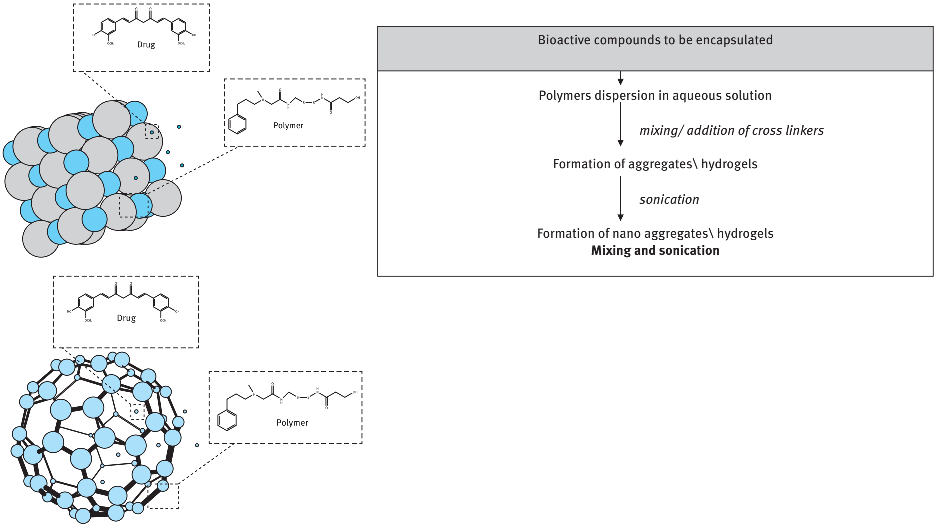

Figure 4.3: Schematic representation and manufacturing methods of nanoaggregates –top- and nanohydrogels –bottom.

Table 4.6: Bioartificial polymeric nanohydrogels and nanoaggregates.

Nanovectors	Composition	Encapsulated drug	Reference
Nanohydrogels	Chitosan-poly (acrylamide-co-methacrylic acid)	Alizarin red Insulin	[78]
	Poly *N*-isopropylacrylamide-chitosan-based nanohydrogels	Anticancer drugs	[79]
Nanoaggregates	Four-arm poly(ethylene glycol),doxorubicin, anti-bcl-2 oligonucleotides	Doxorubicin Anti-bcl-2 oligonucleotides	[80]

with 1,2-diol structure, similar to insulin) in order to find potential application in self-regulated insulin delivery with enhanced sensitivity toward glucose [78]. Jaiswal et al. synthesized poly *N*-isopropylacrylamide – CS-based NHYs encapsulating iron oxide (Fe_3O_4) magnetic nanoparticles through free radical polymerization of the acrylate in presence of CS. These NHSs are spherical shaped with size ranging from 50 nm to 200 nm on the base of the feed ratios of CS. The encapsulation of Fe_3O_4 nanoparticles into poly *N*-isopropylacrylamide–CS based NHYs is confirmed by transmission electron microscopy. This system shows optimal magnetization, good specific absorption rate and excellent cytocompatibility, finding potential applications in hyperthermia treatment of cancer and targeted drug delivery [79]. Yoon et al. produced self-assembled NAGs co-encapsulating doxorubicin and oligonucleotides through the conjugation of four-arm poly(ethylene glycol) with doxorubicin and anti-bcl-2 oligonucleotides. These conjugates are hydrophobically self-assembled into NAGs in aqueous solutions. Elemental scanning of the products reveals a core-shell structure with the drug located at the core of the vectors and the genetic materials at the shell. Analysis by dynamic light scattering and electron microscopy proves the complete disappearance of the particles under reducing conditions and the liberation of oligonucleotides at low pH. *In vitro* studies confirm the uptake of drug and oligonucleotides in cells treated with NAGs [80]. Table 4.6 recaps the described nanovectors (Table 4.6).

4.2.3 Micelles (MCs) and solid lipid nanoparticles (SLNs)

Micelles (MCs) are colloidal dispersions belonging to a large family of systems consisting of particulate matter (the “dispersed phase”), distributed within a continuous phase (the “dispersion medium”), usually constituted by water. MCs form spontaneously at certain concentration (critical micelle concentration) and temperature (critical micelle temperature) values from amphiphilic or surface active agents. Usually, these vehicles have particle size ranging between 5 and 100 nm [81, 82]. Regarding the structure, the hydrophobic fragments of amphiphilic molecules form the core of MCs, while hydrophilic fragments the shells. The formation of MCs is driven by the decrease of free energy in the system because of the removal of hydrophobic fragments from the continuous phase, and the re-establishing of hydrogen bond network in water. Moreover, additional energy results from the formation of van der Waals bonds between hydrophobic blocks in the core of the formed MCs [83]. MCs possess high stability both *in vitro* and *in vivo*, good biocompatibility and are able to solubilize a broad variety of poorly soluble pharmaceuticals through the interaction of the lipophilic substances with their hydrophobic core [84]. Many of these drug-loaded vehicles are currently at different stages of preclinical and clinical trials [85]. Micellar nano-drug delivery systems have increased water solubility, improved bioavailability, reduction of toxicity, enhanced permeability across the physiological barriers, substantial changes in drug biodistribution, extended blood half-life and protection from degradation [86]. Moreover, MCs have spontaneous interstitial penetration into the body compartments with leaky vasculature (tumors and infarcts) [87]. Active targeting of MCs is obtained through surface chemical attachment of driving molecules [88]. MCs are prepared simply dissolving the amphiphiles in water. These vectors are thermodynamically stabilized against disassembly if the amphiphilic concentration remains above the CMC. While, upon dilution below the CMC, MCs disassemble with a rate depending on the structure of the amphiphiles and on the interactions between the chains [89]. The encapsulation of molecules is obtained dissolving the substance into the micellar solution [89]. A further method of MCs preparation, useful to encapsulate non-water soluble molecules, is the thin-film hydration method. The amphiphilic copolymer and the lipophilic drug are dissolved in organic solvent. Then, the apolar eluent is removed to get the drug-containing lipid membrane. This film is resuspended in a polar solvent for nano-MCs self-assembly. The driving force of this process is the hydrophobic effect between the non-polar segments of the polymers. The hydrophobic effect also plays an important role in the drug encapsulation, stabilizing the intermolecular interaction between the substance and the hydrophobic segment [90]. SLNs are colloidal carrier systems, generally spherical in shape, composed of a high melting point lipids, as a solid core, coated by aqueous surfactants. The core lipids are fatty acids, acylglycerols and waxes, whereas phospholipids, sphingomyelins, bile salts and sterols are utilized as stabilizers [91]. SLNs are useful for the delivery of poor water soluble drugs [92]. The particle diameters are in the range of 10–1000 nm. SLNs are characterized by high biocompatibility, high bioavailability, physical stability, protection of incorporated labile drugs from degradation, excellent tolerability, prevention of problems related with multiple routs of administration, avoidance of the use of organic solvents during the preparation, formation of films over the skin showing occlusive properties and absence of problems concerning large-scale production and sterilization [93, 94]. However, common disadvantages of SLNs are particle growth, unpredictable gelation tendency, uncertain diffusion of the drug within the lipid matrix of the vector, unexpected dynamics of polymorphic transitions and inherent low incorporation rate due to the crystalline structure of the solid lipid [95, 96]. SLNs are prepared through homogenization, solvent-evaporation, microemulsion and film-ultrasound dispersion techniques. In the homogenization method, the homogenizers push a liquid with high pressure (100–2000 bar) through a narrow gap. The high shear stress and cavitation forces disrupt the particles down to the submicron range. This technique is carried in hot or cold conditions. Hot homogenization requires temperatures above the melting point of the lipid and necessitates the preparation of a pre-emulsion of the drug loaded lipid melt with the aqueous emulsifier. Higher temperatures result in lower particle sizes. In cold conditions, the drug containing lipid melt is cooled and dispersed into a cold surfactant solution. This pre-suspension is homogenized at or below room temperature, breaking the lipids in solid nanoparticles. In the solvent-evaporation method, the lipids are dissolved in a water-immiscible organic solvent that is emulsified in an aqueous solvent. The nanoparticles dispersion is obtained upon evaporation of the eluent that leads to lipid precipitation. The microemulsion technique is operated stirring a mixture of low melting fatty acids, emulsifiers and water, at 65–70 °C. This hot liquid is dispersed in cold water (2–3 °C) under stirring. The high-temperature gradient facilitates rapid lipid crystallization and prevent aggregation. Finally, in the film-ultrasound dispersion method, the lipid and the drug are put into suitable organic solution that is evaporated to form a lipid film. The following addition of an aqueous solvent results in an emulsion that is sonicated giving SLNs with uniform particle size [97]. A recap of the production methods for both MCs and SLNs is available in Figure 4.4. Bioartificial polymers are widely used in the preparation of both these vesicular systems. For example, Zhang et al. used the core crosslinking method to generate MCs able to increase curcumin delivery to HeLa cells (immortalized cancer cells) *in vitro* and improve tumor accumulation *in vivo*. These MCs are designed with folic acid-PEG as the hydrophilic unit, pyridyldisulfide as the crosslinkable and hydrophobic unit, and disulfide bond as the crosslinker. Such nanovectors show spherical shape with a diameter of 91.2 nm and high encapsulation efficiency. Cytotoxicity effectiveness is demonstrated by the high cellular uptake and the positive *in vitro* antitumor studies. The linkage with folate targets the curcumin against cancer cells and enhances the *in vivo* efficacy of these MCs [98]. Similarly, Lee et al. produced pH-sensitive polymeric MCs composed of poly(l-histidine), PEG and poly(L-lactic acid) block copolymers with folate conjugation, delivering adriamycin. These MCs are investigated for pH-dependent drug release, folate receptor-mediated internalization and cytotoxicity using MCF-7 cells (human breast adenocarcinoma cell line) *in vitro*. These nanovectors show accelerated drug release only at acidic pH. Moreover, the conjugation with folic acid enhances tumor cell kill due to folate receptor-mediated tumor uptake [99]. Li et al. reported linear PEG and dendritic cholic acids block copolymers MCs stabilized with boronate esters at the core–shell interface for efficient anticancer drug delivery. Such system is loaded with paclitaxel to assess its capacity to retain the encapsulated drug under physiological conditions and release the payload when triggered by the lower pH value of the tumor environment or by the presence of competitive diols (e.g. mannitol). This nanovector shows minimal premature drug release at physiological

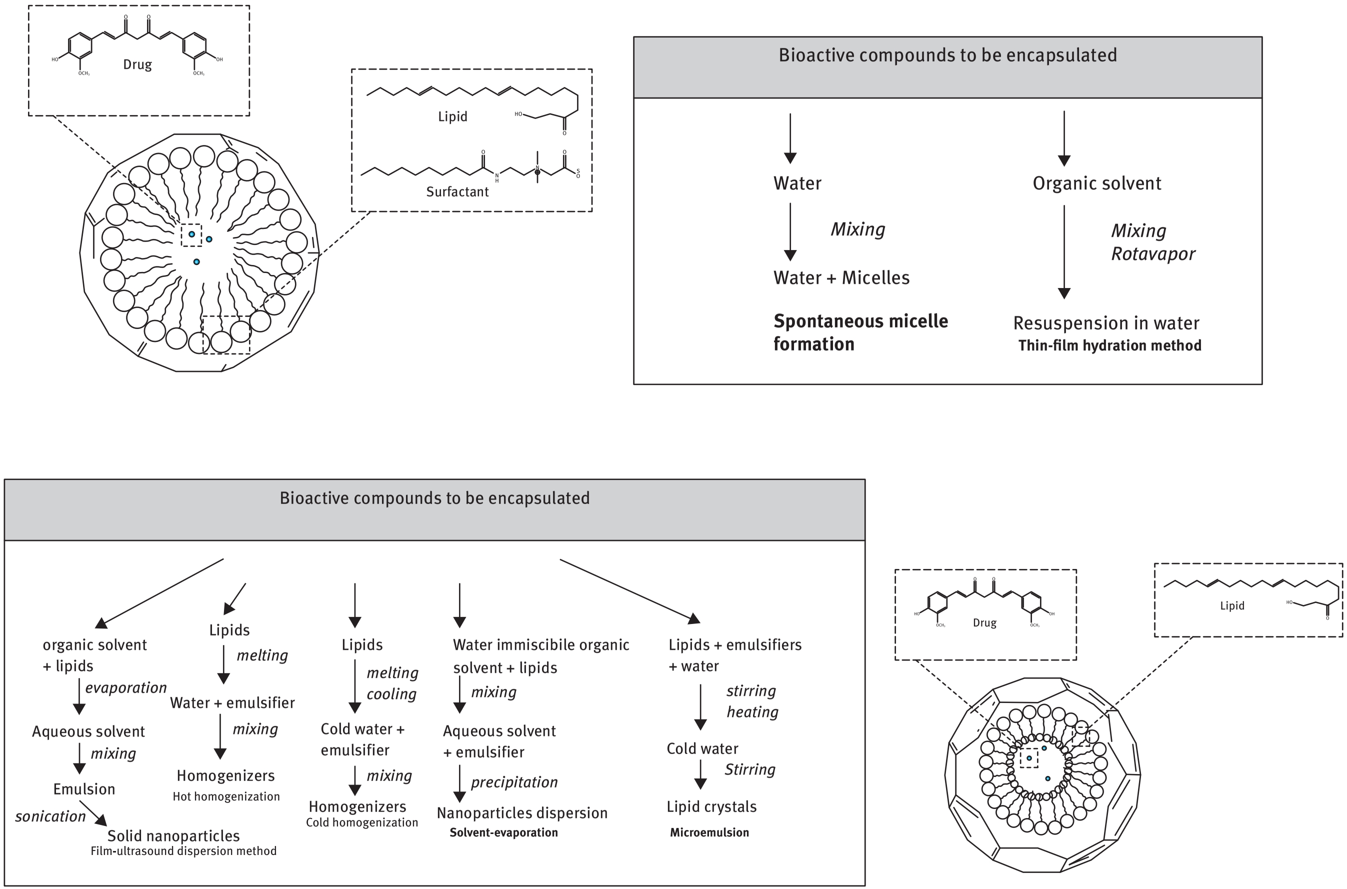

Figure 4.4: Schematic representation and manufacturing methods of micelles –left- and solid lipid nanoparticles –right.

glucose level and physiological pH values in blood circulation and simple activation at the acidic tumor microenvironment or by the additional intravenous administration of mannitol as an on-demand triggering agent [100]. Paclitaxel-loaded mixed polymeric MCs consisting of poly(ethylene glycol) distearoyl phosphoethanolamine conjugates, solid triglycerides and cationic lipofectin lipids were prepared by Wang et al. Optimized MCs have average size of about 100 nm, and zeta-potential of about −6 mV. Such vehicles are stable when stored at 4°C or at room temperature. Release of paclitaxel starts at 37 °C and, approximately, 16 % of the drug is dispensed in 72 h. *In vitro* anticancer effects of the nanovectors are evaluated using human mammary adenocarcinoma (BT-20) and human ovarian carcinoma (A2780) cell lines. The results show enhanced anti-cancer activity due to the ability of the MCs to escape from endosomes and enter the cytoplasm of BT-20 and A2780 cancer cells [101]. Lee et al. developed paclitaxel-loaded sterically stabilized SLNs for parenteral administration. These nanovectors, prepared using the hot homogenization method, are composed of trimyristin as a solid lipid core and egg phosphatidylcholine and pegylated phospholipid as stabilizers. The particles are spherical in shape, with sizes and zeta potentials of around 200 nm and −38 mV. Paclitaxel is loaded to the solid cores at a w/w ratio of 6 % with high encapsulation efficiency. *In vitro* drug release studies show a slow sustained release and high cytotoxicity on OVCAR-3 human ovarian cancer cell line and MCF-7 breast cancer cell line [102]. Gao et al. prepared poly(ethylene glycol)/phosphatidyl ethanolamine (PEG–PE) conjugates for the solubilization and delivery of various poorly soluble anticancer drugs such as m-porphyrin, tamoxifen and taxol. These MCs are stable and have the size of 10 to 40 nm [103]. Wong et al. investigated the in vivo efficacy, unwanted toxicity and loco-regional distribution of doxorubicin-loaded polymer-lipid hybrid nanoparticles formulation in a murine solid tumor model after intratumoral injection. These SLNs are prepared by dispersing the drug in stearic acid and tristearin, with subsequent addition of the hydrolyzed polymers of epoxidized soybean oil to enhance doxorubicin incorporation into the lipids. This formulation is injected intratumorally in murine solid tumors of approximately 0.3 g. *In vivo*, SLNs-treated tumors develop substantially larger central necrotic regions compared to the untreated tumors, with minimal systemic toxicity [104]. Kukowska-Latallo et al. produced polyamidoamine dendritic polymers conjugated to folic acid as targeting agent for methotrexate. These conjugates are injected intravenous into immunodeficient mice bearing human KB tumors overexpressing the folic acid receptors, resulting in high internalization into the tumor cells [105]. Table 4.7 acts as a recap of the described nanosystems.

4.2.4 Nanofibers

Nanofibers (NFs) are fibers with diameters less than 100 nanometers that exhibit special properties due to the extremely high surface to weight ratio, low density, high pore volume and tight pore size [106]. These properties make NFs suitable for

Table 4.7: Bioartificial polymeric micelles and solid lipid nanoparticles.

Nanovectors	Composition	Encapsulated drug	Reference
Micelles	Folic acid – polyethylene glycol and pyridyldisulfide	Curcumin	[91]
	Poly(l-histidine), polyethylene glycol and poly(L-lactic acid) block copolymers with folate conjugation	Adriamycin	[92]
	Linear polyethylene glycol and dendritic cholic acids block copolymers stabilized with boronate esters	Paclitaxel	[93]
	Poly(ethylene glycol)-distearoyl phosphoethanolamine conjugates, solid triglycerides and cationic lipofectin lipids	Paclitaxel	[94]
	Poly(ethylene glycol)/phosphatidyl ethanolamine	m-porphyrin, tamoxifen and taxol	[95]
Solid lipid nanoparticles	Trimyristin, egg phosphatidylcholine and pegylated phospholipid	Paclitaxel	[96]
	Stearic acid, tristearin, hydrolyzed polymer of epoxidized soybean oil	Doxorubicin	[97]
	Polyamidoamine dendritic polymers conjugated with folic acid	Methotrexate	[98]

applications ranging from medical (e.g. drug delivery systems) to industrial and high-tech fields (e.g. aerospace, capacitors, transistors, battery separators, energy storage, fuel cells) [106]. In nanomedicine, NFs are widely used due to their similarity to the extracellular matrix (ECM), the possibility to use several materials for their synthesis (in fact, natural and synthetic polymers along with several solvent systems are effectively used to create NFs) and the possibility to change their architecture in regard to porosity, diameter, mechanical properties, structure arrangement and structure functionalization [107]. The synthetic techniques for NFs are self-assembly, phase separation and electrospinning. All of these techniques require the preparation of a homogeneous drug–polymer solution that is loaded in the electrospinning machine (electrospinning technique), is simply mixed (self-assembly method) or is treated to obtain gelation and freeze-drying (phase separation) (Figure 4.5) [106, 107]. Research about NFs as drug delivery systems is at the early stage of exploration and most of the works focus on the sustained release profiles of model drugs (e.g. small molecules, herbs, proteins, DNA, genes and vaccines) using biodegradable hydrophilic, hydrophobic or amphiphilic polymers and, recently, BPMs [108]. Zhang et al. reported degradable heparin-poly (ε-caprolactone) fiber mats fabricated by electrospinning. The highly sulfated heparin heteropolymer remains homogenous in the spinning solution and is distributed throughout the fabricated polymers. The NFs release heparin for 14 days with a diffusionally controlled kinetics over this period. The drug retains its biological properties and functionality [109]. Chew et al.

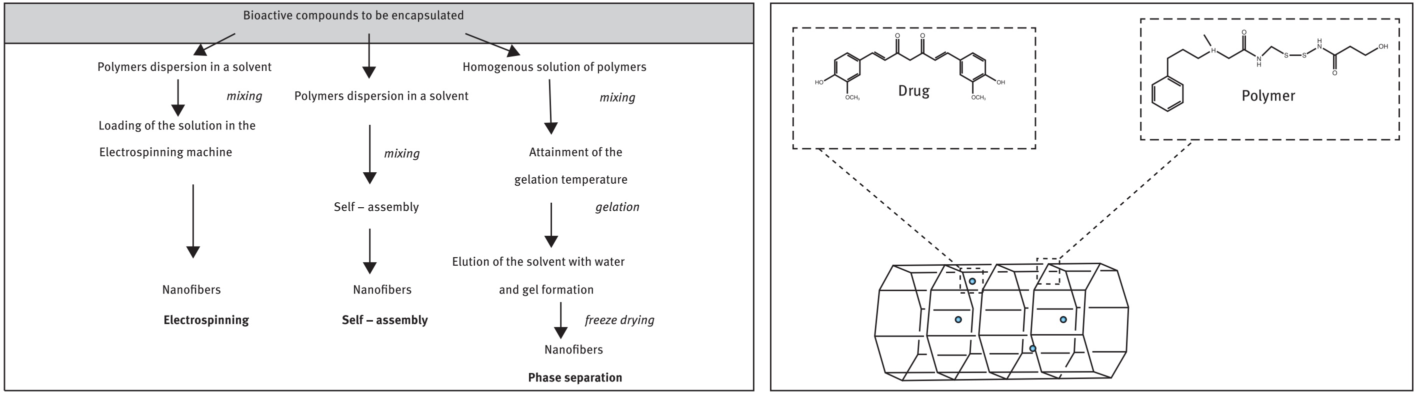

Figure 4.5: Schematic representation and manufacturing methods of nanofibers.

investigated the encapsulation of human β-nerve growth factor (NGF), stabilized in BSA carrier proteins, in a copolymer of ε-caprolactone and ethyl ethylene phosphate. The proteins are randomly dispersed throughout the electrospun fibrous mesh in an aggregated form. The sustained release of NGF by diffusion is detectable for at least 3 months and the bioactivity of the drug is retained throughout this period [110]. Feng et al. produced CS polyethylene oxide NFs with uniform diameter of 112 nm and the potential modulation of CS viscosity and surface tension through the use of different CS molecular weight and polyethylene oxide quantities. These vehicles exhibit excellent biocompatibility with hepatocytes [111]. Similarly, Bhattarai et al. reported that CS\polyethylene oxide nanofibrous scaffolds promote the attachment of human osteoblast and chondrocytes, maintaining their characteristic morphology and viability. This matrix is of particular interest for tissue engineering, drug delivery and tissue remodeling [112]. Moreover, Subramanyan et al. prepared CS\polyethylene oxide NFs for cartilage tissue engineering. These scaffolds are used for cell attach and deliver of growth factors [113]. Park et al. produced chitin/poly glycolic acid NFs with BSA coating to improve human epidermal fibroblasts attach and spread [114]. Shalumon et al. developed bioactive and biocompatible NFs composed of carboxymethyl cellulose\polyvinyl alcohol blend. Such nanomaterials are tested for cytotoxicity and cell attachment, resulting in a safe application for tissue engineering and drug delivery [115]. Nanofibrous scaffold of CS\polyvinyl alcohol and carboxyethylchitosan\polyvinyl alcohol are also prepared by Zhou et al. These materials, tested on L929 fibroblast culture, have good cell attachment and growth [116]. CS hydroxyapatite nanofibrous scaffolds are reported by Yang et al. This nanomaterial significantly stimulates the bone forming ability due to the excellent osteoconductivity of hydroxyapatite [117]. Finally, Junkasem et al. described the fabrication of α-chitin whisker-reinforced poly(vinyl alcohol) NFs by electrospinning. The α-chitin whiskers are prepared from α-chitin flakes by acid hydrolysis. Such vectors exhibit average length and width of about 549 and 31 nm, respectively. The incorporation of the chitin whiskers within the poly(vinyl alcohol) is verified by infrared spectroscopy and thermogravimetry, resulting in an increased Young's modulus of the bioartificial polymer of about 4–8 times compared to the unmodified poly(vinyl alcohol) [118]. Table 4.8 summarizes the described bioartificial polymeric NFs (Table 4.8).

Table 4.8: Bioartificial polymeric nanofibers.

Nanovectors	Composition	Encapsulated drug	Reference
Nanofibers	Heparin-poly (ε-caprolactone) fiber mats	Heparin	[102]
	Copolymer of bovine serum albumin (BSA) ε-caprolactone and ethyl ethylene phosphate	β-nerve growth factor	[103]
	Chitosan polyethylene oxide	Generic drug	[104]

4.3 Conclusion

This chapter analyzes the advantages of the use of bioartificial polymers as carriers and the main strategies used for their design. Despite the enormous progresses in this field, more studies are required for the fully evaluation of these nanovectors in complex organisms and for the characterization of the pharmacodynamic and pharmacokinetic of the loaded drugs. Moreover, progresses in polymer chemistry are introducing a wide range of functionalities in the BPM nanostructures leading to a second generation of bioartificial polymer therapeutics based on novel and heterogeneous architectures with higher molecular weight and predictable structures, in order to achieve greater multivalency and increased loading capacity. Therefore, research on bioartificial polymeric nanovectors is an "on-going" field capable of attracting medical interest.

References

[1] Lazzeri L. Trends in polymer science. Cambridge, UK: Elsevier Trends Journals, 1996.

[2] Barbani N, Lazzeri L, Lelli L, et al. Physical and biological stability of dehydro-thermally crosslinked collagen—Poly(vinyl alcohol) blends. J Mater Science Mater Med. 1994;5:882–886.

[3] Cascone MG. Dynamic–mechanical properties of bioartificial polymeric materials. Polym Int. 1997;43:55–69.

[4] Williams DF. On the nature of biomaterials. Biomaterials. 2009;30:5897–5909.

[5] Ratner BD, Bryant SJ. Biomaterials: where we have been and where we are going. Annu Rev Biomed Eng. 2004;6:41–75.

[6] Scotchford CA, Cascone MG, Downes S, Giusti P. Osteoblast responses to collagen-PVA bioartificial polymers in vitro: the effects of cross-linking method and collagen content. Biomaterials. 1998;19:1–11.

[7] Langer R, Tirrell DA. Designing materials for biology and medicine. Nature. 2004;428:487–492.

[8] Joyce Y, Wong JD. Biomaterials. Boca Raton, FL: CRC Press, 2007.

[9] Long Y. Biodegradable polymer blends and composites from renewable resources. New Jersey, USA: John Wiley & Sons, 2009.

[10] Sionkowska A. Natural polymers as components of blends for biomedical applications. In: Severian Dumitriu VP, editors. Polymeric biomaterials: structure and function Vol. 1. Boca Raton, FL: CRC Press, 2013.

[11] Parthasarathy M, Sethuraman S. Hierarchical characterization of biomedical polymers. In: Laurencin CT, Deng M, editors. Natural and synthetic biomedical polymers. Oxford, UK: Elsevier, 2014:33–42.

[12] Martina M, Hutmacher DW. Biodegradable polymers applied in tissue engineering research: a review. Polym Int. 2007;56:145–157.

[13] Nair LS, Laurencin CT. Biodegradable polymers as biomaterials. Prog Polym Sci. 2007;32: 762–798.

[14] Ulery BD, Nair LS, Laurencin CT. Biomedical applications of biodegradable polymers. J Polymer Sci B Polymer Phys. 2011;49:832–864.

[15] Place ES, George JH, Williams CK, Stevens MM. Synthetic polymer scaffolds for tissue engineering. Chem Soc Rev. 2009;38:1139–1151.

[16] Bostrom A, Löfstedt RE. Nanotechnology risk communication past and prologue. Risk Anal Off Publ Soc Risk Anal. 2010;30:1645–1662.

[17] Koodali RT, Klabunde KJ. Nanotechnology: fundamental principles and applications. In: Kent AJ, editors. Handbook of industrial chemistry and biotechnology. Boston, MA: Springer US, 2012:249–263.

[18] Drexler KE. Engines of creation. London, UK: Fourth Estate, 1996.

[19] Huang C, Notten A, Rasters N. Nanoscience and technology publications and patents: a review of social science studies and search strategies. J Technol Transfer. 2010;36:145–172.

[20] Jain KK. Drug delivery systems – an overview. In: Jain KK, editor. Drug delivery systems. Totowa, NJ: Humana Press, 2008:1–50.

[21] Davies AG, Thompson JM. Advances in nanoengineering: electronics, materials and assembly. London, UK: Imperial College Press, 2007.

[22] Mansur HS. Quantum dots and nanocomposites. Wiley Interdiscip Rev Nanomed Nanobiotechnol. 2010;2:113–129.

[23] Arzt E, Gorb S, Spolenak R. From micro to nano contacts in biological attachment devices. Proc Natl Acad Sci. 2003;100:10603–10606.

[24] Soppimath KS, Aminabhavi TM, Kulkarni AR, Rudzinski WE. Biodegradable polymeric nanoparticles as drug delivery devices. J Controlled Release Off J Controlled Release Soc. 2001;70:1–20.

[25] Takeuchi H, Yamamoto H, Kawashima Y. Mucoadhesive nanoparticulate systems for peptide drug delivery. Adv Drug Deliv Rev. 2001;47:39–54.

[26] Panyam J, Labhasetwar V. Biodegradable nanoparticles for drug and gene delivery to cells and tissue. Adv Drug Deliv Rev. 2003;55:329–347.

[27] Cao X, Lai S, Lee LJ. Design of a self-regulated drug delivery device. Biomed Microdevices. 2001;3:109–117.

[28] Cheng CJ, Tietjen GT, Saucier-Sawyer JK, Saltzman WM. A holistic approach to targeting disease with polymeric nanoparticles. Nat Rev Drug Discov. 2015;14:239–247.

[29] Faraji AH, Wipf P. Nanoparticles in cellular drug delivery. Bioorg Med Chem. 2009;17: 2950–2962.

[30] Doshi N, Mitragotri S. Designer biomaterials for nanomedicine. Adv Funct Mater. 2009;19: 3843–3854.

[31] Kamaly N, Xiao Z, Valencia PM, Radovic-Moreno AF, Farokhzad OC. Targeted polymeric therapeutic nanoparticles: design, development and clinical translation. Chem Soc Rev. 2012;41:2971–3010.

[32] Kumari A, Yadav SK, Yadav SC. Biodegradable polymeric nanoparticles based drug delivery systems. Colloids Surf, B. 2010;75:1–18.

[33] Champion JA, Mitragotri S. Role of target geometry in phagocytosis. Proc Natl Acad Sci USA. 2006;103:4930–4934.

[34] Sahoo B, Devi KS, Banerjee R, Maiti TK, Pramanik P, Dhara D. Thermal and pH responsive polymer-tethered multifunctional magnetic nanoparticles for targeted delivery of anticancer drug. ACS Appl Mater Interfaces. 2013;5:3884–3893.

[35] Nagavarma BV, Yadav HK, Ayaz A, Vasudha LS, Shivakumar HG. Different techniques for preparation of polymeric nanoparticles- A review. Asian J Pharm Clin Res. 2012;5:16–23.

[36] Dutta RK, Sharma PK, Kobayashi H, Pandey AC. Functionalized biocompatible nanoparticles for site-specific imaging and therapeutics. In: Kunugi S, Yamaoka T, editors. Polymers in nanomedicine. Berlin, Germany: Springer Berlin Heidelberg, 2012:233–275.

[37] Albanese A, Tang PS, Chan WC. The effect of nanoparticle size, shape, and surface chemistry on biological systems. Annu Rev Biomed Eng. 2012;14:1–16.

[38] Li YP, Pei YY, Zhang XY, Gu Z, Zhou Z, Yuan W, et al. PEGylated PLGA nanoparticles as protein carriers: synthesis, preparation and biodistribution in rats. J Controlled Release. 2001;71: 203–211.

[39] Amit Singh GG, Sharma PK. Nanospheres: a novel approach for targeted drug delivery system. Int J Pharm Sci Rev Res. 2010;5:84–88.
[40] Anton N, Benoit JP, Saulnier P. Design and production of nanoparticles formulated from nano-emulsion templates-a review. J Controlled Release Off J Controlled Release Soc. 2008;128: 185–199.
[41] Storm G, Belliot SO, Daemen T, Lasic DD. Surface modification of nanoparticles to oppose uptake by the mononuclear phagocyte system. Adv Drug Deliv Rev. 1995;17:31–48.
[42] Scherrmann JM, Temsamani J. The use of pep: tran's vectors for the delivery of drugs into the central nervous system. Int Congress Ser. 2005;1277:199–211.
[43] Sarti S, Bordi F. Polymeric hollow micro and nanospheres for biotechnological applications: a focused review. Mater Lett. 2013;109:134–139.
[44] Shive MS, Anderson JM. Biodegradation and biocompatibility of PLA and PLGA microspheres. Adv Drug Deliv Rev. 1997;28:5–24.
[45] Yow HN, Routh AF. Formation of liquid core–polymer shell microcapsules. Soft Matter. 2006;2: 940–949.
[46] Pinto Reis C, Neufeld RJ, Ribeiro AJ, Veiga F. Nanoencapsulation I. Methods for preparation of drug-loaded polymeric nanoparticles. Nanomed Nanotechnol Biol Med. 2006;2:8–21.
[47] Galindo-Rodriguez S, Allemann E, Fessi H, Doelker E. Physicochemical parameters associated with nanoparticle formation in the salting-out, emulsification-diffusion, and nanoprecipitation methods. Pharm Res. 2004;21:1428–1439.
[48] Prabhakar VT, Yadav A, Ratan R. Magic magic bullets - nanocapsules in future medicine. Int J Pharma Sci. 2013;3:303–308.
[49] Guterres SS, Alves MP, Pohlmann AR. Polymeric nanoparticles, nanospheres and nanocapsules, for cutaneous applications. Drug Target Insights. 2007;2:147–157.
[50] Moghimi SM, Hunter AC, Murray JC. Long-circulating and target-specific nanoparticles: theory to practice. Pharmacol Rev. 2001;53:283–318.
[51] Khoee S, Yaghoobian M. An investigation into the role of surfactants in controlling particle size of polymeric nanocapsules containing penicillin-G in double emulsion. Eur J Med Chem. 2009;44:2392–2399.
[52] Radtchenko I, Sukhorukov G, Mohwald H. A novel method for encapsulation of poorly water-soluble drugs: precipitation in polyelectrolyte multilayer shells. Int J Pharm. 2002;242:219–223.
[53] Mora-Huertas CE, Fessi H, Elaissari A. Polymer-based nanocapsules for drug delivery. Int J Pharm. 2010;385:113–142.
[54] Whelan J. Nanocapsules for controlled drug delivery. Drug Discovery Today. 2001;6:1183–1184.
[55] Barratt GM. Therapeutic applications of colloidal drug carriers. Pharm Sci Technolo Today. 2000;3:163–171.
[56] Karode SK, Kulkarni SS, Suresh AK, Mashelkar RA. New insights into kinetics and thermodynamics of interfacial polymerization. Chem Eng Sci. 1998;53:2649–2663.
[57] Puglisi G, Fresta M, Giammona G, Ventura CA. Influence of the preparation conditions on poly(ethylcyanoacrylate) nanocapsule formation. Int J Pharm. 1995;125:283–287.
[58] Dustgani A, Farahani EV, Imani M. Preparation of chitosan nanoparticles loaded by dexamethasone sodium phosphate. Iran J Pharm Sci. 2008;4:111–114.
[59] Rao JP, Geckeler KE. Polymer nanoparticles: preparation techniques and size-control parameters. Prog Polym Sci. 2011;36:887–913.
[60] Quintanar-Guerrero D, Allémann E, Fessi H, Doelker E. Preparation techniques and mechanisms of formation of biodegradable nanoparticles from preformed polymers. Drug Dev Ind Pharm. 1998;24:1113–1128.

[61] Vauthier C, Dubernet C, Fattal E, Pinto-Alphandary H, Couvreur P. Poly(alkylcyanoacrylates) as biodegradable materials for biomedical applications. Adv Drug Deliv Rev. 2003;55:519–548.

[62] Bellotti E, Barbani N, Cascone MG, Cristallini C. Development and characterization of new intelligent nanoparticles for drug targeting. In: R. Alessandro, editor Biocompatible materials for medicine. Mantova, Italy: Universitas Studiorum, 2014:187–190.

[63] Cui W, Lu X, Cui K, Niu L, Wei Y, Lu Q. Dual-responsive controlled drug delivery based on ionically assembled nanoparticles. Langmuir ACS J Surf Colloids. 2012;28:9413–9420.

[64] Remant Bahadur KC, Thapa B, Xu P. pH and redox dual responsive nanoparticle for nuclear targeted drug delivery. Mol Pharm. 2012;9:2719–2729.

[65] Barick KC, Singh S, Jadhav NV, Bahadur D, Pandey BN, Hassan PA. pH-responsive peptide mimic shell cross-linked magnetic nanocarriers for combination therapy. Adv Funct Mater. 2012;22:4975–4984.

[66] Zhao Z, Huang D, Yin Z, Chi X, Wang X, Gao J. Magnetite nanoparticles as smart carriers to manipulate the cytotoxicity of anticancer drugs: magnetic control and pH-responsive release. J Mater Chem. 2012;22:15717–15725.

[67] Cheng J, Teply BA, Sherifi I, Sung J, Luther G, Gu FX, et al. Formulation of functionalized PLGA-PEG nanoparticles for in vivo targeted drug delivery. Biomaterials. 2007;28:869–876.

[68] Patil YB, Toti US, Khdair A, Ma L, Panyam J. Single-step surface functionalization of polymeric nanoparticles for targeted drug delivery. Biomaterials. 2009;30:859–866.

[69] Farokhzad OC, Jon S, Khademhosseini A, Tran TN, Lavan DA, Langer R. Nanoparticle-aptamer nanoparticle-aptamer bioconjugates: a new approach for targeting prostate cancer cells. Cancer Res. 2004;64:7668–7672.

[70] Schiffelers RM, Ansari A, Xu J, Zhou Q, Tang Q, Storm G, et al. Cancer siRNA therapy by tumor selective delivery with ligand-targeted sterically stabilized nanoparticle. Nucleic Acids Res. 2004;32:e149.

[71] Cho CS, Cho KY, Park IK, Kim SH, Sasagawa T, Uchiyama M, et al. Receptor-mediated delivery of all trans-retinoic acid to hepatocyte using poly(L-lactic acid) nanoparticles coated with galactose-carrying polystyrene. J Controlled Release Off J Controlled Release Soc. 2001;77:7–15.

[72] Soppimath KS, Tan DC, Yang YY. pH-triggered thermally responsive polymer core–shell nanoparticles for drug delivery. Adv Mater. 2005;17:318–323.

[73] Shu S, Zhang X, Wu Z, Wang Z, Li C. Gradient cross-linked biodegradable polyelectrolyte nanocapsules for intracellular protein drug delivery. Biomaterials. 2010;31:6039–6049.

[74] Robinson JR, Mlynek GM. Bioadhesive and phase-change polymers for ocular drug delivery. Adv Drug Deliv Rev. 1995;16:45–50.

[75] Gurtler F, Gurny R. Patent literature review of ophthalmic inserts. Drug Dev Ind Pharm. 1995;21:1–18.

[76] Ahmed EM. Hydrogel: preparation, characterization, and applications: a review. J Adv Res. 2015;6:105–121.

[77] Sharma VK, Jain A, Soni V. Nano-aggregates: emerging delivery tools for tumor therapy. Crit Rev Ther Drug Carrier Syst. 2013;30:535–563.

[78] Ullah F, Othman MB, Javed F, Ahmad Z, Akil HM, Rasib SZ. Functional properties of chitosan built nanohydrogel with enhanced glucose-sensitivity. Int J Biol Macromol. 2016;83:376–384.

[79] Jaiswal MK, Banerjee R, Pradhan P, Bahadur D. Thermal behavior of magnetically modalized poly(N-isopropylacrylamide)-chitosan based nanohydrogel. Colloids Surf, B. 2010;81:185–194.

[80] Yoon S, Kim WJ, Yoo HS. Dual-responsive breakdown of nanostructures with high doxorubicin payload for apoptotic anticancer therapy. Small (Weinheim an Der Bergstrasse, Germany). 2013;9:284–293.

[81] Tanford C. The hydrophobic effect: formation of micelles and biological membranes, 2nd ed Somerset, NJ: John Wiley & Sons, 1980.

[82] Ruckenstein E, Nagarajan R. Critical micelle concentration. Transition point for micellar size distribution. J Phys Chem. 1975;79:2622–2626.

[83] Jones M, Leroux J. Polymeric micelles – a new generation of colloidal drug carriers. Eur J Pharm Biopharm. 1999;48:101–111.

[84] Torchilin VP. Micellar nanocarriers: pharmaceutical perspectives. Pharm Res. 2007;24:1–16.

[85] Cabral H, Kataoka K. Progress of drug-loaded polymeric micelles into clinical studies. J Controlled Release Off J Controlled Release Soc. 2014;190:465–476.

[86] Torchilin VP. Structure and design of polymeric surfactant-based drug delivery systems. J Controlled Release Off J Controlled Release Soc. 2001;73:137–172.

[87] Gabizon AA. Liposome circulation time and tumor targeting: implications for cancer chemotherapy. Adv Drug Deliv Rev. 1995;16:285–294.

[88] Torchilin VP. Targeted polymeric micelles for delivery of poorly soluble drugs. Cell Mol Life Sci CMLS. 2004;61:2549–2559.

[89] Allen C, Maysinger D, Eisenberg A. Nano-engineering block copolymer aggregates for drug delivery. Colloids Surf, B. 1999;16:3–27.

[90] Ai X, Zhong L, Niu H, He Z. Thin-film hydration preparation method and stability test of DOX-loaded disulfide-linked polyethylene glycol 5000-lysine-di-tocopherol succinate nanomicelles. Asian J Pharm Sci. 2014;9:244–250.

[91] Wissing SA, Muller RH. A novel sunscreen system based on tocopherol acetate incorporated into solid lipid nanoparticles. Int J Cosmet Sci. 2001;23:233–243.

[92] Schwarz C, Mehnert W, Lucks JS, Müller RH. Solid lipid nanoparticles (SLN) for controlled drug delivery. I. Production, characterization and sterilization. J Controlled Release. 1994;30:83–96.

[93] Muller RH, Mader K, Gohla S. Solid lipid nanoparticles (SLN) for controlled drug delivery - a review of the state of the art. Eur J Pharmaceutics Biopharm. 2000;50:161–177.

[94] Muller RH, Radtke M, Wissing SA. Solid lipid nanoparticles (SLN) and nanostructured lipid carriers (NLC) in cosmetic and dermatological preparations. Adv Drug Deliv Rev. 2002;54 Suppl 1 S131–S155.

[95] Attama AA, Muller-Goymann CC. Effect of beeswax modification on the lipid matrix and solid lipid nanoparticle crystallinity. Colloids and Surf, A. 2008;315:189–195.

[96] Parhi R, Suresh P. Preparation and characterization of solid lipid nanoparticles-a review. Curr Drug Discov Technol. 2012;9:2–16.

[97] Ekambaram P, Hasan Sathali AA, Priyanka K. Solid lipid nanoparticles: a review. Scientific Rev Chem Communications. 2012;2:80–102.

[98] Zhang Y, Zhou J, Yang C, Weiwei W, Liping C, Fan H, et al. Folic acid-targeted disulfide-based cross-linking micelle for enhanced drug encapsulation stability and site-specific drug delivery against tumors. Int J Nanomed. 2016;11:1119–1130.

[99] Lee ES, Na K, Bae YH. Polymeric micelle for tumor pH and folate-mediated targeting. J Controlled Release. 2003;91:103–113.

[100] Li Y, Xiao W, Xiao K, Berti L, Juntao L, Tseng HP, et al. Well-defined, reversible boronate crosslinked nanocarriers for targeted drug delivery in response to acidic ph values and cis-diols. Angew Chem Int Ed. 2012;51:2864–2869.

[101] Wang J, Mongayt D, Torchilin VP. Polymeric micelles for delivery of poorly soluble drugs: preparation and anticancer activity in vitro of paclitaxel incorporated into mixed micelles based on poly(ethylene glycol) -lipid conjugate and positively charged lipids. J Drug Target. 2005;13:73–80.

[102] Lee MK, Lim SJ, Kim CK. Preparation, characterization and in vitro cytotoxicity of paclitaxel-loaded sterically stabilized solid lipid nanoparticles. Biomaterials. 2007;28:2137–2146.

[103] Gao Z, Lukyanov AN, Singhal A, Torchilin VP. Diacyllipid-polymer micelles as nanocarriers for poorly soluble anticancer drugs. Nano Lett. 2002;2:979–982.

[104] Wong HL, Rauth AM, Bendayan R, Wu XY. In vivo evaluation of a new polymer-lipid hybrid nanoparticle (PLN) formulation of doxorubicin in a murine solid tumor model. Eur J Pharm Biopharm Off J Arbeitsgemeinschaft Fur Pharmazeutische Verfahrenstechnik Ev. 2007;65: 300–308.

[105] Kukowska-Latallo JF, Candido KA, Cao Z, Nigavekar SS, Majoros IJ, Thomas TP, et al. Nanoparticle targeting of anticancer drug improves therapeutic response in animal model of human epithelial cancer. Cancer Res. 2005;65:5317–5324.

[106] Pisignano D. Structural and surface properties of polymer nanofibers and their applications. In: Dario Pisignano, editor. Polymer nanofibers: building blocks for nanotechnology. Cambridge, UK: The Royal Society of Chemistry, 2013:189–235.

[107] Pham QP, Sharma U, Mikos AG. Electrospinning of polymeric nanofibers for tissue engineering applications: a review. Tissue Eng. 2006;12:1197–1211.

[108] Huang ZM, Zhang YZ, Kotaki M, Ramakrishna S. A review on polymer nanofibers by electrospinning and their applications in nanocomposites. Compos Sci Technol. 2003;63: 2223–2253.

[109] Yu DG, Zhu LM, White K, Branford-White C. Electrospun nanofiber-based drug delivery systems. Health. 2009;01:67–75.

[110] Chew SY, Wen J, Yim EK, Leong KW. Sustained release of proteins from electrospun biodegradable fibers. Biomacromolecules. 2005;6:2017–2024.

[111] Feng ZQ, Leach MK, Chu XH, Wang YC, Tian T, Shi XL, et al. Electrospun chitosan nanofibers for hepatocyte culture. J Biomed Nanotechnol. 2010;6:658–666.

[112] Bhattarai N, Edmondson D, Veiseh O, Matsen FA, Zhang M. Electrospun chitosan-based nanofibers and their cellular compatibility. Biomaterials. 2005;26:6176–6184.

[113] Subramanian A, Vu D, Larsen GF, Lin HY. Preparation and evaluation of the electrospun chitosan/PEO fibers for potential applications in cartilage tissue engineering. J Biomater Sci Polym Ed. 2005;16:861–873.

[114] Park KE, Kang HK, Lee SJ, Min BM, Park WH. Biomimetic nanofibrous scaffolds: preparation and characterization of PGA/chitin blend nanofibers. Biomacromolecules. 2006;7:635–643.

[115] Shalumon KT, Binulal NS, Selvamurugan N, Naira SV, Menona D, Furuikeb T, et al. Electrospinning of carboxymethyl chitin/poly(vinyl alcohol) nanofibrous scaffolds for tissue engineering applications. Carbohydr Polym. 2009;77:863–869.

[116] Zhou Y, Yang D, Chen X, Xu Q, Lu F, Nie J. Electrospun water-soluble carboxyethyl chitosan/poly(vinyl alcohol) nanofibrous membrane as potential wound dressing for skin regeneration. Biomacromolecules. 2008;9:349–354.

[117] Yang D, Jin Y, Zhou Y, Ma G, Chen X, Lu F, et al. In situ mineralization of hydroxyapatite on electrospun chitosan-based nanofibrous scaffolds. Macromol Biosci. 2008;8:239–246.

[118] Junkasem J, Rujiravanit R, Supaphol P. Fabrication of α-chitin whisker-reinforced poly(vinyl alcohol) nanocomposite nanofibres by electrospinning. Nanotechnology. 2006;17:4519–4528.

Valentina Marturano, Pierfrancesco Cerruti and Veronica Ambrogi

5 Polymer additives

Keywords: antimicrobial agents, flame retardants, polypropylene

5.1 Introduction

5.1.1 Role of polymer additives

In the present era, every activity of our life revolves around polymers and plastic materials. However, pristine polymeric materials possess unsuitable properties for such a wide range of commodity and specialty applications. The properties of a macromolecule can be tailored by incorporation of additives in their formulation, to improve both their processability and end-use [1]. Natural rubber, extracted from a *hevea* tree, was already in use by the Mayans long before the discovery and colonization of the Americas to fabricate balls or to waterproof clothes and shoes. In 1755, the French engineer and botanist François Fresneau published what is acknowledged as the first paper about rubber (submitted to the *Académie Royale des Sciences*) [2], reporting that crude rubber possessed the valuable properties of elasticity, plasticity, strength, durability, electrical non-conductivity and water resistance; however it hardened in winter, softened and became sticky in summer, it was not resistant to solvents and smelled bad. Natural rubber, named *latex* for its milky appearances, did not find its application until Charles Goodyear discovered that the addition of sulphur dramatically improved its properties, in a process called plastic vulcanization [3]: this was the first example of how additives can dramatically improve polymer properties. Polymer research and development necessarily evolves in parallel with additives technologies, especially if we consider that plastics are progressively more involved in sophisticated applications. Polymer formulations have to be accurately designed to meet the critical requirements that engineers face every day in key sectors, such as Automotive, Aeronautics, Smart Devices, Healthcare and Energy Production and Storage. According to the definition given by the European Community, an additive is “a substance which is incorporated into plastics to achieve a technical effect in the finished product, and is intended to be an essential part of the finished article.” With this chapter, we want to provide an insight into key functional additives for the end-use application of plastics. This means leaving out both structural additives (such as fibres, fillers, etc.) and processing aids (such as slipping agents, lubricants, etc.). According to the *Allied Market Research* report, the global plastic additives were

https://doi.org/10.1515/9783110469745-005

valued for $41.4 billion in 2013 and are expected to generate revenue of $57.8 billion by 2020. Also, in terms of volume, it was estimated at 12,619.8 KTons in 2013 and is expected to reach 17,071.7 KTons by 2020. The top six categories of additives with higher market demand were recognized to be plasticizers, flame retardants (FRs), impact modifiers, antioxidants, antimicrobials and UV stabilizers [4].

The European Union industrial policy is pushing industrial and academic world toward the development of sustainable alternatives to fossil-fuel based products declaring the bio-based products sector to be a priority area with high potential for future growth, reindustrialization, and addressing societal challenges [5]. In this frame, bio-based polymers have shown a steady growth over the past years, and obviously this trend has involved the search for additives "green" and not oil-based, to obtain all bio-based polymer formulations. For this reason, in this chapter, for each class of polymer additive, novel bio-based alternatives will be mentioned.

5.1.2 Additives incorporation in polymer formulation

The additives for polymer formulation are commonly found in several forms, either in solid (powders, flakes, beads, granulate, spheres, emulsions) or, more rarely, in liquid state. The final shape of the additive is influenced by the production method, namely extrusion, pelletizing, grinding, spraying or flaking.

A greater awareness of the drawbacks related to fine dust and particulate characterizes modern safety protocols; for this reason, the current trend involves modification of traditional manufacturing technologies, to provide more environmentally acceptable products endowed with greater safety, and easier to handle and mix [6]. Top challenges of polymer compounding are dust reduction, dispersion quality enhancement and dosing optimization. Ideally, additives should possess spherical form (with diameters ranging between 500 and 1,500 μm), they should ensure high homogeneity and dispersibility, suitable mechanical resistance and no segregation in the polymer matrix [7].

Over the last 15 years, additive masterbatches (i. e. concentrates containing a higher level of additives dispersed in the parent polymer) have become very popular alternatives to pure additives and have found a very wide range of applications, e. g. FRs, impact modifiers, antimicrobials, colour masterbatches, etc. The use of concentrated additive masterbatches has several advantages, if compared with pure additives, in terms of better dosability, ease of handling, homogeneous mixing, safety, additive protection and improvement of performance. Masterbatches overcome the problems of pure additives that usually require specific handling and weighted choice of processing conditions to optimize mixing/dispersing/dissolving processes.

As mentioned before, only a few additives (vitamin E is one of them) are introduced into the polymer in their liquid state, because liquids usually require different handling approach, often incompatible with high-temperature mixing technologies.

A novel technique of incorporation of viscous liquids and low-melting additives in the polymer has recently been reported [8]. The technique involves the introduction of highly concentrated liquid or temperature-sensitive additives (e. g. antistatic agents, lubricants, antioxidants, UV stabilisers, pigments and fragrances) in high-porosity carriers, namely low density polyethylene (LDPE), which allows for a very good dispersion, thanks to its spherical shape.

The incorporation of additives in the polymer matrix can be carried out in different stages of the polymer processing: during polymer production inside the reactor, during the processing stage of the finished polymer pellets by mixing or blending. Additives can also be directly applied to the surface of the finished product. The handling of solid additives has largely been reviewed [9]. For example, stabilizing additives are typically introduced during the manufacturing stage of the raw material, while high-performance additives (e. g. FRs) are introduced during the compounding stage. For specialty applications, reactive compounding techniques are employed to chemically bind reactive additives to the polymeric backbone. Virtually, from very few basic plastic types, the range of recipes and formulations is virtually inexhaustible [7].

5.2 Plasticizers

Plasticizers have been used as polymer additives since the nineteenth century; however, the human kind has known the plasticizing effect of water for thousands of years. As a matter of fact, the first clay figure found in Europe dates back to 24,000 BC, making pottery most likely the first human activity involving plasticizers. The Council of the International Union of Pure and Applied Chemistry (IUPAC) defined a plasticizer as a substance or material incorporated in a material (usually a plastic or elastomer) to increase its flexibility, workability or distensibility. By this definition, a plasticizer may reduce the melt viscosity, lower the temperature of a second order transition or lower the elastic modulus of the product.

Poly(vinyl chloride) (PVC) is the third most widely produced synthetic plastic polymer, after polyethylene and polypropylene (PP). Unmodified PVC is mainly employed in the construction industry (e. g. pipes, door and window components, etc.) where its natural rigidity is needed. However, the addition of organic molecules, known as plasticizers, can provide increased flexibility, extensibility and processability [10].

In 2014, the global plastic market involved 8.4 MTons of plasticizers, of which 80–90 % was employed in the PVC industry. The physical action of plasticizers produces a reduction of Young’s modulus, density, melt viscosity and glass transition temperature of the polymer, while they enhance the final product flexibility, deformation at break and toughness [11, 12]. For this reason, flexible PVC can be used in many applications where it can replace rubber and polyolefins, such as electrical cable insulation, inflatable products, packaging, etc.

The mechanism of plasticization involves the formation of secondary bonds between plasticizer and polymer chains, where they act like "spacers," increasing the distance of neighbour chains, hindering their interaction and increasing their mobility.

5.2.1 Mechanism of plasticisation

The concept of polymer plasticization has been adequately explained, starting from 1930s, with several theories. The classical theories are very elementary, as they were developed in the first part of twentieth century, when the knowledge on polymers was still limited.

- The LUBRICITY THEORY was developed by Kilpatrik [13] and Houwink [14] among others, in the 1940s. Plasticizers were defined as molecules with one segment strongly attracted by the polymer and another acting as lubricant. The plasticizer molecules hinder polymer–polymer interactions (van der Waals forces) between neighbour polymer chains causing a decrease in mechanical rigidity, and the plasticized formulation results in a more flexible and deformable material.
- The GEL THEORY was introduced by Aiken in parallel with the lubricity theory [15]. According to this theory, the plasticized polymer exists in an intermediate state between solid and liquid, so-called *gel state*, characterized by relatively weak secondary attractive forces. These bonding forces acting between plasticizer and polymer are easily overcome by applied external stresses, allowing the plasticized polymer to flex, elongate or compress.
- The FREE VOLUME THEORY was developed later on [16] to explain the decrease in glass transition temperature of plasticized polymers. Free volume is typically defined as the difference in specific volume between temperature T and reference temperature of absolute zero. Free volume is caused by motion of polymer end or side groups, or internal polymer motions. Unplasticized PVC at room temperature (below its glass transition temperature) shows limited motions of any kind and results in a very hard and rigid material. As plasticizers are added to the polymer, free volume is increased and various movements in the polymer chains are suddenly allowed, lowering the glass transition.
- MECHANICISTIC THEORY OF PLASTICIZATION considers the association between polymer and plasticizer as impermanent and variable. While the association can be formed and disrupted, the "strength" of each association depends on the type and quantity of plasticizer added to the formulation. The "antiplasticization" effect is therefore explained, considering that at high plasticizer loadings, plasticizer–plasticizer interactions are dominant over polymer–plasticizer interactions.

5.2.2 Classification of plasticizers

Gel theory allows plasticizers to be classified in *primary* and *secondary*, basing on the quality of the polymer–plasticizer interaction, which is strictly related to the leaching and/or migration of plasticizer molecules from polymer matrix. *Primary plasticizers* have solubility parameters close to those of polymer and are able to rapidly gel the polymer in the temperature range used during the processing step. In this case, they have a scarce tendency to "bleed" from the plasticized material. On the contrary, *secondary plasticizers* have lower gelation capacity and limited compatibility with the polymer. Therefore, after plasticization process, two separate phases can be distinctly identified: the partially plasticized polymer and the completely plasticized polymer. If a stress is applied to these materials, the resulting deformation will appear inhomogeneous, because the actual deformation occurs only in the plasticizer-rich phase. In addition to the loss of mechanical properties, another key issue of diffusion of the plasticizer is its intrinsic toxicity, which may represent a hazard for the outside environment [17]. Therefore, primary plasticizers can be used as the sole component of the plasticizer formulation, while secondary plasticizers are blended with primary ones to improve the final material properties, but are never employed alone.

The classification of plasticizers is most commonly based on their chemical composition in two classes: phthalates and non phthalates. It is now widely recognized that phthalate exposure may constitute a hazard for human health. As phthalate plasticizers are not chemically bound to PVC, they can leach, migrate or evaporate into indoor air and atmosphere, foodstuff, other materials, etc. Consumer products containing phthalates can result in human exposure through direct contact and use, indirectly through leaching into other products, or general environmental contamination [18, 19].

5.2.2.1 Phthalate plasticizers

Phthalate plasticizers are basically phthalate esters whose chemical structure is represented in Figure 5.1. Phthalates are colourless liquids, their solubility in oil, hexane and most organic solvents makes them unfortunately/likely soluble in some body fluids such as saliva or blood plasma. Two of the most commonly used plasticizers for PVC are diethylhexyl phthalate (DEHP) and diisononyl phthalate (DINP). Considering their chemical structures, reported in Table 5.1, it can be easily understood why DEHP, which remains the most used plasticizer in medical applications, has been substituted by DINP in children healthcare products. DINP is formed by longer hydrocarbon chains, possesses higher molecular weight, and therefore presents lower solubility and slower migration rates.

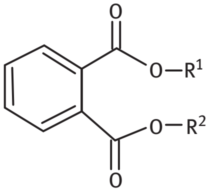

Figure 5.1: Chemical structure of a phthalic ester.

Table 5.1: Common phthalates with acronym, chemical structure and primary applications.

Phthalate name	**Abbreviation**	**Substituting group**	**Applications**
Di-*n*-butyl phthalate	DBP	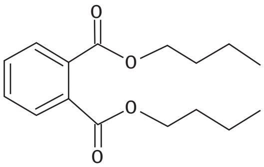	PVC, PVA and rubber
Diethylhexyl phthalate	DEHP	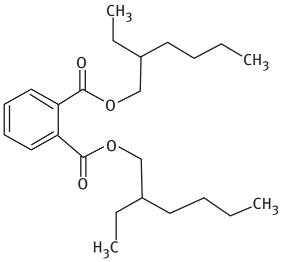	PVC (dolls, shoes, raincoats, clothing, medical devices, plastic tubing and intravenous storage bags)
Diisononyl phthalate	DINP	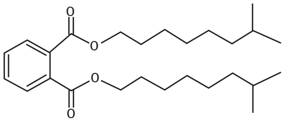	PVC (Teethers, rattles, balls, spoons, toys, gloves, drinking straws)
Diisodecyl phthalate	DIDP	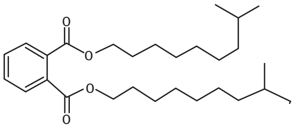	PVC (electrical cords, leather for car interiors and PVC flooring)
Benzyl butyl phthalate	BBP	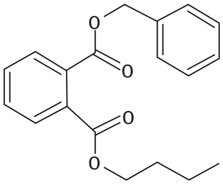	PVC, polyurethane, polysulfide (vinyl flooring, sealants, adhesives, car care products, automotive trim, food conveyor belts, food wrapping material and artificial leather)

The health risks related with the use of DEHP in PVC medical devices were reviewed by Tickner et al. [20]; moreover, DEHP has been shown to affect the development of the male reproductive system of laboratory animals [21].

However, the plasticizing efficiency is inversely proportional to chain branching. In other words, the plasticizing effect is stronger for shorter chains since the branched structure accounts for an increase in viscosity. In Table 5.1, the most commonly used phthalate plasticizers are listed, together with the chemical structure and main application.

5.2.2.2 Non-phthalate plasticizers

Other chemical compounds, potentially employed as phthalate replacement, are generally classified as non-phthalate plasticizers. In this class are included phosphoric esters, citric esters, adipates or sebacates, trimellitic esters and benzoates. Some of the listed compounds (such as adipates) are already widely used in PVC artefacts, others are solely used in niche products because their high price would not allow their use in commodity applications. Most of these alternative plasticizers are not well studied with regard to their potential effects on human health and the environment. Although many of these alternatives show promising application potential, significant exposure may lead to adverse health effects [22].

5.2.3 Bio-based plasticizers

To date, several bio-based plasticizers were tested as PVC secondary plasticizers. For example, Lim et al. [23] reported the use of palm oil-based alkyd in PVC as a co-plasticizer to dioctyl phthalate (DOP) and DINP, resulting in an enhancement of mechanical and thermal properties of the formulation. Bouchareb and Benaniba [24] also reported good results in the use of epoxidized sunflower oil as secondary plasticizer for PVC in combination with DEHP. Some plasticizer formulations based on esters of di-fatty acids have been patented [25] and are commercially available (e. g. Syncroflex TM by Croda).

Leaving aside PVC applications, natural-based products have been widely reviewed as plasticizers for bio-polymer films of different nature, such as polysaccharides (starch, cellulose, pectins, chitosan, etc.), microbial polyhydroxyalcanoates (PHAs) and polyhydroxybutyrates (PHBs) and polylactic acid (PLA). In addition to water, the most commonly used plasticizers are glycerol, polyols (such as sorbitol or xylitol) and vegetable oils [26].

5.3 Flame retardants

In the presence of heat and oxygen, all organic materials engage in a process called combustion, which constitutes the “living” force of nature on our planet. Not only combustion is at the basis of energy production of every living cell, in a controlled process known as cellular respiration, but also the ability to control fire was a dramatic change in the habits of early humans, the first of many ways by which mankind has exploited a combustion reaction in its favour. Combustion of fossil fuels is currently the chief source of energy for humanity; however, man has learned some harmful effect of fossil fuel combustion.

Like other organic substrates, polymers usually burn. Combustion of hydrocarbon macromolecules leads to the scission of polymeric chains in smaller units, which eventually are small enough to become volatile and be released in the atmosphere. These small units, formed by elements such as nitrogen, oxygen, sulphur, fluorine and chlorine, are potentially harmful [27]. For this reason, FRs are added to polymer formulations. Over 175 different FRs are on the market today and fall into three major chemical groups: halogenated, organo-phosphorous and inorganic [28].

5.3.1 Halogenated FRs

Chlorine and bromine are the only halogens used as FRs in synthetic plastic formulations, since fluorine and iodine are unsuitable for this application. Brominated flame retardants (BFRs) are by far the most widely used FRs, because they are more effective, cost less and have wider application. From an environmental point of view, however, BFRs are highly resistant to chemical, biological and photolytic degradation and are capable of long-range migration and bioaccumulation in living tissues. As a matter of fact, contamination of terrestrial and marine environment with BFRs has been widely documented [29] and traced back even to deserted location such as the Arctic [30].

BFRs can vary widely in chemical structure, from aliphatic to aromatic carbon substrates that have been per-halogenated (all hydrogens replaced with bromine atoms). In Table 5.2, the five classes of BFRs most commonly found in polymer formulations are listed, together with their chemical structure.

The mechanism of action of these FRs takes place in the gas state, induced by the high combustion temperatures. The molecules react with the radicals formed during the combustion process, according to the following reactions:

Step 1. High-energy OH and H radicals are formed by chain branching;
Step 2. The halogenated FR breaks down:
$RX \rightarrow R + X$(where X is either chlorine or bromine)
Step 3. The halogen radical reacts with hydrogen from the polymer chain to form hydrogen

Table 5.2: Common brominated flame retardants (BFRs) with acronym, chemical structure and primary applications.

Name	Abbreviation	Chemical structure
Tetrabromobisphenol-A	TBBP-A	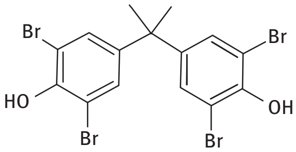
Hexabromocyclododecane	HBCD	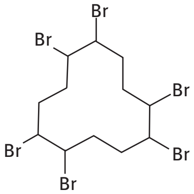
Poly-brominated diphenyl ethers (BDEs)	Penta-BDE	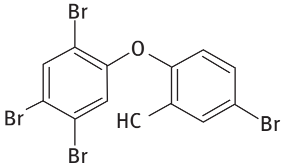
	deca-BDE	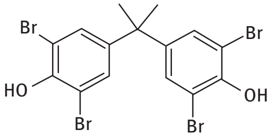

halide:
X + RH → R + HX
Step 4. Hydrogen halide interferes with the chain mechanism, high-energy H and OH

radicals are replaced with low-energy X radicals.
$HX + H \rightarrow H_2 + X$
$HX + OH \rightarrow H_2O + X$
Step 4. The hydrogen halide is regenerated by reaction with hydrocarbon:
X + RH → R + HX

5.3.2 Phosphorus-based FRs

This class of FRs incorporates phosphorus into their structure (PFRs), which can vary according to phosphorus oxidation states (0, +3, +5) [31]. The mechanism of action of PFRs in gas phase is very similar to that of BFRs. Once again, hydrogen and hydroxyl radicals can be replaced by less energetic radicals or combined to form harmless gaseous products. However, differently from BFRs, PFRs are also able to act in condensed phase by enhancing char formation, yielding intumescence (foaming-up) or formation of inorganic glasses [32]. In fact, PFRs are most commonly known as *char formers*, because during the burning process they produce phosphoric acids, which, reacting with the substrate, produce a char that acts as a protection of the substrate itself. Most used PFRs are reported in Table 5.3, their main area of application is in polyamides, polyesters, polyolefins and polystyrene (PS) formulations, especially in electrical and electronic insulation components [33].

5.3.3 Inorganic FRs

Inorganic flame retardants (IFRs) typically include aluminium and magnesium hydroxide ($Al(OH)_3$ and $Mg_2(OH)_4$). The mechanism of action of these compounds deeply differ from organic FRs. IFRs, in fact, cannot evaporate by effect of the combustion heat; however, they can decompose in non-flammable gases (mostly water [34]) by endothermic reactions [35]. Currently, aluminium hydroxide is the most commonly employed IFR, due to low cost and good compatibility with most plastic materials, especially PVC and PE. $Al(OH)_3$ decomposition occurs between 180 and 200 °C according to the endothermic reaction reported below:

$$2\mathrm{Al(OH)}_3 \rightarrow \mathrm{Al_2O_3} + 3\mathrm{H_2O}$$

The endothermic decomposition of aluminium hydroxide primarily leads to the cooling of polymer and the formation of a protective layer of aluminium oxide. Moreover, the formation of water vapour decreases the oxygen concentration near the surface, hindering the combustion reaction.

Magnesium hydroxide ($Mg_2(OH)_4$) has the same flame retardancy effect of aluminium hydroxide, but a different range of decomposition temperature (300–330 °C); therefore, it can be employed in engineering polymers, such as PPs and polyamides (PA), which are usually processed at higher temperatures.

5.3.4 Bio-based FRs

Most of the commercially available FR formulations have adverse effect in the environment, because their chemical components are capable of leaching and

Table 5.3: Common phosphorous-based flame retardants (PFRs) with acronym, chemical structure and primary applications.

Name	Acronym	Chemical structure
Triaryl phosphates	–	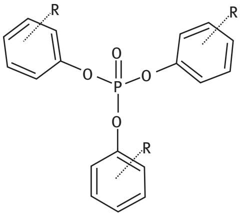
Resorcinol bis(diphenylphosphate)	RDP	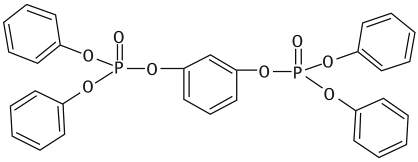
Tris(chloropropyl) phosphate	TCPP	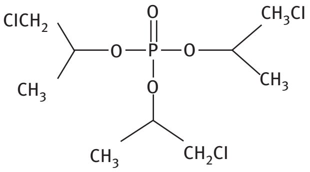
Phosphinic acid derivatives	–	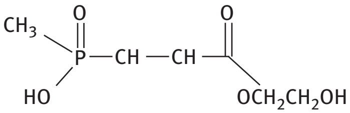
Ammonium polyphosphate	APP	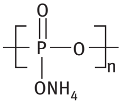
Red phosphorous	–	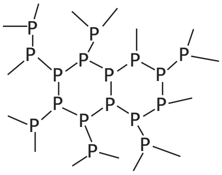

bio-accumulation, contaminating water and fields and polluting the atmosphere.

In most cases, IFRs that contain minerals very common in nature, such as aluminium and magnesium hydroxide, are actually produced through synthetic procedures using bauxite as a rough material. It was estimated that the total volume of natural IFRs ranged around 37 TTon/year (2010), constituting only about 5 % of all mineral filler FRs [36].

It has been found that the addition of natural zeolites to thermoplastic polymers provides a synergistic effect on traditional FRs [37]. However, a more sustainable approach is pushing towards all bio-based formulations. Das and Karak [38] suggested that the incorporation of nanoclays in a vegetable oil-based epoxy resin would provide self-extinguishing properties. The most extensively studied nanoclays in use are based on montmorillonite, exfoliated and added to the polymer matrix in flaky shapes [39].

Another natural material involved in FR formulations is cellulose. Not only cellulose is the world's most abundant, renewable, inexpensive and biodegradable polymer, it is also prone to chemical modification. Phosphorus can be covalently attached to the cellulose chain, forming phosphorylated cellulose derivatives whose flame retardancy action takes place during heating, dehydrating the polysaccharide molecules and promoting the consequent char formation [40].

5.4 Impact modifiers

Most plastic materials suffer from excessive brittleness; in other words they break without significant deformation when subjected to a stress. Unmodified PVC or PS are brittle at room temperature, polyamides and polyolefins instead are ductile at room temperatures and become brittle at low temperatures. An impact modifier is needed whenever the polymer does not meet impact requirements in the specific application.

Rubber toughening of PVC was introduced in the 1930s and 1940s and involved the addition of small amounts of acrylonitrile–butadiene copolymer elastomer (NBR) and other elastomeric materials [41]. The traditional purpose of impact modifiers is to absorb the impact energy by inducing plastic deformation before craze or crack propagation can occur.

In general, impact modifiers are elastomeric or rubbery in nature, with a lower modulus compared to the polymer matrix and a low glass transition temperature (T_g). The rubbery phase should also show good compatibility to the host polymer and a fine particle size distribution.

Impact modifiers can be either incorporated in the polymerization reaction (e. g. acrylonitrile-butadiene-styrene (ABS) block copolymers [42]) or incorporated as solid particulate in the processing step as particles. In Table 5.4, the most common impact modifiers are listed with their relative contribution to the global market [43], while chemical composition of the most common classes of impact modifiers, with their chemical structure and commercial trade names are listed in **Table 5.5**.

Table 5.4: Global market contribution of the most common impact modifiers.

Impact modifier	Contribution to global market
ABS – acrylonitrile-butadiene-styrene terpolymers	45 %
MBS – methacrylate-butadiene-styrene terpolymers	
Acrylics	30 %
Elastomers	10 %
CPE – Chlorinated polyethylene	10 %
Others	5 %

Table 5.5: Chemical composition of the most common classes of impact modifiers, their chemical structure, commercial name and suppliers available in the market.

Class of impact modifiers	Chemical composition	Chemical structure	Trade name (Supplier)
Butadiene-based modifiers	Acrylonitrile-butadiene-styrene	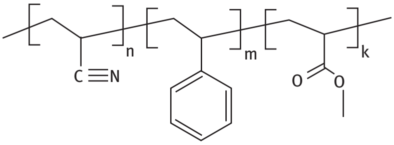	Blendex® 333 (Galata Chemicals)
	Methacrylate-butadiene-styrene	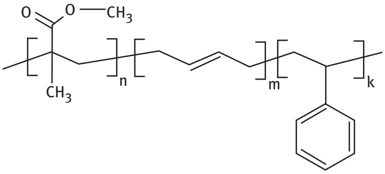	Paraloid™ EXL-2678 (Dow Chemical)
Acrylic modifiers	Acrylonitrile-styrene-acrylate	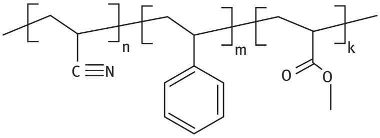	Shinepoly™ LP2068 (Shine Polymer Technology)
Elastomers	Ethylene-propylene copolymer	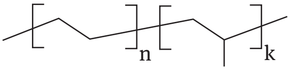	Elvaloy® HP 4051 (Du Pont)

5.4.1 Butadiene based graft copolymers

Butadiene based graft copolymers constitute alone 45 % of the global impact modifiers market. Their success in mainly due to their very low T_g (–80 °C). On the other side, one of the main drawbacks is their sensitivity to thermal and oxidative degradation, due to the presence of double bonds in diene polymers. During processing step and final application, the polymer undergoes severe temperature stress and UV and oxygen exposure; therefore, the formulations should include also suitable antioxidants (see Section 5.5) [44].

5.4.1.1 ABS modifiers

By far the most used graft terpolymer, ABS earns its unique properties by the combinations of the three components: soft rubbery effect is provided by butadiene while acrylonitrile and styrene give the terpolymer the polarity needed for compatibilization to the polymer matrix. As mentioned before, the butadiene chain is susceptible to UV degradation and requires protection while the acrylonitrile brings rigidity and chemical resistance. ABS is very reliable in a wide range of temperatures (between −20 and 80 °C), it is very light and prone to be injection moulded and extruded, as well as 3D printed. For these reasons, ABS has found a wide range of applications in engineering polymers in buildings and constructions, automotive, electronics and many others. A drawback of ABS impact modifiers stands in the development of carcinogenic chemicals and ultrafine particles during the process and final disposal [45, 46].

5.4.1.2 MBS modifiers

Similar to ABS, MBS (methacrylate-butadiene-styrene) impact modifiers are produced according to two different procedures: copolymerization of styrene and methyl methacrylate in the presence of polybutadiene or polymerization of methyl methacrylate in the presence of a styrene butadiene rubber. Once again, butadiene makes these materials susceptible to UV degradation and limits their use to indoor applications. The presence of methacrylate instead of acrylonitrile provides a unique transparency to the polymer but at the same time reduces its chemical resistance. MBS modifiers are mainly applied in PVC in transparent and opaque packaging applications such as impact resistant bottles, packaging films and electrical covers [47]. MBS impact modifiers demonstrated a significant impact-modifying effect at low temperatures. However, in many cases, the addition of a large amount of the MBS impact modifiers is required to enhance impact strength [48].

5.4.2 Acrylic modifiers

PVC formulations directed to outdoor applications require special attention in order to achieve long-time structural and aesthetical properties. In this frame, acrylic modifiers are probably the most widely used impact modifiers as they overcome the problems associated with the limited resistance to weathering phenomena, typical of ABS and MBS. The typical chemical structure of this class of modifiers is that of a graft terpolymer of methyl methacrylate-butyl acrylate-styrene or acrylonitrile-styrene-acrylate. Other advantages of such formulations are the high impact strength, good heat resistance and good thermal stability [49].

5.4.3 Elastomers

The impact strength of polyolefins can be optimized by introducing in the homopolymer formulations a wide variety of elastomers such as ethylene-propylene copolymer (EPM) or ethylene-propylene diene terpolymer (EPDM). The investigation on macroscopic and morphological properties of PP/impact modifiers blends dates back to the 1970s [50].

5.5 Antioxidants and UV stabilizers

5.5.1 Antioxidants

The resistance of polymeric materials to weathering is a key issue if we take into account the wide range of applications in which plastic products are exposed to outdoor environment. Weathering does not simply result in aesthetic decay, such as discoloration, but also changes in mechanical properties. Weathering phenomena includes mainly thermal- or UV light-induced oxidative phenomena, as well as day/night or seasonal temperature variation, humidity and atmospheric contamination with highly corrosive elements [51].

Starting from the 1940s, the phenomenon of polymer degradation *via* oxidation has been the centre of scientific research in parallel with the spread of polymeric materials in many specialty and commodity applications. The degradation process involves the oxygen-induced formation of reactive oxygen species (ROS), also known as free radicals, which eventually leads to the modification of the macromolecular structure by chain scission or crosslinking. This process is frequently called autoxidation because it proceeds by an autoaccelerated radical chain mechanism.

In the initiation step, a hydrogen atom is extracted by an excited oxygen or a free radical from the hydrocarbon chain, forming an organic radical. Further reaction of organic radicals with oxygen leads to the formation of polymer hydroperoxides (ROOH). Consequently, hydroperoxides and their decomposition products are responsible for the changes in molecular structure and molar mass of the polymer, which are manifested in practice by the loss of mechanical properties (e. g. impact, flexure, tensile, elongation) and by the variation in the physical properties of polymer surface (e. g. loss of gloss, reduced transparency, cracking, yellowing, etc.).

During autoxidation, the radical reaction cyclically goes through four steps: initiation, propagation, branching and termination, as described in Figure 5.2. During the initiation step (Figure 5.2-1), the primary alkyl radical is formed from

Chain initiation

$$\left.\begin{array}{l}\mathrm{R{-}H}\\ \mathrm{R{-}R}\end{array}\right\}\mathrm{R}\bullet \qquad (1)$$

Chain propagation

$$\mathrm{R}\bullet + \mathrm{O_2} \longrightarrow \mathrm{ROO}\bullet \qquad (2)$$

$$\mathrm{ROO}\bullet + \mathrm{RH} \longrightarrow \mathrm{ROOH} + \mathrm{R}\bullet \qquad (3)$$

$$\mathrm{RO}\bullet + \mathrm{RH} \longrightarrow \mathrm{ROH} + \mathrm{R}\bullet \qquad (4)$$

$$\bullet\mathrm{OH} + \mathrm{RH} \longrightarrow \mathrm{H_2O} + \mathrm{R}\bullet \qquad (5)$$

Chain branching

$$\mathrm{ROOH} \longrightarrow \mathrm{RO}\bullet + \bullet\mathrm{OH} \qquad (6)$$

$$\mathrm{2ROOH} \longrightarrow \mathrm{RO}\bullet + \mathrm{ROO}\bullet + \mathrm{H_2O} \qquad (7)$$

Chain termination

$$\mathrm{R}\bullet + \mathrm{ROO}\bullet \longrightarrow \mathrm{ROOR} \qquad (8)$$

$$\mathrm{R}\bullet + \mathrm{R}\bullet \longrightarrow \mathrm{R{-}R} \qquad (9)$$

$$\mathrm{R}\bullet + \mathrm{RO}\bullet \longrightarrow \mathrm{R{-}O{-}R} \qquad (10)$$

Figure 5.2: General diagram of autoxidation (Polymer additives handbook, Zweifel).

polymer interaction with molecular oxygen [9]. The formed polymeric radical P• further reacts with molecular oxygen forming the peroxy intermediate radical POO• (Figure 5.2-2**)**. The rate-determining step in autoxidation can be identified in the abstraction of a hydrogen, corresponding to the disruption of a C-H bond, which stabilizes the formed peroxy radical POO•(Figure 5.2**-**3). Chain termination is promoted, in oxygen deficiency conditions, by combination of the various radical species shown in Figure 5.2 – 8, 9 and 10.

Oxidative degradation in polymers can be inhibited by addition in the polymer formulation of proper stabilizing additives, called antioxidants (AOs). In Figure 5.3, the cyclical degradation mechanism is schematized, highlighting the reactive species (polymer and peroxy radicals, and hydroperoxides) susceptible of the intervention of such additives in different steps of the reaction.

AOs are generally classified into two groups, according to their protection mechanism [52]:

- Primary antioxidants also known as chain-breaking antioxidants. These AOs are able to scavenge free radicals via a process called chain-breaking electron donor mechanism. Two classes of primary AO can generally be identified: radical scavengers (chain-breaking acceptors) and H-donors (chain-branching donors).
- Secondary antioxidants are able to decompose hydroperoxides (POOH) forming inert secondary products and therefore are also known as hydroperoxide decomposers.

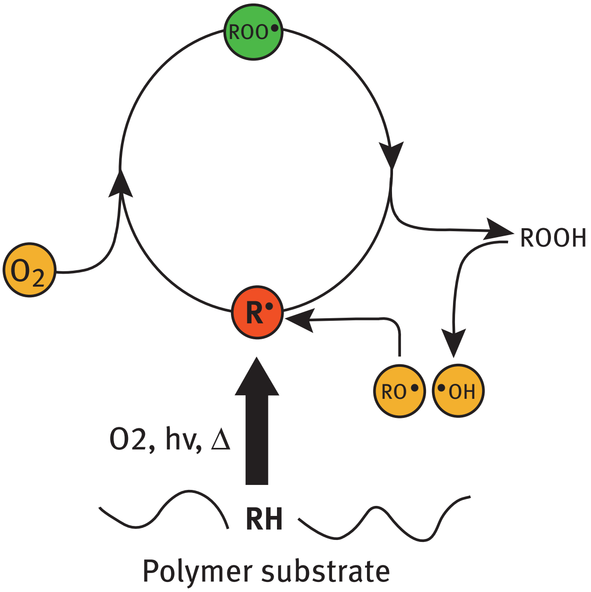

Figure 5.3: Autoxidation mechanism as represented in Zweifel, 1988.

5.5.1.1 Radical Scavengers

The reaction of radical scavenging induces the immediate disruption of the autoxidation mechanism. It is extremely difficult to scavenge alkoxy (RO•) or hydroxyl (•OH) radicals because they are extremely reactive [53]; therefore, the mechanism of action of radical scavengers is focused on the stabilization of carbon centred alkyl radicals (R•). Lactones and acrylated bis-phenols are the most effective classes of scavengers.

Lactones are a class of cyclic esters suitable as alkyl radical scavengers, in particular benzofuranone derivatives are very effective even in low concentrations [54]. Their mechanism of actions is described in Figure 5.4.

Other very effective radical scavengers are the acrylated bis-phenols; this class of stabilizers are widely used in styrene copolymers (such as SBS), preventing the degradation or crosslinking that often occurs during the processing steps. Their mechanism of action is similar to the one studied in hindered phenols, and is schematized in Figure 5.5.

5.5.1.2 H-donors

Usually containing aromatic or phenolic rings, these antioxidants donate a hydrogen atom (H) to the free radicals formed during oxidation. H-donor therefore becomes a radical itself but is able to reach stabilization via resonance delocalization of the electron within the aromatic ring [55]. In case further abstraction of a hydrogen from

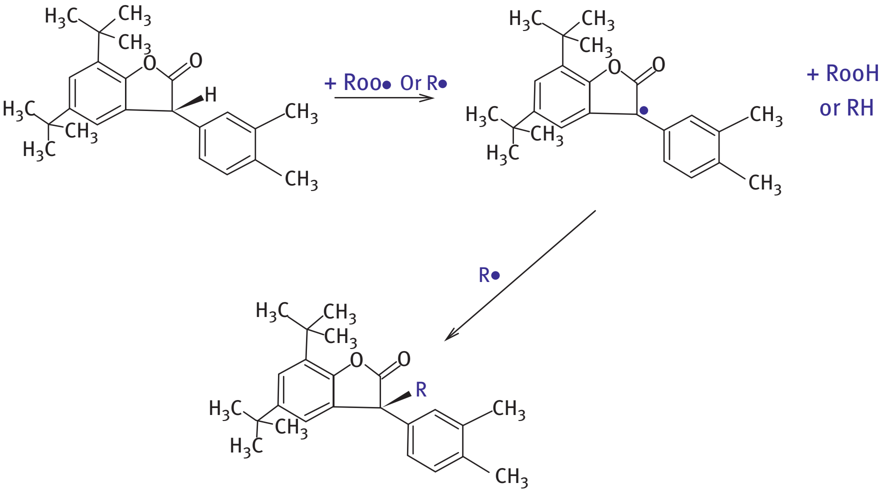

Figure 5.4: Radical scavenging activity of benzofuranone derivatives.

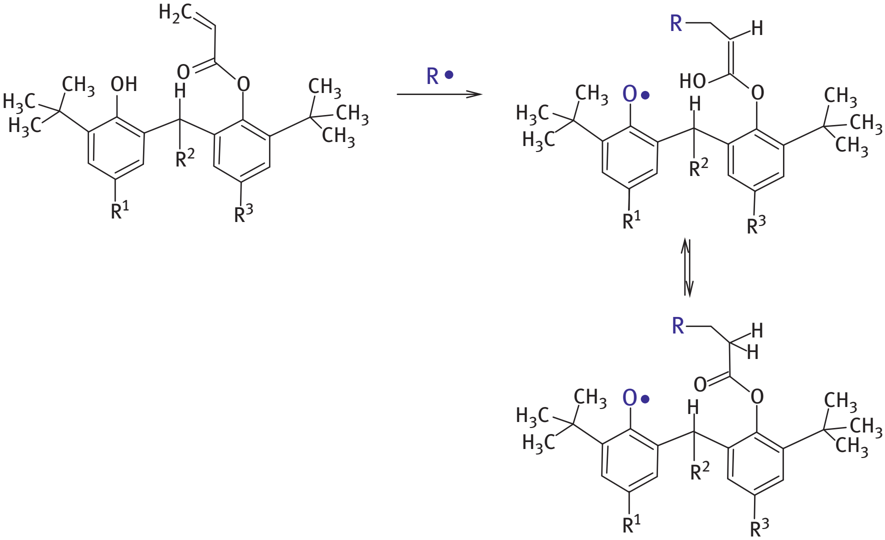

Figure 5.5: Radical scavenging activity of acrylated bis-phenols.

polymeric backbone results hindered, the H-donor is considered suitable as polymer additive [56]. Two of the most effective H-donor compounds are aromatic amines and hindered phenols. Aromatic amines, in particular secondary aromatic amines and diamines, are the most efficient hydrogen donors; however, their application in

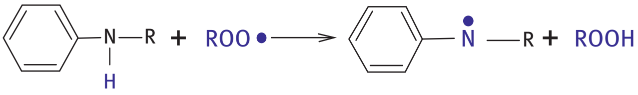

Figure 5.6: Deactivation of ROO* radicals by means of secondary aromatic amines.

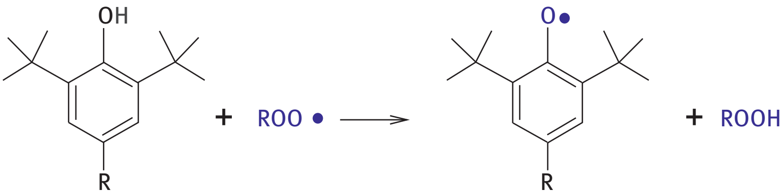

Figure 5.7: Deactivation of ROO* radicals by hindered phenols.

plastics is limited for their carcinogenic effect known since the 1970s [57]. The reaction of deactivation of peroxy radicals by secondary aromatic amines is reported in Figure 5.6.

The safety issues related to the aromatic amines make hindered phenols the most widely used stabilizers for polymers. The antioxidant effect of natural phenols, such as α-tocopherol (vitamin E), is widely reported in literature [58].

Often used in combination with secondary antioxidants, phenolic stabilizers are offered in an extensive range of molecular weights, product forms and functionalities. They are effective during both processing and long-term aging, and many have the Food and Drug Administration (FDA) approvals. The reaction of radical deactivation involving hindered phenols is represented in Figure 5.7 [59].

The phenoxy radicals generated are very stable due to their ability to build numerous mesomeric forms.

5.5.1.3 Hydroperoxide decomposers

Hydroperoxide decomposers belong to the class of secondary antioxidants; these compounds are able to convert the hydroperoxide radicals into non-radical stable products. Their use in combination with primary antioxidants often yields synergistic stabilization effects. According to their general mechanism, the hydroperoxide group (ROOH) is reduced to an alcohol group (ROH) while the decomposer is oxidized. The most widely used classes of hydroperoxide decomposers are organic compounds containing phosphorous and sulphur, respectively, called organophosphorous and thiosynergists.

Organophosphorus compounds are extremely effective stabilizers during polymer melt processing and are commonly used in formulations containing a primary antioxidant, especially hindered phenols. The reaction of organophosphorous

$$(RO)_3\text{—}P + ROOH \longrightarrow (RO)_3\text{—}P{=}O + ROH$$

Figure 5.8: Decomposition of hydroperoxides by means of organophosphorus compounds.

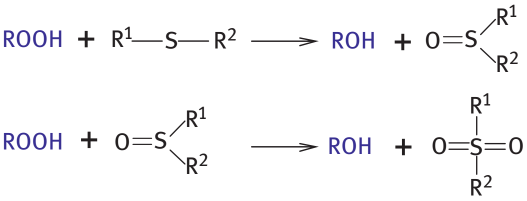

Figure 5.9: Decomposition of hydroperoxides by means of thiosynergists.

antioxidants is reported in Figure 5.8. Accordingly, phosphites or phosphonites are oxidized to phosphates, while hydroperoxides are reduced [60].

One of the main drawbacks of these compounds is their easy hydrolysis in contact with water that eventually leads to the formation of acidic species. The application of these additives is therefore limited to applications that do not involve metal parts. To overcome this issue, acid scavengers are usually added to the formulation or the organophosphorous compound is replaced with another hydrolysis-resistant additive.

Thiosynergists are sulphur-based organic molecules, typically thio-esters. According to their mechanism of action, reported in Figure 5.9, the thiosynergist molecule is transformed into a variety of oxidized sulphur products (e. g. sulfenic and sulfonic acid), while hydroperoxides are reduced to alcohols in an overstoichiometric reaction [61].

Thiosynergists, different from the organophosphorous compounds, are very efficient for long-term thermal aging applications.

5.5.2 UV stabilizers

For polymers employed in outdoor applications, the absorption of photons from sunlight radiation (e. g. wavelengths ranging from 100 nm to about 1 mm including ultraviolet, visible and infrared radiation) is inevitable and eventually leads to the oxidative degradation of photosensitive molecules [62]. The mechanism, called photooxidation, is triggered by light and proceeds similarly to what reported in Section 5.5 for oxidation of polymers.

The stabilization of polymers against the adverse effect of sunlight involves the inhibition or retardation of photochemical processes in polymers and plastics. This retardation can be achieved by reducing the rate of photoinitiation or the kinetic chain length of the propagation stage of the photooxidation mechanism. Visible and infrared light are rather unharmful; therefore photostabilization of polymer items involves the protection against destructive reactions mainly caused by high-energy UV radiation [63]. UV stabilizers can be classified into three main classes:

5.5.2.1 UV absorbers

UV absorbers interact with the first step of the photooxidation process by absorbing the harmful UV radiation (300–400 nm) before it reaches the photosensitive moieties in the polymer. In other words, these compounds are able to provide energy dissipation before photosensitization can occur. UV absorbers are characterized by excellent light stability; therefore, they are modified but not destroyed in the stabilization process [64]. Energy dissipation mechanism reckon on the conversion of harmful UV radiation into harmless infrared radiation or heat that is dissipated through the polymer matrix. Carbon black is one of the most effective and commonly used light absorbers, as well as rutile titanium oxide which is ineffective for radiation below 315 nm, the so-called UV-B radiation.

Compounds with good filtrating action, such as hydroxyaromatic UV stabilizers (such as hydroxybenzophenone and hydroxyphenylbenzotriazole), are successfully used and their absorption characteristics are widely reported in the literature [65, 66]. Other UV absorbers include oxanilides for polyamides, benzophenones for PVC and benzotriazoles and hydroxyphenyltriazines for polycarbonate [67].

Schematization of the energy dissipation mechanism of the β-diketone avobenzone UV absorber is reported in Figure 5.10. The reaction involves the reversible formation of a six-membered hydrogen bonded ring and the equilibrium between the two tautomeric forms provides a facile pathway for deactivation of the excited state induced by the absorption of light.

5.5.2.2 Quenchers

This class of UV absorbers provides deactivation of photosensitive groups in their excited state (singlet and or triplet) before the disruption of molecular bonds can occur [62]. Quenching is a diffusion-controlled process and is effective in polymer protection only if the photosensitive moiety in its triplet state has a long half-life and

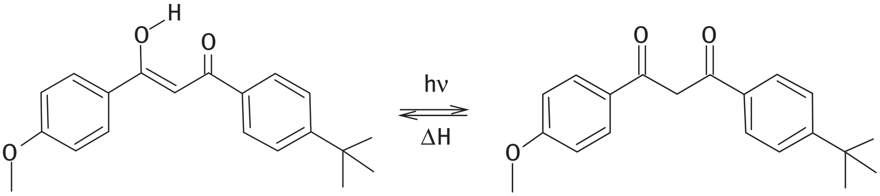

Figure 5.10: Energy dissipation mechanism occurring in avobenzones UV absorbers.

$$D^* + A \longrightarrow D + A^*$$

$$A^* \longrightarrow A + \textit{Energy}\ \ \textit{(heat or light emission)}$$

Figure 5.11: Schematization of the quenching reaction.

if the quencher is freely diffusible [68]. The quenching reaction is represented in Figure 5.11, where an excited chromophoric group in a polymer (donor, D*), responsible for the initiation step in the photodegradation of the polymer, is deactivated by an acceptor molecule (quencher, A) [69]:

Metal complexes, particularly those based on nickel, are very effective quenchers for their relatively low extinction coefficient in the near UV region. Nickel chelates, for example, are able to quench the triplet state of carbonyl groups in polyolefins. These chelates have been tested for photostabilization of polyisobutylene, polybutadiene [70] as well as PS [71].

5.5.2.3 Hindered Amine Light Stabilizers

Hindered amine light stabilizers (HALS) mechanism of action involves trapping of free radicals formed during the photooxidation of a polymeric material, hindering the propagation of the photodegradation process [72]. The ability of HALS to scavenge radicals created by UV absorption is explained by the formation of nitroxyl radicals through a process known as the Denisov cycle, reported in Figure 5.12 [73]. During UV irradiation, when oxygen (from air) and radicals ($R^\bullet$) are made available, hindered piperidine, the model compound for HALS, is able to produce hindered piperidinoxy radicals, which are able to further trap other radicals in a cyclic reaction.

Currently, a wide range of HALS products are commercially available; however, they all share the 2,2,6,6-tetramethylpiperidine ring structure [74]. HALS are some of the most effective UV stabilizers for commodity and specialty plastics.

5.5.3 Natural antioxidants

It is widely recognized that synthetic antioxidants are very effective and highly stable. However, one of the main drawbacks is their derivation from oil-based

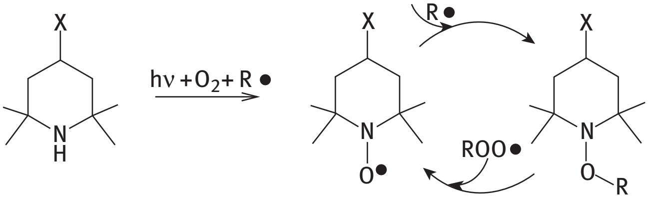

Figure 5.12: Schematization of mechanism of radical scavenging of hindered piperidine.

products, together with their potentially harmful interaction with the human metabolism, especially in food contact applications. Bio-based materials are able to provide a valid alternative source for antioxidants. The search for safe and effective naturally occurring antioxidants has been mainly focused on tocopherols, vitamin C, carotenoids and phenolic compounds [75].

These products have shown very different mechanism of oxidative inhibition; however, they all react stabilizing ROS species, secondary products of plant photosynthesis, making them unharmful.

Tocopherols, for example, are Vitamin E constituents exclusively synthesized by plants, present in seed oil, leaves and other green parts [58].

Tocopherols can act both by a chain-breaking donor and acceptor mechanism, as well as singlet oxygen ($^1O_2$) quenchers. The two mechanisms mentioned above have not been completely elucidated; however involvement of quinone structures has been proposed by Cuppett et al. [76], while Clough et al. [77] claimed about formation of tocopherol hydroperoxide derivative as an intermediate product. These two reaction schemes are reported in Figure 5.13 and Figure 5.14, respectively.

Up to this date, the antioxidant activity of several natural products has been reported in both commercial polymers, such as PE [78] and PP [79] as well as bio-based polymers, such as PHB [80], MaterBi [81] or PLA [82, 83]. Successful attempts prove that the substitution of oil-based products with their natural and renewable

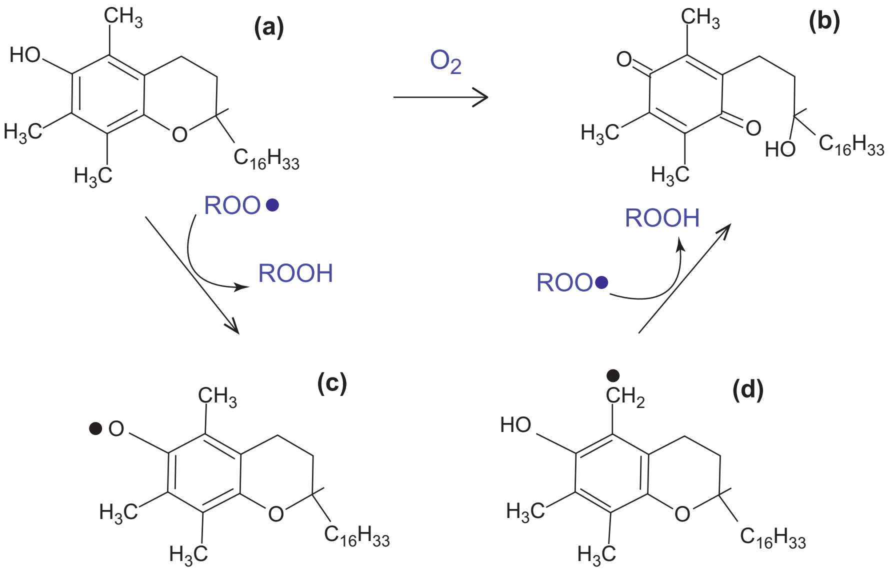

Figure 5.13: (a) α-tocopherol oxidation to (b) α-tocopheryl quinone through semi-quinone intermediates (c,d).

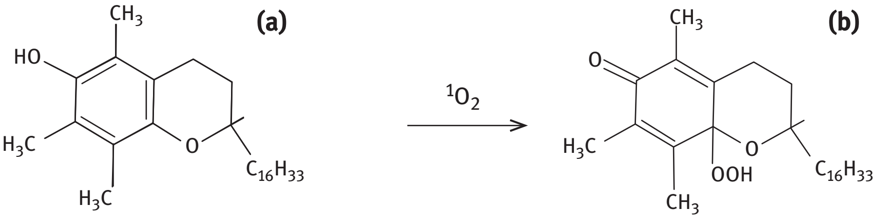

Figure 5.14: Singlet oxidation of (a) a-tocopherol to (b) hydroperoxydienone [76].

counterparts will indeed be possible in the future and has the potential to reach industrial scale.

5.6 Antimicrobials

Under favourable conditions, plastic materials support the growth of microorganisms such as viruses, bacteria and fungi (yeasts and moulds) [84]. Even those plastics that would not normally promote microbial growth can be used in environments that sustain microorganism life or proliferation, for example water or fertile soil [85].

In the modern era, where plastic recycling or disposal is a serious issue, biodegradation can represent a desirable feature. However, bio-stability and prevention of health hazards during both shelf life and final use of plastic artefacts are key factors to take into account in engineering polymer formulations. To overcome these problems, antimicrobial additives are added to the polymer formulation. It is necessary to underline that not all the antimicrobial additives are biocides, i. e. have the ability to kill bacteria or fungi, but many of them are simply biostatic agents, able to hinder the reproduction of the microorganisms.

Antimicrobial additives are mostly used in medical fields and food packaging applications. Therefore, the main requirement of antimicrobial (AM) additives is low toxicity to human and environment in both processing and end-use stages. Moreover, ideal AM additives have to be compatible with processing aids and other additives involved in plastic formulation and should not affect the properties or aesthetic appearances of the final artefact.

There are several ways to classify AM additives; however, they can generally fit in two general classes based on their chemical composition and mechanism of action: organic and inorganic AM agents [86].

5.6.1 Organic antimicrobial agents

Organic antimicrobial agents are typically small molecules able to migrate over time from the bulk to the polymer surface to introduce an antimicrobial effect at the polymer surface. The variable interaction between the organic AM molecules and the polymer matrix represents the pushing force for migration.

One of the advantages of polymer-based antimicrobial systems is that the migration of the AM molecule on the surface can be controlled, so that microbial growth kinetics and antimicrobial activity at the product's surface can be properly modeled. However, the migration of the AM additives eventually leads to their leaching out of the polymer. For this reason, organic AM agents fit application in disposable items rather than durable goods with longer lifespans. Another drawback of these compounds is the limited food contact approval for organic based systems. Once again, the primary concern is their mobility and solubility in food simulants; therefore inorganic based technologies are generally considered more suitable for direct food contact. Organic AM systems are also thermally unstable; many compounds decompose in the typical processing temperature range and in other cases a temperature increase may cause excessive mobilization and consequently high loss rates of AM agents from the plastic.

The most common organic AM agents are organometallic compounds, in particular arsenic-based materials, such as oxybisphenoxarsine (OBPA), are acknowledged as very efficient and cost-effective. As a matter of fact, the use of arsenic-based compounds dates back to the 1930s in the United States. where the *Bordeaux mixture* was first employed in bio-stabilization of plastic materials. On the other hand, arsenic is universally perceived as hazardous material; for this reason the spread of arsenic-based compounds will always receive poor trust from the market. The demand for alternative formulations, such as the isothiazoline family or triclosan (chlorinated diphenyl ether), is growing rapidly [86]. Successful application of organic AM systems is soft PVC. Pristine PVC owns an intrinsic resistance to microbial attacks; however, plasticizers, fillers, pigments and other carbon-based additives used in PVC formulations become nutrients for microorganisms, especially when the final product is employed in wet environments such as shower curtains, paddling pools, etc. For this reason, AM organic agents are commercially available in formulation dissolved in other additives, such as plasticizers. Table 5.6 shows examples of organic antimicrobial products, together with their chemical structure and composition, supplier and typical applications.

5.6.2 Inorganic antimicrobial agents

Inorganic antimicrobial agents exploit metal ions for their intrinsic biocidal activity. The main difference between organic and inorganic AM agent is that the latter do not have the possibility to migrate but they are immobilized in the polymer matrix. The antimicrobial effect of silver ions has long been recognized, dating back to the Ancient Rome. Not only inorganic AM agents are capable of inhibiting microbial growth, but they are also very effective biocides.

Table 5.6: Organic antimicrobial agents listed with their chemical composition and structure, suppliers and applications.

Trade name	Chemical composition	Chemical structure	Supplier	Applications
Triclosan	5-chloro-2-(2,4-dichlorophenoxy) phenol	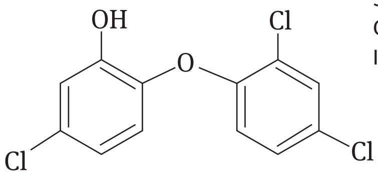	Spec-Chem Industry	Chopping boards, kitchen utensils, sponges, gloves, medical devices, toys, food containers.
Intercide® ABF-2 BBP	Solution of OBPA in DIDP plasticizer carrier	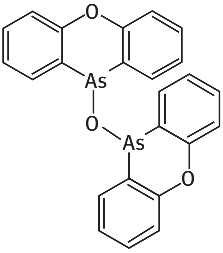	Akcros Chemicals	Flooring, roofing, coated fabrics, wall covering and leather cloth, PVC flexible films, foils and sheets.
Vinyzene™ IT-4000 DIDP	4,5-dichloro-2-n-octyl- isothiazolinone in DIDP plasticizer carrier	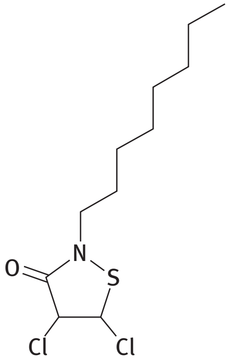	Dow Chemical	PVC Decking, Fencing, Fabrics (Fibres/ Textiles/ Carpets), Refrigerators inserts, films and sheets

Their mechanism of action involves the binding of the metal ion to the cell membrane of the microorganism, causing an unbalance in the diffusion in and out of the cell. Once inside the cell, the ions start a process of enzymatic denaturation, targeting thiol groups on the proteins, which rapidly leads to the loss of cell functional ability and eventually to cell death [87]. In order to be incorporated in the polymer matrix, the highly mobile metal ions are bonded to a delivery system, which allows minute quantities of ions to be released through a process of ion exchange at

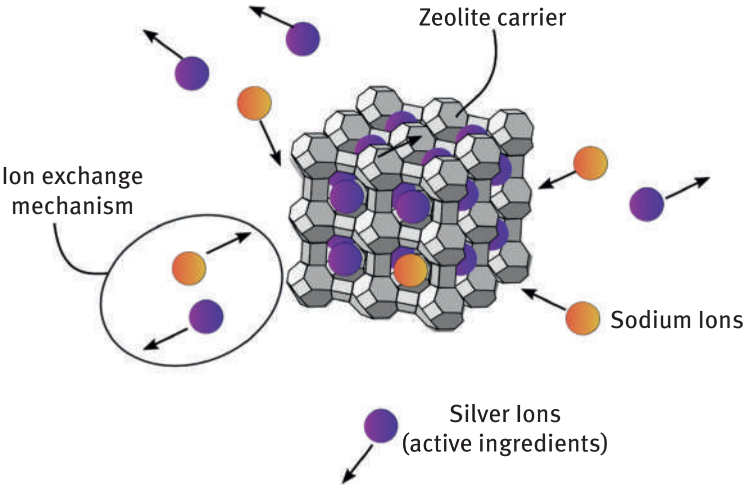

Figure 5.15: Ion exchange mechanism in antimicrobial zeolites loaded with silver ions.

the plastic's surface, as depicted in Figure 5.15 for the case of zeolites loaded with silver ions.

The main advantage of such a mechanism is that the ions are continuously made available over the lifetime of the plastic artefact. Moreover, inorganic systems are characterized by a very good thermal stability that makes them suitable in a wide range of application in different polymer formulations.

The inorganic AM market currently includes releasing systems based on ceramic glasses, doped titanium dioxides or zeolites as carriers. One current trend in inorganic AM polymer additives is the used of nano-sized particles as carriers and delivery systems. Their high aspect ratio (lamellae, flakes, spheres) could offer a higher ion release rate but brings on adverse issues such as possible toxicity, excessive discoloration resulting from rapid oxidization and the increased complexities of producing nano-scale active grades. Currently, nano-silver is not recognized by the US Environmental Protection Agency and its application is therefore forbidden [88].

5.6.3 Natural antimicrobial additives for polymers

The concerns related to the use of arsenic-based products and nanotechnologies as antimicrobial additives for plastics, especially in food-packaging applications, have pushed academic and industrial world towards the development and rediscovery of plant extract as antimicrobial agents. Since prehistoric times, man has learned to exploit different spices and herbs, not only for food flavouring but also for their antiseptic and medicinal properties. Among others, basil is a popular culinary herb used extensively for

Table 5.7: Classification of natural antimicrobial agents.

Class	Composition	Targeted microorganism	Reference
Bacteriocins (especially Nisin)	Peptidic antimicrobial compounds synthesized by different bacteria	*Listeria innocua*	Hoang et al. (2010) [92]
		Listeria monocytogenes	Jin (2010) [93]
		Salmonella spp.	Santiago-Silva et al. (2009) [94].
Enzymes (lysozyme)	Naturally occurring enzyme produced by humans and many animals, it has activity against bacterial cellular structure	*Alicyclobacillus acidoterrestris*	Buonocore et al. (2005) [95]
		Micrococcus lysodeikticus	Appendini and Hotchkiss (1997) [96]
Phytochemicals (essential oils and plant extracts)	Oregano or Citral essential oils	*E. coli, Salmonella enterica* and *L. monocytogenes*	Muriel-Galet et al. 2013 [97]
	Basil essential oil	*E. coli*	Suppakul et al. (2003b) [90]
	Grapefruit seed extract	*E. coli* and *L. monocytogenes*	Luther et al. (2007) [98]

many years in food flavouring. Its essential oil is known to have very powerful antimicrobial activity [89], and possible applications in food packaging have been forecasted [90]. Naturally derived antimicrobial agents are becoming increasingly more important in antimicrobial packaging as they present a perceived lower risk to the consumers. Other than plant extracts, bacteriocins and enzymes are also used in antimicrobial packaging. Natural antimicrobials belonging to the above-mentioned classes are listed in Table 5.7, together with examples of targeted microorganism [91].

References

[1] Harper CA. Handbook of plastics technologies: the complete guide to properties and performance. New York, USA: McGraw-Hill, 2006.

[2] Hauser EA. A contribution to the early history of India-rubber. François Fresneau (1703–1770). Rubber Chem Technol. 1938;11:1–4.

[3] United States Patent 3633 (1844) by Charles Goodyear improvements in India-rubber fabrics.

[4] World Plastics Additives Market – Opportunities and Forecasts, 2012–2020. Mar 2016. Accessed: 10Mar2016 https://www.alliedmarketresearch.com/plastic-additives-market.

[5] Bio-based products. Feb 2016. Accessed: 27Feb2016 http://ec.europa.eu/growth/sectors/biotechnology/bio-based-products/index_en.htm.

[6] Weinekötter R, Gericke H. Mixing of solids. Berlin, Germany: Springer Science & Business Media, 2013.

[7] Bart JCJ. Additives in polymers: industrial analysis and applications. Chichester: John Wiley & Sons, 2006.

[8] Bruens C, Nieland R, Stanssens D. New performance additives from DSM. Polym Polym Compos UK. 1999;7:581–587.

[9] Zweifel H. Plastics additives handbook. Munich, Germany: Hanser Publishers, 2000.

[10] Titow MV. PVC technology. Berlin, Germany: Springer Science & Business Media, 2012.

[11] Chanda M, Roy SK. Plastic technology handbook, 4th Boca Raton, FL: CRC Press, 2007.

[12] Štěpek J, Daoust H. Additives for plastics. Berlin, Germany: Springer Science & Business Media, 1983.

[13] Kilpatrick A. Some relations between molecular structure and plasticizing effect. J Appl Phys. 1940;11:255–261.

[14] Houwink R. Proceedings of the XI congress of pure and applied chemistry, London; 1947; 575–583.

[15] Aiken W, Alfrey T, Janssen A, Mark H. Creep behavior of plasticized vinylite VYNW. J Polymer Sci. 1947;2:178–198.

[16] Ramos-Devalle L, Gilbert M. PVC/plasticizer compatibility: evaluation and its relation to processing. J Vinyl Technol. 1990;12:222–225.

[17] Miller E. Introduction to plastics and composites. Basel, Switzerland: Marcel Dekker, 1996.

[18] Heudorf U, Mersch-Sundermann V, Angerer J. Phthalates: toxicology and exposure. Int J Hyg Environ Health. 2007;210:623–634.

[19] Guo Y, Kurunthachalam K. Challenges encountered in the analysis of phthalate esters in foodstuffs and other biological matrices. Anal Bioanal Chem. 2012;404:2539–2554.

[20] Tickner JA, Schettler T, Guidotti T, McCally M, Rossi M. Health risks posed by use of di-2-ethylhexyl phthalate (DEHP) in PVC medical devices: a critical review. Am J Ind Med. 2001;39: 100–111.

[21] Kortenkamp A, Faust M. Combined exposures to anti-androgenic chemicals: steps towards cumulative risk assessment. Int J Androl. 2010;33:463–474.

[22] Wypych G. PVC degradation & stabilization, 2nd Toronto, Canada: ChemTec Publishing, 2008.

[23] Lim KM, Ching YC, Gan SN. Effect of palm oil bio-based plasticizer on the morphological, thermal and mechanical properties of poly (vinyl chloride). Polymers. 2015;7:2031–2043.

[24] Bouchareb B, Benaniba MT. Effects of epoxidized sunflower oil on the mechanical and dynamical analysis of the plasticized poly (vinyl chloride). J Appl Polym Sci. 2008;107:3442–3450.

[25] Rao N, Kaujalgikar S, Chaudhary BI, Bhide S, Morye S, Agashe S. Epoxidized fatty acid alkyl ester plasticizers and methods for making epoxidized fatty acid alkyl ester plasticizers US Patent WO2014061026 A1.

[26] Vieira MGA, da Silva MA, dos Santos LO, Beppu MM. Natural-based plasticizers and biopolymer films: a review. Eur Polym J. 2011;47:254–263.

[27] Morgan AB, Gilman JW. An overview of flame retardancy of polymeric materials: application, technology, and future directions. Fire Mater. 2013;37:259–279.

[28] Alaee M, Wenning RJ. The significance of brominated flame retardants in the environment: current understanding, issues and challenges. Chemosphere. 2002;46:579–582.

[29] de Wit CA. An overview of brominated flame retardants in the environment. Chemosphere. 2002;46:583–624.

[30] Muir DCG, de Wit CA. Trends of legacy and new persistent organic pollutants in the circumpolar arctic: overview, conclusions, and recommendations. Sci Total Environ. 2010;408:3044–3051.

[31] Levchik SV, Weil ED. A review of recent progress in phosphorus-based flame retardants. J Fire Sci. 2006;24:345–364.

[32] Bernhard S. Phosphorus-based flame retardancy mechanisms – Old hat or a starting point for future development? Materials. 2010;3:4710–4745.

[33] Le Bras M, Bourbigot S, Camino G, Delobel R. Fire retardancy of polymers: the use of intumescence. Cambridge, UK: The Royal Society of Chemistry, 1998.

[34] Horn WE. Inorganic hydroxides and hydroxycarbonates: their function and use as flame-retardant additives. New York, USA: Marcel Dekker, 2000.

[35] Troitzsch JH. Overview of flame retardants: fire and fire safety, markets and applications, mode of action and main families. Role in fire gases and residues. Chem Today. 1998;16:18–24.

[36] Morgan AB, Wilkie CA. The non-halogenated flame retardant handbook. New York, USA: John Wiley & Sons, 2014.

[37] Demir H, Arkış E, Balköse D, Ülkü S. Synergistic effect of natural zeolites on flame retardant additives. Polym Degrad Stab. 2005;89:478–483.

[38] Das G, Karak N. Thermostable and flame retardant Mesua ferrea L. seed oil based non-halogenated epoxy resin/clay nanocomposites. Prog Org Coatings. 2010;69:495–503.

[39] Papaspyrides CD, Kiliaris P. Polymer green flame retardants: a comprehensive guide to additives and their applications. Amsterdam, Netherlands: Elsevier, 2014.

[40] Pan H, Qian X, Ma L, Song L, Hu Y, Liew KM. Preparation of a novel biobased flame retardant containing phosphorus and nitrogen and its performance on the flame retardancy and thermal stability of poly (vinyl alcohol). Polym Degrad Stab. 2014;106:47–53.

[41] Seymour LW, Duncan R, Strohalm J, Kopeček J. Effect of molecular weight (Mw) of N-(2-hydroxypropyl) methacrylamide copolymers on body distribution and rate of excretion after subcutaneous, intraperitoneal, and intravenous administration to rats. J Biomed Mater Res. 1987;21:1341–1358.

[42] Daly LE. Composition of butadiene-acrylonitrile copolymer and styrene-acrylonitrile copolymer U.S. Patent No. 2,439,202. Washington, DC: U.S. Patent and Trademark Office, 1948.

[43] Markarian J. Impact modifiers: how to make your compound tougher. Plastic Addit Compound. 2004;6:46–49.

[44] Paul DR, Newman S. Polymer blends. New York, USA: Academic, 1978.

[45] Stephens B, Azimi P, El Orch Z, Ramos T. Ultrafine particle emissions from desktop 3D printers. Atmos Environ. 2013;79:334–339.

[46] Rutkowski JV, Levin BC. Acrylonitrile–butadiene–styrene copolymers (ABS): pyrolysis and combustion products and their toxicity – A review of the literature. Fire Mater. 1986;10:93–105.

[47] Titow WV. PVC plastics: properties, processing, and applications. Berlin, Germany: Springer Science & Business Media, 2012.

[48] Tseng WT, Lee JS. Functional MBS impact modifiers for PC/PBT alloy. J Appl Polym Sci. 2000;76: 1280–1284.

[49] Larsson BE, Ryan CF, Souder LC. U.S. Patent No. 3,655,825. U.S. Patent and Trademark Office, 1972 Washington, DC.

[50] Karger-Kocsis J, Kallo A, Szafner A, Bodor G, Senyei ZS. Morphological study on the effect of elastomeric impact modifiers in polypropylene systems. Polymer. 1979;20:37–43.

[51] Kockott D. Natural and artificial weathering of polymers. Polym Degrad Stab. 1989;25:181–208.

[52] Rabek JF. Photostabilization of polymers: principles and applications. Amsterdam, Netherlands: Elsevier, 1990.

[53] Galano A, Macías-Ruvalcaba NA, Medina Campos ON, Pedraza-Chaverri J. Mechanism of the OH radical scavenging activity of nordihydroguaiaretic acid: a combined theoretical and experimental study. J Phys Chem. 2010;114:6625–6635.

[54] Meng X, Chen W, Xin Z, Wu C. Effect of benzofuranone on degradation and mechanical properties of polypropylene in processing. J Vinyl Additive Technol 2016. published online. DOI:10.1002/vnl.21535.

[55] Nawar WF. Lipids. In: Fennema O, editors. Food chemistry, 3rd New York, USA: Marcel Dekker, 1996:225–320.

[56] Pospíšil J. Chemical and photochemical behaviour of phenolic antioxidants in polymer stabilization – A state of the art report, part I. Polym Degrad Stab. 1993;40:217–232.

[57] Kriek E. Carcinogenesis by aromatic amines. Biochimica et Biophysica Acta (Bba) Reviews on Cancer. 1974;355:177–203.

[58] Kamal-Eldin A, Appelqvist LÅ. The chemistry and antioxidant properties of tocopherols and tocotrienols. Lipids. 1996;31:671–701.

[59] Ingold KU, Pratt DA. Advances in radical-trapping antioxidant chemistry in the 21st century: a kinetics and mechanisms perspective. Chem Rev. 2014;114:9022–9046.

[60] Schwetlick K. Mechanisms of antioxidant action of organic phosphorus compounds. Pure Appl Chem. 1983;55:1629–1636.

[61] Chien JCW, Boss CR. Sulfur compounds as synergistic antioxidants. J Polymer Sci A-1: polymer Chem. 1972;10:1579–1600.

[62] Yousif E, Haddad R. Photodegradation and photostabilization of polymers, especially polystyrene: review. SpringerPlus. 2013;2:398.

[63] Shalaby SW. Radiative degradation of synthetic polymers: chemical physical, environmental, and technological considerations. J Polym Sci Macromol Rev. 1979;14:419–458.

[64] Yousif E. Photostabilization of thermoplastic polymers. Saarbrücken, Germany: Lambert Academic Publishing, 2012.

[65] Ranby BG, Rabek JF. Photodegradation, photo-oxidation, and photostabilization of polymers. New York, USA: Wiley, 1975.

[66] Allen NS, McKellar JF. Photochemistry of dyed and pigmented polymers. London, UK: Applied Science Publishers, 1980.

[67] Allen NS, Edge M. Fundamentals of polymer degradation and stabilization. New York, USA: Elsevier, 1992.

[68] Heller HJ. Protection of polymers against light irradiation. Eur Polym J. 1969;5:105–132.

[69] Rabek JF. Photostabilization of polymers, principles and applications. London, UK: Elsevier, 1990.

[70] Lala D, Rabek J. Polymer photodegradation: mechanisms and experimental methods. Polym Degrad Stabilization. 1980;3:383–391.

[71] George GA. The mechanism of photoprotection of polystyrene film by some ultraviolet absorbers. J Appl Polym Sci. 1974;18:117–124.

[72] Gijsman P, Hennekens J, Tummers D. The mechanism of action of hindered amine light stabilizers. Polym Degrad Stab. 1993;39:225–233.

[73] Hodgson JL, Coote ML. Clarifying the mechanism of the Denisov cycle: how do hindered amine light stabilizers protect polymer coatings from photo-oxidative degradation?. Macromolecules. 2010;43:4573–4583.

[74] Bottino FA, Cinquegrani AR, Di Pasquale G, Leonardi L, Orestano A, Pollicino A. A study on chemical modifications, mechanical properties and surface photo-oxidation of films of polystyrene (PS) stabilized by hindered amines (HAS). Polym Test. 2004;23:779–789.

[75] Lugasi A. Natural antioxidants chemistry, health effects, and applications. Champaign, IL: AOCS Press, 1997.

[76] Cuppett S, Schnepf M, Hall C. Natural antioxidants – Are they a reality? In: Shahidi F., editors. Natural antioxidants: chemistry, health effects, and applications. Champaign: AOCS Press, 1979:12–24.

[77] Clough RL, Yee BG, Foote CS. Chemistry of singlet oxygen. 30. The unstable primary product of tocopherol photooxidation. J Am Chem Soc. 1979;101:683–686.

[78] Tátraaljai D, Major L, Földes E, Pukánszky B. Study of the effect of natural antioxidants in polyethylene: performance of β-carotene. Polym Degrad Stab. 2014;102:33–40.

[79] Ambrogi V, Cerruti P, Carfagna C, Malinconico M, Marturano V, Perrotti M, et al. Natural antioxidants for polypropylene stabilization. Polym Degrad Stab. 2011;96:2152–2158.

[80] López-Rubio A, Lagaron JM. Improvement of UV stability and mechanical properties of biopolyesters through the addition of β-carotene. Polym Degrad Stab. 2010;95:2162–2168.

[81] Cerruti P, Santagata G, Gomez d'Ayala G, Ambrogi V, Carfagna C, Malinconico M, et al. Effect of a natural polyphenolic extract on the properties of a biodegradable starch-based polymer. Polym Degrad Stab. 2011;96:839–846.

[82] Byun Y, Kim YT, Whiteside S. Characterization of an antioxidant polylactic acid (PLA) film prepared with α-tocopherol, BHT and polyethylene glycol using film cast extruder. J Food Eng. 2010;100:239–244.

[83] Agustin-Salazar S, Gamez-Meza N, Medina-Juàrez LÀ, Soto-Valdez H, Cerruti P. From nutraceutics to materials: effect of resveratrol on the stability of polylactide. ACS Sustainable Chem Eng. 2014;2(6):1534–1542.

[84] Dankert J, Hogt AH, Feijen J. Biomedical polymers-Bacterial adhesion, colonization, and infection. CRC Crit Rev Biocompatibility. 1986;2:219–301.

[85] Nichols D. Biocides in plastics. Shawbury, United Kingdom: iSmithers Rapra Publishing, 2004 .

[86] Jones A. Choosing antimicrobial additives for plastics. Plastics Addit Compound. 2009;11: 26–28.

[87] Sharma R. Enzyme inhibition: mechanisms and scope. Rijeka, Croatia: INTECH Open Access Publisher, 2012 .

[88] Duncan TV. Applications of nanotechnology in food packaging and food safety: barrier materials, antimicrobials and sensors. J Colloid Interface Sci. 2011;363:1–24.

[89] Hussain AI, Anwar F, Sherazi STH, Przybylski R. Chemical composition, antioxidant and antimicrobial activities of basil (Ocimum basilicum) essential oils depends on seasonal variations. Food Chem. 2008;108:986–995.

[90] Suppakul P, Miltz J, Sonneveld K, Bigger SW. Antimicrobial properties of basil and its possible application in food packaging. J Agric Food Chem. 2003;51:3197–3207.

[91] Irkin R, Esmer OK. Novel food packaging systems with natural antimicrobial agents. J Food Sci Technol. 2015;52:6095–6111.

[92] Hoang LC, Chaine A, Gregoire L, Wache Y. Potential of nisin incorporated sodium caseinate films to control Listeria in artificially contaminated cheese. Food Microbiol. 2010;27:940–944.

[93] Jin T. Inactivation of Listeria monocytogenes in skim milk and liquid egg white by antimicrobial bottle coating with polylactic acid and nisin. J Food Sci. 2010;75:83–88.

[94] Santiago-Silva P, Soares NFF, Nobrega JE, Junior MAW, Barbosa KBF, Volp ACP, et al. Antimicrobial efficiency of film incorporated with pediocin (ALTA 2351) on preservation of sliced ham. Food Control. 2009;20:85–89.

[95] Buonocore GG, Conte A, Corbo MR, Sinigaglia M, Del Nobile M. Mono and multilayered active films containing lysozyme as antimicrobial agent. Innovative Food Sci Emerg Technol. 2005;6: 459–464.

[96] Appendini P, Hotchkiss JH. Immobilization of lysozyme on food contact polymers as potential antimicrobial films. Packaging Technol Sci. 1997;10:271–279.

[97] Muriel-Galet V, Cerisuelo JP, Lopez-Carballo G, Aucejo S, Gavara R, Hernandez-Munoz P. Evaluation of EVOH-coated PP films with oregano essential oil and citral to improve the shelf-life of packaged salad. Food Control. 2013;20:137–143.

[98] Luther M, Parry J, Moore J, Meng J, Zhang Y, Cheng Z, et al. Inhibitory effect of Chardonnay and black raspberry seed extracts on lipid oxidation in fish oil and their radical scavenging and antimicrobial properties. Food Chem. 2003;104:1065–1073.

Anna Trojanowska, Adrianna Nogalska, Ricard Garcia Valls,
Marta Giamberini and Bartosz Tylkowski

6 Technological solutions for encapsulation

Abstract: Encapsulation offers broad scope of applications. It can be used to deliver almost everything from advanced drugs to unique consumer sensory experiences; it could be also employed as a protection system or a sensing material. This cutting-edge technology undergoes rapid growth in both academic and industrial conditions. Research in this matter is continuing to find a new application of microcapsules as well as to improve the methods of their fabrication. Therefore, in this review, we focus on the art of the encapsulation technology to provide the readers with a comprehensive and in-depth understanding of up-to-day development of microcapsule preparation methods. Our goal is to help identify the major encapsulation processes and by doing so maximize the potential value of ongoing research efforts.

Keywords: encapsulation technologies, microcapsules, polymerization reactions

6.1 Introduction

According to science, encapsulation, developed roughly 65 years ago, is a major interdisciplinary research technology [1]. In general, capsules are circular cross-section shape particles with certain free volume inside, where a core material can be allocated. As shown in Figure 6.1, the core material can be also called an internal phase, a filler, a matrix or an active. Encapsulation may be as well explained in the frames of supramolecular chemistry as a process where a guest molecule is confined inside the cavity of a host and leads to the formation of a capsule. Capsules with a diameter size between 1 nm and 1,000 nm are named nanocapsules, while the capsules with a size rage 1–1,000 µm and above (> 1 mm) are called microcapsules and macrocapsules, respectively [2, 3].

Capsules can exhibit different morphologies depends on a material used for their fabrication, although also the preparation technique has a significant impact on their final outcome [4]. Depending on the structure of the capsules, they can be characterized as continuous core/shells, polycore capsules, continuous core capsules with more than one layer of shell material and the matrix type, where encapsulated agent is incorporated within the shell material. Representation of aforementioned structures of the capsules is shown in Figure 6.2[5]. Relying on the preparation method used, different morphologies are formed. Rough approximation of the capsule's size range obtained by each technique is presented in Table 6.1.

https://doi.org/10.1515/9783110469745-006

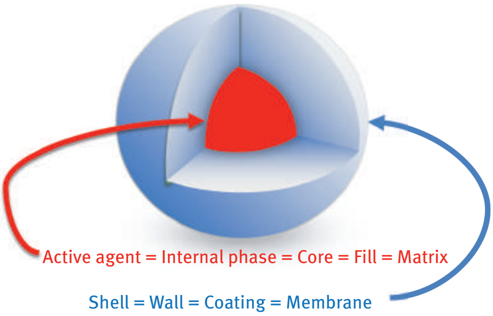

Figure 6.1: Microcapsule.

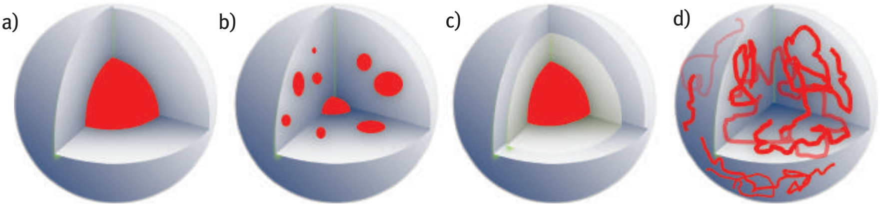

Figure 6.2: Microcapsules morphologies: (a) continuous core/shells, (b) polycore capsules, (c) continuous core capsules with more than one layer of shell material, and (d) the matrix type capsules.

Table 6.1: Capsules size range determined by the preparation technique.

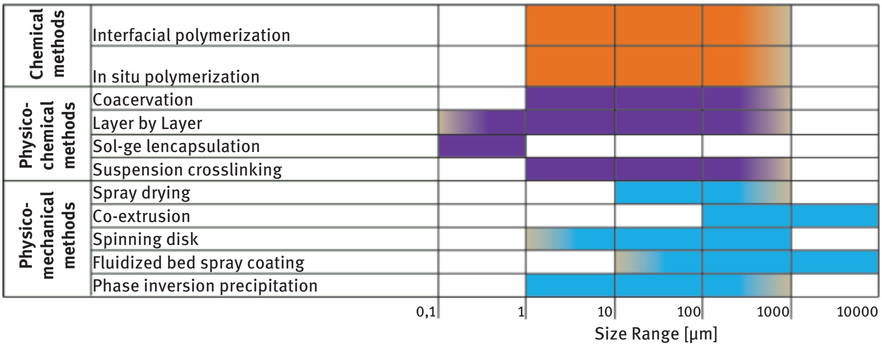

		0,1–1	1–10	10–100	100–1000	1000–10000
Chemical methods	Interfacial polymerization		🟧	🟧	🟧	
	In situ polymerization		🟧	🟧	🟧	
Physico-chemical methods	Coacervation		🟪	🟪	🟪	
	Layer by Layer	🟪	🟪	🟪	🟪	
	Sol-ge lencapsulation	🟪				
	Suspension crosslinking		🟪	🟪	🟪	
Physico-mechanical methods	Spray drying			🟦	🟦	
	Co-extrusion				🟦	🟦
	Spinning disk		🟦	🟦	🟦	
	Fluidized bed spray coating			🟦	🟦	🟦
	Phase inversion precipitation		🟦	🟦	🟦	

Size Range [μm]

Encapsulation is a dynamic research field due to novel technologies, production paths and demand for innovative applications. Running a search on “encapsulation”, over 80,000 records can be found up to date, by the use of Web of Science tool (Figure 6.3). Since 1953, when Green and Schleicher patented the first method for

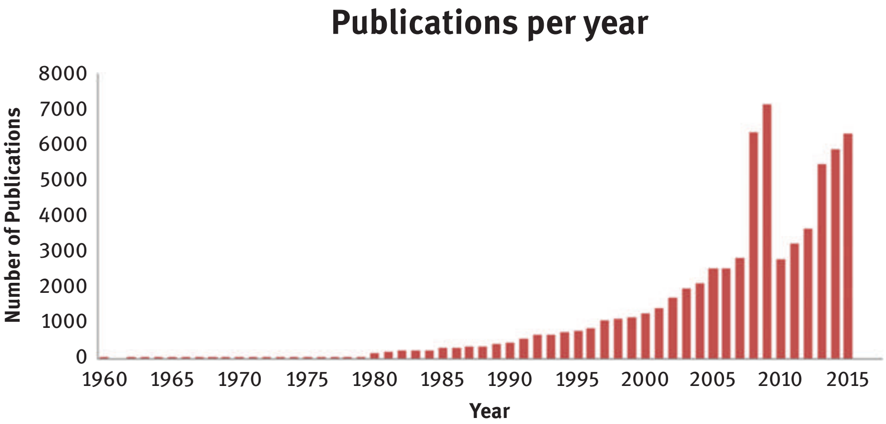

Figure 6.3: Publications per year on "encapsulation" (tool used: Web of Science, May 2016).

microcapsule preparation, different techniques for microcapsules fabrication have been developed.

This review does not pretend to cover the abundant published literature on the subject, but to be representative of the observed tendencies in capsule fabrication for consumer good products, medicine, food chemistry, agriculture, etc. The first part of this review is dedicated to describe chemical methods, such as interfacial polymerization and *in situ* polymerization (suspension, emulsion, dispersion polymerization), while the second one provides detailed information about physicochemical methods, such as coacervation, layer-by-layer (LbL) assembly, sol–gel encapsulation and suspension cross-linking. Finally, we will dedicate the third part to describe physicomechanical methods, such as spray-drying, co-extrusion and phase-inversion precipitation.

6.2 Chemical methods

Chemical methods involve sphere fabrication along with various polymerization reactions. This indicates that the starting materials in these cases are monomers or prepolymers. Further subdivision of these techniques along with a short description is detailed below [6].

6.2.1 Interfacial polymerization

Generally, the interfacial polymerization employs two monomers to react at the interface of a droplet, which lead to the formation of a capsule, as shown in Figure 6.4[7, 8]. [9]. The first to report interfacial polymerization technology was

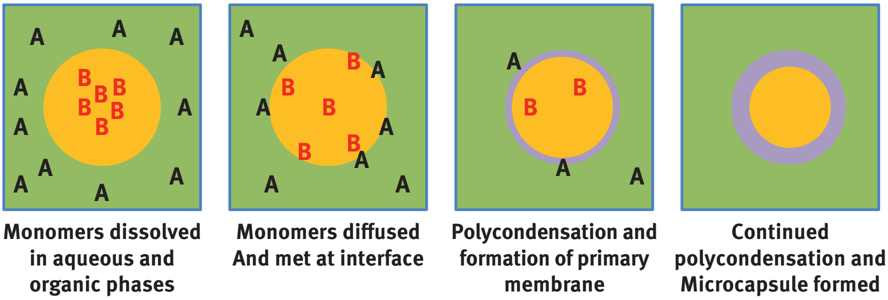

Figure 6.4: Graphical simplification of interfacial polymerization general procedure.

an American polymer scientist – Dr. Morgan from Dupont Nemour Company – who together with his research group published a series of articles in 1959 [10–13]. A few years later, the technology has been expanded, and since 1960 this method has been widely employed for encapsulation; however, the first patent that describes the basic methodology of this process was filled-in by Beestman and co-inventors in 1983 [14]. Since then, the method has been improved significantly.

Interfacial polymerization's tunable conditions make it applicable to various camps, e. g. agrochemicals, self-healing, pharmaceutics and cosmetics. Mainly four groups of polymers have been considered by researchers utilizing this technique: polyamides, polyurethanes, polyureas and polyesters [15]. Interfacial polymerization can be classified as a relatively simple, flexible and low-cost methods; thus, it is a valid method for industrial capsule manufacturing. Nevertheless, it seems that the process is still not well understood, e. g. the effect of the temperature, catalyst, surfactant and active ingredient are not entirely clear [16, 17]. One of major advantages of the interfacial polymerization techniques is its controllable character. Capsule mean size and membrane thickness can be directly designed. For instance, an interesting method of emulsification by the use of micropore metal membranes was proposed by Richard Holdich and his group [18]. The authors were able to directly control the size and homogeneity of the produced droplets, which were the matrices for the capsule shells.

Tylkowski et al. [19] fabricated microcapsules based on a new liquid crystalline lightly cross-linked polyamide, in which the state of order can be triggered by means of external stimuli, such as temperature and light. Figure 6.5 shows the scanning electron microscope (SEM) image of microcapsules prepared by the authors with toluene as a filler, deposited on a millipore teflon filter and dried at room temperature. The microcapsules appear separated, well-formed and globe shaped but deflated. According to the authors, this evidence can be related to the entrapped toluene evaporation in the high-vacuum conditions (10×10^{-2} mbar) employed in sample preparation. Figure 6.5(b) shows the SEM image of one of the

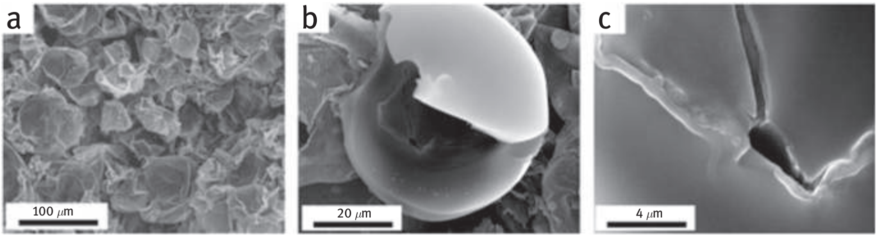

Figure 6.5: SEM micrographs of: (a) polyamide microcapsules containing toluene as a filler; (b) a single microcapsule after fracturing in liquid nitrogen; and (c) detail of the fractured surface. Wall thickness: 180 nm. Reprinted from European Polymer Journal, 45/5, Bartosz Tylkowski,Malgorzata Pregowska,Emilia Jamowska,Ricard Garcia-Valls,Marta Giamberini, Preparation of a new lightly cross-linked liquid crystalline polyamide by interfacial polymerization. Application to the obtainment of microcapsules with photo-triggered release, 1420-1432, Copyright (2009), with permission from Elsevier.

microcapsules after fracturing in liquid nitrogen, while Figure 6.5) shows the details of the fractured surface. The outer surface appears smooth and dense and few heterogeneity can be seen on the inner face. In the case of other polyamide capsules synthesized by the authors, one side of the shell appeared smooth, while the other one possessed a cellular structure [20]. An explanation for the dissymmetric structure of this kind of shell structure was proposed by Janssen and Nijenhuis [21, 22]: the wall of the capsules consists of a polymer formed by a polycondensation reaction at the oil/water interface; at or close to the organic side of the interface the reaction between monomers takes place and the polymer precipitates at the interface. This results in the production of a thin top layer of polymer, through which water and hydrophilic compounds (such as the diamine) can diffuse; as a consequence, the monomers proceed reacting under the formation of the sub-layer. The above-mentioned authors observed, in an oil-in-water dispersion, the appearance of little droplets which coalesce on the organic side of the membrane which is filling with water. This phenomenon is stopped by the polymer precipitation at their surface, which leads to the formation of a cellular inner structure; the longer the reaction time, the more heterogeneous is the inner surface of the membrane: for reaction times lower than 3 h, as in our case, the internal and external surfaces were found relatively homogeneous and smooth [23]. Incorporation of azobenzene photosensitive molecules into a capsule shell has also been performed by Marturano and co-workers [24]. The authors reported for the first time a straightforward route for the preparation of solid shell polymer nanocapsules with controlled UV-triggered release. A miniemulsion interfacial polymerization technique has been employed by the authors to prepare lightly cross-linked polyamide capsules with a hydrophobic liquid core. Based on the presented data, it can be concluded that an appropriate selection of surfactant type, its concentration and processing conditions allowed tailoring the size of the resulting nanocapsules. Podshivalov et al. [25] have studied an influence of agitation speed on the size of the capsules obtained by the interfacial polymerization process. The authors have utilized polyuthane–urea microcapsules containing galangal essential oil as a filler. The investigators performed the polymerization at the oil–water interface in oil–water emulsion. According to the authors, threshold value of agitation speed (4,000 rpm/min) was a decisive condition of the microcapsule size. Moreover, they reported that at higher agitation speed, the break-up of oil droplets strongly increases. As expected, higher agitation rate resulted in smaller size of microcapsules and with a narrower size distribution. A new type of poly(vinyl alcohol)(PVA)–polyurea composite microcapsules, containing isophorone diisocyanate as a core material, has also been successfully prepared via PVA-mediated interfacial polymerization in an oil-in-water emulsion by He and co-workers [26]. The authors reported a facile and versatile preparation protocol of robust microcapsules by using commercial and cost-effective raw materials. Prepared spherical microcapsules with a core content of ~80 wt% exhibited reliable service life and water resistance. Furthermore, the authors reported that investigated microcapsules possess enough mechanical stiffness for postprocessing. As stated in the publication, designed microcapsule shells were able to rupture when the crack approached, releasing the self-healing agent for crack healing. According to the authors, developed microcapsules exhibit remarkable performance for corrosion protection, and they could be used in structural materials with the ability to atomically heal cracks.

6.2.2 *In situ* polymerization

In situ polymerization is a broad concept that includes: (1) suspension polymerization, (2) emulsion polymerization and (3) dispersion polymerization. The literal translation of *in situ* means “in place,” which in terms of polymer science means in reaction mixture. Both the chemical methods presented in this review – interfacial polymerization and *in situ* polymerization – include polymerization reactions; however, in case of the *in situ* polymerization monomer or prepolymer are present only in the single phase of the reaction mixture, whereas in the interfacial polymerization each of the liquid phases contains at least one reactive monomer [6]. A clear division among the terms “suspension,” “emulsion,” “dispersion,” and “precipitation” as used in reference to heterogeneous polymerization systems was proposed by Arshady [27].

6.2.2.1 Suspension polymerization

The term suspension polymerization was very well-defined by Vivaldo-Lima and co-workers [28], who described it as a process in which monomer or monomers, relatively insoluble in water, is (are) dispersed as liquid droplets with steric stabilizer and vigorous stirring (which is maintained during polymerization) to produce polymer particles as a dispersed solid phase. Initiators soluble in the liquid monomer phase are employed in this polymerization process. In case when particle porosity is not required, the suspension polymerization is also known as pearl and bead polymerization. The main challenge in this technique is the formation of an as uniform as possible dispersion of monomer droplets in the aqueous phase with controlled coalescence of these droplets during the polymerization process. Based on the data collected by Vivaldo-Lima and co-workers, the microcapsule fabricated by this process typically have diameters in a range of 10 µm to 5 mm, which are strongly influenced by the following parameters: the interfacial tension, the degree of agitation and the design of the stirrer/reactor system govern the dispersion of monomer droplets. Moreover, the presence of suspending agents (e. g. stabilizers) hinders the coalescence of monomer droplets and the adhesion of partially polymerized particles during the course of polymerization, so that the solid beads may be obtained in the similar spherical form in which the monomer was previously dispersed in the water phase. Commercially available beads with a size above 10 µm can be easily separated from the suspension by filtration or/and sedimentation and then applied as a part of a final commercial products [29].

A very interesting paper was published by Sánchez-Silva et al. [30] in which the authors compared a laboratory scale and a pilot plant conditions for suspension-like polymerization process for the microencapsulation of paraffin wax by polystyrene. The authors carried out both designed experiments in water using polyvinylpyrrolidone, as a suspension agent, and benzoyl peroxide, as an initiator. According to the researchers, the suspension-like polymerization is an easy and an efficient method for microcapsule production at both scales. However, the scientists strongly underline that the condition of the reaction requires high temperature (108 °C) and 6 hours to complete the reaction, not counting the time required for the maintenance of the experimental setup.

Another impressive example of suspension polymerization microencapsulation was reported by Supsakulchai, Nagai and Omi [31]. The scientists encapsulated inorganic materials, such as titanium dioxide (TiO_x), in polystyrene-based matrix. In a frame of the presented project, the authors first prepared an emulsion by glass membrane emulsification process, then they performed polymerization step and finally they recover capsules by centrifugation. To favor the TiO_2 dispersion stability in the oil phase, the authors applied two strategies. The first one was based on an addition of a co-monomer, 2-ethylhexyl acrylate, while the second one was created by adding the same co-monomer, however, in the presence of a cross-linking agent, such as a divinyl benzene. It should be mentioned that by using both the approaches the authors obtained uniform composite particles with the average diameters in a range 20–25 µm. The method used by the authors allows mass production in one batch, easy modification of the capsule walls, flexibility of monomer selection and cross-linked polymers applicable as advantages and undesirable sub-micron aggregates and the possibility of phase separation during the polymerization step as the process drawbacks.

6.2.2.2 Emulsion polymerization

Emulsion polymerization occurs when monomer is added dropwise to the solution of core material and surfactant (emulsion). Katampe et al. [32] have used this type of encapsulation technique to fabricate microcapsules by enwrapping an oily core material in an amine–formaldehyde condensation product formed by *in situ* polymerization. Their invention included a synthetic viscosity modifier (cross-linked polymer of acrylic acid) which was added to the aqueous phase of the oil-in-water emulsion. According to the investigators, this component allows the production of a more uniform, controlled, relatively small-size microcapsules. Bonetti et al. [33] optimized the semicontinuous emulsion polymerization protocol to synthesize poly(*n*-butylacrylate)@polystyrene nanocapsules. The authors developed a novel variation of the emulsion polymerization encapsulation, which includes two-step process. First, the core-forming monomer was emulsified in a continuous phase. Subsequently, the polymerization of the nanodroplets was initiated by 2,2-azobisisobutyronitrile and the second monomer was added (during a second step). The authors highlighted that by employing these biologically friendly solvent method (by using i. e. water), they got microcapsules with a size diameter in an order of 10^2 nm.

6.2.2.3 Dispersion polymerization

Dispersion polymerization takes place when the monomer, initiator and dispersant are present in the same batch. Great influence in this process has a solvent, which needs to be sufficient for all aforementioned substrates but it does not dissolve a produced polymer; thus the polymer will precipitate in it [34]. Lee et al. [35] patented the microencapsulation of a pigment dispersed with a polymeric dispersant and a polymerization initiator in an aqueous solvent system. The innovation of the presented patent based on two or more additions of monomers led to the polymerization and subsequent thicker shell formation. According to the authors, two (or more)-step dispersion polymerization technique provides microcapsules with high amount of encapsulating polymers around the pigment, thus with improved mechanical properties in comparison to the one-step dispersion polymerization technique. Bourgeat-Lami and Jacques Lang [36] have employed dispersion polymerization to encapsulate silica beads with styrene in an aqueous ethanol medium using poly(*N*-vinyl pyrrolidone) as a stabilizer and 2,2-azobis (isobutyronitrile) as an initiator. To promote encapsulation on the surface of the beads, the authors treated the silica with 3-(trimethoxysilyl) propyl methacrylate, which was grafted onto its surface. Polymerization reaction was performed in a batch process, in the ethanol/water

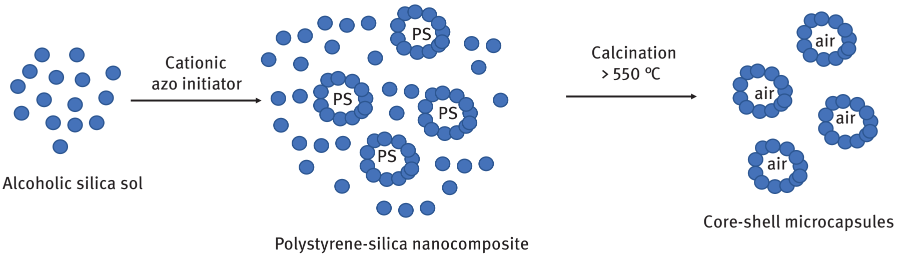

Figure 6.6: A schematic representation of submicrometer-sized polystyrene–silica nanocomposite particles production and their transformation into core/shell microcapsules by a calcinations.

mixture. Silica beads that gave the most satisfactory results had 450 nm of diameter; nevertheless, even the synthesis that utilized those beads led to the creation of the composites that contained more than one silica bead per composite. Mostly, the composites contained up to four silica beads. Micrometer-sized silica-stabilized polystyrene latex particles and submicrometer-sized polystyrene–silica nanocomposite particles have been prepared by Schmid and co-workers [37]. The investigators used the dispersion polymerization of styrene in alcoholic media in the presence of a commercial 13 or 22 nm alcoholic silica sol as the sol stabilizing agent. The authors reported that micrometer-sized near-monodisperse silica-stabilized polystyrene latexes were obtained when the polymerization was initiated by a nonionic initiator (2,2-azobisisobutyronitrile), while submicrometer-sized polystyrene–silica nanocomposite particles were produced by using a cationic azo initiator. At the end of the process, the particles were transformed into core/shell microcapsules by a calcination as illustrated in Figure 6.6.

6.3 Physicochemical methods

Physicochemical methods involve procedures where chemical interaction occurs along with various physical transformation to shape the capsules.

6.3.1 Coacervation

Coacervation is the first method concerning encapsulation technology protected by an international patent law. This pioneer method was developed and described by Green & Schleicher, from the National Cash Register Company, Dayton, USA, who in 1953 filled in a US Patent# 2730456 by a title: Manifold record material. The inventors encapsulated trichlorodiphenyl inside microscopic gelatin capsules by coacervate forces. Since then, the coacervation has been defined as a process in which “an active agent is distributed within the homogenous polymer solution, and by triggering coacervation colloidal polymer aggregates (coacerates) are formed on the outer surface of an active agent droplet." The process can be initiated by varying one or more of parameters of the system, such as temperature, pH or the composition of the reaction mixture (addition of water-miscible nonsolvent or salt). In case of the aforementioned patent, the coacervation was initiated by the addition of sodium sulfate salt.

Coacervation techniques are divided into two subgroups, which differ in the mechanism of the phase separation:

- simple coacervation – occurs when a selected polymer for microcapsule preparation is salted out or desolvated.
- complex coacervation – is achieved by a complexation of two or more oppositely charged polyelectrolytes. The method is presented schematically in Figure 6.7. It is a four-step process: (A) dispersion of the core material in homogenous two-different-polymer solution, (B) initial agglomeration of polyelectrolytes after triggering the coacervation, (C) coacervation of polymer on the surface of the core and (D) wall hardening.

During the last decades, several different research groups have improved the complex coacervation method. Dardelle and co-workers [38] have modified it to produce capsules with improved barrier properties for encapsulated material. First, the authors mixed selected polymers with various types of solid particles (kaolin, silica, Fe_2O_3). Then, they introduced a core material to the particle/polymer complexes, and the obtained hybrid coacervate sol gained a desired viscosity that allowed the aggregates to deposit on the core material to form the capsule shell. In other respects, Kumar et al. [39] patented a novel coacervation process in which the core material/polymer complexes were exposed to one or more coacervation agents in at least two distinctive stages. In this way, the inventors were able to produce capsules with a consistent particle size using easily scalable process. Baker and Ninomiya [40] developed a complex coacervation method, in which to achieve high core-content capsules and avoid unwanted agglomeration, the authors introduced two additional steps. First, they mixed a core material with a coacervation adjuvant (such as an ionizable colloid, an ionic surfactant, or an ionizable long-chain organic compound) prior to emulsification process, and then, after gelation step, the authors

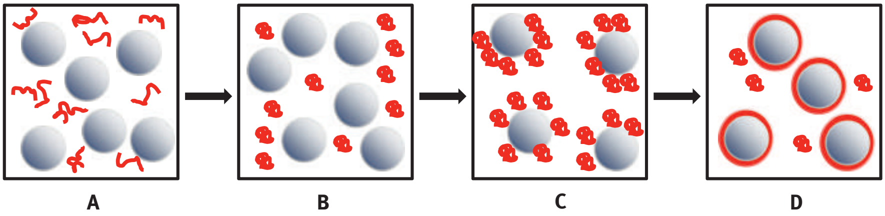

Figure 6.7: Schematic overview over the principal process steps in the capsules production by complex coacervation.

introduced a water-soluble wax that initiated hardening of produced capsule walls. Based on numerous published articles and reviews [41–44], it could be summarized that the coacervation processes during the last years became a widely used encapsulation method, due to their simplicity, low cost and reproducibility. Moreover, these methods can be easily scaled-up to fabricate microcapsule at the industrial setup. Nevertheless, these techniques need a constant attention and an adjustment of operating conditions (such as stirring, viscosity, pH and temperature). Besides, by using these methods, unwanted capsule agglomeration has been commonly observed.

6.3.2 Layer by layer

LbL assembly method was for the first time reported by Caruso & Crusco and Möhwald in 1998 [45]. The method was based on the self-assembling of oppositely charged polyelectrolytes on the outer surface of colloidal particles. The inventors prepared hollow silica and silica–polymer spheres with diameters between 720 and 1,000 nm by consecutively assembling silica nanoparticles and polymer onto colloids and subsequently removing the templated colloid either by calcination or by decomposition upon exposure to solvents. Scanning and transmission electron microscopy images reported by the authors demonstrated that the wall thickness of the hollow spheres can be readily controlled by varying the number of nanoparticle–polymer deposition cycles. Moreover, the authors stated that the capsule size and shape can be determined by the morphology of the templating colloid. The LbL technique can offer capsules with a broad permeability coefficient spectrum that can be tailored depending on the desired application, which includes biosensor, catalyst, agriculture, drug carrier, etc. Active targeting of nanoscale drug carriers can improve tumor-specific delivery; however, cellular heterogeneity both within and among tumor sites is a fundamental barrier to their success. Promising studies in this field have been carried out by Dreaden and co-workers [46], who described a tumor microenvironment-responsive LbL polymer drug carrier that actively targets tumors based on two independent mechanisms: (1) pH-dependent cellular uptake at hypoxic tumor pH and (2) hyaluronan-directed targeting of cell-surface CD44 receptor – well-characterized biomarker for breast and ovarian cancer stem cells. Hypoxic pH-induced structural reorganization of hyaluronan–LbL nanoparticles was a direct result of the nature of the LbL electrostatic complex and led to targeted cellular delivery *in vitro* and *in vivo*, with effective tumor penetration and uptake.

As illustrated in Figure 6.8, the nanoscale drug carriers selectively bound CD44 and diminished cancer cell migration *in vitro* while co-localizing with the CD44 receptor *in vivo*. Because these LbL nanoparticle systems are simple, provide means of modular design and can provide enhanced blood half-life and enhanced tumor targeting, hyaluronan–LbL nanoparticles are promising candidates for targeted drug

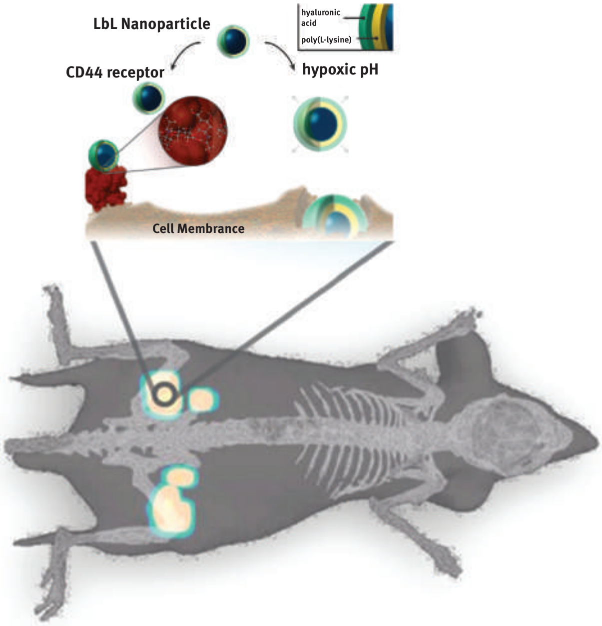

Figure 6.8: Schematic illustration of bimodal tumor targeted delivery.

delivery to solid tumors for number of significant cancer types. The ability to target multiple tumor cell populations without the use of additional drug carrier may circumvent resistance from selective pressure while improving safety and treatment outcomes from actively targeted nanomedicines.

Tao, Li and Möhwald [47] reported that LbL capsules containing an azo dye in their shell permitted photochemical control of the permeability of the capsule wall. In this investigation, the microcapsule shell was built by an azo dye – Congo red (CR) – and different polymers, including poly(styrenesulfonate, sodium salt) (PSS), poly-(allylamine hydrochloride) (PAH) and poly(diallyldimethylammonium chloride) (PDDA).

Figure 6.9 illustrates the general protocol which have been used for the LbL self-assembly of PDDA/CR onto the (PSS/PAH)3/PSS shells templated on melamine formaldehyde (MF) latex particles. In order to analyze morphology change of the microcapsule shell before and after irradiation caused by trans-cis photoisomerization of azobenzene moieties incorporated in the capsule shell, the authors employed scanning force microscopy (SFM). Furthermore, the optical changes of the capsules were verified by using confocal laser scanning microscopy and SFM. All results generated by the authors provide useful insights into the photochemical reaction mechanisms on the self-assembled PDDA/CR composite capsules and release of encapsulated material. This kind of capsule

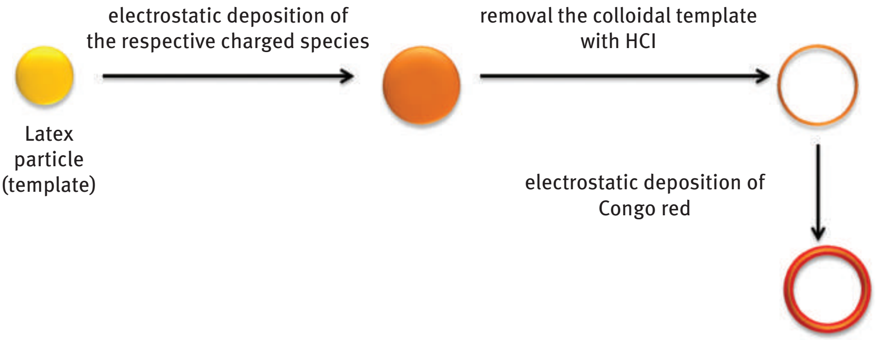

Figure 6.9: General procedure for the fabrication of hollow LbL self-assembly capsules composed of PDDA/CR onto the (PSS/PAH)3/PSS shells templated on the MF latex particles.

with photo-controlled permeability could be of particular interest for applications in drug delivery, photocatalysis, optical materials and related medical areas such as photodynamic therapy or skin care. The concept of photosensitive microcapsules has also been studied by Bédard and co-workers [48] who constructed the microcapsules containing azobenzene moieties through LbL self-assembly of sodium salt of azobenzene, poly(vinylsulfonate) and PAH; however, contrary to Möhwald and co-workers, they investigated how *trans-cis* isomerization of the azo moieties influences the permeability changes of the shell and on encapsulation of the active material instead of its release during light irradiation. According to the authors, incorporation of azobenzene groups can cause shrinking of the microcapsule wall, increase their permeability and as a consequence encapsulate required materials. More recent examples using stimuli-responsive capsules based on azobenzene moieties in the capsule wall are deeply contemplated in [49].

Very interesting approaches have been performed by Hammond and Zhiyong [50] who designed nanosized capsules that exhibit a multifunctionality. The authors used (1) gold nanoparticles as core materials – which act as imaging and drug revisers and (2) therapeutic agents – which are allocated within 2 nm sized LbL capsule wall.

LbL assembly is an extremely valuable, economic and versatile technique for capsule formation. Final material properties can be easily tailored through the thoughtful selection of the active agent, coating material and assembly conditions. LbL as much as it is beneficial has one current limitation which is the standard manual, where numerous time-consuming centrifugation and resuspension are needed to perform the layering steps. Björnmalm et al. [51] overcome this problem introducing a novel fully flow-based technique using tangential flow filtration, which can make the process scalable, controllable and automatable production.

6.3.3 Sol–gel encapsulation

Sol–gel encapsulation is an abbreviation for “solution-gelling.” The term stands for the process where sol is added to the precursor solution, and by alternating physicochemical factors the material is gelled and hardened into the shape of the capsules [52]. Broadly speaking, sol–gel processes can be divided into six steps: hydrolysis, condensation, gelation, ageing, drying and densification [53]. Sol–gel encapsulation techniques have been widely used [53–56]; however, in this review, we focus on the capsules prepared by the use of organosilanes which are extensively studied nowadays due to their surface functionalities and processing conditions (pH, gelation time, etc.). Organosilanes are also compatible with various biomolecules, such as drugs, proteins, antibodies, enzymes, nucleic acids, prokaryotic and eukaryotic cells, which makes silica and its derivatives a suitable capsule material for bioapplications. The most studied sol–gel methods for encapsulation of biological materials, which have been reported in literature, are hydrolysis and condensation of alkoxides, such as tetramethyl orthosilicate or tetraethyl orthosilicate [57–59]. The conventional routes can lead to decrease or total inhibition of the activity of entrapped biomolecules, due to the formation of an alcohol as a byproduct. Bhatia et al. [60] developed an aqueous sol–gel process in which sodium silicate was used as a precursor and the gelation phase was performed at neutral pH and room temperature. By applying the designed methodology, the authors were able to preserve the activities of encapsulated enzymes: high horseradish peroxidase and glucose-6-phosphate at values of specific activity upon immobilization 73 % and 36 %, respectively, after encapsulation. Moreover, the authors reported that encapsulated enzymes exhibited a pH-dependent behavior that is different from that of free enzymes. According to the authors, the silica matrixes offer a number of advantages over conventional organic polymers as immobilization platforms for biosensors owing to their superior mechanical strength, chemical inertness, hydrophilic nature and, above all, optical transparency.

Mikosch and Kuehne [61] have established experimentally optimized conditions of colloid and sol–gel co-assembly for directly printed colloidal crystals. The authors used mixtures of 50 vol % of colloids to 50 vol % of 1,2-bis(triethoxysilyl)ethane (BTES) as the sol–gel precursor which led to the best results, with an efficient encapsulation of colloidal crystals with BTES. According to the authors, the developed method is easily scalable and could be adopted for inkjet printing of colloids, as well as for convective assembly (Figure 6.10).

The optimized conditions for co-assembly will facilitate the production of inkjet-printable photonic crystals that will ultimately lead to self-assembled laser resonators and filters, which can be precisely positioned and patterned into desired structures.

Figure 6.10: Artistic representation of the drop-casting and coassembly process. Reprinted with permission from (61). Copyright (2016) American Chemical Society.

6.3.4 Suspension cross-linking

Microcapsule formation by this technique involves dispersion of an aqueous solution of the polymer-containing core material in an immiscible organic solvent (suspension/dispersion medium) in the form of small droplets. The suspension medium contains a suitable stabilizer to maintain the individuality of the droplet/ microcapsules. The droplets are subsequently hardened by covalent cross-linking and are directly converted to the corresponding microcapsules. The cross-linking process is accomplished either thermally (at >500 C) or using a cross-linking agent (formaldehyde, terephthaloyl chloride, etc.). Suspension cross-linking is a versatile method and can be adopted for microencapsulation of soluble, insoluble, liquid or solid materials and to produce both micro- and nanocapsules [62]. Suspension polymerization reactions generally produce particles with a broad or bimodal size distribution. Bead particles, which are the intended product from a suspension polymerization, with diameters in the range of 10 μm–5 mm, are usually accompanied with unintended smaller particles [63]. Many aspects of suspension polymerizations have been reviewed in the literature [27–29, 64, 65]. The history of suspension cross-linking process originates from the pioneering work in three independent areas of applied polymer research in the late 1960s, which are very well-described in a review published by Arshady [66]. In 1969, Rhodes and co-workers [67] and Pasqualini et al. [68] reported the use of suspension cross-linking for the preparation of albumin microspheres for diagnostic investigations. At about the same period, Khanna and Speiser [69] fabricated epoxy resin microcapsules by cross-linking (curing) of the molten polymer in silicone oil. In 1971, work on the improvement of hydrophilic polymer supports for chromatography led to the development of suspension cross-linking procedures for the preparation of cross-linked procedures for the preparation of cross-linked agarose microspheres by Porath and co-workers [70] and cross-linked cellulose beads by Chimbo and Brown [71].

Suspension cross-linking procedure have been widely used for the preparation of polysaccharide-based polymer supports for chromatography and biomedical applications. Suspension cross-linking has also been the method of choice for the production radiolabeled albumin microspheres as diagnostic imaging reagents. The main challenge of suspension process is the tendency during polymerization for the viscous and adhesive droplets and pearls to agglomerate or to stick to each other, which leads to serious trouble from heat build-up and the formation of large polymer masses [72]. The control of size and size distribution of particles can be achieved by adjusting the reaction parameters, such as stirring speed, reaction temperature, composition and type of reactor system. In general, vigorous stirring, higher temperatures, higher catalyst concentrations and faster polymerization result in finer granules of product. However, too much agitation also may be harmful and may give beads deformed or containing holes because of stirring in of gas. If very effective suspending agents are used in corresponding amounts, quite fine granules result even at low rates of stirring. Addition of suspending agents or suspension stabilizers to the aqueous phase can prevent the agglomeration and sticking together during polymerization and can make the process dependable. Among good suspending agents are found water-soluble high polymers (the so-called protective colloids) such as PVA, polyvinylpyrrolidone, polyacrylic acid or natural gums [63]. Regulation of the encapsulated material release is still a challenging task for science nowadays. There have been many studies analyzing this matter, e. g. Dini et al. [73] published the preparation method of chitosan microspheres loaded with a drug hydroquinone. They have proved that the release of the drug was correlated with the degree of cross-linking. Therefore, by adjustment of the cross-linking agent used in the preparation step, in this case glutaraldehyde, control over drug release is possible.

6.4 Physicomechanical methods

Physical methods do not involve any polymerization reactions considering that the starting materials in these cases are polymers, thus broadly speaking only the formation of shape occur. Few examples of these techniques are listed below.

6.4.1 Spray-drying

Drying is the oldest known method for removing a liquid from wet bulk materials. Already in the older Stone Age, people have dried food to store it for a long time. In the seventeenth and eighteenth centuries, various substances were usually dried by hot air or smoke. In the nineteenth century, the drying by vacuum or by spraying was developed. A century later, the drum dryer and vacuum-freeze dryer were invented [74].

Spray-drying is a process where liquid phase (emulsion, suspension or solution) is forced to form droplets by an atomizer or a spray nozzle. In the advanced developed part of the devise, droplets are dried by the hot air and solidified capsules are created and collected. A schematic representation of this technology is shown in Figure 6.11.

This method has been widely used since the nineteenth century in the industry due to its simplicity, flexibility and consistent particle size distribution and the system can be fully automated [75]. Nevertheless, spray-drying operation presents several drawbacks such as low thermal efficiencies, nozzle clogging and high maintenance costs. Moreover, product loss has been commonly observed, due to the agglomeration of capsules and material sticking to the internal chamber walls. Also, it is highly unlikely to obtain capsules of smaller size than 100 µm [76–78]. Therefore, the process calls for various optimizations. Maury et al. [79] studied the effects of spray-drying parameters on the material yield at laboratory scale spray-dryer. According to the authors a cyclone with the narrow outlet duct is more convenient at laboratory scale spray-dryer. Whereas the T_{inlet}/T_{outlet} was pointed

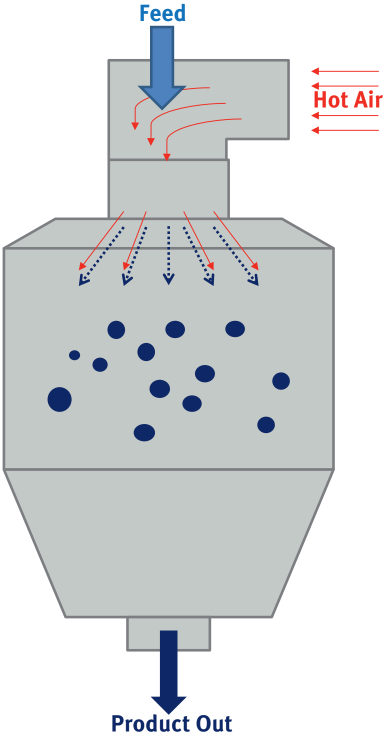

Figure 6.11: Schematic representation of basic spray-drying procedure.

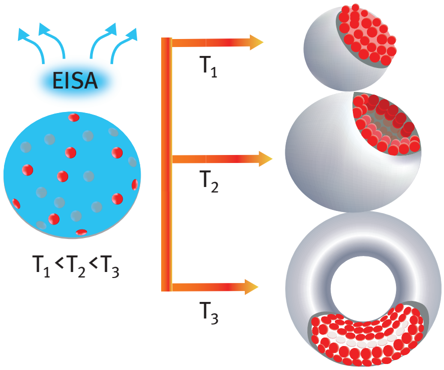

Figure 6.12: Graphical representation of spray-dried capsule’s morphologies obtained with different drying temperatures. Reprinted (adapted) with permission from (80). Copyright (2016) American Chemical Society.

out to be the most important operatory condition to optimize the product yield. This parameter cannot be too high because in other case the inside walls of the spray-dryer reaches the temperature higher than the sticky point of the material. The authors measured that when the parameter exceeds by approximately >10 °C, a product loss is observed. Biswas et al. [80] demonstrated that the morphology of spray-dried nanostructured microcapsules can simply be tuned by controlling the drying temperature, as illustrated in Figure 6.12.

At lower temperature, the nanoparticles are assembled compactly forming spherical granules. In such a case, the size distribution of the granules gets narrowed down with respect to that of the initial droplets. Increase in temperature leads to the formation of larger hollow capsules with nanoparticles packed as a thinner shell. This is because of the preferential motion of the nanoparticles in droplet under a temperature gradient. At still higher temperature, subsequent buckling of the shell leads to the formation of toroidal granules. Polydispersity in granular size increases with temperature. Evolution of capsule shape corroborates with the Surface Evolver computer model, based on buckling of the elastic shell taking into consideration the rate of drying. Statistically averaged local volume fraction of the packed nanoparticles in the capsules remains nearly temperature independent, even though the external morphology changes significantly from sphere to toroid. Scattering experiments indeed differentiate between the two apparent structural correlations that can lead to larger capsule size at higher temperatures. The authors established that increase in capsule size with temperature and consequent buckling are due to the existence of an internal hollow core and not because of the formation of nonconsolidated fractal-like aggregates.

The aim of the research studies performed by Drusch and co-workers [81] was to identify principal parameters determining the oxidative stability of microencapsulated fish oil. The authors prepared the capsules by spray-drying using different types of *n*-octenylsuccinate-derivatized starch, gum Arabic, sugar beet pectin, sodium caseinate and/or glucose syrup. They identified two principal components to classify the different microcapsules accounting for up to 79 % of the variance as shown in Figure 6.13. The principal components were determined by physicochemical parameters reflecting the emulsifying ability of the encapsulant and the drying behavior of the parent emulsion. Microcapsules, which were identified by principal component analysis to be significantly different, exhibited a low stability upon storage,

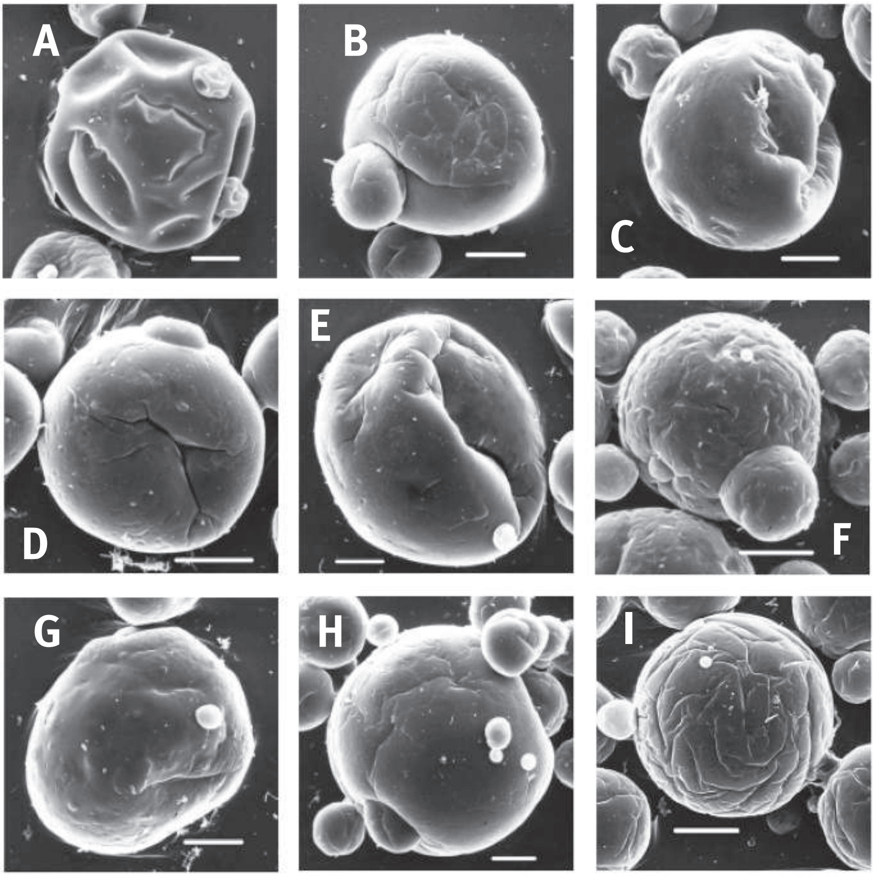

Figure 6.13: Scanning electron micrographs of microencapsulated fish oil spray-dried at 180/70 °C (A, nOSA-starch type 1; B, nOSA-starch type 1/glucose syrup; C, nOSA-starch type 2; D, nOSA-starch type 2/glucose syrup; E, nOSA-starch type 1/gum Arabic; F, gum Arabic; G, sugar beet pectin; H, caseinate/glucose syrup, 1/4; I, caseinate/glucose syrup, 1/19). White bar = 10 μm. Reprinted (adapted) with permission from (81). Copyright (2007) American Chemical Society.

showing that the principal components and, thus, the underlying physicochemical parameters analyzed in the present study are correlated with core material stability. Bertolini and co-workers [82] have investigated the stability of monoterpenes encapsulated in gum Arabic by spray-drying. The authors used the following core materials: citral, linalool, β-myrcene, limonene and β-pinene at concentrations of 10, 20 and 30 % with respect to the wall material. The authors observed that the chemical functionality, associated with the solubility and diffusion through the forming matrix, determines the degree of retention in the production of capsules by spray-drying, in the case of monoterpenes encapsulated in gum Arabic. The order obtained was hydrocarbon > aldehyde > alcohol for monoterpenes with similar molecular weights. Hydrocarbons with the same molecular weight ($C_{10}H_{16}$) and similar solubilities presented different yields in the drying process. According to the authors, these differences were associated with the molecular structures of the monoterpene isomers. The observed order was bicyclic > monocyclic > acyclic, demonstrating the contribution of steric factors to retention in addition to the ability to undergo polarization.

Under this investigation, the products encapsulated in gum Arabic showed a reduction in content during the shelf-life study at controlled temperature. There was little variation in the content during the first 20 days, but after this there was an accentuated and variable loss for the majority of the monoterpenes studied. The observed order of retention was β-pinene > citral > limonene > β-myrcene > linalool.

A novel route for fast, scalable and continuous assembly of highly monodispersed core–shell microencapsulates was presented by Liu et al. [83], who used Eudragit RS (a co-polymer of ethyl acrylate, methyl methacrylate and a low content of methacrylic acid ester with quaternary ammonium groups) as the main shell component and silica as the core component. Because the core–shell architecture could be formed directly by evaporation-induced self-assembly during the single-step spray-drying process, no prolonged chemical reactions or organic solvents were needed. The investigators demonstrated that the microcapsule wall thickness can be easily tuned by adjusting the ratio of the materials in the precursors. The resultant microencapsulates were shown to encapsulate almost 100 % of the active component (in this case, a water-soluble compound, rhodamine B), while the release rates could be directly correlated to the microstructures. This study provides a new scope for practical synthesis of hybrid nanocomposites and functional heterostructures, including core–shell structures with distinct controlled release properties for each section.

6.4.2 Co-extrusion

Co-extrusion was first patented in 1957 and in future was developed by the group that originally patented the technique [84]. It is a process where dual fluid stream is pumped through the nozzle. One of the liquids contains core material and the other

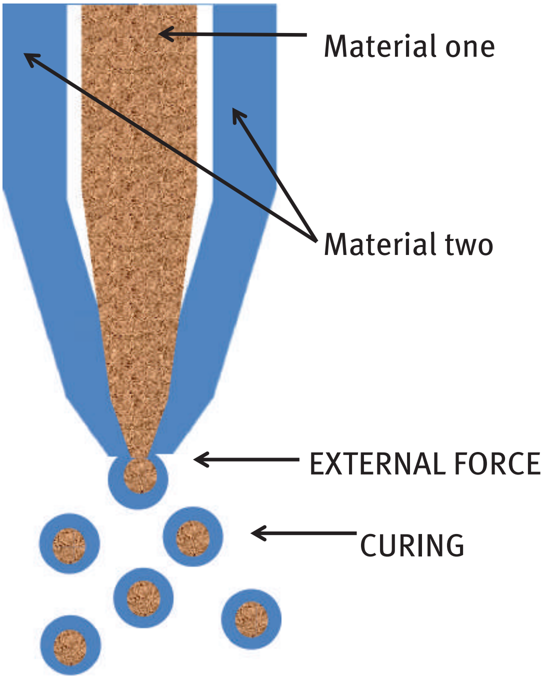

Figure 6.14: Schematic of a co-extrusion process.

wall material. Droplet is formed by the vibrations applied at the exit of the concentric tubes. Then, the droplet undergoes solidification by chemical cross-linking, cooling or solvent evaporation [85]. A schematic representation of co-extrusion is shown in Figure 6.14.

Depending on the device, a monocentric or concentric nozzle system is used, which produces different types of microcapsules, respectively, by extrusion and co-extrusion. The concentric system presents internal and external nozzles that allow the production of reservoir-type microcapsules [86]. Extrusion microencapsulation has been used almost exclusively for the encapsulation of volatile and unstable flavors in glassy carbohydrate matrices. The main advantage of this process is the very long shelf-life imparted to normally oxidation-prone flavor compounds, such as citrus oils, because atmospheric gases diffuse very slowly through the hydrophilic glassy matrix, thus providing an almost impermeable barrier against oxygen. Shelf-lives of up to 5 years have been reported for extruded flavor oils, compared to typically 1 year for spray-dried flavors and a few months for un-encapsulated citrus oils [87]. Very recently, Pasukamonset et al. [88] published very interesting results concerning the microencapsulation of phenolic extracts of *Clitoria ternatea* (CT) petal flower extract through the extrusion method of alginate with calcium chloride ($CaCl_2$). The authors reported that the encapsulation efficiency varied in the range from 74 ± 1 % to 85 ± 1 % depending on the percentage of CT (5–20 %), alginate (1–2 %) and $CaCl_2$ (1.5–5 %). The results showed that the optimized condition of CT-loaded alginate beads (CT beads) was as follows: 10 % CT, 1.5 % alginate and 3 % $CaCl_2$ (w/v). Under this condition, the maximal antioxidant capacity of 11.7 ± 0.1 mg gallic acid equivalent/g_{beads} and the encapsulation efficiency of 84.8 ± 0.4 % were obtained. Moreover, the provided results demonstrated that the prepared microcapsules possessed smooth surface shape with a particle size distribution of 985 ± 0.5 µm. Without any doubts, this report provides a novel food-grade encapsulation formulation to improve the stability as well as the biological activity of plant polyphenols. Recently, Shinde et al. [89] evaluated the co-extrusion using alginate and apple skin polyphenols to protect *Lactobacillus acidophilus* in a milk beverage at 4 °C. The authors decided to employ probiotic bacteria and polyphenols for microcapsule preparation due to their great demand in food products. Lactic acid bacteria have been used to ferment or culture foods for at least 4,000 years. The bacteria have been used in particular in fermented milk products from all over the world, including yoghurt, cheese, butter, buttermilk, kefir and koumiss. Probiotics are defined as “live microorganisms which, when, administered in adequate amounts, confer a health benefit on the host” [89] and polyphenols possess antioxidant capacity, anti-inflammatory and anticarcinogenic properties, as well as protective effects against a variety of chronic diseases [90–93]. The results published by Shinde et al. [89] indicated that the co-extrusion technology was efficient to protect probiotics after 50 days of storage, due to very low decrease on cell viability. Very recently, Silva et al. [94] reported exciting results concerning encapsulation of *Lactobacillus paracasei* BGP-1 probiotic dispersed into sunflower oil or coconut fat by using the co-extrusion process. Under this study, the authors used alginate or alginate-shellac blend as capsule shell materials and fluidized bed or lyophilization as post-treatment processes to dry the capsules. By using the co-extrusion method, Silva et al. [94] have been able to prepare capsules with a diameter between 0.71 and 0.86 mm, which encourage their application in solid foods, such as cereal bars, dark chocolate and mixed nuts. The authors reported that after 60 days of storage at 25 °C, the viability of probiotic loaded into capsules dried by fluidized bed was up to 6 log CFU/g, corresponding to 90 % of the initial probiotic population. In addition, the formulation produced with alginate-shellac and coconut fat was the most effective at improving probiotic survival in simulated gastrointestinal fluids, mainly by reducing the porosity of microcapsules, in which 7.5 log CFU/g of probiotics (95 %) survived at the end of the assay. Thus, according to the authors, immobilization of probiotics in coconut fat co-extruded with alginate-shellac blend followed by fluidized-bed drying is a promising technology to protect and extend the viability of probiotics in functional foods.

Wang et al. [95] investigated a co-extrusion as a feasible approach of a canola oil encapsulation with alginate and alginate–high methoxyl pectin. The authors have also studied how conditions of co-extrusion affect capsule characteristics, core oil stability and retained phenolic content. They discovered that flow rates of core and shell are the critical parameters to create stable spherical oil beads. The authors demonstrated that the shell wall composition is responsible for the bead size, core oil stability and retained phenolic content. He and co-workers [96] have used a minifluicid device to fabricate calcium alginate capsules by extrusion (Figure 6.15).

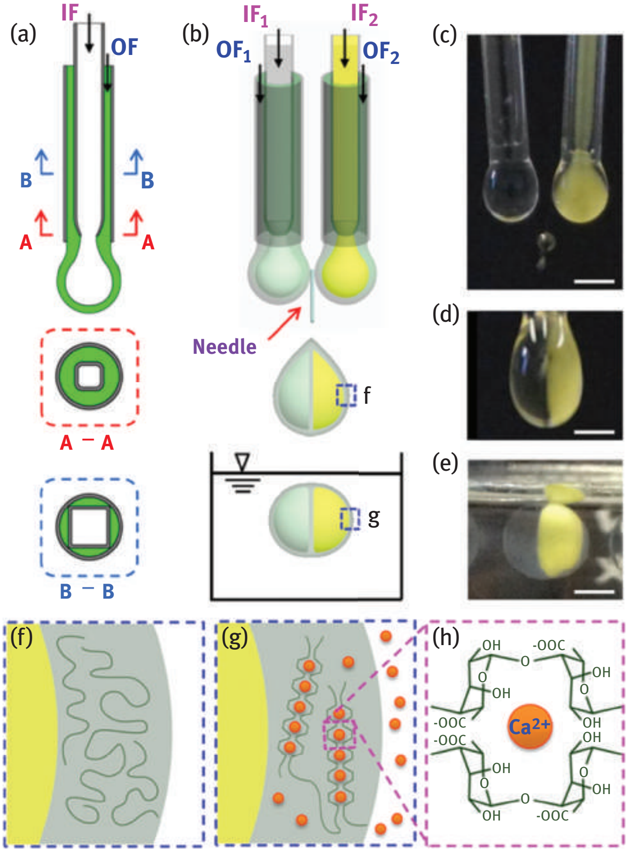

Figure 6.15: Coextrusion minifluidic devices for fabrication of dual-compartmental Ca–Alg capsules. (a) Schematic illustration of the coextrusion minifluidic device for fabricating water-in-water (W/W) droplets. (b) Schematic illustration showing the combination of two coextrusion minifluidic devices for fabricating the dual-compartmental Ca–Alg capsules. (c–e) Digital photos showing the generation of two different W/W droplets at the outlets of the devices (c), the coalescence of the two W/W droplets triggered by the stainless steel needle (d), and the formation of dual-compartmental Ca–Alg capsules in the $Ca(NO_3)_2$ solution (e). Folic acid (yellow color) is added in the core compartment of one W/W droplets for labeling. The scale bars are 2.5 mm. (f–h) Schematic illustrations showing the cross-linking mechanism of alginate in the shell solution (f) by cross-linking with Ca^{2+} from the $Ca(NO_3)_2$ solution (g) via formation of egg-box structures (h). Reprinted (adapted) with permission from (96). Copyright (2016) American Chemical Society.

The authors reported that this novel approach offers an impressive control level over the volume and number of multiple compartments by adjusting flow rates and numbers of orifices of the device. Dual-compartmental capsules obtained by the authors contained one-half shell with a constant release rate and the other half shell with a temperature-dependent release rate. Therefore, the authors fabricated capsules with different permeability rates, which makes them a huge potential for various advanced applications as a multifunctional material. Nevertheless, the size of the capsules needs to be decreased, because now it is situated in the mm range, and it is an insuperable obstacle for many application.

6.4.3 Fluidized-bed spray coating

Originally developed as a pharmaceutical technique, fluidized-bed coating is now increasingly being applied in the food industry to fine-tune the effect of functional ingredients and additives. The main benefits of such miniature packages, called microcapsules, include increased shelf-life, taste masking, ease of handling, controlled release and improved esthetics, taste and color. Fluidized-bed coating increasingly supplies the food industry with a wide variety of encapsulated versions of food ingredients and additives. Compared to pharmaceutical fluidized-bed coating, food industry fluidized-bed coating is more obliged to cut production costs and, therefore, should adopt a somewhat different approach to this rather expensive technology. Solid particles are suspended in a temperature and humidity-controlled chamber of high-velocity air where the coating material is atomized [1, 24]. Though fluidized-bed drying offers a lot of advantages, freeze and spray-drying are preferred drying techniques for probiotic microencapsulation. Compared to lyophilization, fluidized-bed drying is more cost effective. Due to an optimal heat and mass transport as well as equal temperature distribution, drying and granulation processes in a fluidized-bed dryer can be carried out at lower temperatures compared to spray-drying which results in higher survival rates of encapsulated bacteria [25]. Further, granulation and coating procedures can be combined within one fluidized-bed drying process. At least, the coating material determines the protection and targeted release properties. Due to their numerous advantages, the fluidized-bed technology has gained significant importance in the last century in many industrial processes. Fluidized beds are particularly advantageous due to the simple solid handling through the fluid-like behavior, intensive solids mixing and the resulting uniform temperature distribution, large exchange surface between solid and gas and high heat transfer value between solid and gas. In most cases, the heat required for the drying process in fluidized beds is provided by means of a preheated fluidizing gas. Moreover, additional thermal energy can be inserted to the process either by immersed heating elements, e. g. steam-heated tubes, or by heating of the fluidization chamber wall. Due to the contact of particles with heated surfaces, additional heat transfer is available leading to process intensification, i. e. higher drying rates due to increased heat transfer area. Lower gas inlet temperature is requested, which is preferable for heat-sensitive products. However, limited number of tubes, influence on flow field and fouling are subject to the limitations of the process intensification by contact heating [74].

6.4.4 Phase-inversion precipitation

Phase-inversion precipitation method comprises mass transfer and phase separation processes which occur when polymeric solution in the form of droplet get in contact with a nonsolvent and the polymer precipitates. Phase-inversion or immersion precipitation is usually isothermal, ternary system. This technique includes involvement of three components: solvent, nonsolvent and polymer. Process begins by dissolving polymer in its solvent and molding it into a wanted shape, for example film or droplet. Then, the solution is immersed in the nonsolvent bath, which will activate the exchange between molecules of solvent and nonsolvent. Transfer between the solvents will inevitably force precipitation of the polymer, resulting in the final porous structure of the obtained membrane [97].

Bogdanowicz and co-workers [98] prepared photoresponsive microcapsules, based on poly(α–methylstilbenesebacoate-co-α-methylstilbeneisophthalate) (P4), containing different core materials, by using a phase-inversion precipitation process. The authors made the hypothesis that phototriggered release from such microcapsules occurs as a consequence of E–Z photoisomerization of α-methylstilbene moieties in the polymer backbone, which forms a microcapsule shell during UV irradiation. Photoresponsive microcapsules were prepared using P4. P4 is a novel nematic liquid-crystalline polymer of our synthesis with a glass transition of 45 °C and clearing point of 238 °C. This polymer possesses an amorphous structure and a reasonably low glass transition value, thanks to the incorporation of isophthaloyl moieties in the polymer backbone. Before preparing and characterizing microcapsules, we performed an exhaustive characterization of a membrane based on the P4 polymer obtained by using conditions as similar as possible to microcapsule preparation. In this way, we tried to simulate the morphology and the behavior of the microcapsule shell under UV irradiation. In order to establish whether microcapsule shell morphology and behavior could be altered as a consequence of photoirradiation, a complete characterization of a flat membrane based on P4 polymer was first carried out by the investigators. By employing Environmental Scanning Electron Microscope studies, the author demonstrated that P4 membrane and microcapsules containing chloroform as filler possessed very similar asymmetric cross-sectional morphologies. The presence of vanillin in chloroform during phase-inversion precipitation process had an influence on the cross-sectional structure of microcapsules containing this perfume. The authors observed that the outer surface morphologies of all prepared microcapsules appeared like a dense film. Based on atomic force microscope investigations, the authors investigated that the P4 film morphology changed drastically as a consequence of its exposure to UV irradiation at 365 nm (i. e. its surface became much smoother and surface roughness was decreased ca. 24 %). This reasonably induced about a 21 % decrease of the water contact angle value. Release experiments, performed by the investigators, showed that vanillin release from microcapsules in water at room temperature was strongly influenced by UV irradiation: in the absence of irradiation, release was negligible, while, when microcapsules were submitted to continuous irradiation with UV light for 35 min, vanillin was quickly released after an induction time of about 20 min. Panisello et al. [99], by use of phase-inversion precipitation, were able to control polysulfone microcapsule morphology through the adjustment of the composition of the precipitation bath. The aforementioned bath was composed of pure water, which is a nonsolvent for a polysulfone, or of a mixture of water and polysulfone solvent. The results obtained by them show that high concentration of a solvent in the nonsolvent bath favors sponge-like structures. Pena et al. [100] investigated polysulfone microcapsules made by the phase-immersion precipitation method. Based on the generated results, the authors proposed a treatment to avoid the presence of the solvent (DMF) in the prepared capsules, and also to increase the amount of the encapsulated material, in this case vanillin. The treatment consists immersing the capsules in a saturated vanillin aqueous solution for 4 days. By following this procedure, the author demonstrated that the DMF can be totally removed from the core of the microcapsule increasing the amount of encapsulated vanillin to around 100 %.

6.5 General conclusions

A survey of the main encapsulation processes is presented. As well seen in this review, through the years, this field of science has done tremendous progress [101]. To provide a good understanding of the up-to-day development of microcapsule preparation methods and polymer structures used as capsule shell materials, information collected from the literature has been summarized in this work. We have highlighted the processes that have been utilized not only in the academic setup, but as well at the industrial scale. Versatility of the techniques available so far offers enormous resources of possible advanced applications. Nevertheless, to further promote the practical application of capsules, improved and automatable setup units as well as cheap polymers for microcapsule walls must be developed. In addition, developing delivery systems which is controlled release process of encapsulated cargo substances still remains an interesting but challenging task.

Funding: The financial support for the Incoming Marie Curie TECNIOspring fellowship from People Programme (Marie Curies Actions) of the Seventh Framework Programme of the European Union (FP7/2007-2013) under REA grant agreement no. 600388 (TECNIOspring programme), and from the Agency for Business Competitiveness of the Government of Catalonia, ACCIÓ, during which the review was prepared, are gratefully acknowledged by Dr. Tylkowski. This article is also available in: Tylkowski, Polymer Engineering. De Gruyter (2017), isbn 978-3-11-046828-1. (Link leads to https://www.degruyter.com/view/product/468928).

References

[1] Fox SW. How did life begin? Science. 1960;132(3421):200–208.

[2] Peña B, Casals M, Torras C, Gumí T, Garcia-Valls R. Vanillin release from polysulfone macrocapsules. Ind Eng Chem Res. 2009;48(3):1562–1565.

[3] Peña B, Panisello C, Aresté G, Garcia-Valls R, Gumí T. Preparation and characterization of polysulfone microcapsules for perfume release. Chem Eng J. 2012; 179:394–403.

[4] Panisello C, Peña B, Gumí T, Garcia-Valls R. Polysulfone microcapsules with different wall morphology. J Appl Polym Sci. 2013; 129(3):1625–1636.

[5] Dubey R. Microencapsulation technology and applications. Def Sci J. 2009;59(1):82–95.

[6] Salaön F. Microencapsulation by interfacial polymerization. In: Mittal V, editor. Encapsulation nanotechnologies. New Jersey, US, Hoboken: John Wiley & Sons, Inc. 2013:137–173.

[7] Chang TMS. Semipermeable microcapsules. Science. 1964;146(3643):524–525.

[8] Torza S, Mason SG. Coalescence of two immiscible liquid drops. Science. 1969;163(3869): 813–814.

[9] Fink GR. Gene-enzyme relations in histidine biosynthesis in yeast. Science. 1964;146(3643): 525–527.

[10] Wittbecker EL, Morgan PW. Interfacial polycondensation. I. J Polym Sci. 1959;40(137):289–297.

[11] Beaman RG, Morgan PW, Koller CR, Wittbecker EL, Magat EE. Interfacial polycondensation. III. Polyamides. J Polym Sci. 1959;40(137):329–336.

[12] Eareckson WM. Interfacial polycondensation. X. Polyphenyl esters. J Polym Sci. 1959;40(137): 399–406.

[13] Morgan PW, Kwolek SL. Interfacial polycondensation. II. Fundamentals of polymer formation at liquid interfaces. J Polym Sci, Part A: Polymer Chem. 1996;34(4):531–559.

[14] Beestman GB, Deming JM. Encapsulation by interfacial polycondensation, ed: Google Patents. 1983.

[15] Raaijmakers MJT, Benes NE. Current trends in interfacial polymerization chemistry. Prog Polym Sci. 2016;63:86–142.

[16] Thies C. Microencapsulation. In: Mark HF, editor. Encyclopedia of polymer science and technology. Hoboken: John Wiley & Sons, Inc., 2002.

[17] Perignon C, Ongmayeb G, Neufeld R, Frere Y, Poncelet D. Microencapsulation by interfacial polymerisation: Membrane formation and structure. J Microencapsul. 2015;32(1):1–15.

[18] Dragosavac MM, Sovilj MN, Kosvintsev SR, Holdich RG, Vladisavljević GT. Controlled production of oil-in-water emulsions containing unrefined pumpkin seed oil using stirred cell membrane emulsification. J Memb Sci. 2008;322(1):178–188.

[19] Tylkowski B, Pregowska M, Jamowska E, Garcia-Valls R, Giamberini M. Preparation of a new lightly cross-linked liquid crystalline polyamide by interfacial polymerization. Application to

the obtainment of microcapsules with photo-triggered release. Eur Polym J. 2009; 45(5):1420–1432.

[20] Danicher L, Frere Y, Le Calve A. Synthesis by interracial polycondensation of polyamide capsules with various sizes. Characteristics and properties. In: Macromolecular Symposia, Conference Paper vol. 151, 2000, pp. 387–392.

[21] Janssen LJJM, Te Nijenhuis K. Encapsulation by interfacial polycondensation. I. The capsule production and a model for wall growth. J Memb Sci. 1992;65(1–2):59–68.

[22] Janssen LJJM, Te Nijenhuis K. Encapsulation by interfacial polycondensation. II. The membrane wall structure and the rate of the wall growth. J Memb Sci. 1992;65(1–2):69–75.

[23] Danicher L, Gramain P, Frère Y, Le Calvé A. Model capsules. I. Synthesis, characteristics and properties of millimetric polyamide capsules. React Funct Polym. 1999;42(1):111–125.

[24] Marturano V, Cerruti P, Carfagna C, Giamberini M, Tylkowski B, Ambrogi V. Photo-responsive polymer nanocapsules. Polymer. 2015;70:222–230.

[25] Podshivalov AV, Bronnikov S, Zuev VV, Jiamrungraksa T, Charuchinda S. Synthesis and characterization of polyurethane–urea microcapsules containing galangal essential oil: Statistical analysis of encapsulation. J Microencapsul. 2013;30(2):198–203.

[26] He Z, Jiang S, Li Q, Wang J, Zhao Y, Kang M. Facile and cost-effective synthesis of isocyanate microcapsules via polyvinyl alcohol-mediated interfacial polymerization and their application in self-healing materials. Compos Sci Technol. 2017;138:15–23.

[27] Arshady R. Suspension, emulsion, and dispersion polymerization: A methodological survey. Colloid Polym Sci. 1992;270(8):717–732.

[28] Vivaldo-Lima E, Wood PE, Hamielec AE, Penlidis A. An updated review on suspension polymerization. Ind Eng Chem Res. 1997;36(4):939–965.

[29] Dowding PJ, Vincent B. Suspension polymerisation to form polymer beads. Colloids Surf A. 2000;161(2):259–269.

[30] Sánchez-Silva L, Carmona M, De Lucas A, Sánchez P, Rodríguez JF. Scale-up of a suspension-like polymerization process for the microencapsulation of phase change materials. J Microencapsul. 2010;27(7):583–593.

[31] Supsakulchai A, Ma GH, Nagai M, Omi S. Preparation of uniform titanium dioxide (TiO2) polystyrene-based composite particles using the glass membrane emulsification process with a subsequent suspension polymerization. J Microencapsul. 2003;20(1):1–18.

[32] Katampe I, Polykarpov AY, Camillus JC. Photosensitive microcapsules containing a synthetic viscosity modifier in the continuous phase, ed: Google Patents, 2005.

[33] Bonetti S, Farina M, Mauri M, Koynov K, Butt HJ, Kappl M, et al. Core@shell Poly(n-butylacrylate)@polystyrene nanoparticles: Baroplastic force-responsiveness in presence of strong phase separation. Macromol Rapid Commun. 2016;37(7):584–589.

[34] Kawaguchi S, Ito K. Dispersion polymerization. In: Okubo M, editors. Polymer particles. Berlin, Heidelberg: Springer. editor 2005:299–328.

[35] Lee HH, Schadt FL, Wolfe MS. Method of preparing encapsulated pigment dispersions with two encapsulation steps, ed: Google Patents. 2014.

[36] Bourgeat-Lami E, Lang J. Encapsulation of inorganic particles by dispersion polymerization in polar media: 2. Effect of silica size and concentration on the morphology of silica–polystyrene composite particles. J Colloids Interface Sci. 1999;210(2):281–289.

[37] Schmid A, Fujii S, Armes SP, Leite CAP, Galembeck F, Minami H, et al. Polystyrene–silica colloidal nanocomposite particles prepared by alcoholic dispersion polymerization. Chem Mater. 2007;19(10):2435–2445.

[38] Dardelle G, Beaussoubre P, Erni P. Hybrid coacervate capsules, ed: Google Patents. 2015.

[39] Kumar R, Troiano G, Ramstack JM, Herbert P, Figa M. Coacervation process, ed: Google Patents. 2008.

[40] Baker R, Ninomiya Y. Coacervation process for microencapsulation and microcapsules prepared by such coacervation process, ed: Google Patents. 1988.

[41] Yuan Y, Kong Z-Y, Sun Y-E, Zeng Q-Z, Yang X-Q. Complex coacervation of soy protein with chitosan: Constructing antioxidant microcapsule for algal oil delivery. LWT Food Sci Technol. 2017;75:171–179.

[42] Jun-Xia X, Hai-Yan Y, Jian Y. Microencapsulation of sweet orange oil by complex coacervation with soybean protein isolate/gum Arabic. Food Chem. 2011;125(4):1267–1272.

[43] Meng F, Wang S, Liu H, Xu X, Ma H. Microencapsulation of oxalic acid (OA) via coacervation induced by polydimethylsiloxane (PDMS) for the sustained release performance. Mater Des. 2017;116:31–41.

[44] Yan C, Zhang W. Chapter 12 – Coacervation processes. In: Gaonkar AG, Vasisht N, Khare AR, Sobel R, editors. Microencapsulation in the food industry. San Diego: Academic Press, 2014: 125–137.

[45] Caruso F, Caruso RA, Mohwald H. Nanoengineering of inorganic and hybrid hollow spheres by colloidal templating. Science. 1998;282(5391):1111–1114.

[46] Dreaden EC, Morton SW, Shopsowitz KE, Choi JH, Deng ZJ, Cho NJ, et al. Bimodal tumor-targeting from microenvironment responsive hyaluronan layer-by-layer (LbL) nanoparticles. ACS Nano. 2014;8(8):8374–8382.

[47] Tao X, Li J, Möhwald H. Self-assembly, optical behavior, and permeability of a novel capsule based on an azo dye and polyelectrolytes. Chem Eur J. 2004;10(14):3397–3403.

[48] Bédard M, Skirtach AG, Sukhorukov GB. Optically driven encapsulation using novel polymeric hollow shells containing an azobenzene polymer. Macromol Rapid Commun. 2007;28(15): 1517–1521.

[49] Bartosz T, Nuno AGB, Krzysztof Artur B, Marta G. Smart microcapsules based on photo-isomerizable moieties. Phys Sci Rev. 2016;1 Retrieved 5 Apr. 2017, from doi:10.1515/psr-2015-0002.

[50] Hammond PT, Poon Z. Stable layer-by-layer coated particles, ed: Google Patents. 2014.

[51] Björnmalm M, Roozmand A, Noi KF, Guo J, Cui J, Richardson JJ, et al. Flow-based assembly of layer-by-layer capsules through tangential flow filtration. Langmuir. 2015;31 (33):9054–9060.

[52] Dave BC, Dunn B, Valentine JS, Zink JI. Sol-gel encapsulation methods for biosensors. Anal Chem. 1994;66(22) 1120A-1127A.

[53] Brinker, C. J.; Hurd, A. J.; Frye, G. C.; Ward, K. J.; Ashley, C. S., Sol-gel thin film formation. *Journal of Non–Crystalline Solids* 1990, 121 (1–3), 294–302.

[54] Rahman IA, Padavettan V. Synthesis of silica nanoparticles by sol-gel: size-dependent properties, surface modification, and applications in silica-polymer nanocomposites—a review. J Nanomater. 2012;2012:15.

[55] Hench LL, West JK. The sol-gel process. Chem Rev. 1990;90(1):33–72.

[56] Ciriminna R, Sciortino M, Alonzo G, Schrijver AD, Pagliaro M. From molecules to systems: sol–gel microencapsulation in silica-based materials. Chem Rev. 2011;111(2):765–789.

[57] Yamanaka SA, Nishida F, Ellerby LM, Nishida CR, Dunn B, Valentine JS, et al. Enzymatic activity of glucose oxidase encapsulated in transparent glass by the sol-gel method. Chem Mater. 1992;4(3):495–497.

[58] Ellerby LM, Nishida CR, Nishida F, Yamanaka SA, Dunn B, Valentine JS, et al. Encapsulation of proteins in transparent porous silicate glasses prepared by the sol-gel method. Science. 1992;255(5048):1113–1115.

[59] Juszczak LJ, Friedman JM. UV resonance Raman spectra of ligand binding intermediates of sol-gel encapsulated hemoglobin. J Biol Chem. 1999;274(43):30357–30360.

[60] Bhatia RB, Brinker CJ, Gupta AK, Singh AK. Aqueous sol–gel process for protein encapsulation. Chem Mater. 2000;12(8):2434–2441.

[61] Mikosch A, Kuehne AJC. Encapsulation of polymer colloids in a sol–gel matrix. Direct-writing of coassembling organic–inorganic hybrid photonic crystals. Langmuir. 2016; 32(11):2567–2573.

[62] Widder KJ, Senyei AE, Sears B. Experimental methods in cancer therapeutics. J Pharm Sci. 1982;71(4):379–387.

[63] Villanova JCO, Ayres E, Carvalho SM, Patrício PS, Pereira FV, Oréfice RL. Pharmaceutical acrylic beads obtained by suspension polymerization containing cellulose nanowhiskers as excipient for drug delivery. Eur J Pharm Sci. 2011;42(4):406–415.

[64] Jahanzad F, Sajjadi S, Brooks BW. Characteristic intervals in suspension polymerisation reactors: An experimental and modelling study. Chem Eng Sci. 2005;60(20):5574–5589.

[65] Brooks B. Suspension polymerization processes. Chem Eng Technol. 2010;33(11):1737–1744.

[66] Arshady R. Microspheres and microcapsules: A survey of manufacturing techniques. Part 1: Suspension cross-linking. Polymer Eng Sci. 1989;29(24):1746–1758.

[67] Rhodes BA, Zolle I, Buchanan JW, Wagner HN. Radioactive albumin microspheres for studies of the pulmonary circulation. Radiology. 1969;92(7):1453–1460.

[68] Pasqualini R, Plassio G, Sosi S. The preparation of albumin microspheres. J Nucl Biol Med. 1969;13(1):80–84.

[69] Khanna SC, Speiser P. Epoxy resin beads as a pharmaceutical dosage form I: Method of preparation. J Pharm Sci. 1969;58(9):1114–1117.

[70] Porath J, Janson J-C, L««S T. Agar derivatives for chromatography, electrophoresis and gel-bound enzymes. J Chromatogr. 1971;60:167–177.

[71] Chitumbo K, Brown W. The separation of oligosaccharides on cellulose gels. J Polym Sci, Part C: Polym Symposia. 1971;36(1):279–292.

[72] Vonka M, Soos M, Storti G. Viscosity and drop size evolution during suspension polymerization. Aiche J. 2016;62(12):4229–4239.

[73] Dini E, Alexandridou S, Kiparissides C. Synthesis and characterization of cross-linked chitosan microspheres for drug delivery applications. J Microencapsul. 2003;20(3):375–385.

[74] Idakiev VV, Lazarova PV, Bück A, Tsotsas E, Mörl L. Inductive heating of fluidized beds: Drying of particulate solids. Powder Technol. 2017;306:26–33.

[75] Percy SL. Improvement in drying and concentrating liquid substances by atomizing, ed: Google Patents. 1872.

[76] Dihora JO, Cetti JR, Witt SE, Li JJ. Spray drying microcapsules, ed: Google Patents. 2015.

[77] Cardozo LS, Tantawy HH, Lickiss JR, Roberts NPS. Spray-drying process, ed: Google Patents. 2011.

[78] Hussain ZJ. High load spray dry encapsulation, ed: Google Patents. 1996.

[79] Maury M, Murphy K, Kumar S, Shi L, Lee G. Effects of process variables on the powder yield of spray-dried trehalose on a laboratory spray-dryer. Eur J Pharm Biopharm. 2005;59(3): 565–573.

[80] Biswas P, Sen D, Mazumder S, Basak CB, Doshi P. Temperature mediated morphological transition during drying of spray colloidal droplets. Langmuir. 2016;32(10):2464–2473.

[81] Drusch S, Serfert Y, Scampicchio M, Schmidt-Hansberg B, Schwarz K. Impact of physicochemical characteristics on the oxidative stability of fish oil microencapsulated by spray-drying. J Agric Food Chem. 2007;55(26):11044–11051.

[82] Bertolini AC, Siani AC, Grosso CRF. Stability of monoterpenes encapsulated in gum Arabic by spray-drying. J Agric Food Chem. 2001;49(2):780–785.

[83] Liu W, Wu WD, Selomulya C, Chen XD. Facile spray-drying assembly of uniform microencapsulates with tunable core–shell structures and controlled release properties. Langmuir. 2011;27(21):12910–12915.

[84] Risch SJ. Encapsulation of flavors by extrusion. In: Flavor encapsulation, vol. 370(ACS Symposium Series, no. 370): American Chemical Society, 1988:103–109.

[85] Nussinovitch A, editor. Liquid-core beads and their applications in food, biotechnology, and other fields. Polymer macro- and micro-gel beads: Fundamentals and applications. Springer-Verlag New York: Springer, 2010:163–189.

[86] Whelehan M, Marison IW. Microencapsulation using vibrating technology. J Microencapsul. 2011;28(8):669–688.

[87] Abbas S, Da Wei C, Hayat K, Xiaoming Z. Ascorbic acid: Microencapsulation techniques and trends—a review. Food Rev Int. 2012;28(4):343–374.

[88] Pasukamonset P, Kwon O, Adisakwattana S. Alginate-based encapsulation of polyphenols from Clitoria ternatea petal flower extract enhances stability and biological activity under simulated gastrointestinal conditions. Food Hydrocoll. 2016;61:772–779.

[89] Shinde T, Sun-Waterhouse D, Brooks J. Co-extrusion encapsulation of probiotic lactobacillus acidophilus alone or together with apple skin polyphenols: An aqueous and value-added delivery system using alginate. Food Bioprocess Technol. 2014;7(6):1581–1596.

[90] Giamberini M, Fernandez Prieto S, Tylkowski B. Microencapsulation, innovative applications 2015. Berlin: Walter de Gruyter GmbH & Co KG.

[91] Tylkowski B, Nowak M, Tsibranska I, Trojanowska A, Marciniak L, Valls RG, et al. Concentration and fractionation of polyphenols by membrane operations. Curr Pharm Des. 2016;22:1–1.

[92] Tylkowski B, Tsibranska I. Polyphenols encapsulation – application of innovation technologies to improve stability of natural products. In: Giamberini M, Prieto SF, Tylkowski B, editors. Microencapsulation, Innovative Applications 2015:97–113.

[93] Tsibranska I, Tylkowski B, Kochanov R, Alipieva K. Extraction of biologically active compounds from Sideritis ssp. L. Food Bioprod Process. 2011;89(4):273–280.

[94] Silva MP, Tulini FL, Ribas MM, Penning M, Fávaro-Trindade CS, Poncelet D. Microcapsules loaded with the probiotic Lactobacillus paracasei BGP-1 produced by co-extrusion technology using alginate/shellac as wall material: Characterization and evaluation of drying processes. Food Res Int. 2016;89(1):582–590.

[95] Wang W, Waterhouse GIN, Sun-Waterhouse D. Co-extrusion encapsulation of canola oil with alginate: Effect of quercetin addition to oil core and pectin addition to alginate shell on oil stability. Food Res Int. 2013;54(1):837–851.

[96] He F, Wang W, He XH, Yang XL, Li M, Xie R, et al. Controllable multicompartmental capsules with distinct cores and shells for synergistic release. ACS Appl Mater Interfaces. 2016;8(13): 8743–8754.

[97] Mulder M. Membrane preparation |phase inversion membranes. In: Wilson ID, editors. Encyclopedia of separation science. Oxford: Academic Press. editors 2000:3331–3346.

[98] Bogdanowicz KA, Tylkowski B, Giamberini M. Preparation and characterization of light-sensitive microcapsules based on a liquid crystalline polyester. Langmuir. 2013;29(5): 1601–1608.

[99] Panisello C, Peña B, Gumí T, Garcia-Valls R. Polysulfone microcapsules with different wall morphology. J Appl Polym Sci. 2013;129(3):1625–1636.

[100] Peña B, Panisello C, Aresté G, Garcia-Valls R, Gumí T. Preparation and characterization of polysulfone microcapsules for perfume release. Chem Eng J. 2012;179:394–403.

[101] Ghosh SK. Functional coatings and microencapsulation: A general perspective. In: Ghosh SK, editor. Functional coatings. Weinheim: Wiley-VCH Verlag GmbH & Co. KGaA. 2006:1–28.

Monissa Paderes, Deepak Ahirwal and Susana Fernández Prieto

7 Natural and synthetic polymers in fabric and home care applications

Abstract: Polymers can be tailored to provide different benefits in Fabric & Home Care formulations depending on the monomers and modifications used, such as avoiding dye transfer inhibition in the wash, modifying the surface of tiles or increasing the viscosity and providing suspension properties to consumer products. Specifically, the rheology modification properties of synthetic and natural polymers are discussed in this chapter. The choice of a polymeric rheology modifier will depend on the formulation ingredients (charges, functional groups), the type and the amount of surfactants, the pH and the desired rheology modification. Natural polymeric rheology modifiers have been traditionally used in the food industry, being xanthan gum one of the most well-known ones. On the contrary, synthetic rheology modifiers are preferably used in paints & coats, textile printing and cleaning products.

Keywords: dye transfer inhibitors, methylcellulose, polymers, rheology modifier, thickener, xanthan gum

7.1 Introduction

In the early days, polymers have found very little value in detergent and cleaning formulations. Phosphate compounds such as sodium triphosphate (STP) (Figure 7.1) and sodium/potassium phosphate were used primarily in detergent formulations in which they comprise them up to 50 % by weight [1–5]. STP provides significant contributions to laundering by performing several crucial functions [2]. They serve as builders by forming complexes with polyvalent cations such as Ca^{2+} and Mg^{2+} ions and as a result water hardness is reduced, thereby boosting the performance of the surfactants [3]. STP also aids in removing, dispersing and suspending the dirt released and ensuring a good powder structure. However, over the years, phosphates were found to stimulate the rapid growth of algae and plants in lakes and other bodies of water, which caused the deterioration of water quality and the recreational value of the lakes [2, 4]. Due to environmental concerns and government regulations and restrictions regarding the use of phosphates, formulators pursued to reinvent the detergent compositions [6]. Decades of efforts and millions of dollars were spent to find safe, high-performing and economical substitutes for phosphates. Some of the potential alternatives [5] that came out of the market include systems that are based on (1) nitrilotriacetate (NTA) [2, 6], (2) sodium citrates [5, 7] and (3) zeolites [8–10] (Figure 7.1).

https://doi.org/10.1515/9783110469745-007

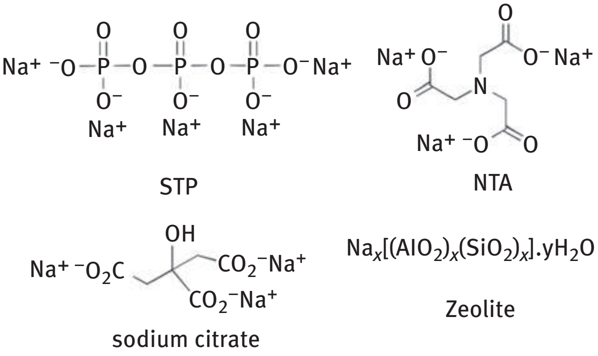

Figure 7.1: Chemical structures of STP, NTA, sodium citrate and general formula of zeolite.

NTA exhibits good cleaning and chelating properties but was later on suspended by National Institute of Environmental Health and Sciences (NIEHS) because it poses detrimental health threats to the development of embryo or what is known as teratogenic effect especially when combined with heavy metals such as cadmium and mercury [2]. Sodium citrate, on the other hand, is environmentally safe and is compatible with cleaning formulations because of its solubility properties. However, in terms of cost and effectiveness, it is generally inferior compared to STP [5, 7].

Zeolite is a synthetic sodium aluminum silicate with the general formula of $Na_x[(AlO_2)_x(SiO_2)_x].yH_2O$ whose primary function is similar to STP, which is to sequester Ca^{2+} and Mg^{2+} ions in wash solutions [9]. In cases where water contains elevated amount of these ions, the zeolite system requires a co-builder, which is water soluble [10]. Polycarboxylates have proven to be the most effective additives for this system. Their function, however, is not via complexation with the hard ions in water, but they aid in the dispersion of calcium salts such as calcium carbonate or phosphate and the soil particulates released during washing. Because these polymeric materials are available at reasonable costs and possess unique and varied multifunctionality, formulators and polymer chemists were prompted to investigate beyond polycarboxylates.

The applications of polymers in household cleaning compositions, both natural and synthetic, have grown tremendously [11, 12]. They have been an important part of detergent formulations for many years now, and 90 % of the polymers used belong to a class of polycarboxylates. The major polycarboxylates used in cleaning products are homopolymers derived from acrylic acid (PAA) and copolymer of acrylic/maleic acid (PAA/MA) (Figure 7.2). They are generally used as sodium salts in phosphate-free detergents to prevent soil redeposition and encrustation. Specialty polymers have also been developed recently [11]. They provide specific and unique benefits to detergent formulations such as enhanced soil release, dye transfer inhibition, modification of rheological properties and many more.

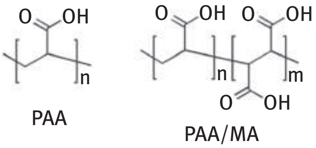

Figure 7.2: Chemical structures of poly(acrylic acid) (PAA) and copolymer of acrylic and maleic acid (PAA/MA).

Most synthetic polymers are toxicologically safe but not biodegradable. They are eliminated from wastewater by precipitation or adsorption to the sludge in sewage treatment facilities [13]. Because natural polymers are renewable and biodegradable to a great extent, they have found broad appeal in detergent industry [14, 15]. Cellulose derivatives such as carboxymethyl cellulose (CMC), xanthan gums and carrageenans were among the first natural polymers to be utilized in detergent formulations. Depending on the desired applications, their physical and chemical properties were readily tailored and fine-tuned by chemical modifications.

In this chapter, we provide an overview of the applications of polymers on fabric and home care formulations. For general households, fabric and home care products include laundry and dishwashing detergents, fabric softeners and hard surface cleaning products such as floor care and bathroom and glass cleaners. Section 7.2 highlights the benefits provided by polymers when incorporated in the product formulations. Specific examples of synthetic and natural polymers that are widely and currently used in the formulations are discussed in detail in Section 7.3.

7.2 Benefits of polymers in fabric and home care formulations

A detergent, in general, is a cleaning agent composed predominantly of surfactant or a mixture of surfactants whose main task is to remove water-insoluble substances like dirt and grease from permeable surfaces (i. e. fabrics and clothes) and/or hard surfaces (i. e. metals, plastics and ceramics). Other than surfactant, a modern detergent formulation normally consists of builders and chelants, co-builders and other polymer additives used for specific washing effects such as soil release and anti-redeposition, dye transfer inhibition and rheology modification [16, 17]. The incorporation of polymers in fabric and home care formulations has provided numerous benefits in enhancing the action and efficiency of detergents, particularly the phosphate-free types. Consequently, the use of these materials, especially the recently developed specialty polymers, has gained increasing attention over the years because they provide specific benefits at a very low percent weight (1 % or less) [11]. Examples of these type of polymers are polyesters based on terephthalic acid which serve as soil release agents, ethylene/propylene glycol-based polymers as anti-redeposition agents and poly(vinylpyrrolidone) as DTIs. Moreover, a detailed description of nathural and synthetic polymeric rheology modifiers is provided in **Section 7. 3**. Some of the benefits provided by the addition of polymers in cleaning compositions are discussed below.

7.2.1 Soil release

The concept of soil release, which refers to the improved removal of soil from fabric during washing by increasing its permeability, was introduced many years ago. Two steps are involved in the general mechanism of soil release process: (1) enhanced penetration of water and detergent solution into the soil/garment interface with the aid of soil release agent and (2) solvation and transport of soil from the fabric to the wash solution by mechanical work [18, 19]. The removal of soil, however, is governed by several factors such as the kind of fabrics and soil particles, the performance of detergent solution, the washing conditions and the mechanical action of water.

Soil in particular includes stains that are water soluble, particulates, oil and grease. The water-soluble stains and the particulates can be easily removed by regular washing, while oil and grease are much more difficult to remove. They require soil release agents to facilitate their removal from the garment and prevent them from spreading on the surface of the fiber. These soil release agents, or what are commonly known as soil release polymers (SRPs), are specific additives that were developed to enable the exclusion of soil from the garments. Recently, a number of SRPs have been commercialized and used in detergent and fabric softener compositions [18, 20]. These polymers are typically low-molecular-weight polyesters that are derived from acrylic acid, terephthalic acid and polyalkylene glycols. Polyacrylates were among the first systems to be used as soil release agents.

The mechanism of action of SRPs is via surface modification wherein they orient themselves in the surface of the garment through adsorption, making it more hydrophilic and easily penetrated by wash liquid, therefore decreasing the affinity of the dirt to the fiber [19]. SRPs do not only improve the soil resistance of the fibers but also enhances the wetting ability with the aqueous cleaning solution especially the polyester fibers. Thus, the effects of SRPs are strongly observed after several treatments of the fabrics.

Oily soils that get impregnated in cotton fabrics are easier to remove than those infused in fabrics woven from synthetic polyester [18]. The cellulosic fibers of cotton fabrics are composed of hydroxyl and carboxyl groups, making them more hydrophilic compared to polyester. High hydrophilicity of cotton fabrics means easy penetrability of the adsorbed soils by water and cleaning solutions, resulting in its fast removal. Methyl and hydroxyalkyl cellulose derivatives are the most common examples of cellulosic soil release agents for cotton [21]. Polyester-containing fabrics, on the other hand, due to its hydrophobic nature absorb oil readily and tenaciously, making the removal of these stains far more challenging. Extensive research to

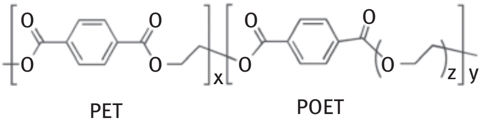

Figure 7.3: Chemical structure of polyethylene terehpthalate (PET)/polyoxyethylene terehpthalate (POET) copolymer.

address this issue has yielded an effective release of soil from polyester fibers with the use of polyethylene terehpthalate (PET)/polyoxyethylene terehpthalate (POET) copolymer (Figure 7.3) [22]. This type of soil release agent has high affinity for synthetic fabrics because its backbone is composed of a mixture of terephthalate residues and ethyleneoxy polymeric units, which closely resembles the materials that comprise the polyester fibers of synthetic fabric.

7.2.2 Dispersant

A dispersant or dispersing agent is used primarily to diffuse and suspend the soil particulates in the washing liquor after they are released from the surfaces or fabrics. They make the dispersion process easier by adsorbing to soil particles, which results in an increase in electrostatic and steric repulsion, thus minimizing clumping, redeposition and scaling onto the garments or hard surfaces [23]. A dispersing additive also provides uniform mixture of particles by preventing them from aggregation and settling at the bottom of the container, thereby ensuring stable formulations and storage.

The efficiency of a polymeric material as a dispersing agent depends on their affinity to the particle surface; therefore charge, size and orientation of the polymer molecule in solution are important factors. Most cleaning products rely on low-molecular-weight polymeric carboxylates as dispersant, which typically take the form of PAA or PAA/MA (Figure 7.2) [23]. Their multiple charges enable them to adsorb at interfaces and act as dispersing agent for soil and inorganic salts and serve as crystal growth inhibitors.

Biodegradable polymeric dispersants were also reported, which include the polyamino acid polymers such as polyaspartate and polysaccharides such as oxidized starch [24]. Poly(vinyl alcohol), polyalkylene glycol and copolymers of alkylene oxide and vinyl acetate are known to be effective dispersing agents for surfaces that are hydrophobic such as garment made from polyester [24].

7.2.3 Anti-redeposition

In a standard laundering process, the detergent removes the soil particles from the fabric and then suspends them in wash solution and prevents these particulates from depositing back onto the surface of the cleaned fabric throughout the washing and rinsing cycle [18]. The resettling of the soil in the textile can occur in all types of fabrics whether hydrophilic or hydrophobic [25]. Examples of fibers made from hydrophilic materials are cotton, linen and rayon, while fabrics like polyester, nylon and acrylic are hydrophobic. Because soil is normally hydrophobic, redeposition is more likely to happen when the surface of the fabric being washed is hydrophobic. However, the degree to which this process occurs is dependent not only on the kind of the fabric being laundered but also on the detergent used, the properties of the soil particles and the washing temperature. Therefore, additives are added to cleaning compositions to enhance the release of soil and/or to inhibit redeposition of the soil.

The chemical agents added to the cleaning formulations, which help minimize and avoid the redeposition process, is known as anti-redeposition polymers (ARDs) [25]. ARDs are usually water soluble and negatively charged. They interact and stabilize the soil in the wash water, thus preventing them from depositing back to the washed garment. There are two ways that these polymeric materials work: (1) the negatively charged ARDs adsorb on the surface of the garment causing an increase in the electrostatic repulsion between the hydrophobic soil molecules and the fabric surface and (2) entrapment of soil particles into a polymer matrix [18].

CMC, a polymer derived from natural cellulose, is one of the first anti-redeposition agents used in detergent systems [26]. This polymeric material is one of the best-known ARD agent applicable to cotton fabrics. The polymeric cellulose acetate, on the other hand, is effective for a broad range of natural and synthetic fabrics. Examples of synthetic polymers that are also used as ARD agents for garments made of cotton are poly(ethylene glycol) and poly(vinyl alcohol) [25].

7.2.4 Dye transfer inhibitors

Another crucial role that polymers perform in washing formulations is as dye transfer inhibitors (DTIs). One of the many challenges in the laundering operations is the possible transfer of dyes from one fabric to another in the wash solution [27], a process known as color transfer. This process occurs when fabrics of different dye colors are washed together. During the wash, a garment can lose some of the dye molecules and resettle on white or differently colored fabrics [28]. The degree to which dye colors leak out of the textile depends on the type of the fabric and dye, the freshness of the garment and the washing conditions. As a result of successive washing, dyed fabrics suffer from color fading.

DTI has become a significant ingredient of detergent formulations. They were developed for two reasons: (1) for color protection and (2) for dye transfer inhibition. As color care additives, they help the fabrics keep their original colors even after multiple washes and prolong the life of the dyed garments. They also inhibit dyes from leaching out of the garment and prevent them from staining another fabric during laundry process.

The polymeric DTIs are known to efficiently reduce the staining of textiles brought by migration of dyes by binding with the free dye molecules in wash solution, which results in the formation of polymer/dye adducts that is water soluble, therefore, allowing to wash many differently colored garments at the same time. DTI also minimizes the release of the dyes from the fabrics by adsorbing onto the surface of the fibers during washing.

The most popular polymer used as DTI in laundry detergents are poly(*N*-vinyl-2-pyrrolidone) (PVP) [29, 30] and poly(vinylpyridine *N*-oxide) (PVP-NO) [31, 32] (Figure 7.4). Both PVP and PVP-NO have moderately high molecular weight and are highly soluble in water. PVP is reported to be particularly effective with synthetic fibers and synthetic cotton blends; however, its efficiency decreases when mixed with anionic surfactants. Poly(vinylpyridine betaine) which contains quaternary nitrogen and carboxylate salt was proven to be effective in laundry detergents containing anionic surfactants (Figure 7.4) [33].

DTIs in general are added up to 0.5 weight % to detergents that are specific for delicate and colored fabrics. Not all DTIs, however, are effective for all dyes. The overall efficiency is highly dependent on the chemical structures of both the dye and DTI.

7.2.5 Rheology modifier

Rheology modifier, also commonly known as viscosifier or thickener, is added to liquid compositions mainly to alter the flow behavior of the formulation, improve the aesthetics and provide specific characteristics to the product [34, 35]. The choice of the most suitable rheology modifier depends on the type of flow required based on the product thickness and pourability, the nature of the formulation as well as the performance attributes of the suspension. The rheology modifiers generally establish suitable rheological characteristics to the liquid products without imparting any

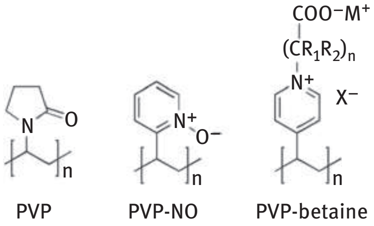

Figure 7.4: Chemical structures of poly(N-vinyl-2-pyrrolidone) (PVP), poly(vinylpyridine N-oxide) (PVP-NO) and poly(vinylpyridine betaine) (R1 and R2 = H, aryl or alkyl).

undesirable properties such as unwanted phase separation and unappealing physical appearance.

Both natural and synthetic polymers have been utilized extensively as rheology modifiers for liquid detergents [35, 36]. There are two ways that these polymeric rheology modifiers can thicken a liquid composition. One is by volume exclusion (or non-associative) and the other is by association mechanism [34]. Associative and non-associative polymers were further discussed in Section 7.3.1. Rheology modifiers that thicken via volume exclusion are normally water-soluble polymers that swell with water. These types of thickeners create viscosity through chain entanglement and particle flocculation. They do not associate with the surfactants or the other particulates present in the formulation. Examples of rheology modifiers under this category include cellulosic ethers such as hydroxyethyl cellulose (HEC) and alkali swellable/soluble emulsions (ASEs) such as copolymers of methacrylic acid and acrylate ester. ASE thickeners are normally acrylic-derived polymers and are pH dependent [34]. They are insoluble at low pH, and as the pH is increased, they become soluble and the particles swell.

Associative rheology modifiers, on the other hand, are those polymers that contain hydrophobic moieties at different levels distributed randomly throughout its main backbone. These hydrophobic functionalities interact with each other via inter- or intramolecular associations, which result in an increase in hydrodynamic volume, therefore increasing the thickening ability of the polymer. The most commonly known associative thickeners are hydrophobically modified alkali soluble emulsions (HASEs) and hydrophobically modified ethoxylated urethanes (HEURs) [34].

Basically, HASEs are hydrophobically modified ASE. They are prepared by the introduction of hydrophobic functional groups onto the acrylate backbone of ASE. Example of HASE polymer is a terpolymer, which contains methacrylic acid, ethyl acrylate (EA) and a hydrophobic group (Figure 7.5) [37]. They retain the pH-dependent

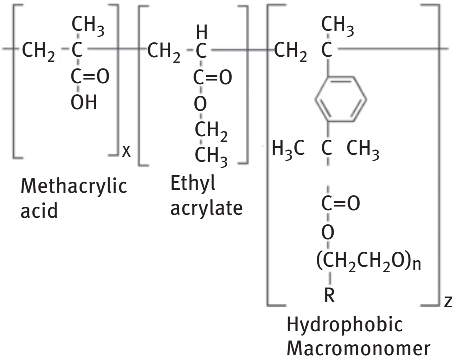

Figure 7.5: Structure of an example of a HASE poymer that contains methacrylic acid, ethyl acrylate and a hydrophobic macromonomer (R = alkyl chain).

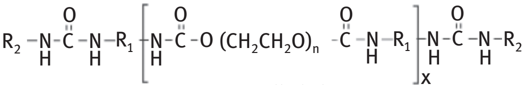

$$R_2-\underset{H}{N}-\overset{O}{\overset{\|}{C}}-\underset{H}{N}-R_1-\left[\underset{H}{N}-\overset{O}{\overset{\|}{C}}-O\,(CH_2CH_2O)_n-\overset{O}{\overset{\|}{C}}-\underset{H}{N}-R_1-\right]_x\underset{H}{N}-\overset{O}{\overset{\|}{C}}-\underset{H}{N}-R_2$$

R_1, R_2 = alkyl chain

Figure 7.6: HEUR polymer based on PEO and diisocyanate capped with amine hydrophobic groups.

behavior of ASE, but in addition to water absorption, they increase the viscosity of the solution by hydrophobic association. These hydrophobic groups can also interact with the other ingredients in solution such as the surfactants, which can contribute to the overall stability of the formulation.

HEURs are non-ionic substances that are typically of low molecular weight and consist of poly(ethylene oxide) (PEO) linked together by diisocyanates and capped at the terminal position by hydrophobic groups (Figure 7.6) [34]. Unlike HASEs, HEURs do not require neutralization to activate their rheology-modifying behavior. Their thickening ability is achieved through hydrophobic interaction between the alkyl groups of the molecule and the other hydrophobic components of the formulation. HEURs have found wide applications in fabric softeners and cleaning products that are purposely formulated for kitchen and bathroom [38].

Some examples of polymeric rheology modifiers that are used nowadays in liquid detergents are discussed in detail in Section 7.3.

7.3 Natural and synthetic polymers

Both natural and synthetic polymers have been widely incorporated in detergent formulations. Their properties could be readily tailored depending on the needs of the household products. For synthetic polymers, the molecular weight, degree of branching and the chemical compositions in the main backbone and side chains are easily controlled and modified. Chemical modifications of natural polymers also demonstrated an improvement in the characteristics and applications relative to the unmodified materials.

7.3.1 Synthetic polymers

Synthetic polymers are frequently used in fabric and home care formulations for surface modifications and as rheology modifiers and DTIs. Broadly, the synthetic water-soluble polymers can be categorized into two types: (i) non-ionic polymers and (ii) charged polymers (polyelectrolytes).

(i) *Non-ionic polymers*: Polar, non-ionic functional groups can impart water solubility if present in sufficient numbers along to the backbone. The key technologies used in consumer products include: (1) polyacrylamide (PAM), (2) PEO, (3) poly(vinyl alcohol)-poly(vinyl acetate) copolymer, (4) poly(*N*-vinylpyrrolidinone), and (5) poly(hydroxyethyl acrylate). Normally, these classes of polymers are radially compatible with any kind of surfactant system (anionic, cationic or zwitterionic).

(ii) *Charged polymers*: Polymers possessing charges along or pendent to the molecular backbone can be classified into two categories based on the behavior in aqueous electrolyte solutions. The first category includes polyelectrolytes, which could be polyanions or polycations, and the second are polyampholytes, polymers that contain both positive and negative charges along the polymer backbone. Electrostatic effects, counterion binding, solvation and local dielectric effects are the factors that govern the phase behavior and solubility of charged polymers in surfactant system. Microstructure of polyelectrolyte can be tailored to allow conformational changes with pH, temperature or added electrolytes. The major parameters that influence the microstructure are: (1) number, type and distribution of charged monomer; (2) hydrophobic/hydrophilic balance; (3) spacing from the backbone and (4) counterion type. Polyelectrolytes are prepared by homo- or copolymerization of appropriate monomers or by modification of functional polymers.

For rheology modification, the described polymers above can be classified into two categories: (1) non-associative polymers and (2) associative polymers [35]. Associative and non-associative polymers have been briefly discussed under rheology modifiers in Section 7.2.5. Here, we would only focus on the main technologies relevant for fabric and home care formulations.

7.3.1.1 Non-associative polymers

Non-associative polymers thicken by structuring the continuous phase and through chain entanglement. These polymers do not interact with surfactant structures, particulates or insoluble emulsion droplets. The key technology in this category are Alkali Swellable Emulsions (ASEs).

7.3.1.1.1 Alkali swellable emulsions

ASEs are carboxyl-containing copolymers that are prepared by the addition polymerization of ethylenically unsaturated monomers (Figure 7.7), and they swell or solubilize to thicken the formulations based on water [37].

The key advantages of ASE are: (1) they are supplied as acidic low viscous latex dispersion which makes them easy to handle on plant scale, (2) they are relatively cheap compared to other technologies, (3) they thicken the alkaline formulation almost immediately (easy dispersion) and this is important as this makes the batch time extremely small compared to most of the natural polymers such as xanthan

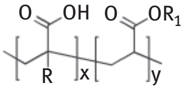

Figure 7.7: Typical chemical structure of ASE. Here R = H, CH3 and most of the commercial ASE contains R1 = -CH2CH3, -CH2CH2CH2CH3.

gum, HEC, etc. and (4) they provide formulation shear-thinning behavior which is important for easy dispensing of fabric and home care products out of the bottle. As with every technology, they also have some limitations such as pH sensitivity, Ca^{2+}, Mg^{2+} and Na^{+} ion sensitivity, and high level of ASE could give formulation a stringing behavior, which can give huge problem in dispensing the product out of the bottle and filling it during production. Some examples of typical commercially available ASE are Rheovis® AS 1130, Rheovis® AS 1125, ACUSOL™ 830 and ACUSOL™ 835.

7.3.1.2 Associative polymers

Associative polymers thicken by two mechanisms that can act simultaneously and synergistically, i. e. hydrodynamic volume of associative polymer and association of the extended hydrophobe groups. When these polymers are in formulation, they make a transient network made up from other hydrophobe groups of polymer and any hydrophobe present in formulation.

7.3.1.2.1 Hydrophobically modified polyacrylamide (HMPAM)

PAM was the first polymer used as a rheology modifier for aqueous solutions [39]. The chemical structure of PAM is shown in Figure 7.8). To achieve a good thickening efficiency, the high molecular weight (M_w>1 MM g/mol) is desired in aqueous solution. The different chemical modification can be employed to improve the properties, e. g. shear resistance, salt compatibility and temperature stability. The partially hydrolyzed polyacrylamide (HPAM) is a good example where HPAM is obtained by copolymerization of sodium acrylate with acrylamide. The chemical structure of HPAM is shown in Figure 7.8) [39]. The presence of electrostatic charges along the polymer backbone is responsible for prominent stretching due to monomer charge repulsion. As a consequence of high stretching of polymer, it leads to a significant increase in viscosity compared to PAM. However, the presence of charges also makes HPAM sensitive to the presence of salt in formulation.

To achieve the best thickening efficiency in formulation with surfactant molecules, HMPAM is frequently used. Figure 7.8(c) shows examples of HMPAM [40]. The high thickening efficiency is a result of association with micelle structure. There are different methods of synthesizing HMPAM such as micellar, homogeneous and heterogeneous copolymerization. PAM is usually prepared via a free radical polymerization in aqueous solution. However, as is evident from the name, HMPAM cannot be synthesized using this technique as the hydrophobic monomer is not soluble in water. In order to disperse the hydrophobic monomer, it is dissolved using a co-solvent or a surfactant (micellar copolymerization) or dispersed without any additives (heterogeneous copolymerization).

The presence of hydrophobic groups suppresses the solubility of the polymer. From the above argument, it is easy to understand that an increase in fraction of hydrophobic groups above a certain percentage will lead to solubility issues, i. e. the polymer is no longer water soluble. Increasing the hydrophobicity of the hydrophobic

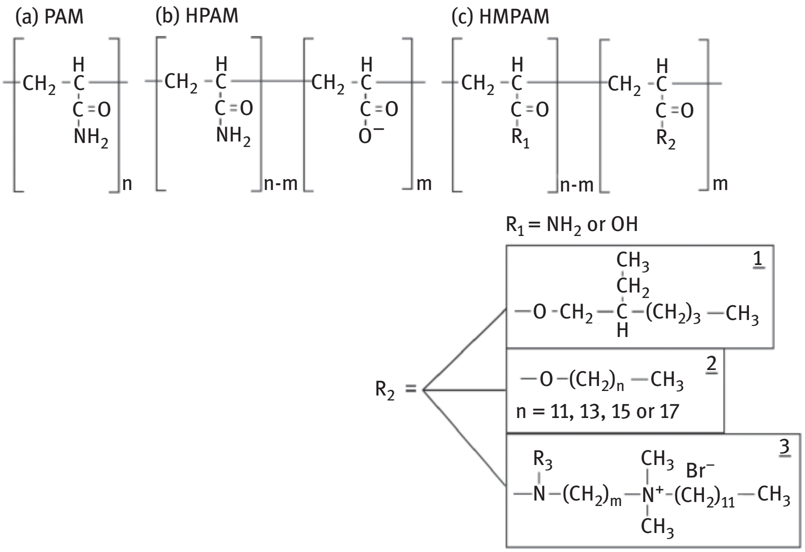

Figure 7.8: Typical chemical structure of hydrophobically modified polyacrylamide (HMPAM).

groups will impart better thickening efficiency as a result of intermolecular association.

The hydrophobic monomer provides interesting rheological properties to the finished product. In the dilute region, intramolecular associations dominate. The hydrodynamic volume is reduced and therefore the viscosity of the subsequent product. When the polymer concentration is increased, the solution ideally moves to the semi-dilute region where intermolecular associations dominate. This leads then to network-like formations (transient network), which significantly increase the viscosity of the solution.

7.3.1.2.2 Hydrophobically modified alkali soluble emulsion

A typical chemical structure of HASE can contain more than three monomers, for example, in addition to acidic group (i. e. methacrylic acid) we could have a small amount of di-acid (maleic acid) and in addition to EA we could have butyl/hexyl acrylates (Figure 7.5) [37]. The HASE polymers differ from ASE in that they also contain long-chain hydrophobic groups in addition to acid groups distributed throughout the polymer chain. The HASE polymers are polyelectrolytes, which have been hydrophobically modified by the introduction of few mol% of hydrophobic group. Comb-like structures where the hydrophobic groups are placed on short PEO side chains randomly distributed along the backbone of the HASE polymer chains are favored. The backbone of the HASE polymers possesses moderate high molecular weight and can reach 100,000 to 500,000 Da.

HASE polymers are synthesized using an emulsion copolymerization process. All the monomers are added to the reaction mixture along with an initiator.

The hydrophobic macro-monomers act as the surfactant for the polymerization reaction. The reaction product of the emulsion polymerization is the HASE polymer. The chief microstructure parameters which plays an important role in modifying the rheology are: (1) charged to un-charged monomer ratio, (2) % of hydrophobic monomer, (3) number of EO units in hydrophobic monomer, (4) length of alkyl chain in hydrophobic monomer, (5) molecular weight and distribution of HASE polyacrylate and (6) the topology of HASE (random or copolymer).

The HASE rheology modifiers are used most frequently in fabric and home care formulations. The main reasons include: (1) the majority of fabric and home care formulations are alkaline and contain anionic surfactant and (2) they are relatively cheap and effective compared to other associative polymers. They could also be compatible with formulations, which contain cationic surfactant. To make the HASE polymer compatible with formulations containing cationic surfactant, the charge density of HASE polymer can be tuned.

The thickening efficiency of HASE in formulation depends on: (1) the intermolecular association of associative monomer, (2) the intramolecular association of associative monomer and (3) the block of EA association (Figure 7.9) [41]. The thickening efficiency improves with intermolecular association. However, intramolecular association of associative monomers and block of EA decreases the thickening efficiency. Typically, it is observed that formulation with HASE polyacrylate viscosity could increase over time. The key factors responsible for increase of viscosity are the hydrolysis of EA unit which could lead to break up of EA block and the intramolecular association leading to intermolecular association. Typical commercially available HASE polyacrylates are Rheovis® AT120, Novethix™ HC200, Capigel™ 98, Novethix™ L10 and Aculyn™ 22.

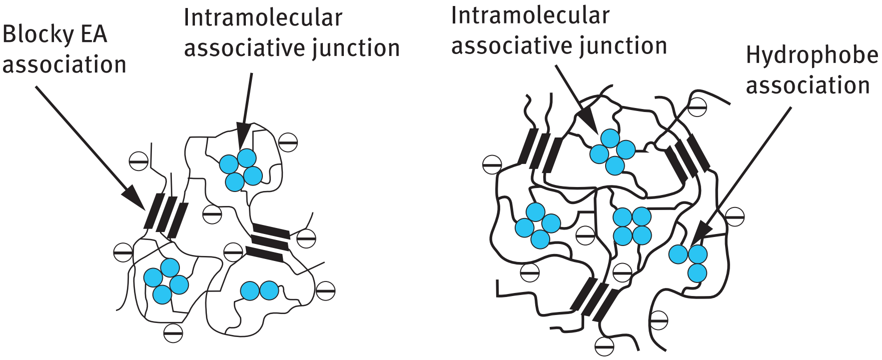

Figure 7.9: The key factors that affects the thickening efficiency of HASE, (1) intermolecular association, (2) intramolecular association, and (3) block of ethyl acrylate (EA). The figure is reproduced from Dai et al. (2005)41 with permission.

7.3.1.2.3 Hydrophobically modified ethoxylated urethane

HEUR polymers are prepared by chain extension of PEO oligomer with a narrow-molecular-weight distribution (MWD) using diisocyanate and end-capping with hydrophobic group. HEUR polymers can be classified into two main classes: step-growth (S-G) HEUR and uni-HEUR. The difference between the two classes relates to the synthesis method and the corresponding MWD of the product. The S-G HEUR involves a procedure where PEO (of a given Mw) is reacted with a large excess of diisocyanate functional groups at both ends. This precursor is subsequently reacted with a hydrophobic group to end-cap both ends, yielding a telechelic polymer. This procedure leads to a HEUR polymer displaying a broad MWD. The procedure for uni-HEUR involves the direct addition of a mono-isocyanate containing a hydrophobic group to the PEO. To this, a hydrophobic group is added. The resulting polymer has a relatively narrow MWD, which is related to that of the parent PEO. The chemical structure of a hydrophobically modified PEO is given in Figure 7.10. Examples of commercially available HEUR are ACRYSOL™ HEUR and Rheosolve 450.

7.3.1.2.4 Hydrophobically modified cellulose derivative

This is the class of semi-synthetic polymers. To synthesize these polymers, the natural polymer is reacted with different kinds of hydrophobic monomer in the presence of initiator. To improve the thickening efficiency, stability and compatibility with different formulations, the natural polymers can be chemically modified, e. g. hydrophobically modified hydroxyethyl cellulose (HM-HEC) [42], hydrophobically modified hydroxypropyl cellulose (HM-HPC) [43], hydrophobically modified ethyl hydroxyethyl cellulose (HM-EHEC) [44] and hydrophobically modified alginate (HM-ALGINATE) [45]. The chemical structure of above examples is shown in Figure 7.11.

The presence of hydrophobic groups on the polymer backbone of the polysaccharides will cause the formation of associations just like HMPAM, HEUR and HASE. The network structure is enhanced due to these groups and hydrophobic associations arise at a very low polymer concentration [42–45]. The improved rheological response

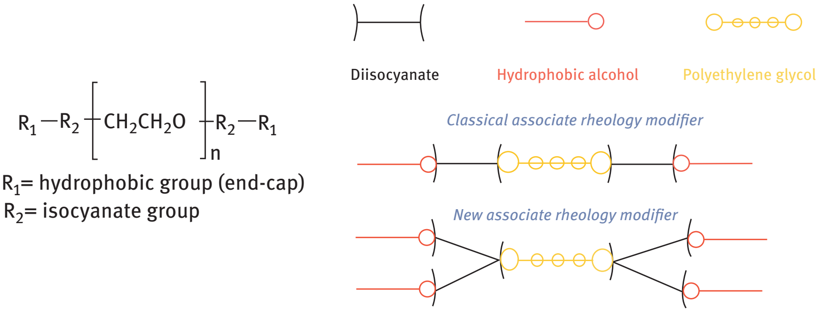

Figure 7.10: Typical chemical structure of HEUR. The isocyanate group acts as a linker between PEO and hydrophobic group.

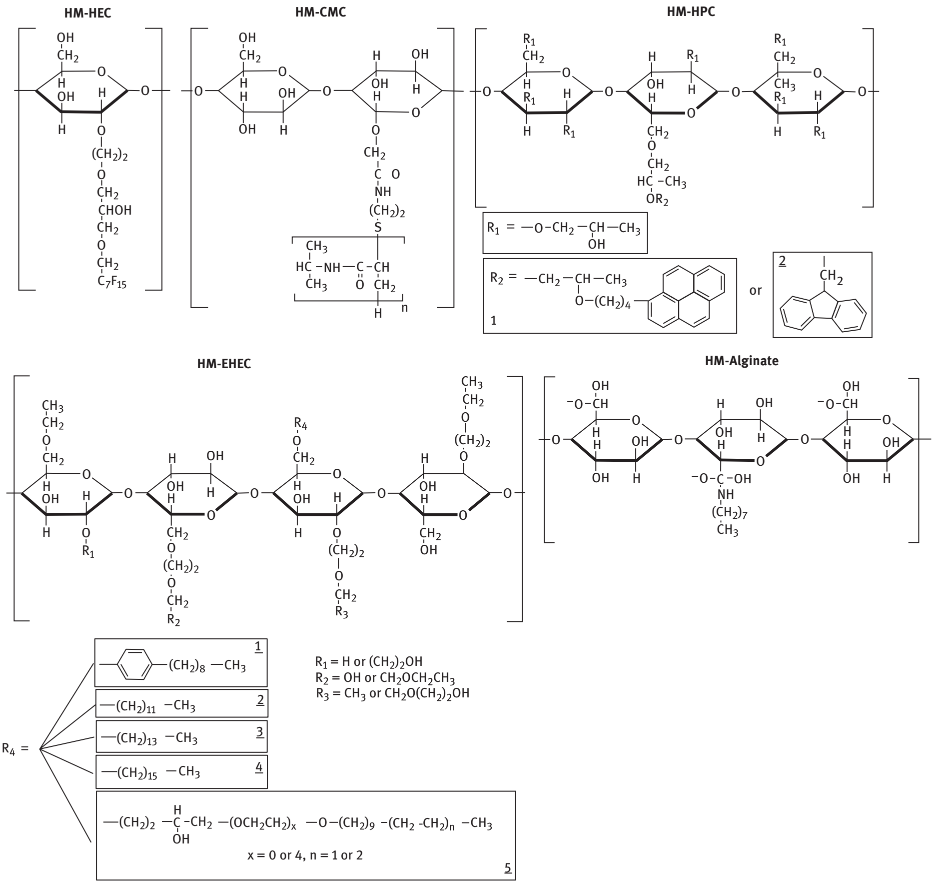

Figure 7.11: Chemical structures of HM-HEC, HM-CMC, HM-HPC, HM-EHEC, and HM-Alginate.

is a result of a formation of strong network compared to unmodified natural polymers. The type of hydrophobic group also affects the strength of the network. Increasing the hydrophobicity will increase the strength. It is also important how the hydrophobic monomers are distributed along the backbone. Inhomogeneous distribution of hydrophobic monomer could lead to a phase separation. The hydrophobic modification decreases the solubility of polymer in aqueous solution.

This class of polymer also imparts pseudoplasticity after certain critical concentration of polymers. In addition, thixotropic behavior is also observed similar to HMPAM. This class of polymer shows an opposite behavior in the presence of salt compared to HMPAM, HEUR and HASE. Indeed, the presence of salt will weaken the electrostatic repulsion. However, this leads to the enhancement of the hydrophobic associations and thus a strengthening of the polymer network. In addition to the presence of salt, the type of salt is also important in defining the thickening efficiency of polymer. The presence of salts that are able to induce a structuring of the water molecules will lead to an enhancement of the viscosity due to the increase in the number of hydrophobic association.

The interaction between hydrophobically modified polymers and a surfactant leads to different behavior depending on the concentration of the surfactant and the type of surfactant (Figure 7.12) [46]. The surfactant molecule will interact with hydrophobic groups forming the mixed micelles. The formation of these mixed micelles will increase the number of hydrophobic microdomains and will enhance interpolymer associations and thus strengthen the polymer network. Increasing the surfactant concentration further will lead to electrostatic repulsions between the mixed micelles and subsequently a drop in the solution viscosity of the formulation. Increasing the surfactant aggregation number in the mixed micelles can counteract the reduction in the solution viscosity at an elevated surfactant concentration. This can be achieved by either adding screening electrolytes or oppositely charged surfactants. A polymer–surfactant formulation employing a surfactant with a lower critical micelle concentration (cmc) will reach a maximum solution viscosity at lower surfactant concentration compared to a surfactant with higher cmc.

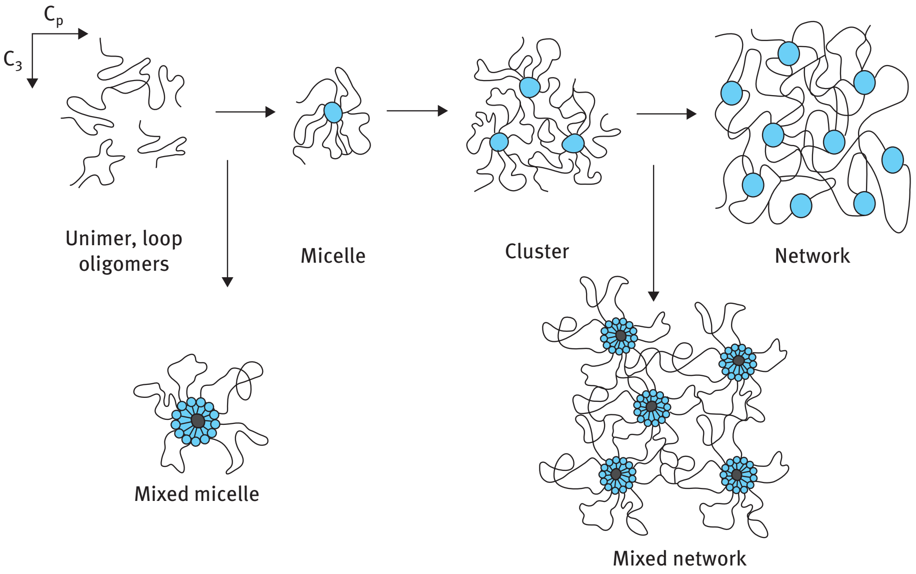

Figure 7.12: The interaction between hydrophobically modified polymers and surfactant which leads to polymer network. Reprinted with permission from Alami et al. Macromoleucles, 1996, 29, 5026. Copyright (1996) American Chemical Society.46.

7.3.2 Natural polymers

Natural polymers are renewable materials that are available in huge quantities. They are economically and environmentally attractive because of their low cost, biodegradability and low toxicity. Similar to synthetic polymers, chemical modifications can be readily achieved on natural polymers which can lead to materials with highly interesting properties. The most common and currently used natural polymers in detergent formulations include cellulose and its derivatives, gums such as xanthan and guar gums and carrageenan.

7.3.2.1 Cellulose

Cellulose is one of the most abundant naturally occurring polymers on earth. It contains a polymeric backbone composed of repeating units of anhydroglucose. Modifications of cellulose were easily accomplished by grafting of long-chain alkyl groups and other functionalities onto the hydroxyl groups [47]. These modifications lead to improved physical, rheological and solution properties. The modified cellulose exhibits increase in water solubility, enhanced viscosity and surface activity. The most common examples of modified cellulose that have been used extensively in the chemical industry are cellulose ethers, which include methylcellulose (MC), hydroxypropyl methylcellulose (HPMC), CMC, HEC and HPC [48]. Each of these cellulosic ethers exhibits unique characteristics and properties. They serve as rheology modifier, anti-redeposition agents, thickeners and stabilizers in cleaning formulations.

7.3.2.1.1 Methylcellulose

MC is a non-ionic polymer that is manufactured by heating the alkali cellulose fibers and treating it with methyl chloride or methyl iodide [49]. MC can be prepared with different degree of substitution (DS). DS refers to the average number of substituents attached to the hydroxyl groups per glucose unit. In theory, the maximum value for DS is 3.0 because there are three reactive hydroxyl units in one glucose ring. Figure 7.13 shows the structure of MC with DS equal to 2.0 [50].

The DS, however, does not only determine the properties (i. e. solubility) of the modified MC but also the distribution of the methoxy group [51, 52]. Typically, the commercially available MC materials have DS between 1.64 and 1.92. MC with DS value at this range is soluble in water and mixed organic solvent/water systems. MC with DS lower than 1.64 produces material that has low water solubility, while those with DS higher than 2.5 are soluble in organic solvents.

MC is compatible with a wide range of ionic species and metallic and inorganic salts because of its non-ionic property. It does not form a complex with these types of salts to form insoluble precipitates. It shows good stability at a pH range of 3 to 11 [34].

MC is marketed under the trade name Benecel™ MC, Methocel™ A and Metolose® SM. It is incorporated in cleaning solutions as thickener and is effective

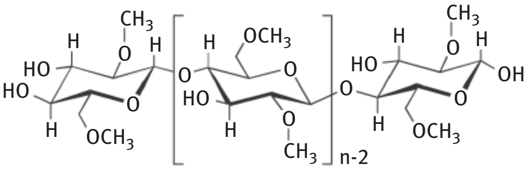

Figure 7.13: Chemical structure of methylcellulose with DS of 2.0.

even at very low dosage (0.5–1 %). MC is reported to help control several important properties of formulations such as rheology, dispersion and water retention. Other benefits that MC provides aside from thickening and stabilizing effect include cold water and organic solubility and gel strength.

7.3.2.1.2 Hydroxypropyl methylcellulose

In the preparation of HPMC, the alkali cellulose fibers are treated with propylene oxide in addition to methyl chloride, to obtain the hydroxypropyl substituents in the hydroxy groups of the anhydroglucose unit (Figure 7.14) [49, 50]. The –OH group of the hydroxypropyl substituent can react further with methyl chloride to form a propylene glycol ether.

HPMC exhibits characteristics that are very similar to MC, but the presence of the hydroxypropyl groups affords hydrophilic domains that are lacking in MC [34]. The HPMC materials that are available in the market consist of varying ratios of methyl and hydroxypropyl groups. They possess different attributes that influence the water and organic solvent solubility and thermal gelation temperature of aqueous solutions. Both MC and HPMC have been utilized as anti-redeposition agents in laundry detergents [53].

7.3.2.1.3 Carboxymethyl cellulose

CMC, also popular under the names cellulose gum, sodium cellulose glycolate and sodium CMC, is the most widely used cellulosic ether. Unlike MC or HPMC, CMC is an anionic polymer. It is synthesized via chemical reaction of cellulose with monochloroacetic acid and subsequent neutralization with sodium salt [49]. An example of a chemical structure of CMC with DS of 1.0 is shown in Figure 7.15.

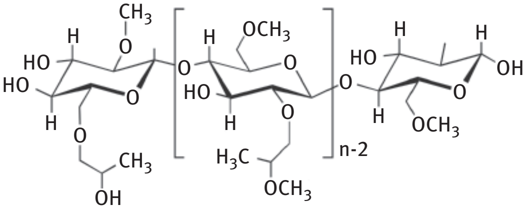

Figure 7.14: Chemical structure of hydroxypropyl methylcellulose (HMPC).

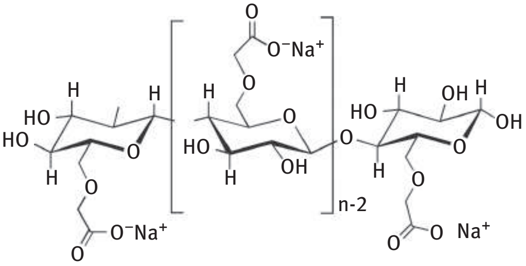

Figure 7.15: Structure of carboxymethyl cellulose (CMC) with DS of 1.0.

The theoretical maximum DS for CMC is also 3.0, but more often than not approximately only half of the hydroxyl units are being substituted with –CH_2COOH groups [34, 49]. The highest level of substitution of CMC that is available in the market is 1.4. The structural stability of formulations induced by CMC is greatly influenced by the concentration of the polymer, while thixotropy generally increases with decreasing DS. CMC is stable over a broad pH range of 4 to 10 and is well suited for most non-ionic and anionic species as well as monovalent and divalent salts [49]. But because of its anionic character, it is generally not compatible with cationic materials.

CMC is used in washing formulations, mainly as anti-redeposition agent, and it is mostly beneficial to the laundering of cotton fabrics [54]. It was reported that the negatively charged carboxyl groups of CMC attract the hydrophobic dirt particles and hold on to them, therefore preventing them from resettling onto the fabrics during the washing process. In addition, CMC also provides effective thickening effects [55] and structural stability on the detergent slurry and liquid soap.

CMC is available in the market as purified and technical grades under the trade name CALEXIS®, CEKOL®, CELFLOW®, CELLUFIX® and FINNFIX®.

7.3.2.1.4 Hydroxyalkyl cellulose

Hydroxyalkyl cellulose derivatives include HEC and HPC. HEC and HPC are both non-ionic and water-soluble polymers. The general structure of HEC is given in Figure 7.16. The hydroxyethyl groups were introduced into the cellulose molecule by treatment with sodium hydroxide followed by ethylene oxide [49, 56]. Subsequently, the ethylene oxide that has previously substituted the hydroxyl group can react further with another ethylene oxide molecule to form an elongated side chain.

The average number of moles of hydroxyethyl and ethoxy units added per anhydroglucose ring is called moles of substitution (MS) [34]. In the case of the structure in Figure 7.16, the value of MS is 2.5 (5 ethylene groups/2 glucose units) and the DS is 1.5 (3 hydroxyl groups substituted/2 glucose units). Because elongation of side chains of ethylene oxide can take place, the MS value can be higher then 3.

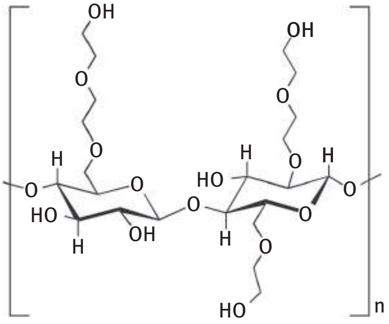

Figure 7.16: Chemical structure of hydroxyethyl cellulose (HEC) with DS of 1.5 and MS of 2.5.

HEC products that are commercially available have DS values ranging from 0.85 to 1.35 and MS values of 1.3 to 3.4. The water solubility of HEC depends on the values of DS and MS. At the values mentioned above, HEC is water soluble. HEC also exhibits good stability with respect to pH (2–11) and temperature and excellent compatibility with other anionic and cationic ingredients [34].

HEC is one of the easiest polymer derivatives to process. It dissolves easily at high temperatures and hydrates very efficiently even with just moderate mixing and agitation. HEC is used as thickening agent in detergent industry and assists in enhancing the silkiness and smoothness of the fabrics. HEC aqueous dispersions are pseudoplastic and thermally reversible. It is commercially available under the trade name Natrosol™ HEC.

The preparation of HPC is similar to HEC, wherein the alkali cellulose is treated with propylene oxide (instead of ethylene oxide for HEC) at high temperatures (Figure 7.17) [49]. A side chain with more than one mole of propylene oxide can also form during the preparation of HPC.

Both HEC and HPC are soluble in water at low temperature. Similar to HEC, HPC also provides rheology control, thickening and stabilizing effects to formulations.

7.3.2.2 Gums

Gums are natural biopolymers that have found broad appeal in detergent industry. They are largely used as thickeners in cleaning compositions. Some of the examples of gums that will be covered in this section are xanthan, guar and locust bean gum.

7.3.2.2.1 Xanthan gum

Xanthan gum is a high-molecular-weight, anionic polysaccharide that is produced by fermentation process using the bacterium *Xanthamonas campestris* [57]. It initially found broad commercial applications in food industry but later on was developed for use in detergent industry [34]. The structural formula of a repeating unit of xanthan gum consists of β-D-(1,4)-glucose molecules in the backbone chain and a

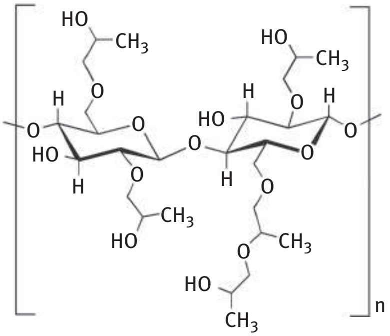

Figure 7.17: Structure of HPC with MS of 2.5 and DS of 2.0.

trisaccharide side chain attached at the O-3 position of every other glucose moiety (Figure 7.18) [49, 57]. The trisaccharide unit is composed of β-D-(1,2)-mannose attached to β-D-(1,4)-glucuronic acid and terminates with β-D-mannose. The inner mannose residue is mostly acetylated at O-6 position and the terminal mannose contains pyruvic acid linked together via keto group at the 4 and 6 positions. The carboxylic acid functionalities at D-glucuronic acid and pyruvic acid make the xanthan gum anionic.

Xanthan gum has high solubility both in hot and in cold water. Xanthan gum solutions are highly pseudoplastic and display a remarkable viscosity even at low polymer concentrations [57, 58]. Their viscosity recovers instantaneously once the shear force is removed. Xanthan gum's shear-thinning behavior provides the desired pour viscosity and improves the stability of the formulation by preventing the suspended particles from settling at the bottom of the container throughout the shelf life of the detergent.

Several factors affect the viscosity of xanthan gum solutions including the dissolution and the measurement temperatures, the pH as well as the concentrations of the polymer and the salt in solution [57]. Generally, the viscosity decreases with increasing temperature. However, it was observed that xanthan gum solutions that

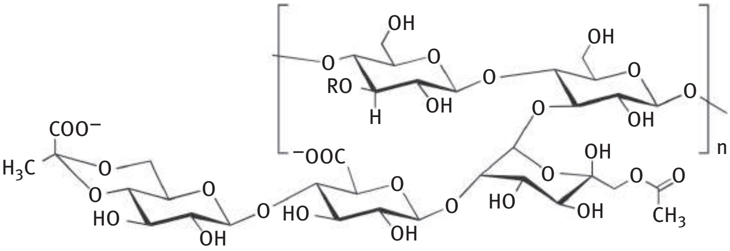

Figure 7.18: Structural formula of a repeating unit of xanthan gum.

were dissolved at moderate temperatures (between 40 and 60 °C) tend to give highly viscous solutions. This observation can be attributed to the change in the conformation of the molecules when the temperature is increased. Xanthan gum molecules were found to adopt two conformations, helix and random coil, depending on the temperatures at which they were dissolved. The conformational shift observed from a low (<40 °C) to high dissolution temperature (>60 °C) corresponds to a helix–coil transition of the backbone with simultaneous release of the lateral chains followed by a progressive decrease of the rigidity of the glucose chain.

The viscosity of the xanthan gum solution is also significantly affected by the amount of the biopolymer added, that is, the higher the concentration the higher the viscosity [57]. This observed behavior was associated with the increase in the molecular dimensions due to an increase in intermolecular interaction. Another significant attribute of xanthan gum solutions is the synergistic increase in viscosity when mixed with other gums such as locust bean and guar gum [59]. This behavior further improves the suspending capability of xanthan gum solution.

Only very few rheology modifiers are stable over an acidic and alkaline pH ranges (pH from 1 to 13), and one of them is the xanthan gum [34, 57]. This property makes it a suitable thickener for cleaning products ranging from acid cleaners to scale removers as well as the conventional alkaline hard surface cleaners and neutral detergents [34]. Xanthan gum also has high tolerance to both monovalent and divalent metal salts in addition to anionic and non-ionic surfactants.

Xanthan gum is widely marketed as KELDENT®, KELFLO®, KELTROL®, KELZAN®, XANTURAL® and XANVIS®.

7.3.2.2.2 Guar gum

Guar gum, also known as guaran, is a water-soluble polysaccharide isolated from the plant called Guar, or cluster bean *Cyamopsis tetragonolobus* that belongs to the family *Leguminosae* [60]. Its backbone is composed of linear chain of D-mannopyranose units linked together by β-(1,4) glycoside linkages with branch points from the 6-positions linked to a single α-D-(1,6)-galactose (Figure 7.19) [61].

Similar to xanthan gum, guar gum also dissolves very quickly in cold and hot water to give highly viscous pseudoplastic solutions even at very low concentrations. However, guar gum solutions are less pseudoplastic compared to xanthan gum. Guar gum solutions display high low-shear viscosity but have strong shear-thinning property [60]. They are thixotropic at high concentrations (1 %) but not at lower concentrations (0.3 %). Because guar gum is a non-ionic biopolymer, it is not easily affected by electrolytes and has high tolerance to basic and acidic environment.

Guar gum has been used effectively as natural thickening agent and stabilizer in detergent compositions. However, there are some disadvantages observed with guar gum solutions such as they tend to give formulations with a stringy rheological property and a hazy physical appearance, which is a result of the residual materials like oils and proteins present in the raw guar gums [34, 49]. These contaminants can

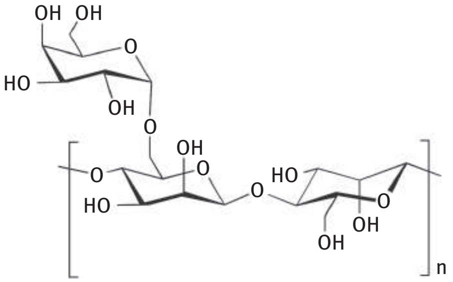

Figure 7.19: Chemical structure of the repeating unit of guar gum.

be removed by repetitive washing of the commercially available guar gums, but this in effect results in an increase in the cost of the product.

Chemical modification of guar gum such as reaction with propylene oxide results in substitution on the hydroxyl groups (Figure 7.20). This functionalized guar gum is called hydropropyl guar (HP-guar) [62]. Compared to hazy solutions obtained from guar gums, this chemically altered compound gave a much clearer aqueous solution [49].

HP-guar displays very similar solution characteristics to those of HPC. It is readily soluble in water and builds high viscosities at low concentrations via the mechanism of chain entanglement. It was reported to act as a foam enhancing agent in liquid detergents [63].

7.3.2.2.3 Locust bean gum

Locust bean gum, also known as Carob bean and Carubin, are extracted from the seed of the carob tree *Ceratonia siliqua* [61]. Its structure is similar to guar gum (Figure 7.20) except that locust bean gum has fewer amount of galactose. For guar gum, there are two mannose residues for every galactose molecule, while for locust bean gum, there are four. For this reason, locust bean gum is less soluble in water and

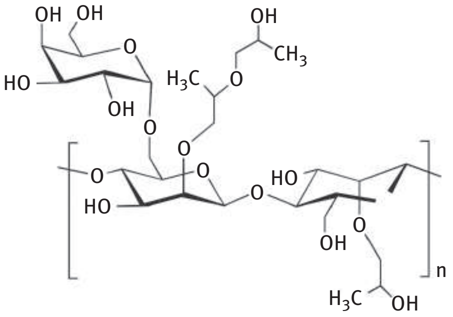

Figure 7.20: Chemically modified guar gum known as hydropropyl guar (HP-guar).

has lower viscosity than guar gum. Heating is usually necessary to obtain solutions of locust bean gum.

Locust bean gum has very similar properties with guar gum. It also has high resistance to ionic strength or broad range of pH because of its non-ionic character. It has been employed as stabilizers in detergent dispersions.

7.3.3 Carrageenan

Carrageenans are family of water-soluble linear polysaccharides extracted from marine red algae (*Rhodophyta*). They are high-molecular-weight polysaccharide ranging from 100 to 1,000 kDa, which contains 15–40 % of sulfate ester groups and alternate units of β-D-1,3-galactose and α-D-1,4-galactose. Seven different variations of carrageenan were identified, but only three of them namely kappa-, iota- and lambda-carrageenans are of commercial interests (Figure 7.21) [49]. These carrageenans were produced by different seaweeds, and the principal differences between these three are the number and position of ester sulfate groups as well as the type of substituents on the α-D-1,4-galactose moiety [64].

The structure of kappa-carrageenan is very similar to iota-carrageenan wherein their galactose residue contains five-membered cyclic ether group between the C3 and C6 carbon atoms, which give them rigid structures (Figure 7.21) [49, 64]. Both of them assume helical conformations and their structures only differ in the presence of extra sulfate ester group in the C2 carbon atom of galactose moiety of iota-carrageenan. Lambda-carrageenan, on the other hand, contains three sulfate groups per two galactose molecules (Figure 7.21) and does not form helical structures like kappa or iota. As a consequence, it does not form gels in aqueous solutions and are mainly used to thicken solutions.

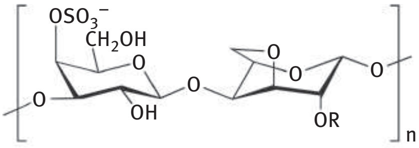

Kappa-Carrageenan, R = H
Iota-Carrageenan, R = SO_3^-

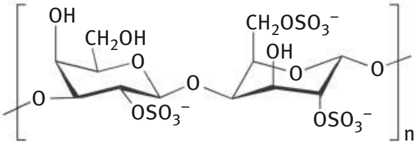

Lambda-Carrageenan

Figure 7.21: Chemical structures of the repeating dimeric units of kappa-, iota- and lambda-carrageenan.

The presence of sulfate esters in carrageenans contributes to their acidity as well as hydrophilicity. The position of the ester sulfate groups also influences their gelling abilities. High amounts of ester sulfate moieties in carrageenans are indicative of high solubility in aqueous solutions and lower gel strength. Both kappa- and iota-carrageenan require high temperatures to dissolve in aqueous solutions, but their sodium salts are readily soluble in cold water. They have the ability to form thermo-reversible gels, which can be attributed to the formation of a three-dimensional double-helix polymer network [65]. When the carrageenans are heated to high temperatures, they exist as random coil. Upon cooling, they build up into double helices, which lead to aggregation forming a three-dimensional gel structures.

The physical properties of the carrageenans are highly dependent on the conformation of the sugar units in the polymer chain and the type of cations present in solution. For example, in the presence of cations such as potassium or calcium ions, kappa- and iota-carrageenans have the ability to form gels in aqueous solutions whereas lambda-carrageenan does not [66]. With potassium salts in aqueous solutions, kappa-carrageenan forms brittle gels, while with calcium salts the iota-carrageenan produces soft and elastic gels. The strength of the gels produced is directly proportional to the concentration of the carrageenan as well as the amount of potassium or calcium salts in solutions. However, the use of excessive quantity of salts weakens the gel. The ionic strength of the solutions also affects the gelling and/or the melting temperatures. When the salt concentration of the aqueous carrageenan solutions in increased, the gelling temperature generally increases.

One of the main concerns encountered with gels that are produced from kappa-carrageenan is the spontaneous separation of water through the surface of gel, a phenomenon known as syneresis [34]. The degree of syneresis increases as the amount of potassium salt in solution is increased. In order to improve this condition, kappa-carrageenan is frequently combined with locust bean gum [67] or guar gum [68]. This combination has shown not just a decrease in the level of syneresis but also a substantial increase in the gel strength, an enhanced texture of the gel, from brittle to elastic, and improvement in water-binding capability. Iota-carrageenan, on the other hand, does not exhibit syneresis.

Iota carrageenan aqueous gels are known to display thixotropic rheological properties at low concentrations, that is, the gels can reorganize to its original form once it is destroyed [64]. This thixotropic property is particularly useful to suspend insoluble particles. Aqueous gels formed with kappa-carrageenan, however, do not display this thixotropic property.

At neutral and basic pH conditions, carrageenan aqueous solutions exhibit good stability. At high temperatures and acidic conditions, the glycosidic linkages of the carrageenans are prone to undergo hydrolysis, causing it to lose its viscosity and gelling capabilities. But once the gel is formed, hydrolysis can no longer take place; therefore it remains stable even at low pH.

Because of the instability of the free sulfonic acid, carrageenans are commonly marketed as the sodium, potassium and calcium salts or a combination of these. They are normally used as thickening, gelling and stabilizing agents [64]. The solution viscosity is strongly influenced by the concentration, the type and molecular weight of carrageenan used, the temperature and the presence of other solutes. Viscosity is directly proportional to the concentration and molecular weight of the carrageenan but inversely proportional to the temperature.

Carrageenans are marketed by CP Kelco under the names: GENULACTA®, GENUGEL®, GENUTINE®, GENUVISCO®, GENU® PLUS and GENU® Texturizer.

7.3.4 Alginates

Alginates are anionic polysaccharides that are extracted from marine brown algae (*Phaephyceae*) [69]. Its structural formula, shown in Figure 7.22, consists of β-D-(1,4)-mannuronic acid and α-L-(1,4)-guluronic acid which can be linked glycosidically as poly(mannuronic acid) and poly(guluronic acid) or mixture of both [49, 69]. The sequence of the mannuronate and glucuronate residues can vary in the naturally occurring alginate depending on the algal source. Alginates owe their highly anionic character to the C6 carboxylate groups of both mannuronic and guluronic acid moieties.

The viscosity of aqueous solutions of alginate is affected by change in pH because of the existence of carboxylic acid groups [49]. The isoelectric point of carboxylic acid is close to pH equal to 4, and this is where the effect of pH on viscosity is most evident. Similar to carrageenans, alginates are not stable at vey low pH because of the tendency of the glycosidic bonds to undergo hydrolysis.

The presence of cations (i. e. calcium ions) in solution also influences the viscosity and gelation of the alginates [70]. Polyvalent cations are known to cause the formation of "junction zones" in alginate solutions. The formation of these junction zones is a result of the interaction between the carboxylic acid substituent of the guluronic acid residues and the calcium ions. These interactions enhance the viscosity of the alginate solutions especially at higher concentration of the cations and eventually cause gel formation. However, a very high amount of the polyvalent

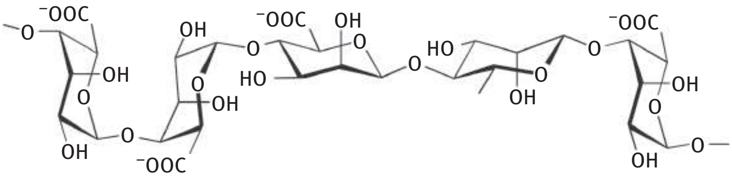

Figure 7.22: Structural formula of repeating unit of alginates which is consists of -D-(1,4)-mannuronic and -L-(1,4)-guluronic acids.

cations can cause the alginic acid to precipitate out of the solution [71]. Alginates, therefore, can be used either as thickeners or gellants depending on the matrix and kind of alginates used. It is marketed under the trade name ZENVIVO™.

7.4 Conclusions

Synthetic and naturally derived polymers have been of great use to fabric and home care products whether in solid or liquid formulations and for manual or machine washings. In addition to conventional cleaning effects, significant improvements and specific benefits have been successfully delivered to detergent formulations with the use of these polymers. The incorporation of these polymeric materials in the cleaning solutions has created one or several effects and offered many novel performance advantages. The synthetic polymer poly(vinyl pyrrolidone), for instance, was developed to effectively inhibit dye transfer in synthetic fabrics. The natural polymer CMC has been used as an efficient anti-redeposition agent after stain removal in household detergents both in washing machines and in hand washing.

The recent developments on synthetic polymers have considerably enhanced the performance attributes of the household products. Polycarboxylates were among the first and most extensively investigated class of synthetic polymers. To get the desired properties, synthetically derived polymers were easily tailored and controlled through modifications of the molecular weight, the degree of branching and chemical functionalities of the polymer main and side chains. The easy manipulation of the characteristics of these materials is one advantage that synthetic polymers have over most natural materials. However, synthetic polymers, particularly the specialty ones, can be costly.

The market price for the natural polymers, on the other hand, is low compared to most synthetic polymers and does not normally affect the final price of the finished products. Hence formulations that are based on these polymers are cost-effective. Various quantities of naturally derived polymer have been used to obtain the preferred properties. Their qualities and versatilities were also further improved by chemical modifications. Most often than not, chemical alterations of these class of polymers lead to materials that are of interesting and remarkable properties.

Manufacturers believed that the future of household formulations is not only linked to enhanced cleaning action but also to sustainability and biodegradability. In general, the goal would be to bring out formulations that would be of sound effects in terms of properties, economic and environmental considerations. Natural polymers have high rate of biodegradability; thus, they can be used in the formulations at the commercial level on a large scale. Synthetic polymers are only biodegradable to some level, but they can be removed from wastewater with the aid of treatment facilities. These amenities can quickly degrade water-soluble polymers by providing high degree of bioactivity. In some cases, this is a limitation that caused synthetic polymers to become comparatively unappealing commercially.

In the following years, we expect that major producers will continue to provide innovations on the finished formulations of fabric and home care products based on evolving needs of the people and trend toward sustainability. The design and development of novel polymeric materials will continue to expand the capabilities and effectiveness of cleaning formulations. Entirely new products with much improved properties will continue to emerge in the market place to better serve the users. These new innovations will involve new chemistry, formulating techniques and functionalities from commercial polymers, whether synthetic, semi-synthetic or natural.

References

[1] Revelle P, Revelle C. The environment: issues and choices for society. Boston: Jones and Bartlett Publishers, 1988.

[2] Hammond AL. Phosphate replacements: problems with the washday miracle. Science. 1971;172:361–363.

[3] Duthie JR. Detergents: nutrient considerations and total assessment. In: Likens GE, editors., editor(s). Nutrients and eutrophication: the limiting- nutrient controversy. Limnology and Oceanography. Lawrence, Kansas: Allen Press, Inc., 1972:205–216.

[4] Agbazue VE, Ekere NR, Shaibu Y. Assessment of the levels of phosphate in detergents samples. Int J Chem Sci. 2015;13:771–785.

[5] Houston CA. Builders in liquid laundry detergents. In: Baldwin AR, editors., editor(s). Second world conference on detergents: looking towards the 90's. Boulder, Urbana, IL: American Oil Chemist's Society, 1987:161–164.

[6] Knud-Hansen C. Historical perspective of the phosphate detergent conflict. Boulder, Colorado: University of Colorado, 1994.

[7] Morgenthaler WW. Builder trends in North American detergent products. In: Baldwin AR, editors., editor(s). Second world conference on detergents: looking towards the 90's. Boulder, Urbana, IL: American Oil Chemist's Society, 1987:165–170.

[8] Pattusamy V, Nandini N, Bheemappa K. Detergent and sewage phosphates entering into lake ecosystem and its impact on aquatic environment. Int J Adv Res. 2013;1:129–133.

[9] Yamane I, Nakazawa T. Development of zeolite for non-phosphated detergents in Japan. Pure Appl Chem. 1986;58:1397–1404.

[10] Andree H, Krings P, Upadek H, Verbeek H. Possibilities of combining zeolite a with different co-builders. In: Baldwin AR, editors., editor(s). Second world conference on detergents: looking towards the 90's. Boulder, Urbana, IL: American Oil Chemist's Society, 1987:148–152.

[11] Bertleff W, Neumann P, Baur R, Kiessling D. Aspects of polymer use in detergents. J Surfactants Deterg. 1998;1:419–424.

[12] Geffroy C. Future trends with polymers in detergency. In: Cahn A, editors., editor(s). 5th world conference on detergents reinventing the industry: opportunities and challenges. Boulder, Urbana, IL: AOCS Press, 2003:75–80.

[13] Hirota R, Kuroda A, Kato J, Ohtake H. Bacterial phosphate metabolism and its application to phosphorus recovery and industrial bioprocesses. J Biosci Bioeng. 2010;109:423–432.

[14] Keshwani A, Malhotra B, Kharkwal H. Natural polymer based detergents for stain removal. World J Pharm Sci. 2015;4:490–508.

[15] Gross RA, Kalra B. Biodegradable polymers for the environment. Science. 2002;297:803–807.

[16] Watson RA. Liquid laundry detergents. In: Showell M, editors., editor(s). Handbook of detergents, part D: formulation. Boca Raton, FL: Taylor & Francis Group, 2006:51–104.

[17] Scialla S. The formulation of liquid household cleaners. In: Showell M, editors., editor(s). Handbook of detergents, part D: formulation. Boca Raton, FL: Taylor & Francis Group, 2006: 153–178.

[18] Anthony J, O'Lenick J. Soil release polymers. J Surfactants Deterg. 1999;2:553–556.

[19] Kissa E. Mechanisms of soil release. Textile Res J. 1981;51:508–513.

[20] Rosie JA, Rodrigues K, Hodgetts RW. A new generation soil-release polymer cotton. In: Cahn A, editors., editor(s). Proceedings of the 4th world conference on detergents: strategies for the 21st century. Boulder, Urbana, IL: AOCS Press, 1999:247–248.

[21] Paul HV, Bruce PJ, Dwight TR. Fabric softener and soil-release composition and method patent US3928213 A 1975. Inventors; Procter & Gamble, assignee.

[22] Nagler M. Soil release promoting pet-poet copolymer, method of producing same and use thereof in detergent composition having soil release promoting property patent US4785060 A 1986. Inventor Colgate-Palmolive Company, assignee.

[23] Swift G. Polymeric dispersants in powdered laundry detergents. In: Showell M, editors., editor(s). Powdered detergents. New York: Marcel Dekker, Inc., 1998:109–136.

[24] Showell M. Introduction to detergents. Handbook of detergents, part d: formulation. New York: Taylor & Francis Group, 2006:1–26.

[25] Diehl FL. Soil anti-redeposition agents, their use and detergent compositions containing same patent US3597416 A 1971. Inventor Procter & Gamble, assignee.

[26] Marco FW, Harris PG. Laundry detergent containing cellulose acetate anti-redeposition agent patent US4235735 A 1980. Inventors; Milliken Research Corporation, assignee.

[27] Carrion FJ. Influence of the dye transfer inhibitors for the washing of softened cotton fabric. J Textile Inst. 2014;105:150–155.

[28] Carrion FJ. The PVP/VI copolymer dye transfer inhibition agent during the washing of the polyester fabric. Tenside Surfactant Deterg. 2013;50:26–30.

[29] Hornby J. PVP: a dye transfer inhibitor for laundry detergents. HAPPI. 1995;32:88–89.

[30] Sterling ME, Dinniwell AR. Dye-transfer-inhibiting systems for use in laundry detergents patent WO9503390A1 1995. Inventors; Procter and Gamble Co., USA. assignee.

[31] Fredj A, Johnston JP, Thoen CAJ. Surfactant-containing dye transfer inhibiting compositions patent US5458809 A 1995. Inventors; The Procter & Gamble Co., assignee.

[32] Busch A, Convents AC. Softening through the wash compositions patent US 5604197 A 1997. inventors; The Procter & Gamble Co., assignee.

[33] Shih JS, Srinivas B, Hornby JC. Water Soluble Dye Complexing Polymers patent US005929175A 1999. Inventors; ISP Investments Inc., Wilmington, Del., assignee.

[34] Reeve P, Tepe T, Shulman J. Rheology modifiers and thickeners for liquid detergents. In: Lai K-Y, editors., editor(s). Liquid detergents, 2nd ed. Boca Raton, FL: Taylor & Francis Group, 2005.

[35] Glass JE, Schulz DN. Polymers as rheology modifiers. Washington, DC: American Chemical Society, 1991.

[36] Rounds RS. Rheology of liquid detergents. In: Lai K-Y, editors., editor(s). Liquid detergents, 2nd ed. Boca Raton, FL: Taylor & Francis Group, 2005.

[37] Horiuchi K, Rharbi Y, Spiro JG, Kazunaga Horiuchi, Yahya Rharbi, John G. Spiro, Ahmad Yekta, Mitchell A. Winnik, Richard D. Jenkins et al. Fluorescence probe studies of hydrophobic domains in a model hydrophobically modified alkali-swellable emulsion (HASE) polymer with C20H41 groups. Langmuir ACS J Surf Colloids. 1999;15:1644–1650.

[38] Ceulemans RA, Block FJ, Hubesch BA. Fabric softener compositions patent EP0799887 A1.. Inventors; Procter & Gamble, assignee. 1997.

[39] Wever DA, Picchioni F, Broekhuis AA. Polymers for enhanced oil recovery: a paradigm for structure–property relationship in aqueous solution. Prog Polym Sci. 2011;36:1558–1628.

[40] Peiffer DG. Hydrophobically associating polymers and their interactions with rod-like micelles. Polymer. 1990;31:2353–2360.

[41] Dai S, Chiu Tam K, Jenkins RD. Dynamic light scattering of semidilute hydrophobically modified alkali-soluble emulsion solutions with different lengths of poly(ethylene oxide) spacer chain. J Polym Sci B Polym Phys. 2005;43:3288–3298.

[42] Kjøniksen A-L, Beheshti N, Kotlar HK, Zhu K, Nyström B. Modified polysaccharides for use in enhanced oil recovery applications. Eur Polym J. 2008;44:959–967.

[43] Gonzales JM, Muller AJ, Torres MF, Saez AE. The role of shear and elongation in the flow of solution of semi-flexible polymers through porous media. Rheologica Acta. 2005;44:959–967.

[44] Hoffman H, Donges R, Ehrler R. Interactions between modified hydroxyethyl cellulose (HEC) and surfactants. Colloid Surf, A. 1996;112:209–225.

[45] Nishikawa K, Yekta A, Pham HH, Winnik MA, Sau AC. Fluorescence studies of hydrophobically modified hydroxyethylcellulose (HMHEC) and pyrene-labeled HMHEC. Langmuir ACS J Surf Colloids. 1998;14:7119–7129.

[46] Alami E, Almgren M, Brown W. Interaction of hydrophobically end-capped poly(ethylene oxide) with nonionic surfactants in aqueous solution. Fluorescence and light scattering studies. Macromolecules. 1996;29:5026–5035.

[47] Habibi Y. Key advances in the chemical modification of nanocelluloses. Chem Soc Rev. 2014;43: 1519–1542.

[48] Majewicz TG, Podlas TJ. Cellulose ethers. In: Kroschwitz JI, Howe-Grant M, editors., editor(s). Kirk-Othmer encyclopedia of chemical technology, 4th ed New York: Wiley, 1993:548–553.

[49] Gruber JV. Polysaccharide-based polymers in cosmetics. In: Goddard ED, Gruber JV, editors., editor(s). Principles of polymer science and technology in cosmetics and personal care. New York: Marcel Dekker, Inc, 1999:325–389.

[50] Farooq A. Rheological modifiers for aqueous solutions. Surfactant Sci Ser. 1999;82:757–785.

[51] Desbrières J, Hirrien M, Ross-Murphy SB. Thermogelation of methylcellulose: rheological considerations. Polymer. 2000;41:2451–2461.

[52] Nasatto P, Pignon F, Silveira J, Duarte M, Noseda M, Rinaudo M. Methylcellulose, a cellulose derivative with original physical properties and extended applications. Polymers. 2015;7:777.

[53] Aszman H, Gomes G, Lee C. Gelled light duty liquid detergent containing anionic surfactants and hydroxypropyl methyl cellulose polymer patent US5565421 A 1996. Inventors; Colgate Palmolive Co., assignee.

[54] Roy MA. Soil anti-redeposition agent patent US3335086 A 1967. Inventor American Cyanamid Co, assignee.

[55] Benchabane A, Bekkour K. Rheological properties of carboxymethyl cellulose (CMC) solutions. Colloid Polym Sci. 2008;286:1173–1180.

[56] Powell GM. Hydroxyethylcellulose. In: Davidson RL, editors., editor(s). Handbook of water-soluble gums and resins. New York: McGraw-Hill, 1980:1–22.

[57] Garcıa-Ochoa F, Santos VE, Casas JA, Gómez E. Xanthan gum: production, recovery, and properties. Biotechnol Adv. 2000;18:549–579.

[58] Zats JL, Knapp S. Viscosity of xanthan gum solutions at low shear rate. J Pharm Sci. 1984;73: 468–471.

[59] Kovacs P. Useful incompatibility of xanthan gum with galactomannans. Food Technol. 1973;27: 26–30.

[60] Chudzikowski RJ. Guar gum and its applications. J Soc Cosmet Chem. 1969;22:43–60.

[61] Whistler RL, Gum G, Gum LB, et al. Natural plant hydrocolloids. Washington, DC: American Chemical Society, 1954:45–50.

[62] Floridi G, Langella V, Li BG, Pelizzari R, Pfeiffer U. Hydroxypropyl guar patent WO2012159972 A1 2012. Inventors; Lamberti Spa, assignee.

[63] Lai K-Y. Foam enhancing agent for light duty detergent patent US4877546 A 1989. Inventor Colgate-Palmolive Company, assignee.

[64] Campo VL, Kawano DF, Silva DB, Carvalho I. Carrageenans: biological properties, chemical modifications and structural analysis – A review. Carbohydr Polym. 2009;77:167–180.

[65] Rochas C, Rinaudo M. Mechanism of gel formation in kappa-carrageenan. Biopolymers. 1984;23:735–745.

[66] Grasdalen H, Smidsroed O. Iodide-specific formation of kappa-carrageenan single helixes. Iodine-127 NMR spectroscopic evidence for selective site binding of iodide anions in the ordered conformation. Macromolecules. 1981;14:1842–1845.

[67] Lundin L, Hermansson AM. Influence of locust bean gum on the rheological behavior and microstructure of k-carrageenan. Carbohydr Polym. 1995;29:91–99.

[68] Turquois T, Rochas C, Taravel FR. Rheological studies of synergistic kappa-carrageenan-carob galactomannan gels. Carbohydr Polym. 1992;17:263–268.

[69] Draget KI, Smidsrød O, Skjåk-Bræk G. Alginates from algae. Biopolymers online. New York: Wiley-VCH Verlag GmbH & Co. KGaA, 2005.

[70] Thom D, Grant GT, Morris ER, Rees DA. Characterization of cation binding and gelation of polyuronates by circular dichroism. Carbohydr Res. 1982;100:29–42.

[71] Jw L, Ashby RD, Day DF. Role of acetylation on metal induced precipitation of alginates. Carbohydr Polym. 1996;29:337–345.

Karolina Wieszczycka and Katarzyna Staszak

8 Polymers in separation processes

Abstract: Application of polymer materials as membranes and ion-exchange resins was presented with a focus on their use for the recovery of metal ions from aqueous solutions. Several membrane techniques were described including reverse osmosis, nanofiltration, ultrafiltration, diffusion and Donnan dialysis, electrodialysis and membrane extraction system (polymer inclusion and supported membranes). Moreover, the examples of using ion-exchange resins in metal recovery were presented. The possibility of modification of the resin was discussed, including hybrid system with metal cation or metal oxide immobilized on polymer matrices or solvent impregnated resin.

Keywords: membrane techniques, ion-exchange resins, metal ion, separation

8.1 Polymers as membranes

8.1.1 Introduction

Membrane techniques are successfully used in the separation in the liquid and gas systems for many years. They are used in scientific researches, but also have numerous applications. One of the criteria for the success of the applied membrane technology is to choose a suitable membrane.

Generally, membranes vary according to the mechanism of separation (solubility–diffusion and sieving), chemical composition (organic and inorganic) and physical structure (symmetric and asymmetric). Depending on the mechanism by which the separation is achieved, membranes are divided into two groups: dense or porous. Operating porous membranes separation is done mechanically, like in the conventional filtration processes. In the process with dense membrane, the selectivity depends on interactions between components of feed solution and membrane material. Membranes, of course, should be stable at the operating temperatures of the process and resist chemical attack by the solution components.

Membranes can be also classified into charged and uncharged type. Ion-exchange membranes have ionic permselectivity and are classified into cation-exchange membranes (CEMs) and anion-exchange membranes (AEMs). In the AEMs, positive-charged groups are fixed; therefore cations are rejected by the positive charge and cannot permeate through the AEM. This is because AEMs are only permeable by anions. The CEMs perform the opposite way compared to anion ones. A similar behaviour, as in ion-exchange membrane, happens in ion-exchange resin. The ion-exchange resins are in the granular form and perform

https://doi.org/10.1515/9783110469745-008

Table 8.1: Comparison of polymeric and ceramic membranes.

	Polymeric membrane	Ceramic membrane
Advantages	– Easy control of the pore forming mechanism;	– Chemical, mechanical and thermal stability;
	– High flexibility;	– Ability of steam sterilization and back flushing; dry storage after cleaning;
	– Low costs;	– High abrasion resistance;
	– Easy to up-scaling and down-scaling of membrane;	– High fluxes and durability;
	– Easy forming properties;	– Bacteria resistance;
	– Selectively transfer of chemical species.	– Possibility of regeneration;
Disadvantages	– Usually high hydrophobicity;	– High costs;
	– Exposure to biofouling;	– Relatively poor control in pore size distribution;
	– Low mechanical strength.	– Low flow rate.

as adsorptive exchange of ions. During the process, the adsorptive capacity of resin is consumed and after certain time period it requires regeneration. In the process with the ion-exchange membrane, the regeneration is unnecessary and allows for continuous use for an extended period of time.

As it was mentioned above, due to the material used, membranes are divided into inorganic membrane (ceramic, glass, metal, zeolite, carbon molecular sieve) or organic membranes (polymer or liquid). The polymeric and ceramic membranes are used most commonly, wherein much of the research works and applications are based on polymer ones. In Table 8.1, the most important advantages and disadvantages of both types of membranes are presented [1, 2].

Among all of the advantages and disadvantages of both types of membranes, using polymeric membranes is supported mainly by economic facts (lower cost of producing) and ease of modification of their surface, which make them suitable in different separation processes. Commercial polymer membranes are formed by different kind of materials [3] – from fully hydrophilic polymers such as cellulose acetate (CA) to fully hydrophobic polymers such as polypropylene (PP) and polyethylene (PE) and some examples of medium properties – polyvinylidene fluoride (PVDF), polyacrylontrile (PAN) and polysulfone (PS)/polyethersulfone (PES) family.

There are some solutions that help to improve the properties of polymeric membranes. Membranes can be modified by using of additives, either as copolymers or by post-treatment, i. e. the incorporation of nanoparticles (inclusion of silver, iron, zirconium, silica, aluminium, titanium, and magnesium) into membranes. Addition of nanoparticles affects the permeability, selectivity, hydrophilicity, conductivity, mechanical strength, thermal stability, antiviral and antibacterial properties of the polymeric membranes [1]. Moreover, surface of membrane can be treated, for example by water-soluble solvents such as acids and alcohols or with ammonia or alkyl compounds (e. g. ethylenediamene and ethanolamine) or be modified by various techniques, such as radical-, photochemical-, radiation-, redox-, and plasma-induced grafting [4].

One of the examples of using polymeric membranes is recovery of metal from aqueous solutions. Several methods are proposed including reverse osmosis (RO), nanofiltration (NF), ultrafiltration (UF), diffusion and Donnan dialysis, electrodialysis (ED) and membrane extraction system, which have been described in detail in the following chapters. These processes are an alternative to conventional metal removal from inorganic effluent processes, such as chemical precipitation, ion exchange, solvent extraction and electrochemical removal.

8.1.2 Reverse osmosis

RO, besides NF, UF and microfiltration, is an example of membrane separation process where driving force is generated by pressure. Depending on the transmembrane pressure (TMP) applied and the type of membranes used in the process, particles of varying size can be separated (Figure 8.1).

RO is the process for removing solvent from a solution using dense membranes. In description of the transport across the membrane in RO system, the solution–diffusion model is proposed with three steps: (i) sorption from the feed solution to the membrane surface, (ii) diffusion through membrane, (iii)

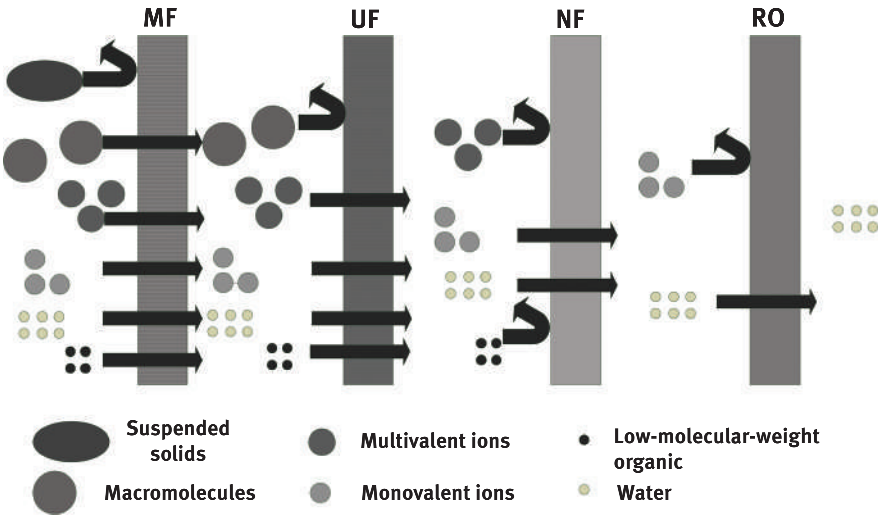

Figure 8.1: Comparison of process where driving force is pressure.

desorption from membrane to permeate solution. Separation in RO occurs due to the difference in solubility and diffusivity rate of dissolved species in solvent. Thus, the selection of the appropriate membrane is very important. Membranes, which are used in RO process, should be freely permeable to water and impermeable to solutes (such as salt ions). Moreover, they should be chemical and high pressure resistant and tolerant to wide ranges of pH and temperature. Generally, in RO, three major types of membranes are used: CA, polyamide and thin- film composite (TFC) with three layers – structural support (e. g. polyester, 120–150 μm thick), a microporous interlayer (e. g. polysulfonic polymer, 40 μm thick) and an ultra-thin barrier layer on the upper surface (e. g. polyamide, 0.2 μm thick).

RO is commonly used in water desalination and ultrapure water production [5, 6]. Moreover, it is proposed to the treatment of industrial wastewater from metal ions. Application of RO to separation of metal ions is shown in Table 8.2.

Results presented in Table 8.2 indicate that RO sufficiently removes the metal ions from the aqueous solutions. The retention depends on the process conditions (TMP, concentration, pH, addition of chelating agent).

8.1.3 Nanofiltration

NF is applied to concentrate multivalent salt solutions and to fractionate salts due to the different charge densities and hydrated sizes of the ions. The mechanism of separation in NF is described both by sieving and by solution–diffusion model. Moreover, during fractionation of dilute salt mixtures by NF, the effect of Donnan force is observed [14]. Additional phenomena can also affect membrane performance, i. e. specific adsorption, reduced dielectric permittivity and hydration [15]. In NF separation of large and uncharged molecules larger than 200 Da, e. g. sugar, sieving effect is observed, while in ion separation – electrostatic force between membrane material and particles should be taken into account. The majority of commercially NF membranes are made of either cellulosic or aromatic polyamide material, like RO membranes. In contrast to RO process, NF membranes are porous and charged, mainly negative. The modification of polymers, in NF membranes, occurs by attachment of some ionic groups to the polymer or by coating a thin layer of e. g. sulfonated polyphenylene oxide on the surface of a porous membrane (support). The most characteristics of NF membranes are low rejection of monovalent ions, high rejection of divalent ions and higher flux compared to RO membranes.

NF is proposed for the removal of multivalent ions in water softening operations, treatment of wastewater from mineral processing, nuclear, metal finishing and metal recycling industries because of its high rejection of multivalent ions, among others metal cations [7] (examples in Table 8.3). Moreover, it

Table 8.2: Examples of metal ion removal by RO.

Metal	Membrane (name, material, supplier)	Results	Ref.
$CuSO_4$ $Cu(NO_3)_2$	*SE RO*, TFC, Sterlitech Co	– Retention is higher than 95 %. – Results independent of the TMP and the kind of salt.	[7]
$CuSO_4$ $Cu(NO_3)_2$	*TW30-1812-50*, polyamide TFC, Filmtec	– Metal concentration has a significant influence on the membrane separation. – The influence of the anions and TMP is observed.	[8]
$Ni(NO_3)_2$ $ZnSO_4$		– Lack of retention results.	
$CuCl_2$	Multilayer TFC aromatic polyamide (*ES20*), Nitto *ULPROM*, Denko	– Retention is higher than 95 % and increases with increasing TMP and pH of feed solution.	[9]
$NiCl_2$		– Increasing concentration of other ions slightly decreased the rejection of metals.	
$Cr(NO_3)_3$ wastewater from the electroplating			
$CuSO_4$ $NiSO_4$	*RE2012-100*, polyamide TFC, CSM	– Retention is about 98.5 %, slightly higher for Cu(II). – Rejection increases by adding chelating agent (Na_2EDTA) up to 99.5 %.	[10]
$CuSO_4$ AsO_4^{3-}, AsO_3^{3-}	Polyamide TFC	– Retention is equal to 91–99 % for As (V) and 20–55 % for As(III), – Rejection depends on the initial concentration and pH.	[11]
$ZnCl_2$ $NiCl_2$	*AG4021FF*, TFC, GE Osmonics	– Retention is equal to 99.3 % for Zn(II) and 98.9 % for Ni(II). – Rejection increases by adding EDTA to 99.7 % and 99.6 %, for Zn(II) and Ni(II), respectively.	[12]
$CuSO_4$ $CdSO_4$	Polyamide	– Retention is equal to 97 % for Cu(II) and 98.5 % for Cd(II). – The explanation of higher cadmium retention – size of the Cd^{2+} is larger than that of Cu^{2+} (the same like in [10]).	[13]

can be used to separate large molecules such as dye, sugars, amino acids and their oligomers.

Based on the results presented in Table 8.3, it can be concluded that polymer NF membranes are capable of removing a high percentage of metal ions.

Table 8.3: Examples of metal ion removal by NF.

Metal	Membrane (name, material, supplier)	Results	Ref.
$CuSO_4$ $Cu(NO_3)_2$	*MPF-44*, proprietary composite, Koch	– Retention higher than 95 %, independent of TMP.	[7]
$CuSO_4$ $CdSO_4$	Polyamide	– Retention of Cu(II) is equal to 84–96 % and that of Cd(II) is equal to 82–97 %.	[13]
$CuSO_4$	GE Osmonics: *Desal KH*, TFC and *Desal-5DK*, TFC, polyamide with polysulfone support;	– Retention is equal to 96–98 %, small changes with different H_2SO_4 concentration for *NF45, NF270* and *Desal-5DK* membranes are observed.	[14]
	DowFilmtec: *NF45* and *NF270*, polyamide;	– *MPF-34* and *Desal KH*, which have been described as more open NF membranes, retain less copper.	
	Koch: *MPF-34*, proprietary composite	– Retention is equal to 69–83 % for *MPF-34*. – Retention is equal to 87–90 % for *Desal KH*.	
$ZnCl_2$	*Nanomax 50*, polyamide arylene on a polysulfone support layer, Millipore Co.	– Retention is equal to 96–99 %, depending on the initial concentration, pH and TMP.	[15]
$CuSO_4$ with 0-2 M H_2SO_4	*DK*, TFC, GE Osmonics *MPF-34*, proprietary composite, Koch	– Retention up to 42 % and 80 % (feed solution with 2 M H_2SO_4) for *MPF-34* and *DK*, respectively. – With increasing of acid concentration, retention of Cu(II) decreases (electromigration effects). – *DK* has a better copper retention and a higher permeate flux than *MPF-34*. However, *MPF-34* has better chemical resistance than *DK*. – Retention of acid lower than 25 % for both membranes (good selectivity between acid and copper).	[16]
$CuCl_2$	*Nanomax 50*, polyamide arylene on a polysulfone support layer, Millipore Co	– Retention up to 55 %, depending on the initial concentration and TMP.	[17]
Pb^{2+}, Cd^{2+}, Cu^{2+}, Cr^{6+} from waters containing sulfate	NF membrane, no data	– Maximum retention of Pb, Cd, Cu and Cr for synthetic samples is equal to 91, 97, 98 and 95 %, and those for real samples were 72, 53, 87 and 99 %, respectively. – Retention of Pb, Cd and Cu decreases with increasing pH and initial metal concentration.	[18]

8.1.4 Ultrafiltration

The separation mechanism of UF is sieving effect; thus porous membranes are used. This technique is applied for the removal of dissolved and colloidal material, mainly in food technology for milk concentration, recovery of proteins from cheese whey, recovery of starch, concentration of egg products and clarification of fruit juice and beer. Moreover, UF processes are used in pharmaceutical, chemical and pulp and paper industries. The most widely used materials for UF membranes are: PS and PES (chemical, thermal and mechanical stability), CA (more hydrophilic – tend to foul more difficult) and polyacrylonitrile (PAN).

In the classical UF, effectiveness of removing of the metal ions is unsatisfactory. When the pore sizes of membranes are larger than dissolved metal ions, these ions would pass easily through UF membranes. However, some results of UF application for metal separation are presented in the literature. Values of retention of Cd(II) ions in UF process with PS membrane are equal to 11 % [19] or 10 % and 15 % for CA and PVDF membrane, respectively [20]. Similarly, weak retention is obtained for Cr(III) ions – 3–5 %, 15–20 % and 15–22 % for CA, PVDF and PES membranes, respectively [21], and for other metal ions, as: Cs(I), Sr(II), Mn(II), Co(II), Cu(II), Zn(II), Cr(III) lower than 20 % (mostly near 10 %) using polyamide (PA, TFC) and PES membranes [22]. The effect of rejection of metal ions in classical UF could be explained by the electrostatic repulsion and the effect of steric exclusion described by Ferry's law [23]. It means that the membrane surface charge significantly influences the separation properties. The surface charge density of a porous membrane is related to the zeta potential of the membrane. The surface charge of all membranes changed from a positive charge to a negative charge as the pH was increased, possibly causing an increase of the membrane repulsive electrostatic force, thereby making it more influential during the membrane process. For example, the comparison of three membranes – PES, PVDF and CA – indicates that their zeta potential is different. PES membranes are neutrally charged or slightly negatively charged (zeta potential slightly below zero), PVDF membrane is more negatively charged (zeta potential from −2 to −10 mV) [24] and CA membrane is the most negative surface charge (zeta potential from −5 to −20 mV) [25]. Transport of positive ions of metal through membrane with negative surface charge is easy as a result of electrostatic attraction, and consequently the retention of these ions is low. This effect was observed in the case of retention of Cr(III) [21] and Cd(II) [20] ions. The value of retention is the lowest for CA membrane, in which the transport of metal through membrane is the easiest one. On the other hand, retention of As(V) ions in the form of anions $H_2AsO_4^-$, $HAsO_4^{2-}$, AsO_4^{3-} is higher for regenerated cellulose (RC) membrane (52 %) in comparison to PES one (5 %) [26]. Much higher value for the retention of arsenic using cellulose membrane could be explained by the negatively charged surface of membrane in the experimental conditions.

Despite these examples of UF of aqueous solutions of metal ions, classical UF is found to be an ineffective method for metal recovery. To obtain high removal efficiency of metal ions, the modification methods of UF – micellar-enhanced ultrafiltration (MEUF) and polymer-enhanced ultrafiltration (PEUF) – were proposed. These two complexation-UF techniques are promising methods for the removal of metal ions and small organic compounds from the aqueous solution.

8.1.4.1 Micellar-enhanced ultrafiltration process

In the MEUF process, the surfactant solution at a concentration higher than the critical micelle concentration (CMC) is added to the solution containing the separated compounds, such as metal ions or low molecular compound. In these conditions, the micelles of surfactants are formed and metal ions and soluble organic compounds can be "captured" by the micelles, with a strong ability to attract through the surface of the micelles or solubilization inside the micelles. Micelles have hydrodynamic diameter significantly larger than the pore diameter of UF membrane, and therefore they are rejected by the membrane together with solubilized/bound contaminants. Permeate contains small amount of unsolubilized contaminants and monomeric form of surfactant. After the process, the surfactant can be recovered by precipitation with one or multivalent counterions [27].

The results presented in Table 8.4 show that MEUF is an effective separation technique to remove metal ions from wastewater. Metal removal efficiency by MEUF

Table 8.4: Examples of metal ion removal by MEUF.

Metal surfactant	Membrane (name, material, supplier)	Results	Ref.
$CdCl_2$ Rofam 10 (non-ionic) SDS (anionic)	CA, PVDF, GE Osmonics	– Retention is equal to 13 % and 15 % for CA, PVDF membrane, respectively in system with Rofam 10. – Retention is equal to 83% and 89 % for CA, PVDF membrane, respectively in system with SDS. – Retention is equal to 88% and 90 % for CA, PVDF membrane, respectively in system with SDS/Rofam 10.	[20]
$Cd(NO_3)_2$ Triton X-100 Brij 35 SDS	PES, Tianjin Motian Membrane Engineering Technology Company	– Retention is equal to 40–70 % for SDS/Brij 35 and 50–70 % for SDS/Triton X-100, depending on the molar ratio of surfactants. – The rejection of Cd(II) in MEUF is enhanced with the higher SDS concentration and moderate Cd(II) concentration.	[28]

(continued)

Table 8.4: (*continued*)

Metal surfactant	**Membrane (name, material, supplier)**	**Results**	**Ref.**
$Cd(NO_3)_2$ $Zn(NO_3)_2$ SDS	PES, Tianjin Motian Membrane Engineering Technology Company	– Retention is equal to 92–98 %, depending on the metal and surfactant.	[29]
$CdCl_2$ $ZnCl_2$ SDS	*Amicon*, regenerated cellulose (RC), PL series, Millipore	– Retention is equal to 98 % for Zn(II) and 99 % for Cd(II). – 84 % of the initial SDS is recovered by precipitation.	[30]
$Cd(NO_3)_2$, $Cu(NO_3)_2$ $Pb(NO_3)_2$, $Zn(NO_3)_2$ cetylpyridinium chloride (CPC)	RC	– Retention for all tested metals is equal to 92–95 %.	[31]
Ni(II) SDS OP-10, nonionic monoalkylphenol polyetoxilate	*OPMN-K*, polyamide *UPM-10*, polysulfonamide *UPM-20*, PS, Vladipor	– Retention is equal to almost 100, 88 and 99 % for *OPMN-K, UPM-20* and *UPM-10*, respectively, in system with SDS. – Retention is equal to 20–40 % and 88–96 % for *UPM-20* in system with OP-10 and SDS/OP-10.	[32]
$Ni(SO_4)_2$, $Cu(NO_3)_2$ $Cd(NO_3)_2$, $Zn(NO_3)_2$ SDS, TWEEN 80, polyoxyethylene sorbitanmonooleate	PES, Hydronautics Nitto Denko Company	– Retention is equal to 83 %, 83 %, 94 %, 98 % for Ni, Cu, Zn, Cd, respectively (total surfactant concentration=4 mM). – Retention increases to almost 100 % with increasing of surfactant concentration.	[33]
$NiCl_2$, $Ni(NO_3)_2$, $CuSO_4$, $CuCl_2$, $Mg(NO_3)_2$, $MgCl_2$, $Zn(NO_3)_2$, $ZnCl_2$, $Cd(CH_3CO_2)_2$, $CdCl_2$, $FeCl_2$ RO90, nonaoxyethylene oleylether carboxylic acid	*PLCC*, RC, Millipore *RC70PP*, RC, Alfa Laval *UC030* and *UC100*, RC, Microdyn Nadir *UP010*, PES, Microdyn Nadir *GR81PP*, PS, Alfa Laval	– Retention of metal ions is >95 %. – The simultaneous removal results in the following order: $Fe^{2+} \sim Cu^{2+} > Cd^{2+} > Zn^{2+} > Ni^{2+} > Mg^{2+}$, which is a result of the different complex binding constants.	[34]

depends on the type and concentrations of the metals and surfactants, pH, ionic strength, type of membrane and operation parameters (TMP, flux, temperature). To obtain the highest retentions of metal ions, surfactants of electric charge opposite to that of the ions to be removed should be used. Thus, to reject metal ions in the form of cations, the anionic surfactants, e. g. sodium dodecyl sulfate (SDS), are added. Because anionic surfactants generally have got high critical micelle concentration, in MEUF process also the mixture of anionic and nonionic surfactant (e. g. Rofam 10, Brij 35, Triton X-100, OP-10) is proposed. The introduction of nonionic surfactant to anionic one usually results in a decrease of CMC [28] and as a consequence less surfactants are necessary to add.

8.1.4.2 Polymer-enhanced UF process

In the PEUF process, the water-soluble metal-binding polymers are used. The ionic forms of metals are complexed by a macroligand and form a macromolecule, to increase their molecular weight. These macromolecules, with a size larger than the pores of the UF membrane, can be rejected by the membrane during UF [35]. Thus, the principles of this process are the same like in MEUF. The only difference is the complexing agent – polymer instead of surfactant. A very important issue in PEUF is proper selection of water-soluble macroligands. Several polymers are proposed: biopolymer e. g. chitosan [36, 37], synthetic macroligands such as carboxyl methyl cellulose [38, 39], diethylaminoethyl cellulose [40], polyvinylethylenimine [41], polyvinyl alcohol [42] and poly(acrylic acid) [43, 44] for removal of metal ions from aqueous solutions. The investigations show that water-soluble polymeric ligands are powerful substances to remove metal ions from aqueous solutions and industrial wastewater in PEUF processes. Some results of metal ion separation by PEUF are presented in Table 8.5.

Table 8.5: Examples of metal ion removal by PEUF.

Metal	Membrane (name, material, supplier)	Polymer	Recovery	Ref.
Cu(II)Ni(II) Cr(III)	*FUS 0181*, PES, MOLSEP® Hohlfasermodule	Carboxy methyl cellulose (CMC)	– Retention is equal to 97.6, 99.5 and 99.1 % for Cu(II), Cr(III), and Ni(II) ions, respectively at c=10 mg/L. – Retention of Cu(II) and Cr(III) ions is high on a wide range of concentration up to 100 mg/L, while Ni(II) ions' retention decreases to 57 %. – Abilities to rejection in the same accordance as complexing abilities of CMC: Cu(II)>Cr(III)⍰Ni(II).	[38]
$CdCl_2$ $CuCl_2$ $ZnCl_2$	*PTGC OMS 10*, PES, Millipore	poly(acrylic acid) (PAA)	– Retention is equal to 75, 80 and 77 % for Cd(II), Cu(II) and Zn(II), respectively (TMP=3 bars) and increases with the increase of TMP and PAA concentrations. – The correction of pH to 5 allows to obtain retention around 80, 93 and 70 % for Cd(II), Cu(II) and Zn(II), respectively. – In the mixture solution, Cu(II) retention is higher than other metal ions.	[44]

(*continued*)

Table 8.5: (*continued*)

Metal	Membrane (name, material, supplier)	Polymer	Recovery	Ref.
$Hg(NO_3)_2$	*HGO1*, PS, GE Osmonics	Polyethyleneimine (PEI)	– Retention is equal to 98 %.	[45]
$Co(NO_3)_2$ $Ni(NO_3)_2$ $Cu(NO_3)_2$ $Zn(NO_3)_2$ $Cd(NO_3)_2$ $Pb(NO_3)_2$	*Biomax PBGC*, PES, Amicon Bioseparations-Millipore Co.	Poly(vinyl sulfonic acid) (PVSA)	– Retention is equal to 20–70 % depending on pH and cleaned or fouled membrane.	[46]
$CdCl_2$	*PTGC OMS 10*, PS, Millipore	Poly(ammonium acrylate)	– Retention increases with polymer concentration and reaches 99 % values at twofold cadmium concentrations.	[47]
$HgCl_2$	PES, Sepro Membranes Inc.	Polyvinylamine (PVAm)	– Retention is equal to 99 %. – PVAm dosage does not affect the Hg(II) rejection considerably.	[48]
$CoSO_4$ $CuSO_4$ $NiCl_2$ $FeCl_3$ $Pb(NO_3)_2$ $CdCl_2$ $ZnCl_2$ $MnCl_2$	*PES-10*, PES, Sepro Membranes.	Polyvinylamine (PVAm)	– Retention is equal to 99 , 97 and 99 % for Pb(II), Cu(II) and Fe(III), respectively. – The temperature and TMP have little effects on metal rejection. – Metal rejection in PEUF is highly correlated to the coordination properties between the polymer and the metals.	[49]
$Ni(NO_3)_2$ $Cu(NO_3)_2$ $Cd(NO_3)_2$	RC, Millipore	Poly(*N*-vinylpyrrolidone-*co*-2-acrylamido-2-methylpropanesulfonate sodium) (PAMPS) poly(VP-*co*-AMPS) poly(vinylpyrrolidone) (PVP)	– Retention of all metals is higher for PAMPS. – The selectivity for Ni(II) for PVP is obtained. – For poly(VP-co-AMPS), selectivity for nickel ions is obtained, and the retention of Cu(II) and Cd(II) increases compared to PVP.	[50]

Depending on the polymer used and the type of separated metal ion, different complexes are formed in the system. For example, the Cr(III) or Ni(II) bond with carboxymethyl cellulose (CMC) by etheroxygen of the hydroxyl group (octahedral geometry), while in Cu(II) complexes, the binding sites are the oxygen of ethoxyl groups and the primary alcoholic O atom of glucopyranose rings (square planar configuration) [38].

8.1.5 Dialysis

Dialysis is a separation process in which a semipermeable membrane separates a feed solution and a receiving solution (dialysate, mainly water). The dialysis membrane should be permeable to selected components in the feed which should be removed and impermeable to remaining components. The driving force for dialysis is difference in the concentration of the solution across the membrane. The best known application of dialysis is its use in the artificial kidney (hemodialysis), where membrane made of cellophane-like material is applied. The typical membrane in dialysis is uncharged and the selectivity of the process is based on the size of the diffusing components. In such process, there is no possibility to separate the metal ions. However, there are specialized dialysis processes where charged membranes are used: diffusion dialysis, Donnan dialysis and ED. These membrane technologies are utilized in the recovery of the metal ions and are described in detail in the following chapters.

8.1.5.1 Diffusion dialysis

As was mentioned above, diffusion dialysis is a subset of dialysis in which the ion-exchange membranes are utilized. This technique is applied to separate acids from salts and bases from salts, depending on the type of membrane: AEM and CEM, respectively. Anions are transported across the AEMs, while membranes are impermeable to cations. However, hydrogen and hydroxyl ions permeate through both types of membrane – AEM and CEM. Their migration occurs by both diffusion and transfer from one water molecule to another, according to the Grotthus mechanism [51]. The principle of separation of acid from the salts (e. g. H_2SO_4 and $ZnSO_4$) is presented in Figure 8.2. There are H^+, Zn^{2+} and SO_4^{2-} ions in the feed solution. To maximize the driving force in the process, generally water is used as a dialysate. Sulfate anions can pass through the AEM, and zinc cations are blocked. Because the radius of H^+ ion is very small and its migration velocity is fast [52], it can be transported across the membrane together with SO_4^{2-}.

Dialysis diffusion is proposed mainly for recovery of acids and alkalis from the discharges from steel production, metal refining, electroplating, non-ferrous metal and tungsten ore smelting, aluminum etching and cation-exchange resin regeneration [53]. Due to these applications, more attention has been placed on AEMs compared to cation-exchange ones. The properties, including structure, charged groups and thickness of the membrane, can affect the diffusion dialysis performances. Typical applications of diffusion dialysis for the separation of the metal ions from acid solutions are presented in Table 8.6.

8.1.5.2 Donnan dialysis

Donnan dialysis is a method of ionic separation using an ion-exchange membrane, in which ions move across the membrane based on Donnan equilibrium [57]. It means

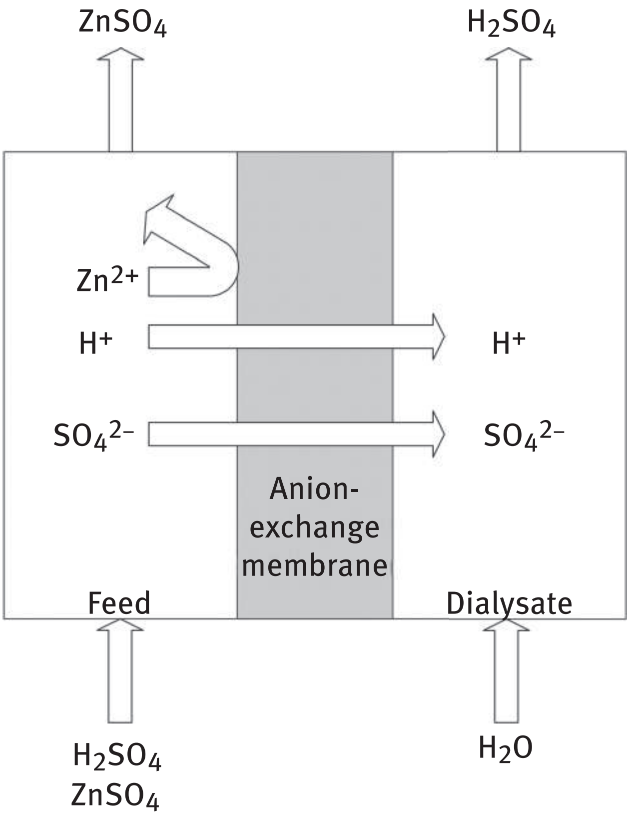

Figure 8.2: Mechanism of separation acids from salts by diffusion dialysis.

that the transport of a counter-ion from the feed solution to the dialysate solution is accompanied by the transport of an equivalent amount on another counter-ion in the opposite direction until reaching Donnan equilibrium (Figure 8.3). The feed solution contains ions that should be removed, and the receiving solution contains the electrolyte with a relatively high concentration.

Generally, this process is used in the separation of inorganic ions, rarely of organic compounds [58]. In contrast to the diffusion dialysis process, in the Donnan dialysis CEMs are used for the recovery of metal (examples presented in Table 8.7). Donnan dialysis with the AEM is applied mainly for the removal of troublesome anions from drinking water. The AEMs (*SB-6407* and *Neosepta*® *AMX*) are proposed, for example, for the removal of nitrate from the aqueous phase [59].

In Donnan dialysis, the thickness of the membrane is not a key issue. The research study [60] shows that under typical hydrodynamic conditions in Donnan dialysis, the boundary layer of the dilute solution poses the major resistance to transport rather than the membrane itself. Thus, even thicker commercial ion-exchange membranes

Table 8.6: Examples of metal ion separation by diffusion dialysis.

Feed solution	Membrane (name, type, material, supplier)	Results	Ref.
Acid: H_2SO_4; ions: As^-, F^-, Cu^{2+}, Zn^{2+}, Fe^{3+}	*Neosepta® AFX*, AEM type, polystyrene-co-divinylbenzene, aminated; Astom Co *S203*, AEM type, chloromethylized polysulfone membrane followed by quaternary amination	– Most of the metal cation can be removed effectively, but the separation of As^- and F^- is comparatively unsatisfactory. – The dialysis of mass transfer coefficient of H_2SO_4 for *AFX* membrane is higher than for *S203* one. However, separation of ions is better for *S203* membrane.	[52]
Acids: HCl, H_2SO_4, HF/HNO_3; ions: Fe^{3+}, Zn^{2+}, Cu^{2+}, Ni^{2+}, Cr^{3+}	*Neosepta® AFN*, AEM type, polystyrene crosslinking and amination; Tokuyama Co	– Recovery of HCl, HNO_3 and H_2SO_4 is equal to 90, 90, and 70 %, respectively. – Fe, Ni, Cr and Cu in the feed waste are rejected effectively, while Zn in HCl solution leaked through the membrane.	[54]
Acid: H_2SO_4; ions: Ni^{2+}, Fe^{3+}	*Selemion CI*, AEM type, DSV Asahi Glass Co	– Recovery of H_2SO_4 increases with the concentration of acid and temperature up to 80 %. – Rejection of Ni^{2+} and Fe^{3+} is equal to 96 % and 99 %, respectively.	[55]
Acid: H_2SO_4; ions: Cu^{2+}	*Neosepta® AFN*, AEM type, polystyrene crosslinking and amination; Tokuyama Co	– H_2SO_4 permeates well through the membrane used, while $CuSO_4$ is efficiently rejected. – Process is very effective at high acid concentrations and low concentrations of $CuSO_4$. – Even at the highest concentration of $CuSO_4$ the rejection is higher than 96 %.	[56]

could be applied in this process. However, electrical properties of the Donann diaysis' membrane have got impact on mass transport during the process. Membrane with low electrical resistance has low resistance to ion diffusion, and that with low electroosmotic water transport has low osmotic water transport [61].

8.1.5.3 Electrodialysis

ED is a membrane process where driving force is generated by an electric potential. Ionized species in the solution are transported through ion-exchange membrane, under the influence of an electric potential. Similar to diffusion dialysis and Donnnan dialysis, the AEMs and CEMs are applied in ED; here however both types of membranes are used simultaneously. The anions migrate

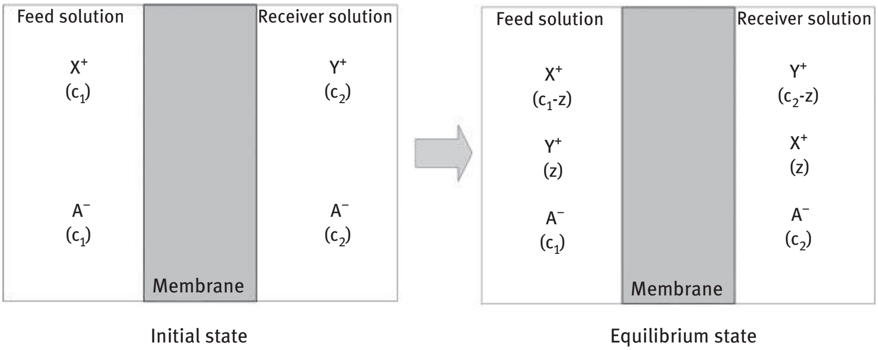

Figure 8.3: Donnan dialysis process with a cation exchange membrane.

toward the anode and the cations toward the cathode, crossing the AEMs and CEMs, respectively. Because the membranes are in the alternate stock, the ions can be separated from the solution. In some chambers, increase of concentration of ions will take place and in other chambers ions will be removed. In

Table 8.7: Examples of metal ion separation by Donnan dialysis.

Feed solution	Receiver solution	Membrane (name, type, material, supplier)	Results	Ref.
Calcite ($CaCO_3$) gypsum ($CaSO_4{\cdot}2H_2O$), or lime softening sludge (Ca^{2+}, Mg^{2+},Na^+, $SO_4{}^{2-}$)	HCl, H_2SO_4, HNO_3 or water	*Nafion*® *117*, CEM type, chemically stabilized perfluorosulfonic acid/ PTFE copolymer in the acid (H^+) form, Dupont Co	– Over 99 % of the hydrogen ions are exchanged in the recovery of up to 20 and 50 % of the Ca and Mg from the lime softening sludge. – Recovery of Ca from synthetic feed suspensions comprised of gypsum or calcite depends on equilibration time and sweep side solution composition.	[62]
Red mud (bauxite wastes of alumina manufacture) containing Al_2O_3, Fe_2O_3, TiO_2, Na_2O, CaO, SiO_2	HCl	Strongly acidic cation-exchange polysulfone with polyester suport, CEM type	– Transport of metals is influenced by the acid concentration. – Flux of ions increases with acid concentration in the receiver solution.	[63]

(*continued*)

Table 8.7: (*continued*)

Feed solution	Receiver solution	Membrane (name, type, material, supplier)	Results	Ref.
$CaCl_2$, $MgCl_2$	NaCl	*Neosepta CMX*, CEM type, homogenous membranes containing sulfonic acid groups as fixed charges, Tokuyama Co *Selemion CMV*, CEM type, homogenous sulfonated styrene divinyl benzene copolymer membrane (PS/DVB) on a PVC backing, Asahi Glass	– Removal of the Ca^{2+} and Mg^{2+} is similar for both membranes and equal to 80–88 %, depending on stream volume ratio and NaCl concentration. – Ionic fluxes for the *Selemion CMV* membrane are higher by about 30 % than those for the *Neosepta CMX* membrane. This result significantly reduces the time of the process.	[64]
Cr(III)/Cr(VI) mixture solutions	NaCl	PP membranes incorporating poly[(ar-vinylbenzyl) trimethylammonium chloride], P(ClVBTA), poly[2-(acryloyloxy)ethyl]trimethylammonium chloride] P(ClAETA), poly(acrylic acid) P(AA), poly(2-acrylamidoglycolic acid) P(AGA), poly(glycidylmethacrylate-N-methyl-D-glucamine) P(GMA-NMG), poly(2-acrylamido-2-methyl-1-propane sulfonic acid) P(AMPS) and poly [sodium (styrene sulfonate)], P(SSNa) are modified via an “in situ” radical polymerization.	– The separation of Cr(III) and Cr(VI) ion mixture by the selective transport properties is obtained. – The Cr(III) ions are selectively separated using MP (SSNa)6 (42 %) respect to 2.5 % for Cr(VI) ions. – The Cr(VI) ions are selectively separated using MP (ClVBTA)6 (61 %) respect to 5.8 % for Cr(III) ions. – Extraction percentage is equal to 1.6–3.1 % and 2.3–2.6 % for Cr (VI) and Cr (III), respectively, using PP membrane.	[65]

Figure 8.4, the principles of ED are presented. A special type of ED process is ED with bipolar membranes (EDBMs). Bipolar membranes consist of a CEM, an AEM and a catalytic intermediate layer to accelerate the splitting of the water into protons and hydroxide ions. This process is proposed for the separation and treatment of organic acids from fermentation broths [66].

ED is used for the production of drinking and process water from brackish water and seawater, treatment of industrial effluents, desalination of organic substances, recovery of useful materials from effluents and salt production [67]. The examples of using ED in metal recovery are presented in Table 8.8.

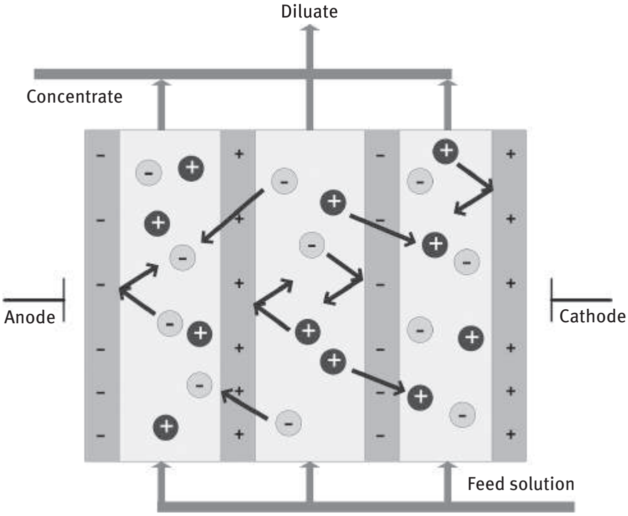

Figure 8.4: Electrodialysis process.

8.1.6 Membrane extraction

Membrane extraction is an alternative process to the classical solvent extraction. In both processes, the same extractants are used. A listing of solvent extraction reagents is given in Table 8.9, together with the proposed mechanism of extraction [72].

In the liquid–liquid extraction process, organic solvents are used, which are often toxic, flammable or otherwise hazardous. As an alternative separation technology, the membrane processes are proposed: bulk liquid membranes (BLMs), emulsion liquid membranes (ELMs), supported liquid membranes (SLMs) and polymer inclusion membranes (PIMs). In the processes with SLMs, the major drawback is their poor stability; in ELMs there is a problem with emulsion breakage. BLMs find application only in theoretical studies because of the low mass transfer rates [73]. The analysis of literature shows that the most popular are PIMs, unfortunately only for laboratory scale, and SLMs, using mainly hollow-fibre membranes, and are described in detail in the following chapters.

8.1.6.1 Polymer inclusion membranes

PIMs have good stability in comparison to other types of the liquid membranes. They are formed by casting solution containing a carrier (extractant, see Table 8.9), a plasticizer, such as o-nitrophenyl octyl ether (NPOE), and a base polymer, such as cellulose triacetate (CTA) or poly(vinyl chloride) (PVC), to form thin, flexible and stable film. The base polymer provides mechanical strength to the membrane. Plasticizer is a solvent for an ion carrier (extractant) and improves the flexibility

Table 8.8: Examples of metal ion separation by electodialysis.

Feed solution	AEM (name, material, supplier)	CEM (name, material, supplier)	Results	Ref.
$Pb(NO_3)_2$	*AR204SXR412* Arak Petrochemical Complex, *Selemion AMV*, poly-styrene-co-divinylbenzene, Asahi Glass	*CR67,MK111*, Ionics Watertown, *Selemion CMV*, homogenous sulfonated styrene divinyl benzene copolymer membrane on a PVC backing, Asahi Glass	– The separation percentage is equal up to 95 %. – With increasing of temperature and voltage, cell performance is improved. – The separation percentage decreased with an increasing flow rate.	[68]
$CuSO_4$ $ZnSO_4$ $Pb(NO_3)_2$ $Cr(NO_3)_3$	*AR204SXR412* Arak Petrochemical Complex, *Selemion AMV*, poly-styrene-co-divinylbenzene, Asahi Glass	*CR67,MK111*, Ionics Watertown, *Selemion CMV*, homogenous sulfonated styrene divinyl benzene copolymer membrane on a PVC backing, Asahi Glass	– Performance of an ED cell is almost independent of the type of ions and only depends on the operating conditions (flow rate, temperature, voltage). – Maximum separation percents are equal to 66, 68, 69, 70, 61 % for Cu^{2+}, Zn^{2+}, Pb^{2+} and Cr^{3+}.	[69]
Gold mine effluent, containing Na^+, Cu^{2+}, Zn^{2+}, K^+, Fe^{3+}, Al^{3+}, Au^+, CN^-, Cl^-	No-name, Qianqiu Environmental Protection & Water Treatment Co	No-name, Qianqiu Environmental Protection & Water Treatment Co	– The highest removal is equal to 99.41 % and 99.83 % for copper and cyanide, respectively. – The results depend on the flow rate, initial concentration and voltage.	[70]
$NiSO_4$ $CoSO_4$	*Neosepta® AHA*, poly-styrene-co-divinylbenzene, aminated; Astom Co	*Nafion® 117*, sulfonated perfluoropolymer, DuPont *SPVDF 4Sb*, sulfonated polyvinyldifluoride, which contains 22 % of styrene.	– The performance of the *SPVDF 4Sb* membrane is slightly better than commercial *Nafion® 117*. – A significant improvement with the use of corrugated membranes on the amounts of metal extracted is observed. – The separation of Ni^{2+} and Co^{2+} with complexing agent (EDTA) by ED is achieved.	[71]

and transport properties of the membrane. Thus, the proper choice of the plasticizer is very important. PIMs are proposed for the removal of organic species and metal ions [74]. Examples of application of PIMs in recovery of metals ions from aqueous solutions are presented in Table 8.10.

Table 8.9: Type of extractants and mechanism of complexation.

Class of extractant	Type	Examples	Mechanism
Acid extractants	Alkyl phosphoric acids	Dialkyl phosphoric acids and sulphur analogs (e. g. D2EHPA)	Acids extract metal ions by a cation-exchange mechanism viz.: $M_{aq}^{n+}+(n+x)(RH)_{org} \leftrightarrow (MR_n \cdot xRH)_{org}+nH_{aq}^{+}$
	Alkylphosphonic acids	2-Ethylhexyl phosphonic acid 2-ethylhexyl ester and sulphur analogs (e. g. PC-88A, Ionquest 801),	
	Alkyl phosphinic acids	Dialkyl phosphinic acids and sulphur analogs (e. g. CYANEX 272, 302 and 301)	
Acid chelating extractants	Hydroxyoximes	Alpha alkaryl hydroxyoximes, β alkaryl hydroxyoximes (Acorga P50, Lix 860)	$Me^{2+}{}_{aq} + HL_{org} \leftrightarrow MeL^{+}{}_{org} + H^{+}{}_{aq}$ $MeL^{+}{}_{org} + HL_{org} \leftrightarrow MeL_{2,org} + H^{+}{}_{aq}$ $MeL_{2,org} + 2HL_{org} \leftrightarrow MeL_{2,org} + HL_{org} + H^{+}{}_{aq}$
	β-diketone	Lix 54	
Basic extractants	Primary amines	Primene JMT, Primene 81R	The extraction is represented by an equation: $RNH_{2org} + H^{+} A^{-}{}_{aq} \leftrightarrow [RNH_3^{+}A^{-}]_{org}$
	Secondary amines	LA-1, LA-2.	
	Tertiary amines	Various Alamines, in particular Alamine 336.	The acid was extracted by amine to form salt: $[RNH_3^{+}A^{-}]_{org} + B^{-}{}_{aq} \leftrightarrow [RNH_3^{+}B^{-}]_{org} + A_{aq}^{-}$
	Quaternary amines	Aliquat 336,	
Solvating extractants	Phosphoric, phosphonic and phosphinic acid esters and thio analogs	Trialkyl phosphine oxides and sulphide (TOPO, CYANEX 921, CYANEX 923) TBP, DBBP, CYANEX 471X.	Trialkyl phosphine oxides can extract both acids and metal complexes while trialkyl phosphine sulphides can extract metal complexes. Thus, their extraction chemistry is as shown, first for acids and second for metal complexes: $m(HX)_{aq} + n(S)_{org} + xH_2O \leftrightarrow ((HX)_m S_n (H_2O)_x)_{org}$ $MX_n + y(S)_{org} \leftrightarrow (MX_n S_y)_{org}$ $HMX_{n+1} + x(S)_{org} \leftrightarrow (HS_x)^{+}(MX_{n+1})_{org}$

8.1.6.2 Supported polymer membranes

SLM process has been designed to apply for the removal of valuable metal ions from various multielement liquid resources. It is one of the promising technologies for possessing the attractive features such as high selectivity and combine extraction and stripping into one single stage, however, this separation system is efficient for aqueous feed with concentration much lower than that can be used in a classical extraction process. SLM acts on nonequilibrium mass-transfer characteristics where

Table 8.10: Examples of metal ion separation by PIMs.

Metal	Composition of PIM	Results	Ref.
$CdCl_2$ in saline or acidic media	Base polymer: CTA	– The transport of Cd is effective in both highly saline and highly acidic media; removal near 80 %.	[74]
	Plasticizers: NPOE, Tris-(2-ethylhexyl)phosphate (TEHP), dibutyl sebacate (99 %) (DBS) Carrier: Aliquat 336	– Because of the absence of plasticizer and low carrier content the transport of the metal is low, but at high amount of carrier, the transport of Cd is possible.	
$FeCl_2$, $FeCl_3$	Base polymer: CTA Plasticizer: NPOE Carrier: Cyphos®IL101, Cyphos®IL104	– Recovery factor of Fe(II) does not exceed 40 %, for – Fe(III) – from 60 % to almost 100 %. – The highest initial flux of Fe(III) and permeability coefficient are obtained for the membrane containing 40 mass % Cyphos® IL 101.	[75]
$CdCl_2$, $CuCl_2$	Base polymer: CTA Plasticizer: NPOE Carrier: Cyphos®IL101, Cyphos®IL104	– Extraction of Cd(II) is very fast and efficient (over 99 %). – The presence of HCl decreases the selectivity coefficient for Cd(II) over Cu(II).	[76]
$K[Ag(CN)_2]Zn(NO_3)_2$	Base polymer: CTA Plasticizer: Bis (2-ethylhexyl) sebacate (BEHS) Carrier: Aliquat 336	– Silver cyanide complex can be efficiently transported from the feed aqueous solutions to the stripping phase (73 %). – Selectivity of separation Zn and Ag is obtained.	[77]

the separation is not limited by the conditions of equilibrium (the mass-transfer reaction involves extraction of metal ions at aqueous feed–membrane interface, diffusion of the metal–ligand complex inside the membrane pores and dissociation of the metal–ligand complex at membrane–strip interface). However, the choice of the extractant has an important role on metal distribution coefficient value, membrane diffusion coefficient value and membrane thickness.

Flat sheet SLM and hollow-fiber SLMs are two commonly used SLM configurations, but only the second one has been designed for industrial application. Hollow-fiber-supported liquid membrane (HF-SLM) has advantages in a large surface area, which enable rapid feed transportation. Moreover, receiving phases are easy to recover. In this separation system, a HF module is used for extraction of metal ions. Inside the shell, there are countless thin fibres running lengthwise whose pores are impregnated with the organic liquid membrane phase. The fiber is a single nonporous material through which the solution present inside cannot be transported. The flow of all streams through the HF module is presented in Figure 8.5.

HF-SLM system can work not only as a single module, but also as a two-module hollow-fibre system, wherein feed phase is piped through one shell and the receiving phase through another. Possibilities of industrial applications of HF-SLM system to separate or recovery of metals ions are shown in Table 8.11.

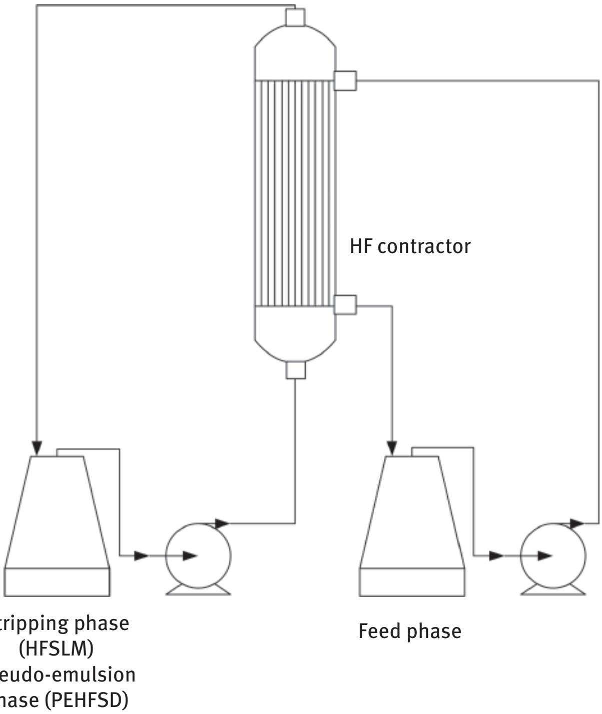

Figure 8.5: Scheme of HF-SLM/PEHFSD system.

An even more innovative version of HF-SLM is a pseudo-emulsion-based hollow-fiber strip dispersion (PEHFSD), wherein the stripping phase is dispersed in the organic membrane phase and a pseudo-emulsion being formed before injection into hollow-fiber module. During this separation, extraction and stripping occur simultaneously in a single hollow-fiber contactor. In PEHFSD, the solute is transported from the feed to the membrane and then to the stripping phase simultaneously. Using this method, the recovery of metal ions even from concentrated solution can proceed efficiently; however, the selectivity of such processes is low.

Table 8.12 lists selected examples of PEHFSD applications.

8.2 Polymer resins

8.2.1 Ion-exchange resin

An ion-exchange resin, similar to ion-exchange membrane, is an insoluble polymer containing positively or negatively charged groups which reacts with the counter-ions of recovered metal. The material has a highly developed structure of pores on the

Table 8.11: HF-SLM systems with their industrial applications.

Metal	Membrane (name, material, supplier)	Carrier	Results	Ref.
Hg(II)	PP, Liqui-Cel Extra-Flow module, Hoechst Celanese, USA	Trioctylamine (TOA) in toluene (2 % (v/v))	– Selective recovery of Hg(II) over As(III). – Stripping solution: NaOH solution; Feed phase: HCl solution	[78]
As(III)	PP, Celgard®x-30 240, Hoechst Celanese, USA	0.75 M (35 %, v/v) Aliquat 336 in kerosene	– As(III) reduction in produced water from the gas separation plant in the Gulf of Thailand. – Stripping solution: 0.5 M NaOH	[79]
U(VI)	PP, Liqui- CelX50: 2.5×8, Hoechst Celanese, USA	1 M di(2-ethylhexyl) isobutyramide in dodecane	– Selective recovery of U(VI) over Th(IV) from THOREX feed. – Stripping solution: distilled water.	[80]
Au(I)	PP, Liqui-Cel 8 cm × 28 cm 5PCG-259, Hoechst Celanese, USA	Mixture of LIX79 +TOPO in heptane	– Selective Au(I) recovery from cyanide solution containing also Fe(II), Cu(I), Ni(II), Ag(I) and Zn(II) (pH range of 9–10.5). – Stripping phase: NaOH solution (pH 12–13).	[81]
V(V)	Liqui-Cel 2.5 × 8 Extra-Flow Membrana-Hoechst Celanese, USA	LIX 84I (2-hydroxy-5-nonylacetophenoneoxime)in kereosene	– V(V) recovery from a multi-metal solution containing V(V), Cu(II), Ni(II), Co(II), Zn(II), Fe(III) and Mg(II).	[82]
Pu(IV)	Liqui-Cel 2.5 × 8 Extra-Flow Membrana-Hoechst Celanese, USA	TBP in dodecane	– Separation and recovery of Pu(VI) from nuclear waste. – Stripping phase: 0.1 M $NH_2OH{\cdot}HCl$ in 0.3 M HNO_3.	[83]
Cr(VI)	PP, Celgard *X10*, Celgard USA	30 % Aliquat 336 and 30 % isodecanol in kerosene	– Cr(VI) recovery from aqueous solutions. Initial Cr(VI) = 2.88 mmol/L, reduction to 71.5 µmol/L – Stripping phase: 1 M NaCl.	[84]

surface, where the ions are trapped or released. Commercially, the most common cation exchangers are the acid-type groups, such as sulfonate (($–SO_3^–$), strong acidic group) and carboxylate groups (($(-C{=}O)O^–$, weak acidic group). Other type of cation-exchange functional units having wide diversity matching different requirements is phosphonic ($-PO_3H_2$), phosphinic ($-PO_2H$), arsonic ($-AsO_3^{-2}$) and selenonic ($-SeO_3^–$) acid groups. In case of the anion-exchange resins functionality groups containing proton-accepting nitrogen and the commonly used functionality are amino groups e. g. ($–N^+(CH_3)_{3)}$ or ($–N^+(CH_3)_2CH_2$ CH_2OH) and much softer amine ($–N(CH_3)_2$). The anion-exchange resin, besides the proton-accepting nitrogen functionality groups, can also have a strong base

Table 8.12: Pseudo-emulsion based hollow-fiber strip dispersion (PEHFSD) applications in metal separation processes.

Metal	Membrane (name, material, supplier)	Carrier	Results	Ref.
Zn(II)	PP, *Liqui-Cel® Extra-Flow 2.5* x *8*, Celgard (USA)	Ionquest 801 (phosphonic acid (2-ethylhexyl)-mono(2-ethylhexyl)ester) in ShellSol D70[a]	– Zn(II) recovery over Ca(II) from sulphate solution at pH of 3. Initial Zn(II) concentration 0.1–1.0 g/L. – Pseudo-emulsion: 10 % Ionquest 801 in ShellSol D70 and 150 g/L H_2SO_4 or 90 g/L Zn(II) + 150 g/L H_2SO_4.	[85]
Zn(II)	PP, *Liqui-Cel® Extra-Flow 2.5* x *8*, Celgard (USA)	TBP in ShellSol D70 or 3-pyridine ketoxime in toluene with decanol (9:1 v/v)	– Zn(II) recovery from chloride solution (HCl or NaCl). – Pseudo-emulsion: TBP in ShellSol D70 and water or 0.1 M 3PC10 in toluene-decanol (9:1 v/v) and 5 % Na_2SO_4 solution.	[86]
Cr(VI)	PP, Liqui-Cel, 8 × 28 cm 5PCG-259, Hoechst Celanese, Charlotte (USA)	0.36 M Cyanex 923 in kerosene[b]	– Cr(VI) recovery from HCl solution with simultaneously reduction to Cr(III). – Stripping solution: hydrazine sulphate.	[87]
Co(II)	PP, Liqui-Cel 2.5x8 5PCG-354, Hoechst Celanese, Charlotte (USA)	0.64 M DP-8R (di (2-ethylhexyl) phosphoric acid) in Exxsol D100[c]	– Efficient recovery of Co(II) from sulphate solution at pH of 5. Selectivity over Li ions is around 25. – Pseudo-emulsion: 0.64 M DP-8R in Exxsol D100 and 0.1 M H_2SO_4.	[88]
Au(I)	PP, Liqui-cel, 8×28 cm 5PCG-259, Hoechst Celanese, Charlotte (USA)	5–10 % LIX79 in heptane	– Selective Au(I) recovery from cyanide solution. Separation over Fe(II), Cu(I), Ni(II), Ag(I) and Zn(II). – Pseudo-emulsion: 12 %LIX-79/heptane and 0.2 M NaOH.	[89]
Cu(II)	PP, *Liqui-Cel® Extra-Flow 2.5x8*, Celgard (USA)	5–10 % Acorga M5640 in ShellSol D70	– Recovery of Cu(II) from sulphate medium. Initial Cu(II) concentration 0.1 or 1.0 g/L. pH =1.4. – Pseudo-emulsion: 2.5–10 % (v/v) Acorga M5640 and 180 g/L H_2SO_4	[90]

[a] Notes: ShellSol D70 consists predominantly of C11–C14 paraffins and naphthenes;
[b] Kerosene is a mixture of paraffins and naphthenes (fractional distillation 150–275 °C);
[c] Exxsol D100 consists predominantly of C12–C15 paraffins, naphthenes and below 2 % aromatic compounds

quaternary phosphonium ($-P^+R_3$) and tertiary sulphonium anion-exchange group ($-S^+R_2$). A limitation of these materials is the selectivity of metal separation especially in case of trace metals in the presence of significant amounts of alkali metals [91]. Most of the selective resins are of the chelating type. This type of material contains mostly as functional groups iminodiacetic ($-N(CH_2COO^-)_2$), dithiocarbamate ($-R_2NCS_2^{-2}$), thiol

(-SH), aminophosphoric ($-NH_2CH_2PO_3^{-2}$) and *bis*-picolylamine (Table 8.13). Chelating resins bind the heavy metals selectively towards the alkali and alkaline earth metals and are efficient, quantitative preconcentrating agents [92].

Available commercially resins are mainly formed via suspension polymerization reaction of styrene in the presence of 1,4-divinylbenzene as a cross-linked agent. As was presented in Table 8.13, the two types of resins can be used: gel and macroporous type. Resins as gel are a cross-linked polymers exhibiting microporosity with pore volumes typically up to 10 or 15 Å. This type of resin is dedicated mainly to sorption of organic substances from water. Macroporous ion-exchange resins are highly cross-linked and have greater porosity and surface area than those of the gel type resins. Unfortunately, because of the high cross-linkage in the matrix, the macroporous resins have greater exposure to potential oxidants than gel resins.

Table 8.13: Physicochemical properties of commercial ion-exchange resins.

Resin	Structure	Polymer	Functional group	Ionic form	Bead size [mm]	Total capacity [meq/g]
Cation-exchange resins						
Lewatit™ S 100	G	Polystyrene	$-SO_3^-$	Na	0.6–0.7	2.0
Amberlite™ IRN77	G	Polystyrene	$-SO_3^-$	H	0.6–0.7	1.9
Dowex™ 88	M	Polystyrene	$-SO_3^-$	Na	0.4–1.2	1.8
Amberlite™ IRP-64	M	Polyacrylic	$(-C{=}O)O^-$	H	0.04–0.15	10
Amberlite™ IRC-50	M	Polyacrylic	$(-C{=}O)O^-$	H	0.3–1.2	10
Anion-exchange resins						
Dowex™ Marathon™ A	G	Polystyrene	$-N^+(CH_3)_3$	Cl	0.4–0.6	4.0
Amberlite™ IRA900	M	Polystyrene	$-N^+(CH_3)_3$	Cl	0.7–0.8	4.2
Lewatit M™ 610	G	Polystyrene	$-N^+(CH_3)_2CH_2CH_2OH$	Cl	0.6–0.7	1.3
Dowex™ 22	M	Polystyrene	$-N^+(CH_3)_2CH_2CH_2OH$	Cl	0.4–0.8	-
Lewatit™ MP 62	M	Polystyrene	$-N(CH_3)_2$	-	0.3–1.3	1.7
Chelating resins						
Dowex™ M4195	M	Polystyrene	*bis*-picolylamine	-	0.30–0.84	35–42*
Amberlite™ IRA743	M	Polystyrene	*N*-methylglucamine	-	0.5–0.7	0.7
Amberlite™ IRC 748	M	Polystyrene	$-NH(CH_2COONa)_2$	Na	0.5–0.7	1.4
Purolite™ S957	M	Polystyrene	$-SO_3^-$ $-PO_3^{-2}$	H	<0.425	18*
Duolite™ GT-73	M	Polystyrene	-SH	H	0.4–0.8	3.9
Diphonix™	G	Polystyrene	-COOH $-PO_3H_2$	H	0.3–0.15	5.3
Duolite™ C467	M	Polystyrene	$-NH_2CH_2PO_3^{-2}$	Na	0.4–1.0	3.5
Purolite™ S920	M	Polystyrene	$-SC(NH_2)_2$	H	0.3–1.2	200*

G = gel (or microporous); M = macroporous (or macroreticular); * g/L
*g of metal/L

The incorporation of functional group to a polymer matrix requires specific synthesis conditions [93]; e. g. sulfonic ion is incorporated via a reaction of a polystyrene resin with a concentrated sulfuric acid, while incorporation of amine or ammonium group is combined mainly with nucleophilic substitution between chloromethyl polystyrene-divinylbenzene copolymer and corresponding amine, nucleophilic substitution between poly(4-vinylpyridine) with halogenated compounds (e. g. benzyl chloride) or by radical polymerization (e. g. synthesis of poly(4-vinylbenzyl)trimethylammonium chloride). Incorporation of phosphonic functionalizing group is prepared by an Arbuzov-type reaction between chloromethyl polystyrene-divinylbenzene copolymers and triethylphosphite, yielding the phosphonate ester, which after hydrolysis gives a phosphonic acid copolymer. Functionalization of acrylic copolymer can be carried out, for example, through an aminolysis of the ester groups in the polymer matrix.

The individual ions present in the sample are retained in varying degrees depending on their different affinity for the resin phase. In the form of a cations, metal ions such as Co(II), Cr(III) and Ni(II) can be removed either with a cation exchanger or with a chelating resin [94–99], but in case of the anionic metal species as in case of Cr(VI) the anionic exchanger is used [100]. The consequence of this phenomenon is the separation of desired metals ions; however, the effectiveness of the process depends on the nature and characteristics of the resin. Ion-exchange process is particularly suitable for purification of metal ions, but the total concentration of dissolved salts in solution must generally be low (<1 g/L). At high concentrations, the exchange potentials for ions diminish and there is more competition for the available exchange sites. Other limitations are their limited radiation and thermal stabilities. Under exposure of both impacts, most organic resins will degrade even at macroscopic level in Table 8.14.

The ion-exchange resins are suitable for the removal of metal anions or cation but mostly with too low selectivity and to improve their separation potential (especially towards alkali and alkaline earth cations), as well as the sorption capacities, metal- or metal oxide-loaded exchange resins have been studied (Table 8.15). In this hybrid system, metal cation (usually Fe(III), Zr(III)) or metal oxide (Fe_3O_4, MnO_2, TiO_2, ZrO_2) have been immobilized on polymer matrices and subsequently studied for heavy metal ion recovery [102]. The metal oxides have been exploited as adsorbents with inner-sphere complexation. Such interaction enables the metal ion complexation with high capacity and specific adsorption towards heavy metals such as As(III) and As(V) [103] in the case of metal-loaded ion-exchange resin, and metal cations have been immobilized on polymer support and subsequently studied for metal ion sorption (As(V), Cr(VI)). The requirement of a polymer matrix for loading with cations is the presence of exchangeable functional group, which enables the coordination of extractable metal ion with loaded metal [104–106]

Table 8.14: Currently marketed ion-exchange resins with examples of their application.

Product name	Polymer	Functional group	Application	Ref.
Amberlite™ IRN77	Polystyrene	$-SO_3H$	Co(II), Cr(III), Ni(II) recovery from synthetic nuclear power plant coolant water. Maximum adsorption capacities at pH 2.75: 1 g/g (Co(II)), 4 g/g (Cr(III)) and 15 g/g (Ni(II)).	[94]
Lewatit™ S 100 Chelex-100	Polystyrene	$-SO_3Na$ $-NH(CH_2COONa)_2$	Cr(III) recovery from aqueous solutions. Maximum ion-exchange capacities at pH of 3.5 and 4.5: 0.39 mmol/g (Lewatit S 100) and 0.29 mmol/g (Chelex-100).	[95]
Amberlite™ IRC 748	Polystyrene	$-NH(CH_2COONa)_2$	Ni(II) recovery from laterite leach tailings (after Co(II) extraction). Maximum ion-exchange capacities: 97.6 mg Ni/g at pH of 4 with low recovery Mg, Na and Fe(III).	[96]
			Ca(II) and Mg(II) recovery from potassium chromate solution. Maximum ion-exchange capacities: 7.21 mg/g (Ca(II)) 27.70 mg/g (Mg(II)).	[97]
Diphonix®	Polystyrene	$-COOH$ $-PO_3H_2$	Separation Zr(III) and Hf(III) from acidic solution. Separation condition: 0.5 M H_2SO_4 at 22 °C with a linear flow rate < 7.5 cm/h.	[98]
Duolite™ GT-73	Polystyrene	$-SH$	Hg(II) removal from waste water generated at The Integrated Defense Melter System (IDMS), located at the Savannah River Site. Initial Hg concentration 0.2–50 µg/L other ions (traces) Al, B, Ca, Li, Mg, Mn, Mo, P, Si, W and Zn. Maximum ion-exchange capacities: 0.1 Mg/g.	[99]
Lewatit™ MP 62 Lewatit™ M 610	Polystyrene	$-N(CH_3)_2$ $-N^+(CH_3)_2CH_2CH_2OH$	Cr(VI) recovery from aqueous solutions. Maximum ion-exchange capacities at pH of 5: 27 mg/g (Lewatit™M 610) 17.1 mg/g (Lewatit™MP 62).	[100]
Dowex™ M-4195	Polystyrene	- *bis*-picolylamine	Cu(II), Co(II), Ni(II) and Pb(II) preconcen-tration from chloride solution. Maximum adsorption capacities at pH 2 were Cu(II) 0.043 mol/L, Ni(II) 0.045 mol/L, Co(II) 0.045 mol/L, Pb(II) 0.010 mol/L desorption condition: solution at pH of 1.4.	[101]

8.2.2 Solvent impregnated resin

The application of reactive extraction for processing dilute aqueous solutions is rather uneconomic. More efficient technique seems to be adsorption on chelating, ion-exchange or enantioselective resins, but those materials are very expensive becuase the preparation is time consuming and difficult. Ideal seem to be linking of the solvent

Table 8.15: Examples of metal ion recovery using hybrid ion-exchange resins.

Product name	Polymer	Functional group	Application	Ref.
Lewatit™ FO 36	Polystyrene	FeO(OH)	Pb(II) recovery from aqueous phase at different pH. Maximum adsorption capacities: 62.5 mmol/g at pH 7.	[107]
ArsenX*np*	Polystyrene	-$N^+(CH_3)_3$ Fe_2O_3	As(III) and As(V) removal from sulfate, fluoride, bicarbonate, and chloride solution. Maximum adsorption capacities: 6.9 mg/g of regenerated resin. Desorption using a warm caustic solution.	[108]
D-001 (HFO-001)	Polystyrene	-SO_3Na Fe_2O_3	Efficient removal of Cd(II), Pb(II) and Cu(II) metals from water and wastewater. Maximum adsorption capacities: 1.6 mmol Pb(II)/g and 1.4 mmol Cu(II) and Cd(II)/g resin. Desorption solution: HCl–NaCl solution (pH 3).	[109]
D-001 (ZrP-001)	Polystyrene	-SO_3Na ZrP (zirconium phosphate)	Selective removal of Pb(II) in the presence of Ca(II). Maximum adsorption capacities: 0.4 g Pb(II)/g resin (total capacity: 0.79 meq/g). Desorption solution: 2 % HNO_3	[110]
Dowex 1×8–400	Polystyrene	-$N^+(CH_3)_3$ MnO_2	As(III) and As(V) removal from sulfate, fluoride, bicarbonate, and chloride solution. Maximum adsorption capacities: 6.9 mg/g of regenerated resin. Desorption using a warm caustic solution.	[111]

extraction supported a selective extractant with ion-exchange process suitable for processing of dilute solutions. The concept includes the incorporation of the extractant into hydrophobic resin, which was first proposed by Warshawsky [112] for metal recovery in hydrometallurgical process. In this study, a hydroxyoxime solvent-impregnated resins (SIRs) was proposed for selective copper removal. This concept of SIRs is based on the physical impregnation of a selected extractant in a porous adsorbent, but the impregnated extractant should behave as in classical reactive extraction process and simultaneously maintain a strong affinity for the polymer matrix.

8.2.2.1 Impregnation procedure

SIR, in which the extractant is incorporated into non-ionic macroreticular polymer structure, can be prepared according to a few types of procedures:

I. “Dry” method has been developed for extractant having strong hydrophilic centres (oximes, ethers, ketones). According to this impregnation procedure, a liquid extractant or as a mixture in polar diluent (acetone, acetonitryle, methanol) is contacted with the polymer in batch mode for few hours; however the period of time is adjusted individually to both reagents and should enable to obtain maximum incorporation of the extractant within the polymer pores. Next the diluent is removed via vacuum evaporation resulting in a polymer–extractant material. Using this method, an adsorption of the extractant on the polymeric can be also observed and that requires additional procedures of washing process.

II. “Wet” impregnation procedure has been developed for strong hydrophobic extractant. According to this procedure, an extractant together with the diluent is incorporated into the polymeric pores resulting in a polymer–extractant–diluent material. During this procedure of impregnation, the polymer support is shaken with extractant–diluent mixture. The next stage was the removal of diluent with remaining extractant.

III. Procedure with a modifier addition. According to this procedure, a diluted extractant in the presence of phase modifier is incorporated into the polymer pores. Goal of the modifier is to promote a water wettability and a simultaneously reduction of too high hydrophobicity of impregnated resin. The added modifier is typically more polar than the extractant and the most commonly used mixtures are acetone, methanol or ethanol with water.

IV. Dynamic column method, according to which the impregnated polymer is placed in a column and fully swelled by the diluent. Then, the extractant solution is fed into the column until the extractant concentration in the outlet is constant. The resulting SIR is finally washed with water. This procedure is directed to materials with analytical application. The choosing of the methods depends mainly on the chemical properties of the extractant, hydrophobicity of polymer support as well as the interaction of extractant–polymer. Both in the industrial and in laboratory scale the most often used polymer supports are a macroreticular polymer resins, mainly series Amberlite, Dovex and Lewatit. The selection of the polymer support is adjusted to the extractant properties to give the optimal balance of hydrophobic versus hydrophilic properties. Moreover, very important is to minimize losses of the extractant to the aqueous phase (e. g. by maintaining enough hydrophilicity or additional coating) and to maximize mass transfer of the solute into the resin pores and between phases, which depends on the complexing properties of the impregnated extractant. The incorporated in a macroreticular polymer structure extractant has a strong affinity towards the polymeric support, but it still behaves as extractant and the extracting properties are as in the liquid state. The immobilization of the extractant on the internal surface of the macroreticular polymer is mainly combined with forces which are responsible to “catching of extractant”–van der Waals forces, π-π interactions and capillary forces [113–116]. Unfortunately, so soft polymer–extractant interactions can cause much higher loss of the extractant than that of classical reactive solvent extraction process. The stability of the resin can be improved by carrying out several impregnation cycles, longer (several hours) or addition wet drying procedure and a post-impregnation encapsulation techniques [117–120]. Using the post-impregnation encapsulation process as loss extractant prevented method enables achieving a much stable material than using other stabilizing procedures. However, supplying a permeable coat around each bead of the resin is difficult and the procedure requires adjusting of the condition and type of coating materials to an impregnated resin.

More stable and selective resins can be obtained by impregnation of ion-exchange materials. For that system, charged or polar functional groups mainly provide hydrophilic character as well as interact with the extractant mainly by covalent binding. So multiple interactions can cause the possibility of strong associations between metal, impregnated extractant and resin functional groups [121].

The impregnated resins can also be obtained by an extractant entrapping directly in polymerization process. The procedure is more difficult especially because of the polymerization procedure, which varies from a type of the extractant, its acidity, viscosity and water-organic diluent activity, as well as, it depends on the initial concentration ratio of monomer and cross-linking agent to initiator. The synthesized beads have gained much attention presently in the metal separation technology due to, in comparison with classical SIRs, a high adsorption capacity, faster kinetics and ease of regeneration. Furthermore, the incorporation of extractant during a polymerization process is a commonly encountered method in an industrial production of SIRs such as Lewatit TP272 [122].

8.2.2.2 Metals recovery with solvent impregnated resin

Mechanism of metal ions recovery with SIR is partially identical as in case of corresponding solvent extraction systems and partially as in case of ion-exchange resin. Kamio et al. [123]. have developed a theoretical model to describe a metal recovery with a microcapsule containing an acidic extractant. The determined kinetic constants for the complex formation reaction are almost the same as that determined for the liquid–liquid extraction system and is supported by Fick's diffusion laws [124, 125]. It was shown that the extraction mechanism of metal ions into a microcapsule progresses through the three processes (Figure 8.6): I. diffusion of metal ion across the aqueous liquid film exists near the surface of a microcapsule; II. intermediated and final extracted complex formation on the surface of a microcapsule, and the last process III. diffusion of extracted complex through resin pores. The extracted complex gradually accumulates at the surface of the resin. The surface of the microcapsule then is saturated with the extracted complex.

8.2.2.3 Application of SIRs in metal recovery

The SIRs show to be effective sorbents for the selective recovery of rare and valuable metals ions from aqueous solutions or separation of toxic element; however, those extraction properties depend mainly on the specific properties of the incorporated extractant (see the mechanisms of extraction presented in Table 8.9). Commercial SIRs being cross-linked polystyrene with an extractant integrated into the resin beads during polymerization process have been evaluated mainly for the processes originally designed for the extractant e. g. separation of uranium and plutonium from mixed actinide residues [126, 127] (Table 8.16).

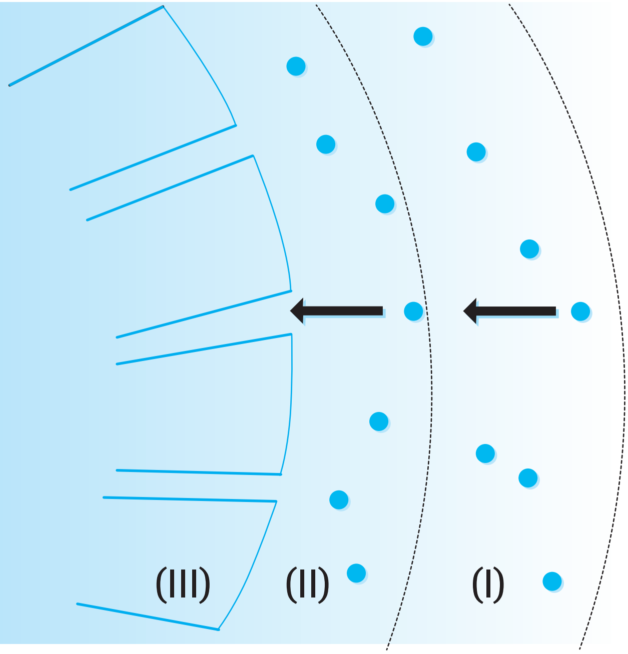

Figure 8.6: Extraction mechanism of metal ions into a microcapsule.

The SIRs have been shown to be effective sorbents for the selective recovery of metal ions from aqueous solutions; however, the industry applications of commercial resins are limited to the few examples. In case of synthetic SIRs prepared usually by the wet impregnation process, the studies are conducted on sorption equilibria of a wide group of transition metals, some metalloids, lanthanides and actinides. So far, the results obtained have led to new technological developments from which the most interesting examples are listed in Table 8.17 and Table 8.18.

Table 8.16: Commercial resins being cross-linked polystyrene containing extractant incorporated into resin beads during polymerization process.

Product name	Matrix	Extractant	Application	Ref.
Lewatit™ OC 1023	Polystyrene	TBP	U(VI) separation from a plutonium–uranium solution (5 M HNO_3 -0.1 M $Fe(SO_3NH_2)_2$) residual plutonium was removed by washing with 0.35-HNO_3 -0.1 M $Fe(SO_3NH_2)_2$ solution. Extraction capacities 10 g/g U 25 g/L Pu. Uranium stripping solution: 0.1 M $Fe(SO_3NH_2)_2$.	[127]

(*continued*)

Table 8.16: (*continued*)

Product name	**Matrix**	**Extractant**	**Application**	**Ref.**
Lewatit™ VP OC 1026	Polystyrene	D2EHPA	Zn(II) separation from a nickel electrolyte prior to electrowinning (Vale's Port Colbourne (Canada) refinery). Metal concentration 10–50 mg/ml Zn, 50–70 mg/L Ni and 0.1–0.3 g/L Co, Selectivity at pH below 3. Extraction capacities 17 mg/g (Zn). 1 M H_2SO_4 Zn(II) separation from electroplating effluent containing Cr(VI). Initial metals concentration 0.52 mg/ml Zn and 0.017 mg/ml Cr, Selectivity at pH of 6.2. Extraction capacities 58 mg/g. Stripping solution: 5 % H_2SO_4 solution.	[128, 129]
Lewatit™ TP 272 Lewatit™ TP 807'84	Polystyrene	Cyanex 272	Co(II) selectively extraction over Ni(II) from sulfate media. Initial Co(II) concentration 59 mg/L, Selectivity at pH range of 4.8–6.0. Extraction capacities 18 mg/g. Stripping solution: H_2SO_4 solution (pH below 2).	[130, 131]
TVEX-TBP	Polystyrene	TBP	Sc(III) extraction from hydrochloric solution. Initial composition 0.08–0.1 Sc, 8 mol/L HCl. Extraction capacities 0.8 mg/g (mol/L TBP). Stripping solution: water. Zr(III) and Hf(III) selective extraction from HNO_3 solution. Extraction capacities 0.7 mol Zr/L TBP and 0.3 mol HF/L of TBP. Resin composition TVEX-65 % TBP. Stripping solution: 30 g/L HNO_3.	[132]
TVEX-TBPHDEHP	Polystyrene	TBP:HDEHP (1:1)	Separation of Bk(IV), Cf(III) and Eu(III) from Am(III) and Cm(III). 95 % of Am separation over Cm (below 1 %) from 0.2 M HNO_3 during one cycle.	[133]
TVEX-DIOMP	Polystyrene	DIOMP (*bis*-isooctyl methyl phosphonate)	Scandium recovery from solutions containing above 4 M HCl. Extraction capacities: 1.4 mol/L of DIOMP (8 M HCl). Stripping solution: diluted HCl.	[134]

Table 8.17: Synthetic resins being cross-linked polystyrene containing acidic extractant incorporated into resin beads during impregnation process.

Commercial name of polymer support	Matrix	Extractant	Application	Ref.
Amberlite™ XAD4	Polystyrene	D2EHPA	Selective Separation of Pb(II) and Cu(II). Resin composition: 30 wt. % of D2EHPA. Initial metals concentration: 0.01 mol/L, pH=2 Metals were separated in 6 batches of contacts.	[135]
Amberlite™ XAD4	Polystyrene	D2EHPA	Separation of Zn(II) and Cu(II) from aqueous sulfate Solutions Resin composition: 40 wt. % of D2EHPA. Initial metal concentration: 1.58 mol/L, pH ranged 1.05–3.34, SO_4^{2-}concentration equal to 0.5 mol/L. Separation can be obtained in either batch or column operation.	[136]
Amberlite™ XAD-1180	Polystyrene	D2EHPA	Extraction of Bi(III) from nitrate medium. Resin composition: 90 wt. % of D2EHPA. Extraction capacities 490.7 mg/g. Stripping solution: concentrated HCl.	[137]
Amberlite™ XAD7	Polyacrylate	D2EHPA-Fe	Extraction of As(V) from aqueous solution. Resin composition: 30 wt.% of D2EHPA-Fe. pH= 9. Extraction capacities 19 µg/g.	[138]
Amberlite™ XAD2, XAD4 Amberlite™ XAD7	Polystyrene Polyacrylate	PC-88A	Extraction of La(III), Sm(III), Tb(III) and Yb(III) from chloride solution. Resin composition: 20 or 50 wt.% of PC-88A. Initial metals concentration: 0.5 mmol/L, pH= 3.5.	[139]
Amberlite™ XAD7	Polyacrylate	Cyanex 301	Extraction of Cd(II) from phosphoric acid (diluted and concentrated). Initial Cd(II) concentration 10 mg/L. Resin composition: 5–14 wt.%. Extraction capacities 11 mg/g. Stripping solution: 5 M HCl.	[140]
Amberlite™ XAD7	Polyacrylate	Cyanex 302	Extraction of Cd(II) and Cu(II) from 40 % phosphoric acid. Initial metals concentration 50 mg/L. Resin composition: 50 wt.% of Cyanex 302. Extraction capacities 27–34 mg/g. Stripping solution: 4 M HCl.	[141]

(*continued*)

Table 8.17: (*continued*)

Commercial name of polymer support	Matrix	Extractant	Application	Ref.
Amberlite™ XAD2	Polystyrene	Cyanex 272 and Cyanex 302	Two fixed-bed columns (XAD-2 – Cyanex 272 (50 wt.%) and XAD-2 Cyanex 302 (15 wt.%)) were successfully used for separation and recovery of from Fe(III), Cd(II) and Ni(II) multicomponent solutions. Initial metals concentration: 10 mg/L, pH= 2 and 8. Stripping solution: 3 M HCl.	[142]

Table 8.18: Synthetic resins being cross-linked polystyrene containing basic extractant incorporated into resin beads during impregnation process.

Commercial name of polymer support	Matrix	Extractant	Application	Ref.
Amberlite™ XAD4	Polystyrene	Trioctylamine (TOA)	Extraction of Au(III), Pt(II) and Pd(II) from 1 M HCl. Initial metal concentration 0.05–0.5 mg/L. Resin composition: 3.5 wt.% of TOA. Extraction capacities 50 μg/g. Stripping solution: 11.9 g/l of N-(dithiocarboxyl) sarcosine diammonium salt (DTCS) in 50 % ethanol.	[143]
Amberlite™ XAD4	Polystyrene	Aliquat 336	Separation of Re(III) from Rd(III) in HNO_3 solution. Initial metal concentration 0.1 g/L. Resin composition: 40 wt.% of Aliquat 336. Extraction capacities of Re 2.0 meq/g.	[144]
Diaion™ HP-20 Diaion™ HP-2 MG.	Polystyrene Polyacrylate	Aliquat 336	Cr(III) extraction from aqueous solution at pH 3 and higher. Initial metal concentration 10 and 20 mg/L. Resin composition: 33 and 50 wt.% of Aliquat 336. Extraction capacities 38(HP-20) ad 40(HP-2 MG) mg/g. Stripping solution: 0.1 M NaOH–0.1 M NaCl.	[145]
Amberlite™ XAD2	Polystyrene	Aliquat 336	Extraction of Pd(II) from HCl solution. Initial metal concentration 0.47 mmol/L. Resin composition: 30–60 wt.% of Aliquat 336. Extraction capacities 64 mg/g (60 % resin, 1MHCl).	[146]

(*continued*)

Table 8.18: (*continued*)

Commercial name of polymer support	Matrix	Extractant	Application	Ref.
Amberlite™ XAD7	Polyacrylate	Cyphos IL 101	Extraction of Zn(II) from HCl solution (optimum 2-4MHCl). Initial metal concentration 20 mg/L. Resin composition: above 30 wt.% of Cyphos IL 101 made process efficient. Extraction capacities 20 mg/g (40 % resin). Stripping solution: water or 0.1 M mineral acid.	[147]
Amberlite™ XAD7	Polyacrylate	Cyphos IL 101	Extraction of Cd(II) from HCl solution (optimum 2-4MHCl). Initial metal concentration 60–100 mg/L. Resin composition: 10–50 wt.% of Cyphos IL 101. Extraction capacities 40–50 mg/g (depended on Cd(II) initial concentration). Stripping solution: water or 0.1 M mineral acid.	[148]

References

[1] Hofs B, Ogier J, Vries D, Beerendonk EF, Cornelissen ER. Comparison of ceramic and polymeric membrane permeability and fouling using surface water. Sep Purif Technol. 2011;79:365–374.

[2] Ng LY, Mohammad AW, Leo CP, Hilal N. Polymeric membranes incorporated with metal/metal oxide nanoparticles: A comprehensive review. Desalination. 2013;308:15–33.

[3] Pearce G. Introduction to membranes: Membrane selection. Filtr Separat. 2007;44:35–37.

[4] Lee KP, Arnot TC, Mattia D. A review of reverse osmosis membrane materials for desalination – Development to date and future potential. J Membr Sci. 2011;370:1–22.

[5] Greenlee LF, Lawler DF, Freeman BD, Marrot B, Moulin P. Reverse osmosis desalination: Water sources, technology, and today’s challenges. Water Res. 2009;43:2317–2348.

[6] Fritzmann C, Löwenberg J, Wintgens T, Melin T. State-of-the-art of reverse osmosis desalination. Desalination. 2007;216:1–76.

[7] Csefalvay E, Pauer V, Mizsey P. Recovery of copper from process waters by nanofiltration and reverse osmosis. Desalination. 2009;240:132–142.

[8] Bakalár T, Búgel M, Gajdošová L. Heavy metal removal using reverse osmosis. Acta Montanistica Slovaca Ročník. 2009;14:250–253.

[9] Ozaki H, Sharma K, Saktaywin W. Performance of an ultra-low-pressure reverse osmosis membrane (ULPROM) for separating heavy metal: Effects of interference parameters. Desalination. 2002;144:287–294.

[10] Mohsen-Nia M, Montazeri P, Modarress H. Removal of Cu2+ and Ni2+ from wastewater with a chelating agent and reverse osmosis processes. Desalination. 2007;217:276–281.

[11] Chan BKC, Dudeney AWL. Reverse osmosis removal of arsenic residues from bioleaching of refractory gold concentrates. Miner Eng. 2008;21:272–278.

[12] Ipek U. Removal of Ni(II) and Zn(II) from an aqueous solution by reverse osmosis. Desalination. 2005;174:161–169.

[13] Qdais HA, Moussa H. Removal of heavy metals from wastewater by membrane processes: A comparative study. Desalination. 2004;164:105–110.

[14] Tanninen J, Mänttäri M, Nyström M. Nanofiltration of concentrated acidic copper sulphate solutions. Desalination. 2006;189:92–96.

[15] Belkhouche NE, Didi MA, Taha S, Farès NB. Zinc rejection from leachate solutions of industrial solid waste – effects of pressure and concentration on nanofiltration membrane performance. Desalination. 2009;239:58–65.

[16] Manis A, Soldenhoff K, Jusuf E, Lucien F.. Separation of copper from sulfuric acid by nanofitration. In: 5th International Membrane Science &Technology Conference, 2003, IMSTEC'03.

[17] Chaabane T, Taha S, Taleb Ahmed M, Maachi R, Dorange G. Removal of copper from industrial effluent using a spiral wound module — Film theory and hydrodynamic approach. Desalination. 2006;200:403–405.

[18] Malakoutian M, Golpayegani AA, Rajabizadeh A. Survey of nanofiltration process efficiency in Pb, Cd, Cr+6 and Cu ions removal from sulfate-containing waters. Water Wastewater. 2015;25: 13–20.

[19] Ennigrou DJ, Gzara L, Ben Romdhane MR. Cadmium removal from aqueous solutions by polyelectrolyte enhanced ultrafiltration. Desalination. 2009;246:363–369.

[20] Staszak K, Karaś Z, Jaworska K. Comparison of polymeric and ceramic membranes performance in the process of micellar enhanced ultrafiltration of cadmium(II) ions from aqueous solutions. Chem Pap. 2013;67:380–388.

[21] Staszak K, Konopczyńska B, Prochaska K. Micellar enhanced ultrafiltration as a method of removal of chromium(III) ions from aqueous solutions. Separ Sci Technol. 2012;47:802–810.

[22] Juang RS, Xu YY, Chen CL. Separation and removal of metal ions from dilute solutions using micellar-enhanced ultrafiltration. J Membr Sci. 2003;218:257–267.

[23] Seymour WB. The preparation of cellophane membranes of graded permeability. J Biol Chem. 1940;134:701–707.

[24] Chen HL, Juang RS. Extraction of surfactin from fermentation broth with n-hexane in microporous PVDF hollow fibers: Significance of membrane adsorption. J Membr Sci. 2008;325:599–604.

[25] Elimelech M, Zhu X, Childress AE, Hong S. Role of membrane surface morphology in colloidal fouling of cellulose acetate and composite aromatic polyamide reverse osmosis membranes. J Membr Sci. 1997;127:101–109.

[26] Gecol H, Ergican E, Fuchs A. Molecular level separation of arsenic (V) from water using cationic surfactant micelles and ultrafiltration membrane. J Membr Sci. 2004;241:105–119.

[27] Li X, Zeng GM, Huang JH, Zhang C, Fang YY, Qu YH, et al. Recovery and reuse of surfactant SDS from a MEUF retentate containing Cd2+ or Zn2+ by ultrafiltration. J Membr Sci. 2009;337:92–97.

[28] Fang YY, Zeng GM, Huang JH, Liu JX, Xu XM, Xu K, et al. Micellar-enhanced ultrafiltration of cadmium ions with anionic-nonionic surfactants. J Membr Sci. 2008;320:514–519.

[29] Huang JH, Zeng GM, Zhou CF, Li X, Shi LJ, He SB. Adsorption of surfactant micelles and Cd2 +/Zn2+ in micellar-enhanced ultrafiltration. J Hazard Mater. 2010;183:287–293.

[30] Landaburu-Aguirre J, Pongrácz E, Perämäk P, Keiski RL. Micellar enhanced ultrafiltration for the removal of cadmium and zinc: Use of response surface methodology to improve understanding of process performance and optimisation. J Hazard Mater. 2010;180:524–534.

[31] Jung J, Yang JS, Kim SH, Yang JW. Feasibility of micellar-enhanced ultrafiltration (MEUF) for the heavy metal removal in soil washing effluent. Desalination. 2008;222:202–211.

[32] Yurlova L, Kryvoruchko A, Kornilovich B. Removal of Ni(II) ions from wastewater by micellar-enhanced ultrafiltration. Desalination. 2002;144:255–260.

[33] Ghadge S, Chavan M, Divekar A, Vibhandik A, Pawar S, Marathe K. Mathematical modelling for removal of mixture of heavy metal ions from waste-water using micellar enhanced ultrafiltration (MEUF) process. Sep Sci Technol. 2015;50:365–372.

[34] Schwarze M, Groß M, Moritz M, Buchner G, Kapitzki L, Chiappisi L, et al. Micellar enhanced ultrafiltration (MEUF) of metal cations with oleylethoxycarboxylate. J Membr Sci. 2015;478: 140–147.

[35] Rether A, Schuster M. Selective separation and recovery of heavy metal ions using water-soluble N-benzoylthiourea modified PAMAM polymers. React Funct Polym. 2003;57:13–21.

[36] Juang RS, Shiau RC. Metal removal from aqueous solutions using chitosan-enhanced membrane filtration. J Membr Sci. 2000;165:159–167.

[37] Llorens J, Pujola M, Sabaté J. Separation of cadmium from aqueous streams by polymer enhanced ultrafiltration: A two-phase model for complexation binding. J Membr Sci. 2004;239:173–181.

[38] Barakat MA, Schmidt E. Polymer-enhanced ultrafiltration process for heavy metals removal from industrial wastewater. Desalination. 2010;256:90–93.

[39] Petrov S, Nenov V. Removal and recovery of copper from wastewater by a complexation–ultrafiltration process. Desalination. 2004;162:201–209.

[40] Trivunac K, Stevanovic S. Removal of heavy metal ions from water by complexation-assisted ultrafiltration. Chemosphere. 2005;64:486–491.

[41] Canizares P, Perez A, Camarillo R. Recovery of heavy metals by means of ultrafiltration with water-soluble polymers: Calculation of design parameters. Desalination. 2002;144:279–285.

[42] Vieira M, Tavares CR, Bergamasco R, Petrus JCC. Application of ultrafiltration-complexation process for metal removal from pulp and paper industry wastewater. J Membr Sci. 2001;194: 273–276.

[43] Zhang YF, Xu ZL. Study on the treatment of industrial wastewater containing Pb2+ ion using a coupling process of polymer complexation-ultrafiltration. Separ Sci Technol. 2003;38: 1585–1596.

[44] Ennigrou DJ, Sik Ali MB, Dhahbi M, Ferid M. Removal of heavy metals from aqueous solution by polyacrylic acid enhanced ultrafiltration. Desalin Water Treat. 2015;56:2682–2688.

[45] Uludag Y, Hö Ö, Yilmaz L. Removal of mercury from aqueous solutions via polymer-enhanced ultrafiltration. J Membr Sci. 1997;129:93–99.

[46] Palencia M, Rivas BL, Pereira E. Metal ion recovery by polymer-enhanced ultrafiltration using poly(vinyl sulfonic acid): Fouling description and membrane-metal ion interaction. J Membr Sci. 2009;345:191–200.

[47] Ennigrou DJ, Gzara L, Romdhane MRB, Dhahbi M. Cadmium removal from aqueous solutions by polyelectrolyte enhanced ultrafiltration. Desalination. 2009;246:363–369.

[48] Huang Y, Du JR, Zhang Y, Lawless D, Feng X. Removal of mercury (II) from wastewater by polyvinylamine-enhanced ultrafiltration. Sep Purif Technol. 2015;154:1–10.

[49] Huang Y, Wu D, Wang X, Huang W, Lawless D, Feng X. Removal of heavy metals from water using polyvinylamine by polymer-enhanced ultrafiltration and flocculation. Sep Purif Technol. 2016;158:124–136.

[50] Valle H, Sánchez J, Rivas BL. Poly(N-vinylpyrrolidone-co-2-acrylamido-2-methylpropanesulfonate sodium): Synthesis, characterization, and its potential application for the removal of metal ions from aqueous solution. J Appl Polym Sci. 2015;132:41272.

[51] Tongwen X, Weihua Y. Industrial recovery of mixed acid (HF+HNO3) from the titanium spent leaching solutions by diffusion dialysis with a new series of anion exchange membranes. J Membr Sci. 2003;220:89–95.

[52] Guiqing Z, Qixiu Z, Kanggen Z. Acid recovery from waste sulfuric acid by diffusion dialysis. J Cent South Univ Technol. 1999;6:103–106.

[53] Luo J, Wu C, Xu T, Wu Y. Diffusion dialysis-concept, principle and applications. J Membr Sci. 2011;366:1–16.

[54] Oh SJ, Moon SH, Davis T. Effects of metal ions on diffusion dialysis of inorganic acids. J Membr Sci. 2000;169:95–105.

[55] Jeong J, Kim MS, Kim BS, Kim SK, Kim WB, Lee JC. Recovery of H2SO4 from waste acid solution by a diffusion dialysis method. J Hazard Mater. 2005;124:230–235.

[56] Palaty Z, Žakova A. Separation of H2SO4+ CuSO4 mixture by diffusion dialysis. J Hazard Mater. 2004;114:69–74.

[57] Donnan FG. The theory of membrane equilibria. Chem Rev. 1924;1:73–90.

[58] Sato K. Effects of the feed solution concentration on the separation degree in Donnan dialysis for binary systems of amino acids. J Membr Sci. 2002;196:211–220.

[59] Altintas O, Tor A, Cengeloglu Y, Ersoz M. Removal of nitrate from the aqueous phase by Donnan dialysis. Desalination. 2009;239:276–282.

[60] Ng PK, Snyder DD. Effect of concentration on ion transport in Donnan dialysis. J Electrochem Soc. 1983;130:2363–2365.

[61] Davis TA. Donnan Dialysis. In Encyclopedia of Desalination and Water Resources; EOLSS Publishers Co, Paris, 2010; Vol. 2, 1701-1707.

[62] Wang Q, Lenhart JL, Walker HW. Recovery of metal cations from lime softening sludge using Donnan dialysis. J Membr Sci. 2010;360:469–475.

[63] Çengeloğlu Y, Kir E, Ersöz M. Recovery and concentration of Al(III), Fe(III), Ti(IV), and Na(I) from red mud. J Coll Interface Sci. 2001;244:342–346.

[64] Wiśniewski J, Różańska A. Donnan dialysis for hardness removal from water before electrodialytic desalination. Desalination. 2007;212:251–260.

[65] Tapiero Y, Sanchez J, Rivas BL. Ion-selective interpenetrating polymer networks supported inside polypropylene microporous membranes for the removal of chromium ions from aqueous media. Polym Bull. 2016;73:989–1013.

[66] Prochaska K, Staszak K, Woźniak-Budych MJ, Regel-Rosocka M, Adamczak M, Wiśniewski M, et al. Nanofiltration, bipolar electrodialysis and reactive extraction hybrid system for separation of fumaric acid from fermentation broth. Bioresour Technol. 2014;167:219–225.

[67] Fu F, Wang Q. Removal of heavy metal ions from wastewaters: A review. J Environ Manag. 2011;92:407–418.

[68] Mohammadi T, Razmi A, Sadrzadeh M. Effect of operating parameters on Pb2+ separation from wastewater using electrodialysis. Desalination. XXXX;167:379–385 .

[69] Mohammadi T, Moheb A, Sadrzadeh M, Razmi A. Modeling of metal ion removal from wastewater by electrodialysis. Sep Purif Technol. 2005;41:73–82.

[70] Zheng Y, Gao X, Wang X, Li Z, Wang Y, Gao C. Application of electrodialysis to remove copper and cyanide from simulated and real gold mine effluents. RSC Adv. 2015;5:19807–19817.

[71] Tzanetakis N, Taama WM, Scott K, Jachuck RJJ, Slade RS, Varcoe J. Comparative performance of ion exchange membranes for electrodialysis of nickel and cobalt. Sep Purif Technol. 2003;30: 113–127.

[72] Flett DS. Solvent extraction in hydrometallurgy: The role of organophosphorus extractants. J Organomet Chem. 2005;690:2426–2438.

[73] Sgarlata C, Arena G, Longo E, Zhang D, Yang Y, Bartsch RA. Heavy metal separation with polymer inclusion membranes. J Memb Sci. 2008;323:444–451.

[74] Pont N, Salvadó V, Fontàs C. Selective transport and removal of Cd from chloride solutions by polymer inclusion membranes. J Membr Sci. 2008;318:340–345.

[75] Baczynska M, Rzelewska M, Regel-Rosocka M, Wisniewski M. Transport of iron ions from chloride solutions using cellulose triacetate matrix inclusion membranes with an ionic liquid carrier. Chem Pap. 2015;70:172–179.

[76] Pospiech B. Application of phosphonium ionic liquids as ion carriers in polymer inclusion membranes (PIMs) for separation of cadmium(II) and copper(II) from aqueous solutions. J Solution Chem. 2015;44:2431–2447.

[77] Iben Nasser I, Ibn El Haj Amor F, Donato L, Algieri C, Garofalo A, Drioli E, et al. Removal and recovery of Ag(CN)2- from synthetic electroplating baths by polymer inclusion membrane containing Aliquat 336 as a carrier. Chem Eng J. 2016;295:207–217.

[78] Sangtumrong S, Ramakul P, Satayaprasert C, Lothongkum AW. Purely separation of mixture of mercury and arsenic via hollow fiber supported liquid membranes. J Ind Eng Chem. 2007;5(7): 751–756.

[79] Pancharoen U, Poonkuma W, Lothongkum AW. Treatment of arsenic ions from produced water through hollow fiber supported liquid membrane. J Alloy Comp. 2009;482:328–334.

[80] Pathak PN, Ansari SA, Prabhu DR, Kanekar AS, Mohapatra PK, Manchanda VK. Selective recovery of uranium from THOREX feed by hollow fibre supported liquid membrane technique containing di(2-ethylhexyl) isobutyramide (D2EHIBA) as the carrier. Radiochim Acta. 2010;98: 259–266.

[81] Kumar A, Haddad R, Benzal G, Ninou R, Sastre AM. Use of modified membrane carrier system for recovery of gold cyanide from alkaline cyanide media using hollow fiber supported liquid membranes: Feasibility studies and mass transfer modeling. J Membr Sci. 2000;174:17–30.

[82] Rout PC, Sarangi K. Separation of vanadium using both hollow fiber membrane and solvent extraction technique – A comparative study. Sep Purif Technol. 2014;122:270–277.

[83] Rathore NS, Sonawane JV, Kumar A, Venugopalan AK, Singh RK, Bajpai DD, et al. Hollow fiber supported liquid membrane: A novel technique for separation and recovery of plutonium from aqueous acidic wastes. J Membr Sci. 2001;189(1):119–128.

[84] Alonso AI, Pantelides CC. Modelling and simulation of integrated membrane processes for the recovery of Cr (VI) with Aliquat 336. J Mem Sci. 1996;110:151–167.

[85] Agarwal S, Reis MTA, Ismael CRM, Carvalho JMR. Zinc extraction with Ionquest 801 using pseudo-emulsion based hollow fibre strip dispersion technique. Sep Purif Technol. 2014;127: 149–156.

[86] Wieszczycka K, Regel-Rosocka M, Staszak K, Wojciechowska A, Reis MTA, Ismael MRC, et al. Recovery of zinc(II) from chloride solutions using pseudo-emulsion based hollow fiber strip dispersion (PEHFSD) with 1-(3-pyridyl)undecan-1-one oxime or tributylphosphate. Sep Purif Technol. 2015;154(5):204–210.

[87] Sonawane JV, Pabby AK, Sastre AM. Pseudo-emulsion based hollow fibre strip dispersion (PEHFSD) technique for permeation of Cr(VI) using Cyanex- 923. J Hazard Mater. 2010;174: 541–547.

[88] Alguacil FJ, Garcia-Diaz I, Lopez F, Sastre AM. Cobalt(II) membrane extraction by DP-8R/Exxsol D100 using pseudo-emulsion based hollow fiber strip dispersion (PEHFSD) processing. Sep Purif Technol. 2011;80:467–472.

[89] Sonawane JV, Pabby AK, Sastre AM. Pseudo-emulsion based hollow fiber strip dispersion: A novel methodology for gold recovery. Aiche J. 2008;54(2):453–463.

[90] Agarwal S, Reis MTA, Ismael MRC, Correia MJN, Carvalho JMR. Application of pseudo-emulsion based hollow fibre strip dispersion (PEHFSD) for the recovery of copper. Sep Purif Technol. 2013;102:103–110.

[91] Fritz JS, Story JN. Selectivity behavior of low-capacity, partially sulfonated, macroporous resin beads. J Chrom A. 1974;90(2):267–274.

[92] DaBrowski A, Hubicki Z, Podkościelny P, Robens E. Selective removal of the heavy metal ions from waters and industrial wastewaters by ion-exchange method. Chemosphere. 2004;56(2): 91–106.

[93] Alexandratos SD. Ion-exchange resins: A retrospective from. Ind Eng Chem Res. 2009;48: 388–398.

[94] Rengaraj S, Kyeong-Ho Y, So-Young K, Jong-Un L, Kyung-Woong K, Moon S-H. Studies on adsorptive removal of Co(II), Cr(III) and Ni(II) by IRN77 cation-exchange resin. J Hazard Mat. 2002;B92:185–198.

[95] Gode F, Pehlivan E. Removal of chromium (III) from aqueous solutions using Lewatit S 100: The effect of pH, time, metal concentration and temperature. J Hazard Mater. 2006;136:330–337.

[96] Mendes FD, Martins AH. Recovery of nickel and cobalt from acid leach pulp by ion exchange using chelating resin. Min Eng. 2005;18(9):945–954.

[97] Yua Z, Qia T, Qua J, Wanga L, Chu J. Removal of Ca(II) and Mg(II) from potassium chromate solution on Amberlite IRC 748 synthetic resin by ion exchange. J Hazard Mat. 2009;167: 406–417.

[98] Smolik M, Jakóbik-Kolon A, Porański M. Separation of zirconium and hafnium using Diphonix® chelating ion-exchange resin. Hydrometallurg. 2009;95:350–353.

[99] Ritter JA, Bibler JP. Removal of mercury from waste water: Large-scale performance of an ion exchange process. Water Sci Technol. 1992;25:165–172.

[100] Gode F, Pehlivan E. Removal of Cr(VI) from aqueous solution by two Lewatit-anion exchange resins. J Hazard Mat. 2005;B119:175–182.

[101] Diniz CV, Doyle FM, Ciminelli VST. Effect of pH on the adsorption of selected heavy metal ions from concentrated chloride solutions by the chelating resin Dowex M-4195. Sep Sci Technol. 2002;37:3169–3185.

[102] Rivas BL, Sánchez J, Urbano BF. Polymers and nanocomposites: Synthesis and metal ion pollutant uptake. Polym Int. 2016;65:255–267.

[103] Hristovski K, Baumgardner A, Westerhoff P. Selecting metal oxide nanomaterials for arsenic removal in fixed bed columns: From nanopowders to aggregated nanoparticle media. J Hazard Mater. 2007;147:265–274.

[104] Kołodyńska D, Kowalczyk M, Hubicki Z, Shvets V, Pavlovich BI. Effect of accompanying ions and ethylenediaminedisuccinic acid on heavy metals sorption using hybride materials Lewatit FO 36 and Purolite Arsen Xnp. Chem Eng J. 2015;276:376–387.

[105] Shao W, Li X, Cao Q, Luo F, Li J, Du Y. Adsorption of arsenate and arsenite anions from aqueous medium by using metal(III)-loaded Amberlite resins. Hydrometallurgy. 2008;91:138–143.

[106] Balaji T, Yokoyama T, Matsunaga H. Adsorption and removal of As(V) and As(III) using Zr-loaded lysine diacetic acid chelating resin. Chemosphere. 2005;59(8):1169–1174.

[107] Ahmadi M, Teymouri P, Setodeh A, Mortazavi MS, Asgari A. Adsorption of Pb (II) from aqueous solution onto Lewatit FO36 nano resin: Equilibrium and kinetic studies. Envir Eng Manag J. 2011;10(10):1579–1587.

[108] Sylvester P, Westerhoff P, Möller T, Badruzzaman M, Boyd O. A hybrid sorbent utilizing nanoparticles of hydrous iron oxide for arsenic removal from drinking water. Environ Eng Sci. 2007;24(1):104–112.

[109] Pan B, Qiu H, Pan B, Nie G, Xiao L, Lv L, et al. Highly efficient removal of heavy metals by polymer-supported nanosized hydrated Fe(III) oxides: Behavior and XPS study. Water Res. 2010;44(3):815–824.

[110] Pan BC, Zhang QR, Zhang WM, Pan BJ, Du W, Lv L, et al. Highly effective removal of heavy metals by polymer-based zirconium phosphate: A case study of lead ion. J Colloid Interface Sci. 2007;310(1):99–105.

[111] Lenoble V, Chabroullet C, Shukry R, Serpaud B, Deluchat V, Bollinger J-C. Dynamic arsenic removal on a MnO2-loaded resin. J Colloid Interface Sci. 2004;280(1):62–67.

[112] Warshawsky A, Berkovitz H. Hydroxyoxime solvent impregnated resins for selective copper extraction. Trans Inst Min Metall Sect C. 1979;88 c36–c43.

[113] Jerabek K, Hankova L, Strikovsky AG, Warshawsky A. Solvent impregnated resins: Relation between impregnation process and polymer support morphology I. Di(2-ethylhexyl)-dithiophosphoric acid. React Funct Polym. 1996;28:201–207.

[114] Cortina JL, Miralles N, Aguilar M, Sastre AM. Solvent impregnated resins containing di(2-ethylhexyl)phosphoric acid. I. Preparation and study of the retention and distribution of the extractant on the resin. Solvent Ext Ion Exch. 1994;12:349–369.

[115] Cortina JL, Miralles N, Sastre AM, Aguilar M, Profumo A, Pesavento M. Solvent impregnated resins containing di(2,4,4-trimethylpentyl)phosphinic acid. I. Comparative study of di(2,4,4-trimethylpentyl)phosphinic acid adsorbed on Amberlite XAD-2 and dissolved in toluene. React Polym. 1993;21:89–101.

[116] Villaescusa I, Salvadó V, De Pablo J, Valiente M, Aguilar M. Liquid-solid extraction of gold(III) from aqueous chloride solutions by macroporous resins impregnated with tributyl phosphine sulfide (Cyanex 471). React Polym. 1992;17(1):69–73.

[117] Kabay N, Cortina JL, Trochimczuk A, Streat M. Solvent-impregnated resins (SIRs) – methods of preparation and their applications. React Funct Polym. 2010;70:484–496.

[118] Muraviev D, Ghantous L, Valiente M. Stabilization of solvent impregnated resin capacities by different techniques. React Funct Polym. 1998;38:259–268.

[119] Alexandratos SD, Smith SD. High stability solvent impregnated resins: Metal ion complexation as a function of time. Solv Extr Ion Exch. 2004;22(4):713–720.

[120] Trochimczuk AW, Kabay N, Arda M, Streat M. Stabilization of solvent impregnated resins (SIRs) by coating with water soluble polymers and chemical crosslinking. React Funct Polym. 2004;59(1):1–7.

[121] Muraviev D, Ghantous L, Valiente M. Stabilization of solvent-impregnated resin capacities by different techniques. React Funct Polym. 1998;38(2-3):259–268.

[122] Vaughan J, Dieters C, Fu Weng BK. Properties of Lewatit® TP272, a commercial solvent impregnated cation exchange resin for cobalt recovery. Miner Eng. 2016;88:2–8.

[123] Kamio E, Matsumoto M, Kondo K. Theoretical development of metal extraction mechanism into an extractant-impregnated microcapsule. Ind Eng Chem Res. 2007;46:255–265.

[124] Juang RS, Lin HC. Metal sorption with extractant-impregnated macroporous resins. 1. Particle diffusion kinetics. J Chem Technol Biotechnol. 1995;62(2):132–140.

[125] Juang RS, Lee SH. Metal sorption with extractant-impregnated macroporous resins. 2. Chemical reaction and particle diffusion kinetics. J Chem Technol Biotechnol. 1995;62(2): 141–147.

[126] Jarvis NV. Small-scale recovery and separation of actinides using tri-n-butyl phosphate extraction chromatography. Solv Extr Ion Exch. 1989;7(6):1077–1088.

[127] Alford CE, Navratil JD. Tributyl-phosphate-impregnated sorbents for plutonium-uranium separations. Golden, CO: Rockwell International Corp.. Rocky Flats Plant XXXX.

[128] Cortina JL, Miralles N, Aguilar M, Sastre AM. Extraction studies of Zn(II), Cu(II) and Cd(II) with impregnated and levextrel resins containing Di(2-ethylhexyl)phosphoric acid. Hydrometallurgy. 1994;36(2):131–142.

[129] Jha MK, Kumar V, Lee J-C. Processing of electroplating effluent for the recovery of zinc and chromium using ion exchange technique. In: Davis B, Free M, editors. Proceedings of International Symposium of resource recycling, 2007, resource recycling. Haevichi, Jeju, S. Korea: TMS (The Minerals, Metals and Materials Society), 2007:77–86.

[130] Vaughan J, Dieters C, Fu W, Byrne K. Properties of Lewatit® TP272, a commercial solvent impregnated cation exchange resin for cobalt recovery. Miner Eng. 2015;88:2–8.

[131] Yoshizuka K, Sakomoto Y, Baba Y, Inoue K. Distribution equilibria in the adsorption of cobalt (II) and nickel(II) on Levextrel resin containing Cyanex 272. Hydromettalurgy. 1990;23(2-3): 309–318.

[132] Korovin V, Shestak Y, Pogorelov Y, Cortina J-L. Solid polymeric extractants (TVEX): Synthesis, extraction characterization and applications for metal extraction process. In: Aguilar M, Cortina J-L, editors. Solvent extraction and liquid membranes: Fundamentals and applications in new materials. London – New York: CRC Press, 2008:261–299.

[133] Kremliakova N, Barsukova KV, Myasoedov BF. Behaviour of transplutonium and rare earth elements on TVEX III. Nitric acid solutions. J Radioanal Nucl Chem. 1988;122(1):3–11.

[134] Korovin VY, Shestak YG. Scandium extraction from hydrochloric acid media by Levextrel-type resins containing di-isooctyl methyl phosphonate. Hydrometallurgy. 2009;95:346–349.

[135] Chen JH, Kao Y, Lin CH, Yang FR. Surface modification of Amberlite XAD-4 resin with D2EHPA by a two-step, solvent–nonsolvent procedure and the application on the selective separation of lead and copper ions. Sep Sci Tech. 2004;39:2067–2090.

[136] Juang R-S, Su J-Y. Separation of zinc and copper from aqueous sulfate solutions using bis(2-ethylhexyl)phosphoric acid-impregnated macroporous resin. Ind Eng Chem Res. 1992;31:2783–2794.

[137] Belkhouche NE, Didi MA. Extraction of Bi(III) from nitrate medium by D2EHPA impregnated onto Amberlite XAD-1180. Hydrometallurgy. 2010;103:60–67.

[138] Negrea A, Ciopec M, Lupa L, Davidescu CM, Popa A, Ilia G, et al. Removal of As-V by Fe-III-loaded XAD7 impregnated resin containing di(2-ethylhexyl) phosphoric acid (DEHPA): Equilibrium, kinetic, and thermodynamic modeling studies. J Chem Eng Data. 2011;56(10): 3830–3838.

[139] Matsunaga H, Ismail A, Wakui Y, Yokoyama T. Extraction of rare earth elements with 2-ethylhexyl hydrogen 2-ethylhexyl phosphonate impregnated resins having different morphology and reagent content. React Func Polym. 2001;49(3):189–195.

[140] Reyes LH, Medina IS, Mendoza RN, Vazquez JR, Rodriguez MA, Guibal E. Extraction of cadmium from phosphoric acid using resins impregnated with organophosphorus extractants. Ind Eng Chem Res. 2001;40(5):1422–1433.

[141] Kabay N, Demircioğlu M, Ekinci H, Yüksel M, Sağlam M, Streat M. Extraction of Cd(II) and Cu(II) from phosphoric acid solutions by solvent-impregnated resins (SIR) containing Cyanex 302. React Func Polym. 1998;38:219–226.

[142] Gonzales MP, Saucedo I, Navarro R, Avila M, Guibal E. Selective separation of Fe(III), Cd(II) and Ni(II) from dilute solutions using solvent impregnated resins. Ind Eng Chem Res. 2001;40(25): 6004–6013.

[143] Saitoh T, Nakane F, Hiraide M. Preparation of trioctylamine-impregnated polystyrene-divinylbenzene porous resins for the collection of precious metals from water. Ind Eng Chem Res. 2007;67(3):247–252.

[144] Moon JK, Han Y, Jung C, Lee E, Lee B. Adsorption of rhenium and rhodium in nitric acid solution by Amberlite XAD4 impregnated with Aliquat 336. Korean J Chem Eng. 2006;23(2):303–308.

[145] Kabay N, Arda M, Saha B, Streat M. Removal of Cr(VI) by solvent impregnated resins (SIR) containing Aliquat 336. React Funct Polym. 2003;54(1–3):103–115.

[146] Rovira M, Hurtado L, Cortina JL, Arnaldos J, Sastre AM. Recovery of palladium(II) from hydrochloric acid solutions using impregnated resins containing Alamine 336. React Funct Polym. 1998;38(2–3):279–287.

[147] Gallardo V, Navarro R, Saucedo I, Avila M, Guibal E. Zinc(II) extraction from hydrochloric acid solutions using Amberlite XAD-7 impregnated with Cyphos IL 101 (tetradecyl(trihexyl) phosphonium chloride). Sep Sci Technol. 2008;43:2434–2459.

[148] Arias A, Saucedo I, Navarro R, Gallardo V, Martinez M, Guibal E. Cadmium(II) recovery from hydrochloric acid solutions using Amberlite XAD-7 impregnated with a tetraalkyl phosphonium ionic liquid. React Funct Polym. 2011;71(11):1059–1070.

Bartosz Tylkowski and Irene Tsibranska

9 Polymer application for separation/filtration of biological active compounds

Abstract: Membrane technology is an important part of the engineer's toolbox. This is especially true for industries that process food and other products with their primary source from nature. This review is focused on ongoing development work using membrane technologies for concentration and separation of biologically active compounds, such as polyphenols and flavonoids. We provide the readers not only with the last results achieve in this field but also, we deliver detailed information about the membrane types and polymers used for their preparation.

Keywords: asymmetric polymeric membranes, polyimide, metal-organic frameworks

9.1 Introduction

Bioactive compounds (BACs) from natural sources, extracted by appropriate solvent and further treated by membrane operations, are promising and intensively investigated area of scientific research in view of BAC separation or concentration. Polymer membranes, as well as the newer class of mixed matrix membranes (MMMs), are attractive for concentrating and/or selectively fractionating BACs contained in aqueous as well as non-aqueous extracts from different natural sources. A large number of potential applications are focused on their solvent resistancy and the ways to improve it, as can be seen in several review articles in the recent years [1–4]. Large areas for realization of these membrane separation techniques are the food industry [5, 6], the concentration and fractionation of value-added products from agro-industrial wastes [7] and the purification of thermally sensitive compounds as active pharmaceutical ingredients (APIs) and catalysts [8]. Among the numerous examples, important ultrafiltration (UF) and nanofiltration (NF) implementations can be cited in the recovery of polysaccharides and polyphenols from winery effluents [9, 10], or the fractionation of olive mill wastewaters [11, 12], where almost all polyphenols were recovered in the permeate solution from nanofiltration and subsequently concentrated by osmotic distillation. The recovery of valuable compounds found as subproducts in diluted effluents through membrane separation and concentration makes them attractive for use in the food, cosmetic and pharmaceutical industry.

https://doi.org/10.1515/9783110469745-009

9.1.1 Membranes used for separation of biologically active compounds

Widely used membranes are asymmetric polymeric membranes, especially in solvent-resistant applications. In general, they are inexpensive for fabrication and easy to scale-up, but their typical drawbacks concern membrane compaction and fouling, as well as thermal and chemical stability. Detailed reviews on the polymeric materials used for membrane preparation could be found in [2, 3]. Their basic configuration of dense selective layer supported by microporous structure, which can be of the same material (the integral type) or from a different one (the thin-film composite type), is the focus of numerous investigations including new membrane materials or membrane modifications. Examples can be found among the most commonly used polymers such as polyimide (PI) [13, 14], polyamide (PA) [15], polyacrylonitrile (PAN) [16], polyphenylsulfone (PPSU) [17, 18], polyether sulphone (PES) [19] and polypyrrole (PPy) [20], as well as in new directions like polyarylene sulfide sulfone (PASS) [21] or cross-linked polybenzimidazole membranes (PBIs) [22]. Enhancement of the membrane performance is searched through improving the permeance of the membrane after crosslinking [14], modulating the hydrophobic–hydrophilic behaviour of the membrane in the search of high rejection and reasonable flux in aqueous media [19], as well as membranes for use in organic media with enlarged ability to withstand harsh chemical environment [22]. In order to obtain higher membrane selectivity, able to serve specific separation needs, new membrane technologies involving molecular imprinting are used [23, 24] which overcome the limitations of the conventional size-exclusion membranes. In the same time, higher flux and preserved rejection values are observed with the molecularly imprinted membranes. Concerning the separation and purification capability in organic solvent medium, MMMs and metal–organic frameworks (MOFs) membranes have a great potential for implementation.

The MMMs are composite organic–inorganic membranes which can be designed to possess good chemical and mechanical stability, as well as rejection and flux and to overcome drawbacks such as flux decline due to compaction of polymeric membranes or their aging [4]. This is achieved by incorporating inorganic nanoparticles into the membrane matrix, which can be visualized as discrete particles in a continuous polymer phase. The connection between these two can be through covalent bonds, van der Waals forces or hydrogen bonds. Various metal oxide nanoparticles – TiO_2, ZnO, Fe_2O_3, Al_2O_3, silica-containing (SiO_2) or carbon fillers – are used. In the area of solvent-resistant nanofiltration, examples can be cited for embedding nanoparticles, containing Cu in PPSU-based membranes [25], Ti in crosslinked PI membranes [26], Zn in PA network [27], as well as zeolites in polydimethylsiloxane [28] or UZM-5 zeolite in PA [15], inorganic organosiloxane in PI [29], etc.

In all these cases, improved membrane compaction resistance was reported, which results in enhanced fluxes and better or unchanged rejection performance as compared to commercially available solvent-resistant polymeric nanomembranes [29] (e. g. Duramem™ 300, Evonik Membrane Technology Ltd Milton Keynes, UK), as well as in better chemical and thermomechanical properties.

Concerning flux decline and rejection with MMM, further development is searched for improving the adhesion between the polymer and the inorganic filler, thus avoiding a possible nonselective void formation. The latter is achieved by using MOFs, i. e. porous crystalline material, containing metal ions/clusters and organic linkers, which posses better affinity towards polymer chains. This structure possesses flexibility and mechanical strength characteristic of the polymer membranes, but incorporates the separation potential of MOFs. Investigations with potential application in organic solvent nanofiltration are directed to MOF–thin-film composite (TFC) membranes, as well as to integrally skinned asymmetric membranes, examples being given in [30, 31]. The TFC membrane structure – ultrathin selective layer and highly porous support – suppose smaller resistance to solvent flux, which is an advantage to integrally-skinned asymmetric membranes. Concerning the membrane morphology, an even MOF distribution throughout the membrane and across the membrane surface is achieved [32], and further possibilities are searched in the use of MOFs with different pore sizes in view of the molecular weight cut-offs. Successful applications of the MMMs are found in:

- In olive oil wastewater treatment [33], the hydrophobicity of the polyethersulfone membrane is modified by the concentration of functionalized multiwall carbon nanotube (F-MWCNT) in the membrane structure, improved antifouling properties were obtained, resulting in reduced flux decline and high rejections through Chemical Oxygen Demand (COD) and total phenols in the olive oil wastewater;
- API purification, employing PI-based membranes incorporating anorganic–inorganic hybrid network (3-aminopropyl trimethoxysilane
- APTMS as crosslinking agent and organosilicone precursor). A review of organic solvent membrane application in the pharmaceutical industry for solvent recovery and API purification is given in [34] including peptide and oligonucleotide production, removal of excess reagents and removal of APIs from organic solvents.

9.1.2 Concentration and purification of bioactive compounds from natural extracts

An area of special interest to this chapter is the application of membrane separations in organic solvents coupled with solid–liquid extraction for production of high-value products from natural plant extracts [35]. The latter are multicomponent with complex chemical structure of the individual compounds depending on the number of aromatic rings, hydroxyl, carboxylic groups, etc., and are characterized by a large molecular weight (MW) distribution and different molecular polarity. Examples are the phenolic compounds and their numerous non-flavonoid and flavonoid representatives, whose MW typically ranges between 100 and over 600 Da. Additional intermolecular solute or solute–solvent interactions can result in bigger molecular structures, which determine the wider use of ultrafiltration and nanofiltration membranes. Examples for such applications and analysis of the separation behaviour depending on the pore sizes of the membrane are reviewed in [36] in order to distinguish the effects of molecular sieving mechanism, polarity and solute–solvent interactions. The authors discuss the possibilities to achieve better flexibility of the membrane or membrane sequence (UF-NF) for particular separations taking into account the biological activity, for instance the removal of “heavier” phenolic classes without affecting the overall antioxidant properties of the permeate. Examples are given concerning successful UF separations of low and high MW: anthocyanins from winery sludge extract; proanthocyanidins from grape seeds extract; pectin from phenols in olive mill wastewater; hydroxycinnamic acids and flavanones from blood orange juice etc. [36].

The multicomponent character and unique bioactive properties of the natural extracts from different plants, sometimes with large MW distribution profile and very different solubility, make them a challenge for membrane separation on a molecular level exploring the potential of organic solvent nanofiltration (OSN).

Table 9.1 summarizes recently reported investigations, representative for the application of polymeric membranes in separating/concentrating biologically active compounds from natural extracts. The interest in combining membrane filtration with solid-phase extraction is to improve the amount of BACs extracted from plant materials provided that membranes with high rejections and reasonable permeate fluxes are selected. By *concentrating* the extracts new potential applications areas are offered for these natural extracts as preservatives and functional ingredients for food, cosmetic, nutraceutical and medical uses. Examples are the concentrated through NF rosemary extract [37]; the almost 100 % retention of anthocyanins in roselle extract using a sequence of UF and NF membranes [38]; the concentration of water–ethanolic extracts from propolis with over 95 % rejections towards flavones, flavonols, flavanones, dihydroflavonols as well as total phenolic substances [39–41]. On the other hand, the possibility for *fractionating* the extracts, thus obtaining fractions enriched in target BACs, is another promising perspective, though it is more difficult for realization. The reason is the complex mechanism involved in pressure-driven membrane separations on a molecular level, where the molecular sieving mechanism is not enough to explain the permeance of the solutes, but also

Table 9.1: Summary of applications of polymeric membranes to separate/concentrate biologically active compounds from natural extracts. Table 9.1.I. Aqueous extracts.

Extracted material	Membrane Proc.	Membrane material (Manufacturer)	MWCO	Filtration module	Composition	Ref.
Grape seeds	UF	Fluoropolymer: FSM0, 15PP (Alfa Laval) Polyethersulphone (PES): UP150 (Nadir) Polyvinylidene difluoride (PVDF): UV050 (Nadir)	150 kDa 50 kDa	Dead-end stirred cell	Total polyphenols (as gallic acid equivalent)	[53]
Jamun seed *Syzygium cumini* (L.)	UF⇒ NF	Polyethersulphone (PES): UF supplied by M/s Alfa Laval Pvt. Ltd., India NF supplied by M/s. Permionics Membranes Pvt. Ltd., India	100 kDa 250 Da	Flat sheet, cross-flow Dead-end stirred cell	Total polyphenols (as gallic acid equivalent); total flavonoids (as quercetin equivalent)	[54]
Roselle extract	UF	Composite polyamide: GE, Thin film: GH, GK (GE Osmonics); Polyethersulphone: UP005, UP020, UP150; UH030, UH050 (Microdyn-Nadir)	1–150 kDa	Flat sheet, cross-flow	Anthocyanins: delphinidin 3-xylo-syl-glucoside (delphinidin 3-sambu-bioside or hibiscin); cyanidin 3-xylosyl-glucoside (cyanidin 3-sambubio-side or ossypicyanin);	[38]
	NF	Polyamide thin-film composite: NF90 (Dow); NF200, NF270 (FILMTEC); Crosslinked polyamide composite: UTC60 (TORAY); Composite: MPF36, MPF34 (Koch); Polyamide polysulfone, thin-film: DL, DK (GE Osmonics); Polyethersulphone: NP010, NP030 (Microdyn Nadir);	150–400 Da			
Bark residues from mate tree	NF	Polyvinylidene difluoride (PVDF) thin-film membrane: Desal HL2521TF (Osmonics, USA)	150–300 Da	Spiral module	Gallic, chlorogenic (5-caffeoyl quinic), 3,4-dihydroxyben zoic, 4,5-dicaffeoyl quinic acid; epigallocatechin gallate	[55, 56]

(*continued*)

Table 9.1: (*continued*)

Extracted material	Mem-brane Proc.	Membrane material (Manufacturer)	MWCO	Filtration module	Composition	Ref.
Soybeans	NF	Polyvinylidene difluoride (PVDF) (GE Osmonics, USA)	150–300	Spiral module	Malonyl and β-glucosides (genistin, daidzin, glycitin), aglycones (daidzein genistein, glycitein)	[57]
Castanea sativa leaves	UF	Modified polyethersulfone (Omega Membranes, Minisette, Pall Filtron)	5 and 10 kDa	Flat sheet, cross-flow incl. batch redilution of the retentate	Flavonoids (quercetin and cirsiliol), phenolic acids (gallic, protocatechuic and vanillic acids) and lignans (medioresinol)	[58, 59]
Olive-extracted oleuropein	NF	Aromatic polyamide on polysulfone support (PA/PS): DK Osmonics Desal, USA; DL Osmonics Desal, USA; Polyethylene glycine (PEG): G10 Osmonics Desal, USA; G5 Osmonics Desal, USA; Silicone on polysulfone support (SB/PS): MPF34 KOCH, USA; MPF36 KOCH, USA; MPF44 KOCH, USA Polyvinyl alcohol (PVA): NTR7250 Nitto Denko Co, JP Sulfonated polyether sulfone (SPES): NTR7410 Nitto Denko Co., JP; NTR7430 Nitto Denko Co., JP; NTR7450 Nitto Denko Co., JP;	150, 300 Da 1–2.5 kDa 200, 1000, 250 Da 300–400 17.5 kDa, 2 kDa, 700–800 Da	Dead-end stirred cell	Oleuropein	[60]

Table 9.1.II: Organic solvents.

Extracted material	Solvent	Process	Membrane material	MWCO	filtration module	Composition	Ref.
Pequi (*Caryocar brasiliense* Camb.)	EtOH–H_2O (95:5 v/v) H2O	NF	Polyamide (PA): NF 90, Filmtec, Dow Chemical Company, Sao Paulo, SP, Brazil)	200–300 Da	Dead-end stirred cell	Polyphenols, carotenoids	[61]
Cotinus coggygria	MeOH; EtOH (azeotr.); EtOH/H_2O (50/50); H_2O	NF	Crosslinked polyimide (Duramem, Evonik, UK)	200–900 Da	Dead-end flat sheet tangential	Polyphenols and flavonoids: gallic acid, catechin, quercetin, rutin	[62]
Persimmon	MeOH	UF	Polysulfone (Tianjin, Tianfang, China)	10 kDa	Hollow fiber	Polyphenols, including condensed tannin	[63]
Sage-Salvia officinalis L. (*Labiaceae* family)	EtOH–H_2O 50 % v/v	UF	Polysulfone (PSF) and polyacrylonitrile (PAN)-based membrane (prepared)	Not specified	Flat sheet tangential	Carnosic acid, carnosol and rosmarinic acid	[64]
Viscum album L. (*Loranthaceae*),	H_2O	UF	Polysulfone (PSF) and polyacrylonitrile (PAN) membrane	Not specified	Flat sheet tangential	Phenolic acids, flavonoids, carotenoids	[64]
Grape marc	EtOH–H_2O 0–100 %	NF	Advanced polyamide, (HAR SpA, Milan, Italy)	470 Da det. exp. with PEG of diff. MW	Spiral wound	Total phenols Catechin Quercetin Epicatechin Rutin	[65]

(*continued*)

Table 9.1.II: (*continued*)

Extracted material	Solvent	Process	Membrane material	MWCO	filtration module	Composition	Ref.
Grape seeds	MeOH-H_2O	NF⇒MF⇒UF NF⇒UF⇒MF⇒ UF (incl. diafil.)	AFC40: Polyamide (PA) ES404: Polyethersulphone (PES); PU608: Polysulphone (PS); PU120: Polysulphone (PS); FP200: Polyvinilidene fluoride (PVDF)	4 kDa 8 kDa 20 kDa 200 kDa	Monotubular	Oligomeric proanthocyani-dins; polyphenolic acids: cinnamic (coumaric, caffeic, ferulic, chlorogenic, neochlorogenic); flavonoids: flavan-3-ol (catechin, epicatechin, their polymers or esters with galactic acid or glucose)	[42]
Propolis,	EtOH–H_2O H_20; EtOH–H_2O	NF	NF90: Polyamide/polysulphone (Osmonics, USA) Crosslinked polyimide (Duramem, Evonik, UK)	180–300 Da 200–900 Da	Spiral wound filtration Dead-end filtration	Phenolic compounds and flavonoids – flavones, flavonols, flavanones, dihydro-flavonols (e. g. pinocembrin, pinobanksin, caffeic acid, quercetin, pinoban-ksin-methilether, p_coumaric acid, crysin)	[39–41, 43]
Sideritis	EtOH	NF	Crosslinked polyimide: Duramem (Evonik, UK): polyimide: StarmemTM 240:	300–500 Da	Dead-end flat sheet, tangential	Chlorogennic acid, lavandulifolioside,verbascoside, leucoseptiside, 7 flavonoid gluosides	[48–50]
St John's wort *(Hypericum perforatum L.)*	EtOH (96 %)	NF	Crosslinked polyimide Duramem (Evonik, UK polyimide: Starmem^{TM} 240	500 Da 400 Da	Dead-end stirred cell	Quercetin; catechin; hyperoside (quercetin 3-o-galactoside); hyperforin; hypericin; quercitrin (quercetin 3-o-rhamnoside); Isoquercitrin (quercetin 3-o-glucoside);	[47, 50]

(*continued*)

Table 9.1.II: (*continued*)

Extracted material	Solvent	Process	Membrane material	MWCO	filtration module	Composition	Ref.
Lemon balm	EtOH–H_2O	NF	Crosslinked polyimide: Duramem (Evonik, UK	200 Da	Dead-end stirred cell	Rosmarinic acid	[47]
Rosemary	EtOH	NF	Crosslinked polyimide: Duramem (Evonik, UK	200–500	Flat sheet, tangential	Rosmarinic acid	[37]
Cocoa seeds	EtOH	NF, RO	Commercial NF and RO membranes: NF: DL, HL (GEOsmonics), NF-90 (Film-tec-Dow). RO: SG (GE-Osmonics), BW-30 (Filmtec-Dow)	Retention charact. provided by manufactures 96–99.5 %	Dead end	Polyphenols (mono to decamers)	[66]
Thymus capitatus	Hexane, Acetonitrile, Methanol	NF UF	Polysulphone and polyamide (NF-DK; Desal 5 DK, Osmonics);		Dead end	Carnosic and rosmarinic acids	[67]
Artichoke (*Cynara scolymus* L.) wastes	EtOH–H_2O	NF	NF270: Polyamide thin-film composite; GE Osmonics: Polyamide; GE Osmonics: Cross-linked aromatic polyamide;	200–400 Da 200 Da 150–300 Da	Flat sheet tangential filtration	Phenolic acids: cynarin (1,5-dicaffeoylquinic acid) and chlorogenic acid (5-caffeoylquinic acid) flavonoid derivatives: Luteolin-7-glucoside, Apigenin-7-glucoside, flavones	[68]

(*continued*)

Table 9.1.II: (*continued*)

Extracted material	Solvent	Process	Membrane material	MWCO	filtration module	Composition	Ref.
Green tea Polyphenon-60	EtOH–H_2O 10–80 %	NF	Polysulphone/polydimethylsiloxane (PSF/PDMS) Desalination Systems, USA, G-5, G-10, G-20 and G-50 membranes; HC-50 and HR98PP, DOW Denmark A/S, Denmark; MPF-60, Abcor Tokyo, Japan and 960PP, DDS Filtration, Denmark.	Rejection characteristic only	Dead-end stirred cell	Polyphenols: catechins	[69]
Eucalyptus globulus bark	EtOH–H_2O 80/20 (v/v)	UF	Polyamide composite: GE 1, GE Osmonic Polyethersulfone PLEAIDE: P5, Orelis Env. Polyvinylidenefluoride: JW 30, GE Osmonic Polysulfone: EW 60.	1 kDa 5 kDa 30 kDa 60 kDa	Flat sheet tangential	Polyphenols	[70]
Tobacco leaves and waste	EtOH	NF	Duramem^{TM} (Evonik, UK): Crosslinked polyimide Starmem^{TM} 240: polyimide	300 Da 400 Da	Dead-end stirred cell	Chlorogenic acid and its isomers neochlorogenicacid (5-o-caffeoylquinic acid) and 4-o-caffeoylquinic acid; Rutin (quercetin-3-o-rutinoside) Kaempferol-3-rutinoside	[50, 71]

component solubility, as well as membrane hydrophobicity, polarity resistance and solute–solvent interactions have to be taken into account. An example could be the phenolic compounds as solute and the hydroethanolic solvent interacting with the nonpolar and polar sides within their molecules [36] which leads to improved solubility and preservation of the antioxidant properties of the latter. Positive examples for fractionation of BACs from multicomponent solutions originating from natural sources are also reported in the literature using membranes with different molecular weight cut-off (MWCO) [12, 42–45].

9.1.3 Recovery of extraction solvents

Successful concentration of the solutes supposes high membrane rejections and possibility for *recovery and direct solvent reuse*. In this case, membrane separation replaces fully or to some extent distillation/evaporation processes, showing improved environmental, safety and economical aspects. Applications of solvent recovery by OSN are reported in the pharmaceutical and the oil industry [46]. Examples are the commercial polymeric OSN membranes (Starmem 122 and Duramem 150), successfully tested for treating pharmaceutical/solvent mixtures [1]; separation of oil from different solvents [2]; solvent recovery from ethanolic extract of rosemary, lemon balm [37, 47] (Duramem 200) and Sideritis (Duramem 300) [48–50] where the reuse of the permeate as solvent proved equal and even better extraction capability and considerably reduced the required solvent volume. This solvent recovery as compared to the traditional distillation process has also the advantage of being a greener alternative for separation of solvents, requesting mild conditions and providing reduced volumes of toxic solvent effluents to the environment and lower energy consumption (the effect being stronger for solvents with higher boiling point). Further development of tighter membranes for removal of small solutes by OSN is pointed out as important in view of solvent purification in fine chemistry processing, in order to explore the potential of OSN as sustainable and competitive to other purification technologies [46].

The use of natural and renewable sources of BACs combined with membrane separation techniques that can be viewed as environmentally friendly makes the whole process to be classified as a green one. In the scope of a green technology also, the production of the polymer membranes has to be taken into account. The latter has been in the focus of recent publications of leading groups in the field of membrane technology and especially in organic media applications – the OSN separation process [46–52]. The idea is to reduce the discharge of hazardous chemicals as waste by replacing toxic solvents with environmentally friendly ones without worsening the membrane performance. Investigations are made with solvent-resistant PI membranes [51] as well as polyether ether ketone

(PEEK) membranes [52] and performed on bench and industrial scales. Concerning the membrane performance, the authors pointed out the need of research and optimization work in scaling-up.

Funding: This chapter was prepared under the projects with financial supports from: the National Science Fund at the Bulgarian Ministry of Education and Science, Contract No DN 07/11/15.12.2016, as well as Incoming Marie Curie TECNIOspring fellowship from People Programme (Marie Curies Actions) of the Seventh Framework Programme of the European Union (FP7/2007-2013) under REA grant agreement no. 600388 (TECNIOspring programme), and from the Agency for Business Competitiveness of the Government of Catalonia, ACCIÓ, which are gratefully acknowledged by the authors.

References

[1] Darvishmanesh S, Firoozpour L, Vanneste J, Luis P, Degreve J, van der Bruggen B. Performance of solvent resistant nanofiltration membranes for purification of residual solvent in the pharmaceutical industry: experiments and simulation. Green Chem. 2011;13:3476–3483.
[2] Vandezande P, Gevers LEM, Vankelecom IFJ. Solvent resistant nanofiltration: separating on a molecular level. Chem Soc Rev. 2008;37:365–405.
[3] Cheng XQ, Zhang YL, Wang ZX, Guo ZH, Bai YP, Shao L. Recent advances in polymeric solvent-resistant nanofiltration membranes. Adv Polymer Technol. 2014;33(S1) E1-E24.
[4] Marchetti P, Solomon MFJ, Szekely GY, Livingston AG. Molecular separation with organic solvent nanofiltration: a critical review. Chem Rev. 2014;114 10735–10806.
[5] Salehi F. Current and future applications for nanofiltration technology in the food processing. Food Bioprod Process. 2014;92:161–177.
[6] Ilame SA, Satyavir VS. Application of membrane separation in fruit and vegetable juice processing: a review. Crit Rev Food Sci Nutr. 2015;55(7):964–987.
[7] Galanakis CM. Emerging technologies for the production of nutraceuticals from agricultural by-products: a viewpoint of opportunities and challenges. Food Bioprod Process. 2013;91: 575–579.
[8] Kim JF, Székely G, Valtcheva IB, Livingston AG. Increasing the sustainability of membrane processes through cascade approach and solvent recovery – pharmaceutical purification case study. Green Chem. 2014;16:133–145.
[9] Giacobbo A, Oliveira M, Duarte ECNF, Mira HMC, Bernardes AM, de Pinho MN. Ultrafiltration based process for the recovery of polysaccharides and polyphenols from winery effluents. Sep Sci Technol. 2013;48:438–444.
[10] Giacobbo A, Bernardes AM, de Pinho MN. Nanofiltration for the recovery of low molecular weight polysaccharides and polyphenols from winery effluents. Sep Sci Technol. 2013;48: 2524–2530.
[11] Garcia-Castello E, Cassano A, Criscuoli A, Conidi C, Drioli E. Recovery and concentration of polyphenols from olive mill wastewaters by integrated membrane system. Water Res. 2010;44: 3883–3892.
[12] Cassano A, Conidi C, Giorno L, Drioli E. Fractionation of olive mill wastewaters by membrane separation techniques. J Hazard Mater. 2013;248–249:185–193.

[13] Soroko I, Sairam M, Livingston AG. The effect of membrane formation parameters on performance of polyimide membranes for organic solvent nanofiltration (OSN). Part C. Effect of polyimide characteristics. J Membr Sci. 2011;381:172–182.

[14] Xu YC, Cheng XQ, Long J, Shao L. A novel monoamine modification strategy toward high-performance organic solvent nanofiltration (OSN) membrane for sustainable molecular separations. J Membr Sci. 2016;497:77–89.

[15] Namvar-Mahboub M, Pakizeh M, Davari S. Preparation and characterization of UZM-5/polyamide thin film nanocomposite membrane for dewaxing solvent recovery. J Membr Sci. 2014;459:22–32.

[16] Wang J, Yue Z, Ince JS, Economy J. Preparation of nanofiltration membranes from polyacrylonitrile ultrafiltration membranes. J Membr Sci. 2006;286:333–341.

[17] Sani NAA, Lau WJ, Ismail AF. Influence of polymer concentration in casting solution and solvent–solute–membrane interactions on performance of polyphenylsulfone (PPSU) nanofiltration membrane in alcohol solvents. J Polym Eng. 2014;34:489–500.

[18] Darvishmanesh S, Jansen JC, Tasselli F, Tocci E, Luis P, Degreve J, et al. Novel polyphenylsulfone membrane for potential use in solvent nanofiltration. J Membr Sci. 2011;379:60–68.

[19] Shahmirzadi MAA, Hosseini SS, Ruan G, Tan NR. Tailoring PES nanofiltration membranes through systematic investigations of prominent design, fabrication and operational parameters. RSC Adv. 2015;5:49080–49097.

[20] Shao L, Cheng X, Wang Z, Ma J, Guo Z. Tuning the performance of polypyrrole-based solvent-resistant composite nanofiltration membranes by optimizing polymerization conditions and incorporating grapheme oxide. J Membr Sci. 2014;452:82–89.

[21] Liu L, Wang X, Wang Y, Li L, Pan K, Yang J, et al. Preparation and characterization of asymmetric polyarylene sulfide sulfone (PASS) solvent-resistant nanofiltration membranes. Mater Lett. 2014;132:11–14.

[22] Valtcheva IB, Kumbharkar SC, Kim JF, Bhole Y, Livingston AG. Beyond polyimide: crosslinked polybenzimidazole membranes for organic solvent nanofiltration (OSN) in harsh environments. J Membr Sci. 2014;457:62–72.

[23] Szekely G, Valtcheva IB, Kim JF, Livingston AG. Molecularly imprinted organic solvent nanofiltration membranes – revealing molecular recognition and solute rejection behavior. React Funct Polym. 2015;86:215–224.

[24] Valtcheva IB, Marchetti P, Livingston AG. Crosslinked polybenzimidazole membranes for organic solvent nanofiltration (OSN): analysis of crosslinking reaction mechanism and effects of reaction parameters. J Membr Sci. 2015;493:568–579.

[25] Sani NAA, Lau WJ, Ismail AF. Polyphenylsulfone-based solvent resistant nanofiltration (SRNF) membrane incorporated with copper-1,3,5-benzenetricarboxylate (Cu-BTC) nanoparticles for methanol separation. RSC Adv. 2015;5:13000–13010.

[26] Soroko I, Livingston A. Impact of TiO2 nanoparticles on morphology and performance of crosslinked polyimide organic solvent nanofiltration (OSN) membranes. J Membr Sci. 2009;343:189–198.

[27] Pal A, Dey TK, Singhal A, Bindala RC, Tewaria PK. Nano-ZnO impregnated inorganic–polymer hybrid thinfilm nanocomposite nanofiltration membranes: an investigation of variation in structure, morphology and transport properties. RSC Adv. 2015;5:34134–34151.

[28] Gevers LEM, Vankelecom IFJ, Jacobs PA. Zeolite filled polydimethylsiloxane (PDMS) as an improved membrane for solvent-resistant nanofiltration (SRNF). Chem Commun. 2005;19:2500–2502.

[29] Siddique H, Rundquist E, Bhole Y, Peeva LG, Livingston AG. Mixed matrix membranes for organic solvent nanofiltration. J Membr Sci. 2014;452:354–366.

[30] Zhu L, Yu H, Zhang H, Shen J, Xue L, Gaob C, et al. Mixed matrix membranes containing MIL-53(Al) for potential application in organic solvent nanofiltration. RSC Adv. 2015;5: 73068–73076.

[31] Campbell J, Davies RP, Braddock DC, Livingston AG. Improving the permeance of hybrid polymer/ metal–organic framework (MOF) membranes for organic solvent nanofiltration (OSN) – development of MOF thin films via interfacial synthesis. J Mater Chem A. 2015;3:9668–9674.

[32] Campbell J, Szekely G, Davies RP, Braddock DC, Livingston AG. Fabrication of hybrid polymer/ metal organic framework membranes: mixed matrix membranes versus in situ growth. J Mater Chem A. 2014;2:9260–9271.

[33] Zirehpour A, Rahimpour A, Jahanshahi M, Peyravi M. Mixed matrix membrane application for olive oil waste water. J Env Manag. 2014;132:113–120.

[34] Buonomenna MG, Bae J. Organic solvent nanofiltration in pharmaceutical industry. Sep Pur Rev. 2015;44(2):157–182.

[35] Tsibranska I, Tylkowski B. Concentration of polyphenols by integrated membrane operations. (DOI (Chapter 11): https://doi.org/10.1515/9783110285666.269) In: Cassano A, Drioli E, editors. Integrated membrane operations in the food production. De Gruyter, 2014:269–294.

[36] Galanakis CM. Separation of functional macromolecules and micromolecules: from ultrafiltration to the border of nanofiltration. Trends Food Sci Technol. 2015;42:44–63.

[37] Peshev D, Peeva L, Peev G, Baptista I, Boam A. Application of organic solvent nanofiltration for concentration of antioxidant extracts of rosemary (Rosmarinus officiallis L.). Chem Eng Res Des. 2011;89(3):318–327.

[38] Cissé M, Vaillant F, Pallet D, Dornier M. Selecting ultrafiltration and nanofiltration membranes to concentrate anthocyanins from roselle extract (Hibiscus sabdariffa L.). Food Res Int. 2011; 44(9):2607–2614.

[39] Tylkowski B, Trusheva B, Bankova V, Giamberini M, Peev G, Nikolova A. Extraction of biologically active compounds from propolis and concentration of extract by nanofiltration. J Membr Sci. 2010;348(1):124–130.

[40] Mello B, Petrus J, Hubinger M. Concentration of flavonoids and phenolic compounds in aqueous and ethanolic propolis extracts through nanofiltration. J Food Eng. 2010;96(4):533–539.

[41] Mello B, Petrus J, Hubinger M. Nanofiltration of aqueous propolis extracts and the effects of temperature, pressure and ph in the concentrated product. Stud Chem Technol (SCPT). 2013;1(4): 55–65.

[42] Santamaría B, Salazar G, Beltrán S, Cabezas JL. Membrane sequences for fractionation of polyphenolic extracts from defatted milled grape seeds. Desalination. 2002;148(1): 103–109.

[43] Tsibranska IH, Peev GA, Tylkowski B. Fractionation of biologically active compounds extracted from propolis by nanofiltration. J Membr Sci Technol. 1:2012;2011 .

[44] Donelian A, de Oliveira PF, Rodrigues AE, Mata VG, Machado RA. Performance of reverse osmosis and nanofiltration membranes in the fractionation and retention of patchouli essential oil. J Supercrit Fluids. 2016;107:639–648.

[45] Cassano A, Cabri W, Mombelli G, Peterlongo F, Giorno L. Recovery of bioactive compounds from artichoke brines by nanofiltration. Food Bioprod Process. 2016;98:257–265.

[46] Szekely G, Jimenez-Solomon MF, Marchetti P, Kim JF, Livingston AG. Sustainability assessment of organic solvent nanofiltration: from fabrication to application. Green Chem. 2014;16:4440–4473.

[47] Peev G, Penchev P, Peshev D, Angelov G. Solvent extraction of rosmarinic acid from lemon balm and concentration of extracts by nanofiltration: effect of plant pre-treatment by supercritical carbon dioxide. Chem Eng Res Des. 2011;89(11):2236–2243.

[48] Tylkowski B, Tsibranska I, Kochanov R, Peev G, Giamberini M. Concentration of biologically active compounds extracted from Sideritis ssp. L. by nanofiltration. Food Bioprod Process. 2011;89(4):307–314.

[49] Tsibranska I, Tylkowski B. Concentration of ethanolic extracts from Sideritis ssp. L. by nanofiltration: comparison of dead-end and cross-flow modes. Food Bioprod Process. 2013;91(2):169–174.

[50] Tsibranska I, Saykova I, Tylkowski B. Flux and rejection behavior in nanofiltration of polyphenols and flavonoids from plant extracts. Sci Works Univ. of Food Technol. 2015; LXII:514–518.

[51] Soroko I, Bhole Y, Livingston A. Environmentally friendly route for the preparation of solvent resistant polyimide nanofiltration membranes. Green Chem. 2011;13:162–168.

[52] da Silva Burgal J, Peeva L, Livingston A. Towards improved membrane production: using low–toxicity solvents for the preparation of PEEK nanofiltration membranes. Green Chem 2016;18: 2374–2384.

[53] Liu D, Vorobiev E, Savoire R, Lanoisellé JL. Intensification of polyphenols extraction from grape seeds by high voltage electrical discharges and extract concentration by dead-end ultrafiltration. Sep Pur Technol. 2011;81(2):134–140.

[54] Balyan U, Sarkar B. Integrated membrane process for purification and concentration of aqueous Syzygium cumini (L.) seed extract. Food Bioprod Process. 2016;98:29–43.

[55] Prudêncio APA, Prudêncio ES, Amboni RDC, Murakami ANN, Maraschin M, Petrus JCC, et al. Phenolic composition and antioxidant activity of the aqueous extract of bark from residues from mate tree (Ilex paraguariensis St. Hil.) bark harvesting concentrated by nanofiltration. Food Bioprod Process. 2012;90(3):399–405.

[56] Murakami ANN, Amboni RDC, Prudêncio ES, Amante ER, de Moraes Zanotta L, Maraschin M, et al. Concentration of phenolic compounds in aqueous mate (Ilex paraguariensis A. St. Hil) extract through nanofiltration. LWT Food Sci Technol. 2011;44(10):2211–2216.

[57] Benedetti S, Prudêncio ES, Mandarino JMG, Rezzadori K, Petrus JCC. Concentration of soybean isoflavones by nanofiltration and the effects of thermal treatments on the concentrate. Food Res Int. 2013;50(2):625–632.

[58] Dias-Reinoso B, Moure A, Domínguez H, Parajó JC. Membrane concentration of antioxidants from Castanea sativa leaves aqueous extracts. Chem Eng J. 2011;175:95–102.

[59] Munekata PES, Franco D, Trindade MA, Lorenzo JM. Characterization of phenolic composition in chestnut leaves and beer residue by LC-DAD-ESI-MS. LWT Food Sci Technol. 2016;68:52–58.

[60] Danmark I, Neves MA, Nabetani H, Isoda H, Sayadi S, Nakajima M. Transport properties of oleuropein through nanofiltration membranes. Food Bioprod Process. 2015;94:342–353.

[61] Machado MT, Mello BC, Hubinger MD. Study of alcoholic and aqueous extraction of pequi (Caryocar brasiliense Camb.) natural antioxidants and extracts concentration by nanofiltration. J Food Eng. 2013;117(4):450–457.

[62] Koleva V, Simeonov E. Solid liquid extraction of phenolic and flavonoid compounds from Cotinus coggygria and concentration by nanofiltration. Chem Biochem Eng Quart. 2015;28(4): 545–551.

[63] Gu HF, Li CM, Xu YJ, Hu WF, Chen MH, Wan QH. Structural features and antioxidant activity of tannin from persimmon pulp. Food Res Int. 2008;41(2):208–217.

[64] Roman GP, Neagu E, Radu GL. Antiradical activities of salvia officinalis and viscum album L. extracts concentrated by ultrafiltration process. Acta Sci Pol Technol Aliment. 2009;8(3): 47–58.

[65] Zagklis DP, Paraskeva CA. Purification of grape marc phenolic compounds through solvent extraction, membrane filtration and resin adsorption/desorption. Sep Pur Technol. 2015;156: 328–335.

[66] Sarmento LA, Machado RA, Petrus JC, Tamanini TR, Bolzan A. Extraction of polyphenols from cocoa seeds and concentration through polymeric membranes. J Supercrit Fluids. 2008;45(1): 64–69.
[67] Achour S, Khelifi E, Attia Y, Ferjani E, Noureddine Hellal A. Concentration of antioxidant polyphenols from Thymus capitatus extracts by membrane process technology. J Food Sci. 2012;77(6) C703-C709.
[68] Rabelo RS, Machado MT, Martínez J, Hubinger MD. Ultrasound assisted extraction and nanofiltration of phenolic compounds from artichoke solid wastes. J Food Eng. 2016;178: 170–180.
[69] Nwuha V. Novel studies on membrane extraction of bioactive components of green tea in organic solvents: part I. J Food Eng. 2000;44(4):233–238.
[70] Baptista EA, Pinto PCR, Mota IF, Loureiro JM, Rodrigues AE. Ultrafiltration of ethanol/water extract of Eucalyptus globulus bark: resistance and cake build up analysis. Sep Pur Technol. 2015;144:256–266.
[71] Tsibranska I, Karabojikova V, Jeliazkov J. Concentration of flavonoids in ethanolic extracts from tobacco leaves through nanofiltration. Bulg Chem Commun 2016;48(4):232.

Justyna Walkowiak-Kulikowska, Joanna Wolska and
Henryk Koroniak

10 Polymers application in proton exchange membranes for fuel cells (PEMFCs)

Abstract: This review presents the most important research on alternative polymer membranes with ionic groups attached, provides examples of materials with a well-defined chemical structure that are described in the literature. Furthermore, it elaborates on the synthetic methods used for preparing PEMs, the current status of fuel cell technology and its application. It also briefly discusses the development of the PEMFC market.

Keywords: proton exchange membrane, proton exchange membrane fuel cells, polymer electrolyte membrane, direct methanol fuel cell, fuel cells, Nafion

10.1 Introduction

Energy development, including energy production, distribution and consumption, is vital to any country that aims at constant progress. Given the steadily growing demand for energy and constantly dwindling resources of such fossil fuels as coal, oil and gas, more and more attention is earned by modern solutions that lead to stabilization of the energy market and reduce emissions, such as is the case with fuel cells (FCs).

Fuel cell technologies have been rapidly growing lately because many scientists find it a promising and efficient power generation alternative. Recently, proton exchange membrane fuel cells or polymer electrolyte membrane fuel cells (jointly abbreviated as PEMFCs) have progressed particularly dynamically. Many research groups seek to develop proton exchange membranes that will give high proton conductivity, low electronic conductivity, low fuel permeability, a low electro-osmotic drag coefficient, good chemical and thermal stability, favourable mechanical properties, sufficient durability, and a competitive cost of manufacture. Polymer membranes are the “heart” of PEM fuel cells, and therefore, chemists investigate new strategies for synthesizing materials that would be suitable for their production. There is no reason to believe that the polymeric membrane revolution will end any time soon. In this review, we elaborate on the synthesis of membranes and describe the different types of polymer systems for PEMFC technology.

https://doi.org/10.1515/9783110469745-010

10.2 Historical background

Despite their modern character, fuel cells have actually been known for more than 150 years [1] (Figure 10.1). The history of fuel cells goes back to the early nineteenth century, when Humphry Davy, a British chemist and physicist, first described in 1801 the concept of a fuel cell. Then, in 1838, "The Philosophical Magazine" published a pioneering paper by Christian Friedrich Schönbein, a German-Swiss chemist, describing the electrochemical reaction between hydrogen and oxygen. In 1842, these previous achievements encouraged William Grove, a British lawyer and amateur scientist, to design the first fuel cell that used hydrogen and oxygen to produce electricity [2]. The device was called a "gas voltaic battery" – now often termed as the

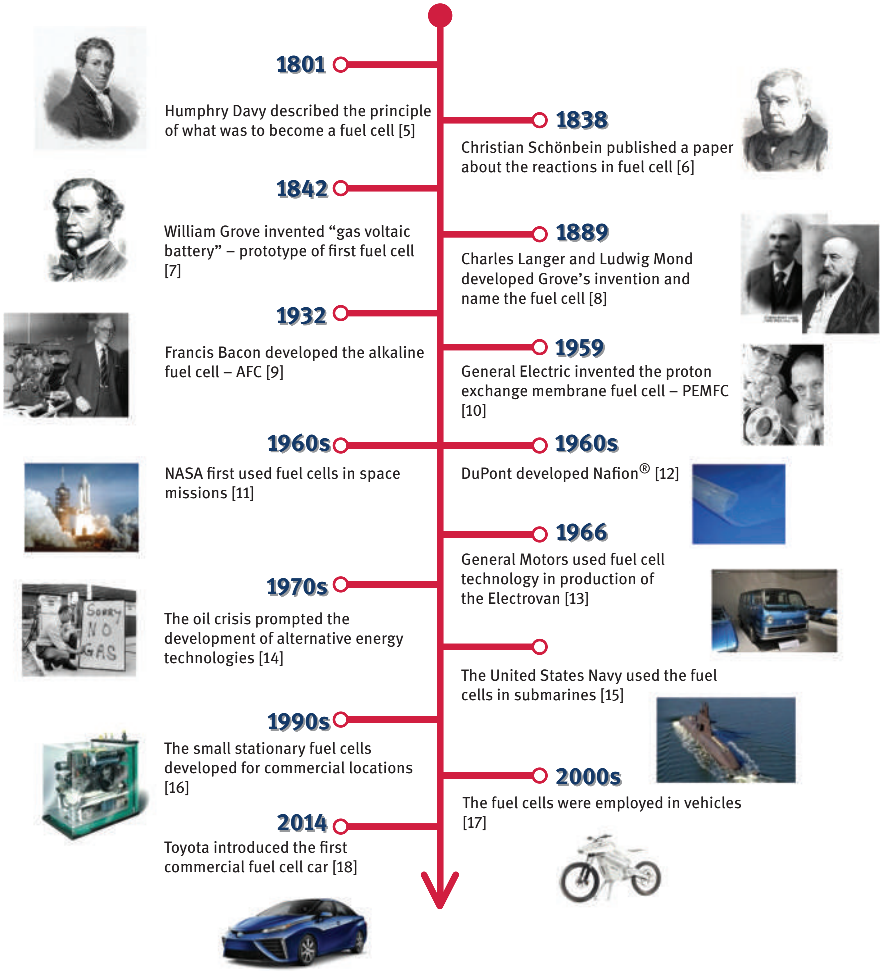

Figure 10.1: History of fuel cells [5–18].

“Grove battery”. It consisted of several cells containing platinum electrodes placed in two small upturned vessels, one filled with hydrogen, the other with oxygen, both immersed in a bath with diluted sulphuric acid as the electrolyte. Problems with the corroding electrodes and instability of the materials, however, rendered Grove’s fuel cell an impractical solution. The term “fuel cell” itself was first used in 1889 by Charles Langer and Ludwig Mond who attempted to build a fuel cell by using air and industrial coal gas. Development of the internal combustion engine pushed the fuel cell technology out of focus for over half a century. Extensive research was resumed in the 1930s, when Francis Bacon, a British chemical engineer, successfully revisited the concept of the fuel cell through a design by Langer and Mond. Already in 1932, Bacon developed a prototype alkaline fuel cell (AFC). He introduced nickel gauze electrodes and used molten potassium hydroxide as the electrolyte, replacing the sulphuric acid [3]. Over almost thirty years Bacon improved the design and presented in 1959 a first practical and operational alkaline fuel cell that could generate 5 kW of energy. The same year another team, working for Allis-Chalmers, built a tractor powered by alkaline fuel cells (AFCs). The machine was widely exhibited across the United States. Meanwhile, Willard Thomas Grubb and Lee Niedrach, working for General Electric, developed an alternative fuel cell technology: proton exchange membrane fuel cells (PEMFCs). The evolution of PEMs for fuel cell applications began in 1955, when GE developed a new fuel cell type based on partially sulphonated polystyrene sulphonic acid membranes. PEMFCs were even employed in the Gemini V space mission. Nonetheless, the Apollo Programme and subsequent space missions of Apollo-Soyuz, Skylab and Space Shuttle used Bacon-designed alkaline fuel cells.

In 1966, General Motors applied the fuel cell technology in ground transportation: the company manufactured the Electrovan, a concept car powered by hydrogen fuel cells. In the late 1960s, DuPont developed the first membrane based on polytetrafluoroethylene and perfluorovinyl ether, known under the tradename Nafion®. More and more companies initiated extensive research programmes aimed at eliminating the obstacles to commercial use of the fuel cell technology. The 1970s were the decade of growing environmental awareness of governments, companies and individuals. The oil crisis combined with the oil embargoes imposed by the Organization of the Petroleum Exporting Countries (OPEC) that began in 1973 refocused all the industrialized countries’ research efforts on the development of alternative methods of energy production. The world sought ways to reduce dependence on petroleum imports. In the 1980s, the United States Navy commissioned studies into the use of FCs in submarines, where their highly efficient, zero-emission, near-silent running offered considerable operational advantages. After some years, in the 1990s, the attention turned to fuel cell technology being used in small stationary applications. The governments of Germany, Japan and the UK offered dedicated funding for the development of new technologies suitable for residential micro-combined heat and power (micro-CHP) purposes. Fuel cells underwent meaningful developments and enhancements, leading to the modernization of various cell types such as a solid oxide fuel cell (SOFC), molten carbonate fuel cell (MCFC) or direct methanol fuel cell (DMFC). The previous decade was characterized by increasing concerns over energy efficiency, energy security and carbon dioxide emissions. In the 2000s, funding for fuel cell research increased remarkably and scientists focused on cost reduction and improving the operational performance to make fuel cells competitive with regard to conventional energy technology. State funding from the European Union, Canada, Japan, South Korea, and the United States had been targeted at fuel cell demonstration and deployment projects, primarily for stationary and transport fuel cells, and the related fuelling infrastructure. In the mid-2000s, buses became a promising application for fuel cells due to the combination of high efficiency, zero-emissions and ease of refuelling. In 2005, Intelligent Energy produced the first ENV (Emissions Neutral Vehicle): a motorcycle prototype completely designed for power fuel cells. The company successfully overcame the miniaturization barriers by employing direct methanol fuel cells (DMFCs) as a power source in portable electronic equipment, for example, portable computers, laptops, or mobile phones. From 2006 to 2009, dozens of fuel cell buses were distributed in the regular public transport service in Europe, China and Australia as a part of the HyFLEET/CUTE project. Finally, the fuel cell technology found an application in a number of vehicle types – cars, vans, buses, forklifts, bikes, scooters, submarines, ferries, electric boats and aircraft. Since 2014, the Toyota Mirai, the first fuel cell car, has been introduced for commercial lease and sale in limited quantities. Mirai in Japanese means “the future”. The car has started a new chapter in the automotive history. In addition, Mercedes, Ford, Mitsubishi, Honda, GM and many other companies have organized exhibitions with concept cars [4].

10.3 Fuel cells

A fuel cell is an energy conversion device that transforms the chemical energy of the reaction that takes place within it directly into electrical energy with the by-products of heat and water [19]. The fuel cell consists of two electrodes: an anode and a cathode that sandwich an electrolyte. Generally, all fuel cell technologies consume hydrogen and oxygen. The hydrogen gas from a fossil fuel and oxygen gas from the air are fed continuously to the anode and cathode, respectively. At the anode, the hydrogen fuel reacts with a catalyst, creating positively charged protons (H^+) and negatively charged electrons (e^-). The electrolyte membrane allows only the positive ions to flow from the anode to the cathode side and acts as an insulator for electrons [3]. These electrons want to recombine on the other side of the membrane to obtain a stable system, so the freed electrons pass through an external electrical circuit and travel to the cathode, while the protons are delivered via the electrolyte. This exchange releases electrical energy. Simultaneously, on the cathode side, as a result of the reaction between the oxygen, electrons from the electrode and protons

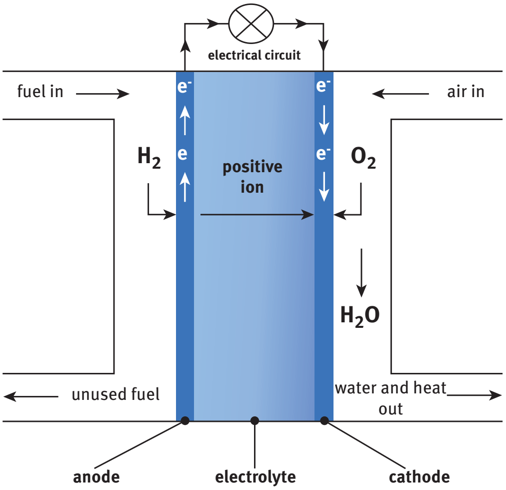

Anode reaction: $2\,H_2 \rightarrow 4\,H^+ + 4\,e^-$

Cathode reaction: $O_2 + 4\,H^+ + 4\,e^- \rightarrow 2\,H_2O$

Overall reaction: $2\,H_2 + O_2 \rightarrow 2\,H_2O$

Figure 10.2: Fuel cell operation diagram.

from the electrolyte, water forms [20]. The structure of a simplified fuel cell is shown in Figure 10.2.

Individual fuel cells can be collected into a unit and connected to each other in series, resulting in a “stack” of cells. The output of the stack can be adjusted by changing the number of individual cells.

Fuel cells are classified, generally, according to the choice of electrolyte and fuel. So far, there have been six major groups of fuel cells, summarized in Table X [20]. There are also other groups of fuel cells which are less popular but which may find specific application in the future such as air-depolarized cells, sodium amalgam cells, biochemical fuel cells, inorganic redox cells, regenerative cells and alkali metal-halogen cells [2]. Based on the literature surveys, the main advantages, disadvantages and suitability for specific applications are briefly presented in forthcoming sections of the review [19, 21–27].

10.3.1 Alkaline fuel cells (AFCs)

Alkaline fuel cells are the oldest fuel cell system. AFCs generate electricity by using an aqueous solution of potassium or sodium hydroxide as the electrolyte [3]. At the anode, hydrogen gas combines with negative charged hydroxyl ions to release water molecules and electrons. These electrons reach the cathode through an external electrical circuit and combine with oxygen and water to form negatively charged OH^- ions that may transfer to the anode through the electrolyte. AFCs generally perform in temperatures between 60 and 200 °C. Two main advantages of AFCs include their quick start and high power density – about 1 kW m^{-3}. The major disadvantage is their sensitivity to carbon dioxide that converts KOH into potassium carbonate. The resultant salt may precipitate on the pores of the electrodes and eventually block them. Moreover, carbonate formation depletes hydroxyl ions from the electrolyte, which reduces the electrolyte conductivity and consequently the cell's performance [3]. Therefore, AFCs typically require the use of pure oxygen or at least purified air, which considerably increases the cell operating costs. Thus, the alkaline fuel cells are rarely used for commercial purposes, though they are employed in other transportation services.

10.3.2 Phosphoric acid fuel cells (PAFCs)

Phosphoric acid fuel cells are a type of cells that use relatively stable, concentrated liquid phosphoric acid as their electrolyte. Since the ionic conductivity of H_3PO_4 is low at low temperatures, PAFCs operating range is about 150–250 °C. The hydrogen oxidized at the anode splits into protons and electrons. The electrons pass through the external electrical circuit, whereas the protons are transferred through the electrolyte. On the cathode side, the redox reaction between positive hydrogen ions, electrons and oxygen gas results in water formation [3].

Unlike AFCs, PAFCs are able to work on hydrogen contaminated with CO_2. However, the presence of CO significantly affects the performance of the cells due to poisoning of the platinum electrode catalyst. Carbon monoxide absorption is reported to arise from the dual site replacement of one H_2 molecule by two CO molecules on the platinum's surface [28]. The sulphur containing compounds can also reduce the effectiveness of PAFCs in result of sulphur adsorption on the electrode's surface [29]. The main advantage of phosphoric fuel cells is their capacity to generate and separate electricity and useful heat at the same time. The process of combined heat and power (CHP) production is termed as cogeneration. The waste heat captured from the cells can be easily used in most commercial and industrial applications. The drawback of PAFC is its high cost of manufacture due to the need for properly dispersed platinum catalyst coating electrodes [30].

10.3.3 Solid oxide fuel cells (SOFCs)

Solid oxide fuel cells (also called *ceramic fuel cells*) are characterized by a solid ceramic electrolyte, which is metallic oxide. Dense yttria stabilized zirconia (YSZ), a crystal structure of zirconium dioxide (ZrO_2) with the addition of yttrium oxide (Y_2O_3), is the most commonly used electrolyte for SOFCs due to its high chemical and thermal stability and good ionic conductivity. The ceramic fuel cells can produce electricity in the range of 600–1000 °C. At the cathode, the oxygen is reduced to oxygen ions O^{2-}. The oxygen ions diffuse into the electrolyte material and migrate to the anode, where they react with the fuel, generally hydrogen and carbon monoxide, producing water and carbon dioxide, as well as heat and electricity [19]. The main advantage of SOFCs is their high operating efficiency of 50–60 %. Furthermore, the waste heat can be recycled to make additional electricity by cogeneration, and hence, CHP operation increases the fuel efficiency by up to 80 %. The SOFC systems have demonstrated minimal air pollutant emissions and low greenhouse gas emissions, but some drawbacks, such as their high cost, very long start-up and cooling-down times, as well as sensitivity to sulphur and other contaminants, significantly limit their use. SOFCs are mainly used for medium and large stationary power applications (ranging to 250 kW capacity) [30].

10.3.4 Molten carbonate fuel cells (MCFCs)

Molten carbonate fuel cells are high temperature cells operating at approximately 600–700 °C. MCFCs use a combination of molten alkali carbonates (lithium or sodium), suspended in a porous, chemically inert ceramic matrix of beta-alumina solid electrolyte (BASE), which is an isomorphic form of aluminium oxide complexed with a mobile ion such as Na^+, K^+ or Li^+ [31]. At the anode, hydrogen gas reacts with the oxidizing agent, namely CO_3^{2-} from the electrolyte. The anode reaction products are water and carbon dioxide, while electrons released to the external circuit are transferred to the cathode, where a reduction reaction of the oxygen and carbon dioxide occurs. As the result of the cathode reaction, carbonate ions are formed and released to the electrolyte.

The major advantages of MCFCs include their high efficiency of 50–60 %, suitability of cheap nickel electrodes for providing sufficient activity, and more efficient than other fuel cells operability with CO containing bio-fuel derived gases [32]. Their main drawback is the corrosive and mobile electrolyte requiring the use of nickel and high-grade stainless steel for the cells’ hardware. Furthermore, the higher operating temperatures promote material problems, impacting the mechanical stability of the fuel cell. The MCFCs have found various stationary and marine applications, where their large size and weight, combined with their long start-up time, matter less.

10.3.5 Direct methanol fuel cells (DMFCs)

Direct methanol fuel cell technology is relatively new when compared to other fuel cell types. Like the PEM fuel cell, the DMFC uses a polymer electrolyte membrane. The system is fuelled with methanol. At the anode, the methanol undergoes an oxidation reaction with water, releasing carbon dioxide, protons and electrons. The protons are transported from the anode through the membrane to the cathode, where they react with oxygen and electrons to form clean water. Water consumed at the anode is reproduced at the cathode. Due to their low efficiency, DMFCs are targeted at portable electronic applications such as cameras or notebook computers, where energy and power density are more important than efficiency, mainly for the capacity range from 1W to 1kW. One of the major advantages is that the anode electrode, made of platinum and ruthenium particles, draws the hydrogen gas from the methanol, thereby reducing the overall cost due to the absence of the reformer [3, 33].

10.3.6 Proton exchange membrane fuel cells (PEMFCs)

The proton exchange membrane fuel cell (also termed the “polymer electrolyte membrane fuel cell”) utilizes a solid polymer membrane as the electrolyte. The PEMFCs have received increasing worldwide attention due to their potential of reducing our energy use, pollutant emission, and dependence on fossil fuels [34]. In PEMFCs, the hydrogen gas is oxidized to form proton ions and eject electrons at the anode. The positive ions pass through the electrolyte membrane, while electrons are forced to flow to the electrical circuit and generate the electricity. In the next step, they flow to the cathode and react with oxygen and H^+ to form clean water.

The “heart” of a single electrolyte fuel cell is the membrane electrode assembly (MEA). It consists of a proton exchange membrane (PEM) and two gas diffusion electrodes (GDE), formed by two catalyst layers (CL) and two porous gas diffusion layers (GDL) [35].

For a properly operating fuel cell, an effective membrane electrode assembly is needed. The MEA plays a crucial role in three transport processes: (i) the transport of protons from the PEM to the CL, (ii) the transport of electrons from the current collector to the CL through the GDL and (iii) the transport of the reactant and product gases to and from the CL and the gas channels [36].

The proton exchange membranes (PEM) are the main subject of this review, as described in the next section. In the gas diffusion electrode (GDE), the important component is the catalyst layer. CT is in direct contact with the membrane and the gas diffusion layer. It is also termed the “active layer”, because it impacts the efficient oxidation of the hydrogen gas. In both the anode and the cathode, the CL is the place of the half-cell reaction in the PEMFC. The layer with the catalyst is where the protons, electrons and gases, so-called three phases, are found (Figure 10.3) [37]. Platinum or platinum alloys are common materials used to produce the catalyst layer. Nowadays, due to the rapid development of the novel sputtering methods, it is possible to reduce the consumption of the noble metal [38–40].

The second component of the gas diffusion electrode is the gas diffusion layer [41]. The porous layer ensures: (i) an effective diffusion pathway of gases to the catalyst, (ii) the removal of the by-produced water outside of the catalyst layer and the prevention of flood, (iii) the storage of water on the surface for conductivity through the membrane, (iv) transfer of the heat during the cell’s operation, (v) sufficient mechanical strength to prevent the membrane electrode assembly expansion in result of water absorption [42]. Typically, the gas

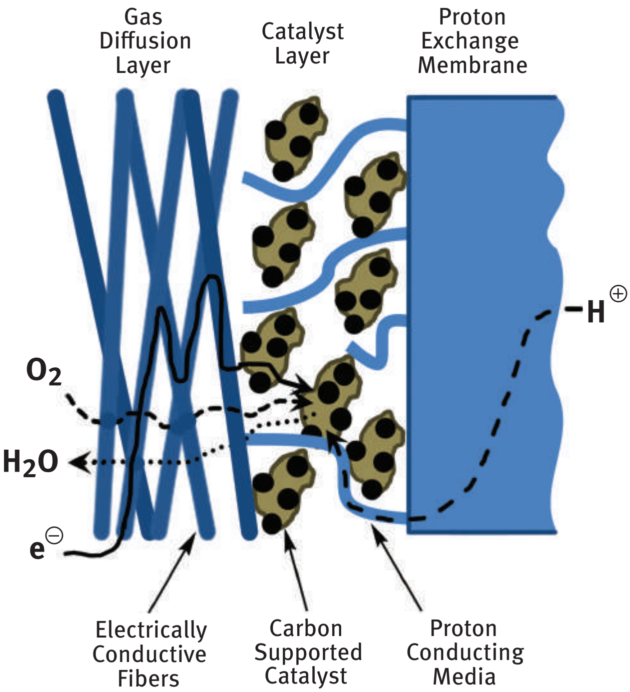

Figure 10.3: Transport of gases, protons and electrons in PEMFCs.

diffusion layers are made of porous carbon paper, or carbon cloth, with a thickness in the range of 100–300 µm [36].

The MEA is typically sandwiched with two bipolar plates (BPs) with a current collector and gas channels [36]. The diagram of a single typical proton exchange fuel cell is shown in Figure 10.4.

The BPs are responsible for the following functions (i) to distribute the fuel and oxidant within the cell, (ii) to facilitate water management within the cell, (iii) to separate individual cells in the fuel stack, (iv) to carry the current away from the cell and (v) to facilitate heat management. The most commonly used BP material is natural or synthetic graphite due to its excellent chemical stability [43].

Proton exchange fuel cells are light weight compact systems, suitable for discontinuous operation at temperatures between 50 °C to 100 °C and above 100 °C to 200 °C for low temperature (LT-PEMFCs) [44] and high temperature (HT-PEMFCs) units [45], respectively. The LT-PEMFC performance is superior to the HT-PEMFC, but only under pure hydrogen conditions [46]. When using hydrogen gas directly from the fuel processor, that is, without any prior purification, poisoning of the catalyst through CO adsorption occurs [47]. Moreover, the low temperature PEMFCs pose serious water management challenges, whereas the high temperature of PEMFCs can operate at dry conditions, and no humidifiers are needed [48].

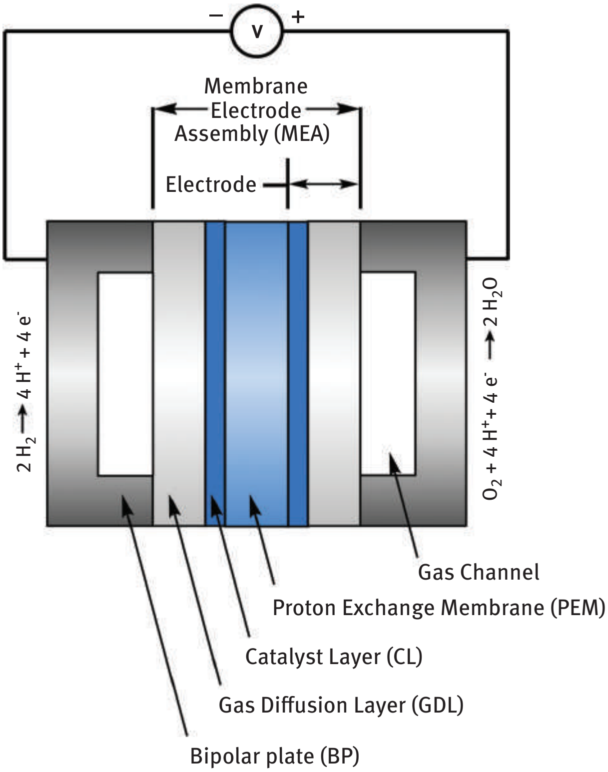

Figure 10.4: Schematic diagram of a proton exchange membrane fuel cell.

Comparison of PEMFCs with the other fuel cell technologies shows that the important advantages of the proton exchange fuel cells are their highest power density, longer lifetime, potentially faster start-up (measured in seconds) and cheaper manufacturing costs (Table 10.1). From the efficiency point of view, the higher working temperature ensures higher efficiency due to the higher reaction rate. What is equally important, the working temperature above 100 °C may cause a decrease in the conductivity of LT-PEMFC induced by vaporizing the water, which plays a vital role in proton transportation in low temperature PEM fuel cells. In this case, better efficiency can be achieved when heat released from the fuel cell is reused in a cogeneration system [49, 50].

Various features make the PEMFCs one of the most promising and attractive technologies for a wide variety of power applications ranging from automotive, through stationary to portable power systems. There are hundreds of companies involved in various aspects of the fuel cell industry, for example, Ballard Power System, United Technologies Corporation, Nuvera, General Electric FCS, Plug Power, Intelligent Energy, Novars, Smart Fuel Cell, Toshiba, Sanyo, and Hydrogenics.

Table 10.1: Comparison of different fuel cell systems [3, 20, 58, 59].

Fuel cell type	**AFC**	**PAFC**	**SOFC**	**MCFC**	**PEMFC**	**DMFC**
Common electrolyte	Solution of potassium hydroxide	Phosphoric acid	Solid ceramic inorganic oxide	Molten potassium or lithium carbonate	Solid polymeric proton exchange membrane	Solid polymer membrane
Anode reaction	$2H_2 + 4OH^- \rightarrow 4H_2O + 4e^-$	$2H_2 \rightarrow 4H^+ + 4e^-$	$2O^{2-} + 2H_2 \rightarrow 2H_2O + 4e^-$	$2H_2 + 2CO_3^{2-} \rightarrow 2H_2O + 2CO_2 + 4e^-$	$2H_2 \rightarrow 4H^+ + 2e^-$	$CH_3OH + H_2O \rightarrow CO_2 + 6H^+ + 6e^-$
Cathode reaction	$O_2 + 2H_2O + 4e^- \rightarrow 4OH^-$	$O_2 + 4H^+ + 4e^- \rightarrow 2H_2O$	$O_2 + 4e^- \rightarrow 2O^{2-}$	$O_2 + 2CO_2 + 4e^- \rightarrow 2CO_3^{2-}$	$O_2 + 4H^+ + 4e^- \rightarrow 2H_2O$	$3O_2 + 12H^+ + 12e^- \rightarrow 6H_2O$
Fuel	Pure H_2	Pure H_2	H_2, CO, CH_4, other hydrocarbons	H_2, CO, CH_4, other hydrocarbons	Pure H_2	CH_3OH
Oxidant	O_2 in air	O_2 in air	O_2 in air	O_2 in air	O_2 in air	O_2 in air
Charge carrier	OH^-	H^+	O^{2-}	CO_3^{2-}	H^+	H^+
Operating temperature (°C)	60–200	150–250	600–1000	600–700	50–200	60–200
Capacity (kW)	10–100	50–1000	<1–3000	<1–1000	<1–250	0.001–100
Electrical Efficiency (%)	60	>40	50–60	>50–60	35–45	30–40
Power density ($W\ m^{-2}$)	~1.0	0.8–1.9	0–1.5	1.5–2.6	3.8–6.5	1.0–2.0
Installation cost (US$ kW^{-1})	1800–1900	2100	3000	2000–3000	<1500	1500–1800
Operation diagram **Schema A**	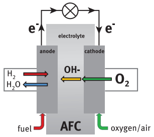	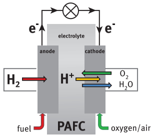	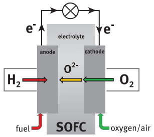	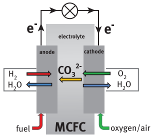	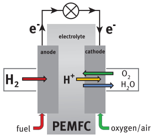	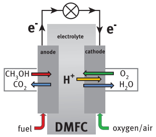

Moreover, a vast range of electronics companies (e.g. Nippon Telegraph, Telephone, Sanyo, Samsung and IBM) and automobile manufactures (e.g. Chrysler, Ford, Renault, Toyota, Nissan, General Motors, BMW, MAN, Hyundai) have presented various applications and prototype vehicles that use PEMFCs [51–57]. Although PEMFCs have been demonstrated in buses, cars, motorcycles and portable power units, there are still many unresolved commercialization issues, especially the manufacturing cost. Nevertheless, PEMFCs are expected to be fully commercialized in the next ten or fifteen years [51].

10.4 Proton exchange membranes for fuel cells

Proton exchange membranes (PEMs) are essential components of membrane electrode assemblies (MEA). A PEM is, generally, a semipermeable membrane made from an ionomeric polymer. Fundamental functions of such proton exchange membranes are as follows: (i) the transport of protons, (ii) the separation of reactants and (iii) electric insulation between the anode and cathode [22]. Common themes critical to all high-performance proton exchange membranes include (i) high ionic conductivity, (ii) low permeability to fuel and oxidants, (iii) a low electro-osmotic drag coefficient, (iv) oxidative, hydrolytic and thermal stability, (v) adequate mechanical properties, allowing to obtain as thin as possible membrane (thickness approximately 10–250 µm), (vi) long lifetime, (vii) low cost and (viii) the capability of fabrication into membrane electrode assemblies (MEAs) [60, 61]. The publication list as shown in Figure 10.5 undoubtedly proves that the polymer electrolyte membranes for fuel cells are objects of intent interest. Recently, the number of publications about PEMs has clearly risen, indicating that the development of polymer membranes is a very active and popular field.

In this section, we will focus on the presentation of the seven main types of materials used in preparing proton exchange membranes. The division is based on

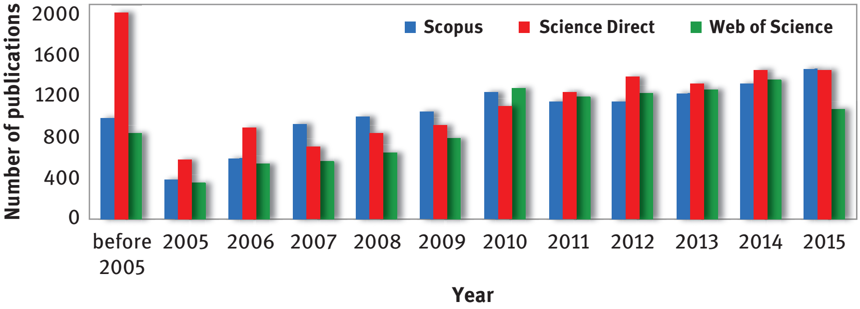

Figure 10.5: The number of publications found in three scientific databases (Scopus, Science Direct, and Web of Science). The search keywords were “proton exchange membrane” and “proton exchange membranes” in all fields.

the differences in the polymer chain structure and the presence of various functional groups. These are: poly(perfluorosulphonic acid) membranes, partially fluorinated and non-fluorinated polystyrene-based membranes, polybenzimidazole/H_3PO_4 membranes, polyphosphazene membranes, sulphonated polyimide membranes, sulphonated poly(arylene ether ketone)-based membranes and natural polymer- and bio-inspired-based membranes. Details of their properties and possible approaches to the synthesis are described in the following sections.

10.4.1 Poly(perfluorosulphonic acid) membranes

Currently, the most commercially applied proton exchange membranes are based on the poly(perfluorosulphonic acids) (PFSAs), also termed as perfluorosulphonic acid ionomers (PFSIs). In the late 1960s, DuPont developed and patented one of the most popular materials, the first from the PFSIs group [62]. The company registered it under the trade name Nafion®. Up to now, Nafion® and its derivatives have been standard materials for polymeric electrolyte fuel cells [63, 64]. Figure 10.6 shows the chemical structures of representative PFSIs [64].

Alternative polymer membranes are almost invariably compared to Nafion®. Generally, such ionomers are free radical initiated amphiphilic copolymers, consisting of hydrophobic polytetrafluoroethylene (PTFE) backbones and regular spaced long perfluorovinyl ether pedant side chains terminated by a hydrophilic sulphonate ionic group. Table 10.2 summarizes the most popular available Nafion® membrane types provided by DuPont.

Other world-class manufacturers have also been involved in the production of Nafion®-like structured perfluorosulphonic acid ionomers, for example, Asahi Chemical Industry (Aciplex®**1b**) or Asahi Glass (Flemion®**1c**), Dow Chemical Company (Dow®**1d**) or 3 M Company (3 M®**1e**). However, Dow® and 3 M® membranes had structures with side chains reduced to tetrafluoroethylenoxysulphonic acid

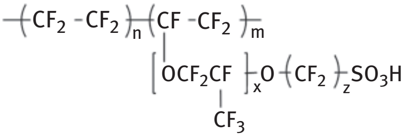

1a-e

1a n = 5-13.5, m = 1000, x = 1, z = 2 for Nafion® 117 membrane
1b x = 0, 1, z = 1-5 for Flemion® membrane
1c n = 1.5-14, x = 0,3, z = 2-5 for Aciplex® membrane
1d n = 3.6-10, x = 0, z = 2 for Dow® membrane
1e n = 3-6, x = 0, z = 3 for 3M® membrane

Figure 10.6: Chemical structures of poly(perfluorosulphonic acids).

Table 10.2: Thickness and basis weight property measurements taken with membrane conditioned to 23 °C, 50 % RH [65, 66].

Nafion® membrane type	Typical thickness [μm]	Basis weight [g m^{-2}]	EW[a] [g]
NR111	25.4	50	1100
NR112	50.8	100	1100
N112	50.8	100	1100
NE1135	88.9	190	1100
N1035	88.9	175	1000
N115	127.0	250	1100
N105	127.0	n.a.	1000
N117	177.8	360	1100
N1110	254.0	500	1100

[a] Note: equivalent weight, mass of dry ionized polymer (g) in the protonic acid form that would neutralize one equivalent of base.

($-OCF_2CF_2SO_3H$) and hexafluoropropylenoxysulphonic acid ($-OCF_2CF_2SO_3H$) functions, respectively [67, 68]. Moreover, in China, the Shanghai Institute of Organic Chemistry has developed its own perfluorosulphonated ionomer membranes used in fuel cells (Shanghai®) [69]. Similarly to Nafion®, all of these perfluorinated sulphonic acid membranes suffer from shortcomings such as low proton conductivity at low hydration and relatively low mechanical strength at elevated temperatures. Moreover, the high cost of production has limited their use. However, Solvay-Solexis has presented a cheaper membrane named Hyflon-Ion H® [70].

Up to now, the perfluorinated sulphonic acid membranes (e.g. Nafion® membrane) have been the most advanced membrane for use in practical fuel cell systems due to their high cell performance and long lifetime over 60 000 h at 80 °C. All of these polyperfluorosulphonic acid membranes are stabile in oxidative and reductive environments. The polymer chain structure provides very good chemical and thermal stability and also enables production of suitable thin membranes, while the negatively charged SO_3^- groups are very appropriate for ion exchange, because sulphonate groups allow for the passage of cations and reject anions due to the occurrence of electrostatic interactions [71, 72].

The water sorption behaviour in PFSI membranes is very important since they can conduct protons only in the humid conditions. With increasing water content, Nafion®-like membrane constituents are characteristically separated into hydrophobic PTFE-region and hydrophilic ionic clusters which contain water, solvated SO_3^- heads and counterions (mainly H^+ but depending on pre-treatment also some Na^+ or K^+). Water-filled clusters are connected by short and narrow nanochannels that form a random cluster network embedded in the surrounding, sponge-like hydrophobic fluorocarbon backbones [73]. The level of hydration is a critical parameter in Nafion®-type membranes, since at temperatures above 100 °C, the water evaporates and these materials significantly decrease in performance [72]. Furthermore, during the production process, strongly toxic and environment-unfriendly intermediates can be formed. One of the main shortcomings of Nafion® series PEMs is their high price due to expensive fluoroorganic compound having to be employed in their synthesis (cost of membrane amounting even to US$ 2500 per square meter for Nafion® N1110 [74]).

10.4.1.1 The proton conduction mechanism in perfluorosulphonic acid ionomers (PFSIs)

Proton conduction is a crucial feature for proton exchange membrane fuel cells to assure high current density. At the molecular level, the proton transfer in hydrated conditions can be described through two principal mechanisms: the proton hopping of the generally named Grotthuss mechanism or a diffusion mechanism.

In the proton hopping mechanism, the protons jump from one hydrolysed ionic site (SO_3^- H_3O^+) to another across the membrane. The proton formed in the oxidation reaction of hydrogen gas at the anode adheres to water molecules and forms provisional hydronium ions. Subsequently, one different proton from the same hydronium ion hops onto the other water molecule. In this mechanism, an ionic region forms specific hydrophilic clusters which swell in the presence of water. As a result, the percolation mechanism for protons can occur [64, 75].

In vehicular mechanisms, the hydrated proton (hydronium ion) diffuses through an aqueous medium in response to an electrochemical difference. The protons attach themselves to a vehicle such as water and diffuse through the medium. In other words, the protons treat the water as a carrier. The rate of such transport depends on the existence of the free volumes within the polymeric chains, as well as on the rate of vehicular diffusion [76]. Moreover, water plays an important role in the proton conductivity by impacting the formation, size, connectivity and strength of the ionic pathways and clusters in the PEMs [75]. When the cluster sizes increase in aqueous conditions, the proton conductivity also increases along with the humidity [59].

The important parameter in the case of membranes based on sulphonated perfluoropolymers, which describes the hydration extent of the proton exchange, is the total number of exchangeable sites for the protons. The parameter indicates the overall proton activity, thus defining the total number of water molecules coordinated per sulphonate group (denoted λ). The hydration extent can be described at a few levels. At the beginning ($\lambda<2$), only small water clusters are observed and Nafion®-based membranes behave like insulators. If λ reaches 2, the percolation threshold of the proton conductivity occurs and the water molecules bond with sulphonate groups on the inner side of the channels and clusters forming specific solvation shells. When the conditions become more humid (λ from 2 to 5), the water clusters and channels become bigger and broader, respectively. With this extent of hydration, some of the water molecules exist in a free form; however, they are strictly limited due to the coordination of hydronium ions by sulphonate groups caused by electrostatic interaction. Subsequently, with more water content (λ between 5 and 7), structural reorganization is observed. The swelling clusters and expanded channels become a partially interconnected network. The continuous path for the conduction of protons begins to be expanded. Furthermore, the existence of free water in the membrane increases, and therefore, an increase in proton conductivity is also noticed. Lastly, the maximum hydration extent is observed, and the distance between SO_3^- groups becomes larger. The Nafion®-like membrane swells, and a well-developed proton transfer network with markedly increased free water content is obtained, as illustrated in Figure 10.7 [23, 77–80].

10.4.2 Partially fluorinated and non-fluorinated polystyrene-based membranes

Chemical synthesis of poly(perfluorosulphonic acid) membranes is challenging due to the safety concerns of the tetrafluoroethylene (TFE) and their high cost combined with the limited availability of perfluorovinylethers. One alternative to the PFSA membranes is the use of styrene or its partially fluorinated derivatives to prepare PEMs. Polystyrene-sulphonic acid (PSSA) membranes are the oldest commercial polymer materials and their evolution began in 1955, when General Electric tested the first polystyrene membranes for PEMFCs [81–83]. Polystyrene-sulphonic acid (PSSA) membranes were used to produce the operational PEM fuel cells that were first ever employed in one of the Gemini programme space flights organized by NASA. The system, however, exhibited low power density, a short lifetime and low mechanical strength. In the practical FC operating conditions, under chemical attack by free radicals, local depolymerization of the polystyrene backbone occurred, resulting in interrupted regularity in the structure, and thus rapid degradation of the membrane material [84]. Reactive intermediates, mainly hydroxyl radicals ($OH^•$) formed during electrochemical conversion in PEMFC, can react with PSSA via abstraction of the

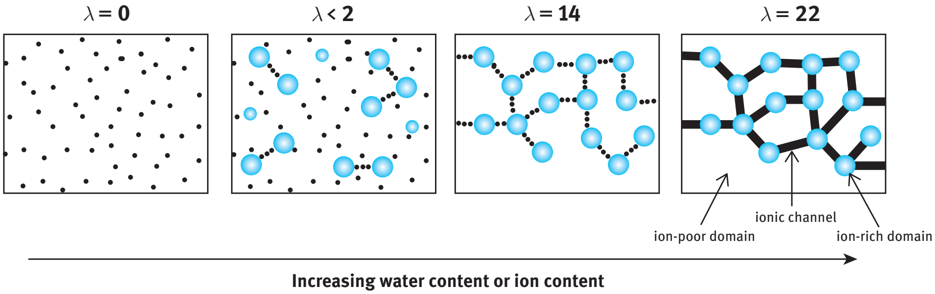

Figure 10.7: Evolution of the membrane structure as a function of water content, λ (moles of water per mole of sulphonic acid sites). The pictures are cross-sectional representations of the membrane, where the white area is the fluorocarbon matrix, the black is the polymer side chain, the grey is the liquid water, and the dotted line is a collapsed channel.

labile tertiary *α*-protons of the polymeric chain **2** leading to the formation of a benzyl radical **3** (Figure 10.8, reaction **A**) and follow-up chain scission and polymer degradation [85]. However, $OH^{\bullet}$ may add very rapidly to the *ortho* position of the aromatic rings, producing the isomeric hydroxycyclohexadienyl radicals **4** (Figure 10.8, reaction **B**). The resulting OH-adduct‡**4** may subsequently form additional highly reactive radicals [86–88].

Despite the fact that PSSA membranes are relatively inexpensive, the conductivity loss occurring during degradation caused that the emergence of Nafion® in the late 1960s reduced interest in the development of polystyrene-based membranes. The call for alternative materials, however, has reinstated the interest in polystyrene-sulphonic acid membranes for FC application. Relatively stable materials were developed by using styrenic monomers that possess substituents other than a labile proton at the *α*-position to the aromatic ring [89]. The preparation of *α*-methylstyrene-based membranes (PMSSAs) and the study of the effect of tertiary hydrogens on their stability in oxidatively aggressive environments by comparison with styrene-based membranes (PSSAs) were first reported by Assink et al. The PMSSAs exhibited higher energy efficiencies and stronger resistance to oxidative degradation conditions [90, 91].

Another strategy involving the introduction of fluorine substituents allowed for the production of various phosphonated or sulphonated poly(*α*,*β*,*β*-trifluorostyrene) membranes. The *α*,*β*,*β*-trifluorostyrene (TFS) monomer synthesis was first reported in 1949 by Cohen et al. [92]. A few years later, the TFS monomer was successfully

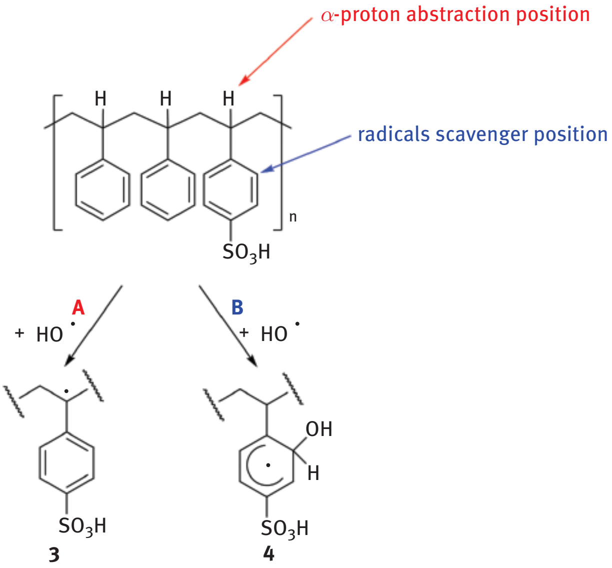

Figure 10.8: The main degradation reactions occur in polystyrene membranes.

homopolymerized under radical conditions [93]. The first sulphonated poly(*α*,*β*,*β*-trifluorostyrene) with an applicability to fuel cells was presented by Hodgdon [94]. Moreover, Ballard Advanced Materials Corporation developed sulphonated *α*,*β*,*β*-trifluorostyrene membranes under the trade name BAM1G and BAM2G (Ballard Advanced Materials 1st and 2nd Generation, respectively). The durability of these ionomeric polymers was limited to approximately 500 h under practical fuel cell operating conditions [71]. Based on previous achievements, Ballard provided a series of sulphonated copolymers of *α*,*β*,*β*-trifluorostyrene with selected *α*,*β*,*β*-trifluorostyrene analogues such as *m*-trifluoromethyl-*α*,*β*,*β*-trifluorostyrene, *p*-sulphonyl fluoride-*α*,*β*,*β*-trifluorostyrene or *p*-fluoro-*α*,*β*,*β*-trifluorostyrene – a group of materials referred to as BAM3G (Ballard Advanced Material 3rd Generation) [95]. BAM3G membranes exhibited performances superior to the Nafion® and Dow® membranes [71]. The main disadvantages of these membranes, however, include the complicated production process for the *α*,*β*,*β*-trifluorostyrene monomer and the difficult postsulphonation procedures [94, 96]. Furthermore, the Ballard Company decided to investigate the potential of phosphonic acid-based PEMs. They presented a preparation of phosphonated *α*,*β*,*β*-trifluorostyrene polymers, their characterization, and indications of their fuel cell performance capabilities [97]. The sulphonated materials showed outstanding performance in both oxygen and air conditions, while the phosphonic acid-type membranes showed excellent performance only in the oxygen fuel cells. The BAM membranes demonstrated good stability, and conductivity values ranging from 5×10^{-2} to 9×10^{-2} S cm^{-1}.

In order to improve the thermal stability of the targeted polystyrene-sulphonic acid membranes, attempts were made to modify the initial physical and chemical properties of the polystyrene via the introduction of various fluorinated styrenic comonomers into the polymer chain. The studies were mostly focused on copolymerization of the styrene with comonomer such as: *β*-fluorostyrene, *α*,*β*,*β*-trifluorostyrene, 3-methyl-*α*,*β*,*β*-trifluorostyrene, 4-methyl-*α*,*β*,*β*-trifluorostyrene, *α*-fluoromethylstyrene, *α*-difluoromethylstyrene and *α*-trifluoromethylstyrene [98–100]. The polymeric materials produced in the copolymerizations of fluorinated *α*-methylstyrenes with styrene exhibited enhanced thermal properties in comparison with the polystyrene homopolymers. An increase of the thermal stability might be attributed to the thermo-oxidative resistance of the styrene carbon α bearing fluorinated methyl groups [101].

The above-presented ionomers are believed to be random systems, both in the chemical composition of the copolymer backbone and with regard to their sulphonic acid attachment. The comparison with sulphonated multiblock copolymers revealed, however, that the latter exhibit a higher proton conducting ability with less dependence on relative humidity. Until recently, many PEMs that contain various block-copolymers with a styrene function were developed including sulphonated poly(styrene-*block*-isobutylene-*block*-styrene) triblock copolymers [102–104], sulphonated polystyrene-*block*-(ethylene-*ran*-butylene)-*block*-polystyrene [105, 106], sulphonated styrene-ethylene copolymers [107], sulphonated polystyrene (ethylene-butylene)-polystyrene triblock copolymers [108] and poly-[norbornenyl-ethylstyrene-*s*-styrene]-poly(*n*-propyl-*p*-styrenesulphonate) (PNS-PSSP) block polymers [109]. The Dais Analytic produced semi-commercial sulphonated styrene-ethylene/butylene-styrene (SSEBS) membranes that are based on the well-known commercial block copolymers containing SEBS blocks (e.g. Kraton® G1650). Unlike the perfluorinated or partially fluorinated ionomers, the Dais membranes suffer from low resistance to an oxidative condition due to the partially aliphatic character of the hydrocarbon backbone structure. Therefore, its operational temperatures should not exceed 60 °C. Nevertheless, they are considerably cheaper to produce than Nafion® and, as a result, offer an affordable alternative for lower cost portable electronics and other low power (≤1kW), room temperature applications [110].

Another strategy involves the modification of existing polymer backbones through chemical or radiation-induced grafting polymerization. Such modification affects the most inherent characteristics only to a small extent and thus offers a effortless route for the preparation of PEMs with desirable properties. The partially fluorinated acid ionomer membranes were typically fabricated by the radiation-induced grafting of a versatile monomer such as styrene onto a highly stable fluoropolymeric matrix with subsequent sulphonic acid functionalization [111]. The common base polymer films employed in the preparation of polystyrene-sulphonic acid-grafted membranes include polytetrafluoroethylene (PTFE, Teflon®), poly(tetrafluoroethylene-*co*-hexafluoropropylene) (FEP), poly-(tetrafluoroethylene-*co*-perfluoropropyl vinyl ether) (PFA), polyvinylidene fluoride (PVDF), poly(vinylidene fluoride-*co*-hexafluoropropylene) (PVDF-*co*-HEP), poly(ethylene-*alt*-tetrafluoroethylene) (ETFE), polyvinyl fluoride (PVF), or polyethylene (PE) [112]. Such membranes offer a higher ion exchange capacity than block membranes and often have physical and electrochemical properties superior to Nafion® but also an inferior fuel cell performance due to the degradation of the ionic domains while operating in a fuel cell environment. As a result, a loss of ion exchange capacity and thus a loss in conductivity were observed. In order to improve the intrinsic chemical stability and extend the durability of the grafted membranes, materials grafted with a substituted styrene sulphonic acid: α,β,β-trifluorostyrene and α-methylstyrene were developed. However, the preparation of such membranes is limited due to their low grafting rate [113]. To address this problem, the substituted styrene sulphonic acid was grafted with other monomers (co-grafted membranes). The most popular non-cross-linking comonomers for such co-grafting procedure were methacrylonitrile (MAN), acrylonitrile (AN), methyl methacrylate (MMA) and methyl acrylic acid (MAA) [114]. An attractive skeleton structure for the co-grafted membranes preparation was provided by poly(ethylene-*alt*-tetrafluoroethylene) (ETFE) [115]. However, all the co-grafted membranes exhibited an increase in membrane water uptake with but a similar ion exchange capacity without any improvement of the conductivity, which was obviously undesirable.

10.4.3 Polybenzimidazole/H_3PO_4 membranes

Generally, the high temperature PEMFCs are known to be very attractive due to their improved catalyst activity, high tolerance to impurities present in the hydrogen fuel such as carbon monoxide, and simplified thermal and water management. In order to obtain a fuel cell system that can operate in limited humidification, above 100 °C, many research groups focus their efforts on producing polymeric membranes for HT-MEA [116]. The use of Nafion® requires humidified conditions, but at an elevated temperature, the water evaporates from the membrane. Under such conditions, Nafion® converts to insulator and becomes useless for the fuel stack. To solve this problem, an aromatic heterocyclic polymer, called polybenzimidazole (PBI), was synthesized by Vogel and Marvel [117]. The PBI consists of an aromatic backbone, which provides excellent thermal stability (with a glass transition temperature reach of 430 °C), good chemical inertness and high mechanical strength. The PBI in and of itself is not a proton conducting polymer and cannot be used as a PEM. In order to ensure the proton conductivity, Savinell et al. presented polybenzimidazole impregnated with phosphoric acid (PA) [118–120]. The use of phosphoric acid was determined due to its thermal stability at a temperature above 100 °C and its ability to conduct protons [121]. So far, such polymers doped with H_3PO_4 are one of the most attractive alternatives to Nafion® for high temperature polymer electrolyte membrane fuel cells [122]. Without humidification, phosphoric acid (PA)-doped *m*-polybenzimidazole (PBI) membranes perform well. Moreover, increase of the temperature and humidity of the reaction gases result in a much improved performance, even above 100 °C.

Fully aromatic PBIs are a well-known group of polybenzimidazoles. Among them, the most popular are the *para*-type poly[2,2’-(*p*-phenylene)-5,50-bisbenzimidazole]) (*p*PBI) **5** and the *meta*-type poly[2,2’-(*m*-phenylene)-5,50-bisbenzimidazole]) (*m*PBI) **6** (Figure 10.9). Such PBIs are mainly synthesized via the polycondensation reactions of aromatic amines and aromatic acids (or their derivatives) and self-condensation reactions involving 3,4-diamino acids [123].

The most systematically studied polybenzimidazoles are those of the mPBI, which has been commercially produced by the Celanese Corporation since 1983 under the trade name PBI®, and poly(2,5-benzimidazole) (ABPBI). Nonetheless, it is well known that the first one has a very rigid molecular structure so its

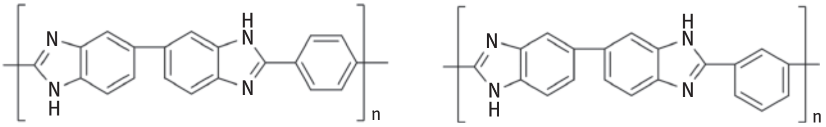

5 **6**

Figure 10.9: Chemical structures of polybenzimidazole polymers.

processability is limited [124]. To date, BASF has introduced other commercially available polybenzimidazole/H_3PO_4 membranes, for example, CeltecL®, CeltecP1000® or CeltecV®.

The proton conductivity mechanism of phosphoric acid (PA)-doped *m*-polybenzimidazole (PBI) membranes (poly-salts) is mainly by the Grotthuss mechanism. Phosphoric acid has an amphoteric character, so it can act as either a proton donor (acid) or a proton acceptor (base). As a result of the dynamic hydrogen bond network, where protons can transfer through the formation and cleavage of bonds, a so-called hopping mechanism is formed (Figure 10.10) [125]. The PBI polymer chain has two basic nitrogen atoms per repeating unit, which may trap two phosphoric molecules. Additional acid molecules absorbed during the doping process accumulate in the free volume of the polymer network. These "free phosphoric acids" are responsible for the proton conductivity of the material.

The conductivity of (PBI/H_3PO_4) poly salts depends on the acid content. A low acid content (up to 2.4 H_3PO_4 per PBI monomer unit) yields conductivities of less than approximately 10^{-4} S cm^{-1} at 160 °C, while a high acid content (11 acid molecules per repeating polymer unit) provides high conductivity values of up to 0.15 S cm^{-1} at 160–180 °C [126, 127].

An increasing phosphoric acid content may encounter several disadvantages, however, including leaching out of H_3PO_4, poisoning of the catalyst, or the inducing of corrosion of the electrodes and bipolar plates in the FC stack [128]. Furthermore, with the increasing acid content, the mechanical properties of the membranes such as their tensile strength and homogeneity become significantly deteriorated [129, 130]. An optimal phosphoric acid content depends on the structure of the membrane polymeric matrix. Improved mechanical properties and enhanced conductivity can be obtained via: cross-linking modification of the linear PBI

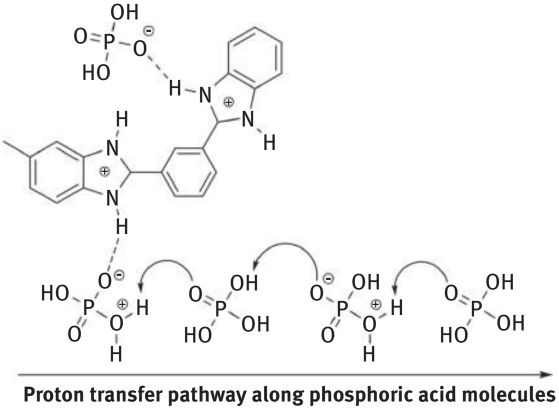

Figure 10.10: Proton conducting mechanism in phosphoric acid (PA) doped polybenzimidazole (PBI).

(using e.g. γ-(2,3-epoxypropoxy)propyltrimethoxysilane (KH560) [131], poly(vinylbenzyl chloride) [132], 1,3-bis(2,3-epoxypropoxy)-2,2-dimethylpropane (NGDE) [133] or dichloromethylphosphinic acid (DCMP) [134] as cross-linkers), modification of the main PBI chain (e.g. using partially fluorinated polybenzimidazoles containing $-C(CF_3)_2-$ junctional groups) [135], or using nanofibres to reinforce the PBI/H_3PO_4 membranes [136].

The phosphoric acid (PA)-doped *m*-polybenzimidazole (PBI) membranes are vulnerable to attack by radicals [126]. The PBI membrane exhibits higher weight loss than Nafion® in reaction with Fenton's reagent. However, the oxidative stability of the PBI membranes was improved as the molecular weight of the PBI polymers increased [137].

10.4.4 Polyphosphazene membranes

An alternative class of polymers for proton exchange membranes is polyphosphazenes. Polyphosphazenes (PPZs) are very unique hybrid polymers that contain a backbone of alternating phosphorus and nitrogen atoms with two organic, inorganic, or organometallic side groups attached to each phosphorus atom (Figure 10.11).

The polymers are of interest to many research groups because of the opportunities they provide for structural diversification via the introduction of a vast range of side groups, which allows obtaining an unprecedented and largely controlled variety of desirable properties [138–140].

PPZs have numerous advantages over conventional hydrocarbon-based polymers. One of the most important is their thermal and chemical stability. Due to the highest oxidation states of nitrogen and phosphorus atoms in the –P=N– backbone, the polyphosphazenes are particularly stable in aggressive oxidative conditions. Moreover, PPZs are characterized by a low glass-transition temperature due to their low barrier to the skeletal free rotation of each phosphorus–nitrogen bond and their high torsional mobility [141]. Other very important advantages of polyphosphazenes are their relatively low cost and facile synthesis routes. The most widely used method is the thermal ring-opening polymerization of chlorophosphazene cyclic trimer, presented by Allcock and Kugel [142–146]. The cyclic trimer –

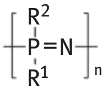

$$\left[-\overset{R^2}{\underset{R^1}{P}}=N- \right]_n$$

$R^1, R^2 =$ Cl
OC_6H_5
$OC_6H_4SO_3H$
OCH_2CF_3
$OC_2H_5OC_2H_5OCH_3$
CH_3
C_6H_5
$NHCH_3$
…

Figure 10.11: General polyphosphaznes structure.

hexachlorocyclotriphosphazene – is polymerized to linear poly(dichlorophosphazene). The subsequent macromolecular substitution with the appropriate nucleophilic reagent allows to obtain polyphosphazene (Figure 10.12). The PPZs containing aryloxy substituents exhibit the best combination of properties [138].

In order to be qualified as typical ion-conducting materials for MEA applications, the phosphazenes polymers need to have acid functionality, which is incorporated into the polymer structure. Polyphosphazenes can be classified according to the type of acidic function they have. Literature reports present that the sulphonic and phosphonic groups can ensure the proton conductivity of PPZs. The first attempt to develop the polyphosphazene solid electrolyte took place in 1984 and was published by Blonsky and Shiver [145]. It was Allcock et al. who reported the first synthesis of polyphosphazenes with sulphonic groups (S-PPZs) which would be a proton-conducting material for fuel cell applications. The authors synthesized the polyphosphazenearylsulphonic acid derivatives. The sulphonation reactions were developed initially with cyclic trimers, then polymers in solution, and, finally, with surfaces made of solid S-PPZs [146].

Pintauro and co-workers showed sulphonation reaction for poly[(3-methylphenoxy)(phenoxy)phosphazene] [147] and poly[bis(3-methylphenoxy)phosphazene] [141]. In result, they obtained a stable material with high ion exchange capacity values (near 2 mmol/g). Furthermore, they developed PEMs with sulphonated poly [bis(3-methylphenoxy)phosphazene] characterized by their high IEC (1.4 mmol/g) [148]. The poly[bis(3-methylphenoxy)phosphazene] with SO_3^- groups allow to understand the specific proton conductivity mechanism. The ion exchange capacity and proton conductivity of the sulphonated membrane increased with increasing water content, finally reaching the maximum conductivity of $0.1\,Scm^{-1}$ at the IEC of 1.6 mmol/g. Moreover, the results clearly indicated that sulphonated PPZs are good proton conductors (comparable to Nafion®) when they swell in water. The hydrophilicity of the –N=P– backbone demonstrated that in this type of a conductor, the proton migration proceeds primarily according to the Grotthuss mechanism [149]. For such a mechanism, the activation energy for proton conduction should vary from 14 to 40 kJ mol^{-1} [150].

Due to the opportunity to incorporate the acidic groups into the polymer structure without the harsh conditions required in the sulphonation process, the phosphonic acid functionalized polyphosphazenes (P-PPZs) are a promising alternative to the sulphonated PPZs. Nonetheless, the literature data show that P-PPZs membranes

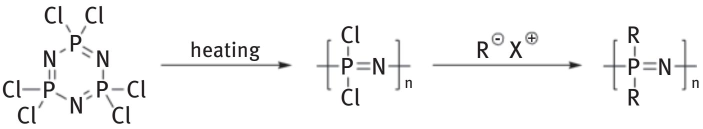

Figure 10.12: Polyphosphazene synthesis method developed by Allcock and Kugel [142–146].

have a lower conductivity than S-PPZs [138]. Another alternative is the use of polyphosphazenes with the sulphonamide group incorporated. Such derivatives have good conductivity and are excellent candidates for MEAs [151].

PEMs containing pure polyphosphazene films have relatively poor mechanical behaviour due to the necessary hydrated conditions. In order to improve such properties, polymer blends were produced. The membranes were synthesized either by cross-linking (e.g. with segments of polybenzimidazole [152] or polyacrylonitryle [153]), or other re-enforcement via a physical mixure (e.g. with PVDF [154]).

10.4.5 Sulphonated polyimide membranes

The aromatic polyimides are compounds containing an imide heterocyclic structure in their backbone. They have found a vast range of applications in many industrial fields due to their excellent thermal stability, high mechanical strength, membranability (good film-forming ability) and significant chemical resistance. These values are required for the electrolyte membrane for proton exchange fuel cells, and thus, sulphonated polyimides (SPIs) have been developed as promising candidates for PEMFCs [155]. Generally, the opportunity to produce significantly less expensive membranes than Nafion® successfully contributed to the polyimide-based materials development. The use of polyimide membranes in FCs applications was first presented by Faure et al. [156]. The most interesting are the more hydrolytically stable six-membered ring (naphthalenic) sulphonated polyimides-based membranes (Figure 10.13) [157, 158].

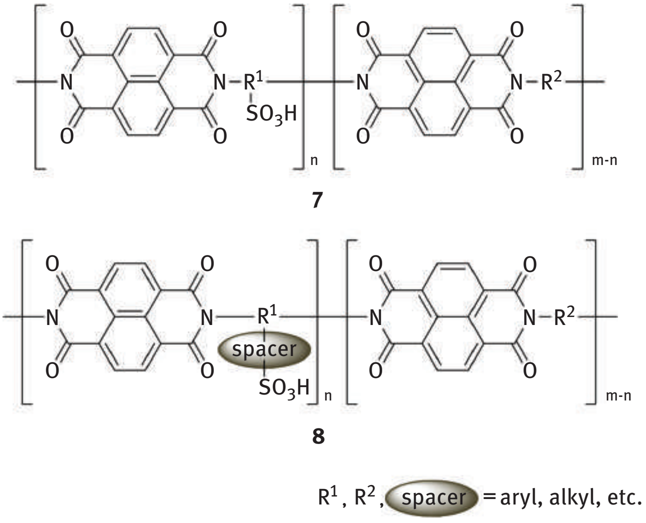

Figure 10.13: Naphthalenic type polyimides containing sulphonic acid moieties attached directly to the polymer main chain **7** and with sulphonated side-chains **8**.

Five-membered heterocyclic (phthalic) polyimides have been also investigated for many years, but under practical fuel cell operating humidity conditions they quickly degrade via hydrolysis due to the lower electron density of the carbonyl carbon atom [71]. Such a step in the degradation of imide is caused by the nucleophilic attack of a hydroxyl anion from water on the electrophilic carbon atom of the carbonyl group. Hydrolytic cleavage of phthalic polyimides results in polyimide chain scission and the formation of units with dicarboxylic acid and free amine functions [159]. Due to the fact that the sulphonic acid group is strongly electron-withdrawing, the distancing its position from the imide moiety is also expected to result in an increase in the hydrolytic stability of the polyimide main chain (Figure 10.13). The polyimide membranes containing sulphonic acid groups attached directly to the polymer backbone (**7**, Figure 10.13) are less stable compared to the polyimides with sulphonated side-chains (**8**, Figure 10.13). In contrast to the SO_3H groups, to improve oxidative and hydrolytic stability of the six-membered ring polyimides-based membranes, sulphonated polyimides bearing trifluoromethyl groups were successfully synthesized. The hydrophobic character of CF_3 moieties protect the imide ring from being attacked by water or radical molecules, despite its strong electron-withdrawing behaviours [160]. Furthermore, the addition of bulky aliphatic groups into the main and side chains of the ionomers significantly improves the hydrolytic stability [161–163]. The addition of a cross-linker or constructing network structure can also increase the resistance to hydrolysis while simultaneously improving the dimensional stability. This may be because cross-linking can reduce the swelling to a greater extent. Sundar et al. used a series of dibromoalkanes (dibromobutane, dibromohexane and dibromodecane) as cross-linking compounds. The cross-linked sulphonated polyimides exhibited higher hydrolytic stability than uncross-linked ones. However, this feature decreased with an increase in the chain length of the cross-linker. This may be due to the higher swelling of the polymers with longer alkyl chain lengths [164]. Other cross-linkers used to obtain membranes with high hydrolysis resistance are as follows: various diols (1,2-ethanediol, 1,4-butanediol, 1,5-pentanediol, 1,6-hexanediol or 1,10-decanediol) [165], poly(ethylene glycol) diacrylate [166] or 1,3,5-tris(4-aminophenoxy) benzene (TAPB) [167]. Another possibility to enhance the water stability of SPIs for fuel cells is to use the SPI membranes employing 4,4'-binaphthyl-1,1',8,8'-tetracarboxylic dianhydride (BTDA) that contains binaphthyl units instead of conventional 1,4,5,8-naphtalene-carboxylic dianhydride (NTDA) with a common aromatic naphtyl function. The improved stability of BTDA-based polyimides was attributed to its unique binaphthalimide structure, which effectively decreases the possibility of a nucleophilic attack leading to hydrolysis [168, 169]. Electron-donating phenoxy [170] or benzophenone groups [171] at the *meta*-position of the imido groups positively impact the hydrolytic stability of producing SPI materials.

The naphthalenic SPI membranes are much more resistant to hydrolysis, but they also have a few drawbacks. They show rather low water stability, which limits their further use in FCs technology [163]. Moreover, the proton conductivity of SPI membranes is low at low humidity levels [172]. Accordingly, in order to overcome the above disadvantages, many researchers have been endeavouring to prepare novel and improved SPI membranes for the proton exchange fuel cells.

10.4.6 Sulphonated poly(arylene ether ketone)-based membranes

The sulphonated poly(arylene ether ketone)-based (SPAEK-based) membranes are a family of sulphonated aromatic main-chain polymers. They are a promising alternative to PEMs due to their wide range of advantages such as good mechanical properties, outstanding thermal and chemical stability, facile processability, high availability and also low cost. The PAEK polymer family includes poly(ether ketone)s (PEKs), poly(ether ketone ketone)s (PEKKs), poly(ether ether ketone)s (PEEKs), poly (ether ether ketone ketone)s (PEEKKs) and poly(ether ketone ether ketone ketone)s (PEKEKKs). The exemplified general structures of the PAEK polymer group are presented in Figure 10.14.

Poly(arylene ether ketone)s are very rigid, inflexible polymers with bulky aromatic rings. These features result in a high glass transition temperature exceeding 200 °C. The aromatic rings support various electrophilic or nucleophilic modifications. To produce membranes for MEAs for fuel cells, active proton exchange sites, such as sulphonic groups, have to be introduced to the poly(arylene ether)s [173]. Of all these suitable materials, the sulphonated poly(ether ether ketone)s (SPEEK) are the focus of many investigations in preparing membranes (Figure 10.15).

The literature reports that sulphonated poly(arylene ether ketone)-based (SPAEK-based) membranes are durable under fuel cell operating conditions and sometimes their lifetime exceeds 3000 h. However, while the higher degree of sulphonation (DS) offers higher proton conductivity, the mechanical stability decreases. Such membranes are vulnerable to radical attacks and degradation processes [174, 175]. The radicals generated during PEMFC operation (mainly $HO^\bullet$) may degrade with the detachment of the sulphonic acid groups and the scission of the polymer chain [176]. Further studies suggested that $HO^\bullet$ may either attack the aromatic ring in the *ortho* position to the alkyl and RO substituents (Figure 10.16, sites **A**), or cause the C–O–C scission (Figure 10.16, site **B**) [177].

Attempts to improve the stability of SPAEK have included optimization of the position of SO_3H. When such an electron-withdrawing group is attached directly to the aromatic ring, it may reduce the electron density of the neighbouring ether function via resonance and increase the susceptibility to hydrolysis of ether linkage [178]. To avoid this potential instability, the sulphonic group should be attached to the pendant chain rather than to the main chain of the polymer [179]. Another way of improving the stability is incorporating hydrophobic perfluorinated blocks in the main-chain of the multi-block aromatic polymer. Strong electron-withdrawing

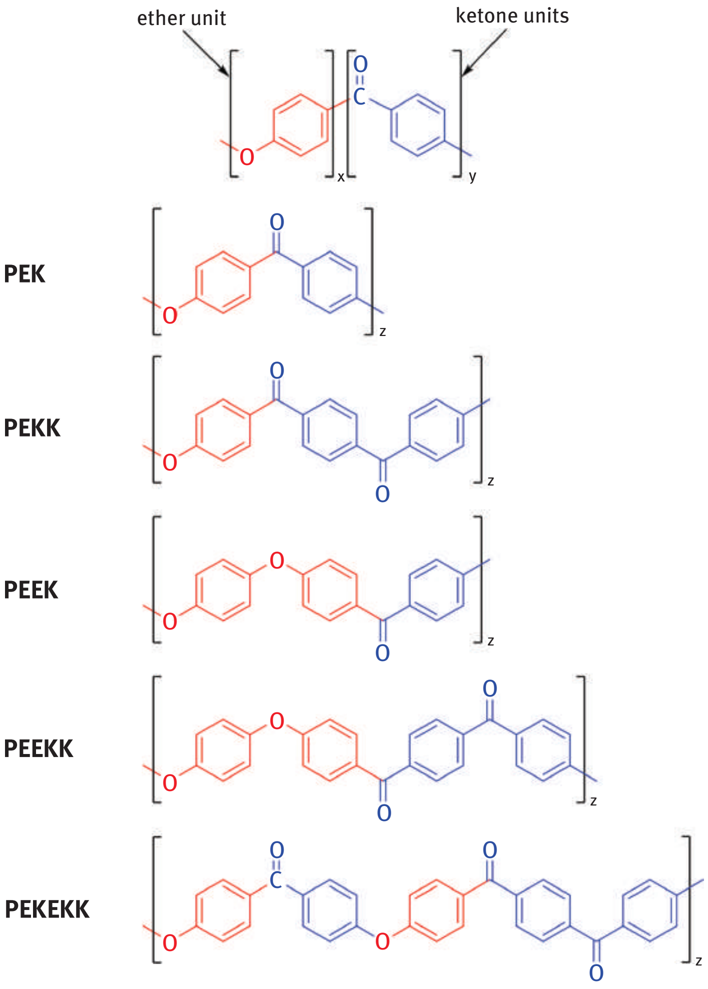

Figure 10.14: General formulas of the poly(arylene ether ketone) (PAEK) family.

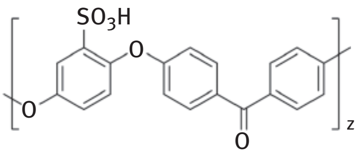

Figure 10.15: The chemical structure of SPEEK.

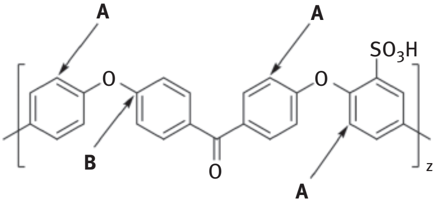

Figure 10.16: The vulnerable sites for HO$^{\bullet}$ radical attacks on SPAEK materials (indicated by arrows).

fluorine atoms can deactivate the aromatic ring and reduce the negative addition reactions of radicals [178].

The proton transport of SPAEK was compared to the corresponding properties of Nafion®. Due to the rigid structure of the aromatic backbone in SPAEK, the hydrophilic channels are narrower than in Nafion®. It results in a reduced dissociation level of the sulphonic groups. Moreover, the narrower channels have numerous cul-de-sacs (dead-end "pockets") which form a slimmer and poorly connected water-filled network and significantly impede proton transfer. Scientific efforts are focused on producing SPEEK with a high proton conductivity, but maintaining the sulphonation on appropriate levels to assure also chemical stability and limited swelling [180]. Currently, SPEEK membranes with conductivity over 0.1 S cm^{-1} are reported [181].

The general approaches for the synthesis of sulphonated poly(arylene ether ketone)s include polymer postmodification and direct copolymerization of sulphonated monomers. The conditions of the first modification reaction are very harsh and sometimes incur difficulties (e.g. a lack of control over the sulphonation level and the final location of the acidic conductivity groups, as well as the possibility of side reactions or degradation of the polymeric chain). Such a transformation was used to obtain the most popular sulphonated poly(arylene ether ketone) – sulphonated Victrex® PEEK [182]. PEEK can be obtained by two main synthetic pathways – electrophilic or nucleophilic substitutions [183]. The first method employs extremely strong acidic conditions, such as a triflic acid (CF_3SO_3H) used as a solvent. Such a media limited the applicability in the industry, however, due to its safety hazards. In contrast, the nucleophilic substitution method may be performed using a wider range of solvents (e.g. dimethyl sulphoxide, sulpholane [184], diphenyl sulphone [185] or *N*-methylpyrrolidone [186]). In the nucleophilic substitution method of PEEK synthesis, a hydroquinone reacted with a 4,4′-dihalobenzophenone (derivative with chlorine or fluorine atoms) in the presence of a potassium carbonate as a base (Figure 10.17).

The direct synthesis of sulphonated monomers for SPEEK membranes seems to be more advantageous than the postsulphonation process. In such a synthesis, side reactions can be avoided or significantly reduced. Moreover, the degree of sulphonation (DS) and position of the sulphonate groups in the aromatic ring may be better controlled.

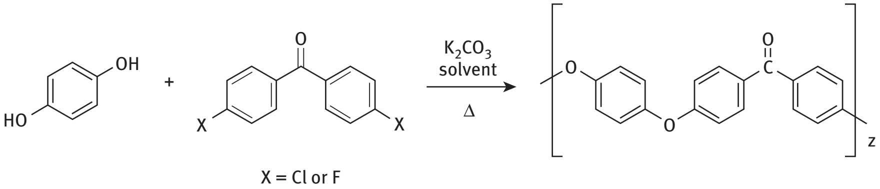

Figure 10.17: The nucleophilic substitution method for synthesizing commercially available PEEK.

In order to improve the performance of SPAEK membranes, various modification strategies were introduced [23].

Cross-linking of poly(ether ether ketone)s improves the thermal stability, mechanical strength and oxidative stability of the membranes. Such membranes exhibit lower water uptake than non-cross-linked materials. Nonetheless, the expanded polymer network and increased cross-linking density may cause a reduction in the proton conductivity and flexibility of the PEMs [187]. Hou et al. presented an excellent review of recent advancements in the development of cross-linking strategy [188]. Literature reports show that cross-linked SPAEK membranes have limited solubility in common solvents and show improved stability. Wang and co-workers prepared an outstanding SPAEK sulphonated poly(ether ether ketone) bearing pendant amino group (Am-SPEEK) membrane with 4,4’-diglycidyl(3,3’-5,5’ -tetramethylbiphenyl) (TMBP) as an epoxy resin cross-linker with a proton conductivity of 0.140 S cm^{-1}(80 °C), i.e. higher than that of Nafion® (0.1 S cm^{-1}) [189]. Li et al. used sulphonated – a novel cross-linker – carboxyl terminated benzimidazole trimer bearing sulphonic acid groups (s-BI). The series of SPEEK/s-BI-n membranes show excellent stability and a low swelling ratio. Furthermore, the authors achieved high proton conductivities exceeding 0.12 S cm^{-1} (60 °C) [190].

The next modification is preparing branched sulphonated poly(ether ether ketone)s. The branched polymers are defined as materials between linear and cross-linking type polymers. Branching allows getting a large free volume for water [191, 192] and increases the proton conductivity of the membranes.

Polymer blending is an appropriable technique for designing materials with enhanced properties. The blends often exhibit better properties than the properties of an unmixed component. The preparation of blend membranes employing organic fillers is a common way to improve the properties of SPAEKs materials due to the simplicity of preparation and easy control of different physical properties. Until now, sulphonated poly(arylene ether ketone)s have been blended with polybenzimidazole (PBI) [193–195], poly(ether sulphone) (PES) [196, 197], sulphonated and silylated polyphenylsulphone [198], sulphonated cyclodextrin [199] poly(vinylidene fluoride) (PVDF) [200–202], poly(vinylidene fluoride-*co*-hexafluoropropylene) (PVDF-*co*-HFP) [202], phosphonated polysulphone [203], 3-aminopropyltriethoxysilane [204], poly(ether sulphone) [205], acrylic acid-*co*-4-vinylimidazole [206], poly(ether imide)

[207, 208], polypyrrole [209], nylon 6 [210], polystyrenesulphonic acid [211], polyacrylonitryle [212], or poly(vinyl alcohol) [213].

The formation of composite SPAEK-based materials with inorganic filler is another technique to enhance the proton conductivity and mechanical stability of membranes. A wide range of heteropolyacids (HPA) and their salts is used as fillers, for example, $H_3PW_{12}O_{40}$, $H_3PMo_{12}O_{40}$, $Na_2HPW_{12}O_{40}$ [214], $CsH_2PW_{12}O_{40}$, $CsH_3SiW_{12}O_{40}$ [215], $Cs_{2.5}H_{0.5}PW_{12}O_{40}/Pt$ [216], $Cs_{2.5}H_{0.5}PW_{12}O_{40}/Pt$ [217], $H_3PW_{12}O_{40}/SiO_2$ [218], $H_3PW_{12}O_{40}$ and MCM-41 [219], $H_4SiW_{12}O_{40}/SiO_2$ or Al_2O_3 [220], $y\text{-}K_9SiW_{10}O_{36}$ [221], $Cs_{2.5}H_{0.5}PW_{12}O_{40}$ [222]. Furthermore, the combination of SPAEK and non-acid zirconium, titanium or silica inorganic fillers was also reported [223–225].

10.4.7 Natural polymer- and bio-inspired-based membranes

Power needs to be generated using environmentally friendly natural materials, so scientists are focusing their efforts on investigating natural or bio-inspired polymeric membranes for the application of FCs. Use of eco-friendly biopolymers in designing electrical devices is not only challenging and interesting, but also important from the environmental safety point of view. Moreover, use of such polymers can significantly decrease the cost of production, often very high compared to typically synthetic materials. Currently, few natural or bio-inspired polymers have been employed as an attractive electrolyte for the membrane electrolyte assemblies [226]. Until now, only few polymers have been reported as suitable biopolymer electrolyte membranes for fuel cell applications. Such natural-based polymers include agar [227], uracil [228, 229], gelatin [230, 231], pectin [226] or cellulose [232–236].

Chitosan (CS) and its derivatives are extensively investigated as some of the most attractive “green” materials for fuel cell applications. CS is a biodegradable, biocompatible, nontoxic, and quite low-cost polymer, offering a vast range of possibilities for simple chemical modifications.

The proton conductivity of Chitosan is low, and it is necessary to enhance its conductivity. In order to produce a conducting material, proton donors may be introduced into the CS matrix by a blending method with various acidic compounds. In result of such modifications, the acid–base complexes are synthesized [111]. Until now, Chitosan has been mixed with various acidic compounds, such as a medronic acid [237], poly(vinyl phosphonic acid) [238], poly(4-styrenesulphonic acid-*co*-maleic acid) (PSSA-MA) [239], acrylic acid-2-acrylamido-2-methylpropane sulphonic acid copolymer [240], oxalic acid [241], poly(acrylic acid) [242], or various heteropolyacids and their salts [243, 244]. Furthermore, the grafting of acidic functions to the backbone of CS may be another effective way to obtain proton conducting materials [245, 246].

The proton conducting mechanism for acid-base complexes with Chitosan in anhydrous conditions is of a Grotthuss-type character. Yamada and Honma have presented proton transfer for Chitosan and medronic acid (MA). The electrostatic

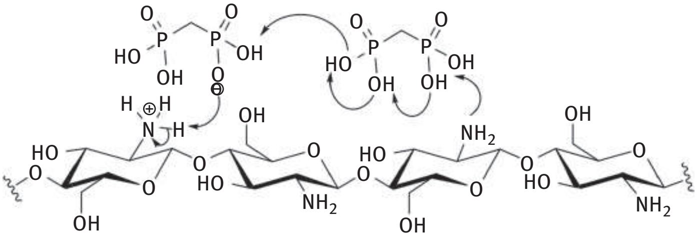

Figure 10.18: The anhydrous proton conducting mechanism of Chitosan-MP composite proposed by Yamada and Honma [237].

interaction of the amino group in Chitosan with the phosphate group in the MA molecule forms a proton defect site. The neighbouring proton in the acid molecule is transferred to the defect site (Figure 10.18) [237]. The hydrated or partially hydrated conditions contribute to the combine vehicle and Grotthuss mechanisms [240].

Recently, the model PEMFC with a CS-based natural membrane has demonstrated some possibilities but a low power density (16 mW cm^{-2} at 75 °C [247]). Therefore, the preparation of such membranes to be efficiently applied in PEMFC is still a challenge for many research groups.

10.5 Synthetic methods of PEMs preparation

As illustrated in the preceding section, many polymer classes of diverse chemical structures and various strategies of the incorporation of protogenic moieties have been explored as electrolyte materials for PEM application. The sulphonic acid moieties arrangement and the acid strength and the character of the connecting unit to the polymer backbone may have a considerable impact on the morphologies of the resultant membrane and subsequently on its physical and chemical properties. Most of the synthetic methods employed in the formation of ionomeric materials lead to the statistical or random distribution of sulphonic acid groups along the backbone chain of the copolymer [22]. The following four different synthetic strategies, allowing for preparations of the ionomer membranes, can be distinguished: (i) postmodification/postsulphonation of existing fluorinated/nonfluorinated polymeric materials (Figure 10.19), (ii) direct polymerization of monomers functionalized by acids (sulphonic mostly) with fluorinated or/and nonfluorinated monomeric units (Figure 10.19), (iii) chemical grafting of sulphonated monomers onto the fluorinated/nonfluorinated backbone (Figure 10.19) and (iv) the stepwise route based on irradiation grafting of monomers onto the fluoropolymer backbone followed by a subsequent postsulphonation (Figure 10.19).

One of the most commonly used and oldest methods that allow to convert the existing polymeric materials into ionomers and to confer their protonic conduction properties is the postsulphonation strategy (Figure 10.19(a)). Postsulphonation has

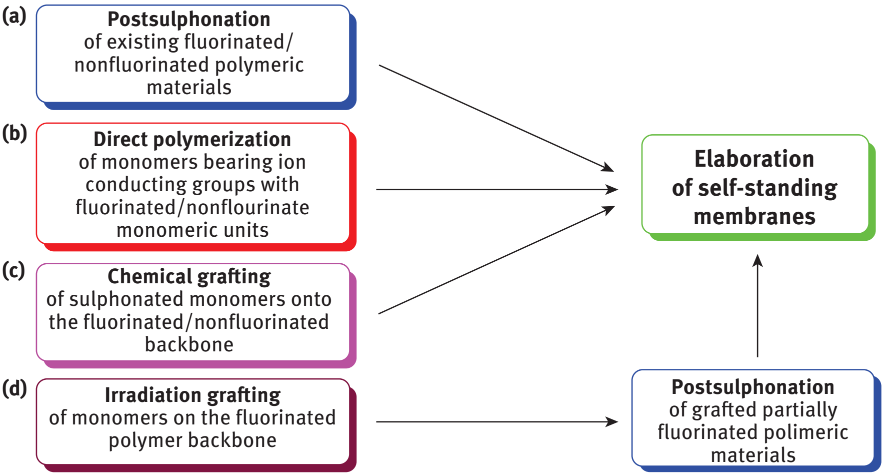

Figure 10.19: Various methodologies of self-standing PEMs preparation.

been employed in the preparation of numerous ionomeric materials for application as PEMs, namely polystyrene-sulphonic acids (PSSA) [81–88], sulphonated poly(α,β,β-trifluorostyrene)s – 1st, 2nd and 3rd generation Ballard Advanced Materials (BAM1G, BAM2G, BAM3G) [71, 95–97], sulphonated poly(benzimidazole)s (SPBI) [248], sulphonated poly(phosphazane)s (S-PPZ) [148–150], sulphonated poly(arylene ether ketone)s (SPEAK) or sulphonated poly(ether ether ketone)s (SPEEK) [173–186]. The postmodification, for example, electrophilic sulphonation, is usually employed to modify polymers with aromatic functional groups either in the lateral position to the polymer backbone or incorporated directly into the polymer main chain. Aromatic polymers easily undergo sulphonation reactions in the presence of concentrated sulphuric acid, fuming sulphuric acid, chlorosulphonic acid, oleum or other sulphur trioxide complexes. Since sulphonation is an electrophilic substitution reaction, its applicability strongly depends on the aromatic ring reactivity, that is, the electron character of the present substituents. Electron-donating groups (EDGs) activate the ring and thus favour the reaction, while electron-withdrawing groups (EWGs) deactivate the ring, so that successful introduction of a sulphonic acid moiety requires a much stronger sulphonating agent. Moreover, the sulphonic acid substituent is preferably introduced to the activated position of the aromatic ring and usually only one $-SO_3H$ group per repeat unit could be achieved. There are several drawbacks of the postsulphonation strategy, mainly (i) the lack of precise control over the location and degree of the functionalization that influences the ion exchange capacity, (ii) a risk of an undesired side-reaction occurrence such as cross-linking via sulphone formation that may result in the reduction of the material proton conducting properties, (iii) a degradation of the polymer chain that may contribute to deterioration of the membranes' mechanical properties. Therefore, a direct polymerization of monomers bearing sulphonic acid groups with nonsulphonated monomers seems to be an optional strategy allowing for the placement of ionic groups on a copolymer backbone in a controlled manner.

Synthesis of sulphonated macromolecular materials for application in PEMs by the direct copolymerization of sulphonated monomers has been alternatively applied in the preparation of nonfluorinated sulphonic acid ionomers such as sulphonated poly(arylene ether)s [174, 249, 250] or sulphonated poly(imid)s [157]. Though synthetically challenging, the direct strategy is considered to be a rigorous and repetitive method of controlling the chemical composition, acid content, and even molecular weight of the resultant sulphonated macromolecules. The direct copolymerization strategy is also commonly used in the preparation of polyfluorosulphonic acid ionomers like Nafion®, Aciplex®, Flemion®, Dow® or 3 M®, the current state-of-the-art membranes for PEMs [62–64, 67, 68]. The perfluorinated copolymers bearing sulphonic acid groups are synthesized in direct free radical copolymerizations of tetrafluoroethylene (TFE) with perfluorinated vinyl ethers terminated by pefluorosuphlonic acid groups (Figure 10.19). However, all these fluorinated membranes are expensive due to the demanding chemical synthesis and the cost or availability of perfluoroether comonomers and suffer from low conductivity at a low water content, moderate glass transition temperatures and the relatively low mechanical strength at elevated temperatures.

Chemical grafting of sulphonated monomers onto the hydrophobic polymer backbone is another approach that has been employed for the preparation of ion containing materials, such as the copolymer consisting of a polystyrene backbone and sodium styrene sulphonate graft chains (PS-*g*-*mac*PSSNa) [251, 252] or a copolymer of sodium styrene sulphonate grafted to a poly(acrylonitrile) backbone (NaSS-*g*-PAN) [253], as well as *N*-benzylsulphonate poly(benzimidazole) (BzS-PBI) [254, 255] (Figure 10.19). The chemical grafting strategy allows for the elaboration of ion conducting membranes formed by potentially well-defined block copolymers with sulphonated and unsulphonated blocks. The chemical structure of such materials with their blocky character results in an increased proton conductivity without an enormous increase in water swelling. Moreover, the comparison of random and graft copolymer properties (proton conductivity, water uptake, mechanical strength or thermal stability) reveals that the polymer structure, that is, selected method of synthesis, enormously impacts the morphology and, therefore, the properties of the resultant materials [22].

Poly(styrene sulphonic acid) grafts have also been attached to per- or partially fluorinated backbones. The materials were synthesized via a stepwise route based on the irradiation grafting of monomers onto a fluoropolymer backbone followed by a subsequent postsulphonation (Figure 10.19). The fluorinated polymers such as poly (tetrafluoroethylene) (PTFE) [112], poly(tetrafluoroethylene-*co*-hexafluoropropylene) (FEP) [256–258], poly(ethylene-*alt*-tetrafluoroethylene) (ETFE) [259], or poly(vinylidene fluoride) (PVDF) [260] were activated by different techniques of irradiation, for example, thermally, in the presence of ozone, from swift heavy ions, electron beam or γ rays. The irradiated polymer films were immersed in styrene solution to graft polystyrene onto the fluorinated backbone, and finally, the non-conducting hydrophobic materials were sulphonated by chlorosulphonic acid. The degree of grafting can be controlled by the concentration of styrene, choice of solvent, temperature and time of grafting.

The synthetic strategies presented above are widely used in the formation of polymers bearing functional moieties for proton conduction [23, 112]. The resulting materials are designed to serve as stand-alone PEM, although they might also be a host for inorganic compounds or organic polymer to afford a proton conducting component in a blend or composite. Preparation of such polymeric systems is a promising technique to improve the membrane ionic conductivity, mechanical strength, water retention and to decrease the fuel permeability, especially at elevated operating temperatures [261]. To overcome the most crucial problem, that is, the severe loss of conductivity at working temperatures above 100 °C, two strategies have been developed. The first approach is based on systems that exhibit a high resistance to dehydration or are capable of maintaining high conductivity with low water content. The other strategy employs systems where media other than water assist the proton transport. Ionomer composite membranes include perfluorosulphonic acid ionomer/polymer matrix membranes (e.g. PTFE/perfluorinated ionomer macrocomposite membrane from W. L. Gore and Associates, Inc. – Gore®Select [262], sulphonated FEP/Nafion hybrid membrane [263], or Nafion/PBI composite membrane doped with phosphoric acid [264]), perfluorosulphonic acid ionomer/inorganic fillers composite membranes (e.g. Nafion/SiO_2 nanocomposite membrane [265], Nafion/TiO_2 composite membrane [266], Nafion/Zirconium phosphate (α-ZrP) composite membrane [267], or Nafion/polyphenylsilsesquioxane (PPSQ) – polysiloxane composite membrane [268]), sulphonated polymer/inorganic proton conductor systems (e.g. most widely studied SPEEK/heteropolyacids (HPA) composite membranes [214–222]), polymer/acid complexes (e.g. PBI/H_3PO_4 based membranes [269], or poly (diallyldimethylammonium-dihydrogenphosphate ($PAMA^+H_2PO_4^-$)/H_3PO_4 blend membrane [270], sulphonated polymer/base complexes (e.g. SPEEK/imidazole or pyrazol complex membranes [271]), or polymer blends (e.g. SPEEK/PBI and ortho-sulphone-sulphonated poly(arylethersulphone (SPSU)/BPI as the acid/base blend membranes [272], or sulphonated poly(phenylene oxide) (SPPO)/PVDF [273]). The current trend is for the composite and hybrid membranes, which combine the properties of both the polymeric matrix and inorganic part.

Cross-linking is another efficient strategy to improve the thermal stability, mechanical strength and oxidative stability, as well as to lower the water uptake of ionomeric membranes. It has been widely employed in modifying the structure of sulphonated aromatic polymers in particular [188, 274]. A cross-linking reaction can be defined as a process where a polymer becomes a dense three-dimensional network by varied interactions, such as covalent bonds, as a result of the chemical reaction (e.g. esterification, addition, Friedel–Crafts reactions and the formation of sulphone $-SO_2-$ bridges), ionic bonds or hydrogen bonds, as well as a combination of covalent and ionic bonds [275]. Chemical cross-linking was employed to modify a wide range of aromatic polymers of potential FC applications including polybenzimidazoles (PBIs) [131–134], polyphosphazenes (PPZs) [152, 153], sulphonated polyimides (SPIs) [164–167], and sulphonated poly(ether ether ketone)s (SPEEKs) [187–190]. Nonetheless, the expanded polymer network and increased cross-linking density may cause a decrease in the proton conductivity and flexibility of the PEMs [187].

10.6 Applications of PEM fuel cell technology

Fuel cells have the potential to replace such conventional power sources as internal combustion engines or batteries due to their high energy efficiencies and low emissions. The efficiency can reach as much as 60 % in electrical energy conversion and an overall 80 % in the cogeneration of electrical and thermal energies. Additionally, fuel cells can significantly reduce (by more than 90 %) or even eliminate pollution – such as in the case of hydrogen-fuelled FCs, where the water forms as a non-polluting by-product, which can further be reused as potable water. Use of the FCs can also eliminate the emission of greenhouse gases, since hydrogen fuel can be produced in an environmentally friendly manner such as through the electrolysis of water driven by renewable energy, and not generated by burning fossil fuels, mostly coal and natural gas. As a consequence, avoiding the need for the usage of conventional carbon-based fuels' (coal, oil and gas) can significantly decrease economic dependence on oil producing countries and, therefore, also provide greater security of energy supply for the user nation. Moreover, most of the fuel cells operate with a low noise level compared to conventional combustion engines, and therefore, they are ideally suited for use within buildings and readily accepted in residential areas. The availability of stationary fuel cells at any location with access to a source of power and water supply essential for producing the hydrogen fuel may result in a decentralization of power grids, the reduction of transmission and distribution losses, and, thus, considerable decrease the grid dependence. Furthermore, unlike batteries, fuel cells exhibit longer operating times that depend on the amount of fuel supplied and not on the capacity of the unit itself, quick recharge by fuelling, no "memory effect" during refuelling – no gradual energy capacity loss after repeated recharging or partial discharging – and a modular design allowing for the easy exchange of cells' parts, and low maintenance costs. Although fuel cells feature outstanding properties, such features as high initial cost and relatively low durability still remain the greatest obstacle to their commercial implementation. Nevertheless, fuel cell technology can compete with the conventional, well-established technologies (internal combustion engines or batteries) in practically all applications [276].

The three major areas of application for fuel cell technology are portable power generation, stationary power generation and power for transportation. A fuel cell's power output parameters depend on several factors, including the type, size, operating temperature and pressure of the supplied gases. As already presented, most often the various types of fuel cells are classified by the electrolyte used. It determines the potential for their application in certain FC technologies through their working temperature (T) profile. The profile impacts such vital characteristics as: (i) efficiency (η): the higher the temperature, the lower the internal resistivity and polarization, and offsetting of the voltage drop in result of the temperature increase, (ii) start-up time (the time needed for reaching the cell's optimal operating temperature) is longer for higher temperatures, (iii) dynamic behaviour: fluctuating temperatures following the changing load lead to a repeated stack material shrinking or expanding and the resultant mechanical stress reduces the fuel cells' lifetime, especially in the case of high temperature units (HTFC) that have ceramic components [277].

The three latter parameters above determine the applicability of specific FC technologies. Figure 10.20 illustrates the dependence quite well: for large stationary applications that require, most of all, high efficiency (with the start-up time and load-following dynamics being less important), MCFC or SOFC are the most suitable types. Mobile and portable equipment, on the other hand, needs short start-up times in any, also sub-zero, temperatures, so PEMFCs would be preferred.

Another criterion for FC technology selection is fuel availability. From the electrochemical point of view, hydrogen is the best fuel; its direct reaction ensures the system's high power density. However, being a gas, the fuel is difficult to handle. As for much easier to manage liquids, only methanol reacts directly at acceptable rates, but its power density is less than 20 % of direct hydrogen fuel cells. Other liquid fuels

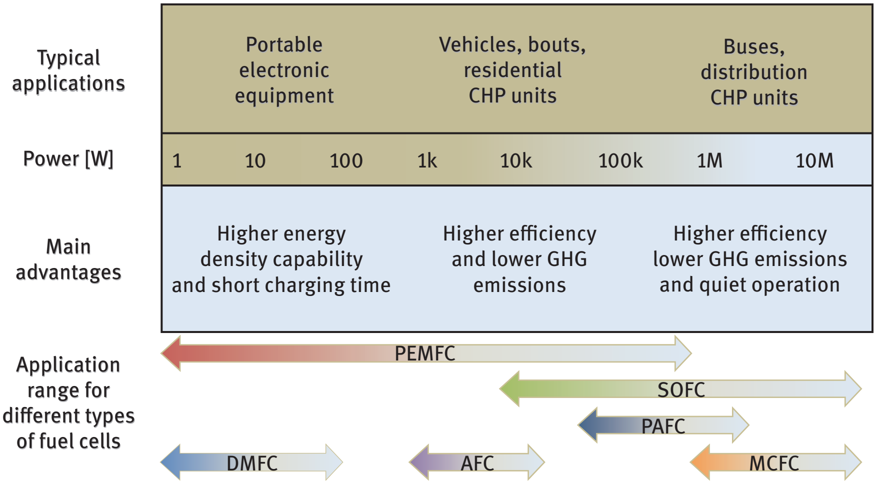

Figure 10.20: Typical applications of different fuel cells' types.

require reforming into H_2-rich gases. This applies also to natural gas (NG), although in this case the advantage is the already existing dense supply network. The conversion process produces catalyst poisons, such as carbon monoxide (CO), that are desorbed in high temperatures, which makes high temperature fuel cells (HT-FCs) the preferred type for the overall reduced cell complexity and ease of handling.

Portable fuel cells can be defined as low power systems being an integral part, or external charging up, of products designed to be moved. Prime candidates for FCs application are small personal electronics (mp3 players, mobile phones, cameras), large personal electronics (laptops, printers, radios), or education kits and toys. Fuel cells also earn much attention as power supply for military applications in portable soldier's appliances or skid mounted generators, or auxiliary power units (APU) for the leisure and trucking industries, as well as portable products (torches, trimmers) or emergency equipment [278]. The typical power range for portable electronic devices is from less than 5 W (micro power application) to 500 W. Portable/micro fuel cells are generally an alternative to batteries and typically are based on either PEM or DMFC technology. These FC applications are mostly driven by the capability of higher energy density, extending a device's operating time, the reduction of noise and emissions, and a short charging time [279]. The market of portable fuel cells is led by the following players: Horizon, myFC, Inteligence Energy, eZelleron, EnyMotion, Truma, Acumtrics, Thoshiba, NEC, Hitachi, Panasonic, Samsung, Sanyo, or LG [277].

Stationary fuel cells are units providing electricity (and sometimes heat), but not designed to be moved. As the prime power source, they are most commonly used in large cogenerated heat and power (CHP) systems, residential applications (resCHP) and uninterrupted power supply solutions (UPS). Development works continue on expanding their functionality by adding absorption chillers to make trigeneration systems that provide heat, power, and a cooling capacity [280]. These would be of particular interest in situations characterized by comparable, seasonally fluctuating demand for heat and cooling power. An additional benefit would be the suitability of oxygen-free exhaust gases for fire prevention. An important feature of this type of FC is their resilience, that is, their ability to mitigate drops and peaks in the demand/supply, which is particularly useful in distributed power grids for absorbing local events, such as blackouts, or for stabilization and backing-up purposes. Stationary FCs make up the body of global FC sales. As reported by Navigant Research, they amounted to over 70 % of the total FC turnover in 2014 [281]. The type is expected to remain most popular, with the annual volume growing from approximately 40,000 in 2014 to 1.25 million in 2022, which translates into a 51.7 % compound annual growth rate (CAGR). One of the most popular types of FCs used for stationary purposes is CHP units. They generate not only power, but also heat that otherwise would be wasted, which increases their total efficiency to 80–95 %. Both types of energy find use in residential applications. Based on either PEM or SOFC technology, the fuel cells have the power output range of 0.5 kW to 10 kW. Residential CHPs are popular in Japan (over 10,000 cumulative units deployed by the end of

2010) and South Korea, although in the second case, their purchase still relies on government subsidies. Another type of stationary FC units belongs to UPS systems. They are used for continuous power supply in case of blackouts, for instance. As for the fuel type used, it differs by region: in Asia the most common fuel is natural gas and LPG, in the United States it is hydrogen, while, in Europe, there have been attempts of fuelling with methanol. Finally, there is a wide range of large stationary primary power source units ranging from 1 to 50 MW. Their main purpose is to take over the power grid function in areas with little or no network, or to extend it by additional nodes in such cases. Based on four FC types (SOFC, MCFC, PEMFC, and PAFC), the systems are mostly provided by manufactures in the United States and Japan. The prime power market of large stationary fuel cells is led by three players such as: Fuel Cell Energy (MCFC systems), Bloom Energy (SOFC systems), and Doosan (prior ClearEdge Power, PAFC systems). Moreover, commercially available PEMFC systems include units for back-up and off-grid power applications from Axane, Ballard, Power Cell, Electro Power Systems, Heliocentris, Horizon, Hydrogenics or ReliOn-Plug Power, as well as for residential CHP usage from Ene-Farm [277].

Fuel cells for transport applications are units designed as the power source for vehicles or for extending their drive range. Their advantages include their zero emissions and considerably higher efficiency than ICE or battery-powered vehicles. The use of FCs has increased the range of electric vehicles (EVs) and reduced the refuelling time (sometimes to as little as a few minutes) compared to battery-based vehicles. Because of the power demand characteristics (short start-up time and high load dynamics), the cell type most often applied is PEMFC. The preferred fuel is hydrogen compressed to 350 or 700 bars, although the availability of fuelling stations is limited. The reason is a lack of feasible technology for on-board processing systems that would produce hydrogen from such liquid fuels as methanol, LPG, gasoline, or diesel. In transport, fuel cells are applied mainly in passenger cars, buses and cargo vehicles but H_2 and O_2-fueled PEMFCs are also successfully used in military submarines, allowing silent underwater operations for up to three weeks without surfacing [279]. Development works continue for light traction vehicles such as golf cars, airport carts, wheelchairs, and motorcycles, bicycles, ships, airplanes, trams and locomotives. Although FC-powered light duty vehicles (LDVs) have not been commonly used so far, the situation started to change in 2014, with Toyota's launch of its Mirai model. The deployment commenced at a few nodes with the required refuelling infrastructure in Germany, Japan, and the United States, but it is expected to spread from these centres as the market grows. Another sector for fuel cells is bus transport. It keeps growing with every new model presented successfully in Europe, Japan, Canada and USA. The capital cost remains high, although it is expected to become comparable to the prices of hybrid diesel buses in the near future. There are also a few niche transport applications, some successfully marketed, such as PEMFC-powered materials handling vehicles, popular in the United States and making up about 90 %

of the category, as well as other applications less commercialized and still under development, such as unmanned aerial vehicles (UAV), e-bikes or trains.

In unit shipment terms, PEM has been the most popular fuel cell technology for a number of years because of its versatility and sizeablity. Measured in megawatts, the distribution between various types is more even due to the contribution from the limited applicability but high power MCFCs and SOFCs commonly used for large stationary applications as the primary source of power. The medium versatility range is characterized by the SOFCs applied in stationary and some portable equipment, while DMFCs, similar to PEMs, are the most "dedicated" technology means useful in small transport units and for power grid extension or back-up purposes (Figure 10.21) [282, 283].

2015 marked a considerable change in the PEM sales trend by power output. Previously stable at about 60 – 70 MW annually, shipments more than doubled that year, reaching 180 MW and making up more than a half of the total fuel cell technology turnover. The sales increased due to the launch of fuel cell electric cars, mostly two models manufactured by Toyota and Hyundai. The growth trend is expected to sustain, especially in that the figures are easy to attribute, knowing the vehicles' power rating of 114 and 100 kW, respectively, and considering the contribution from forklift trucks' (FLT) and buses' stacks as well as other transport applications. The impact of the few hundred vehicles on the global sales structure clearly illustrates the size of the current fuel cells market [283].

Nonetheless, the automotive sector is not the only source of the sector's growth: micro-CHPs continue to gain in popularity in Japan and, to an extent, in Europe, as UPS solutions or grid extension nodes. Although dominated by Japanese and Canadian companies, the market is being entered into by new players such as

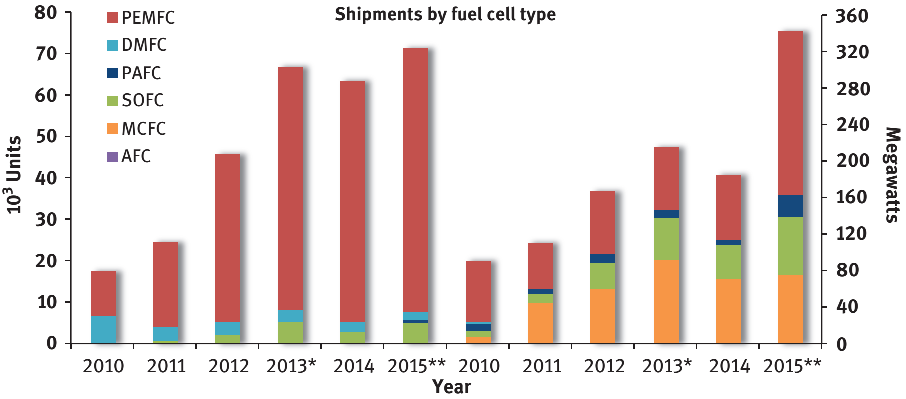

Figure 10.21: Market development of various fuel cell types based on sales from 2010 to 2015 in units and by power output (MW). * *Uncorrected Fuel Cell Today forecast from 2013* [282]. ** *Uncorrected E4tech forecast from 2015* [283].

American Altergy or ReliOn. Japanese PEM technology finds its use also in European micro-CHPs (Viessmann and Baxi/Senertec), although there are companies that prefer other solutions, such as Elcore marketing its own patented high temperature PEMs [283].

Fuel cell technology has proven feasible in a number of applications: as CHPs, remote or back-up sources of power, or for vehicle propulsion. It has successfully handled such challenges as the matter of having sufficient power density or problems with the durability of specific applications. Nonetheless, the cost of the inevitable technology is still too high, and its further reduction requires significant research and investment in its development.

10.7 Summary and future perspectives

This review presents the most important research on alternative polymer membranes with ionic groups attached, provides examples of materials with a well-defined chemical structure that are described in the literature, and elaborates on the synthetic methods used for preparing PEMs and the current status of fuel cell technology and its application. It also briefly discusses the development the PEMFC market.

The growing FC market is a clear driver for the scientific community to continue working on the development of inexpensive and efficient materials for the membranes. The two main barriers to global commercialization of PEM fuel cells are their durability and cost of production. Recently, we have seen considerable progress in this respect, and the two attributes can be successfully used for illustrating the current status of PEMFC technology, as set in the targets of the U.S. Department of Energy for: (1) durability: (i) for transportation applications, 5000 h by 2020, and, ultimately, 8000 h, (ii) for distributed generation and micro-CHP fuel cell systems on natural gas or liquid petroleum gas (5kW), 60,000 h by 2020 and (iii) for medium-sized CHP systems (100 kW–3 MW), 80,000 h by 2020 [284]; the currently achieved figures for the three applications are: less than 4000 h (2015, 285], 6000 h (2011) and 30,000 h (2011), respectively [286] and (2) the cost: (i) for transportation applications, \$40/kW in 2020, and, ultimately \$30/kW, and (ii) for the distributed power and CHP, \$1000/kW to \$1500/kW by 2020, depending on the size and application [284]. The cost of power in fuel cell transport systems was \$53/kW in 2015 [285]. Moreover, DOE completed the set of targets with the maximum efficiency: 65 % for transportation, 45 % electric efficiency for micro-CHP systems, and 50 % electric efficiency and 90 % CHP efficiency for medium-sized combined heat and power fuel cell stacks.

The cost of FCs needs to be reduced by over 40 %, but for the manufacturing plants the current figure of \$53/kW translates into as much as over a half of the total system cost, and it has not been reduced considerably in the recent years [284]. The biggest cost component of the overall FC system is the membrane, followed by the catalyst. The only way to make catalyst production less expensive is to reduce the content of the platinum, but no significant progress has been reported recently in this respect. That makes lowering the cost of membranes the main method of limiting the total FC cost, that is, the change required for global marketing and popularization of the inevitable solution [287].

Although for availability and applicability reasons Nafion and similar polyperfluorosulphonic acid membranes still remain the best researched materials in properties' terms, little is known about their manners of synthesizing, chemical composition and molecular weight. Even if they exceed their alternatives with regard to many vital properties, it might be required to compromise such attributes as a favourable conductivity profile, and develop alternative membranes that could well offset the loss with potential other advantages, such as thermal stability, durability, applicability in a wider range of conditions (especially humidity), limited swelling, lower fuel crossover, and, especially, lower cost of production and operation. Given the current status of research on and interest in PEM membranes, they remain the most promising, certainly in the short run, future solution to the challenges presently faced.

References

[1] Fuel Cell Today Industry Review. Fuel cells: a history, 2011. March 2011. Available at:. 22March2016 http://www.fuelcelltoday.com/history.

[2] Boudghene Stambouli A, Traversa E. Fuel cells, an alternative to standard sources of energy. Renew Sustain Energy Rev. 2002;6:297–306.

[3] Kirubakaran A, Jain S, Nema RK. A review on fuel cell technologies and power electronic interface. Renew Sustain Energy Rev. 2009;13:2430–2440.

[4] Cleantech magazine: Fuel Cell Special. March 2010. March222016 http://www.cleantechinvestor.com/portal/2010-issue-5.html.

[5] http://quotesgram.com/humphry-davy-quotes/#jjYgzy9nwn.

[6] http://www.sil.si.edu/digitalcollections/hst/scientific-identity/CF/display_results.cfm?alpha_sort=s.

[7] https://pl.wikipedia.org/wiki/William_Grove.

[8] https://sites.google.com/site/d1b2tpetersonjschleisman/historical-info.

[9] http://www.britannica.com/biography/Francis-Thomas-Bacon.

[10] http://americanhistory.si.edu/fuelcells/pem/pem2.htm.

[11] http://www.nasa.gov/centers/dryden/Features/sts-1_31st_anniversary_prt.htm.

[12] http://fuelcellstore.com/Chemours/nafion-211.

[13] http://www.conceptcarz.com/z19151/GMC-Electrovan-Experimental.aspx.

[14] http://www.sociologydiscussion.com/economics/1979-oil-crisis-that-led-to-the-liberalisation-of-indian-economy/991.

[15] http://www.fuelcelltoday.com/analysis/analyst-views/2013/13-07-03-fuel-cells-and-submarines.

[16] http://www.energysavingadvisor.co.uk/micro-chp/how-micro-chp-technologies-work.

[17] http://www.intelligent-energy.com/our-divisions/automotive/case-studies/the-env-fuel-cell-motorcycle/.

[18] http://www.samar.pl/wiadomosci/wodorowa-toyota-mirai-z-nowa-technologia?locale=pl_PL.

[19] Mark Ormerod R. Solid oxide fuel cells. Chem Soc Rev. 2003;32:17–28.

[20] Mekhilefa S, Saidurb R, Safari A. Comparative study of different fuel cell technology. Renew Sustain Energy Rev. 2012;16:981–989.

[21] en.wikipedia.org: fuel cell. March 2016. March232016 https://en.wikipedia.org/wiki/Fuel_cell.

[22] Hickner MA, Ghassemi H, Kim YS, Einsla BR, McGrath JE. Alternative polymer systems for proton exchange membranes (PEMs). Chem Rev. 2004;104:4587–4612.

[23] Zhang H, Shen PK. Recent development of polymer electrolyte membranes for fuel cells. Chem Rev. 2012;112:2780–2832.

[24] Wang Y-J, Qiao J, Bakerb R, Zhang J. Alkaline polymer electrolyte membranes for fuel cell applications. Chem Soc Rev. 2013;42:5768–5787.

[25] Pachauri RK, Chauhan YK. Various control schemes of power management for phosphoric acid fuel. Electr Power Energy Syst. 2016;74:49–57.

[26] Kulkarni A, Giddey S. Materials issues and recent developments in molten carbonate fuel cells. J Solid State Electrochem. 2012;16:3123–3146.

[27] Akbari E, Buntat Z, Nikoukar A, Kheirandish A, Khaledian M, Afroozeh A. Sensor application in Direct Methanol Fuel Cells (DMFCs). Renew Sustain Energy Rev. 2016;60:1125–1139.

[28] Vogel W, Lundquist J, Ross P, Stonehart P. Reaction pathways and poisons–II: the rate controlling step for electrochemical oxidation of hydrogen on Pt in acid and poisoning of the reaction by CO. Electrochim Acta. 1975;20:79–93.

[29] Chin D-T, Howard PD. Hydrogen sulphide poisoning of platinum anode in phosphoric anode in phosphoric acid fuel cell electrolyte. J Electrochem Soc. 1986;133:2447–2450.

[30] U.S. Department of Energy Office of Fossil Energy, National Energy Technology Laboratory. Phosphoric acid fuel cell. Fuel cell handbook (Seventh Edition). Morgantown, USA: EG&G Technical Services, Inc., 2004:5–24.

[31] Ovshinsky SR, Venkatesan S, Corrigan DA. United States Patent Application Publication. Pub. No.: US 2006/0204830 A1 Molten carbonate fuel cell.

[32] Farooque M, Maru HC. Fuel cells – the clean and efficient power generators. Proc IEEE. 2001;89:1819–1829.

[33] Garcia BL, Sethuraman VA, Weidner JW, White RE, Dougal R. Mathematical model of direct methanol fuel cell. J Fuel Cell Scitechnol. 2004;1:43–48.

[34] Millington B, Du S, Pollet BG. The effect of materials on proton exchange membrane fuel cell electrode performance. J Power Sources. 2011;196:9013–9017.

[35] Schweiss R-B. Membrane electrode assembly, SGL Carbon, German Patent Application WO/2016/005257 2016.

[36] Litster S, McLean G. PEM fuel cell electrodes. J Power Sources. 2004;130:61–76.

[37] Ma S, Chen Q, Jøgensen FH, Stein PC, Skou EM. ^{19}F NMR studies of Nafion™ionomer adsorption on PEMFC catalysts and supporting carbons. Solid State Ionics. 2007;178:1568–1575.

[38] O'Hayre R, Lee SJ, Cha SW, Prinz FB. A sharp peak in the performance of sputtered platinum fuel cells at ultra-low platinum loading. J Power Sources. 2002;109:483–493.

[39] Cuynet S, Caillard A, Kaya-Boussougou S, Lecas T, Semmar N, Bigarre J, et al. Membrane patterned by pulsed laser micromachining for proton exchange membrane fuel cell with sputtered ultra-low catalyst loadings. J Power Sources. 2015;298:299–308.

[40] Ozdemir OK. Effect of sputtering power on the electrochemical properties of low loaded Pt catalysts for PEM fuel cell. Electrochemistry. 2015;83:76–79.

[41] Cindrella L, Kannan AM, Lina JF, Saminathan K, Hoc Y, Lind CW, et al. Gas diffusion layer for proton exchange membrane fuel cells–A review. J Power Sources. 2009;194:146–160.

[42] Morgan JM, Datta R. Understanding the gas diffusion layer in proton exchange membrane fuel cells. I. How its structural characteristics affect diffusion and performance. J Power Sources. 2014;251:269–278.

[43] Hermann A, Chaudhuri T, Spagnol P. Bipolar plates for PEM fuel cells: a review. Int J Hydrogen Energy. 2005;30:1297–1302.

[44] Au SF, Hemmes K, Woudstra N. The influence of operating temperature on the efficiency, of combined fuel cell and power systems. J Electrochem Soc. 2002;7:879–885.

[45] Chandan A, Hattenberger M, El-Kharouf A, Du S, Dhir A, Self V, et al. High temperature (HT) polymer electrolyte membrane fuel cells (PEMFC) – A review. J Power Sources. 2013;231: 264–278.

[46] Authayanun S, Mamlouk M, Scott K, Arpornwichanop A. Comparison of high-temperature and low-temperature polymer electrolyte membrane fuel cell systems with glycerol reforming process for stationary applications. Appl Energy. 2013;109:192–201.

[47] Das SK, Reis A, Berry KJ. Experimental evaluation of CO poisoning on the performance of a high temperature proton exchange membrane fuel cell. J Power Sources. 2009;193:691–698.

[48] Scott K, Pilditch S, Mamlouk M. Modelling and experimental validation of a high temperature polymer electrolyte fuel cell. J Appl Electrochem. 2007;37:1245–1259.

[49] Barelli L, Bidini G, Gallorini F, Ottaviano A. An energetic–exergetic analysis of a residential CHP system based on PEM fuel cell. Appl Energy. 2011;88:4334–4342.

[50] Oh S-D, Kim K-Y, Oh S-B, Kwak H-Y. Optimal operation of a 1-kW PEMFC-based CHP system for residential applications. Appl Energy. 2012;95:93–101.

[51] Wee J-H. Applications of proton exchange membrane fuel cell systems. Renew Sustain Energy Rev. 2007;11:1720–1738.

[52] Schaller KV, Gruber C. Fuel cell drive and high dynamic energy storage systems – Opportunities for the future city bus. Fuel Cells Bull. 2000;3:9–13.

[53] Panik F. Fuel cells for vehicle applications in cars-bringing the future closer. J Power Sources. 1998;71:36–38.

[54] Kawatsu S. Advanced PEFC development for fuel cell powered vehicles. J Power Sources. 1998;71:150–155.

[55] Lloyd AC. The California fuel cell partnership: an avenue to clean air. J Power Sources. 2000;86:57–60.

[56] Weiner SA. Fuel cell stationary power business development. J Power Sources. 1998;71:61–64.

[57] Gasteiger HA, Panels JE, Yan SG. Dependence of PEM fuel cell performance on catalyst loading. J Power Sources. 2004;127:62–71.

[58] Pachauri RK, Chauhan Y. A study, analysis and power management schemes for fuel cells. Renewable and Sustainable Energy Reviews. 2015;43:1301–1319.

[59] Kim DJ, Jo MJ, Nam SY. A review of polymer-nanocomposite electrolyte membranes for fuel cell application. Journal of Industrial and Engineering Chemistry. 2015;21:36–52.

[60] Chang H, Koschany P, Lim C, Kim J. Materials and processes for light weight and high power density PEM fuel cells. J New Mater Electrochem Syst. 2000;3:55–59.

[61] Bae JM, Honma I, Murata M, Yamamoto TM, Ogata N. Properties of selected sulphonated polymers as proton-conducting electrolytes for polymer electrolyte fuel cells. Solid State Ionics. 2002;147:189–194.

[62] Connolly DJ, Gresham WF. US Patent 3,282,875 1966. Fluorocarbon vinyl ether polymers.

[63] Peighambardoust SJ, Rowshanzamir S, Amjadi M. Review of the proton exchange membranes for fuel cell applications. Inter J Hydrogen Energy. 2010;35:9349–9384.

[64] Gabbasa M, Sopian K, Fudholi A, Asim N. A review of unitized regenerative fuel cell stack: material, design and research achievements. Inter J Hydrogen Energy. 2014;39:17765–17778.

[65] Yang Y, Siu A, Peckham TJ, Holdcroft S. Structural and morphological features of acid-bearing polymers for PEM fuel cells. Adv Polym Sci. 2008;215:55–126.

[66] Rao V, Kluy N, Ju W, Stimming U. Proton-conducting membranes for fuel cells. In: Pabby AK, Rizvi SSH, Sastre Requena AM, editors. Handbook of membrane separations: chemical, pharmaceutical, food and biotechnological applications, 2nd ed Boca Raton, FL: CRC Press, 2015;567–614.

[67] Eisman GA. The application of dow chemical's perfluorinated membranes in proton exchange fuel cells. J Power Sources. 1990;29:389–398.

[68] Rivard LM, Pierpont D, Freemeyer HT, Thaler A, Hamrock SJ. Development of a new electrolyte membrane for PEM fuel cells. Fuel cell seminar, Florida, USA: Miami Beach, 2003.

[69] Du X, Yu J, Yi B, Han M, Bi K. Performances of proton exchange membrane fuel cells with alternate membranes. Phys Chem Chem Phys. 2001;3:3175–3179.

[70] Arcella V, Troglia C, Ghielmi A. Hyflon ion membranes for fuel cells. Ind Eng Chem Res. 2005;44:7646–7651.

[71] Savadogo O. Emerging membranes for electrochemical systems. Part I. Solid polymer electrolyte membranes for fuel cell systems. J New Mat Electr Sys. 1998;1:47–66.

[72] Savadogo O. Emerging membranes for electrochemical systems. Part II. High temperature composite membranes for polymer electrolyte fuel cell (PEFC) applications. J Power Sources. 2004;127:135–161.

[73] Eikerling M, Kornyshev AA, Stimming U. Electrophysical properties of polymer electrolyte membranes: a random network model. J Phys Chem B. 1997;101:10807–10820.

[74] Ion Power. April 2016. April122016 http://www.nafionstore.com.

[75] Seger B, Vinodgopal K, Kamat PV. Proton activity in nafion films: probing exchangeable protons with methylene blue. Langmuir. 2007;23:5471–5476.

[76] Hogarth WHJ, Diniz da Costa JC, Lu GQ. Solid acid membranes for high temperature (140 °C) proton exchange memebrane fuel cells. J Power Sources. 2005;142:223–237.

[77] Smitha B, Sridhar S, Khan AA. Solid polymer electrolyte membranes for fuel cell applications – a review. J Membr Sci. 2005;259:10–26.

[78] Gebel G. Structural evolution of water swollen perfluorosulphonated ionomers from dry membrane to solution. Polymer. 2000;41:5829–5838.

[79] Wu D, Paddison SJ, Elliott JA. Effect of molecular weight on hydrated morphologies of the short-side-chain perfluorosulphonic acid membrane. Macromolecules. 2009;42:3358–3367.

[80] Deluca NW, Elabd YA. Polymer electrolyte membranes for the direct methanol fuel cell: a review. J Polym Sci Part B Polym Phys. 2006;44:2201–2225.

[81] Grubb WT. Fuel cell 1955. US Patent 2,913,511.

[82] Grubb WT. Batteries with solid ion exchange electrolytes i. Secondary cells employing metal electrodes. J Electrochem Soc. 1959;106:275–278.

[83] Grubb WT, Niedrach LW. Batteries with solid ion-exchange membrane electrolytes II. Low-temperature hydrogen-oxygen fuel cells. J Electrochemsoc. 1960;107:131–135.

[84] Wakizoe M, Velev OA, Srinivasan S. Analysis of proton exchange membrane fuel cell performance with alternate membranes. Electrochim Acta. 1995;40:335–344.

[85] Gubler L, Dockheer SM, Koppenol WH. Radical (HO•, H• and HOO•) formation and ionomer degradation in polymer electrolyte fuel cells. J Electrochemsoc. 2011;158 B755–B769.

[86] Yu J, Yi B, Xing D, Liu F, Shao Z, Fu Y, et al. Degradation mechanism of polystyrene sulphonic acid membrane and application of its composite membranes in fuel cells. Phys Chemchem Phys. 2003;5:611–615.

[87] Dockheer SM, Gubler L, Bounds PL, Domazou AS, Scherer GG, Wokaunb A, et al. Damage to fuel cell membranes. Reaction of HO• with an oligomer of poly(sodium styrene sulphonate) and subsequent reaction with O2. Phys Chemchem Phys. 2010;12:11609–11616.

[88] Dockheer SM, Gubler L, Koppenol WH. Reactions of the tetraoxidosulphate(•) and hydroxyl radicals with poly(sodium α-methylstyrene sulphonate). Phys Chemchem Phys. 2013;15: 4975–4983.

[89] Fan Q, Hussain H. 2008. High stability membrane for proton exchange membrane fuel cells. US Patent 7,323,265.

[90] Assink RA, Arnold C, Hollandsworth RP. Preparation of oxidatively stable cation-exchange membranes by the elimination of tertiary hydrogens. J Membr Sci. 1991;56:143–151.

[91] Zu J, Liu R, Wei Y, Wang P, Fu H, Tang F, et al. Pulse radiolysis investigation of •OH and •H radicals initiated degradation reaction of sulphonated aromatics as model compounds for proton exchange membrane. Res Chem Intermed. 2016;42:2883–2898.

[92] Cohen SG, Wolosinski HT, Scheue PJ. α,β,β-Trifluorostyrene and α-chloro-β,β-difluorostyrene. J Am Chem Soc. 1949;71:3439–3440.

[93] Prober M. The synthesis and polymerization of some fluorinated styrenes. J Am Chem Soc. 1953;75:968–973.

[94] Hodgdon RB. Polyelectrolytes prepared from perfluoroalkylaryl macromolecules. J Polym Sci Part A. 1968;6:171–191.

[95] Wei J, Stone C, Steck AE. 1995. Trifluorostyrene and substituted trifluorostyrene copolymeric compositions and ion-exchange membranes formed therefromUS Patent 5,422,411.

[96] Kerres JA. Development of ionomer membranes for fuel cells. J Membr Sci. 2001;185:3–27.

[97] Stone C, Daynard TS, Hu LQ, Mah C, Steck AE. Phosphonic acid functionalized proton exchange membranes for pem fuel cells. J New Mater Electrochem Sys. 2000;3:43–50.

[98] Yegorova YI, Smirnova ZA, Dukukina AF. The synthesis and polymerization (copolymerization) of fluorinated styrenes – III. The preparation and properties of copolymer of vinyl monomers with styrene fluorinated in the side chain. Vysokomolsoyed. 1964;7:1187–1189.

[99] Walkowiak J, Martinez del Campo T, Ameduri B, Gouverneur V. Syntheses of mono-, di-, and trifluorinated styrenic monomers. Synthesis. 2010;11:1883–1890.

[100] Walkowiak-Kulikowska J, Kanigowska J, Koroniak H. α-(Difluoromethyl)styrene: improved approach to grams scale synthesis. J Fluorine Chem. 2015;179:175–178.

[101] Walkowiak-Kulikowska J, Szwajca A, Boschet F, Gouverneur V, Ameduri B. Iodine transfer copolymerization of fluorinated α-methylstyrenes with styrene using 1-iodoperfluorohexane as the chain transfer agent. Macromolecules. 2014;47:8634–8644.

[102] Elabd YA, Napadensky E, Sloan JM, Crawford DM, Walker CW. Triblock copolymer ionomer membranes Part I. Methanol and proton transport. J Membr Sci. 2003;217:227–242.

[103] Elabd YA, Napadensky E. Sulphonation and characterization of poly(styrene-isobutylene-styrene) triblock copolymers at high ion-exchange capacities. Polymer. 2004;45: 3037–3043.

[104] Lawton JS, Budil DE. Spin probe ESR study of cation effects on methanol and DMMP solvation in sulphonated poly(styrene-isobutylene-styrene) triblock copolymers at high ion-exchange capacities. Macromolecules. 2010;43:652–661.

[105] Elamathi S, Nithyakalyani G, Sangeetha D, Ravichandran S. Preparation and evaluation of ionomeric membranes based on sulphonated-poly(styrene_isobutylene_styrene) membranes for proton exchange membrane fuel cells (PEMFC). Ionics. 2008;14:377–385.

[106] Kim J, Kim B, Jung B. Proton conductivities and methanol permeabilities of membranes made from partially sulphonated polystyrene-block-poly(ethylene-ran-butylene)-block-polystyrene copolymers. J Membr Sci. 2002;207:129–137.

[107] Serpico JM, Ehrenberg SG, Fontanella JJ, Jiao Z, Perahia D, McGrady KA, et al. Transport and structural studies of sulphonated styrene–ethylene copolymer membranes. Macromolecules. 2002;35:5916–5921.

[108] Muller F, Ferreira CA, Franco L, Puiggali J, Aleman C, Armelin E. New sulphonated polystyrene and styrene–ethylene/butylene–styrene block copolymers for applications in electrodialysis. J Phys Chem B. 2012;116:11767–11779.

[109] Chen L, Hallinan DT, Jr Eladb YA, Hillmyer MA. Highly selective polymer electrolyte membranes from reactive block polymers. Macromolecules. 2009;42:6075–6085.

[110] Trogadas P, Ramani V. Membrane and MEA development in polymer electrolyte fuel cells. In: Zaidi SMJ, Matsuura T, editors. Polymer membranes for fuel cells. New York, USA: Springer, 2009:253–280.

[111] Gubler L. Polymer design strategies for radiation-grafted fuel cell membranes. Adv Energy Mater. 2014;4:1300827.

[112] Kraytsberg A, Ein-Eli Y. Review of advanced materials for proton exchange membrane fuel cells. Energy Fuels. 2014;28:7303–7330.

[113] Momose T, Yoshioka H, Ishigaki I, Okamoto J. Radiation grafting of α,β,β-trifluorostyrene onto poly(ethylene-tetrafluoroethylene) film by preirradiation method. II. Properties of cation-exchange membrane obtained by sulphonation and hydrolysis of the grafted film. J App Polymsci. 1989;38:2091–2101.

[114] Jetsrisuparb K, Balog S, Bas C, Perrin L, Wokaun A, Gubler L. Proton conducting membranes prepared by radiation grafting of styrene and various comonomers. Eur Polym J. 2014;53:75–89.

[115] Gubler L, Slaski M, Wallasch F, Wokaun A, Scherer GG. Radiation grafted fuel cell membranes based on co-grafting of α-methylstyrene and methacrylonitrile into a fluoropolymer base film. J Membr Sci. 2009;339:68–77.

[116] Sannigrahi A, Ghosh S, Maity S, Jana T. Polybenzimidazole gel membrane for the use in fuel cell. Polymer. 2011;52:4319–4330.

[117] Vogel H, Marvel CS. Polybenzimidazoles, new thermally stable polymers. J Polym Sci Part A Polym Chem. 1961;50:511–539.

[118] Savinell RF, Litt MH. Proton conducting polymers used as membranes 1994. US Patent 5,525,436.

[119] Wainright JS, Wang JT, Weng D, Savinell RF, Litt M. Acid-doped polybenzimidazoles: a new polymer electrolyte. J Electrochem Soc. 1995;142 L121–L123.

[120] Wang JT, Savinell RF, Wainright J, Litt M, Yu H. A H_2/O_2 fuel cell using acid doped polybenzimidazole as polymer electrolyte. Electrochim Acta. 1996;41:193–197.

[121] Bai H, Li Y, Zhang H, Chen H, Wu W, Wang J, et al. Anhydrous proton exchange membranes comprising of Chitosan and phosphorylated graphene oxide for elevated temperature fuel cells. J Membr Sci. 2015;495:48–60.

[122] Borup R, Meyers J, Pivovar B, Kim YS, Mukundan R, Garland N, et al. Scientific aspects of polymer electrolyte fuel cell durability and degradation. Chem Rev. 2007;107:3904–3951.

[123] Wang Y, Chen L, Yu J, Zhu J, Shi Z, Hu Z. Strong and conductive polybenzimidazole composites with high graphene contents. RSC Adv. 2013;3:12255–12266.

[124] Hou S, Wang X, Zhang X. Fabrication and wet spinning of a fully aromatic meta-polybenzimidazole. High Perform Polym. 2016;28:288–295.

[125] Zeis R. Materials and characterization techniques for high-temperature polymer electrolyte membrane fuel cells. Beilstein J Nanotechnol. 2015;6:68–83.

[126] Yang JS, Cleemann LN, Steenberg T, Terkelsen C, Li QF, Jensen JO, et al. High molecular weight polybenzimidazole membranes for high temperature PEMFC. Fuel Cells. 2014;14:7–15.

[127] Kawahara M, Morita J, Rikukawa M, Sanui K, Ogata N. Synthesis and proton conductivity of thermally stable polymer electrolyte: poly(benzimidazole) complexes with strong acid molecules. Electrochim Acta. 2000;45:1395–1398.

[128] Mamlouk M, Scott K. The effect of electrode parameters on performance of a phosphoric acid-doped PBI membrane fuel cell. Int J Hydrogen Energy. 2010;35:784–793.

[129] Perry KA, More KL, Payzant EA, Meisner RA, Sumpter BG, Benicewicz BC. A comparative study of phosphoric acid-doped m-PBI membranes. J Polymsci Part B Polym Phys. 2014;52:26–35.

[130] Ergun D, Devrim Y, Bac N, Eroglu I. Phosphoric acid doped polybenzimidazole membrane for high temperature PEM fuel cell. J Appl Polym Sci. 2012;124 E267–E277.

[131] Wang S, Zhao C, Ma W, Zhang N, Zhang Y, Zhang G, et al. Silane-cross-linked polybenzimidazole with improved conductivity for high temperature proton exchange membrane fuel cells. J Mater Chem A. 2013;1:621–629.

[132] Yang J, Aili D, Li Q, Cleemann LN, Jensen JO, Bjerrum NJ, et al. Covalently cross-linked sulphone polybenzimidazole membranes with poly(vinylbenzyl chloride) for fuel cell applications. ChemSusChem. 2013;6:275–282.

[133] Wang S, Zhang G, Han M, Li H, Zhang Y, Ni J, et al. Novel epoxy-based cross-linked polybenzimidazole for high temperature proton exchange membrane fuel cells. Int J Hydrogen Energy. 2011;36:8412–8421.

[134] Noye P, Li Q, Pan C, Bjerrum NJ. Cross-linked polybenzimidazole membranes for high temperature proton exchange membrane fuel cells with dichloromethylphosphinic acid as a cross-linker. Polym Adv Technol. 2008;19:1270–1275.

[135] Li QF, Rudbeck HC, Chromik A, Jensen JO, Pan C, Steenberg T, et al. Properties degradation and high temperature fuel cell test of different types of PBI and PBI blend membranes. J Membr Sci. 2010;347:260–270.

[136] Li HY, Liu YL. Polyelectrolyte composite membranes of polybenzimidazole and crosslinked polybenzimidazole polybenzoxazine electrospun nanofibers for proton exchange membrane fuel cells. J Mater Chem A. 2013;1:1171–1178.

[137] Lobato J, Canizares P, Rodrigo MA, Linares JJ, Aguilar JA. Improved polybenzimidazole films for H3PO4-doped PBI-based high temperature PEMFC. J Membr Sci. 2007;306:47–55.

[138] Allcock HR, Wood RM. Design and synthesis of ion-conductive polyphosphazenes for fuel cell applications: review. J Polym Sci Part B Polym Phys. 2006;44:2358–2368.

[139] Allcock HR. Polyphosphazene elastomers, gels, and other soft materials. Soft Matter. 2012;8: 7521–7532.

[140] Allock HR. Generation of structural diversity in polyphosphazenes. Appl Organomet Chem. 2013;27:620–629.

[141] Tang H, Pintauro PN, Guo Q, O'connor S. Polyphosphazene membranes. III. Solid-state characterization and properties of sulphonated poly[bis(3-methylphenoxy)phosphazene. J Appl Polym Sci. 1999;71:387–399.

[142] Allcock HR, Kugel RL. Synthesis of high polymeric alkoxy and aryloxyphosphonitriles. J Am Chem Soc. 1965;87:4216–4217.

[143] Allcock HR, Kugel RL, Valan KJ. Phosphonitrilic compounds. VI. High molecular weight poly (alkoxy-and aryloxyphosphazenes). Inorg Chem. 1966;5:1709–1715.

[144] Allcock HR, Kugel RL. Phosphonitrilic compounds. VII. High molecular weight poly (diaminophosphazenes). Inorg Chem. 1966;5:1716–1718.

[145] Blonsky PM, Shiver DF. Polyphosphazene solid electrolytes. J Am Chem Soc. 1984;106: 6855–6856.

[146] Allcock HR, Fitzpatrick RJ, Salvati L. Sulphonation of (aryloxy)- and (arylamino)phosphazenes: small-molecule compounds, polymers, and surfaces. Chem Mater. 1991;3:1120–1132.

[147] Wycisk R, Pintauro PN. Sulphonated polyphosphazene ion-exchange membranes. J Membr Sci. 1996;119:155–160.

[148] Guo Q, Pintauro PN, Tang H, O'Connor S. Sulphonated and crosslinked polyphosphazene-based proton-exchange membranes. J Membr Sci. 1999;154:175–181.

[149] Tang H, Pintauro PN. Polyphosphazene membranes. IV. Polymer morphology and proton conductivity in sulphonated poly[bis(3-methylphenoxy)phosphazene. J Appl Polym Sci. 2001;79:49–59.

[150] Sone Y, Ekdunge P, Simonsson D. Proton conductivily of Nafion 117 as measured by a four-electrode AC Impedance Method. J Electrochem Soc. 1996;143:1254–1259.

[151] Chalkova E, Zhou X, Ambler C, Hofmann MA, Weston JA, Allcock HR, et al. Sulphonimide polyphosphazene-based H2/O2 fuel cells. Electrochem Solid-State Lett. 2002;5:A221–A222.

[152] Wycisk R, Lee JK, Pintauro PN. Sulphonated polyphosphazene-polybenzimidazole membranes for DMFCs. J Electrochem Soc. 2005;152 A892–A898.

[153] Carter R, Wycisk R, Yoo H, Pintauro PN. Blended polyphosphazene/polyacrylonitrile membranes for direct methanol fuel cells. Electrochem State-Solid Lett. 2002;5:A195–A197.

[154] Hofmann MA, Ambler CM, Maher AE, Chalkova E, Zhou XY, Lvov SN, et al. Synthesis of polyphosphazenes with sulphonimide side groups. Macromolecules. 2002;35:6490–6493.

[155] Zhang Y, Yue M, Chen Y. Proton exchange membrane based on sulphonated polyimide for fuel cells: state-of-the-art and recent developments. Adv Mater Res. 2011;239:3032–3038.

[156] Faure S, Pineri M, Aldebert P, Mercier R, Sillion B. US Patent 6,245,881 1996. Sulphonated polyimides membranes prepared with them, and fuel cell device that includes these membranes.

[157] Genies C, Mercier R, Sillion B, Petiaud R, Cornet N, Gebel G, et al. Stability study of sulphonated phthalic and naphthalenic polyimide structures in aqueous medium. Polymer. 2001;42:5097–5105.

[158] Liu C, Li L, Liu Z, Guo M, Jing L, Liu B, et al. Sulphonated naphthalenic polyimides containing ether and ketone linkages as polymer electrolyte membranes. J Membr Sci. 2011;366:73–81.

[159] Jang W, Lee C, Sundar S, Shul JG, Han H. Thermal and hydrolytic stability of sulphonated polyimide membranes with varying chemical structure. Polym Degrad Stab. 2005;90: 431–440.

[160] Zhang Q, Li Q. Synthesis and characterization of sulphonated polyimides containing trifluoromethyl groups as proton exchange membranes. Chin J Chem. 2011;29:1460–1466.

[161] Okamoto K, Yin Y, Yamada O, Islam MN, Honda T, Mishima T, et al. Methanol permeability and proton conductivity of sulphonated co-polyimide membranes. J Membr Sci. 2005;258: 115–122.

[162] Asano N, Aoki M, Suzuki S, Miyatake K, Uchida H, Watanabe M. Aliphatic/aromatic polyimide ionomers as a proton conductive membrane for fuel cell applications. J Am Chem Soc. 2006;128:1762–1769.

[163] Asano N, Miyatake K, Watanabe M. Hydrolytically stable polyimide ionomer for fuel cell applications. Chem Mater. 2004;16:2841–2843.

[164] Sundar S, Jang W, Lee C, Shul Y, Han H. Crosslinked sulphonated polyimide networks as polymer electrolyte membranes in fuel cells. J Polym Sci Pol Phys. 2005;43:2370–2379.

[165] Park HB, Lee CH, Sohn JY, Lee JM, Freeman BD, Kim HJ. Effect of crosslinked chain length in sulphonated polyimide membranes on water sorption, proton conduction, and methanol permeation properties. J Membr Sci. 2006;285:432–443.

[166] Seo J, Jang W, Lee S, Han H. The stability of semi-interpenetrating polymer networks based on sulphonated polyimide and poly(ethylene glycol) diacrylate for fuel cell applications. Polym Degrad Satbil. 2008;93:298–304.

[167] Tin Y, Yamada O, Hayashi S, Tanaka K, Kita H, Okamoto KI. Chemically modified proton-conducting membranes based on sulphonated polyimides: improved water stability and fuel-cell performance. J Polym Sci Part A Polym Chem. 2006;44:3751–3762.

[168] Li N, Cui Z, Zhang S, Li S, Zhang F. Preparation and evaluation of a proton exchange membrane based on oxidation and water stable sulphonated polyimides. J Power Sources. 2007;172: 511–519.

[169] Yan J, Huang X, Moore HD, Wang CY, Hickner MA. Transport properties and fuel cell performance of sulphonated poly(imide) proton exchange membranes. Int J Hydrogen Energy. 2012;37:6153–6160.

[170] Zhang F, Li N, Zhang S, Li S. Ionomers based on multisulphonated perylene dianhydride: synthesis and properties of water resistant sulphonated polyimides. J Power Sources. 2010;195:2159–2165.

[171] Zhang F, Li N, Zhang S. Preparation and characterization of sulphonated poly(arylene-conaphthalimide)s for use as proton exchange membranes. J App Polym Sci. 2010;118: 3187–3196.

[172] Guo X, Fang J, Watari T, Tanaka K, Kita H, Okamoto K. Novel sulphonated polyimides as polyelectrolytes for fuel cell application. 2. Synthesis and proton conductivity of polyimides from 9,9-bis(4-aminophenyl)fluorene-2,7-disulphonic acid. Macromolecules. 2002;35: 6707–6713.

[173] Iulianelli A, Basile A. Sulphonated PEEK-based polymers in PEMFC and DMFC applications: a review. Int J Hydrogen Energy. 2012;37:15241–15255.

[174] Alberti G, Casciola M, Massinelli L, Bauer B. Polymeric proton conducting membranes for medium temperature fuel cells (110-160 °C). J Membr Sci. 2001;185:73–81.

[175] Kreuer KD. On the development of proton conducting polymer membranes for hydrogen and methanol fuel cells. J Membr Sci. 2001;185:29–39.

[176] Lawrence J, Yamaguchi T. The degradation mechanism of sulphonated poly(arylene ether sulphone)s in an oxidative environment. J Membr Sci. 2008;325:633–640.

[177] Panchenko A, Dilger H, Möller E, Sixt T, Roduner E. In situ EPR investigation of polymer electrolyte membrane degradation in fuel cell applications. J Power Sources. 2004;127: 325–330.

[178] Hou H, Di Vona ML, Knauth P. Durability of sulphonated aromatic polymers for proton-exchange-membrane fuel cell. Chem Sus Chem. 2011;4:1526–1536.

[179] Hu Z, Yin Y, Chen S, Yamada O, Tanaka K, Kita H, et al. Synthesis and properties of novel sulphonated (co)polyimides bearing sulphonated aromatic pendant groups for PEFC applications. J Polym Sci Part A Polym Chem. 2006;44:2862–2872.

[180] Chen Y, Meng Y, Wang S, Tian S, Chen Y, Hay AS. Sulphonated poly(fluorenyl ether ketone) membrane prepared via direct polymerization for PEM fuel cell application. J Membr Sci. 2006;280:433–441.

[181] Swier S, Chun YS, Gasa J, Shaw MT, Weiss RA. Sulphonated poly(ether ketone ketone) ionomers as proton exchange membranes. Polym Eng Sci. 2005;45:1081–1091.

[182] Roziere J, Jones DJ. Non fluorinated polymer materials for proton exchange membrane fuel cell. Annu Rev Mater Res. 2003;33:503–555.

[183] Gunaratne HQN, Langrick CR, Puga AV, Seddon KR, Whiston K. Production of polyetheretherketone in ionic liquid media. Green Chem. 2013;15:1166–1172.

[184] Johnson RN, Farnham AG, Clendinning RA, Hale WF, Merriam CN. Poly(aryl ethers) by nucleophilic aromatic substitution. I. Synthesis and properties. J Polym Sci Part A-1. 1967;5: 2375–2398.

[185] Attwood TE, Dawson PC, Freeman JL, Hoy LRJ, Rose JB, Staniland PA. Synthesis and properties of polyaryletherketones. Polymer. 1981;22:1096–1103.

[186] Toriida M, Kuroki T, Abe T, Hasegawa A, Takamatsu K, Taniguchi Y, et al. Polyether ketone and method for production thereof. Eur Pat EP. 2002;1464662:1.

[187] Jeong MH, Lee KS, Lee JS. Cross-linking density effect of fluorinated aromatic polyethers on transport properties. Macromolecules. 2009;42:1652–1658.

[188] Hou H, Di Vona ML, Knauth PJ. Building bridges: crosslinking of sulphonated aromatic polymers – A review. J Membr Sci. 2012;423–424:113–127.

[189] Wang J, Zhao C, Zhang L, Li M, Ni J, Wang S, et al. Cross-linked proton exchange membranes for direct methanol fuel cells: effects of the crosslinker structure on the performances. Int J Hydrogen Energy. 2012;37:12586–12596.

[190] Li M, Zhang G, Xu S, Zhao C, Han M, Zhang L, et al. Cross-linked polyelectrolyte for direct methanol fuel cells applications based on a novel sulphonated cross-linker. J Power Sources. 2014;255:101–107.

[191] Matsumura S, Hlil AR, Du N, Lepiller C, Gaudet J, Guay D, et al. Ionomers for proton exchange membrane fuel cells with sulphonic acid groups on the end-groups: novel branched poly(ether-ketone)s with 3,6-ditrityl-9H-carbazole end-groups. J Polym Sci Part A Polym Chem. 2008;46:3860–3868.

[192] Park HS, Seo DW, Choi SW, Jeong YG, Lee JH, Kim DI, et al. Preparation and characterization of branched and linear sulphonated poly(ether ketone sulphone) proton exchange membranes for fuel cell applications. J Polym Sci Part A Polym Chem. 2008;46:1792–1799.

[193] Kerres J, Ullrich A, Meier F, Haring T. Synthesis and characterization of novel acid–base polymer blends for application in membrane fuel cells. Solid State Ionics. 1999;125:243–249.

[194] Kerres J, Tang CM, Graf C. Improvement of properties of poly(ether ketone) ionomer membranes by blending and cross-linking. Ind Eng Chem Res. 2004;43:4571–4579.

[195] Zhang H, Li X, Zhao C, Fu T, Shi Y, Na H. Composite membranes based on highly sulphonated PEEK and PBI: morphology characteristics and performance. J Membr Sci. 2008;308:66–74.

[196] Wu HL, Ma CC, Liu FY, Chen CY, Lee SJ, Chang CL. Preparation and characterization of poly (ether sulphone)/sulphonated poly(ether ether ketone) blend membranes. Eur Polym J. 2006;42:1688–1695.

[197] Lim SS, Daud WR, Jahim JM, Ghasemi M, Chong PS, Ismail M. Sulphonated poly(ether ether ketone)/poly(ether sulphone) composite membranes as an alternative proton exchange membrane in microbial fuel cells. Int J Hydrogen Energy. 2012;37:11409–11424.

[198] De Bonis C, D'Epifanio A, Di Vona ML, D'Ottavi C, Mecheri B, Traversa E, et al. Proton conducting hybrid membranes based on aromatic polymers blends for direct methanol fuel cell applications. Fuel Cells. 2009;4:387–393.

[199] Yang T, Liu C. SPEEK/sulphonated cyclodextrin blend membranes for direct methanol fuel cell. Int J Hydrogen Energy. 2011;36:5666–5674.

[200] Jung HY, Park JK. Blend membranes based on sulphonated poly(ether ether ketone) and poly(vinylidene fluoride) for high performance direct methanol fuel cell. Electrochim Acta. 2007;52:7464–7468.

[201] Li Z, Xi J, Zhou H, Liu L, Wu Z, Qiu X, et al. Preparation and characterization of sulphonated poly(ether ether ketone)/poly(vinylidene fluoride) blend membrane for vanadium redox flow battery application. J Power Sources. 2013;237:132–140.

[202] Inan TY, Dogan H, Unveren EE, Eker E. Sulphonated PEEK and fluorinated polymer based blends for fuel cell applications: investigation of the effect of type and molecular weight of the fluorinated polymers on the membrane's properties. Int J Hydrogen Energy. 2010;35: 12038–12053.

[203] Abu-Thabit NY, Shaikh AA, Zaidi SM, Javaid MK. Novel sulphonated poly(ether ether ketone)/ /phosphonated polysulphone polymer blends for proton conducting membranes. J Mater Res. 2010;27:1958–1968.

[204] Xue Y, Fu R, Wu C, Lee JY, Xu T. Acid–base hybrid polymer electrolyte membranes based on SPEEK. J Membr Sci. 2010;350:148–153.

[205] Gao Q, Wang Y, Xu L, Wang Z, Wei G. Proton-exchange sulphonated poly(ether ether ketone)/sulphonated phenolphthalein poly(ether sulphone) blend membranes in DMFCs. Chin J Chem Eng. 2009;17:934–941.

[206] Jithunsa M, Tashiro K, Nunes SP, Chirachanchai S. Poly(acrylic acid-co-4-vinylimidazole)/sulphonated poly(ether ether ketone) blend membranes: a role of polymer chain with proton acceptor and donor for enhancing proton transfer in anhydrous system. Int J Hydrogen Energy. 2011;36:10384–10391.

[207] Mikhailenko SD, Zaidi SMJ, Kaliaguine S. Electrical properties of sulphonated polyether ether ketone/polyetherimide blend membranes doped with inorganic acids. J Polym Sci Pol Phys. 2000;38:1386–1395.

[208] Liu S, Wang L, Ding Y, Liu Y, Han X, Somg Y. Novel sulphonated poly (ether ether keton)/polyetherimide acid-base blend membranes for vanadium redox flow battery applications. Electrochim Acta. 2014;130:90–96.

[209] Li X, Liu C, Xu D, Zhao C, Wang Z, Zhang G, et al. Preparation and properties of sulphonated poly(ether ether ketone)s (SPEEK)/polypyrrole composite membranes for direct methanol fuel cells. J Power Sources. 2006;162:1–8.

[210] Cui W, Kerres J, Eigenberger G. Development and characterization of ion-exchange polymer blend membranes. Sep Purif Technol. 1998;14:145–154.

[211] Yang T, Meng L, Huang NJ. Synthesis of sulphonated (ether ether ketone) based membranes containing poly(4-styrenesulphonic acid) and its excellent performance for direct methanol fuel cells. J Power Sources. 2013;224:132–138.

[212] Wang J, Yue Z, Economy J. Preparation of proton-conducting composite membranes from sulphonated poly(ether ether ketone) and polyacrylonitrile. J Membr Sci. 2007;291:210–219.

[213] Yang T. Preliminary study of SPEEK/PVA blend membranes for DMFC applications. Int J Hydrogen Energy. 2008;33:6772–6779.

[214] Zaidi SMJ, Mikhailenko SD, Robertson GP, Guiver MD, Kaliaguine S. Proton conducting composite membranes from polyether ether ketone and heteropolyacids for fuel cell applications. J Membr Sci. 2000;173:17–34.

[215] Oh SY, Yoshida T, Kawamura G, Muto H, Sakai M, Matsuda A. Proton conductivity and fuel cell property of composite electrolyte consisting of Cs-substituted heteropoly acids and sulphonated poly(ether–ether ketone). J Power Sources. 2010;195:5822–5828.

[216] Zhang Y, Zhang H, Bi C, Zhu X. An inorganic/organic self-humidifying composite membranes for proton exchange membrane fuel cell application. Electrochim Acta. 2008;53:4096–4103.

[217] Peighambardoust SJ, Rowshanzamir S, Hosseini MG, Yazdanpour M. Self-humidifying nanocomposite membranes based on sulphonated poly(ether ether ketone) and heteropoly acid supported Pt catalyst for fuel cells. Int J Hydrogen Energy. 2011;36:10940–10957.

[218] Colicchio I, Wen F, Keul H, Simon U, Moeller M. Sulphonated poly(ether ether ketone)–silica membranes doped with phosphotungstic acidMorphology and proton conductivity. J Membr Sci. 2009;326:45–57.

[219] Bello M, Javaid Zaidi SM, Rahman SU. Proton and methanol transport behaviour of SPEEK/TPA/MCM-41 composite membranes for fuel cell application. J Membr Sci. 2008;322:218–224.

[220] Ismail AF, Othman NH, Mustafa A. Sulphonated polyether ether ketone composite membrane using tungstosilicic acid supported on silica–aluminium oxide for direct methanol fuel cell (DMFC). J Membr Sci. 2009;329:18–29.

[221] Ponce ML, Prado LAS, Silva V, Nunes SP. Membranes for direct methanol fuel cell based on modified heteropolyacids. Desalination. 2004;162:383–391.

[222] Dogan H, Inan TY, Unveren E, Kaya M. Effect of cesium salt of tungstophosphoric acid (Cs-TPA) on the properties of sulphonated polyether ether ketone (SPEEK) composite membranes for fuel cell applications. Int J Hydrogen Energy. 2010;35:7784–7795.

[223] Tchicaya-Bouckary L, Jones DJ, Roziere J. Hybrid polyaryleetherketone membranes for fuel cell apilcations. Fuel Cells. 2002;2:40–45.

[224] Yin B, Yu L, Jiang B, Wang L, Xi J. Nano oxides incorporated sulphonated poly(ether ether ketone) membranes with improved selectivity and stability for vanadium redox flow battery. J Solid State Electrochem. 2016;20:1271–1283.

[225] Yin Y, Xu T, He G, Jiang Z, Wu H. Fabrication of sulphonated poly(ether ether ketone)-based hybrid proton-conducting membranes containing carboxyl or amino acid-functionalized titania by in situ sol-gel process. J Power Sources. 2015;276:271–278.

[226] Mishra RK, Datt M, Banthia AK, Majeed ABA. Development of novel pectin based membranes as proton conducting material. Int J Plast Technol. 2012;16:80–88.

[227] Raphael E, Avellaneda CO, Manzolli B, Pawlicka A. Agar-based films for application as polymer electrolytes. Electrochim Acta. 2010;55:1455–1459.

[228] Yamada M, Honma I. Biomembranes for fuel cell electrolytes employing anhydrous proton conducting uracil composites. Biosens Bioelectron. 2006;21:2064–2069.

[229] Yamada M, Honma I. An anhydrous proton conductor based on lactam-lactim tautomerism of uracil. Chem Phys Chem. 2004;5:724–728.

[230] Pawlicka A, Mattos RI, Lima JF, Tambelli CE, Magon CJ, Donoso JP. Magnetic resonance and conductivity study of a gelatin-based polymer gel electrolyte. Electrochim Acta. 2011;57: 187–191.

[231] Mattos RI, Pawlicka A, Lima JF, Tambelli CE, Magon CJ, Donoso JP. Magnetic resonance and conductivity study of gelatin-based proton conductor polymer electrolytes. Electrochim Acta. 2010;55:1396–1400.

[232] Lopes LVS, Machado GO, Pawlicka A, Donoso JP. Nuclear magnetic resonance and conductivity study of hydroxyl ethylcellulose based polymer gel electrolytes. Electrochim Acta. 2005;50: 3978–3984.

[233] Harun NI, Ali RM, Ali AMM, Yahya MZA. Dielectric behaviour of cellulose acetate-based polymer electrolytes. Ionics. 2012;18:599–606.

[234] Gadim TDO, Figueiredo AGPR, Rosero-Navarro NC, Vilela C, Gamelas JAF, Barros-Timmons A, et al. Nanostructured bacterial cellulose–poly(4-styrene sulphonic acid) composite membranes with high storage modulus and protonic conductivity. Appl Mater Interfaces. 2014;6: 7864–7875.

[235] Choi Y-J, Ahn Y, Kang M-S, Jun H-K, Kim IS, Moon S-H. Preparation and characterization of acrylic acid-treated bacterial cellulose cation-exchange membrane. J Chem Technol Biotechnol. 2004;79:79–84.

[236] Lin CW, Liang SS, Chen SW, Lai JT. Sorption and transport properties of 2-acrylamido-2-methyl-1-propanesulphonic acid-grafted bacterial cellulose membranes for fuel cell application. J Power Sources. 2013;232:297–305.

[237] Yamada M, Honma I. Anhydrous proton conductive membrane consisting of Chitosan. Electrochim Acta. 2005;50:2837–2841.

[238] Göktepe F, Çelik SU, Bozkurt A. Preparation and the proton conductivity of chitosan/poly(vinyl phosphonic acid) complex polymer electrolytes. J Non-Cryst Solids. 2008;354:3637–3642.

[239] Seo JA, Koh JH, Roh DK, Kim JH. Preparation and characterization of crosslinked proton conducting membranes based on chitosan and PSSA-MA copolymer. Solid State Ionics. 2009;180:998–1002.

[240] Jiang Z, Zheng X, Wu H, Wang J, Wang Y. Proton conducting CS/P(AA-AMPS) membrane with reduced methanol permeability for DMFCs. J Power Sources. 2008;180:143–153.

[241] Fadzallah IA, Majid SR, Careem MA, Arof AK. A study on ionic interactions in chitosan–oxalic acid polymer electrolyte membranes. J Membr Sci. 2014;463:65–72.

[242] Gümüsoglu T, Arı GA, Deligöz H. Investigation of salt addition and acid treatment effects on the transport properties of ionically cross-linked polyelectrolyte complex membranes based on chitosan and polyacrylic acid. J Membr Sci. 2011;376:25–34.

[243] Cui Z, Liu C, Lu T, Xing W. Polyelectrolyte complexes of chitosan and phosphotungstic acid as proton-conducting membranes for direct methanol fuel cells. J Power Sources. 2007;167: 94–99.

[244] Xiao Y, Xiang Y, Xiu R, Lu R. Development of cesium phosphotungstate salt and chitosan composite membrane for direct methanol fuel cells. Carbohydr Polym. 2013;98:233–240.

[245] Xiang Y, Yang M, Guo Z, Cui Z. Alternatively chitosan sulphate blending membrane as methanol-blocking polymer electrolyte membrane for direct methanol fuel cell. J Membr Sci. 2009;337:318–323.

[246] Tripathi BP, Shahi VK. Functionalized organic-inorganic nanostructured N-p-carboxy benzyl chitosan-silica-PVA hybrid polyelectrolyte complex as proton exchange membrane for DMFC applications. J Phys Chem B. 2008;112:15678–15690.

[247] Ramırez-Salgado J. Study of basic biopolymer as proton membrane for fuel cell systems. Elelctrochim Acta. 2007;52:3766–3778.

[248] Asensio JA, Sanchez EM, Gomez-Romero P. Proton-conducting membranes based on benzimidazole polymers for high-temperature PEM fuel cells. A chemical quest. Chem Soc Rev. 2010;39:3210–3239.

[249] Noshay A, Robeson LM. Sulphonated polysulphone. J Appl Polym Sci. 1976;20:1885–1903.

[250] Johnson BC, Yilgor I, Tran C, Iqbal M, Wightman JP, Lloyd DR, et al. Synthesis and characterization of sulphonated poly(acrylene ether sulphones). J Polym Sci: Polym Chem Ed. 1984;22:721–737.

[251] Ding J, Chuy C, Holdcroft S. A self-organized network of nanochannels enhances ion conductivity through polymer films. Chem Mater. 2001;13:2231–2233.

[252] Ding J, Chuy C, Holdcroft S. Enhanced conductivity in morphologically controlled proton exchange membranes: synthesis of macromonomers by sfrp and their incorporation into graft polymers. Macromolecules. 2002;35:1348–1355.

[253] Chuy C, Ding J, Swanson E, Holdcroft S, Horsfall J, Lovell KV. Conductivity and electrochemical ORR mass transport properties of solid polymer electrolytes containing poly(styrene sulphonic acid) graft chains. J Electrochem Soc. 2003;150 E271–E279.

[254] Glipa X, El Haddad M, Jones DJ, Rozier J. Synthesis and characterisation of sulphonated polybenzimidazole: a highly conducting proton exchange polymer. Solid State Ionics. 1997;97:323–331.

[255] Gieselman MB, Reynolds JR. Water-soluble polybenzimidazole-based polyelectrolytes. Macromolecules. 1992;25:4832–4834.

[256] Gupta B, Buchi F, Scherer GG, Chapiro A. Materials research aspects of organic solid proton conductors. Solid State Ionics. 1993;61:213–218.

[257] Gupta B, Buchi FN, Scherer GG, Chapiro A. Development of radiation-grafted FEP-g-polystyrene membranes: some property–structure correlations. Polym Adv Technol. 1994;5: 493–498.

[258] Buchi FN, Gupta B, Haas O, Scherer GG. Study of radiation-grafted FEP-G-polystyrene membranes as polymer electrolytes in fuel cells. Electrochim Acta. 1995;40:345–353.

[259] Chuy C, Basura VI, Simon E, Holdcroft S, Horsfall J, Lovell KVJ. Electrochemical characterization of ethylenetetrafluoroethylene-g-polystyrenesulphonic acid solid polymer electrolytes. Electrochem. Soc. 2000;147:4453–4458.

[260] Flint SD, Slade RCT. Investigation of radiation-grafted PVDF-g-polystyrene-sulphonic-acid ion exchange membranes for use in hydrogen oxygen fuel cells. Solid State Ionics. 1997;97: 299–307.

[261] Hogarth M, Glipa X. Report issued by Johnson Matthey Technology Centre to the ETSU on behalf of the Department of Trade and Industry as ETSU F/02/00189/REP, DTI/Pub UNR 01/893 2001. High temperature membranes for solid polymer fuel cells.

[262] Bahar B, Cavalca C, Cleghorn S, Kolde J, Lane D, Murthy M, et al. Effective selection and use of advanced membrane electrode powerassemblies. New Mater Electrochem Syst. 1999;2: 179–182.

[263] Sato Y, Fujii K, Mitani N, Matsuura A, Kakigi T, Muto F, et al. Development of sulphonated FEP–Nafion hybrid proton exchange membranes for PEFC. Nucl Instrum Methods, Sect B. 2007;265: 213–216.

[264] Zhai YF, Zhang HM, Zhang Y, Xing DM. A novel H_3PO_4/Nafion–PBI composite membrane for enhanced durability of high temperature PEM fuel cells. J Power Sources. 2007;169:259–264.

[265] Tang H, Wan Z, Pan M, Jiang SP. Self-assembled Nafion–silica nanoparticles for elevated-high temperature polymer electrolyte membrane fuel cells. Electrochem Commun. 2007;9: 2003–2008.

[266] Chen SY, Han CC, Tsai CH, Huang J, Chen-Yang YW. Effect of morphological properties of ionic liquid-templated mesoporous anatase TiO_2 on performance of PEMFC with Nafion/TiO_2 composite membrane at elevated temperature and low relative humidity. J Power Sources. 2007;171:363–372.

[267] Hou HY, Sun GQ, Wu ZM, Jin W, Xin Q. Zirconium phosphate/Nafion115 composite membrane for high-concentration DMFC. Int J Hydrogen Energy. 2008;33:3402–3409.

[268] Nam SE, Kim SO, Kang Y, Lee JW, Lee KH. Preparation of Nafion/sulphonated poly (phenylsilsesquioxane) nanocomposite as high temperature proton exchange membranes. J Membr Sci. 2008;322:466–474.

[269] Seel DC, Benicewicz BC, Xiao L, Schmidt TJ. High-temperature polybenzimidazole-based membranes. In: Vielstich W, Yokokawa H, Gasteiger HA, editors. Handbook of FUEL CELLS–FUNDAMENTALS, TECHNOLOGY AND APPLICATIONS. Hoboken, NJ: John Wiley and Sons. Vol. 5: advances in Electocatalysis, Materials, Diagnostics and Durability, Chapter 19 2009.

[270] Trogodas P, Ramani V. Membrane and MEA development in polymer electrolyte fuel cells. In: Zaidi SMJ, Matsuura T, editors. Handbook of polymer membranes for fuel cells. New York, NJ: Springer. Chapter 11 2009:267–268.

[271] Kreuer KD, Fuchs A, Ise M, Spaeth M, Maier J. Imidazole and pyrazole-based proton conducting polymers and liquids. Electrochim Acta. 1998;43:1281–1288.

[272] Walker M, Baumgärtner KM, Kaiser M, Kerres J, Ullrich A, Räuchle E. Proton-conducting polymers with reduced methanol permeation. J Appl Polym Sci. 1999;74:67–73.

[273] Cabasso I, Yuan Y, Mittelsteadt C. Blend membranes based on sulphonated poly(phenylene oxide) for enhanced polymer electrochemical cells 1999. US Patent 5,989,742.

[274] Kerres JA. Blended and cross-linked ionomer membranes for application in membrane fuel cells. Fuel Cells. 2005;5:230–247.

[275] Li H, Zhang G, Wu J, Zhao C, Jia Q, Lew CM, et al. A facile approach to prepare self-crosslinkable sulphonated poly(ether ether ketone) membranes for direct methanol fuel cells. J Power Sources. 2010;195:8061–8066.

[276] Wang Y, Chen KS, Mishler J, Cho SC, Cordobes Adroher X. A review of polymer electrolyte membrane fuel cells: technology, applications, and needs on fundamental research. Applied Energy. 2011;88:981–1007.

[277] Garche J, Jorissen L. Applications of fuel cell technology: status and perspectives. Electrochem Soc Intereface. 2015;24 Summer:39–43.

[278] Thampan T, Shah D, Cook C, Novoa J, Shah S. Development and evaluation of portable and wearable fuel cells for soldier use. J Power Sources. 2014;259:276–281.

[279] Hagiwara A, Sotouchi H. Potential applications of fuel cells. In: Ohta T, editors. Energy carriers and conversion systems with emphasis on hydrogen - volume II. Oxford, UK: EOLSS Publisher/UNESCO, 2009:356–362.

[280] Badami M, Portoraro A. Performance analysis of an innovative small-scale trigeneration plant with liquid desiccant cooling system. Energy Buildings. 2009;41:1195–1204.

[281] Stationary Fuel Cells, Fuel cells for Prime Power, Large CHP, Residential CHP, and UPS Applications: global Market Analysis and Forecasts, Navigant Research http://www.navigantresearch.com/research/stationary-fuel-cells.

[282] Carter D, Wing J. The Fuel Cell Industry Review. July 2013. July32016. http://www.fuelcelltoday.com/analysis/industry-review.

[283] Hart D, Lehner F, Rose R, Lewis J. The Fuel Cell Industry Review. July 2015. July32016. http://www.fuelcellindustryreview.com.

[284] Papageorgopoulos D. Fuel cells sub-program overview. DOE hydrogen and fuel cells program. July262016. 2015. Annual Progress Reporthttps://www.hydrogen.energy.gov/pdfs/progress15/v_0_papageorgopoulos_2015.pdf.

[285] Papageorgopoulos D. Fuel cells program area - plenary presentation. Annual Merit Review and Peer Evaluation Meeting, 2016. June6-102016 https://www.hydrogen.energy.gov/pdfs/review16/fc000_papageorgopoulos_2016_o.pdfJuly262016.

[286] Papageorgopoulos D. U.S. DOE Activities Related to Fuel Cell Durability. 2nd INTERNATIONAL WORKSHOP ON DEGRADATION ISSUES OF FUEL CELLS, Thessaloniki, Greece; 2016. 21/09/2016 http://iet.jrc.ec.europa.eu/fuel-cells/sites/fuel-cells/files/files/documents/events/u.s._doe_activities_related_to_fuel_cell_durability_-_d._papageorgiopoulos.pdfJuly262016.

[287] DOE Fuel Cell Technologies Office Record 15015: fuel Cell System Cost. July 2015. July252016. https://www.hydrogen.energy.gov/pdfs/15015_fuel_cell_system_cost_2015.pdf.

Adrianna Nogalska, Anna Trojanowska and Ricard Garcia-Valls

11 Membrane contactors for CO_2 capture processes – critical review

Abstract: The use of membrane contactor in industrial processes is wide, and lately it started to be used in CO_2 capture process mainly for gas purification or to reduce the emission. Use of the membrane contactor provides high contact surface area so the size of the absorber unit significantly decreases, which is an important factor for commercialization. The research has been caried out regarding the use of novel materials for the membrane production and absorbent solution improvements. The present review reveals the progress in membrane contactor systems for CO_2 capture processes concerning solution for ceramic membrane wetting, comparison study of different polymers used for fabrication and methods of enzyme immobilization for biocomposite membrane. Also information about variety of absorbent solutions is described.

Keywords: membrane contactors, CO_2 capture, polymeric membranes

11.1 Introduction

The content of carbon dioxide in the atmosphere has increased since the industrial revolution (started in 1750) by 40 % according to The International Panel of Climate Change (Figure 11.1) [1]. The major human activity sources of CO_2 emission are power and industry sectors, which generate 60 % of total emission. Burning fossil fuels in power plants, oil refineries and other large industrial facilities release the biggest amount of carbon dioxide to the air. Besides the combustion, emission occurs during petrochemical processes, manufacture of metals from ores with use of carbon, thermal decomposition of limestone in cement production and fermentation process in alcohol making. Even if natural sources of CO_2 emissions are larger than human, increased content of carbon dioxide affects the balance in nature and causes the climate change [1]. More than 100 countries have adopted a global warming limit of 2 °C or below as a guiding principle for it mitigation efforts to reduce climate change risks, impacts and damages [2]. Unfortunately, simulations shows that even though the emission will stop, the consequences will be an irreversible change for 1,000 years after, such as atmosphere warming, precipitation changes or sea level rise [3].

The CO_2 capture is an efficient process if we are taking into consideration a CO_2 emission source with its high concentration. In order to contribute to the wellness of

https://doi.org/10.1515/9783110469745-011

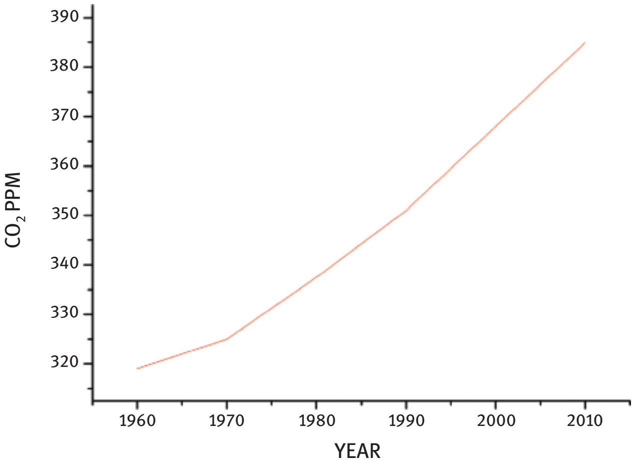

Figure 11.1: Chart showing the increase of atmospheric concentration during years 1958–2010 [1].

the environment, few ways of the elimination of the CO_2 excess from the air were proposed, like the use of algal cultures and sea weed as negative emission technologies [4] or use of CO_2 captured directly from the air as reagent in green synthetic strategy [5]. Due to low efficiency, the low-concentration carbon dioxide capture process is still a rarely discussed subject and requires development.

Very effective and widely commercially used during flue gas purification CO_2 capture method is the amine base scrubbing [6]. Amine-based system uses the chemical absorption of CO_2 into metanolamine. It takes place in a two-compartment system: first CO_2 from the flue gas stream is absorbed in the absorber and then desorbed in stripper as concentrated gas so the amine is regenerated. The heat needed for desorption is very high and it is the most expensive part of the process. Nevertheless, researchers are coming with new ideas constantly searching for improvements.

There are a number of patents released during the last decade with inventions concerning CO_2 removal from the gas streams by precipitation techniques [7–9] or by separation with membranes [10–14]. The absorbent systems for removing CO_2 from exhaust gases by precipitation consist of absorbents such as a mixture of amine and amino acid salts (AASs), metal oxides or bicarbonates which are contacted with CO_2-containing gas stream, what results in a precipitation of different solids. The bicarbonate salts are then withdrawn from the absorber compartment and regenerated in desorber by for example applying heat. The inventors claim that the CO_2 capture efficiency is higher than conventional amine scrubbing with higher CO_2 removal ability per cycle and less solvent vaporization loss. The membrane technology used for CO_2 capture is based on the separation processes in mixed gases – CO_2/N_2 and CO_2/CH_4 in flue gas and nature gas. The inventors have come up with new composite materials for the membrane preparation, e. g. polyimide-poly(ethylene glycol) copolymer membrane, polyvinylamine/polyaniline mixed matrix membranes or a metal organic framework membrane among the others. Membranes work as selective barriers which allow the passage of CO_2 and contribute to the formation of CO_2 reach permeate on the other side.

Fixed CO_2 can be later used for several applications and further processes depending on its form. For example, precipitated product can be used as a material for a construction, cement, or to produce aggregate so the CO_2 cannot escape back to the atmosphere. Whereas a pure, gaseous product is used in chemical synthesis. The scientific world notes the potential use of the CO_2 as a source of green energy production, especially being interested in recycling of the carbon dioxide by its conversion to the methanol or hydrocarbons and further use of it as a fuel in e. g. direct methanol fuel cell [15].

Lately, use of membrane contactors found interest due to a possible decrease of the absorber unit size and as a consequence, lower prize of the system production and exploration. This review focused on the use of gas–liquid membrane contactor systems in CO_2 capture processes. We summarize the state of art in the technology including novel materials and process improvement approaches. Three different membrane types – ceramic, polymeric and biocomposite, as well as variety of absorbents solutions – are presented.

11.2 Membrane contactors

Membrane contactors (Figure 11.2) are used in separation processes due to a number of advantages, e. g.: they provide large gas–liquid contact area which helps reducing the contactor size and weight, they are easy scale-up and have compact configuration, what's more the driving force is a difference in the concentration gradient; thus there is no need to apply pressure and this excludes flooding problem.

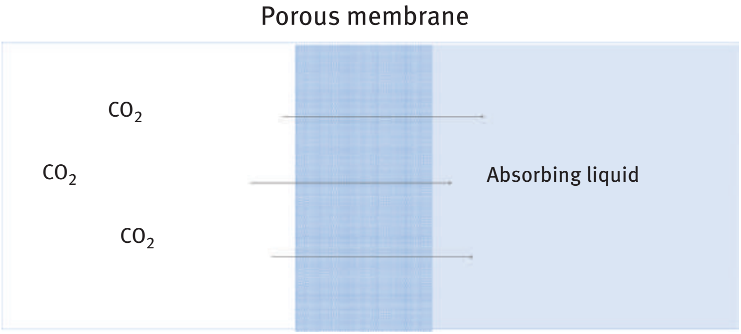

Figure 11.2: Schematic representation of gas–liquid membrane contactor for CO_2 capture.

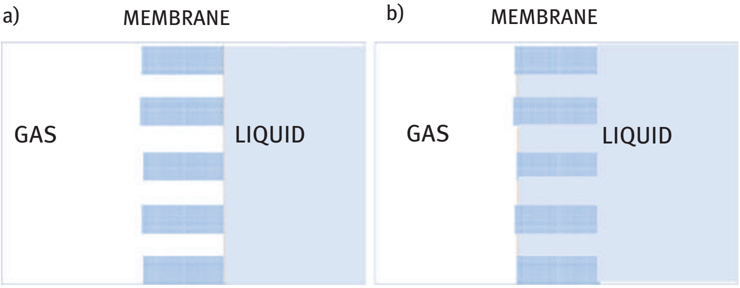

Figure 11.3: Gas–liquid membrane contactor in dry (a) and wet (b) modes. The contact surface area is marked with red color.

Selection of compatible membrane and absorbent is crucial for the efficiency of the system. The membrane has to be stable chemically and physically so it will not undergo degradation. But the most important factor is overcoming the wetting problem. It is true that high porosity and the open structure are good for the flux; unfortunately they can contribute to the membrane wetting. For a proper performance, membrane pores should stay dry and open for the gas, because it helps to keep the large contact area (Figure 11.3). Thus, the best solution is to choose the membrane with high hydrophobicity and the absorbent solution with high surface tension. Besides, absorbent should exhibit high affinity to the gas so its gas absorption capacity will be high as well as the selectivity and it should be also compatible with the rest components of the system having e. g. non-corrosive properties. Whereas, the membrane mostly has to provide high gas permeability by having large open spaces within the structure.

11.3 Membranes

11.3.1 Ceramics

Ceramic membranes possess superior chemical and thermal stability over polymeric ones. The most common materials used for the fabrication of ceramic membranes for the CO_2 capture systems are metal oxides, especially alumina and silica. Unfortunately, hydroxide groups situated on their surface results in high hydrophilicity of the material. Thus, the researchers are focused mostly on improvement of the membrane hydrophobicity in order to overcome the wetting problem and come with new superhydrophobic ceramic (SC) membrane contactors. The fluoroalkysilane (FAS) grafting is the method usually used for the hydrophobicity improvement. The FAS reacts with OH-groups from e. g. silica and increases the surface hydrophobicity (Figure 11.4).

For instance, Magnone et al. [16] performed the grafting directly on an alumina hollow-fiber membrane contactor with a high-symmetric distribution of

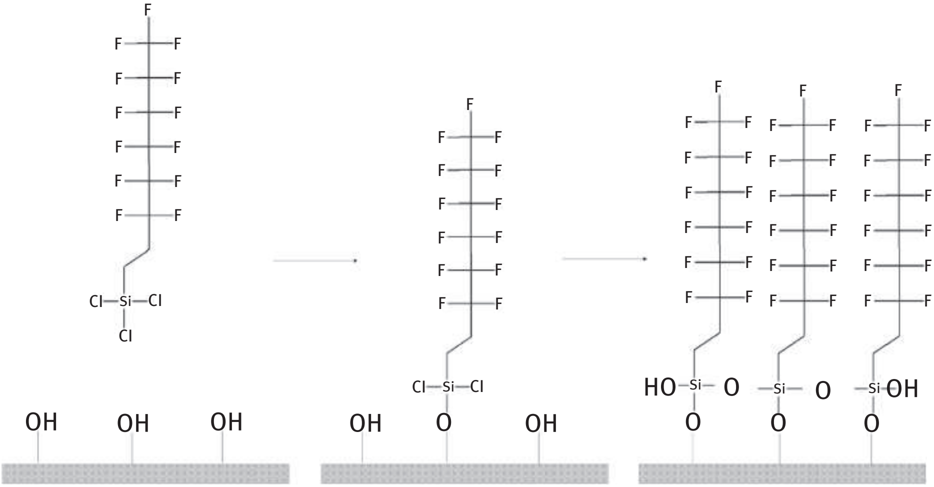

Figure 11.4: Exemplary reaction of surface hydroxyl groups with fluoroalkylsilane.

morphological elements. The modified membrane achieved a CO_2 absorption flux of about 5.4×10^{-3} mol/m^{2}s at room temperature with a single-symmetric ceramic membrane, which is considerably higher compared to other conventional polymeric membrane for CO_2 absorption into MEA solutions.

Lin et al. [17] reported that pore wetting by amine solution was decreasing CO_2 absorption flux into an alumina membrane. The author's approach consisted in coating the macroporous alumina tubular membrane surface with mesoporous silica aerogel by sol-gel reaction and shrinking of the pore size. Afterward, the membrane undergoes grafting with FAS. The achieved contact angle with four grafting reached the value of 139 degrees showing the improvement of the membrane hydrophobicity. Prepared membranes have high CO_2 flux 0.6 mmol/m^{2}s and were stable for 24 h. Compared to the analogue flat membranes, the tubular membranes provide a larger surface area, which results in higher CO_2 recovery up to 100 %.

Another material for SC preparation is a mullite ($3Al_2O_32SiO_2$), which combines alumina and kaolin. Abdulmunen et al. [18] proposed the preparation of grafted kaolin–alumina hollow-fiber membrane. Using low-cost materials, provides obtainment of membranes with high porosity and hydrophobicity what contributes to a high performance. The membrane was prepared by extrusion and sintering technique from a suspension of kaolin and alumina mixture followed by grafting with FAS with a contact angle of 142 degrees.

In order to overcome the wetting and the fouling problem in liquid gas membrane contactor systems, Yu et al. [19] fabricated the SC membrane from alumina tube with ZrO_2 which was followed by grafting. The authors suggested also a periodic drying of the membrane to ensure constant and high CO_2 removal efficiency. The ceramic membrane is considered as a cheaper material, which gives improved results and has anti-wetting and anti-fouling features, thanks to the drying. After being grafted with FAS, the ceramic membrane exhibited a contact angle value of 153° and a slightly lower permeance because the grafted FAS reduces the pore size of the membrane.

11.3.2 Polymers

Comparison between different polymeric membranes was done by Fabien Porcheron and the group. The authors studied a number of polymers: polypropylene (PP), nylon, polytetrafluoroethylene (PTFE) and polyvinylidene fluoride (PVDF). Studies show that the membranes are hydrophobic; unfortunately, they notice the decrease of contact angle up to 0 degrees on nylon and PVDF after aging with absorbent solution in high temperature for 1 week. The results are in agreement with thermogravimetric analysis (TGA), thermomechanical analysis (TMA) and infrared spectroscopy (IR) analysis, where only PP and PTFE membranes did not reveal any changes caused by aging. Gas permeability test shows that the more porous is the material the better results it gives. According to the researcher, the PTFE membrane provides the best performance with high efficiency among the studied materials, due to its structure and stability [20].

The main studied section in the field are materials, mainly new materials for membrane preparation or improvements of existing ones. The most important membrane feature to improve in gas–liquid contactors operation is its hydrophobicity. A research group from China was trying to achieve it, incorporating graphene nanosheets into PVDF membrane. The modification induced a more porous sublayer structure, where the particles were visible and the surface roughness increased. Thus, contact angle increased only on the bottom surface. The hybrid membrane enhances the CO_2 absorption only when the more hydrophobic surface was facing the absorbent. The wetting problem was overcome so the long-term efficiency of system was achieved [21].

Fashand et al. [22] decided to use PVC for the first time in the gas–liquid contacting process for CO_2 capture. The relatively cheap material provides membrane with high hydrophobicity and a structure adequate for its use in the process, such as large macrovoids and reduced wall thickness. Thanks to good processability, high absorption efficiency was achieved by optimization of take-up speed during spinning process.

Besides concentrating about materials, researchers are concerning also the use of different modules. There is a theoretical study treating about the difference in CO_2 removal performance by flat-sheet membrane contactor (FSMC) and hollow-fiber (HFMC) polymeric membrane contactor with use of amine aqueous solutions. For the studied conditions, FSMC showed better results. Nevertheless, the authors admit that before choosing a suitable module a number of factors should be considered, such as membrane properties and operating parameters [23]. Francis Bougie and Iliuta [24] have studied the possibility of use of more than one FSMC for CO_2 removal from a gas mixture. The author designed an experiment, which consists of connecting up to three polymeric membrane contactors, so the outlet absorbent liquid was directed to the inlet of next compartment. Generated results indicated that there is a proportional increase in the CO_2 flux with the number of membranes. Moreover, the authors demonstrated that there is a possibility to add as many membranes as needed to achieve the absorbent solution saturation.

11.3.3 Biocomposite

According to Fick's law, increase of local CO_2 concentration on the membrane side will result in enhancing the CO_2 absorption by the system. To achieve it, scientists are modifying the membrane surface, by for example incorporation of biomolecules. Most commonly used enzyme for CO_2 capture studies is carbonic anhydrase. The protein is situated in leaf and it is responsible for catalysis of CO_2 hydration (1) for photosynthesis. Besides, we can find it in blood, where it helps to keep the pH balance. The catalyzed reaction involves two-step mechanism. The first step (2) is the nucleophilic attack of a zinc-bound hydroxide ion on CO_2. The second step (3) is the regeneration of the active site by ionization of the zinc-bound water molecule and removal of a proton from the active site.

$$CO_2 + H_2O \leftrightarrow HCO^{3-} + H^+ \tag{11.1}$$

$$Zn^{2+}OH^- + CO_2 \leftrightarrow Zn^{2+} + HCO^{3-} \tag{11.2}$$

$$Zn^{2+} + H_2O \leftrightarrow H^+ + Zn^{2+}OH^- \tag{11.3}$$

Unfortunately, the biomimetic systems suffer one main disadvantage: enzyme incorporation into a synthetic support usually results in decrease in its activity caused by, among the others, structural or functional changes. The researchers are applying different incorporation techniques to overcome this issue.

One option is use of nanoparticles to covalently bond the enzyme. This approach was investigated by Jingwei Hou et al. [25] Biocatalytic TiO_2 nanoparticles with covalently immobilized carbonic anhydrase were used to prepare superhydrophobic PP membrane by sol–gel coating and surface modification with perfluorodecyltriethoxysilane (PDTS). Results showed that enzyme remain high in activity and the biocatalytic membrane contactor exhibits reusability of 10 cycles.

Another method, used by Joel K. J. Yong et al. [26], includes the electrostatic adsorption of carbonic anhydrase by layer-by-layer assembly on polimeric membrane surface. The films were applied to the shell side of the hollow-fiber membranes by static mode where membrane remains in solution and by forcing polyelectrolites across the membrane. Results show the formation of thin films only on the surface, without penetration to the inside pores. This caused another improvement – the pore wetting was significantly reduced and finally the CO_2 hydration was enhanced in all examined cases.

Ya-Tao Zhang et al. [27] studied the performance of membrane reactors consisting of PVDF hollow-fiber membranes aligned parallel with nanocomposite hydrogel with immobilized CA between them. As the porous network of the hydrogel contained free water, which is crucial for proper functioning of the enzyme, the enzymatic activity remained up to 76 %. The obtained reactor effectively separates CO_2 from mixed gas streams of low concentration with 30 h of durability.

11.4 Absorbents

Absorbents are playing a crucial role in membrane contactor systems as they are the only selective part of the compartment and the effectivity of the system depends mostly on the affinity of the liquid to CO_2. A number of solutions were studied (Figure 11.5), especially bases and amines and their salts, but monoethanolamine solution is still the most commonly used reference absorbent.

The theoretical study conducted by Subham Paul and the group [23] about the use of single and blended amines, considering aqueous solutions of MEA, DEA, MDEA and AMP, as absorbent solutions for CO_2 capture by FSMC,

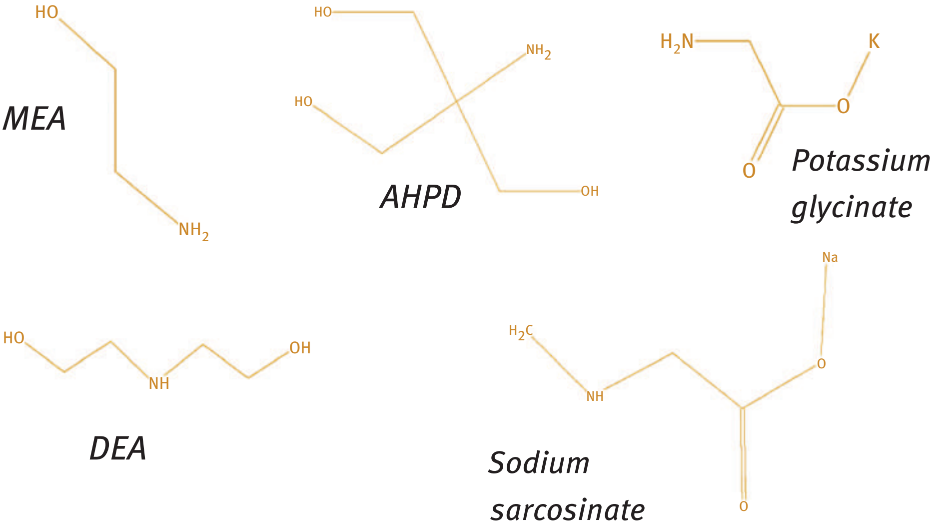

Figure 11.5: Amines used in CO_2 absorption studies.

proves that MEA has the highest absorption flux rate among single amines and the increase in its concentration in blends results in increase of absorbtion rate as well.

The use of aqueous amine solution was investigated also by Francis Bougie and Iliuta [24], who incorporated piperazine (Pz) as activator of CO_2 removal from CO_2/N_2 gas mixture by aqueous 2-amino-2-hydroxymethyl-1,3-propanediol (AHPD) in polymeric FSMC comparing his results with MEA solution. Pz is a secondary diamine activator, which has a good absorption and regeneration capacity and, thanks to its high surface tension, has a potential to decrease the membrane wetting. The activated absorbent solution showed better performance than single AHPD solution, but similar absorption flux for MEA solution.

AASs such as potassium glycinate, sodium glycinate, potassium sarcosine and sodium sarcosine, were compared with MEA and NaOH by Nihmiya Abdul Rahim and Al-Marzouqi [28]. The AAS solutions show better CO_2 absorption performance unfortunately only in low molar ratios, because decreased pH enhances the release of CO_2 reaction.

Muhammad Saeed [29] used zinc complex to promote the K_2CO_3 absorption in a contactor system. The Zn–cyclen complex is mimicking carbonic anhydrase (the enzyme mention in biocomposite membrane section), but according to the studies it is more stable and has a longer lifetime compared with the natural enzyme. Promotion of the absorbent results in a 10-fold improvement of the adsorption rate.

11.5 Conclusions

In this review, we revealed the current state of art of membrane contactors for CO_2 capture technology, covering different membrane materials, hydrophobicity improvements methods and process efficiency enhance approaches including the use of biological molecules and summary of absorbent solutions in use.

References

[1] IPCC. In: Stocker D., Qin G.-K., Plattner M., Tignor S.K., Allen J., Boschung A., Nauels Y., Xia V. Bex, Midgley P.M., editors. *Climate Change* 2013: *The Physical Science Basis*, ed. T.F. Contribution of Working Group I to the Fifth Assessment Report of the Intergovernmental Panel on Climate Change Vol. Chapters: 6. Cambridge, United Kingdom and New York, NY, USA: Cambridge University Press. TPM 2013.

[2] Malte Meinshausen NM, Hare W, Raper SC, Frieler K, Knutti R, Frame DJ, et al. Greenhouse-gas emission targets for limiting global warming to 2 6C. Nature. 2009;458:1158–1163.

[3] Susan Solomon GK, Knutti R, Friedlingstein P. Irreversible climate change due to carbon dioxide emissions. PNAS. 2009;102(6):1704–1709.

[4] Diana Moreira JC. Atmospheric CO2 capture by algae: negative carbon dioxide emission path. Bioresour Technol. 2016;215:371–379.

[5] Wendong Zhang FD, Zhang W. Capture of atmospheric CO_2into (BiO)2CO_3/graphene or grapheneoxide nanocomposites with enhanced photocatalytic performance. Appl Surf Sci. 2015;358:75–83.

[6] Anand B. Rao ES. A technical, economic, and environmental assessment of amine-based CO_2 capture technology for power plant greenhouse gas control. Environ Sci Technol. 2002;36: 4467–4475.

[7] Donald W (CA) Way J Douglas (US) Bard Allen J (US) Danziger Robert (US) Ryan Cecily (US) Fernandez Miguel (US), C.B.U.Y.A.U.T.P.B.U.O.S.U.F.K.U.G.R.J.U.D.V.U.K. Methods of sequestering CO2. E.P. Application, Editor 2010.

[8] (US), C.B.R.U.B.M.U.S.J.U.C.C. Carbon sequestration methods and systems, and compositions produced thereby. Blue Planet Ltd. E.P. Application, Editor 2016.

[9] Dakhil FR. IT) Carbon dioxide capture and storage system. United States: Dakhil Farouk, 2016.

[10] Ryul[KR], L.J.W.K.L.K.S.K.P.S. Method for capturing and converting carbon dioxide from exhaust gas and apparatus for capturing and converting carbon dioxide from exhaust gas. L.C. CORP[KR], Editor 2013.

[11] +, W.Z.Z.S.Z.J.Q.Z.W.J. Preparation of polyvinylamine/polyaniline mixed matrix membranes used for separation of gas containing carbon dioxide. U.T. +, Editor.

[12] Dehong YJ. Preparation method of metal organic framework membrane for CO_2 separation. U.D. TECH, Editor 2013.

[13] Polyimide-poly(Ethylene Glycol) copolymer membrane for separating carbon dioxide and method of manufacturing the same 2015.

[14] HIRANABE Ryuichiro (Toray Industries Inc., -., Sonoyama 1-chome, Otsu-sh, Shiga 58, 〒5208558, JP) HANAKAWA Masayuki (Toray Industries Inc., 1-1, Sonoyama 1-chome, Otsu-sh, Shiga 58, 〒5208558, JP) KAWAKAMI Tomonori (Toray Industries Inc., 1-1, Sonoyama 1-chome, Otsu-sh, Shiga 58, 〒5208558, JP) *CARBON-DIOXIDE-SEPARATING MEMBRANE* W.P. Application, Editor. 2013, TORAY INDUSTRIES, INC. (1-1 Nihonbashi-Muromachi 2-chome, Chuo-ku Tokyo, 66, 〒1038666, JP) Japan.

[15] George A. Olah AG, Prakash GK. Chemical recycling of carbon dioxide to methanol and dimethyl ether: from greenhouse gas to renewable, environmentally carbon neutral fuels and synthetic hydrocarbons. J Org Chem. 2009;74(2):487–498.

[16] Edoardo Magnone HJL, Che JW, Park JH. High-performance of modified Al2O3 hollow fiber membranes for CO2 absorption at room temperature. J Ind Eng Chem. 2016;42:19–22.

[17] Yi-Feng Lin JM, Qian Y, Tung KL. Hydrophobic fluorocarbon-modified silica aerogel tubular membranes with excellent CO_2 recovery ability in membrane contactors. Appl Energy. 2015;154: 21–25.

[18] Mohammed Abdulmunem Abdulhameed MH, Ismail AF, Matsuura T, Harun Z, Rahman MA, Puteh MH, et al. Carbon dioxide capture using a superhydrophobic ceramic hollow fibre membrane for gas-liquid contacting process. J Clean Prod. 2017;140:1731–1738.

[19] Xinhai Yu LA, Yang J, Tu ST, Yan J. CO2 capture using as uperhydrophobic ceramic membrane contactor. J Memb Sci. 2015;496:1–12.

[20] Fabien Porcheron DF, Favre E, Nguyen PT, Lorain O, Mercier R, Rougeau L. Hollow fiber membrane contactors for CO2 capture: from lab-scale screening to pilot-plant module conception. Energy Procedia. 2011;4:763–770.

[21] Xiaona W, Liang Wang BZ, Zhang Z, Zhang H, Zhao X, Guo X. Hydrophobic PVDF/graphene hybrid membrane for CO_2 absorption in membrane contactor. J Memb Sci. 2016;520:120–129.

[22] Hossein Fashandi AG, Saghafi R, Zarrebini M. CO2absorption using gas-liquid membrane contactors made of highly porous poly(vinyl chloride) hollow fiber membranes. Int J Greenhouse Gas Control. 2016;52:13–23.

[23] Subham Paul AK, Mandal B. Theoretical studies on separation of CO2 by single and blended aqueous alkanolamine solvents in flat sheet membrane contactor (FSMC). Chem Eng J. 2008;144:352–360.

[24] Francis Bougie II, Iliuta MC. Flat sheet membrane contactor (FSMC) for CO2 separation using aqueous amine solutions. Chem Eng Sci. 2015;123:255–264.

[25] Jingwei Hou MY, Mohammada M, Zhang Y, Razmjou A, Chen V. Biocatalytic gas-liquid membrane contactors for CO2 hydration with immobilized carbonic anhydrase. J Memb Sci. 2016;520:303–313.

[26] Joel K. J. Yong GW, Caruso F, Kentish SE. In situ layer-by-layer assembled carbonic anhydrase-coated hollow fiber membrane contactor for rapid CO_2 absorption. J Memb Sci. 2016;514: 556–565.

[27] Ya-Tao Zhang LZ, Chen HL, Zhang HM. Selective separation of low concentration CO2 using hydrogel immobilized CA enzyme based hollow fiber membrane reactors. Chem Eng Sci. 2010;65:3199–3207.

[28] Nihmiya Abdul Rahim NG, Al-Marzouqi M. Absorption of CO2 from natural gas using different amino acid salt solutions and regeneration using hollow fiber membrane contactors. J Nat Gas Sci Eng. 2015;26:108–117.

[29] Muhammad Saeed LD. Post-combustion CO2 membrane absorption promoted by mimic enzyme. J Memb Sci. 2016;499:36–46.

Maciej Staszak

12 Modeling and simulation of membrane process

Abstract: The article presents the different approaches to polymer membrane mathematical modeling. Traditional models based on experimental physicochemical correlations and balance models are presented in the first part. Quantum and molecular mechanics models are presented as they are more popular for polymer membranes in fuel cells. The initial part is enclosed by neural network models which found their use for different types of processes in polymer membranes. The second part is devoted to models of fluid dynamics. The computational fluid dynamics technique can be divided into solving of Navier-Stokes equations and into Boltzmann lattice models. Both approaches are presented focusing on membrane processes.

Keywords: Fuel cell, two (D2Q9) and three (D3Q19) dimensional physical space, neutron layers

12.1 Introduction

Physical phenomena is subject to many different modeling methods. This chapter is organized to give a general view of the modeling approaches, aims, capabilities, and limitations especially for polymer membrane systems. As a preferable engineering view of the modeling task the text describes two general cases from geometric perspective, zero- and higher dimensional modeling. The traditional design approach is to use zero-dimensional description of simulated entity which is less computationally demanding. The zero-dimensional methods involve classical correlations for membrane fluxes, transmembrane pressures estimations, resistances, retentions, etc. The zero-dimensional approach also involves the microscopic-level description of the phenomena modeled, e.g. by quantum or molecular analysis where the answer obtained corresponds to some indefinite point location rather than spatial distribution of resultant variables. On the other hand, modeling performed for two- or three-dimensional geometries becomes more popular for the process systems designers due to fast development of computers and numerical algorithms. This approach is generally based on hydrodynamic level of process description. Two fundamentally different, higher dimensional methods are described in the text, the more traditional finite volume method and lattice Boltzmann method. The first is derived based on discretization of Navier–Stokes equations of flow while the second relies on Boltzmann particle distribution function, which is a multidimensional function of position and momentum of fluid ensemble.

https://doi.org/10.1515/9783110469745-012

Both methods of phenomena description, zero and higher dimensional, are important and are further discussed in details for polymer membrane systems, divided into several appropriate subtopics.

12.2 Zero-dimensional modeling

The zero-dimensional modeling refers to the traditional technique of simulation and design approach in which the problem stated is formulated as a lumped parameter model. This approach considers any simulated and modeled phenomena as the entity with constant parameters over space analyzed. In such a case no spatial distribution of any of the variables modeled is taken into account. This approach is used in many important areas of design when there is a need to estimate key process variables, e.g. flowrates, temperatures, concentrations, pressures, and so forth. However, there is a smooth border between zero- and higher dimensional problems as many of the correlations used in this approach contain some important sizes of simulated entity, e.g. channel length, membrane width, pores diameter, and so forth. But the approach itself is still zero dimensional due to its governing equations of lumped formulation.

12.2.1 Basic modeling description

The most fundamental approach considers entering and exiting masses from subjected space. The mass, energy, and/or momentum streams are balanced over analyzed entity, the process is described by appropriate constitutive relation and model is formulated typically in terms of algebraic, but sometimes also differential, equations. In the membrane systems the mass balance involved is included implicitly, during the derivation of some specified formulation. The general approach to model the porous and nonporous membranes is similar but there are some differences due to their morphology. In details the model construction is dependent mainly on the membrane filtration mode due to specific flows schemes. Two basic modes are commonly used when considering the flows arrangement, namely dead-end and cross-flow setup (Figure 12.1). Several prediction models have been proposed as constitutive relation for the membrane permeate flux for the aforementioned modes of filtration.

One of the earliest approaches to the membrane transportation process is the orifice model for a pore which utilizes the Sampson [1] equation for the flow through the orifice q_{orifice}.

$$q_{orifice} = \frac{r^3 \Delta P}{3\mu} \tag{12.1}$$

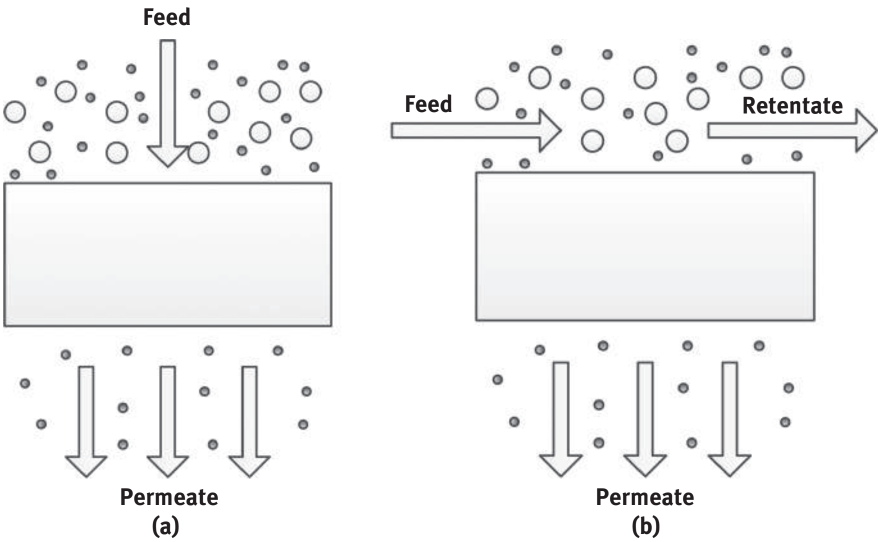

Figure 12.1: Cross-flow and dead-end membrane configuration setup.

where μ is the fluid viscosity and ΔP is transmembrane pressure. Applying fractional pore area A_p/A_m and the pore radius r, the flux q across membrane can be obtained:

$$q = \frac{r}{3\pi\mu} \frac{A_p}{A_m} \Delta P \tag{12.2}$$

The resistance-in-series model assumes that the resistances exerted on flowing fluid by the porous media can be presented in the form of sum of resistances. The flux in the membrane filtration can be described by governing equation given as:

$$q = \frac{\Delta P}{R_m + R_{pl} + R_c} \tag{12.3}$$

In the above relation q is the permeate flux with the units of velocity (discharge per unit area), ΔP is the pressure applied, R_m membrane resistance, R_{pl} concentration polarization (CP) layer resistance, and R_c is the cake resistance. The most problematic variable to be estimated when incorporating equation into modeling procedure is CP layer resistance. This resistance depends on amount of retained particles in layer considered and on the particle–membrane material interactions. Furthermore, the particles amount depends on the permeate flux which is then intrinsically coupled with its value so cannot be determined without prior knowing the permeate flux. It was presented [2] that pressure drop over the CP layer is constant in the case when the cake layer exists on the surface of the membrane. This pressure drop is called critical pressure ΔP_c and can be determined by the relationship:

$$\Delta P_c = \frac{3kT}{4\pi r^3} N_{Fc} \tag{12.4}$$

where r is the radius of the particle, N_{Fc} is the critical filtration number. N_{Fc} is the critical value of the filtration number at which the cake layer begins to appear. The filtration number N_F is defined as the ratio of the energy required to transport a particle from the surface of the membrane into the bulk suspension to the thermal, dissipative energy of the particle. Details on derivation and relation of filtration number to the Einstein–Stokes equation, combined with the correction factor for high particle concentration from Hapell cell model, can be found in the literature [3].

For membrane filtration process, Darcy law (5) can also be considered as a constitutive relation. This approach formulates the flux q in terms of pressure gradient across the membrane, k permeability of the membrane, and μ fluid viscosity.

$$q = \frac{-\kappa}{\mu} \nabla p \tag{12.5}$$

The flux q refers to the total cross section of the membrane and thus to obtain the actual average velocity u in the porous media it must be divided by the membrane porosity ϕ:

$$u = \frac{q}{\phi} \tag{12.6}$$

The process of filtration has the intrinsic dynamic nature. The time evolution of membrane filtration is mainly due to fouling phenomenon. Several stages of fouling are classified, and mechanisms proposed as well. The typical dynamics of the filtration resembles the flux changes during time. Initially high flux corresponds to the situation when almost pure solvent is transported across membrane. This period is characterized by short duration time and fast drop of the flux. Succeeding stage is represented by long-term gradual flux decline, and finally the last period of the process is indicated by the steady-state flux. Initial or last stage might sometimes be difficult to observe due to high rate of the process dynamics or long time of steady-state approach.

12.2.1.1 Standard blocking model

The model is also referred as pore blocking model. The rate of change of number of pores that are available for fluid transportation at any time of the process can be given by relation:

$$\frac{dn}{dt} = -f_b \frac{u_0 C_0 n}{n_0} \tag{12.7}$$

In the above n represents number of non-blocked pores accessible by the fluid per unit of area of the membrane surface. The variable f_b is the number of pores that can be blocked by a unit volume of particles. The C_0 is the initial particle concentration in the feed stream. The indices 0 refer to the initial values of specified variables. The analytical solution to the above is:

$$n = n_0 e^{-f_b \frac{u_0 C_0}{n_0} t} \tag{12.8}$$

Thus two time-dependent component fluxes can be identified, the flux by unblocked pores and flux by blocked pores. The dynamics of the total flux can thus be given:

$$u = \underbrace{u_0 e^{-f_b \frac{u_0 C_0}{n_0} t}}_{\text{unblocked pores}} + \underbrace{u_{b0} \left(1 - u_0 e^{-f_b \frac{u_0 C_0}{n_0} t} \right)}_{\text{blocked pores}} \tag{12.9}$$

where u_{b0} is the flux for the blocked membrane.

12.2.1.2 Cake formation model

For incompressible cakes the Carman-Kozeny [4] equation relates pressure drop with velocity and membrane details:

$$\frac{\Delta p}{L} = \frac{180\mu}{\Phi_s^2 D_p^2} \frac{(1-\varepsilon)^2}{\varepsilon^3} u_s \tag{12.10}$$

Equation commonly used to estimate specific cake resistance r_c reads:

$$r_c = \frac{180\mu(1-\varepsilon)^2}{D_p^2 \varepsilon^3} \tag{12.11}$$

In the above equation, μ is the viscosity of the fluid, ε is the porosity of the solid cake, D_p diameter of the particle, u_s superficial velocity, Φ_s is the sphericity of the particles in the cake. The time required for 99 % reduction of the initial flux is given by:

$$t = \frac{(10^4 - 1) R_{bm} c_g}{2 r_c u_0 c_0} \tag{12.12}$$

where c_g is the particle concentration on the surface of the cake layer, c_0 is the particle concentration in the bulk (feed) fluid, R_{bm} is the resistance of the blocked membrane and u_0 is the initial velocity (to the clean surface of the membrane).

12.2.1.3 Physicochemical model

The model with a fouling limitation applied is given in the form that reads [5]:

$$R_f = R^*(1 - p\ \exp\ (-qc^r t)) \tag{12.13}$$

where R^* is the long-term fouling resistance, p, q, and r are specific constants. The variable p renders very fast initial increase in the resistance, due to the substance adsorption at the surface of the membrane which causes blocking of the pores. The q and r variables render the curvature of the time evolution of the hydraulic resistance of the membrane. R^* is given by a Langmuir or Freundlich isotherms and is a function of bulk concentration and solution pH. Equation 12.13 represents typical correlative approach where the specific variables must be experimentally obtained for individual membrane type.

12.2.1.4 Reaction model

The assumption of Langmuir–Hinshelwood kinetics for the buildup of an adsorbed layer on the membrane surface [6] and leads to the description of the dynamics of its thickness l:

$$\frac{dl}{dt} = k_1(l_0 - l)C_w - k_2 l \tag{12.14}$$

The C_w is the concentration of the separated substance at the membrane surface. The kinetic constants k_1 and k_2 refer to the rate of its deposition and removal respectively. The solution to the above reads:

$$l(t) = \frac{k_1 C_w l_0}{k_1 C_w + k_2} + e^{-(k_1 C_w + k_2)t}\left(l_0 - \frac{k_1 C_w l_0}{k_1 C_w + k_2}\right) \tag{12.15}$$

The values of kinetic constants can be obtained by means of nonlinear fit numerical methods versus experimental data of cake thickness formation.

By solving classical diffusion equation of Fick's second law, other formulation can also be given:

$$\frac{dl}{dt} = k_r C_b{}^2 \exp\left(\frac{2\Delta P}{k_m \mu (R_m + l/p)}\right) \tag{12.16}$$

where ΔP is the pressure across the membrane, μ is the viscosity, p is permeability of the filtrated substance, l represents thickness of the layer, C_b bulk concentration of the substance, and R_m is the membrane resistance. The kinetic constants represented by k_r and k_m refer to the deposition and removal process respectively. The solution to the above problem can only be done on the numerical basis.

12.2.1.5 Maxwell permittivity model

Gas separation by selective transport through mixed matrix polymeric membranes is commonly used technique for gaseous mixtures treatment. Chung et al. [7] suggested to use Maxwell permittivity model [8] originally aimed to predict the material resistance to external electric field. The effective permeability of composite membrane can be formulated in terms of component permeabilities of continuous P_c and dispersed phases P_d:

$$P_{eff} = P_c \frac{P_d + 2P_c - 2\phi_d(P_c - P_d)}{P_d + 2P_c - \phi_d(P_c - P_d)} \tag{12.17}$$

The above model is a simple approach that accounts for dilute suspension of spherical particles. The variable ϕ_d is the dispersed (polymer) phase volume fraction. Some modifications of the above approach have been proposed [9] to account for more realistic behavior. The diffusion coefficient for gas in membrane pores is then given by Knudsen diffusion coefficient that reads:

$$D_{AK} = 9.7 \cdot 10^{-5} r \sqrt{\frac{T}{M_A}} \left(1 - \frac{d_g}{2r}\right) \tag{12.18}$$

where r is the effective pore radius expressed in Å, T is the absolute temperature, M_A is the molecular mass of the gas, and d_g is the diameter of the gas molecules also expressed in Å. The value of the permeability of the combined sieve (P_d) and interface (P_i) void can be used along with the continuous polymer phase permeability (P_c) to obtain a predicted permeability P_{3MM} for the three-phase mixed matrix materials by applying the Maxwell equation:

$$P_{eff} = P_c \frac{P_{eff} + 2P_c - 2(\phi_d + \phi_i)(P_c - P_{eff})}{P_{eff} + 2P_c - (\phi_d + \phi_i)(P_c - P_{eff})} \tag{12.19}$$

The variable ϕ_d is the dispersed (polymer) phase volume fraction and ϕ_i is the volume fraction of the interface void.

12.2.1.6 Modeling dense membranes

The nonporous membranes, i.e. for reverse osmosis [10], modeling shares the same principia of mass conservation as the porous, they differ in the form of constitutive relations although. The key process governing the transport through the membrane material is the solution-diffusion mechanism. The performance of the process depends on the selectivity φ_M of the membrane which is defined by:

$$\varphi_M = 1 - \frac{C_p}{C_w} \tag{12.20}$$

where C_w and C_p are the concentration of diluted substance in the feed and permeate, respectively. The flux of permeate J_P can be calculated by relationship:

$$J_P = \frac{j_m \Delta P_m}{\varphi_M^{\omega}} \tag{12.21}$$

where the thermodynamic function to compute a maximum value of the selectivity coefficient of the membrane reads:

$$\varphi_M = 1 - \exp\left(\frac{\Delta W}{k_B T}\right) \tag{12.22}$$

In eq. 12.21 the variable j_m is the impermeability coefficient of the membrane, and ΔP_m is the operating pressure. The ω is an empirical coefficient that depends on the physical properties of the material and the operation conditions. The ΔW is the component of power of osmotic process expended for transporting ions across the membrane, T is the temperature of the fluid, and k_B is the Boltzmann constant. The flow through the membrane under the operating pressure ΔP_m, including impurities, depends on the hydraulic resistances of the membrane R_m and the deposit layer (cake) R_c:

$$J_v = j_m \frac{\Delta P_m}{\mu_c (R_c \delta_c + R_m \delta_m)} \tag{12.23}$$

where the d_c and d_m are the cake and membrane thicknesses, μ_c is the dynamic viscosity of the deposit layer.

The steady state and dynamics for dense membranes can also be modeled by considering that the driving force of the process is entirely of diffusive nature [11]. In this case the flux of specie i^{th} is related with diffusion coefficient and specific formulation of driving force which includes corresponding permeabilities $p_{i,\text{perm}}$ and $p_{i,\text{feed}}$ difference:

$$J_i = \frac{S_i}{L \cdot \mathrm{H}_i} D_i (p_{i,feed} - p_{i,perm}) \tag{12.24}$$

where D_i is the diffusion coefficient of specie i^{th}, S_i is the sorption coefficient, H_i is Henry constant, and L is the membrane thickness. The postulated dynamic description relies on variation of diffusion coefficient and permeabilities by introducing their functional forms dependent on time, $D_i(t)$ and $p_{i,\mathrm{perm}}(t)$. Such mathematical simplification is valid only with assumption that diffusion coefficient is independent of diffusing specie concentration which is valid for dilute solutions. This statement is postulated by the authors [11] exclusively by particular formulation of Fick's second law for time evolution of specie concentration in membrane material:

$$\frac{\partial c}{\partial t} - \frac{\partial}{\partial x}\left(D(t)\frac{\partial c}{\partial x}\right) = 0 \tag{12.25}$$

The initial condition for the above reads:

$$c(x,0) = 0 \tag{12.26}$$

which formulates that no diffusing specie is contained inside the membrane in the initial moment of the process. The boundary conditions read:

$$\begin{cases} c(0,t) = c_1 \\ -D(t)\dfrac{\partial c(L,t)}{\partial x} = J(t) \end{cases}$$

that depicts that at the membrane surface (x=0) there is some initial concentration c_1 of the solute, and at the downstream surface of the membrane there is a flux $J(t)$ given by the partial pressure in the permeate channel during the process.

12.2.1.7 Models dependent on membrane configuration

12.2.1.7.1 Hollow fiber module

The hollow fiber modules are specific types of membranes in which the key constituent is their longitudinal character of the process. Starting from Fick's diffusion law the longitudinal development of solute concentration for laminar flow is given by relation dependent on the distance z from inlet [12]:

$$C_m(z) = C_{A,i}\left(1 - \exp\left(-\frac{4k_L z}{u_L d}\right)\right) \tag{12.27}$$

where $C_{A,i}$ is the bulk concentration of specie A^{th}, k_L is the mass transfer coefficient, d is the diameter of the fiber, u_L liquid velocity. The average of the above distributed concentration $C_m(z)$ can be obtained [13] by calculating the integral average along the z axis, to give C_A:

$$C_A = \frac{C_{A,i}}{L}\left(L + \frac{u_L d}{4k_L}\left(\exp\left(-\frac{4k_L z}{u_L d}\right) - 1\right)\right) \tag{12.28}$$

12.2.1.7.2 Spiral-wound module

Spiral-wound membranes are typically used for reverse osmosis process. To estimate the concentrations in permeate following equations are proposed [14]:

$$C_p(z) = C_i\left(1 + \frac{J_v(z)/B_s}{e^{J_V(z)/k_i}}\right)^{-1} \tag{12.29}$$

where k_i is the mass transfer coefficient at z location, and z is the location of feed (z=0) and outlet channel of module length L (z=L). The J_v evaluated at the same z locations is given by:

$$J_v(z) = \frac{A_W \Delta P(z)}{1 + \frac{A_W R}{B_s} T \cdot C_p} \tag{12.30}$$

where B_s is the solute mass transfer coefficient, A_W is the solvent mass transfer coefficient, C_p is the concentration of solute in the permeate, T is the temperature, R is universal gas constant, ΔP is transmembrane pressure at predefined z locations.

12.2.1.7.3 Capillary module

The capillary modules are commonly used for membrane distillation. The mathematical model [15] of such a unit operation must account for mass and also for heat balance equations, to enable the power requirement calculation. The formulations of equations presented below confirm also flat configuration of the membrane. The flux F expressed by the mass balance equation reads:

$$F = 1.064\left(\frac{r_p \varepsilon}{\delta \tau}\right)\sqrt{\frac{M_w}{RT_m}}(P_m - P_d) \tag{12.31}$$

where r_p is the pore size, ε is the porosity of the membrane, δ is the membrane thickness, τ is the pore tortuosity, P_d is the pressure at the vacuum side, P_m is the water vapor pressure at the membrane surface temperature T_m, M_w is the water molecular weight and R is the gas constant.

Heat balance equation reads:

$$\rho c_p S > \left(\frac{d(vT_f)}{dA_{mb}} - \frac{T_{ref} dv}{dA_{mb}}\right) = -F\Delta \mathrm{H}_v \tag{12.32}$$

where c_p is the specific heat, T_{ref} is the reference temperature and ΔH_v the heat of vaporization of water. The model can be used to calculate the energy requirements and distillate yield flat and capillary modules.

12.2.1.8 Summary

The presented section outlines the broad spectrum of model approaches that are based on traditional engineers and designers techniques of membrane processes description. The modeling and the designing procedure are the tasks that employ the same tools but take different view of the process considered. The correlations presented can be used to make a simulation if some initial data like feed source, feed quality, feed/product flow, and required product quality are given. Then having selected the flow configurations and membrane elements type and setup, one can determine whether the process works as expected. The design procedure on the other hand implicates a specific results to be obtained, namely the material and geometry estimation of the membrane itself. Both views, the modeling and the design, are essentially the same regarding the theoretical and mathematical description of the process but target different needs. Most of the presented formulations are based on correlated experimental results applied to equation of mass or momentum balances. In general, the fundamental disadvantage of the models based on experimental measurements or any specific material constants obtained under particular conditions is their higher, compared to other approaches, tendency to decrease the accuracy and/or reliability when performing calculations for systems that differ significantly from systems for which they were originally established. Many correlations are designed for some specific range of temperatures, pressures, and so forth and beyond these ranges they might not be reliable source of knowledge about the system. The exception from such typical correlative issues might be to rely only on fundamental physicochemical data which do not depend on the system conditions (e.g. critical pressures, temperatures, or volumes of species involved). The mathematical approaches and models presented in next parts of this chapter address this problem because their fundamental approach is not to rely on actual, narrow range specific parameters.

12.2.2 Molecular modeling

Molecular modeling covers methods, algorithms, and numerical approaches which can be applied to model the molecules and atoms behavior. Its typical use is to study molecular systems varying from small to large molecular systems and material entities. The typical analysis done by molecular modeling is a phenomenon at atomistic level of the matter. In general this type of analysis can be done on the basis of molecular mechanics or quantum chemistry approach. Molecular mechanics applies laws of classical mechanics to render the interactions between atoms and molecules while quantum approach utilizes quantum theory to describe behavior of molecules, atoms, and subatomic particles. While the molecular mechanics involves atoms and bigger entities the quantum approach accounts also for electrons in the atomic structure. Both approaches are entirely different, with molecular mechanics being less accurate but faster and quantum modeling much more realistic but also with higher computational demands. There exists also approaches combined that couple the molecular and quantum mechanics in single algorithms [16] referred to as QM/MM (quantum mechanics/molecular mechanics).

12.2.2.1 Quantum mechanics models in polymer membranes

The underlying fundament of all quantum methods is Schrödinger equation which defines molecules in terms of interactions among nuclei and electrons and depicts geometry of the molecules by structure satisfying minimum energy requirement. The time dependent Schrödinger equation reads:

$$E\Psi(r,t) = \hat{H}\,\Psi(r,t) \tag{12.33}$$

In the above the Ψ represents wave function representing quantum state of the molecule, atomic, or subatomic system. A single wave function covers at once all the particles in the system analyzed. There are many different wave functions for single system though, each of them representing appropriate description, in a chosen coordinate system. Every of the distinct representatives express all observable elements of information about the state (e.g. position, translational momentum, orbital angular momentum, spin, total angular momentum, energy). $\hat{H}$ is the Hamiltonian operator that acts on a function Ψ. The Hamiltonian corresponds to the kinetic and potential energies of a system and is the summation of all energies for every particle in the given spatial configuration at an instant time. The Schrödinger equation cannot be solved directly and approximations must be used in order to obtain results. The most commonly approximation used in order of increasing simplifications applied are as follows. The Born–Oppenheimer approximation with the assumption that the atomic nuclei do not move and only electrons kinetic energy, and the nuclei–nuclei charge interactions are accounted for. The Hartree–Fock approximation is further simplification that assumes no interaction between electrons themselves. This leads to formulation of atomic (and molecular) orbitals which can be related to stationary state of wave function for an electron in atom or molecule. The orbitals render the structure of the atom or molecule as if all the electrons formed the molecule shape without electron–electron interactions, which obviously is a simplification. The LCAO approximation (Linear Combination of Atomic Orbitals) is used in Hartree–Fock approximation to render the linear combination of atomic orbitals to further calculate the molecular orbitals by their quantum superposition. The molecular orbitals are expressed in the sense of so-called basis sets which are the linear combinations of a set of functions. The basis set is created of a finite number of orbitals, centered at each atomic nucleus within the molecule. The Hartree–Fock approximation is applicable to molecules composed from up to hundreds of atoms. Assuming no electron–electron interactions and treating every electron as independent of each other leads to overestimating of electron repulsion energy which consequently render as too high total energy of the system calculated. To overcome this problem a correlated models were proposed in which the electron correlation accounts for coupling the electrons motions that result to decrease the repulsion energy of electron–electron interactions. Lower repulsion energy estimated leads to lowering the total energy. The density functional models propose approximate correlation by an explicit term formulated on the basis of Density Functional Theory. The main assumption of this approach is the fact that the sum of the correlation energies of uniform electron cloud can be evaluated based on its density. The density functional models are usually appropriate to estimate equilibrium, geometries of transition-states, and vibrational frequencies. The density functional models reveal some serious deficiencies with regard to energetics of reaction. Due to this problem the Configuration Interaction Models were introduced in which the “auxiliary” wavefunction terms corresponding to excited states are additionally included with regards to Hartree–Fock method. The Configuration Interaction Method approaches the exact Schrodinger equation solution if the basis set applied is more complete (covers wider range of possible wavefunction states). The importance of using more complete basis sets arises due to size consistency, where typical problem is that the solution to the energy of two infinitely separated particles is not double the energy of the single particle. Due to the high demand on computing power these methods are limited to relatively small systems, however. The simplest model offering improvement over Hartree–Fock method is Moller–Plesset theory of second order (MP2). Also higher order models MP3, MP4 were formulated but they are limited to small systems. The MP2 method is practical for molecules of moderate size, although.

The basis sets mentioned earlier are functions introduced first by Slater [17] to give a description of electron orbitals. Slater type orbital (STO-xG, where x is the number of Gaussian functions) basis sets are simplest sets of Gaussian functions representing orbitals. It is significant that the same number of Gaussian functions is used to represent core and valence orbitals. They give rough estimation for orbitals but are much less computationally demanding. Pople et al. [18] formulated more complex basis sets named split valence basis sets. This formulation represents the valence orbitals by more than one basis function due to the fact that valence orbitals take main part in molecular bonding. A lot of basis sets are discussed in the references [19–23].

Due to the complexity of the quantum calculation it is typically not possible to perform the calculations by homebrew computer codes, instead a commercial (Gaussian, Jaguar, etc.), academic (e.g. Gamess, Firefly) or free General Public License (CP2K, PUPIL) codes are used.

Taking into account polymer membranes the main research area where the quantum modeling calculations are mostly involved are polymeric membranes in fuel cell simulations, namely proton exchange membrane fuel cell, PEMFC (Figure 12.2). Fuel cell is an electrochemical device that transforms the chemical energy into the electrical energy without any assistance of additional component. Principal elements of a single PEM fuel cell are: membrane, catalyst layer, gas

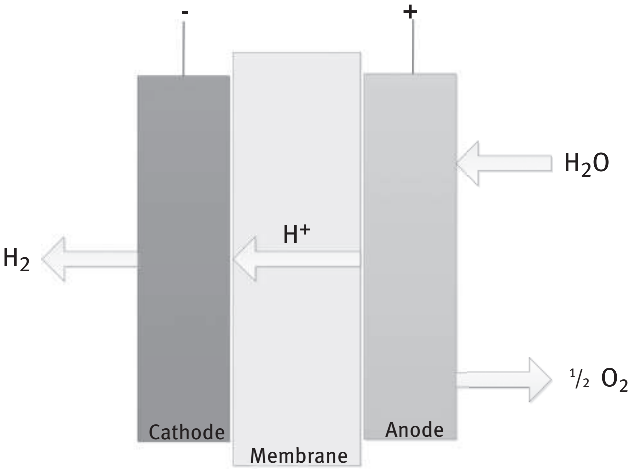

Figure 12.2: Fuel cell typical setup.

diffusion layer (also referred to as porous transport layer), current collectors, and flow channels. Such membranes are often denoted as polymer electrolyte membranes or proton exchange membranes. The hydrogen is the fuel for the PEMFC and the hydrogen ion, proton is the charge carrier.

The anode reaction reads:

$$H_2 \longrightarrow 2H^+ + 2e^- E = 0V \frac{dE}{dT} = 0mVK^{-1} \tag{12.34}$$

The cathode reaction reads:

$$\frac{1}{2}O_2 + 2H^+ + 2e^- \longrightarrow H_2O \ E = 1.2291V \ \frac{dE}{dT} = -0.8456mVK^{-1} \tag{12.35}$$

The overall reaction is then given by stoichiometry:

$$H_2 + \frac{1}{2}O_2 \longrightarrow H_2OE = 1.2291V\frac{dE}{dT} = -0.8456mVK^{-1} \tag{12.36}$$

The anode reaction reads:

The cathode reaction reads:

The overall reaction is then given by stoichiometry:

One of the most popular membrane material present on the market is Nafion, which is sulfonated tetrafluoroethylene based fluoropolymer-copolymer ($RF[OCF_2CF(CF_3)_2]_nOCF_2CF_2SO_3H$). Nafion is most often formed as a thin foil and used as a protons transporting membrane, namely ionomer, while being a barrier for electrons or anions. This material exhibits also high thermal and chemical resistance.

Yu et al. [24, 25] simulated chemical mechanisms of degradation of Nafion using JAGUAR 7.0 code. They incorporated Density Functional Theory to formulate the potential energy surfaces for various possible reactions accounting for intermediates which could be created when Nafion is exposed to molecular hydrogen, molecular oxygen, or protons in the presence of the platinum catalyst. The B3LYP (Becke, three-parameter, Lee-Yang-Parr) exchange-correlation functional was used with 6-311G** basis set (six Gaussian primitive function for core orbitals, and a linear combination of two basis function for each valence orbitals, the stars indicate extension to the main basis set by adding double polarization functions). Based on the results three mechanisms by which OH radical species formed on a platinum surface lead to degradation of Nafion polymer were proposed and experimentally validated by F NMR and mass spectroscopy.

Sakai et al. [26] used Gaussian software commercial tool to model the deprotonation reaction of the sulfonic group (SO_3H) in a hydrocarbon membrane, as a new proton conductor for polymer electrolyte membranes (PEM) of polymer electrolyte fuel cells (PEFC). Similarly as case previously described 6-311+G(d, p) basis set was used at the B3LYP density functional theory level. The difference in basis set is presented by the plus sign meaning that the diffuse function is used for *p* and *d* orbitals. The diffuse functions are of high significance for anions to describe the electrons that are at longer distances from the nuclei. The quantum model was used to investigate and simulate the behavior of the sulfonic group of sulfonic acid $C_6H_5SO_3H$ as a model of a hydrocarbon membrane. As the concluding statement the following two properties were noticed as the main factors decreasing proton conductivity at low hydration levels: sulfonic acid has low acidity because deprotonation of SO_3H group and protonation of SO_3^- anion occur with the same probability; and the SO_3^- anion of sulfonic acid binds strongly with the $H3O^+$ in comparison with short side chain perfluorosulfonic acid. Paddison et al. [27] presented earlier similar study using B3LYP/6-311G** level density functional theory to perform modeling of a hydrocarbon polymer membrane ($CF_3CF(O(CF_2)_2SO_3H)(CF_2)_nCF(O(CF_2)_2SO_3H)CF_3$, where $n = 5$, 7, and 9). The quantum simulation performed exposed that the number of water molecules needed to connect the sulfonic acid groups is a proportional function of the number of fluoromethylene groups in the main chain, with one, two, and three water molecules needed to connect the sulfonic acid groups in parts with $n = 5$, 7, and 9, respectively. It is also worth noting that the simulation was performed with explicit addition of water molecules to each of the polymeric fragments (an implicit approach would be to replace intermolecular interactions by so-called averaged field), which allowed to conclude that the minimum number of water molecules required to affect proton transfer also increases as the number of separating tetrafluoroethylene units in the main chain is increased. These quantum modeling calculations provided the results that might be used to evaluate the impact of changes of polymer chemistry on proton conduction, including the side chain length and acidic functional group.

There are also modeling studies which are based on approaches which in their background rely on quantum calculations. One of such approach is COSMO model (conductor-like screening model) which is used for estimating the electrostatic interaction between a molecule and a solvent. This model belongs to continuum solvation or averaged field group of models. The main concept is to approximate the solvent presence by a dielectric continuum, surrounding the molecules. The COSMO method can be used with Hartree–Fock methods or density functional theory calculations. The extensions for real solvents allow to estimate the chemical potentials of substances in liquids which consequently leads to other thermodynamic equilibrium properties (such as solubility, activity coefficients, vapor pressures, partition coefficients and free solvation energies) calculations. The example of the use of such an approach is the work of Shah et al. [28] They used a COSMO-SAC model (conductor-like screening model – segment activity coefficient) to estimate the structure–properties relationships between the polymer structure and membrane performance. The GGA/VWN-BP functional setting and the DNPv4.0.0 basis set was used. The generalized gradient approximation (GGA) takes into account variations in the density by including the gradient of the density in the functional. The Vosko-Wilk-Nusair [29] (VWN) is the correlation for many electron system of the spin-polarized homogeneous electron gas. The VWN correlation energy per particle of homogenous electron gas improves the theory and experiment agreement. The VWN-BP represents the Becke-Perdew version of the VWN functional. The model can successfully predict two component sorption from single component sorption data. The model functions poorly in the case of some polar solvent/polar polymer combinations, however.

12.2.2.2 Molecular mechanics models in polymer membranes

Molecular mechanics describes molecules and chemical bonds based on van der Waals and Coulombic interactions. This approach utilizes classical mechanics laws to model the molecular systems.

The molecular mechanics approach expresses the energetic state of a molecule in terms of a sum of contributions resulted from deviations from an ideal molecular state of lowest energy. The summation is taken over stretch contributions (bond distances), bend contributions (bond angles) and torsion contributions (torsion angles) of mechanical state of molecular system. Additional terms are the contributions due to van der Waals and Coulombic (non-bonded) interactions. Stretches and bends contributions of molecular bonds are formulated in terms of Hook’s law forms. Torsion contributions need to reflect the torsional potential periodicity which takes the form of trigonometric functionals that accounts for such behavior. The energy of torsion can be formulated in terms of Fourier series which allow to account for energy differences in cis and trans conformers or between planar and perpendicular conformers. The van der Waals and Coulombic interactions summation formulate the non-bonded interactions terms. Some explicit summation terms might also be included to account for such interactions as hydrogen bonding. The van der Waals interactions are formulated as a summation of attractive and repulsive components. The Coulombic term is formulated to take the charges interactions into account.

The advantage of molecular mechanics models over quantum approach is their greater ability to transfer the geometrical variables between molecules, and expectable parameters dependence on atomic hybridization. This makes the molecular mechanics approach to be easier when applying initial geometrical guess to a numerical solving procedure and allows to perform faster calculations. In practice the computational load increases linearly with the size of molecular system modeled (which is not the case for quantum mechanics). The parametrization of molecular models is also important advantage over quantum approach. On the other hand the simplicity of the molecular mechanics models imposes some limitation when comparing with quantum approach. The most important limitation is that molecular mechanics allow to represent only the equilibrium states (geometries and conformations) of the molecular systems. The parametrization of functionals describing force fields has not yet been done to comply with nonequilibrium molecular states. The next limitation is that the molecular mechanics cannot describe the electron distributions in molecules which is an important feature when simulating chemical reactions. Consequently, the underlying principal nature of molecular mechanics modeling is its approximation character, for which the accuracy depends on quality of the parameters used and on the classifications of relations between molecules. This is typical that for such an approach going beyond the range of parametrizations, i.e. describing some new molecular structures, is expected to be burdened with high and difficult to estimate error.

The extension to molecular mechanics approach is molecular dynamics, which besides of the molecular mechanics interactions, consist on solving, typically on numerical basis, the classical equations of motion. After the calculation of potential energy field, the forces acting on the molecules are computed. Applying the Newton's equations of motions to the molecular system results in a molecular momenta estimation which consequently leads to movement patterns of molecules. Such a system of differential equations is solved using specified step-by-step numerical algorithm of integration. The differential equations set is typically characterized by high stiffness (relation of fast to slow dynamic components of the process simulated) and special numerical treatment is needed. Historically the Gear's algorithm [30] was designed for such systems, which is the two step method assembled of explicit Adams and implicit backward differentiation formula. Recently Verlet algorithm [31] is used to solve this problem, which is purposely designed to integrate the equations of motion.

As an example the effects of molecular structure on the polymer membrane process is studied by means of molecular mechanics calculations by Shen et al. [32] The molecular mechanics models require to input initial structure of the modeled molecular system. For the polymers a heuristic method [33] can be used, which consist on building the structure from monomers and locating them randomly in computational space. Authors examined the rejection mechanisms for contaminants in polyamide reverse osmosis process and based on the molecular dynamics calculations concluded that the solute rejection is positively correlated with the Van der Waals size of the dehydrated solutes due to decreasing accessible intermolecular volume between polymer chains of the membrane with solute size. Devanathan et al. [34] performed an *ab initio* study (from first principles) of proton transport in Nafion polymer membrane. One of the most fundamental problems in proton transport is that it does not follow diffusive transport of water molecules but make use of surrounding hydrogen bonded clusters. For complex molecular systems, such as those which appear in proton exchange membranes, molecular dynamics methods that aim to explain proton transport accurately need to capture this dynamical behavior. The study was conducted for different hydration levels: dry, hydrated, and saturated fuel cell membrane. In the confined environment of the membrane, the protonic defect exists as $H_5O_2^+$, $H_7O_3^+$, and $H_9O_4^+$ cations for the three hydration levels respectively. As the hydration levels increases, the barrier for proton transport from contact ion pair to solvent separated ion pair decreases, the water molecules form a penetrating cluster, which allows the proton to hop through the water cluster structure contacting multiple sulfonate groups of Nafion polymer. The estimated by means of molecular dynamics diffusion coefficient for proton transfer is equal to $0.9 \cdot 10^{-5}$ cm^2/s, which for high hydration levels stands in accordance with experimental trends, as stated by authors.

The diffusive transport in four polymer membranes is investigated on the basis of molecular dynamics by Ling et al. [35] to give the estimation of diffusion coefficients in this process. Based on diesel components the study presented the modeling calculations that allowed to investigate the micro diffusion mechanism inside polymer membranes. Authors took into account three key factors affecting the diffusional transfer: interaction energy between molecule and polymer membrane, fractional free volume of the membrane and mobility of polymer chains. The mean square displacement formulation was used to calculate the diffusion coefficient from the results obtained:

$$MSD = \langle (r_i(t) - r_i(0))^2 \rangle = \frac{1}{t} \sum_{\tau=1}^{t} \left(r(\tau) - r(0)\right)^2 \tag{12.37}$$

where $r_i(t)$ is the spatial coordinate of molecule i at time t, and $r_i(0)$ is the initial spatial coordinate of molecule i. The diffusion coefficient is calculated from Einstein formula:

$$MSD = 2dDt^{\alpha} \tag{12.38}$$

where d is the dimensionality of the Brownian movement (space dimensionality), t is the time over which the diffusion coefficient value D is averaged. The power law exponent α is in normal diffusion regime (the diffusing molecules jump between individual free spaces in the polymer membrane) equal unity. The calculated diffusion coefficients were of order 10^{-9}, m^2/s which is in good accordance with presented experiments for materials investigated.

12.2.2.3 Summary

In general quantum and molecular mechanics simulations even of idealized polymer membranes can provide valuable guidance by predicting the performance of candidate systems as a function of the structural and compositional factors that influence transport properties. Results obtained from such calculations, even if semiquantitative, can be used to give directions of synthesis toward suitable materials among the increasing number of potential polymers combinations. The modeled and calculated wave function representing the state of molecule can effectively be related to chemically valuable concepts such as atoms in molecules, functional groups, bonding, the theory of Lewis pairs and the valence bond model [36].

12.2.3 Neural networks modeling

Artificial neural network is the class of models where the fundamental algorithms resemble biological neural networks learning process. The neural network model is a type of approximation algorithm which is used to estimate functions that depend on large number of variables. The structure of artificial neural network is based on its key element – neuron that is typically presented by some mathematical function which recalculates and transfers variable values (information). The neurons that are used in neural network are interconnected and are capable of exchanging information between each other. The neural connections are characterized by weights which are tuned during the learning process, making the neural networks adaptive to data sets presented for the learning process. The artificial neural network is constructed from interconnected neurons, and typically takes the form of neuron layers.

The three-layered connection of neurons is an example of neural network model (Figure 12.3). The first layer, input layer, contains input neurons which transmit data to the second, hidden layer of neurons. The hidden layer can be assembled of any number of neural layers. The hidden layer transfers the information to the output layer to give result of calculations. Each connection, so-called synapse, stores a numerical weight which transforms data during the process of its transmission. The artificial neural network can be characterized uniquely by three elements: the pattern of interconnections between layers of neurons and neurons themselves, the algorithm of weights updating at the synapses, and activation function which recalculates and transforms the input signal to its output value. A simplest neural network consisting of single neuron is referred to as perceptron. It takes a number of binary

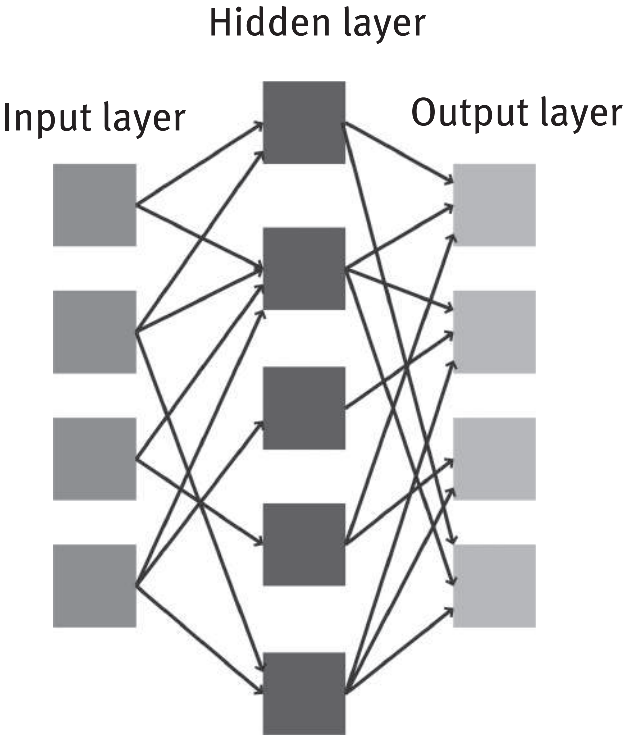

Figure 12.3: Example of neural network setup connections between neutron layers.

inputs and produces single binary output and is used to solve the classifications problems. A multilayer perceptron is a composite of several (at least two) perceptrons aligned in layers. More sophisticated neuron formulations were introduced as for example sigmoid neuron. Instead of binary inputs/outputs, a continuous activation function is defined which works in the variable range <0; 1>, and is called sigmoid function:

$$\sigma(z) = \frac{1}{1+e^{-z}} \tag{12.39}$$

In the case the sigmoid neuron contains N inputs with corresponding weights w_j and bias b applied the formulation of activation function reads:

$$\sigma(z) = \frac{1}{1+\exp\left(-\sum_{j=1}^{N} w_j x_j - b\right)} \tag{12.40}$$

The particular choice of activation function determines the neural response to the neural network and has impact on its learning properties and capabilities.

Fundamental feature of neural network is its ability to learn based on teaching data sets. The process aims to find optimal solution for the specified task. For this purpose a cost function is defined which is a measure of particular solution distance from the optimal one. It is the key task of learning algorithms to minimize the cost function in the solution space. The least squares method defined on the observed data and neural network output is a typical approach characterizing the cost function. There are three learning paradigms, namely supervised learning, unsupervised learning and reinforcement learning. In supervised learning the two sets of paired data are given over which the neural network is trained to find optimal synapses weights, that match the presented, teaching data. The unsupervised learning is the process where for particular teaching data set the specific cost function chosen is minimized. The cost function is of arbitrary choice that should reflect any of the data features. In reinforcement learning the teaching data set is not given, instead so-called software agent (that is a computer program communicating with the environment) acts on the studied environment at some time t and observes its reaction. The aim of this action is to determine a scheme that minimizes measure cost function in long term. The neural network models are able to approximate, predict, or recognize specific behavior; they are also capable of making generalizations exceeding boundaries of range for which they were trained.

Lobato et al. [37] present a study in which three different types of neural networks are tested to model a polybenzimidazole-based polymer electrolyte membrane fuel cell. Multilayer Perceptron (MLP), Generalized Feedforward Network (GFF), and Jordan Elman Network (JEN) were used having as common characteristic the supervised learning control. The training and validation data set consisted of 16 series of experimental data where 10 % of the whole set were preserved for validation phase, which was not used for training the neural network purposes. The neural networks had three input variables: conditioning temperature, the operating temperature and electric potential, and three outputs: the electric current density, the cathode resistance and the ohmic resistance. The best prediction was reached by MLP network as determined at the validation stage, which was the simplest network used in the study. All three neural networks exhibited good accordance with experimental results, although.

Modeling the performance of Nafion type fuel cell was also subject of the study by Lee et al. [38] The aim of this analysis was to obtain an empirical model including process variations to estimate the performance of fuel cells without complex calculations. Artificial neural network were trained to fit experimental data obtained in a single cell in H_2/air operation using Nafion 115 and Nafion 1135 membrane electrolytes. The models presented accounted for the current density, the gas pressure, temperature, humidity, and utilization to cover operating processes. The multilayer feed forward neural network was used with two cases of activation function for neurons, linear and tangent sigmoid function:

$$f = x, \; f = \frac{2}{1 + \exp(-2x)} - 1. \tag{12.41}$$

Due to the multilayered network construction the output of the j^{th} hidden layer unit is given by:

$$h_j = f\left(\sum_{i=1}^{n_i} w'_{ji} x_i + b'_j\right) \tag{12.42}$$

where w'_{ji} is the weight of connection from i^{th} input unit to j^{th} hidden layer unit and b'_j is the bias value for j^{th} hidden layer unit. The output value from the network is given by:

$$y = f\left(\sum_{j=1}^{n_h} w_j h_j + b\right) \tag{12.43}$$

where w_j is the weight of synapse from j^{th} hidden layer unit to output unit and b is the bias for output unit. Finally the weights are adjusted to minimize sum of squares error SSE:

$$SSE = \sum_{p=1}^{n_p} (t_p - y_p)^2 \tag{12.44}$$

$$\begin{cases} \rho \dfrac{\partial u}{\partial t} = -\rho u \cdot \nabla u - \nabla p + \rho g \\ \nabla \cdot u = 0 \end{cases} \tag{12.45}$$

In the above the variable $\mathbf{u}$ is the velocity vector, ρ is the fluid density, $\mathbf{g}$ is the acceleration vector. The first equation states that the rate of change of force vector exerted on fluid volume $\rho \cdot \partial \mathbf{u} / \partial t$ equals: the negative value of advective (sometimes referred to as convective) component of flow due to the fluid's bulk motion $\rho \mathbf{u} \cdot \nabla \mathbf{u}$; the negative value of pressure gradient ∇p acting on the analyzed fluid volume; and bodyforces $\rho \mathbf{g}$ exerted on a fluid volume. The bodyforces source term can be of different nature, typically due to gravity but also centrifugal, magnetic or porous media resistance forces can be taken into account. The second equation presenting zeroth divergence of velocity vector means that there are no source or sinks in the volume analyzed. The key weakness of the equation is its idealization due to the absence of constitutive relation. For the fluids in motion it is very important to account for their real behavior by including the relation between forces applied (stress) and deformations observed (strain) on the fluid volume. This term was introduced by Navier and Stokes independently, extending the Euler's equation and is referred to as stress-strain relation. For compressible fluids (most general case) the constitutive relation is presented in the form of total stress tensor **σ** (containing axiatoric and deviatoric components) that reads:

$$\sigma = \lambda(\nabla \cdot u)I + \tau \tag{12.46}$$

where *λ* is the bulk viscosity which originates from the drag forces created by volumetric change (compressibility effects). The identity matrix **I** was introduced during derivation due to fluid isotropic properties related to axiatoric component of the stress. The deviatoric component **τ** of the stress tensor **σ** originates from the viscous drag forces developing in fluid in motion:

$$\tau = \mu(\nabla u + \nabla u^T) \tag{12.47}$$

The deviatoric stress tensor **τ** describes the state of stress at a point inside a fluid in the deformed state. The deviatoric stress (apart from axiatoric which is an uniform stress) has dissipative nature and is referred to as diffusion of momentum term. The variable *μ* is the viscosity of the fluid.

Any source of vector or tensor quantity is indicated by the its divergence, therefore the divergence of the stress tensor describes the force transport component that results from the viscous nature of the fluid. The divergence of deviatoric stress tensor **τ** reads:

$$\nabla \cdot \tau = \mu \nabla \cdot (\nabla u + \nabla u^T) = \mu \nabla^2 u \tag{12.48}$$

$$\frac{\partial u}{\partial t} + u \cdot \nabla u = -\frac{1}{\rho} \nabla p + \mu \nabla^2 u + \frac{1}{3} 1mu\mu \nabla (\nabla \cdot u) + g. \tag{12.49}$$

which finally leads to the formulation of Navier–Stokes equation:

The above equation is valid for constant viscosity *Δ* which does not depend on strain rate (Newtonian fluids). Another terms that appear in this equation: $\Delta\nabla^2\mathbf{u}$ is the momentum diffusion, the gradient of the divergence of velocity $\nabla(\nabla\cdot\mathbf{u})$ – the resultant vector field presents the measure of the changes of the source/sink of the velocity vector field of the fluid volume. The Navier–Stokes equation itself describes the velocity field of the fluid modeled.

The mass continuity equation might also be considered. The solution of conservation of mass equation:

$$\frac{\partial \rho}{\partial t} + \nabla \cdot (\rho u) = 0 \tag{12.50}$$

results in scalar field describing mass distribution in the fluid volume. The equation describes the fact that the rate of change of mass $\partial\rho/\partial t$ inside specified volume of fluid equals the difference between masses entering and exiting $\nabla\cdot(\rho\mathbf{u})$ this volume. For the multicomponent flows additional diffusive terms must be accounted for:

$$\frac{\partial\rho}{\partial t} + \nabla \cdot (\rho u) = \nabla \cdot (D\nabla\rho) \tag{12.51}$$

where $\nabla\cdot(D\nabla\rho)$ is the measure of the changes of flux due to diffusion, D is the diffusion coefficient. In case of reactive flows the equation might preferably be expressed using molar basis and for nonequimolar chemical reaction additional source term S should be introduced.

12.3.1.1 Finite volume method

A practical realization of solution algorithms to the Navier–Stokes equations is a finite volume method widely known as CFD. The finite volume refers to the discretization approach used, which is most popular in fluid dynamics simulation software packages. The governing form of the finite volume equation reads:

$$\frac{\partial}{\partial t}\iiint_{\mathrm{V}} \mathrm{Q}dV + \iint_{A} \mathrm{F}d\mathrm{A} = 0 \tag{12.52}$$

which formulates the principia that changes in time are balanced by changes in space. The vector of conserved variables $\mathbf{Q}$ is integrated over a volume V, while fluxes vector $\mathbf{F}$ is integrated over boundary surface $\mathbf{A}$ surrounding fluid volume V.

The Navier–Stokes equation solution is obtained by applying appropriate discretization scheme over time, for time derivative of function u:

$$\frac{\partial u_i}{\partial t} = \frac{u_i^n - u_i^{n-1}}{\Delta t} \tag{12.53}$$

In this way the partial differential equation is discretized to give ordinary differential equations set. The spatial derivatives follow similar schema (although different schema are used), for the x component of u:

$$\left(\frac{\partial u}{\partial x}\right)_x = \frac{u_{I,J} - u_{I-1,J}}{\Delta x} \tag{12.54}$$

The above scheme represents a general guideline of discretization. In typical practice the geometry of analyzed object is constructed by spatial mesh which can be assembled of number of cells. Such volumetric cells can be chosen as tetrahedrons, wedges, prisms, hexahedrons and polyhedrons for three-dimensional cases. For modeling in two dimensions it is typical to use triangles, rectangles or quadrilateral to represent the space of the flow. It is important to mention that the geometric primitives used are of convex type.

The process of mesh creation is the preprocessing stage where a decision is made about the sizes and shapes of boundaries, eventually moving or rotating bodies, and the type and size of the mesh cells used. This is crucial to the accuracy of the solution for the cell size not to be larger than the smallest process phenomena to be tracked and simulated. From this point it is evident that to be able to solve or represent very small flow effects one should also use very small cell sizes, which in turn would increase the cells number. Because the differential equations are discretized over the cells producing corresponding number of algebraic equations, the higher number of cells results in larger equations set to be solved. Consequently as a reason of increasing demands on accuracy, decreasing size of cells produces CFD models that require more time to reach the solution. This is a problem of tradeoff between the demanded accuracy and computing load when performing the step of preprocessing. The preprocessed mesh is then a base of the core step – the processing that consists on applying the iterative algorithms to obtain the solution for steady or transient states of the flow. The final stage is to postprocess the results obtained to analyze them. It can be the graphical representation of the flows but also calculation of several process variables, e.g. calculating flowrates, pressure drops, or chemical reaction rates.

Reformulating the Navier–Stokes eq. (50) to account for transport through porous media an additional source force term **S** must be introduced:

$$\rho\frac{\partial u}{\partial t}+\rho u\cdot\nabla u=-\nabla p+\rho\mu\nabla^2 u+\rho\frac{1}{3}\mu\nabla(\nabla\cdot u)+\rho g+\rho S \tag{12.55}$$

which accounts for the resistance effects when modeling permeate flux. For any type of membrane, polymer, ceramic, and so forth when the sieve transport is considered the most straightforward way to calculate the **S** resistance term is to use Darcy equation.

$$\nabla p_{Darcy}=-\frac{\mu}{\alpha}u \tag{12.56}$$

and inertial losses factor:

$$\nabla p_{inertial}=R\frac{1}{2}\rho|u|u \tag{12.57}$$

In the above formulation the multiplication of both the vector **R** (inertial resistance factor which for non-isotropic media depends on direction) and vector **u** is a scalar product. The velocity vector magnitude is designated by $|\mathbf{u}|$. The resistance term **S** in the Navier–Stokes equation is the summation of both component resistances. For the case when the membrane material can be assumed to be isotropic, then the geometric direction i^{th} component of **S** reads:

$$S_i = R_i \frac{1}{2} \rho |u| u_i - \frac{\mu}{\alpha_i} u_i \tag{12.58}$$

The variable α is the permeability and R is the inertial resistance factor. For the isotropic case the indexes are omitted. The simple and straightforward estimation of both the parameters can be done on the basis of experimental measurements of the flows and pressures across the membrane [40]. Inertial resistance term R can be calculated based on measurements of the permeate flux q subject to changing transmembrane pressure Δp:

$$R = \frac{\Delta p}{q \cdot \mu} \tag{12.59}$$

Having calculated the R coefficient and knowing the membrane thickness L the permeability coefficient is obtained by relation:

$$\alpha = -\frac{L}{R} \tag{12.60}$$

Many software tools aimed for CFD calculations which allow fluid transport in porous media simulation, provide specific interface to enter these component resistances, in different range of functionality, however (e.g. Ansys/Fluent allows for vector resistance specifications while CFX allows only a scalar definition, concerning version 16.0).

Pellerin et al. [41] used Darcy law to simulate a two-dimensional case of membrane flux. The fluid flow outside membrane is simulated using closure model for turbulence effects (density-weighted ensemble-averaged, which is a simpler case of Reynolds averaged stress model). The membrane itself is simulated as an isolated entity by the laminar flow approach with velocity calculated on the basis of Darcy equation. The two-dimensional space was constructed by regular mesh of squares which formulated simple discretization problem of finite differences approach. The results were compared to analytical models of Berman [42] and Gupta [43]. The model proposed and both literature models show similar results which support it accuracy.

The CFD simulation of porous membrane of fuel cell is presented by Wang et al. [44] For the first time, the polarization curve and flowing components concentration distributions encompassing both single- and two-phase regimes of the air cathode are presented. The liquid and vapor transfer is governed by capillary transport mechanism and molecular diffusion, respectively, due to negligible small air velocity within the porous electrode. Authors applied following simplifying assumptions to the CFD model presented: the gas diffusion is isotropic and homogeneous, and characterized by an effective porosity and permeability of the porous media; the catalyst layer is treated as an infinitely thin surface for oxygen reduction at the membrane interface forming water; the cell is at isothermal conditions; the gas phase is an ideal mixture. The model construction allows for algorithmic coupling to predict the transition between the single and two phase regimes of flow. The two-phase model is appropriate to model the air cathode of both hydrogen and direct-methanol fuel cells.

The three-dimensional model of polymer membrane fuel cell was presented by Siversten et al. [45] The model proposed was non-isothermal model for proton exchange membrane fuel cells, which was implemented into a CFD code. The model algorithm presented allows for parallelization of the computing architecture. The convective and diffusive transport mechanism was accounted for which allows to present the concentration distribution of components. Appropriate energy balance is used to render the distributed heat generation associated with the electrochemical reaction in the cathode and anode. Authors implemented the modeling procedure in commercial tool Fluent 6.1 by the use of so-called user-defined functions, which allows to program own algorithms using C programming language. The modeling algorithm included flow channels and membrane itself. For the membrane the electro-neutrality was assumed, which is a valid assumption for fully humidified polymer material. The heat transport through the membrane for N-component mixture is calculated by the energy balance equation that reads:

$$\nabla \cdot (u \cdot (\rho E + \rho)) = \nabla \left(k_{eff} \nabla T - \sum_{j=1}^{N} \mathrm{H}_j J_j + \tau_{eff} \cdot v \right) + S_h \tag{12.61}$$

where E is the total energy, k_{eff} is the effective conductivity, $\mathbf{J}_j$ is the diffusive flux and H is the enthalpy of the j^{th} specie. The effective stress tensor matrix is designated by $\boldsymbol{\tau}_{eff}$ (is the volume average of the stress matrix [46] as given by (48)) and S_h is the source term for energy per unit volume and unit time which may include the heat of reaction. A general thermodynamic approach is used to model the transport in the membrane material. The current density of protons j is given by:

$$j = -L_{++} \nabla \phi_m - L_{+w} \nabla \mu_w \tag{12.62}$$

where L_{++} is the specific proton conductivity [47] (assumed at value 13.375 S/m), ϕ_m is the local potential, Δ_w is the local chemical potential of water. The water flux is given by:

$$N_w = -L_{w+} \nabla \phi_m - L_{ww} \nabla \mu_w \tag{12.63}$$

The L variables are the Onsager coefficients, and can be related by L_{+w}=L_{w+}. They can be estimated by the equation:

$$L_{w+} = \frac{\xi}{F} \tag{12.64}$$

where ξ is the number of water molecules transported with each proton (value of 3 is used). The variable F is the Faraday constant. The variable L_{ww} is not discussed in the paper unfortunately, the reader is referred to master thesis of Sivertsen [48]. The l_{mem} variable is used (permeability of the membrane, $2.35{\cdot}10^{-7}$ $\mathrm{mol^2 s/m^{-3} kg^{-1}}$):

$$l_{mem} = L_{ww} - \frac{L_{+w}L_{+w}}{L_{ww}} \tag{12.65}$$

The number of cells of a mesh constituting the space of simulation was total of 546,000. Such a mesh resolution is typically sufficient to obtain accurate and reliable results. Global comparisons show that the model and experimental results are in good accordance. The study also demonstrates that altering the conductivity modifies the current distribution by changing the relative influence of electrode potential to activation overpotentials (measure of electrode polarization).

Wiley et al. [49] present a two-dimensional study to compare the CFD simulations results with previous literature experimental data. The developed approach was a general purpose model of concentration polarization and fluid flow in pressure driven membrane separation processes. The model treats the channels as a typical space of flow with no slip boundary conditions at the walls. The membrane wall is treated differently although, where the tangential velocity component is applied to be zero and normal component of velocity (entering the space of membrane material) u_w is defined by:

$$u_w = u_0\left(1 - \beta\frac{c_w}{c_0}\right) \tag{12.66}$$

where u_0 is the velocity at channel inlet, c_w is the concentration at the wall, c_0 is the channel inlet concentration. The coefficient β is given by Brian [50] as:

$$\beta = \frac{R\pi_0}{\Delta P - R\pi_0} \tag{12.67}$$

and R (fractional component rejection/retention):

$$R = 1 - \frac{J}{c_w u_w} \tag{12.68}$$

where J is the component flux through membrane. The variable π_0 is the osmotic pressure of the feed solution, and ΔP is transmembrane pressure.

The normal velocity u_w to the membrane surface can also be given by relation of Doshi et al. [51]:

$$u_w = \frac{u_0 B_1}{h \cdot Sc}\left(1 - B_2 \frac{c_w}{c_0}\right) \tag{12.69}$$

although no further details are given referring constants B_1 and B_2. The variable h represents the half flow channel height, and Sc is the Schmidt number. The main concept is to balance the convective flux in the channel with the diffusive flux in the membrane material, taking into account that not all of the fluid pass through the membrane. This last is taken into account by R rejection coefficient. Finally the balance equation at the feed side of the membrane reads:

$$D\frac{\partial c}{\partial y} + u_w R c_w = 0 \tag{12.70}$$

and for the permeate side:

$$D\frac{\partial c}{\partial y} + u_w c_p = (1 - R) c_w u_w \tag{12.71}$$

where D is the diffusion coefficient in the membrane (the term $D\partial c/\partial y$ formulates the diffusive flux along y axis). The CFD model developed contains specific equations for the cases studied, but it can be changed to cover any combination of variations in wall flux, rejection, viscosity and diffusivity.

12.3.2 Boltzmann lattice models

The Boltzmann lattice method is completely different method of solving Navier–Stokes equations than the finite volume approach. The method is based on the Boltzmann equation which describes the statistical behavior of a non-equilibrium thermodynamic system. The equation in the principal formulation can be stated as:

$$\frac{\partial f}{\partial t} = \left(\frac{\partial f}{\partial t}\right)_{force} + \left(\frac{\partial f}{\partial t}\right)_{diffusion} + \left(\frac{\partial f}{\partial t}\right)_{collisions} \tag{12.72}$$

In the above formulation f is the distribution function which quantifies particles per unit volume in single-particle phase space. It is a function of six scalar coordinates of phase space of position and momentum components: $(\mathbf{r}, \mathbf{p})$ =

(x, y, z, p_x, p_y, p_z) which is parametrized by time t. The *force* term relates to the forces of external origins exerted on the particles, the *diffusion* term characterizes the diffusion of particles, and *collisions* is the collision term – describing for the forces appearing between particles in collisions. The specific formulation of this equation reads:

$$\frac{\partial f}{\partial t} + \underbrace{\frac{p}{m} \cdot \frac{\partial f}{\partial r}}_{diffusion} + \underbrace{F \cdot \frac{\partial f}{\partial p}}_{force} = \left(\frac{\partial f}{\partial t}\right)_{collisions} \tag{12.73}$$

where m is the mass of the particles ensemble with which the function f is associated. Vector $\mathbf{F}$ is the external forces vector (e.g. force due to gravity), vector $\mathbf{p}$ is the momentum vector, vector $\mathbf{r}$ is the position of the particle. The term for collisions cannot be formulated generally. The simplest model of collisions between particles is due to Bhatnagar, Gross and Krook [52] which assumes that the effect of molecular collisions is to shift the distribution function f being in non-equilibrium state back to a Maxwellian equilibrium distribution function f_0, with the rate proportional to the molecular collision frequency υ:

$$\frac{\partial f}{\partial t} + \frac{p}{m} \cdot \frac{\partial f}{\partial r} + F \cdot \frac{\partial f}{\partial p} = \nu(f_0 - f) \tag{12.74}$$

Considering the mixture of the N components the general formulation for k^{th} specie reads:

$$\frac{\partial f_k}{\partial t} + \frac{p_k}{m_k} \cdot \frac{\partial f_k}{\partial r_k} + F \cdot \frac{\partial f_k}{\partial p_k} = \sum_{j=1}^{N} \frac{1}{m_j} \int\int \sigma(\Omega) \left| \frac{p_k}{m_k} - \frac{p_j}{m_j} \right| (f_k' f_j' - f_k f_j) d\Omega d^3 p_j \tag{12.75}$$

where apostrophe superscripted variables refer to the state after collision. The variable Ω is the solid scattering angle, the term $\sigma(\Omega)$ is the differential cross section for collision with the scattering angle Ω.

The Lattice Boltzmann model refers to a small differential volume in six-dimensional space of position and momentum. The idea goes further in problem reduction with the postulate that the particle (or fluid ensemble) is restricted to move in specific directions only or stay at rest. For the case of two physical dimensions of fluid calculations, these directions $e_{\vec{i}}$ (or referred also as microscopic velocities) are symmetrically distributed straight paths (Figure 12.4).

The designations refer to the physical dimensions D and number of directions chosen Q over which the movement is quantified. For presented case of D2Q9 lattice the microscopic velocities are defined by:

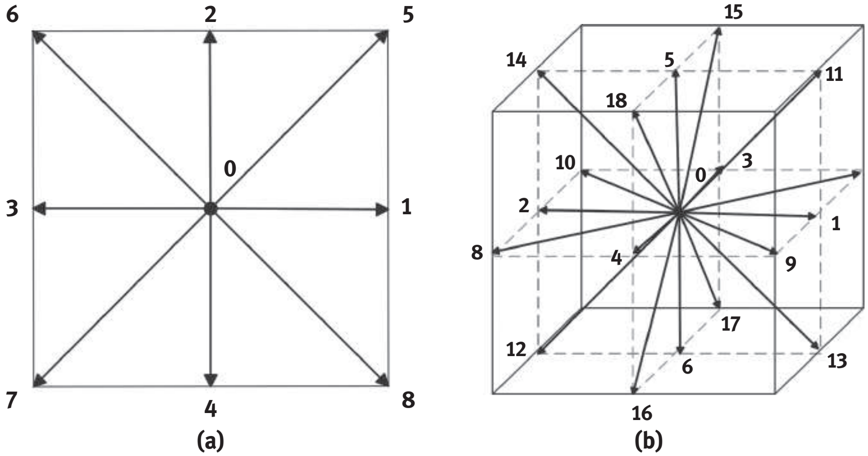

Figure 12.4: Lattice Boltzmann microscopic speed directions setup for two (D2Q9) and three (D3Q19) dimensional physical space.

$$e_i = c \times \begin{cases} (0,0) & i=0 \\ (1,0),(0,1),(-1,0),(0,-1) & i=1,2,3,4 \\ (1,1),(-1,1),(-1,-1),(1,-1) & i=5,6,7,8 \end{cases} \tag{12.76}$$

where c is the lattice speed:

$$c = \frac{\Delta x}{\Delta t} \tag{12.77}$$

The value of ∇x is the lattice cell geometric size (geometric discretization size), the ∇t is the time step of transient discretization. The resultant value of velocity for given lattice cell with N_{dir} directions is then the macroscopic velocity $\mathbf{u}(\mathbf{x}, t)$ which is given as the average weighted by distribution function f_i:

$$u(x,t) = \frac{1}{\rho}\sum_{i=1}^{N_{dir}} f_i \vec{e}_i \tag{12.78}$$

while density ρ is given by the summation of the distribution function:

$$\rho(x,t) = \sum_{i=1}^{N_{dir}} f_i \tag{12.79}$$

The Lattice Boltzmann method can be regarded as a particular finite difference method for solving the Boltzmann transport equation on a lattice. The key explanation why this approach can function as a method for fluid simulations is that the Navier–Stokes equations can be derived from the discrete equations by the Chapman–Enskog expansion [53].

Park et al. [54] apply the lattice Boltzmann method to the multi-phase flow phenomenon in the inhomogeneous gas diffusion layer of a polymer electrolyte membrane fuel cell. The D2Q9 lattice was used to represent the two-dimensional process of flow and D3Q15 for three physical dimensions. The Stokes/Brinkman [55] model formulation was used to describe the flow in porous media:

$$\mu_e \nabla^2 \langle u \rangle - \frac{\mu}{K_{tow}} \langle u \rangle = \nabla \langle P \rangle \tag{12.80}$$

The operator $\langle\rangle$ on the velocity $\mathbf{u}$ and pressure P designates volume-average in the porous region. $\mathbf{K}_{tow}$ is the tensor of permeability for the fiber bundles, and μ_e is the effective viscosity. The Brinkman equation reduces to Darcy's law at distant locations from the void spaces when velocity gradients are small. The permeability in the above equation is expressed in the form of tensor to account for isotropy of the porous media, which can be represented in the form of matrix of k_{ij} permeability elements:

$$K_{tow} = \begin{bmatrix} k_{xx} & k_{xy} & k_{xz} \\ k_{yx} & k_{yy} & k_{yz} \\ k_{zx} & k_{zy} & k_{zz} \end{bmatrix} \tag{12.81}$$

The permeability tensor elements on the diagonal (k_{xx}, k_{yy}, k_{zz}) represent the components of permeability corresponding to pressure force acting in the direction of flow. The off-diagonal permeability tensor elements (k_{xy}, k_{xz}, k_{yx}, k_{yz}, k_{zx}, k_{zy}) account for the flow rate dependence on pressure forces in orthogonal directions. Equation 12.73 is coupled with the continuity equation:

$$\nabla \cdot u = 0 \tag{12.82}$$

The construction of lattice Boltzmann model is done by formulating the collision term according to BGK method [52], with time discrete advancement function defined as:

$$f_i(x + e_i \Delta t, t + \Delta t) - f_i(x, t) = -\frac{f_i(x, t) - f_i^{eq}(x, t)}{\tau_v} \tag{12.83}$$

where ∇t is the numerical time step, τ_υ is the relaxation time. The equilibrium distribution function f_i^{eq} at given time step depends on density ρ and velocity $\mathbf{u}$ at location $\mathbf{x}$ is given by:

$$\omega_i = \begin{cases} 4/9 & i=0 \\ 1/9 & i=1,2,3,4 \\ 1/36 & i=5,6,7,8 \end{cases} \tag{12.84}$$

The microscopic velocities are formulated by Cartesian coordinates given by definition:

$$e_i = \begin{cases} (0,0) & i=0 \\ c\left(cos\ \frac{i-1}{2}\pi, sin\ \frac{i-1}{2}\pi\right) & i=1,2,3,4 \\ \sqrt{2}c\left(cos\ \frac{i-4\frac{1}{2}}{2}\pi, sin\ \frac{i-4\frac{1}{2}}{2}\pi\right) & i=5,6,7,8 \end{cases} \tag{12.85}$$

which resembles the definition given by formulation (77).

The three-dimensional construction of the lattice is formed used 15 microscopic speeds defined by the matrix:

$$e_i = c\times \begin{cases} (0,0,0) & i=0 \\ (\pm 1,0,0),(0,\pm 1,0),(0,0,\pm 1) & i=1,2,\ldots,5,6 \\ (\pm 1,\pm 1,\pm 1) & i=7,8,\ldots,13,14 \end{cases} \tag{12.86}$$

The equilibrium distribution function f_i^{eq} reads:

- for zeroth microscopic speed:

$$f_0{}^{eq}(\rho,u) = \rho\left(\frac{1}{8} - \frac{u\cdot u}{3}\right) \tag{12.87}$$

- for orthogonal directions of microscopic speeds, *i*=1..6:

$$f_i^{eq}(\rho,u) = \rho\left(\frac{1}{8} + \frac{e_i\cdot u}{3} + \frac{(e_i\cdot u)^2}{2} - \frac{u\cdot u}{6}\right) \tag{12.88}$$

- for non-orthogonal microscopic speeds, *i*=7..14:

$$f_i^{eq}(\rho,u) = \rho\left(\frac{1}{64} + \frac{e_i\cdot u}{24} + \frac{(e_i\cdot u)^2}{16} - \frac{u\cdot u}{48}\right) \tag{12.89}$$

For the porous media lattice Boltzmann model is modified to account for Brinkman equation by incorporating the force term $\mathbf{F}_B$ that reads:

$$F_B = s(x)\frac{\tau F(x,t)}{\rho(x,t)} \tag{12.90}$$

and:

$$U = u(x,t) + F_B \tag{12.91}$$

The term **U** exchanges the velocity **u** in formulation for equilibrium distribution function f_i^{eq}. The variable s(x,t) indicates the porous media (=1) or void (=0) of the space of the flow.

The force term **F**(**x**,*t*) which is needed to recover the Brinkman equation reads:

$$F(x,t) = -\beta\rho(x,t)u(x,t) \tag{12.92}$$

where the β parameter describes the momentum sink magnitude due to resistance of porous media. Finally the lattice Boltzmann equation according to Brinkman porous material description reads:

$$\nu\nabla^2 u - \beta u = \frac{1}{\rho}\nabla P \tag{12.93}$$

in which the β parameter:

$$\beta = \frac{\nu}{K_{tow}} \tag{12.94}$$

In the above the viscosity υ and permeability tensor are expressed in lattice units [56].

Han et al. [57] presents the results of the two-dimensional simulation concerning the polymer membrane of fuel cell although no specific details concerning mathematical procedure taken are given in the study. The transport is considered in two regimes: flow in microporous layer and in gas diffusion layer. The numerical investigations concentrate primarily on liquid water transport in flooding conditions. The water entering the porous regions is generally driven by the capillary forces through the contact with the solid material. Numerical results acquired for the cases with and without the perforated cavity in the porous layers were compared. For the case without the perforated cavity, water randomly penetrates through the porous regions and finally appears as two small droplets at the surface of the channel. For the case with the hole in the porous layer, water transports favorably through this void space and appears as a relatively large liquid droplet at the open end. This liquid transport phenomenon is caused by the smaller capillary pressure requirement and less flow resistance in the large perforated pore. The perforated pores can therefore function as a suitable water transport pathway and contribute in liquid water removal.

Kim et al. [58] investigated liquid water transport in the microporous layer and gas diffusion layer of polymer electrolyte membrane fuel cells by lattice Boltzmann method. Application of the model for two-phase systems with porous geometry that emulates the process in multilayer porous transport layers. The model was built for two-dimensional physical space. Apart from the typical lattice Boltzmann setup (D2Q9) the approach to calculate collision function is aimed at the liquid–liquid and liquid–solid interactions. The collision function for the j^{th} component and i^{th} microscopic speed applied reads:

$$\Omega_{i,j}(x,t) = -\frac{1}{\tau_j}\left(f_{i,j}(x,t) - f_{i,j}^{eq}(x,t)\right) \tag{12.95}$$

where τ_j is relaxation time corresponding to viscosity of specie j^{th} given by:

$$\mu_j = c_s{}^2\left(\tau_j - \frac{1}{2}\right) \tag{12.96}$$

The variable c_s is the speed of sound in the media simulated. The equilibrium distribution function is then given by:

$$f_{i,j}^{eq}(\rho,u) = \omega_i\rho_j\left(1 + \frac{e_i\cdot u_j^{eq}}{c_s{}^2} + \frac{(e_i\cdot u_j^{eq})^2}{2c_s{}^4} - \frac{u_j^{eq}\cdot u_j^{eq}}{2c_s{}^2}\right) \tag{12.97}$$

The equilibrium velocity of the specie j^{th} is formulated by considering the rate of momentum change due to the fluid–fluid and fluid–solid interaction forces $\Sigma\mathbf{F}_j$. In the study the $\Sigma\mathbf{F}_j$ does not account for gravitational and buoyancy forces, and is given by:

$$u_j^{eq} = u + \frac{\tau_\sigma}{\rho_j}\sum^{F_j} \tag{12.98}$$

The rate of net momentum change due to the fluid–fluid interactions $\mathbf{F}_j^{int}$ are given by:

$$F_j^{int}(x) = -\psi_j(x)\sum_k G_{j,k}(x,x')\sum_i \omega_i\psi_k(x+e_i\Delta t)e_i \tag{12.99}$$

where ψ_j is the effective number density for specie j^{th} and is equal to its density ρ_j for multiphase lattice Boltzmann model. The function $G_{j,k}(\mathbf{x},\mathbf{x'})$ is the Green function [59] which relates the interactions between specie j^{th} at $\mathbf{x}$ location and $\mathbf{x'}$ location, that reads:

$$G_{j,k}(x,x') = \begin{cases} 0, & |x-x'| > |e_i| \\ G_{j,k}, & |x-x'| = |e_i| \end{cases} \tag{12.100}$$

which means that only the nearest particle interactions are considered, the coefficient $G_{j,k}$ is defined to account for the strength of the interaction between components j and k. The $G_{j,k}$ determines the repulsion strength between particles belonging to different species and can be used to fine tune the surface tension between phases. For critical value of $G_{j,k}$ the repulsion forces are not strong enough to keep the two fluids separated and start to form single phase system [60]. The fluid–solid interactions are considered by the relation:

$$F_j^{ads}(x) = -\psi_j(x)\sum_i G_j^{ads}\omega_i s(x+e_i\Delta t)e_i \tag{12.101}$$

where G_j^{ads} is the adsorption coefficient for specie j^{th}. The G_j^{ads} controls the strength of the fluid wettability of the solid surface. The function $s(\mathbf{x}+\mathbf{e}_i\nabla\ t)$ attains value 1 for solid neighbor location and 0 for fluid neighborhood.

The model studied presents creation of water clusters inside the porous media. Also extraordinary transient behavior of the liquid water near the microporous layer/gas diffusion layer interface and the gas diffusion layer/gas channel interface was realized from the lattice Boltzmann simulations of highly hydrophobic multilayer porous transport layers.

12.3.2.1 Summary

CFD methods are valuable tools for process engineers in the design and simulation fields. The differential models, commonly referred to as CFD, aim to solve the Navier–Stokes equation in its discretized form. The advantage of this approach is the ability to use a variety of discretization schemes that suits the geometrical and process needs. The discretization which is dependent on the mesh construction is always a source of error which can be minimized by proper tuning the cell sizes, shapes and types. This formulation of the fluid dynamics approach is not able to predict the thermodynamics of the simulated entity, however. On the other hand, the lattice Boltzmann method, by proper use of collision operator, is able to predict specific thermodynamic behavior of the fluids simulated, e.g. the existence of multiphase system. Such possibility, in order to be incorporated into traditional discrete approach, needs to be accounted for by separate models, for example volume of fluid model of multiphase flow, which further enlarges the formulation and computing demand. One of the key benefits of lattice Boltzmann method for simulating fluid flows as compared to traditional numerical methods is their aptitude to efficiently model interfaces between two or more fluids. Both the fluid dynamics approaches, however totally different, can successfully be incorporated into modeling and simulations of membrane systems.

References

[1] Sampson RA. On Stokes's current function. Phil Trans R Soc Lond A. 1891;182:449–518.

[2] Song L, Elimelech M. Theory of concentration polarization in crossflow filtration. J Chem Soc Faraday Trans. 1995;91(19):3389–3398.

[3] Happel J, Brenner H. Low Reynolds number hydrodynamics. Englewood Cliffs: Prentice Hall, 1965.

[4] McCabe WL, Smith J, Harriott P. Unit operations of chemical engineering.. New York: McGraw-Hill Education, 2005.

[5] Aimar P, Baklouti S, Sanchez V. Membrane – solute interactions: Influence on pure solvent transfer during ultrafiltration. J Memb Sci. 1986;29(2):207–224.

[6] Velicangil O, Howell IA, Le MEH, Zeppelin AL. Ultrafiltration of protein solutions. Annals NY Acad Sci. 1981;369–355.

[7] Chung T-S, Jiang LY, Li Y, Kulprathipanja S. Mixed matrix membranes (MMMs) comprising organic polymers with dispersed inorganic fillers for gas separation. Prog Polym Sci. 2007; 32(4):483–507.

[8] Maxwell JC. Treatise on electricity and magnetism. London: Oxford University Press, 1873.

[9] Mahajan R, Burns R, Schaeffer M, Koros WJ. Challenges in forming successful mixed matrix membranes with rigid polymeric materials. J Appl Poly Sci. 2002;86:881–890.

[10] Slesarenko VV. Modelling of RO installations for wastewater treatment plants. Pac Sci Rev. 2014;16(1):40–44 2014. ISSN 1229-5450.

[11] Fraga SC, Trabucho L, Brazinha C, Crespo JG. Characterisation and modelling of transient transport through dense membranes using on-line mass spectrometry. J Memb Sci. 2015;479:213–222.

[12] Kreulen H, Smolders CA, Versteeg GF, Van Swaaij WPM. Microporous hollow fibre membrane modules as gas-liquid contactors Part 2. Mass transfer with chemical reaction. J Memb Sci. 1993;78(3):217–238.

[13] Dindore VY, Brilman DWF, Versteeg GF. Hollow fiber membrane contactor as a gas–liquid model contactor. Chem Eng Sci.60(2):467–479 2005.

[14] Sundaramoorthy S, Srinivasan G, Murthy DVR. An analytical model for spiral wound reverse osmosis membrane modules: Part II – Experimental validation. Desalination. 2011; 277(1–3):257–264.

[15] Criscuoli A, Carnevale MC, Drioli E. Modeling the performance of flat and capillary membrane modules in vacuum membrane distillation. J Memb Sci. 2013;447:369–375.

[16] Warshel A, Levitt M. Theoretical studies of enzymic reactions: Dielectric, electrostatic and steric stabilization of the carbonium ion in the reaction of lysozyme. J Mol Biol. 1976;103(2):227–249.

[17] Slater JC. Atomic shielding constants. Phys Rev. 1930;36:57.

[18] Ditchfield R, Hehre WJ, Pople JA. Self-consistent molecular-orbital methods IX. An extended Gaussian-type basis for molecular-orbital studies of organic molecules. J Chem Phys. 1971; 54(2):724–728.

[19] Levine IN. Quantum chemistry.. Englewood Cliffs, NJ: Prentice Hall, 1991.

[20] Hehre WJ. A guide to molecular mechanics and quantum chemical calculations. Irvine, CA: Wavefunction, Inc, 2003.

[21] Cramer CJ. Essentials of computational chemistry.. Chichester: John Wiley & Sons, Ltd, 2002.

[22] Jensen F. Introduction to computational chemistry.. New York: John Wiley and Sons, 1999.

[23] Quinn CM. Computational quantum chemistry: An interactive introduction to basis set theory, 1st ed London: Academic Press, 2002

[24] Yu TH, Sha Y, Wei-Guang Liu BV, Merinov PS, Goddard WA. Mechanism for degradation of Nafion in PEM fuel cells from quantum mechanics calculations. J Am Chem Soc. 2011; 133(49):19857–19863.

[25] Yu TH, Liu W-G, Sha Y, Merinov BV, Shirvanian P, Goddard III WA. The effect of different environments on Nafion degradation: Quantum mechanics study. J Memb Sci. 2013;437: 276–228.

[26] Sakai H, Tokumasu T. Quantum chemical analysis of the deprotonation of sulfonic acid in a hydrocarbon membrane model at low hydration levels. Solid State Ionics. 2015;274:94–99.

[27] Paddison SJ, Elliott JA. Molecular modeling of the short-side-chain perfluorosulfonic acid membrane. J Phys Chem A. 2005;109(33):7583–7593.

[28] Shah MR, Yadav GD. Prediction of sorption in polymers using quantum chemical calculations: Application to polymer membranes. J Memb Sci. 2013;427:108–117.

[29] Vosko SH, Wilk L, Nusair M. Accurate spin-dependent electron liquid correlation energies for local spin density calculations: A critical analysis. Can J Phys. 1980;58(8):1200.

[30] Gear GW. Numerical initial value problems in ordinary differential equations. Englewood Cliffs, NJ: Prentice-Hall, 1971.

[31] Verlet L. Computer “experiments” on classical fluids. I. Thermodynamical properties of Lennard –Jones molecules. Phys Rev. 1967;159:98–103.

[32] Shen M, Keten S, Lueptow RM. Rejection mechanisms for contaminants in polyamide reverse osmosis membranes. J Memb Sci. 2016;509:36–47.

[33] Edward Harder D, Walters E, Bodnar YD, Faibish RS, Roux B. Molecular dynamics study of a polymeric reverse osmosis membrane. J Phys Chem B. 2009;113(30):10177–10182.

[34] Devanathan R, Idupulapati N, Baer MD, Mundy CJ, Dupuis M. Ab initio molecular dynamics simulation of proton hopping in a model polymer membrane. J Phys Chem B. 2013;117(51): 16522–16529.

[35] Ling C, Liang X, Fan F, Yang Z. Diffusion behavior of the model diesel components in different polymer membranes by molecular dynamic simulation. Chem Eng Sci. 2012;84:292–302.

[36] Bader R. Atoms in molecules: A quantum theory. New York: Oxford University Press, 1994.

[37] Lobato J, Cañizares P, Rodrigo MA, Linares JJ, Piuleac C-G, Curteanu S. The neural networks based modeling of a polybenzimidazole-based polymer electrolyte membrane fuel cell: Effect of temperature. J Power Sources. 2009;192(1):190–194.

[38] Lee W-Y, Park G-G, Yang T-H, Yoon Y-G, Kim C-S. Empirical modeling of polymer electrolyte membrane fuel cell performance using artificial neural networks. Int J Hydrogen Energy. 2004;29(9):961–966.

[39] Chakraborty S, Dasgupta J, Farooq U, Sikder J, Drioli E, Curcio S. Experimental analysis, modeling and optimization of chromium (VI) removal from aqueous solutions by polymer-enhanced ultrafiltration. J Memb Sci. 2014;456:139–154.

[40] Staszak M, Staszak K. Computational fluid dynamics (CFD) modelling of porous, ultrafiltration membranes. J Membr Separation Technol. 2013;2(1):36–46.

[41] Pellerin E, Michelitsch E, Darcovich K, Lin S, Tam CM. Turbulent transport in membrane modules by CFD simulation in two dimensions. J Memb Sci. 1995;100(2):139–153.

[42] Berman AS. Laminar flow in channels with porous walls. J Appl Phys. 1953;24:1232–1235.

[43] Gupta BK, Levy EK. Symmetrical laminar channel flow with wall suction. Trans ASME J Fluids Eng. 1976;98:469–474.

[44] Wang ZH, Wang CY, Chen KS. Two-phase flow and transport in the air cathode of proton exchange membrane fuel cells. J Power Sources. 2001;94(1):40–50.

[45] Sivertsen BR, Djilali N. CFD-based modelling of proton exchange membrane fuel cells. J Power Sources. 2005;141(1):65–78.

[46] Dhont JKG. An introduction to dynamics of colloids. Amsterdam: Elsevier, 1996.

[47] Janssen GJM. A phenomenological model of water transport in a proton exchange membrane fuel cell. J Electrochem Soc. 2001;148(12):A1313–A1323.

[48] Sivertsen BR. CFD-based modelling of proton exchange membrane fuel cellsNorwegian University of Science and Technology, 2003, Master's thesis.

[49] Wiley DE, Fletcher DF. Techniques for computational fluid dynamics modelling of flow in membrane channels. J Memb Sci. 2003;211(1):127–137.

[50] Brian PLT. Concentration polarization in reverse osmosis desalination with variable flux and incomplete salt rejection. Ind Eng Chem Fundam. 1965;4(4):439–445.

[51] Doshi MR. The effect of concentration dependent viscosity and diffusivity on concentration polarization in reverse osmosis flow systems. AIChE Symp Ser. 1971;68:124.

[52] Bhatnagar PL, Gross EP, Krook M. A model for collision processes in gases. I. Small amplitude processes in charged and neutral one-component systems. Phys Rev. 1954;94(3):511–525.

[53] Bardos C, Ukai S. The classical incompressible Navier-Stokes limit of the Boltzmann equation. Math Models Methods Appl Sci. 1991;01(02):235–257.

[54] Park J, Li X. Multi-phase micro-scale flow simulation in the electrodes of a PEM fuel cell by lattice Boltzmann method. J Power Sources. 2008;178(1):248–257.

[55] Park J, Matsubara M, Li X. Application of lattice Boltzmann method to a micro-scale flow simulation in the porous electrode of a PEM fuel cell. J Power Sources. 2007;173(1):404–441.

[56] Latt J. Hydrodynamic limit of lattice Boltzmann equationsUniv. Genève, 2007 – Sc. 3846-2007/03/09, PhD thesis.

[57] Han B, Meng H. Numerical studies of interfacial phenomena in liquid water transport in polymer electrolyte membrane fuel cells using the lattice Boltzmann method. Int J Hydrogen Energy. 2013;38(12):5053–5059.

[58] Kim KN, Kang JH, Lee SG, Nam JH, Kim C-J. Lattice Boltzmann simulation of liquid water transport in microporous and gas diffusion layers of polymer electrolyte membrane fuel cells. J Power Sources. 2015;278:703–717.

[59] Shan X, Doolen G. Multicomponent lattice-Boltzmann model with interparticle interaction. J Stat Phys. 1995;81(1):379–393.

[60] Parmigiani A.. Lattice Boltzmann calculations of reactive multiphase flows in porous mediaUniversite de Geneve, 2010. PhD thesis.

Bartosz Tylkowski, Anna Trojanowska, Martyna Nowak,
Lukasz Marciniak and Renata Jastrzab

13 Applications of silver nanoparticles stabilized and/or immobilized by polymer matrixes

Abstract: Nanomaterials frequently possess unique and noticeably changed physical, chemical and biological properties compared to their macro scaled corresponding item. Utilization of nanoparticles habitually requires the construction of integrated chemical systems. Most popular of these are polymer-supported nanoparticles. In this review, we provide the reader with the last developments and breakthrough technologies concerning silver nanoparticles (AgNPs), one of the most comprehensively studied nanomaterials, considering the polymer types and processes used for the nanocomposite membranes preparation.

Keywords: silver, nanoparticle, biofouling

13.1 Nanotechnology

In today's world, nanoparticles (NPs) and nanotechnology have attracted the attention of the scientific community globally and have emerged as a fast developing and fascinating area of research. In December 1959, Nobel Laureate – Prof. Richard Feynman – gave an infamous lecture entitled "*There's plenty of room at the bottom*" at the California Institute of Technology during a meeting with the American Physical Society. During this meeting, Prof. Feynman for the first time mentioned a process which could potentially manipulate individual atoms and molecules and hence advance the field of synthetic chemistry. He was one of the first to recognize the potential of nanoscale materials for industrial society. In 1974, in order to describe the process of moving or manipulating atoms at the nanoscale (1–100 nm), this type of technology was officially termed as "nanotechnology" [1], and since that year, it has been defined as follows [2]:

> Nanotechnology is the design, characterization, production and application of structures, devices and systems by controlling shape and size at nanometer scale.

NPs, the building blocks for nanotechnology, are engineered materials with at least one dimension less than 100 nm. They may have one (e. g. nanolayers), two (nanowires and nanotubes) or three dimensions on the nanoscale (quantum dots, NPs and metal NPs). NPs may provide solutions to technological and environmental challenges in the areas of solar energy conversion, catalysis, medicine,

https://doi.org/10.1515/9783110469745-013

biotechnology, biological labeling, environmental, water treatment, photography, photonics, optoelectronics and surface-enhanced Raman scattering (SERS) detection [3–5]. Moreover, functionalized, biocompatible and inert nanomaterials have potential applications in cancer diagnosis and therapy [6]. A recent survey found that more than 247 nanomaterial-based medical products have been approved by the USA Food and Drug Administration (FDA) and are currently in various stages of clinical study. Their intended uses range from the treatment of clinically unrespectable cancers to the preparation of antibacterial hand gels to the regeneration of heart tissue. At the same time, common themes emerge when discussing nanomaterials in medicine. Indeed, one of the biggest issues is how to translate nanomaterials from the laboratory to the clinic effectively [7]. This increasing demand must be accompanied by "green" synthesis methods. In the global efforts to reduce generated hazardous waste, "green" chemistry and chemical processes are progressively integrating with modern developments in science and industry. Implementation of these sustainable processes should adopt the 12 fundamental principles of green chemistry:

1/Prevention – It is better to prevent waste than to treat or clean up waste after it has been created.

2/Atom Economy – Synthetic methods should be designed to maximize the incorporation of all materials used in the process into the final product.

3/Less Hazardous Chemical Syntheses – Wherever practicable, synthetic methods should be designed to use and generate substances that possess little or no toxicity to human health and the environment.

4/Designing Safer Chemicals – Chemical products should be designed to affect their desired function while minimizing their toxicity.

5/Safer Solvents and Auxiliaries – The use of auxiliary substances (e. g. solvents, separation agents, etc.) should be made unnecessary wherever possible and innocuous when used.

6/Design for Energy Efficiency – Energy requirements of chemical processes should be recognized for their environmental and economic impacts and should be minimized. If possible, synthetic methods should be conducted at ambient temperature and pressure.

7/Use of Renewable Feedstocks – A raw material or feedstock should be renewable rather than depleting whenever technically and economically practicable.

8/Reduce Derivatives – Unnecessary derivatization (use of blocking groups, protection/deprotection, temporary modification of physical/chemical processes) should be minimized or avoided if possible, because such steps require additional reagents and can generate waste.

9/Catalysis – Catalytic reagents (as selective as possible) are superior to stoichiometric reagents.

10/Design for Degradation – Chemical products should be designed so that at the end of their function they break down into innocuous degradation products and do not persist in the environment.

11/Real-time analysis for Pollution Prevention – Analytical methodologies need to be further developed to allow for real-time, in-process monitoring and control prior to the formation of hazardous substances.

12/Inherently Safer Chemistry for Accident Prevention – Substances and the form of a substance used in a chemical process should be chosen to minimize the potential for chemical accidents, including releases, explosions and fires.

These principles were first articulated in 1998 as a set of tools to help the design scientist to anticipate downstream issues at the earliest stage of a Research & Development effort [8]. They were geared to guide in minimizing the use of unsafe products and maximizing the efficiency of chemical processes. Hence, any synthetic route or chemical process should address these principles by using environmentally benign solvents and nontoxic chemicals [9, 10]. Conventionally, nanomaterials are synthesized using either chemical or physical methods which include sol process, micelle, chemical precipitation, hydrothermal method, electrochemical techniques, pyrolysis and chemical vapor deposition. Some of these methods are easy and make available control over crystallite size by restoring the reaction environment. But problem still exists with the general stability of the product and in achieving monodisperse nanosize using these methods. Investigations have shown that the size, morphology, stability and chemical and physical properties of the metal NPs are strongly influenced by the experimental conditions, the kinetics of interaction of metal ions with reducing agents and adsorption processes of stabilizing agent with metal NPs. Therefore, the design of a synthesis method in which the size, morphology, stability and properties are controlled has become a major field of interest [11, 12].

Nanomaterials often show unique and considerably changed physical, chemical and biological properties compared to their macroscaled counterparts [13]. Utilization of NPs often requires the construction of integrated chemical systems. Most popular of these are polymer-supported NPs. In this chapter, we provide the reader with the last developments and breakthrough technologies concerning silver nanoparticles (AgNPs) applications in antifouling properties for water and wastewater treatment; SERS enhancement; catalysis and medicine. According to literature and patent reports, AgNPs represent one of the most comprehensively studied nanomaterials [14].

13.2 Silver nanoparticles

Silver, known in metallic form since antiquity, has very early been recognized by mankind for its antimicrobial properties, a phenomenon observed, for example, in the context of drinking water (a silver coin in a well), food (silver cutlery, water storage recipients) and medicine (silver skull plates, teeth). Silver compounds were also shown to be useful. For example, dilute solutions of silver nitrate served long, and still do in some countries, as antimicrobial ointment to be instilled into newborn babies' eyes to prevent contraction of gonorrhea from the mother. Used frequently until the middle of the twentieth century, silver and its compounds were then replaced by the newly discovered antibiotics and nearly forgotten for almost 50 years [11, 15]. Moreover, in the recent past, AgNPs have received enormous attention of the researchers due to their extraordinary defense against wide range of microorganisms and due to the appearance of drug resistance against commonly used antibiotics. AgNPs are used just about everywhere, including in cosmetics, socks, food containers, detergents, sprays and a wide range of other products to stop the spread of germs.

13.2.1 Polymeric composite membranes containing silver nanoparticles for antifouling properties during water and wastewater treatment

Membrane applications in water and wastewater treatment have increased steadily over the past few years due to improved membrane design, smaller footprint and reliable effluent quality. Microfiltration membranes, in particular, have shown promise as a cost-effective alternative to conventional water treatment, as pretreatment for nanofiltration (NF) and reverse osmosis (RO) and as key components in membrane bioreactors. Despite this potential, organic fouling and biological fouling remain problematic for membranes. Fouling increases operating and replacement costs and compromises membrane performance. The abundance of natural organic matter (NOM) in natural waters makes organic fouling of membrane processes in water treatment inevitable; biofouling is considered more problematic since bacteria can reproduce at the membrane surface, create biofilms and cause additional fouling.

To solve the membrane biofouling problems, a variety of reactive functional materials, such as hydrophilic, charged, photocatalytic or biocidal materials, have been introduced into the ultra- and microfiltration membranes. These materials can reduce membrane biofouling by adhesion inhibition (hydrophilic, charged matters) of hydrophobic foulants or decomposition (biocidal, photocatalytic, positively charged matters) of microbial foulants. Although these material's properties endow good antifouling properties to the water treatment membrane, a number of limitations have been associated with these materials, including stability (autoxidation), pH dependence (losing their charge by deprotonation) and membrane degradation [16]. Exceptionally, among the biocidal materials, AgNPs display strong inhibitory and biocidal properties against a variety of microorganism types with long time periods. Significant efforts have been devoted to introducing AgNPs into polymeric membrane substrates to form AgNPs/membrane nanocomposite. Both *in situ* and *ex situ* methods have been developed to incorporating AgNPs into the membrane surface.

13.2.1.1 *In situ* methods

Under the *in situ* approach, with the aid of reducing agents, the synthesis of AgNPs occurred on the membrane surface sequestering silver ions [17]. For example, the negatively charged carboxylic groups sequestered Ag^+ on the polyamide surface of

RO membrane, and the silver ions were reduced by sodium borohydride ($NaBH_4$) to form AgNPs [18]. However, the Ag loading amount was very low, and the formed AgNPs were loosely bound on the surface and were easily washed out. Mussel-inspired dopamine chemistry has opened a new route to modify all types of inorganic and organic substrates with controllable film thickness and durable stability [19]. Polydopamine (PDA) has stimulated extensive research in the membrane surface functionalization for antifouling purpose [20, 21]. Interestingly, PDA has been found to reduce Ag^+ ions to Ag and to synthesize AgNPs *in situ* on different substrates without any other reducing agent [22]. Furthermore, Lee and co-authors [19] demonstrated that the O- and N-sites of PDA can serve as anchors for the AgNPs to enhance the durability of AgNPs on the surfaces via metal coordination. Consequently, PDA chemistry may pave a simple, yet universal way to immobilize AgNPs on various membrane surfaces for antibiofouling purpose.

Recently, Tang et al. [23] reported that the surface modifications with PDA and AgNPs formed *in situ* can reduce the propensity of polysulfone membranes for bacterial adhesion and growth. Under these studies, the surface of a polysulfone membrane was modified with a bioinspired PDA film followed by the *in situ* formation of AgNPs to mitigate membrane biofouling. According to the authors, the PDA modification enhanced the membrane's bacterial anti-adhesive properties by increasing the surface hydrophilicity, while AgNPs imparted strong antimicrobial properties to the membrane. The authors demonstrated that the AgNPs could be generated on the membrane surface by simply exposing the membrane to $AgNO_3$ solutions. Indeed, the Ag^+ ions were reduced by the catechol groups in PDA; the AgNP mass loading increased with exposure time, and the AgNPs were firmly immobilized on the membrane through metal coordination. Generated results shown that during leaching tests, the concentrations of Ag^+ ions released were 2–3 orders of magnitude lower than the established contaminant limit for drinking water, thereby providing a safe antimicrobial technology.

Huang et al. [24] have also *in situ* immobilized AgNPs on polysulfone ultrafiltration membrane via PDA deposition. The authors have used a silver ammonia aqueous solution ($Ag(NH_3)_2OH$) for AgNPs) *in situ* reduction and demonstrated that the adhesive and reductive PDA layer existing on the membrane surface induced the reduction of Ag^+ on the site of surface without surface pore blockage, and also favored to the firm attachment and uniform distribution of AgNPs onto the membrane. Under this study, the prepared AgNPs-PDA/PSf membranes were characterized by mean of: X-ray photoelectron spectroscopy (XPS), scanning election microscope (SEM), atomic force microscopy (AFM), water contact angle measurement and thermogravimetric analysis (TGA). Obtained results indicated that AgNPs were immobilized on the surface as well as the top layer cross-section of the membranes. The authors reported that the increase of Ag^+ ion concentration led to an increase in the size and density of AgNPs anchored onto the membrane. Moreover, the authors reported that compared with PSf membrane, AgNPs-PDA/PSf membrane showed higher water flux, slower flux decline rate during BSA solution filtration and higher flux recovery ratio after simple water flushing. In mean that prepared AgNPs-PDA/PSf membrane possessed excellent stability with little release of silver during the filtrate operation or static immersion in water for 12 days. Besides, published results clearly demonstrated that the AgNPs-PDA/PSf membrane displayed excellent antibacterial and antibiofouling properties against *Escherichia coli* and *Bacillus subtilis*.

Just a while ago, a simple and facile approach was developed by Liu and Hu [25] to *in situ* generate AgNPs on the thin-film composite forward osmosis (TFC FO) membrane. The authors also have applied a Mussel-inspired dopamine chemistry to grow PDA coating on both surfaces of polysulfone support membranes, followed by the generation of AgNPs upon a simple dip coating in silver nitrate aqueous solution, as illustrated in Figure 13.1.

The authors demonstrated that the AgNPs have a controllable effect on the membrane performances including the water flux and reverse salt flux in the FO test mode. The water flux and salt permeability of the membranes were tested using a custom laboratory-scale cross-flow FO test system in layer faces the draw solution (AL-DS) membrane orientation. The authors reported that the water flux decreased from 17.49 ± 0.42 to 14.56 ± 0.75 L m^{-2} h^{-1} and 13.31 ± 0.95 L m^{-2} h^{-1}, and the reverse salt flux decreased from 34.64 ± 2.6 to 28.24 ± 3.61 g m^{-2} h^{-1} and 22.39 ± 0.54 g m^{-2} h^{-1}, for pristine, PDA coated, and AgNP generated membranes, respectively. The obtained results confirmed that the PDA coating decreased the water flux and the reverse salt flux by 16.75 % and 18.48 %, and the AgNP generation decreased the water flux and the reverse salt flux further by 8.58 % and 20.71 %. Therefore, the authors concluded that the PDA coatings have stronger effect on decreasing the water flux than the AgNP generation, whereas the AgNP generation has more benefits on suppressing the reverse

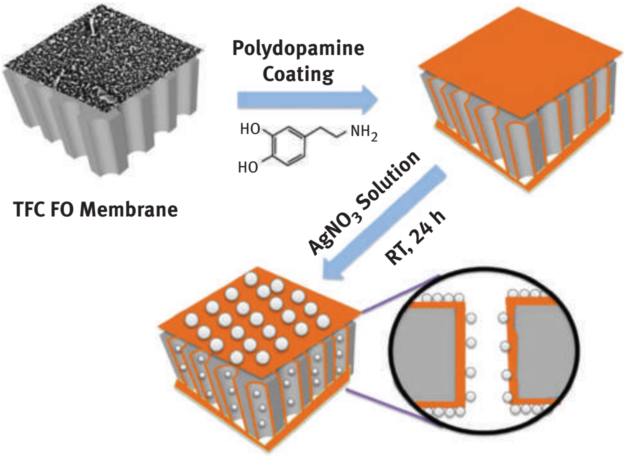

Figure 13.1: *In situ* synthesis procedure of silver nanoparticles on both sides of TFC FO membrane. Reprinted with permission from [25]. Copyright (2016) American Chemical Society.

salt flux than the PDA coatings. The authors demonstrated the water flux and reverse salt flux could be tailored via controlling the formation of PDA coating by adjusting the immersion time of membranes in 3,4-dihydroxyphenylalanine (DOPA) solution. The published results suggest that the water flux and the reverse salt flux of the TFC FO membranes can be further optimized to achieve controllable effect through optimizing the thickness of the PDA film and the growth of AgNPs. Without any doubts, the presented results shed new light on the development of a simple, universal and applicable approach for constructing long-lasting biofouling-resistant membrane surfaces.

Application of *in situ* method for the formation of AgNPs in a TFC FO membrane structure has also been explored by Soroush and co-workers [26]. The authors have modified a surface of TFC FO membranes by AgNPs in the presence and absence of graphene oxide (GO) nanosheets to impart biocidal properties to the membranes, as it shown in Figure 13.2.

The generated results showed that the abundance of oxygen-containing functional groups in GO makes it suitable for anchoring Ag^+ ions and governing the size, shape and distribution of AgNPs. Instead, the presence of GO resulted in the formation of smaller and uniformly distributed AgNPs as well as increased silver loading, higher stability and enhanced ion release control. The authors reported that the membranes modified by both GO and Ag exhibited improved (98 %) bacterial inactivation when compared to that of only Ag-modified (80 %) or GO-modified membranes (50 %). Moreover, the investigators reported that after release of Ag ion from GO-Ag-modified membranes for 7 days, AgNP regeneration was conducted in a manner identical to the *in situ* Ag formation procedure. Furthermore, after regeneration, the membrane regained nearly all of its antibacterial properties and 75 % of its initial silver loading.

Madhavan and co-workers [27] incorporated AgNPs into isoporous membranes manufactured by a phase inversion method using a polystyrene-*b*-poly(4-vinylpyridine) (PS-*b*-P4VP) block copolymer. Under this investigation, the AgNPs were obtained by promoting pyridine–silver ion interactions, followed by reaction with a reducing agent.

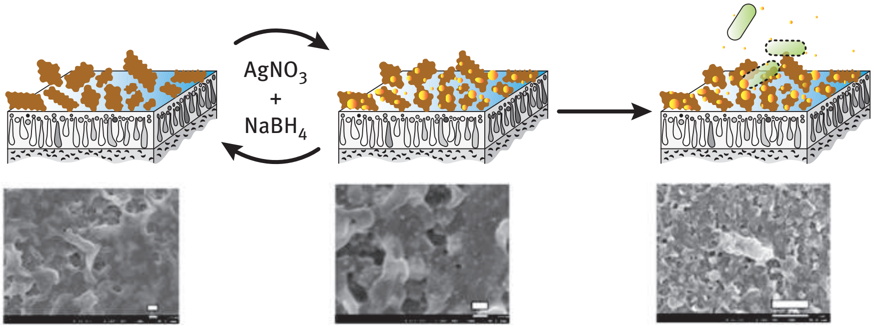

Figure 13.2: Modification of TFC FO membranes surface. Reprinted with permission from [26]. Copyright (2016) American Chemical Society.

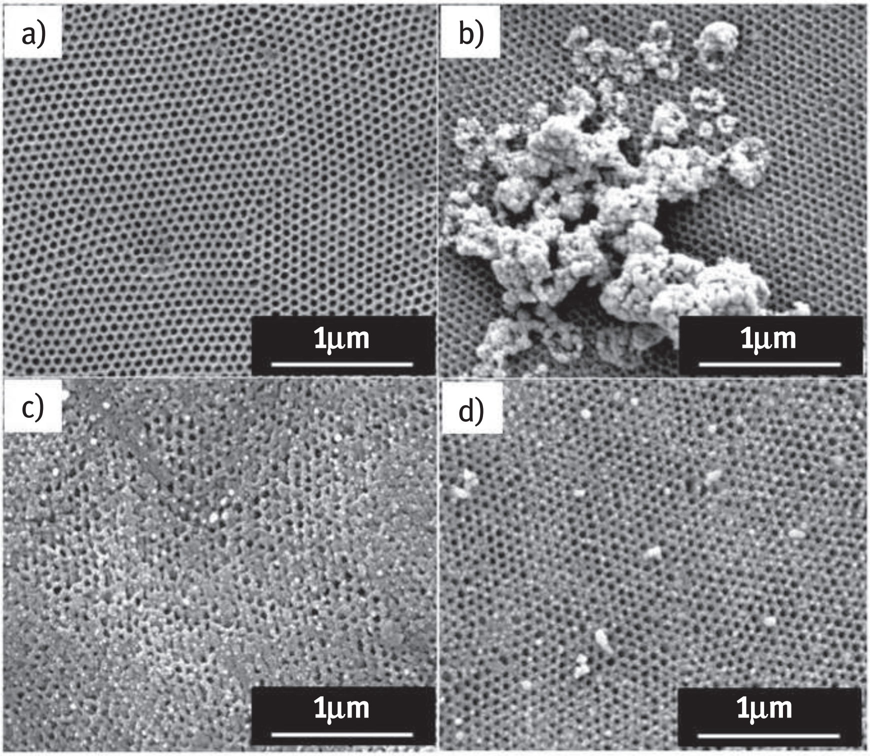

Figure 13.3: SEM images of a (a) plain PS-*b*-P4VP membrane and membranes with Ag nanoparticles prepared at (b) pH 2.1, (c) pH 7 and (d) pH 9 with 1.0 mM $AgNO_3$ solution. Reprinted with permission from [27]. Copyright (2014) American Chemical Society.

As shown in Figure 13.3, the AgNP deposited on the membrane at pH 9 with 1.0 mM $AgNO_3$ solution show well-distributed membrane morphology. Moreover, antibacterial tests performed by the authors show that the NPs have strong biocidal activity and they might be a suitable candidate for practical application. Indeed, flow cytometry measurements, used in this study, demonstrated that, after 72 h of incubation of the membrane systems with *P. aeruginosa*, the proportion of viable cells compared to the control (in absence of AgNPs) was around 20 %.

Mishra et al. [28] disclosed an *in situ* synthesis method for preparing silver nanoclusters (AgNCs) embedded in chitosan–polyethylene glycol (CS–PEG) membranes. Under this investigation, the synthesis of AgNCs in CS–PEG matrix was accomplished by the mild *in situ* reduction of silver ions created upon refluxing $AgNO_3$ in the mixed CS–PEG aqueous solution at 90 °C for 6 h, confirmed by a clear golden yellow color of the resulting colloidal system. The authors observed that in the absence of PEG, reduction was very slow and no substantial color change was noted while varying pH from 3 to 7 at 90 °C up to 8 h; however, in the presence of

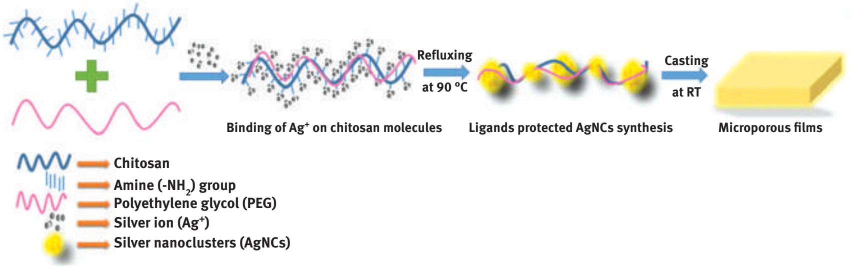

Figure 13.4: Formation mechanism of AgNCs in CS-PEG solution. Reprinted with permission from [28]. Copyright (2016) American Chemical Society.

PEG, reduction was faster and at pH 7.0 ± 0.3, CS–PEG matrix color changed to golden yellow within 6 h.

Figure 13.4 shows the possible mechanism of AgNC synthesis in CS–PEG solution. The pH of the mixed solution was adjusted to 7.0 ± 0.3 by adding of CH_3COOH and NaOH. The Ag^+ ions initially coordinated with the nonprotonated electron donor amine groups of CS are subsequently stabilized as AgNCs during reduction process that occurs on heating. A multiple array of characterization techniques, employed by the investigators, confirmed the formation of fluorescent AgNCs with sizes of ~3 nm uniformly distributed in CS–PEG matrix. Moreover, exhausted characterization confirmed that the AgNCs play an active role in determining the fraction and interconnectivity of the microporous membranes. Furthermore, reported results showed that the presence and increasing contents of AgNCs enhanced the mechanical stability of membranes and decreased their susceptibility to degradation in the presence of lysozyme and H_2O_2. Moreover, the presence and increasing concentrations of AgNCs hindered biofilm formation against *Escherichia coli* (Gram negative) and *Staphylococcus aureus* (Gram positive) and enabled a sustainable release of an anti-inflammatory drug naproxen *in vitro* until 24 h. The overall results gathered and reported in this work make the AgNC-impregnated CS–PEG membranes highly promising multifunctional devices combining efficient antibacterial activity in antifauling studies and biocompatibility with active local drug delivery.

Investigations carried out by Diagne et al. [29] were addressed to reduce both organic and biological fouling by modifying the surface of commercially available poly(ether sulfone) (PES) membranes using the polyelectrolyte multilayer modification method with poly(styrenesulfonate) (PSS), poly(diallyldimethylammonium chloride) (PDADMAC), and AgNPs (nanoAg) integrated onto the surface as stable, thin films. The authors reported that the PSS increases the hydrophilicity of the membrane and increases the negative surface charge, while integration of nanoAg into the top PSS layer imparts biocidal characteristics to the modified surface.

AgNPs have also been coated directly onto polymer membrane substrates to form AgNP/membrane nanocomposite. Nisola et al. [30] have coated polyether-*block*-

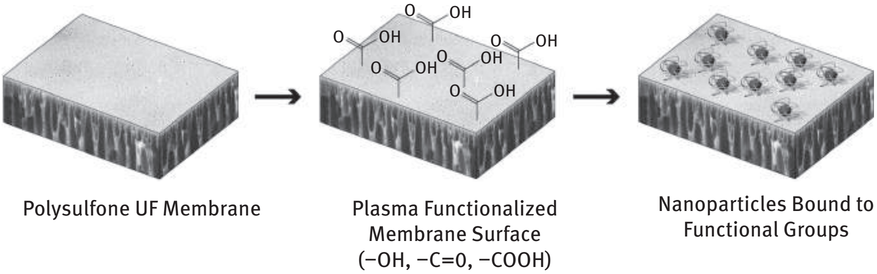

Figure 13.5: Scheme of polysulfone membrane fictionalization with encapsulated AgNPs. Reprinted with permission from [31]. Copyright (2011) American Chemical Society.

polyamide copolymer (PEBA) dense film containing AgNPs onto ultrafiltration polysulfone membranes; however, the practical utility of these methods has been limited by the low efficiency of AgNP deposition onto the membrane surfaces. The authors demonstrated that the immobilized AgNPs can be easily released (or leached) from the membranes owing to the lack of interaction between AgNPs and membrane.

Meagan and coworkers [31] described the preparation of AgNP/membrane nanocomposites in which the AgNPs were electrostatically assembled on the membrane, as shown in Figure 13.5.

The membrane was prepared by means of the assembly between the AgNPs encapsulated with the positively charged polyethyleneimine (PEI) and the polysulfone membrane functionalized with the negative charged carboxylic acid. Electrostatic interactions were useful for depositing the AgNPs on the membrane substrate; however, the AgNPs were eventually released from the membrane due to the weakness of the electrostatic attraction between the AgNPs and the membrane. Stable and robust bonds between the AgNPs and the membrane are important for ensuring the preparation of safe, ecofriendly, stable, antibiofouling and high-efficiency membranes.

Nanosilver has been incorporated into cellulose acetate [32] and polyimide [33] membranes; however, the long-term effectiveness of the incorporated nanosilver in preventing biofouling during continuous filtration has not been addressed.

13.2.1.2 *Ex situ* methods

This silver loss resulted in a significant loss of antibacterial and antiviral activity. Thus, successful fabrication of nanoAg-impregnated membranes needs to allow for the release of sufficient silver ions for microbial control while preventing a rapid depletion of silver. The unwanted loss of the AgNPs from the membrane brings about the deterioration in the desired properties such as an antibiofouling property and a membrane lifetime. Most problematic of all, the AgNPs released from the membrane can penetrate easily into the human body and can produce cell damage and cancer.

The *ex situ* method generally involves two steps including the synthesis of AgNPs first and their immobilization on the membrane surface, requiring either AgNPs or membrane surface being functionalized to promote their strong bonding. Conventionally, AgNPs have been synthesized using either chemical or physical methods which include sol process, micelle, chemical precipitation, hydrothermal method, electrochemical techniques, pyrolysis and chemical vapor deposition. Some of these methods are easy and make available control over crystallite size by restoring the reaction environment. But problem still exists with the general stability of the product and in achieving monodisperse nanosize using these methods. Investigations have shown that the size, morphology, stability and properties (chemical and physical) of the metal NPs are strongly influenced by the experimental conditions, the kinetics of interaction of metal ions with reducing agents and adsorption processes of stabilizing agent with metal NPs. Therefore, the design of a synthesis method in which the size, morphology, stability and properties are controlled has become a major field of interest [11, 12].

Kwak and co-workers have studied metal–polymer (cellulose [34] or poly(vinylidene fluoride) [35]) fabrics nanocomposite, in which AgNPs have been covalently assembled onto a thiolated polymer fabric. The author reported that the thiol group in the thiolated cellulose formed a robust covalent bond with the Ag atoms on the surface of the metal NPs, thereby significantly reducing the number of metal NPs released from the fabric during washing [34]. Furthermore, the same authors showed [35] that the AgNP–poly(vinylidene fluoride) (Ag–PVDF) membrane nanocomposites have a sustainable antibiofouling property through the covalent assembly of the AgNPs onto the PVDF membrane surface via a thiol end-functionalized amphiphilic block copolymeric linker, as illustrated in Figure 13.6. To this end, the thiol end-functionalized amphiphilic block copolymer as a covalent linker between the AgNPs

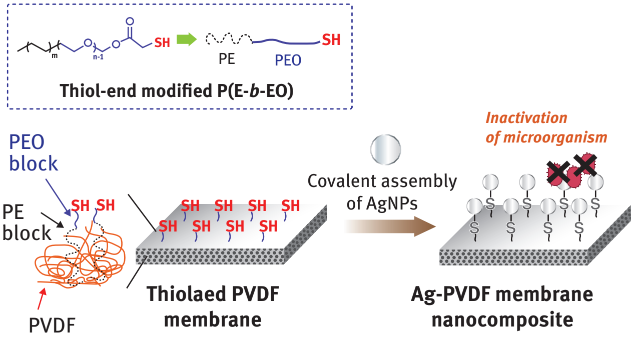

Figure 13.6: Sustainable anti-biofouling ultrafiltration membrane nanocomposites by covalently immobilizing silver nanoparticles (AgNPs) onto poly(vinylidene fluoride) (PVDF) membrane mediated by a thiol-end functional amphiphilic block copolymer linker. Reprinted with permission from [31]. Copyright (2011) American Chemical Society.

and the membrane was physically anchored onto the membrane via hydrophilic–hydrophobic phase recognition of the amphiphilic linkers during the membrane fabrication process, resulting in the thiolated PVDF membrane. AgNPs then covalently bound to the thiolated PVDF membrane via a simple impregnation process. Surprisingly, the resulting Ag–PVDF membrane nanocomposite did not release detectable amounts of AgNPs from the membrane, and the membrane displayed excellent antibiofouling property. This makes them tremendously attractive in applications ranging from high-efficiency membrane to ecofriendly water purification systems.

The same concept of silver–composite membrane formation via the Ag–S chemical bonding has also been carried out by Yin et al. [36]. The authors reported that the AgNPs with approximately 15 nm in diameter were effectively attached to the surface of polyamide TFC membrane via covalent bonding, with cysteamine as a bridging agent. Gusseme et al. [37] immobilized the silver nanopraticles in polyvinylidene fluoride membranes and investigated the disinfection capacity toward virus in water. However, the researchers were mainly focused on application of antibiofouling performance of AgNPs in membrane fabrication, but the hydrophilicity of membrane surface provided by AgNPs has rarely been reported. Li et al. [38] immobilized AgNPs on the surface of poly(vinylidene fluoride)-g-poly(acrylic acid) (PVDF-g-PAA) membranes obtaining composite membranes with excellent surface hydrophilicity and outstanding antifouling performance. Under this investigation, the authors first prepared the PVDF membranes by a classical method-immersion precipitation inversion process. Then by using a physisorbed free radical grafting technique, they grafted a PAA brush on PVDF membrane surface. Next, they decorated the membrane with Ag ions by immersion of the grafted membrane in a silver nitrate solution. After this step, the silver ions were coordinately bonded with the carboxyl group of PAA. In order to get the Ag-PVDF-g-PAA membranes, the silver ions were further reduced with $NaBH_4$, as illustrated in Figure 13.7.

Unfortunately, the approaches that have been performed by Kwak and co-workers [34, 35], as well as by Yin and co-workers [39] or Li and co-workers

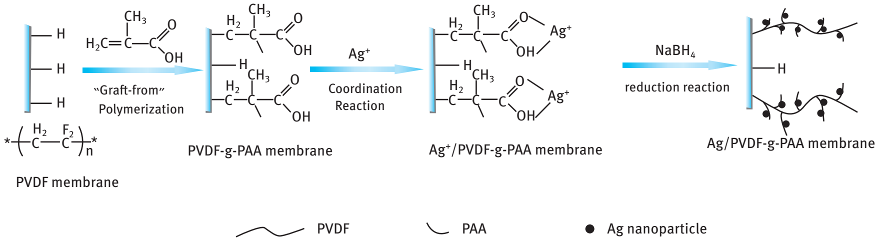

Figure 13.7: Silver modification of PVDF membrane.

[38], require the membrane surface having certain functionalities to immobilize AgNPs, and they are not applicable to most of other different membranes.

13.2.2 Polymeric stabilized silver nanoparticles for SERS properties

Raman spectroscopy arises from the inelastic light scattering by molecular vibrations, which could provide "fingerprint" information for molecular diagnostics [40]. However, the inherently low scattering intensity of conventional Raman spectroscopy limits its widespread applicability. Over the last few decades, surface-enhanced Raman spectroscopy (SERS) has received intense attention because of its great potential for ultrasensitive detection down to the single-molecular level that are often found in art materials that exhibit a highly fluorescent background occurring when the studied materials are excited in the visible and near infrared (NIR) in spontaneous Raman scattering measurements [41–43]. It is well-known that the extremely large electromagnetic SERS enhancement (proportional to field enhancement to the fourth power) up to 10^{10} has been theoretically predicted and experimentally demonstrated for small areas called as "hot spots" [44–46]. Because SERS "hot spots" usually reside in the interstitial voids of metal NPs and metal structures with intersections, bifurcations and high radius of curvatures, exquisite preparation of metal NPs with controlled size and morphology and delicate manipulation of the NP assemblies are required in order to maximize the sensitivity of the prepared SERS platforms. To this objective, various designs of SERS-active substrates have been reported, such as roughened metal substrates, metal NP assemblies, porous or holey substrates and even semiconductor-based substrates. However, SERS substrates must be reproducible, highly sensitive and facile for fabrication and have site-independent "hot spots," while most of the above-mentioned candidates require relatively complicated and expensive manipulations [24]. The polymer engineering opens a new path for NP assembling and their successive application in SERS technologies. Illustrative examples include the synthesis of Ag/poly(butyl acrylate) composites using microemulsions [47], the preparation of poly(methyl methacrylate) durable plastic films using an Ag/PVP colloid [48], incorporation of AgNPs in soft polymers to produce active SERS substrates [49] and the preparation of Ag/bionanocomposites using cellulose [50], chitosan [51] or sporopollenin [52]. It is important to underline that most of the polymer–AgNP matrix preparations are based on *in situ* methods. Some of the most exciting examples are described below.

Recently, Yan et al. [53] reported a facile synthesis of homogeneous AgNPs fully covering the polyaniline (PANI) membrane surface simply by introducing organic acid in the $AgNO_3$ reaction solution, as an improved technique to fabricate well-defined Ag nanostructures on PANI substrates through a direct chemical deposition method described in [54]. The authors found that the chemical nature of the acid is crucial to create a homogeneous nucleation environment for Ag growth, where, in this case, homogeneous AgNPs that are assembled by Ag nanosheets are produced with the assistance of succinic acid and lactic acid, but only scattered AgNPs with camphorsulfonic acid. According to the authors, improved surface wettability of PANI membranes after acid doping may also account for the higher surface coverage of Ag nanostructures. The authors reported that the Ag nanostructures fully covering the PANI surface, and they are extremely sensitive in the detection of a target analyte, 4-mercaptobenzoic acid (4-MBA), using SERS, with a detection limit of 10^{-12} M. The authors believe the facilely fabricated SERS-active substrates based on conducting polymer-mediated growth of Ag nanostructures can be promising in the trace detection of chemical and biological molecules.

Li and co-workers have focused their investigation on the development of sensitive detection methods for environmental antibiotics monitoring due to the increasing pollution of aquatic environments by antibiotics. Recently, the authors published very interesting results concerning a preparation of AgNPs and carbon nanotube-intercalated graphene oxide laminar membranes (AgNPs/CNT-GO membranes) (Figure 13.8) for enrichment and SERS detection of antibiotics [55].

The achieved results show that the prepared Ag NPs/CNT-GO membranes exhibit a high enrichment ability because of the π–π stacking and electrostatic interactions of GO toward antibiotic molecules, which enhance the sensitivity of SERS measurements and enable the antibiotics to be determined at sub-nM concentrations. In addition, the nanochannels created by the intercalation of CNTs into GO layers result in an eightfold enhancement in the water permeance of Ag NPs/CNT-GO membranes compared to that of pure GO membranes. More importantly, the obtained Ag NPs/CNT-GO membranes exhibit high reproducibility and long-term stability. The presented results show that the spot-to-spot variation in SERS intensity was less than 15 %, and the SERS performance can be maintained for at least 70 days. The Ag NPs/

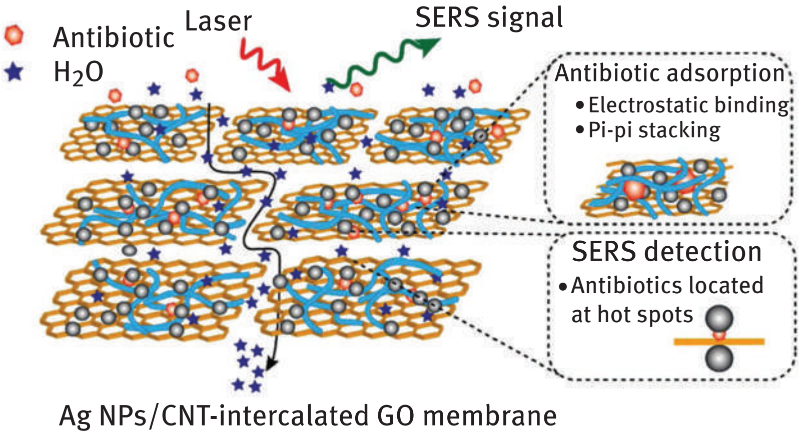

Figure 13.8: Scheme of AgNPs/CNT-GO membranes for SERS detection of antibiotics. Reprinted with permission from [54]. Copyright (2016) American Chemical Society.

CNT-GO membranes were also used for SERS detection of antibiotics in real samples. The results showed that the characteristic peaks of antibiotics were obviously recognizable. Thus, the authors expect that the reported ultrasensitive SERS detection of antibiotics can improve practical applications of Ag NPs/CNT-GO in environmental analysis.

Mondal et al. [56] have decorated PANI fibers with AgNPs by using a solution-dipping technique. Then, the authors evolved the fibers as sensitive materials for the detection of trace amounts of 4-mercaptobenzoic acid and rhodamine 6 G as an analyte of SERS. The investigators reported that the developed decorated fibers possess a down detection limit to nanomolar concentrations with excellent recyclability. Furthermore, the authors demonstrated that synthesized fiber composites can be apply simultaneously as an active SERS substrate and a superior catalyst for reduction of 4-nitrothiophenol. Figure 13.9 shows an SEM micrograph of Ag/PANI fiber and SERS enhancements.

Polymers whose behavior is sensitive to external stimuli are attracting great interest as they might add complementary functionalities to the composite of the SERS active metal. Accordingly, Au/Ag nanorods in thermoresponsive hydrogel networks [57] or mechanical responsive Ag-loaded agarose gels [58] have been reported as substrates that show a SERS behavior dependent on “hot spots” induced by the synergistic action of the plasmonic metal nanostructures and the external stimuli responsive polymer. Trindade and co-workers have focused their investigation on the development of κ-carrageenan-based nanocapsules containing nanometals and SERS platforms. The authors have shown that κ-carrageenan can incorporate diverse types of inorganic NPs via encapsulation in the biopolymer structures [59–61]. Recently, the investigators reported that blended nanocomposites of Ag have been prepared in order to obtain new analytical SERS platforms [62]. According to the authors, because of κ-carrageenan tunable colloidal behavior between the sol–gel state, carrageenans are foreseen as interesting matrices to

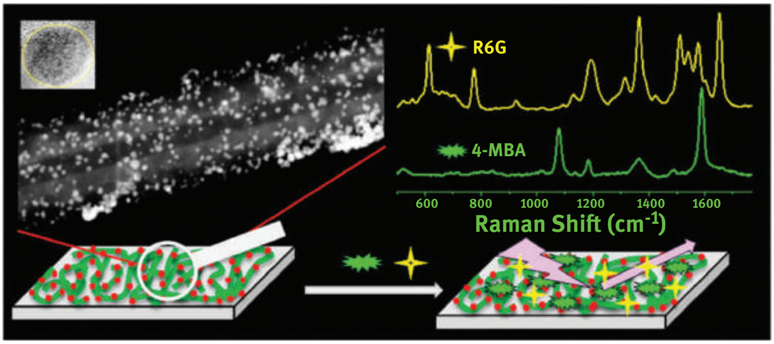

Figure 13.9: SEM micrograph of Ag /polyaniline fiber and SERS enhancements. Reprinted with permission from [56]. Copyright (2015) American Chemical Society.

develop thermosensitive SERS substrates provided that there is the ability to create dynamic hot spots by varying the gelation conditions. The authors demonstrated that the rheological behavior of Ag-containing hydrogels influences their performance as SERS platforms. The published results provided new insights into SERS associated with changes on the rheological behavior of chemical environments comprising active metal surfaces such as AgNPs. Furthermore, the authors provided a possible mechanism that correlates the gel strength of the biopolymer matrix with the SERS signal, as consequence of the formation of metal nanojuntions caused by the closer proximity of AgNPs as the biopolymer chains interaction. The authors believe that reported results can motivate research on the design of thermosensitive polymers that use rheological parameters for controlling the analytical sensitivity when used as SERS substrates.

13.2.3 Polymeric stabilized silver nanoparticles as catalyst

As mentioned in the beginning of this chapter in recent years, the synthesis of metal nanostructures using noble metals has gathered notable attention. Especially, polymer-embedded metal NPs seem to have special advantages that, in addition to providing stabilizing and protecting effects to metal NPs, polymers also offer unique possibilities for enhancing access of reactants to catalytic sites by way of a preconcentration effect, thereby exerting synergism in catalytic activities. An efficient and widespread way of synthesis of aromatic amines is the reduction of nitroaromatics using catalysts. Metal NPs have been used widely for the catalytic reduction of nitroaromatics in the presence of $NaBH_4$ [63].Various mono- and bi-metal NPs such as Ag, Pt, Au, Au–Ag, Pt/C and Ni–Pt have been used for the catalytic conversion of nitroaromatics into their corresponding amino compounds. Generally, Pt, Pd, Au and its bi-metal NPs are expensive and are considered to have better catalytic activity than AgNPs. However, Ag is the cheapest metal available among them. Hence, the preparation of catalytically more active AgNPs over other noble metal NPs through a simple procedure is of significance in this field of research. Viswanathan and Ramaraj [64] developed a simple protocol for silver ion reducing by using dopamine in the presence of the polyelectrolyte poly[acrylamide-*co*-(diallyldimethylammonium chloride)] (PADA) and amine-functionalized silane. The authors have used the polymer-stabilized AgNPs as catalyst for the reduction of 4-nitrophenol (4-NP). Reported results demonstrated that interestingly dopamine-reduced AgNPs show better catalytic activity ($k=10.99\times10^{-3}\ s^{-1}$) than those reduced using the conventional reducing agent $NaBH_4$ ($k=4.16\times10^{-3}\ s^{-1}$) toward the reduction of 4-NP.

Jayabal and Ramaraj have also developed a simple method for the preparation of bimetallic gold/silver nanorods embedded in amine functionalized silicate sol–gel matrix (Au/Ag–TPDTNRs) in the aqueous medium [63]. The authors have used N^1-[3-trimethoxysilyl)propyl]diethylene triamine (TPDT) as a reducing as well as stabilizing agent to prepare the Au/Ag–TPDTNRs. Furthermore, the authors have investigated the Au/Ag–TPDTNR application for a catalytic reduction of nitrobenzene. The catalytic activity of the Au/Ag–TPDTNRs was evaluated by studying the catalytic reduction of nitrobenzene to aniline upon the addition of $NaBH_4$ in an aqueous solution. The Au/Ag–TPDTNRs was found to be a good catalyst when compared to the Au–TPDTNRs and AuNRs for the reduction of nitrobenzene to aniline at room temperature. According to the authors, the enhanced catalytic activity of Au/Ag–TPDTNRs is due to the synergistic effect of Au and Ag present in the bimetallic Au/Ag–TPDNRs. The reaction rate constants (k) are estimated to be 0.4050, 0.2515 and 0.1235 min^{-1} for Au/Ag–TPDTNRs, Au–TPDTNRs and AuNRs, respectively. The electrocatalytic reduction of nitrobenzene at pH 7 using the Au/Ag–TPDTNRs modified electrode was also investigated by the authors and compared with the Au–TPDTNRs. The generated results showed that the higher electrocatalytic activity of Au/Ag–TPDTNRs is due to the synergistic effect of Au and Ag present in the bimetallic Au/Ag–TPDTNRs. The results of the reported study demonstrated that the Au/Ag–TPDNRs are efficient catalysts for the catalytic reduction of nitrobenzene.

The use of smart polymer microgels as microreactors for the synthesis of AgNPs and for stabilizing them is increasing due to the unique combination of tunable optical and catalytic properties of AgNPs and responsive behavior of the microgels. *N*-isopropylacrylamide (NIPAM)-based microgels are generally used for *in situ* fabrication of AgNPs [65]. AgNPs fabricated with microgels have been widely used as catalysts for various organic reactions due to their easy synthesis, control over size and shape of NPs, open network of microgels for diffusion of reactants toward the surface of NPs, long-term stability, good reusability, non-toxicity, low cost, easy availability, quasi-homogeneous catalytic nature and tunable catalytic activity [66]. Liu et al. [67] synthesized AgNPs inside poly (NIPAM) microgels by *in situ* reduction method and used this hybrid system for catalytic reduction of 4-NP in aqueous medium. The authors reported that the catalytic activity of AgNPs can be tuned by swelling and de-swelling of the hybrid microgels. Dong et al. [68] fabricated AgNPs in poly(*N*-isopropylacrylamide-*co*-acrylic acid) microgels and explained the stability of AgNPs inside the network on the basis of the electron donor–acceptor concept. Khan et al. [69] used poly(*N*-isopropylacrylamide-*co*-methacrylic acid) microgels as microreactors for the fabrication of AgNPs for catalytic applications. The amide groups in NIPAM and acrylamide units of P(NIPAM-*co*-AAm) microgels may act as ligand to stabilize the AgNPs inside the network, and the hybrid system can be used as a catalyst for various reactions in aqueous medium. The copolymerization of NIPAM with acrylamide can not only increase the volume phase transition temperature of the microgels to increase their catalytic temperature range but it may also increase the diffusion of hydrophilic reactants from outside to inside the network. These ideas stimulated Begum and co-workers [70] to fabricate AgNPs in P(NIPAM-*co*-AAm) microgels for catalytic application. Under this investigation, the uniformly loaded AgNPs were found to be stable for a long time due to donor–acceptor interaction between amide groups of polymer network and AgNPs. The hybrid microgels were successfully used by the authors as a catalyst for rapid reduction of 4-Nitrophenol (4-NP) into 4-aminophenol (4-AP) in aqueous medium. They reported that the apparent rate constant increased with increasing concentration of catalyst and $NaBH_4$. The hybrid system reported in the publication has a potential to be used as a catalyst for many other organic reactions. According to the authors, provided results could inspire others researchers to fabricate NPs of other metals like Pt, Pd, Ru, etc., inside P (NIPAM-*co*-AAm) microgels, and these hybrid systems may be used in future as catalysts for reduction of nitroarenes and other systems. According to the investigators, developed hybrid microgels can also be used for applications other than catalysis.

13.2.4 Silver polymer-based material in medical applications

Implant associated and joint replacement bacterial infections are high at 1.0–4.0 % and are one of the most serious complications in orthopedic surgery because they are extremely difficult to treat and result in increased morbidity and significantly worse outcomes [71–73]. Bone infection, also called osteomyelitis, can result when bacteria invade a bone. Treatment of osteomyelitis usually requires surgical debridement and prolonged antimicrobial therapy. The rising incidence of infection with multidrug-resistant bacteria, in particular methicillin-resistant *S. aureus* (MRSA), however, limits the antimicrobial treatment options available [74]. Therefore, AgNPs have been incorporated into plain poly(methyl methacrylate) bone cement, used for the secure attachment of joint prostheses hip and knee replacement surgery, as a way to reduce bacterial resistance [72, 75]. Soo and co-workers have investigated incorporating AgNPs into poly(lactic-co-glycolic acid) (PLGA) grafts as a potential for implant and fixation material in orthopedic and orthodontic surgery [76, 77]. The authors demonstrated that metallic nanosilver particles (with a size of 20–40 nm)–(PLGA) composite grafts have strong antibacterial properties [76]. In addition, nanosilver particle–PLGA composite grafts did not inhibit adherence, proliferation, alkaline phosphatase activity or mineralization of on growth MC3T3-E1 pre-osteoblasts compared to PLGA controls. Furthermore, the authors reported that the nanosilver particles did not affect the osteoinductivity of bone morphogenetic protein 2 (BMP-2). Infected femoral defects implanted with BMP-2 coupled 2.0 % nanosilver particle–PLGA composite grafts healed in 12 weeks without evidence of residual bacteria. In contrast, BMP-2-coupled PLGA control grafts failed to heal in the presence of continued bacterial colonies. The obtained results indicated that nanosilver of defined particle size is bactericidal without discernible *in vitro* and *in vivo* cytotoxicity or negative effects on BMP-2 osteoinductivity, making it an ideal antimicrobial for bone regeneration in infected wounds. Moreover, the same research group has evaluated AgNP/PLGA-coated stainless steel alloy (SNPSA) as a potential antimicrobial implant material [77]. The authors reported that SNPSA exhibited strong antibacterial activity *in vitro* and *ex vivo* and promoted MC3T3-E1 pre-osteoblast proliferation and maturation in vitro. Furthermore, SNPSA implants induced osteogenesis while suppressing bacterial survival in contaminated rat femoral canals. The generated results pointed out that SNPSA has simultaneous antimicrobial and osteoinductive properties that make it a promising therapeutic material in orthopedic surgery.

Catheters used in the hospital setting have a high propensity for infection, which can lead to unwanted complications. Thus, AgNPs have been investigated as a method of reducing biofilm growth on catheters. Recently, polyurethane catheters have been modified with a coat of AgNPs to create effective antibacterial catheters [78]. Silver-coated catheters prepared by Roe et al. [79] showed significant *in vitro* antimicrobial activity and prevented biofilm formation using *Escherichia coli, Enterococcus, Staphylococcus aureus*, coagulase-negative *staphylococci, Pseudomonas aeruginosa* and *Candida albicans*. Approximately 15 % of the coated silver eluted from the catheters in 10 days *in vivo*, with predominant excretion in faces (8 %), accumulation at the implantation site (3 %) and no organ accumulation (≤0.1 %). Moreover, multiple studies have reported that AgNP-coated catheters can effectively reduce bacteria for up to 72 h in animal models [78, 80]. A clinical pilot study performed by Lacknerand co-workers was focused on investigating the prevention of catheter-associated ventriculitis (CAV) with AgNPs. The authors did not find any incidence of CAV, and all cerebrospinal fluid cultures were negative in the 19 patients that received a AgNP-coated catheter [81]. On the contrary, in the control group of 20 patients by using the catheter without AgNPs, five were positive for CAV [81].

AgNPs have also been applied to dental medicine. The oral environment is considered to be an asperous environment for restored tooth structure. Recurrent dental caries is a common cause of failure of tooth-colored restorations. Bacterial acids, microleakage and cyclic stresses can lead to deterioration of the polymeric resin–tooth bonded interface. Research on the incorporation of cutting-edge anticaries agents for the design of new, long-lasting, bioactive resin-based dental materials is a demanding and provoking work. Released antibacterial agents such as AgNPs, nonreleased antibacterial macromolecules (DMAHDM, dimethylaminohexadecyl methacrylate) and released acid neutralizer amorphous calcium phosphate nanoparticles (NACP) have shown potential as individual and dual anticaries approaches. Melo and co-workers [82] performed an exhausted investigations on AgNP synthesis, and their future incorporated into all the dental materials required to perform a composite restoration: dental primer, adhesive and composite (Figure 13.10).

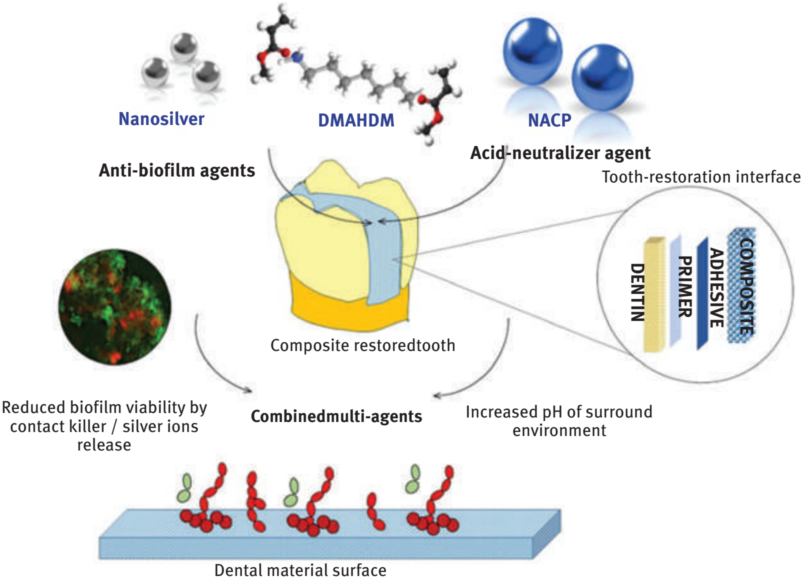

Figure 13.10: Incorporation of AgNPs into dental structure. Reprinted with permission from [82]. Copyright (2016) American Chemical Society.

The authors focused on combining different dental materials loaded with multiagents to improve the durability of the complex dental bonding interface. A combined effect of bacterial acid attack and fatigue on the bonding interface simulated the harsh oral environment. Human saliva-derived oral biofilm was grown on each sample prior to the cyclic loading. The oral biofilm viability during the fatigue performance was monitored by the live–dead assay. Damage of the samples that developed during the test was quantified from the fatigue life distributions. Results achieved by the authors indicate that the resultant multiagent dental composite materials were able to reduce the acidic impact of the oral biofilm, thereby improving the strength and resistance to fatigue failure of the dentin–resin bonded interface. Besides, studies performed by Melo et al. [82] showed that dental restorative materials containing multiple therapeutic agents of different chemical characteristics can be beneficial toward improving resistance to mechanical and acidic challenges in oral environments. Akhavan et al. [83] reported that incorporation of AgNPs into orthodontic adhesives could increase or maintain the shear bond strength of an orthodontic adhesive while simultaneously increasing its resistance to bacteria. A recent study carried out by researchers Zmudzkin and co-workers [84] demonstrated that integration of AgNPs into dental composites could reduce the microbial colonization of lining materials, enhancing the antifungal efficiency. Similarly, AgNP amalgamation into endodontic fillings displays an increased antibacterial effect against

Streptococcus milleri, Staphylococcus aureus and *Enterococcus faecalis* [85]. Degrazia et al. [86] investigated an effect of AgNPs on the physicochemical and antimicrobial properties of an orthodontic adhesive. The authors found that the addition of AgNP solutions to Transbond™ XT adhesive primer inhibited *Streptococcus mutans* growth without compromising the chemical and physical properties of the adhesive.

Funding: The financial support for the Incoming Marie Curie TECNIOspring fellowship from People Programme (Marie Curies Actions) of the Seventh Framework Programme of the European Union (FP7/2007-2013) under REA grant agreement no. 600388 (TECNIOspring programme), and from the Agency for Business Competitiveness of the Government of Catalonia, ACCIÓ, during which the chapter was prepared, is gratefully acknowledged by Dr. Tylkowski.

References

[1] Srivastava V, Gusain D, Sharma YC. Critical review on the toxicity of some widely used engineered nanoparticles. Ind Eng Chem Res. 2015;54:6209–6233.

[2] Yang W, Peters JI, Williams RO. Inhaled nanoparticles–a current review. Int J Pharm. 2008;356: 239–247.

[3] Gurunathan S, Kalishwaralal K, Vaidyanathan R, Venkataraman D, Pandian SR, Muniyandi J, et al. Biosynthesis, purification and characterization of silver nanoparticles using Escherichia coli. Colloids Surf B. 2009;74:328–335.

[4] Tolaymat TM, El Badawy AM, Genaidy A, Scheckel KG, Luxton TP, Suidan M. An evidence-based environmental perspective of manufactured silver nanoparticle in syntheses and applications: A systematic review and critical appraisal of peer-reviewed scientific papers. Sci Total Environ. 2010;408:999–1006.

[5] Skrabalak SE, Xia Y. Pushing nanocrystal synthesis toward nanomanufacturing. ACS Nano. 2009;3:10–15.

[6] Sun X, Huang X, Yan X, Wang Y, Guo J, Jacobson O, et al. Chelator-free 64Cu-integrated gold nanomaterials for positron emission tomography imaging guided photothermal cancer therapy. ACS Nano. 2014;8:8438–8446.

[7] Mitragotri S, Anderson DG, Chen X, Chow EK, Ho D, Kabanov AV, et al. Accelerating the translation of nanomaterials in biomedicine. ACS Nano. 2015;9:6644–6654.

[8] Jessop PG, Trakhtenberg S, Warner J. The twelve principles of green chemistry, innovations in industrial and engineering chemistry. American Chemical Society, 2008; 1000:401–436 DOI:10.1021/bk-2009-1000.ch012 ACS Symposium Series.

[9] Anastas PT, Kirchhoff MM. Origins, current status, and future challenges of green chemistry. Acc Chem Res. 2002;35:686–694.

[10] Anastas PT, Zimmerman JB. Peer reviewed: Design through the 12 principles of green engineering. Environ Sci Technol. 2003;37 94A–101A.

[11] Abbasi E, Milani M, Fekri Aval S, Kouhi M, Akbarzadeh A, Tayefi Nasrabadi H, et al. Silver nanoparticles: Synthesis methods, bio-applications and properties. Crit Rev Microbiol. 2016;42:173–180.

[12] Solanki JN, Murthy ZVP. Controlled size silver nanoparticles synthesis with water-in-oil microemulsion method: a topical review. Ind Eng Chem Res. 2011;50:12311–12323.

[13] Abou El-Nour KMM, Eftaiha AA, Al-Warthan A, Ammar RAA. Synthesis and applications of silver nanoparticles. Arabian J Chem. 2010;3:135–140.

[14] Anjum S, Abbasi BH, Shinwari ZK. Plant-mediated green synthesis of silver nanoparticles for biomedical applications: Challenges and opportunities. Pakistan J Bot. 2016;48:1731–1760.

[15] Tang Q, Liu J, Shrestha LK, Ariga K, Ji Q. Antibacterial effect of silver-incorporated flake-shell nanoparticles under dual-modality. ACS Appl Mater Interfaces. 2016;8:18922–18929.

[16] Rana D, Matsuura T. Surface modifications for antifouling membranes. Chem Rev. 2010;110: 2448–2471.

[17] Li X, Pang R, Li J, Sun X, Shen J, Han W, et al. In situ formation of Ag nanoparticles in PVDF ultrafiltration membrane to mitigate organic and bacterial fouling. Desalination. 2013;324:48–56.

[18] Ben-Sasson M, Lu X, Bar-Zeev E, Zodrow KR, Nejati S, Qi G, et al. In situ formation of silver nanoparticles on thin-film composite reverse osmosis membranes for biofouling mitigation. Water Res. 2014;62:260–270.

[19] Lee H, Dellatore SM, Miller WM, Messersmith PB. Mussel-inspired surface chemistry for multifunctional coatings. Science. 2007;318:426–430.

[20] Li Y, Su Y, Zhao X, He X, Zhang R, Zhao J, et al. Antifouling, high-flux nanofiltration membranes enabled by dual functional polydopamine. ACS Appl Mater Interfaces. 2014;6: 5548–5557.

[21] Jiang J, Zhu L, Zhu L, Zhang H, Zhu B, Xu Y. Antifouling and antimicrobial polymer membranes based on bioinspired polydopamine and strong hydrogen-bonded poly(n-vinyl pyrrolidone). ACS Appl Mater Interfaces. 2013;5:12895–12904.

[22] Cong Y, Xia T, Zou M, Li Z, Peng B, Guo D, et al. Mussel-inspired polydopamine coating as a versatile platform for synthesizing polystyrene/Ag nanocomposite particles with enhanced antibacterial activities. J Mater Chem B. 2014;2:3450–3461.

[23] Tang L, Livi KJT, Chen KL. Polysulfone membranes modified with bioinspired polydopamine and silver nanoparticles formed in situ to mitigate biofouling. Environ Sci Technol Lett. 2015;2:59–65.

[24] Huang L, Zhao S, Wang Z, Wu J, Wang J, Wang S. In situ immobilization of silver nanoparticles for improving permeability, antifouling and anti-bacterial properties of ultrafiltration membrane. J Memb Sci. 2016;499:269–281.

[25] Liu Z, Hu Y. Sustainable antibiofouling properties of thin film composite forward osmosis membrane with rechargeable silver nanoparticles loading. ACS Appl Mater Interfaces. 2016;8: 21666–21673.

[26] Soroush A, Ma W, Cyr M, Rahaman MS, Asadishad B, Tufenkji N. In situ silver decoration on graphene oxide-treated thin film composite forward osmosis membranes: Biocidal properties and regeneration potential. Environ Sci Technol Lett. 2016;3:13–18.

[27] Madhavan P, Hong P-Y, Sougrat R, Nunes SP. Silver-enhanced block copolymer membranes with biocidal activity. ACS Appl Mater Interfaces. 2014;6:18497–18501.

[28] Mishra SK, Raveendran S, Ferreira JMF, Kannan S. In situ impregnation of silver nanoclusters in microporous Chitosan-PEG membranes as an antibacterial and drug delivery percutaneous device. Langmuir. 2016;32:10305–10316.

[29] Diagne F, Malaisamy R, Boddie V, Holbrook RD, Eribo B, Jones KL. Polyelectrolyte and silver nanoparticle modification of microfiltration membranes to mitigate organic and bacterial fouling. Environ Sci Technol. 2012;46:4025–4033.

[30] Nisola GM, Park JS, Beltran AB, Chung W-J. Silver nanoparticles in a polyether-block-polyamide copolymer towards antimicrobial and antifouling membranes. RSC Advances. 2012;2:2439–2448.

[31] Mauter MS, Wang Y, Okemgbo KC, Osuji CO, Giannelis EP, Elimelech M. Antifouling ultrafiltration membranes via post-fabrication grafting of biocidal nanomaterials. ACS Appl Mater Interfaces. 2011;3:2861–2868.

[32] Chou WL, Yu DG, Yang MC. The preparation and characterization of silver-loading cellulose acetate hollow fiber membrane for water treatment. Polym Adv Technol. 2005;16:600–607.

[33] Deng Y, Dang G, Zhou H, Rao X, Chen C. Preparation and characterization of polyimide membranes containing Ag nanoparticles in pores distributing on one side. Mater Lett. 2008;62: 1143–1146.

[34] Park SY, Chung JW, Priestley RD, Kwak S-Y. Covalent assembly of metal nanoparticles on cellulose fabric and its antimicrobial activity. Cellulose. 2012;19:2141–2151.

[35] Park SY, Chung JW, Chae YK, Kwak SY. Amphiphilic thiol functional linker mediated sustainable anti-biofouling ultrafiltration nanocomposite comprising a silver nanoparticles and poly (vinylidene fluoride) membrane. ACS Appl Mater Interfaces. 2013;5:10705–10714.

[36] Yin J, Yang Y, Hu Z, Deng B. Attachment of silver nanoparticles (AgNPs) onto thin-film composite (TFC) membranes through covalent bonding to reduce membrane biofouling. J Memb Sci. 2013;441:73–82.

[37] De Gusseme B, Hennebel T, Christiaens E, Saveyn H, Verbeken K, Fitts JP, et al. Virus disinfection in water by biogenic silver immobilized in polyvinylidene fluoride membranes. Water Res. 2011;45:1856–1864.

[38] Li J-H, Shao X-S, Zhou Q, Li M-Z, Zhang -Q-Q. The double effects of silver nanoparticles on the PVDF membrane: Surface hydrophilicity and antifouling performance. Appl Surf Sci. 2013;265: 663–670.

[39] Li S, Sun H, Wang D, Hong J, Tao S, Yu H, et al. Enhanced chemiluminescence of the luminol-AgNO3 system by Ag nanoparticles. J Biolumin Chemlumin. 2012;27:211–216.

[40] Bryche J-F, Bélier B, Bartenlian B, Barbillon G. Low-cost SERS substrates composed of hybrid nanoskittles for a highly sensitive sensing of chemical molecules. Sens Actuators B. 2017;239: 795–799.

[41] Choi H-K, Park W-H, Park C-G, Shin -H-H, Lee KS, Kim ZH. Metal-catalyzed chemical reaction of single molecules directly probed by vibrational spectroscopy. J Am Chem Soc. 2016;138: 4673–4684.

[42] Aioub M, El-Sayed MA. A real-time surface enhanced Raman spectroscopy study of plasmonic photothermal cell death using targeted gold nanoparticles. J Am Chem Soc. 2016;138:1258–1264.

[43] Cialla D, Pollok S, Steinbrücker C, Weber K, Popp J. SERS-based detection of biomolecules. Nanophotonics. 2014;3:383–411.

[44] Song J, Wang F, Yang X, Ning B, Harp MG, Culp SH, et al. Gold nanoparticle coated carbon nanotube ring with enhanced Raman scattering and photothermal conversion property for theranostic applications. J Am Chem Soc. 2016;138:7005–7015.

[45] Ansar SM, Li X, Zou S, Zhang D. Quantitative comparison of Raman activities, SERS activities, and SERS enhancement factors of organothiols: Implication to chemical enhancement. J Phys Chem Lett. 2012;3:560–565.

[46] Schultz ZD, Marr JM, Wang H. Tip enhanced Raman scattering: Plasmonic enhancements for nanoscale chemical analysis. Nanophotonics. 2014;3:91–104.

[47] Pinheiro PC, Fateixa S, Nogueira HI, Trindade T. SERS study on adenine using a Ag/poly (t-butylacrylate) nanocomposite. Spectrochim Acta Part A. 2013;101:36–39.

[48] Lin W. A durable plastic substrate for surface-enhanced Raman spectroscopy. Appl Phys A. 2011;102:121–125.

[49] Kim Nam-Jung, Lin Mengshi, Hu Zhiqiang, Li Hao. Evaporation-controlled chemical enhancement of SERS using a soft polymer substrate. Chemical Communications. 2009;(41):6246–6246. DOI:10.1039/B907504F.

[50] Marques PAAP, Nogueira HIS, Pinto RJB, Neto CP, Trindade T. Silver-bacterial cellulosic sponges as active SERS substrates. J Raman Spectrosc. 2008;39:439–443.

[51] Potara M, Gabudean A-M, Astilean S. Solution-phase, dual LSPR-SERS plasmonic sensors of high sensitivity and stability based on chitosan-coated anisotropic silver nanoparticles. J Mater Chem. 2011;21:3625–3633.

[52] Joseph V, Schulte F, Rooch H, Feldmann I, Dorfel I, Osterle W, et al. Surface-enhanced Raman scattering with silver nanostructures generated in situ in a sporopollenin biopolymer matrix. Chem Commun. 2011;47:3236–3238.

[53] Yan J, Han X, He J, Kang L, Zhang B, Du Y, et al. Highly sensitive surface-enhanced Raman spectroscopy (SERS) platforms based on silver nanostructures fabricated on polyaniline membrane surfaces. ACS Appl Mater Interfaces. 2012;4:2752–2756.

[54] Xu P, Mack NH, Jeon S-H, Doorn SK, Han X, Wang H-L. Facile fabrication of homogeneous 3D silver nanostructures on gold-supported polyaniline membranes as promising SERS substrates. Langmuir. 2010;26:8882–8886.

[55] Qu LL, Liu -Y-Y, Liu M-K, Yang G-H, Li D-W, Li H-T. Highly reproducible Ag NPs/CNT-intercalated GO membranes for enrichment and SERS detection of antibiotics. ACS Appl Mater Interfaces. 2016;8:28180–28186.

[56] Mondal S, Rana U, Malik S. Facile decoration of polyaniline fiber with Ag nanoparticles for recyclable SERS substrate. ACS Appl Mater Interfaces. 2015;7:10457–10465.

[57] Contreras-Caceres R, Pastoriza-Santos I, Alvarez-Puebla RA, Perez-Juste J, Fernandez-Barbero A, Liz-Marzan LM. Growing Au/Ag nanoparticles within microgel colloids for improved surface-enhanced Raman scattering detection. Chemistry. 2010;16:9462–9467.

[58] Abalde-Cela S, Auguie B, Fischlechner M, Huck WTS, Alvarez-Puebla RA, Liz-Marzan LM, et al. Microdroplet fabrication of silver-agarose nanocomposite beads for SERS optical accumulation. Soft Matter. 2011;7:1321–1325.

[59] Daniel-da-Silva AL, Pinto F, Lopes-da-Silva JA, Trindade T, Goodfellow BJ, Gil AM. Rheological behavior of thermoreversible kappa-carrageenan/nanosilica gels. J Colloid Interface Sci. 2008;320:575–581.

[60] Daniel-da-Silva AL, Fateixa S, Guiomar AJ, Costa BF, Silva NJ, Trindade T, et al. Biofunctionalized magnetic hydrogel nanospheres of magnetite and kappa-carrageenan. Nanotechnology. 2009;20:355602.

[61] Daniel-da-Silva AL, Trindade T, Goodfellow BJ, Costa BFO, Correia RN, Gil AM. In situ synthesis of magnetite nanoparticles in carrageenan gels. Biomacromolecules. 2007;8:2350–2357.

[62] Fateixa S, Daniel-da-Silva AL, Nogueira HIS, Trindade T. Raman signal enhancement dependence on the gel strength of Ag/hydrogels used as SERS substrates. J Phys Chem C. 2014;118:10384–10392.

[63] Jayabal S, Ramaraj R. Bimetallic Au/Ag nanorods embedded in functionalized silicate sol–gel matrix as an efficient catalyst for nitrobenzene reduction. Appl Catal A: Gen. 2014;470: 369–375.

[64] Viswanathan Perumal, Ramaraj Ramasamy. Preparation of polyelectrolyte-stabilized silver nanoparticles for catalytic applications. Polymer International. 2016 7 5;66(3):342–348. DOI:10.1002/pi.5178.

[65] Farooqi Zahoor H., Naseem Khalida, Ijaz Aysha, Begum Robina. Engineering of silver nanoparticle fabricated poly (N-isopropylacrylamide-co-acrylic acid) microgels for rapid catalytic reduction of nitrobenzene. Journal of Polymer Engineering. 2016 1 1;36(1). DOI:10.1515/polyeng-2015-0082.

[66] Lu Y, Mei Y, Drechsler M, Ballauff M. Thermosensitive core–shell particles as carriers for Ag nanoparticles: Modulating the catalytic activity by a phase transition in networks. Angew Chem Int Ed. 2006;45:813–816.

[67] Liu -Y-Y, Liu X-Y, Yang J-M, Lin D-L, Chen X, Zha L-S. Investigation of Ag nanoparticles loading temperature responsive hybrid microgels and their temperature controlled catalytic activity. Colloids Surf A. 2012;393:105–110.

[68] Dong Y, Ma Y, Zhai T, Shen F, Zeng Y, Fu H, et al. Silver nanoparticles stabilized by thermoresponsive microgel particles: synthesis and evidence of an electron donor-acceptor effect. Macromol Rapid Commun. 2007;28:2339–2345.

[69] Khan SR, Farooqi ZH, Ajmal M, Siddiq M, Khan A. Synthesis, characterization, and silver nanoparticles fabrication in N-isopropylacrylamide-based polymer microgels for rapid degradation of p-nitrophenol. J Dispersion Sci Technol. 2013;34:1324–1333.

[70] Begum Robina, Farooqi Zahoor H., Ahmed Ejaz, Naseem Khalida, Ashraf Sania, Sharif Ahsan, Rehan Rida, et al. Catalytic reduction of 4-nitrophenol using silver nanoparticles-engineered poly(N -isopropylacrylamide-co -acrylamide) hybrid microgels. Applied Organometallic Chemistry. 2016 8 14;31(2):e3563–e3563. DOI:10.1002/aoc.3563.

[71] Alt V, Bechert T, Steinrücke P, Wagener M, Seidel P, Dingeldein E, et al. An in vitro assessment of the antibacterial properties and cytotoxicity of nanoparticulate silver bone cement. Biomaterials. 2004;25:4383–4391.

[72] Liu X, Man HC. Laser fabrication of Ag-HA nanocomposites on Ti6Al4V implant for enhancing bioactivity and antibacterial capability. Mater Sci Eng C. 2017;70:1–8.

[73] Murphy Maxwell, Ting Kang, Zhang Xinli, Soo Chia, Zheng Zhong. Current Development of Silver Nanoparticle Preparation, Investigation, and Application in the Field of Medicine. Journal of Nanomaterials. 2015;2015:1–12. DOI:10.1155/2015/696918.

[74] Mohiti-Asli M, Molina C, Diteepeng T, Pourdeyhimi B, Loboa EG. Evaluation of silver ion-releasing scaffolds in a 3D coculture system of MRSA and human adipose-derived stem cells for their potential use in treatment or prevention of osteomyelitis. Tissue Eng. 2016;22: 1258–1263.

[75] Van De Belt H, Neut D, Schenk W, Van Horn JR, Van Der Mei HC, Busscher HJ. Infection of orthopedic implants and the use of antibiotic-loaded bone cements. Acta Orthop Scand. 2001;72:557–571.

[76] Liu Y, Zheng Z, Zara JN, Hsu C, Soofer DE, Lee KS, et al. The antimicrobial and osteoinductive properties of silver nanoparticle/poly (dl-lactic-co-glycolic acid)-coated stainless steel. Biomaterials. 2012;33:8745–8756.

[77] Zheng Z, Yin W, Zara JN, Li W, Kwak J, Mamidi R, et al. The use of BMP-2 coupled – Nanosilver-PLGA composite grafts to induce bone repair in grossly infected segmental defects. Biomaterials. 2010;31:9293–9300.

[78] Paladini F, Pollini M, Deponti D, Di Giancamillo A, Peretti G, Sannino A. Effect of silver nanocoatings on catheters for haemodialysis in terms of cell viability, proliferation, morphology and antibacterial activity. J Mater Science: Mater Med. 2013;24:1105–1112.

[79] Roe D, Karandikar B, Bonn-Savage N, Gibbins B, Roullet JB. Antimicrobial surface functionalization of plastic catheters by silver nanoparticles. J Antimicrob Chemother. 2008;61: 869–876.

[80] De Mel A, Chaloupka K, Malam Y, Darbyshire A, Cousins B, Seifalian AM. A silver nanocomposite biomaterial for blood-contacting implants. J Biomed Mater Res. 2012;100A:2348–2357.

[81] Lackner P, Beer R, Broessner G, Helbok R, Galiano K, Pleifer C, et al. Efficacy of silver nanoparticles-impregnated external ventricular drain catheters in patients with acute occlusive hydrocephalus. Neurocrit Care. 2008;8:360–365.

[82] Melo MA, Orrego S, Weir MD, Xu HHK, Arola DD. Designing multiagent dental materials for enhanced resistance to biofilm damage at the bonded interface. ACS Appl Mater Interfaces. 2016;8:11779–11787.

[83] Akhavan A, Sodagar A, Mojtahedzadeh F, Sodagar K. Investigating the effect of incorporating nanosilver/nanohydroxyapatite particles on the shear bond strength of orthodontic adhesives. Acta Odontol Scand. 2013;71:1038–1042.

[84] Chladek G, Kasperski J, Barszczewska-Rybarek I, Zmudzki J. Sorption, solubility, bond strength and hardness of denture soft lining incorporated with silver nanoparticles. Int J Mol Sci. 2013;14:563–574.

[85] Magalhães APR, Santos LB, Lopes LG, Estrela CRDA, Estrela C, Torres EM, Bakuzis AF, Cardoso PC, Carrião MS. Nanosilver application in dental cements. ISRN Nanotechnol. 2012;2012:6.

[86] Degrazia FW, Leitune VCB, Garcia IM, Arthur RA, Samuel SMW, Collares FM. Effect of silver nanoparticles on the physicochemical and antimicrobial properties of an orthodontic adhesive. J Appl Oral Sci. 2016;24:404–410.

Tomasz Runka

14 Spectroscopic properties of polymer composites

Keywords: carbon materials, polymers, Raman and IR spectroscopy

14.1 Introduction

Polymers and polymer composites have been present in human life for a long time. Every day, we use many objects made of polymers, e. g. disposable tableware made of polyethylene (PE) or polypropylene (PP) are with us during the family picnics and holiday trips. We drink water from plastic bottles, eat using plastic cutlery, and so on. On the other hand, we see polymers and polymer composites as essential parts in equipment at homes, public buildings, cars, aircrafts, and different machines. Moreover, the role of these materials has become significant for our organisms. Nowadays, polymeric biomaterials play important roles in medicine for example as resorbable substrates for tissue regeneration control, construction implants of tailored mechanical properties and controlled resorption time, construction of prostheses, dental materials, artificial coronary vessels, a drug carrier, biostable joining elements, surgical sutures, and dressing materials. The polymers most often used in medical applications are polyvinyl chloride (PVC), polyvinylidene chloride (PVDC), polystyrene (PS), PE, polytetrafluoroethylene (PTFE), PP, polymethyl methacrylate (PMMA), polycarbonate (PC), and many others.

Moreover, biomaterials are generally made of polymer composites. Additionally, they can include metals and metal alloys (e. g. Fe, Co, Cr-Ti, and amalgams), ceramic materials (e. g. bioglass and hydroxyapatite) or possibly cells and human tissues.

Generally, it is worth noting that organic–inorganic hybrid materials such as polymer-ceramics and polymer-carbon very often are applied as biomaterials or materials used in electronics and optoelectronics.

According to literature, essential and very often used components of polymer composites are different allotropic forms of carbon, e. g. graphene, graphene nanoribbons (GNRs), and single- or multiwalled carbon nanotubes (MWCNTs). Thus, owing to interesting electronic and mechanical properties of GNRs, they have become promising materials for preparation of conductive composites for applications as transparent electrodes, heat circuits, and supercapacitors [1]. On the other hand, chemical modification of graphene by photopolymerization with styrene results in self-organized intercalative growth and delamination of graphene with few layers. Such composites are extremely promising for a wide range of

https://doi.org/10.1515/9783110469745-014

mechanical, thermal, and electrical applications [2]. An interesting report was that on electron field emission (FE) from reduced graphene oxide (rGO):poly(3-hexylthiophene) (P3HT) composite layers [3]. Reduced graphene oxide can also have potential applications in vacuum microelectronic devices, such as microwave power amplifiers and FE-based electronic devices such as flat panel FE displays (FEDs) [4–6]. Graphene fibers provide new ways to study interfacial interactions between the polymer and graphene for producing high-performance graphene-enhanced polymer nanocomposites. As an example, transcrystallization of isotactic polypropylene (iPP) surrounding the graphene fibers can be shown. The results indicate that fabrication of effective graphene-enhanced polymer nanocomposites can be used for various emerging applications [7]. Graphene-based polymer composites are also developed for potential use in biomedical applications. Soft biomedical polymers can be strengthened by incorporating graphene in the polymer matrix for use in hard tissue applications such as orthopedic repair and regeneration in the form of fracture fixation devices, tissue scaffolds, etc. [8].

Another form of carbon used as fillers in polymer composites or hybrid materials is carbon nanotube (CNT), generally due to its extremely high Young’s modulus, stiffness, and flexibility. Considering first single-walled carbon nanotubes (SWCNTs) as a candidate for application in producing composite materials, it should be noted that successful application requires well-dispersed nanotubes with good adhesion to the host matrix, which is not easy to realize. Moreover, weak nanotube–polymer interactions result in poor interfacial adhesion, which can cause nanotube aggregation within the matrix. A novel approach to in situ composite synthesis, by attachment of PS chains to full-length pristine SWCNTs without disrupting the original structure, has been proposed [9]. For some applications, solid-phase deposition of CNTs at the site of action is realized, but for other ones solution-phase processing and manipulation are required to achieve appropriate assemblies, orientations, and homogeneous dispersion of CNTs within host materials [10, 11]. In the last decade, the interest has been focused on functionalization of CNTs and especially SWCNs with various organic, inorganic, and organometallic structures using both covalent and noncovalent approaches [12, 13]. Multifunctional nanotube–polymer composites (e. g. SWCNT/MWCNT-polycarbonate (PC)/polystyrene (PS)) have been developed mainly due to improvement in mechanical and thermal properties and an increase in electrical conductivity [14–16]. The interest in transparent and flexible conductors as components of various devices used, e. g. as paper displays and plastic solar cells, has resulted in novel CNT/polymer composites (e. g. PS, PMMA, P3HT) with highly aligned nanotubes inside. The composite films obtained show high optical transparency, robust flexibility, and excellent conductivity [17, 18]. Polymer colloids with an interfacial coating of purified SWCNs have been synthesized from length- and type-sorted SWCNTs. Such composite particles exhibit electrical conductivities comparable to or higher than those of bulk SWCNT–polymer composites at nanotube loadings lower by more than 1 order of magnitude, maintaining unique electronic and optical characteristics of the parent SWCNT solution with potential applications as microelectronic and microoptical components [19]. In the last few years, hybrid nanocomposites containing SWCNTs and ordered polyaniline (PANI) have been prepared through in situ polymerization reaction. The SWCNT–PANI nanocomposites show both higher electrical conductivity and Seebeck coefficient than pure PANI, which could be attributed to the enhanced carrier mobility in the ordered chain structures of PANI. Such nanocomposites with thermoelectric effect (TE) have great potential for applications in both power generation in waste heat recovery systems and solid-state cooling or heating devices [20].

Hybrid materials fabricated on the basis of polymers and allotropic forms of carbon constitute a wide group of composite materials; however, other groups of hybrid materials synthesized from polymers and metals, metal oxides and metal alloys have been discussed in the past decade. Ordered mesostructured materials fabricated from polymerizable silica species and organic structure-directing agents, such as amphiphilic block copolymers or charged surfactants, are important examples of self-assembling hybrids. However, optical devices made from silica have a limited refractive index (n = 1.43) and must be supported by ultralow refractive index materials when efficient waveguiding is important [21]. One of the innovations proposed for fabrication of ordered self-assembling optical hybrids required replacing the silica framework with a higher refractive index material, such as titania [22, 23]. Dye-doped hybrid waveguides with trifluoroacetate-modified titania frameworks and high effective index of refraction (n = 1.6–1.7) have been fabricated [23, 24]. Commodity polymers such as PC films and polyester (PET) filaments are selectively functionalized through UV oxidation and then used as templates to control the nucleation and growth of ZnO nanorods and microplates forming periodically ordered microarrays directly out of aqueous solution. Such a process allows preparation of materials for biomimetics and makes this strategy more technologically applicable [25]. On the other hand, metal-insulator core-shell structure has been employed to fabricate composites with high dielectric constant and low energy losses. An example is Zn-ZnO/polyvinylidene fluoride (PVDF) composite with enhanced dielectric constant due to duplex interfacial polarizations induced by metal–semiconductor interface and semiconductor–insulator interface. Such polymer-based dielectric composites with conductive fillers have potential applications in electric power systems and electronic devices [26]. Thermally conducting but electrically insulating polymer-based composites have been widely used in electronic devices. Such composites are mostly manufactured by introducing highly thermally conducting particles such as ceramics, metals, or metal oxides into a polymer matrix. Examples are hexagonal boron nitride (hBN) platelets widely used as the reinforcing fillers for enhancement of thermal conductivity of polymer-based composites [27].

The above-mentioned groups of different composite materials and their applications are far from exhausting all materials reported in literature and in the following, spectroscopic characterization of only chosen polymer composites is given.

14.1.1 Review of results

Among different spectroscopic techniques, Raman spectroscopy is a noninvasive and powerful tool for investigation of different materials. For quite a long time, Raman spectroscopy was mainly dedicated to fundamental research, but development of instrumentation (laser miniaturization, CCD detection, Rayleigh filters, high-resolution holographic gratings and data processing software) has rendered it a general characterization method. An important breakthrough in the development of Raman spectrometers was integration with optical microscope, ensuring spatial resolution of less than 1 μm, upon visible excitation. It is worth noting that infrared absorption spectroscopy is complementary to Raman spectroscopy; however, it is not as versatile, useful and informative as Raman spectroscopy. Moreover, standard equipment of today's Raman microscopes is a motorized stage allowing Raman mapping and depth profiling of the sample.

A wide group of polymer composite materials contains allotropic forms of carbon, such as graphene flakes, carbon nanoribbons, or CNTs. Raman spectroscopy is known as a very useful technique to study compounds containing carbon allotropes. It is one of the few techniques sensitive to the full range of structural states present in this class of materials, from perfectly crystalline to amorphous. Raman spectroscopy allows distinction between diamond, graphite, graphene, or CNT through the measurement of a single spectrum. The common crystalline phases of carbon yield very simple spectra: diamond (sp^3 hybridization) gives a strong single mode of T_{2g} symmetry at 1,332 cm^{-1}, whereas graphite (sp^2 hybridization) gives doubly degenerated E_{2g} modes at 42 and 1,582 cm^{-1}. The latter is referred to as G band and corresponds to vibration in graphene planes, whereas the former corresponds to weak interplanar Van der Waals interactions [28]. Two additional modes called D and D' (the letter stands for "disorder") are detected whenever flaws/defects appear in the structure. D' mode results from the splitting of the G band and appears around 1,620 cm^{-1}, at the value at which the dispersion curve of graphite is the flattest. The intensity ratio of G to D' bands depends on the proportion of distorted graphene planes [29]. D band results from the resonant enhancement of the modes from graphite dispersion curves, having the same wavevector k as the incident photons. This assignment provided an explanation for some peculiarities of the D band, such as its excitation dependence [30]. A SWCNT can be considered as a cylinder of graphene of a few nanometers in diameter and a length ranging from tens of nanometers to millimeters. The properties of SWCNT are different and depend on the cylinder diameter and rolling direction. The number of Raman-active modes of SWCNT depends on the symmetry of the tube but is independent of its diameter. In fact, only four to five Raman bands are observed. Two of them recorded at around 1,600 cm^{-1} are assigned to G^{+} and G^{-}; however, the mode at around 1,350 cm^{-1} is attributed to defect-induced vibration (D mode). Moreover, in the Raman spectrum of SWCNT, besides D, G (G^{+}, G^{-}), and D* (marked also in literature as 2D) modes, a low wavenumber radial breathing mode (RBM) is detected in the range 80–350 cm^{-1} [31].

14.1.2 Polymer composites with graphene

Owing to the unusual mechanical properties of graphene (Young's modulus of an order of 1 TPa), production of reinforced high-performance composites based on polymer and graphene seems to be possible. Upon a composite deformation, internal stress is induced and in such materials stress is transferred from polymer matrix to the monolayer graphene. Raman spectroscopy is one of the best techniques for characterization of both graphene and its deformations. The positions of Raman bands in the graphene spectra shift with stress and the stress-induced Raman bands shifts can be used for determination of the stress in the material and in consequence for estimation of its effective Young's modulus [32, 33]. It is important to evaluate and compare the levels of reinforcement in polymer nanocomposites by exfoliated graphene flakes made of different numbers of layers. Many authors have reported that the shift of Raman bands for the nanocomposites containing multilayer graphene flakes is smaller than that for the material with monolayer graphene. Moreover, the band shift rate for multilayer graphene without a top coat (i. e. polymer is deposited on only one surface of the flake) is very low [34, 35]. Gong et al. have discussed the influence of tensile strain on vibrational spectra of monolayer and bilayer graphene flakes before and after applying the SU-8 top coat (SU-8 is an epoxy resin). The changes in the peak position of 2D Raman band vs. strain for coated and uncoated monolayer and bilayer graphene on PMMA polymer beam are presented in Figure 14.1.

It is well known that the 2D band from the spectrum of bilayer graphene consists of four components and should be fitted using four lines. As seen in Figure 14.2(a), a red shift of four components of 2D band is observed. Comparing the slopes of 2D1A and 2D2A components recorded for bilayer graphene to those recorded monolayer graphene, one can notice very similar dependence of the 2D component position as a function of strain. To avoid problems with orientation of the graphene flake, the measurements were carried out for the same flake coated with mono-, bi-, and trilayer of graphene, which ensures the same orientation of the flake toward the laser light polarization. The shift of the adjacent monolayer region is shown for comparison in Figure 14.2(a) (open circles) [33]. Figure 14.2(b) shows changes in the position of 2D band vs. strain for four different coated graphene structures, i. e. mono-, bi-, tri-, and other multilayers of graphene. The 2D band was fitted in all cases with a single Lorentzian line shape function, to compare the shift of the maximum of this band.

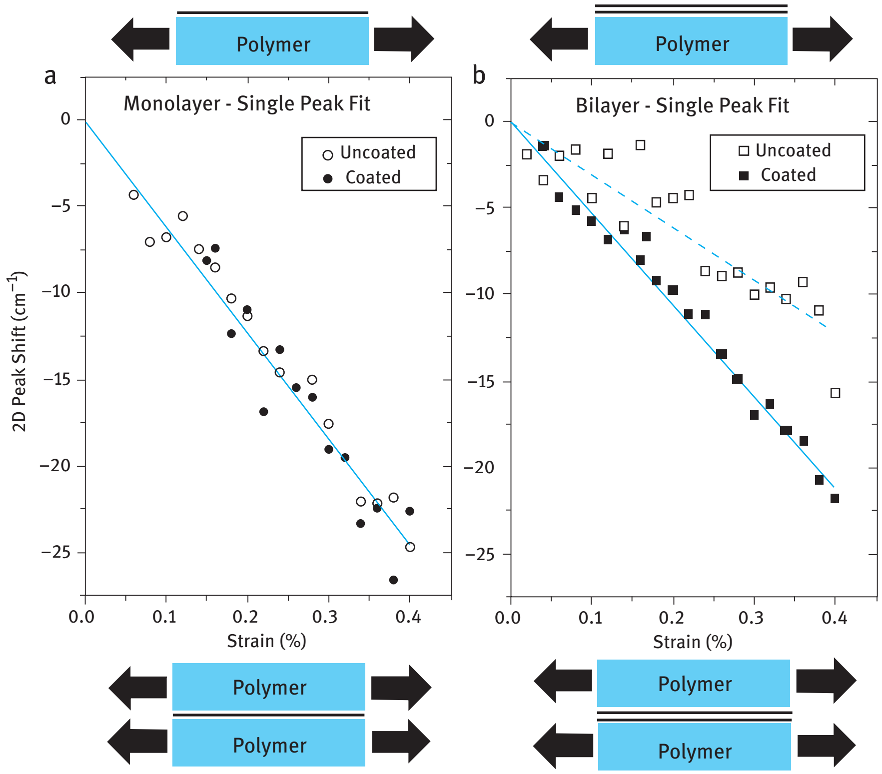

Figure 14.1: The change in the 2D peak position vs. strain for graphene (band was fitted to single peak) upon deformation of PMMA beam. (a) Graphene monolayer, (b) bilayer deformed before and after coating with SU-8. Schematic diagrams of the deformation of uncoated (above) and coated (below) graphene are also included. Adapted with permission from ACS NANO 6 (2012) 2086-2095. Copyright (2012) American Chemical Society [33].

The slope of 2D band maximum for mono- and bilayer materials is comparable but somewhat lower for the trilayer material. However, the slope for multilayer graphene is significantly lower.

A shift of 2D band can be also caused by a change in the measurement conditions, e. g. different wavelength, different relative orientation of graphene lattice to the straining direction, and direction of polarization of laser light. Gong at al. have performed a systematic study for more than 30 different graphene flakes on polymer beams in different orientations, with different numbers of layers, both uncoated and with a polymer coat, recording changes in the 2D band position upon deformation. For uncoated samples, a decrease in the band shift rate ($d\omega_{2D}/d\varepsilon$ in cm^{-1}/% strain) was noted when the number of layers increased from one to three, from −48.8 to −32.4, respectively. The value obtained for a multilayer uncoated flake was −37.4 but with a high error ±8.2. The shift rate obtained for uncoated graphite flake was very

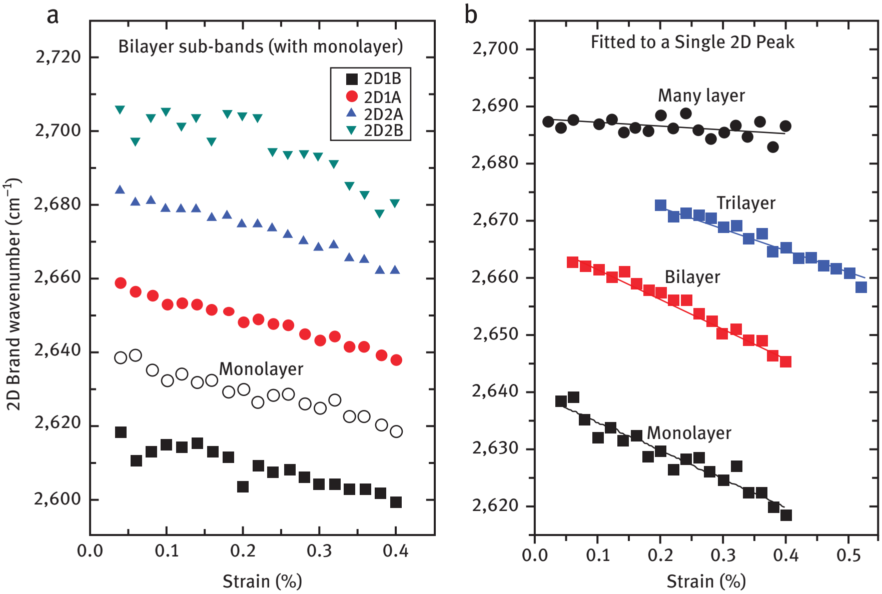

Figure 14.2: The wavenumbers of four components of 2D band vs. strain for bilayer graphene and monolayer region on the same flake (a). The strain dependence of the wavenumber of 2D band for adjacent mono- bi- and trilayers regions on the same graphene flake (2D peaks were fitted with a single Lorentzian shape function) (b). Adapted with permission from ACS NANO 6 (2012) 2086-2095. Copyright (2012) American Chemical Society [33].

low and equaled −3.0. For coated specimens, the band shift rates observed were generally higher and reached from −57.7 to −46.6 cm^{-1}/% strain for the samples with a single layer and that with three layers, respectively. Additionally, the differences between mono- and bilayer flakes were comparable within the limits of experimental error. The value obtained for a multilayer coated flake was −40.2 cm^{-1}/% strain, but similarly as for uncoated specimen, it was charged with a high experimental error ±14.2 cm^{-1}/% strain. For coated graphite, the band shift rate is 0 cm^{-1}/% strain. Since the shift of the 2D band with strain ($d\omega_{2D}/d\varepsilon$ in cm^{-1}/% strain) is proportional to the effective Young's modulus of graphene, it follows that, if the polymer–graphene interface remains undisturbed, the mentioned above band shift rates are an indication of the efficiency of internal stress transfer within the graphene layers. Concluding, it has been established that although there is good stress transfer between the polymer matrix and a monolayer graphene, monolayer graphene is not the optimum material to use for reinforcement of graphene-based polymer nanocomposites. Similarly, in bilayer material, good stress transfer between polymer matrix and graphene is observed, and there is no slippage between the layers for fully encapsulated material. Less efficient stress transfer has been found for trilayer and other multilayer graphene due to slippage between the internal layers, indicating that such materials will have a lower effective Young's modulus than either monolayer or bilayer graphene in polymer-based nanocomposites [33].

Young et al. have demonstrated a possibility of using Raman mapping for investigation of strain distribution in graphene flake and stress transfer from the polymer matrix (PMMA beam) to a graphene monolayer for model composites sample [36]. It was found that the shift rate with strain of 2D band was $-61 \pm 2\,\mathrm{cm}^{-1}/\%$ strain showing good stress transfer between underlying polymer and a graphene monolayer. Moreover, a significant broadening of 2D band is observed as a result of deformation. However, it should be mentioned that broadening or even splitting of 2D band strongly depends on the angle between the direction of laser light polarization and high-symmetry directions in graphene.

In order to avoid discrepancies in interpretation, the direction of the laser light polarization was parallel to the strain axis in the graphene monolayer for all measurements. Figure 14.3 presents Raman maps of the strain in graphene monolayer at different

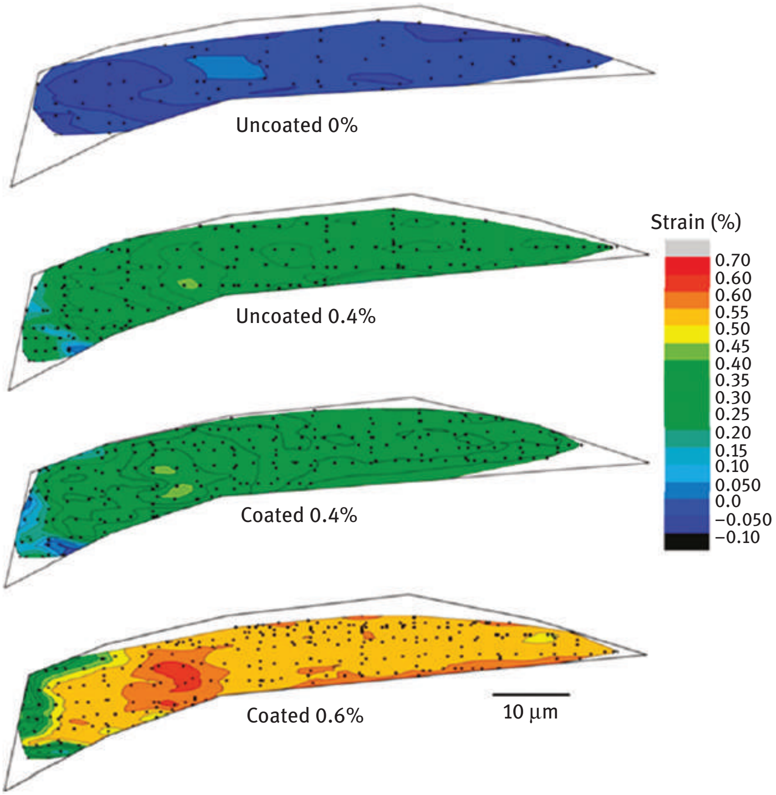

Figure 14.3: Raman maps of strain over the graphene monolayer at different levels of strain, in the uncoated and coated states. Adapted with permission from ACS NANO 5 (2011) 3079-3084. Copyright (2011) American Chemical Society [36].

strain levels applied in horizontal direction along the flake. Scale bar shows the relationship between the color of maps and graphene strain. The contour of the graphene flake around the maps is also shown. The black dots on the maps represent the points at which measurements were carried out. As seen from Figure 14.3, the first two maps were obtained for applied strains of 0 % and 0.4 % for graphene on PMMA beam without SU-8 top coating. These maps indicate that the strain in graphene is relatively uniform with some evidence of lower strain at the left-hand end at 0.4 % strain. Then, the specimen was unloaded, coated with SU-8, and reloaded to 0.4 % and 0.6 % strain, and Raman maps were obtained (see Figure 14.3). It is seen from Figure 14.3 that at 0.4 % strain the graphene strain distribution is virtually identical in both the uncoated and coated samples. Increasing the applied strain to 0.6 % strain causes the strain in the graphene to increase to around 0.6 % strain over most of the monolayer, with a lower level of strain at the left-hand end. The distribution of strain over a linear region along the middle of the long axis of the monolayer is presented in Figure 14.4. The increase in strain at the right-hand tip of the tapering monolayer can be explained in the same way as for the fibers in composites with differently shaped ends [36, 37]. If the fiber has a square end in cylindrical fiber, there is a gradual decrease in fiber strain toward the end of the fiber (left-hand end of graphene flake), whereas if the fiber has a conical tip, then for high-modulus reinforcements the strain actually rises as the fiber tapers (right-hand end of graphene flake) and drops to zero only very close to the end of the tip [37].

Further significant information related to stress transfer to the graphene monolayer at higher strain can be gathered from the Raman maps of strain in graphene (see Figure 14.5).

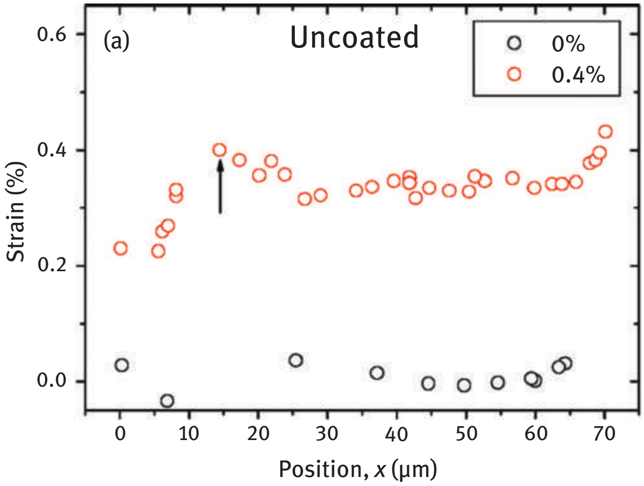

Figure 14.4: Variation in the strain in the graphene along the middle of the long axis of the monolayer for uncoated specimen. Adapted with permission from ACS NANO 5 (2011) 3079-3084. Copyright (2011) American Chemical Society [36].

As shown, the strain is relatively uniform around 0.15 % in the relaxed state, whereas if the applied strain is increased to 0.8 %, the strain distribution becomes very nonuniform in the graphene monolayer. Further analysis carried out for the specimen reloaded to 0.6 % applied strain (Figure 14.5) indicates that variation of strain along the middle of the long axis of the graphene flake changes quasi-periodically with the repetition within 10–20 µm. After repeated relaxation of the sample, the strain is less uniform than for the originally relaxed sample. After further reloading to 0.6 % applied strain, the strain distribution is very similar to that obtained for 0.8 % applied strain, but it is different than that obtained for the initially loaded specimen in which the distribution of strain was relatively uniform (see Figure 14.3). It probably indicates that the specimen was damaged by loading up to 0.8 % strain and the damage was retained on reloading to the lower strain [36]. The results presented by Young et al. indicated that Raman mapping can be used for the analysis of

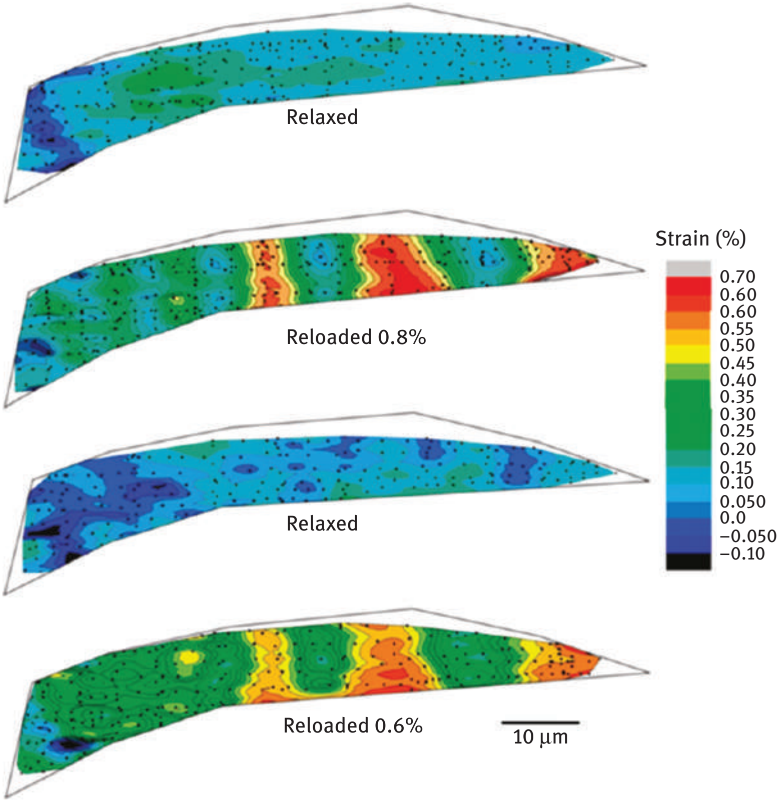

Figure 14.5: Raman maps of strain over the coated graphene monolayer in the relaxed states and reloaded to 0.8% and 0.6% strain. Adapted with permission from ACS NANO 5 (2011) 3079-3084. Copyright (2011) American Chemical Society [36].

strain distribution in specimens containing graphene and allows following the levels of reinforcement in such systems with high precision.

14.1.3 Polymer composites with carbon nanotubes

Owing to the application potential of CNTs in the production of molecular wires, the next generation of electronic devices, fibers with exceptionally high tensile length, novel thermoelectric materials, etc., new high-performance composite materials have been recently reported by many authors.

Yao et al. [20] have studied hybrid nanocomposites containing SWCNTs and PANI prepared in a simple one step by in situ polymerization reaction. Because of excellent electrical properties of SWCNTs much better than those of MWCNTs, resulting from fewer structure defects in the SWCNTs, both electrical conductivity and Seebeck coefficient of highly ordered chain structure of SWCNT/PANI nanocomposite are much enhanced with increasing SWCNT content. In this in situ polymerization process, the PANI could be considered to grow along the surface of SWCNTs because of the strong π–π interactions between the two components. Meanwhile, the chain packing of PANIs is also ordered due to the template effect of 1D nanostructured CNTs. Transmission electron Microscopy (TEM) and SEM images of SWCNT/PANI powder containing 25 wt % SWCNT are shown in Figure 14.6. The composites show nanocable structure in which a bundle of SWCNTs were coated and bounded by PANI.

Moreover, both X-ray diffraction and Raman spectra analyses confirmed the ordered chain packing of PANIs. Raman spectra analysis gives evidence for the ordering of PANI along SWCNT. As follows from Figure 14.7, the Raman spectrum

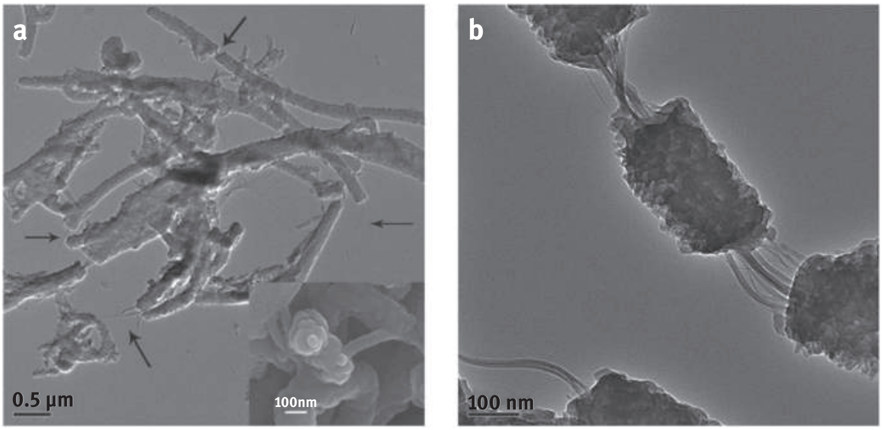

Figure 14.6: TEM images for SWCNT/PANI composites with 25 wt % SWCNT. Inset of (a) is the SEM top view of the nanocable. Adapted with permission from ACS NANO 4 (2010) 2445-2451. Copyright (2010) American Chemical Society [20].

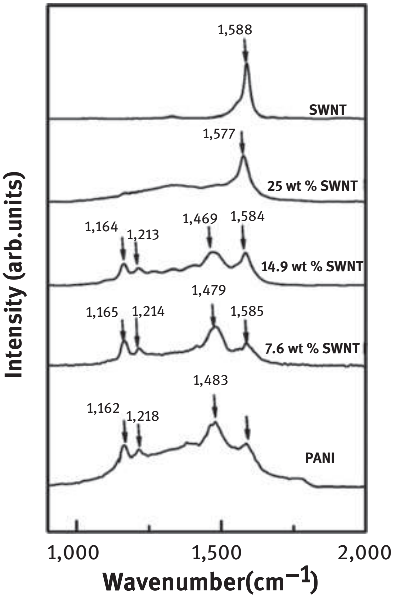

Figure 14.7: Raman spectra of SWCNT/PANI composites with different SWCNT content excited with 632.8 nm laser wavelength. Adapted with permission from ACS NANO 4 (2010) 2445-2451. Copyright (2010) American Chemical Society [20].

of pure CNTs shows a strong peak at 1,588 cm^{-1} assigned to the G band (in-plane stretching E_{2g} mode). For the pure PANI, C–H bending of the quinoid/benzenoid ring at 1,162 cm^{-1}, weak C–N stretching at 1,218 cm^{-1}, C=N stretching of the quinoid ring at 1,483 cm^{-1}, and C–C stretching of the benzenoid rings at 1,590 cm^{-1} are observed. It is worth noting that the intensity of modes at 1,483 cm^{-1} and 1,164 cm^{-1} decreases with increasing SWCNT content with a simultaneous increase in the intensity of the mode at 1,590 cm^{-1}. The decrease in the intensity of modes at 1,164 cm^{-1} and 1,483 cm^{-1} with increasing SWCNT content is attributed to the site-selective interactions between the quinoid rings and CNTs, which induce the chemical transformation of quinoid rings to benzenoid rings and cause the conformational changes of PANI from a coil-like structure to an extended one.

Increasing intensity of mode at 1,590 cm^{-1} suggests a decrease in the quinoid unit concentration and an increase in the benzenoid unit concentration. Moreover, it has been also found that all modes at 1,218, 1,483, and 1,590 cm^{-1} shift to the lower wavenumbers after addition of SWCNTs, which may result from the additional π–π conjugated interactions between the PANI and SWCNTs that induce the red shift of Raman modes. The ordered structures result in the increase in carrier mobility. In consequence, both electrical conductivity and Seebeck coefficient of the PANI-based polymer composites are dramatically improved as compared with those of pure PANI.

However, the thermal conductivities of the composites, even with high SWCTN content, do not change much and still keep very low values, which is attributed to the phonon scattering effect of nanointerfaces produced by the SWCNT/PANI nanocable structure [20, 38].

Successful applications of composites reinforced by addition of SWCNTs require well-dispersed nanotubes with good adhesion to the host matrix, which, unfortunately, is not easily realized. The reason for this is related to poor solubility of SWCNTs and weak nanotube–polymer interactions, and the poor adhesion causes nanotube aggregation within the matrix. One approach to in situ composite synthesis is the attachment of PS chains to full-length pristine SWCNTs without disrupting the original structure. Anionic polymerization process requires no nanotube pretreatment and works well with as-produced SWCNTs. In such a process, well-defined composites with a homogeneous dispersion of nanotubes were obtained. Carbanions are introduced on the SWCNT surface by treatment with the anionic initiators that serve to exfoliate the bundles and provide initiating sites for the polymerization of styrene (see Figure 14.8). When styrene is added, both free *sec*-butyllithium and the nanotube carbanions initiate polymerization, resulting in an intimately mixed composite system. The polymerization was terminated using degassed *n*-butanol, and the composite was recovered by precipitation with methanol [9].

Evidence for formation of carbanions and subsequent attachment of PS chains was obtained using Raman spectroscopy. The Raman spectra of pristine SWCNTs, butylated SWCNTs, and PS-grafted SWCNTs are presented in Figure 14.9.

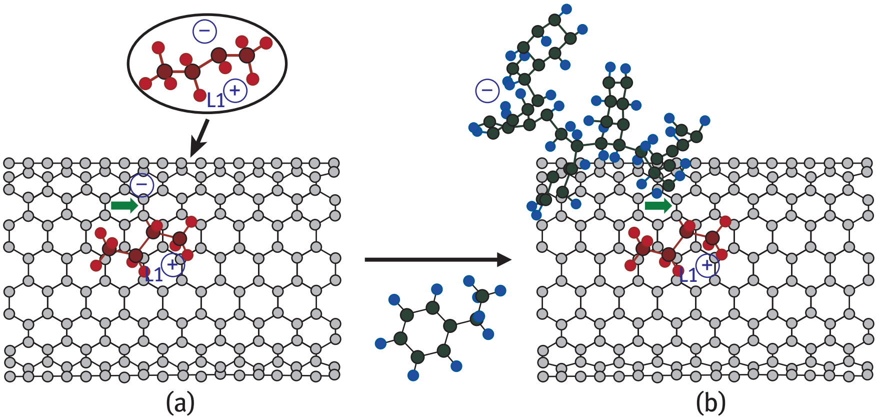

Figure 14.8: Schematic (not to scale) process of carbanions formation and subsequent initiation of polymerization: (a) section of SWCNT sidewall showing *sec*-butyllithium addition to a double bond (green arrow indicates the bond to which it adds) and formation of anion via transfer of charge; (b) the carbanions attacks the double bond in styrene and transfer the negative charge to the monomer. Successive addition of styrene results and a living polymer chain is formed. Adapted with permission from J. Am. Chem. Soc. 125 (2003) 9258-9259. Copyright (2003) American Chemical Society [9].

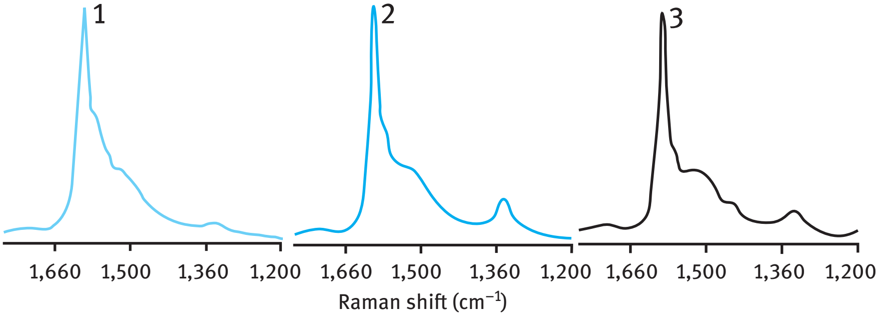

Figure 14.9: Raman spectra of (1) pristine SWCNTs, (2) butylated SWCNTs, and (3) PS-grafted SWCNTs recorded with 514.5 nm excitation laser wavelength. Adapted with permission from J. Am. Chem. Soc. 125 (2003) 9258-9259. Copyright (2003) American Chemical Society [9].

Apart from two characteristic Raman-active modes recorded for SWCNTs (E_{2g} and RBM), the third mode marked as D band, indicative of disorder or sp^3 character within the nanotube framework, is detected at about 1,320 cm^{-1}. As shown in Figure 14.9, the intensity of D band with respect to E_{2g} mode at about 1,580 cm^{-1} is indicative of the extent of covalent modification of the nanotube surface. In the Raman spectra of butylated and PS-grafted SWCNTs, the relative intensity of the D band increases when compared to that recorded for pristine SWCNTs. Analysis of the RBM wavenumbers was inconclusive because of the presence of characteristic C–X bending modes of PS in the same region, and no useful information could be obtained. Excessive chemical modification of the nanotube surface can lead to degradation of the nanotube mechanical strength and also result in the loss of electronic structure. It has been reported that nanotube electronic structure can be retained at low levels of functionalization [9, 39].

Li et al. [40] have reported the application of the Huisgen cycloaddition to functionalization of SWCNTs with PS. To achieve a high degree of functionalization, they chose to introduce alkyne groups on the nanotube surface using the Pschorr-type arylation, which was shown to modify a significant proportion of carbons within the nanotube sidewall. Subsequent introduction of PS was achieved by first installing an azide functionality at the polymer chain end. The Cu(I)-catalyzed formation of 1,2,3-triazoles by coupling azide-terminated polymer and alkyne-functionalized SWCNTs was found to occur in an efficient manner under a variety of favorable conditions. It resulted in relatively high nanotube graft densities, full control over polymer molecular weight, and good solubility in organic solvents [40].

Raman spectroscopy was not only used to verify the structural integrity of the modified SWCNT materials, but also to get the information on the degree of nanotube functionalization. Figure 14.10 presents the Raman spectra of pristine SWCNTs (A), alkyne-functionalized SWCNTs (B), and PS-functionalized SWCNTs (C). Spectrum A exhibits the characteristic RBM at about 250 cm^{-1} and tangential G mode at about

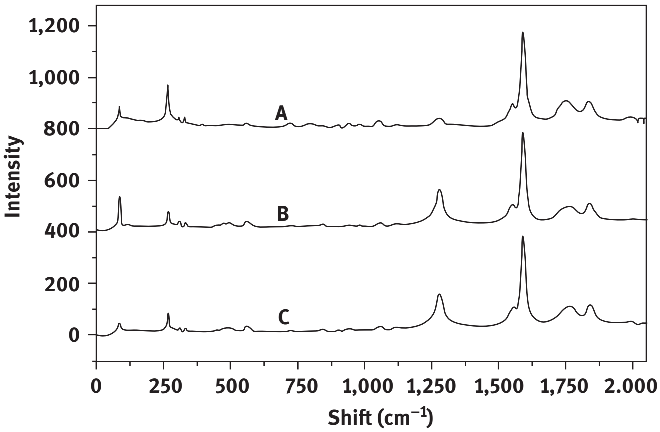

Figure 14.10: Raman spectra of (A) pristine SWCNTs, (B) alkyne-functionalized SWCNTs, and (C) polystyrene-functionalized SWCNTs. Adapted with permission from J. Am. Chem. Soc. 127 (2005) 14518-14524. Copyright (2005) American Chemical Society [40].

1,590 cm^{-1}. In addition, weak disorder band at about 1,290 cm^{-1} can be observed, indicating the presence of a small number of sp^3 hybridized carbons within the nanotube framework. Intensity of disorder band D increases dramatically relative to both the radial breathing and tangential modes, indicating that a large number of sp^2 hybridized carbons have been converted to sp^3 hybridization. The intensity of tangential mode also increased with respect to that of the RBM. Upon reaction with azide-functionalized PS, the intensity of the disorder band relative to the RBM and G modes remained unchanged, as expected, because the click reaction does not alter the hybridization of carbon atoms within the nanotube framework [40].

IR spectroscopy provided the information about the structures appended to the surface of the SWCNTs, which is not available from Raman data. Figure 14.11 presents the IR spectra of unmodified SWCNTs (spectrum A), the alkyne-functionalized SWCNTs (spectrum B), and the polymer-functionalized SWCNTs (spectrum C).

In spectrum A of unmodified SWCNTs, only one band around 3,500 cm^{-1} is recorded and assigned to trace the amount of water present in KBr used for preparation of pellet. However, spectrum B shows small, but clearly noticeable, signals at 2,120 and 3,280 cm^{-1}, corresponding to the C–C and C–H stretching vibrations of appended terminal alkyne functionalities, respectively. Additionally, the signals corresponding to the C–C and C–H stretches of the aromatic ring that serves as a linker between the nanotubes and the alkyne functionality can be seen at 1,660 and 2,920 cm^{-1}, respectively. Upon cycloaddition, the IR spectrum of the product (see Figure 14.11, spectrum C) bears the bands characteristic of PS, indicating that the polymer was grafted. Although the alkyne band at 2,120 cm^{-1} is weak, magnification of the three spectra in the spectral range 2,000–2,250 cm^{-1} indicates that it was not present prior to the

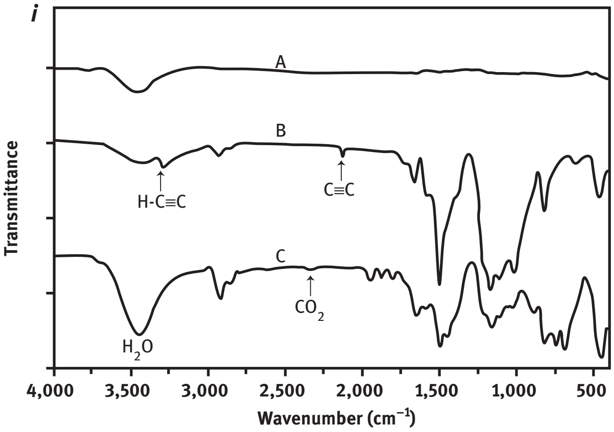

Figure 14.11: IR spectra of (A) pristine SWCNTs, (B) alkyne-functionalized SWCNTs, and (C) polystyrene-functionalized SWCNTs. Adapted with permission from J. Am. Chem. Soc. 127 (2005) 14518-14524. Copyright (2005) American Chemical Society [40].

reaction with *p*-aminophenyl propargyl ether or after the Huisgen cycloaddition. The disappearance of the alkyne stretching after the click coupling indicates that most of the alkynes must have been consumed during this reaction, although the low intensity of this IR absorption makes the quantitation of conversion difficult [40].

Yao et al. [13] have investigated the use of atom transfer radical polymerization (ATRP), which has been shown to be a highly versatile technique for the controlled radical polymerization of acrylate-based monomers from the surface of the CNTs. The nanotubes functionalized with poly(methyl methacryalte) were found to be insoluble, while those functionalized with poly(*tert*-butyl acrylate) were soluble in a variety of organic solvents. The resulting polymerized nanotubes were analyzed among others by IR and Raman spectroscopy.

Figure 14.12(A) presents the IR spectrum of a SWCNT specimen after 48 h of polymerization with MMA, clearly indicating the expected carbonyl stretching vibrational modes at about 1,730 cm^{-1} and C–H stretching at about 2,950 cm^{-1} attributed to nanotube-attached PMMA. The presence of CNTs in this residue was confirmed by Raman spectroscopy (Figure 14.12(B)), which revealed a tangential G band characteristic of them at about 1,590 cm^{-1} and RBMs at 184 and 205 cm^{-1}, corresponding to 1.2 and 1.1 nm diameter tubes, respectively. The peak at 1,338 cm^{-1} corresponds to the presence of relatively small amount of sp^3-hybridized carbon atoms, formed as a result of sidewall functionalization.

This combination of IR and Raman data indicates that both components are present in the sample and cannot be separated by washing with good polymer solvents. It should be noted that in control experiment, in which nanotubes were mixed with preformed PMMA, filtration and washing resulted in complete removal of

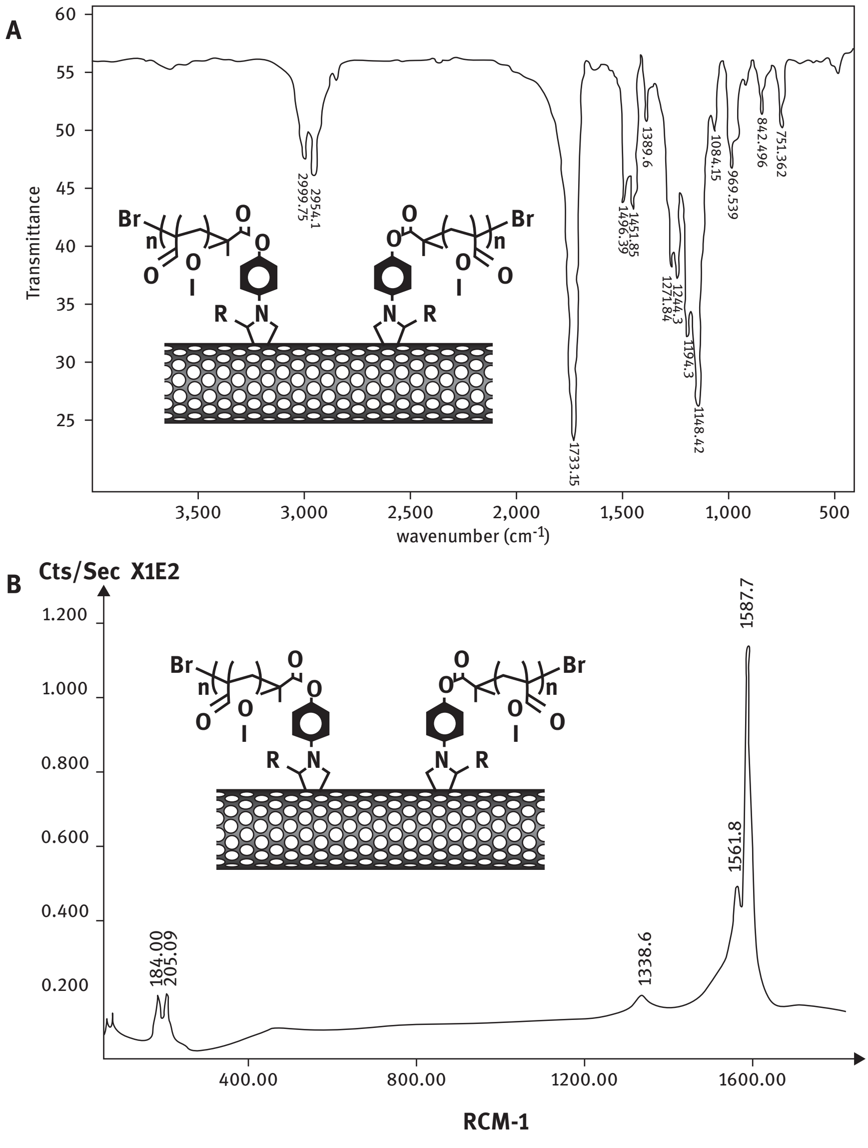

Figure 14.12: IR spectrum (A), Raman spectrum (B) of SWCNT-PMMA polymerized product. Adapted with permission from J. Am. Chem. Soc. 125 (2003) 16015-16024. Copyright (2003) American Chemical Society [13].

the free polymer from nanotube residue, as indicated by the absence of IR stretches at about 1,730 and 2,900 cm^{-1} [13].

The IR and Raman spectra of poly(*tert*-butyl acrylate)-functionalized SWCNTs are presented in Figure 14.13(A) and (B). Characteristic bands at about 1,730 and

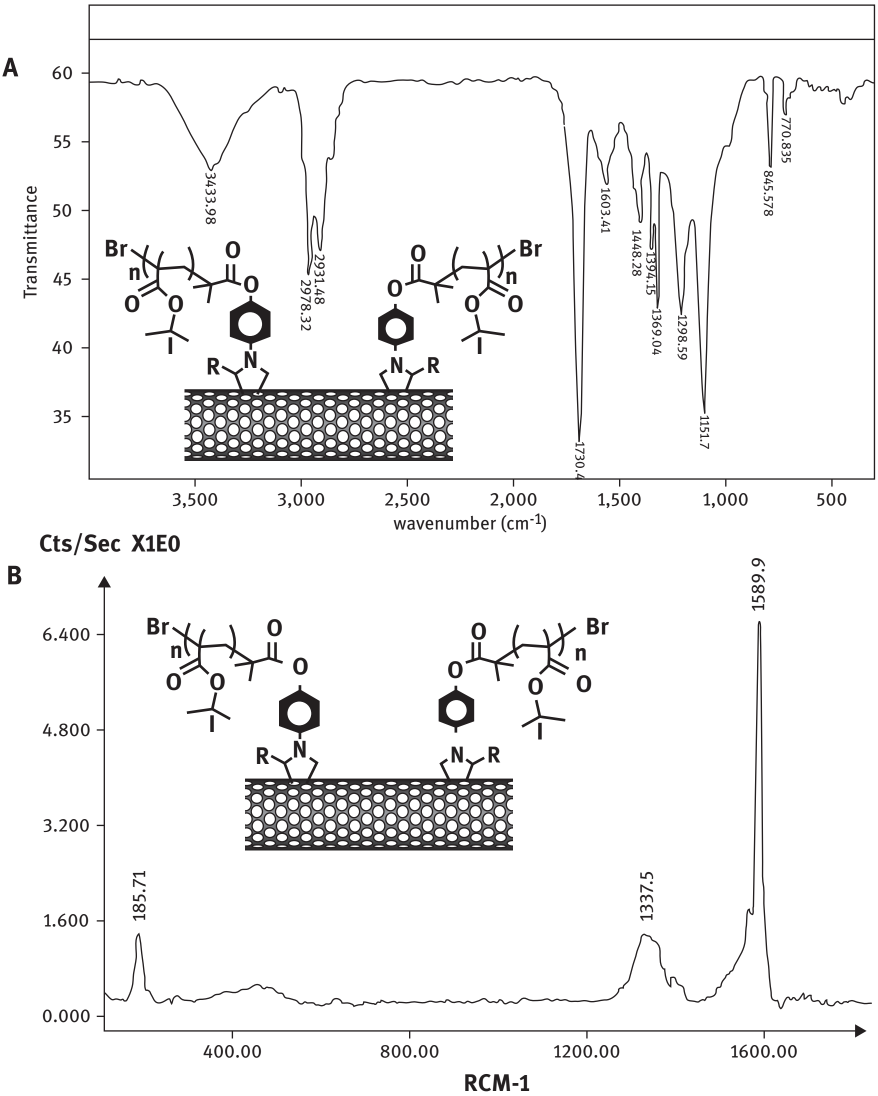

Figure 14.13: IR spectrum (A), Raman spectrum (B) of poly(tert-butyl acrylate)-functionalized SWCNTs nanocomposite. Adapted with permission from J. Am. Chem. Soc. 125 (2003) 16015-16024. Copyright (2003) American Chemical Society [13].

2,950 cm^{-1} attributed to stretching vibrations in the IR absorption spectrum indicate the presence of polymer, while the Raman bands detected at about 185 and 1,590 cm^{-1} correspond to the RBMs and tangential modes of SWCNT. It is not entirely clear why the RBM in this sample corresponds solely to nanotubes having a diameter of 1.2 nm, but this is likely due to heterogeneity of different batches of starting material. In addition, there is the band at 1,338 cm^{-1} corresponding to the presence of sp^3-hybridized carbon atoms within the nanotubes formed as a result of the functionalization process. This disorder peak is proportional to the extent of nanotube functionalization.

14.1.4 Polymer composites with GNRs

Polymer-functionalized graphene nanoribbons (PF-GNRs) can be promising low-cost materials that could be useful for transparent electrodes and heat circuits, electroactive polymer/graphene supercapacitors, and conductive nanocomposites. The synthetic strategy for the one-pot synthesis of PF-GNRs is shown in Figure 14.14. MWCNTs were converted into edge-negatively charged polymerization macroinitiators via intercalation and splitting. On the basis of the proposed mechanism, it is assumed that the edges of the split tubes are lined by aryl anions and associated to them metal cations. Moreover, anionic polymerization of vinyl monomers starting at

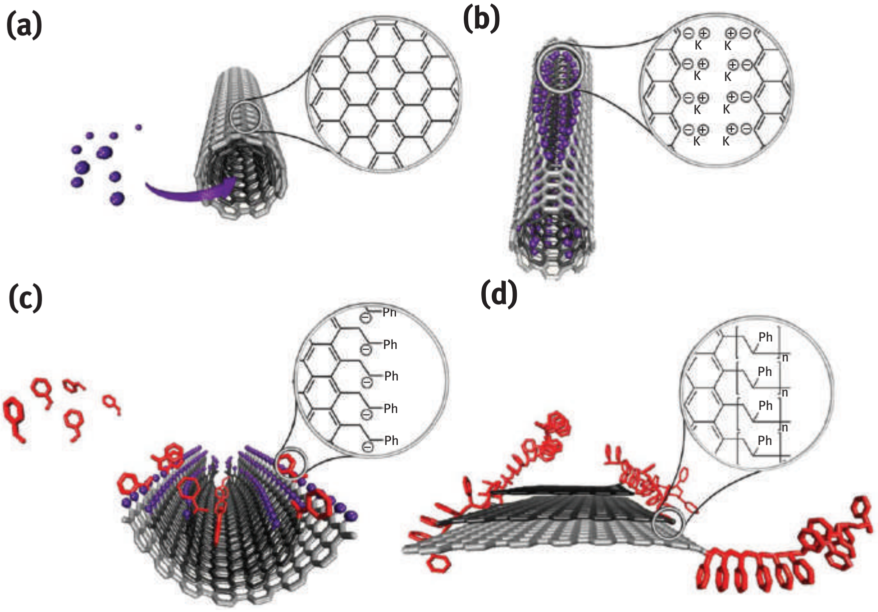

Figure 14.14: Reaction scheme for the one-pot synthesis of functionalized GNRs. (a) The NWCNTs are intercalated with potassium naphthalenide (blue dots). (b) A longitudinal fissure is formed in the walls of the MWCNTs due to expansion caused by intercalation of THF-stabilized potassium ions into the MWCNT host. The edge radicals would be immediately reduced to the corresponding anions under the reducing conditions. (c) Polymerization of styrene (for instance) assists in exfoliation of MWCNTs. (d) PF-GNRs are formed upon quenching. Adapted with permission from ACS NANO 7 (2013) 2669-2675. Copyright (2013) American Chemical Society [1].

the negatively charged GNR edges results in PF-GNRs. The potassium naphthalenide liquid-phase intercalation is described below along with the relevant methodology. Briefly, MWCNTs, potassium metal, naphthalene, and THF (tetrahydrofuran) are placed in a Schlenk flask and subjected to three freeze–pump–thaw cycles to remove oxygen. The intercalation of solvent-stabilized potassium cations into MWCNTs may lead to expansion of the *d*-space between MWCNT layers, causing the MWCNTs to partially or fully split. The fissures in the sidewalls of the MWCNTs serve as the starting points for vinyl or epoxide monomers to anionically polymerize from the GNR edges. Because of polymerization probably proceeding between the GNR layers, only a small amount of olefin is needed to effect the exfoliation of the MWCNTs. The nonattached polymer was removed by extracting the raw product with boiling chloroform in a Soxhlet extractor [1].

Raman spectroscopy was used to characterize the graphitic structure of the PF-GNRs. An increase in the intensity of the D band over the G band from 0.15 for MWCNTs to 0.35 PF-GNRs was observed in Figure 14.15.

Upon splitting of MWCNTs, a prominent D band is an indication of disorder in the graphene structure due to the high edge content. The disordered structure also results in slight broadening of the G band and the 2D band, as well as a combination of D + G bands at 2,700 cm^{-1} in PF-GNRs. However, a splitting of the G band, corresponding to an intercalated graphitic structure, is not observed in the Raman spectrum, implying that little residual intercalants, if any, or solvents are left between the PF-GNRs [1].

To explore the flexibility of the proposed protocol, two other sources of MWCNTs, NanoTechLabs MWCNTs (NTL MWCNTs) and Bayer MWCNTs (Baytubes), were subjected to the reaction to compare the results to those obtained

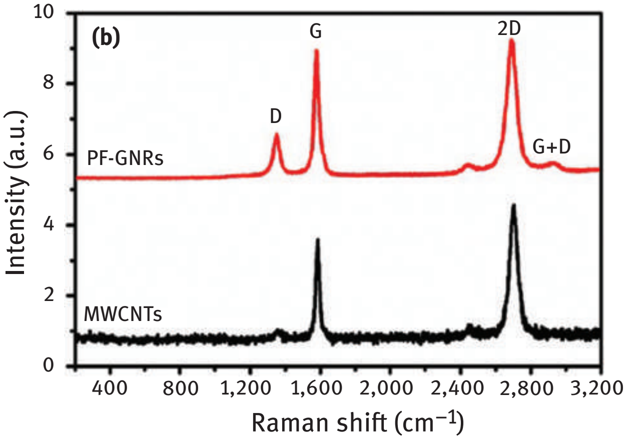

Figure 14.15: Raman spectra of PF-GNRs and starting MWCNTs. Adapted with permission from ACS NANO 7 (2013) 2669-2675. Copyright (2013) American Chemical Society [1].

when the Mitsui MWCNTs were used in the former two experiments. Upon liquid-phase intercalation followed by polymerization, NTL MWCNTs were split but not further flattened to form GNRs (Figure 14.16(a)). With the Baytubes MWCNTs, although some partially flattened GNRs could be identified, most of the MWCNTs remained intact (Figure 14.16(b)).

Raman spectroscopy was used to differentiate the degree of disorder in the structure of the host materials by calculating the intensity ratio of D to G band. The ratio of intensities of disorder-induced D band to that of crystalline G band, I_D/I_G is 0.15 for Mitsui MWCNTs, 0.27 for NTL MWCNTs, and 0.92 for Baytubes, as shown in Figure 14.17.

Defect sites on graphite do not favor the formation of well-defined intercalation structure and thus, the complete exfoliation of highly defective Baytubes by

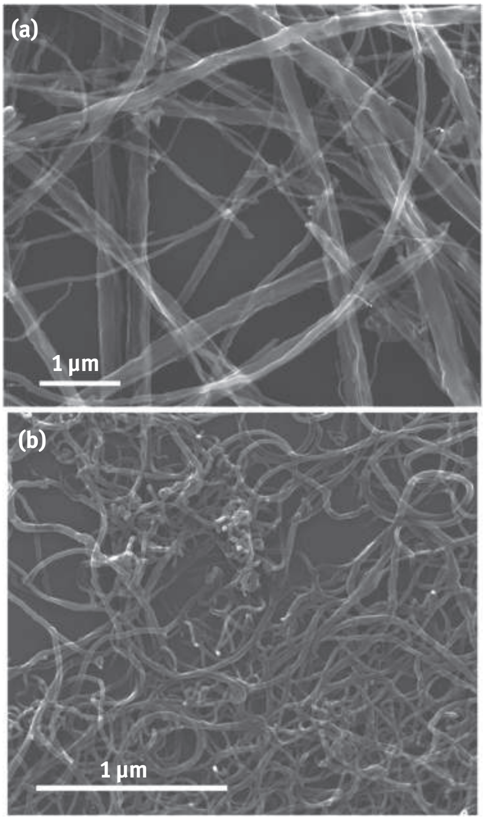

Figure 14.16: (a) SEM image of NTL MWCNTs treated with potassium naphthalenide in THF followed by addition of styrene. (b) SEM image of Baytubes treated with potassium naphthalenide in THF followed by the addition of styrene. Adapted with permission from ACS NANO 7 (2013) 2669-2675. Copyright (2013) American Chemical Society [1].

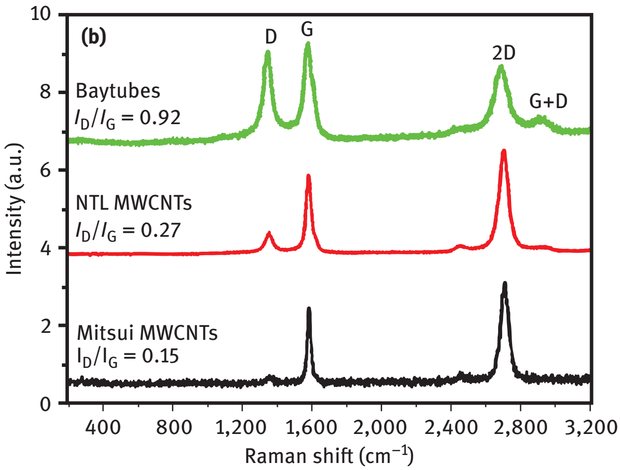

Figure 14.17: Raman spectra of Mitsui MWCNTs, NTL MWCNTs and Baytubes. Adapted with permission from ACS NANO 7 (2013) 2669-2675. Copyright (2013) American Chemical Society [1].

intercalation is likely to be more difficult. This is corroborated by recent work on reductive alkylation of MWCNTs with potassium naphthalenide, in which the outer surface of highly defective MWCNTs ($I_D/I_G > 1$) was functionalized with decanoic acid and ribbon-like structure was observed in the SEM images. Although NTL MWCNTs have fewer defects, flattening of ultra-long split tubes may require further treatment. Most NTL MWCNTs remained split and stacked rather than completely flattened. It is difficult to precisely establish the structural threshold (i. e. the critical value for I_D/I_G) that should be used to predict if the MWCNTs can be split and exfoliated; however, it is noteworthy that the higher the degree of graphitization of the carbon host or the less defective the carbon host, the easier the exfoliation of the MWCNTs via intercalation. The PF-GNRs or split tubes could be used for reinforcing polymers, since the sword-in-sheath type failure of MWCNTs due to interlayer slip could be retarded owing to the entangled polymer chains anchored at the edges. Through the compatibilizing appended polymer chains, the load might be effectively transferred from the polymer matrix to the rigid PF-GNRs, thus making stronger composites [1].

14.1.5 Examples of other polymer composites

Hybrid materials, the composites that combine attractive qualities of dissimilar materials, have received great interest because of a wide range of mechanical, electronic, biological, and optical application. Boettcher et al. [24] have reported the synthesis and characterization of highly ordered, stable, titania-based hybrid optical materials, fabricated from self-assembling block copolymers (P123 or F127) and trifluoroacetic acid (TFAA)-modified titania precursors, from molecular to macroscopic length scale. To achieve a deep understanding of a hybrid material's structure, it is necessary to investigate a hierarchy of size scales with a diverse array of analysis techniques. Analysis on molecular level considering bonding interactions can be carried out using IR and Raman spectroscopy. In the intermediate mesoscale size regime, SAXS (small-angle X-ray scattering) and TEM are used to understand the assembly and structure of ordered hexagonal and cubic mesostructures. The chemical bonding mode between the carboxylic acid groups and the titanium centers was investigated by IR and Raman spectroscopy, among the most well-developed analytical techniques for the characterization of organometallic complexes. The IR vibrations of the hybrid sample were assigned by comparison with the IR spectra of the individual components as well as literature sources [41]. The observed IR/Raman spectra show TFA–Ti asymmetric ($\nu_{as} = 1{,}653\,\text{cm}^{-1}$) and symmetric ($\nu_{sym} = 1{,}464\,\text{cm}^{-1}$) carboxylate stretching vibrational modes (see Figure 14.18).

Low-intensity stretching vibrations of free TFAA at $1{,}781\,\text{cm}^{-1}$ are apparent in the freshly dipped films but completely disappear within 20 min of drying at room temperature. Identical vibrational transitions are observed in the ethanolic precursor solution. The difference between carboxylate stretching modes wavenumbers $\Delta = \nu_{as} - \nu_{sym}$ is useful in identifying the bonding mode of the carboxylate ligand (see Figure 14.19).

Generally, monodentate complexes (Figure 14.19(A)) exhibit Δ values much higher than those of the corresponding ionic structure (i. e. sodium trifluoroacetate). Bidentate chelating complexes (Figure 14.19(B)) exhibit Δ values significantly

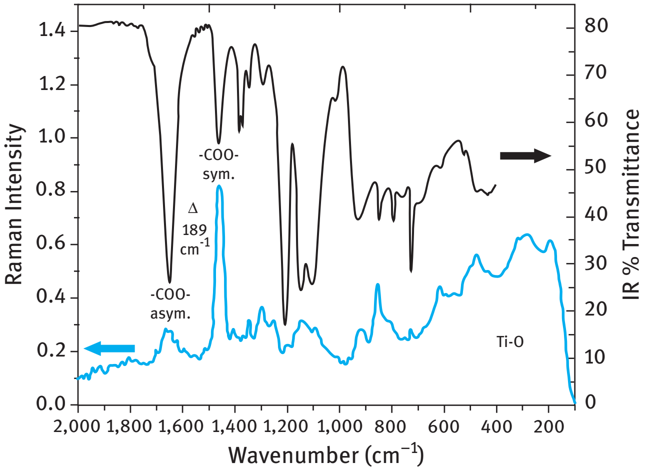

Figure 14.18: IR/Raman spectra of the hybrid material. TFA carboxylic acid stretches are indicative of bidentate bridging/chelation of the titanium center, and Ti–O stretches suggest rutile-like coordination in the amorphous inorganic. Adapted with permission from J. Am. Chem. Soc. 127 (2005) 9721-9730. Copyright (2005) American Chemical Society [24].

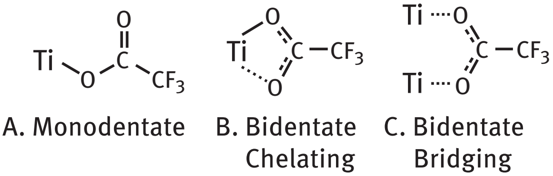

Figure 14.19: Carboxylate coordination modes. Adapted with permission from J. Am. Chem. Soc. 127 (2005) 9721-9730. Copyright (2005) American Chemical Society [24].

smaller than the ionic values, and bridging complexes (Figure 14.19(C)) have the delta values less than, but close to, the ionic value. The observed Δ value for the hybrid material is 189 cm^{-1}, much smaller than that for isolated hydrogen bonded dimers (345 cm^{-1}) or the sodium salt (252 cm^{-1}). This establishes that TFA binds to the titanium center in a bidentate bridging or chelating fashion (Figure 14.19(C) or (B)), both in solution and in the final hybrid. Because chelation (Figure 14.19(B)) strains the ~120° free carboxylate OCO bond angle, it is supposed that the TFA ligands bridge adjacent oxo/hydroxybridged titanium atoms (Figure 14.19(C)) within the amorphous hybrid material. The three broad, full-width-at-half-maximum (fwhm) 50–100 cm^{-1}, Raman modes positioned at about 600, 475, and 280 cm^{-1} (see Figure 14.18) can be attributed to the Ti–O– network [42] and correspond approximately to the three vibrational transitions of the rutile phase of TiO_2 (612, 447, 232 cm^{-1}) [43]. The shoulder peaks in this region were identified as corresponding to structural deformations of the TFA ligand. The Raman data suggest that the nearest neighbor environment around the central Ti ions consists of an octahedral "rutile-like" oxygen coordination, consistent with previous studies on acetic acid-modified titanium alkoxides. The lack of long-range order between complexed titania species leads to an overall amorphous network [24].

Conducting polymers can be expected to serve as molecular wires connecting organic molecules and electrodes; therefore, many attempts have been made to elucidate the properties of single conducting polymer chains [44, 45]. Confinement of polymer chains in porous materials is a feasible method to isolate single polymer chains, permitting the study of their properties, such as conductivity and fluorescence of macromolecules in nanochannels of zeolites, nanoporous silicas, and organic crystalline hosts [46–49]. Kitao et al. [50] have reported the incorporation of polysilane into the nanochannels of porous coordination polymers (PCPs) as individual chains. Polysilanes exhibit unique optical and electrical properties, such as backbone electronic transition with UV-vis absorption, high quantum yield of fluorescence, and high mobility of charge carriers [51, 52], which are attributed to delocalization of σ-electrons along the main chains. The conformation of polymer chain, which is sensitive to temperature and to solvent, strongly influences the σ-conjugation system. However, the σ-conjugation of polysilane becomes inefficient under UV exposure because of photodegradation. Therefore, improvement in photostability is highly desirable for light-emitting devices and solar cells [53].

Host–guest composites of 1⊃PMPrS were fabricated by inclusion of polymethylpropysilane (PMPrS) in the nanochannels of two PCPs with distinct channel size (Figure 14.20). The used PCPs can be described by the following chemical formula $[Al(OH)(L)]_n$ in which the ligand (L) corresponds to 2,6-naphthalenedicarboxylate (DUT-4, marked as 1a) and 4,4'-biphenyldicarboxylene (DUT-5, marked as 1b), see Figure 14.20.

The molecular conformation of PMPrS encapsulated in PCP was investigated using Raman spectroscopy. Figure 14.21 presents the room temperature Raman spectra of 1a, 1b, 1a⊃PMPrS, 1b⊃PMPrS and bulk PMPrS and Raman spectra of bulk PMPrS and 1a⊃PMPrS recorded at 80 °C. The intensity of the peak corresponding to the symmetric stretching vibrations ν(Si–C) at about 670 cm^{-1} strongly depends on the main chain conformation. The relative intensity of this peak increases with increasing amount of s-trans conformation. The intensity of the ν(Si–C) peak of

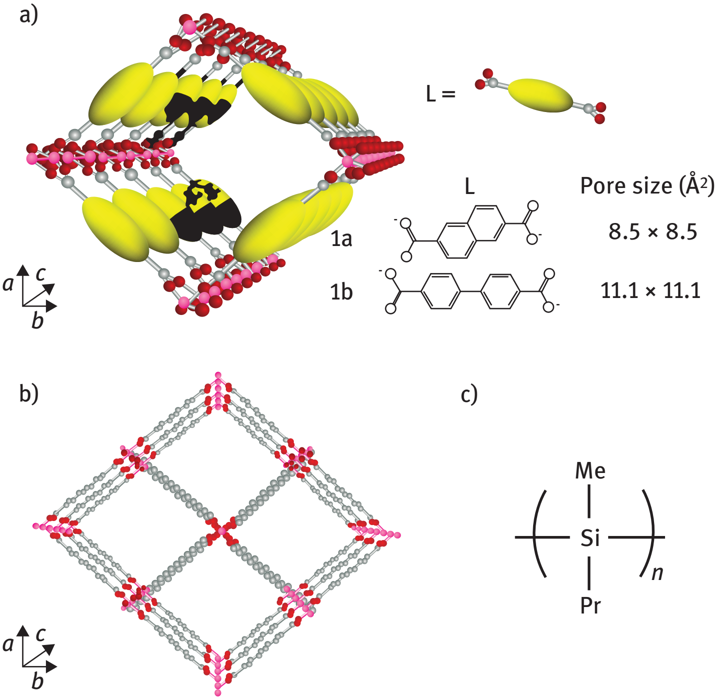

Figure 14.20: (a) Schematic image of nanochannel structures of PCP hosts. [Al(OH)L]n (Al, pink; O, red; C, gray; 1a, L = 2,6-naphthalenadicarboxylate; 1b, L = 4,4'-biphenyldicarboxylate). (b) X-ray structures of 1a (Al, pink; O, red; C, gray). Hydrogen atoms are omitted for clarity. (c) Molecular structure of polymethylpropylsilane. Adapted with permission from J. Am. Chem. Soc. 137 (2015) 5231-5238. Copyright (2015) American Chemical Society [50].

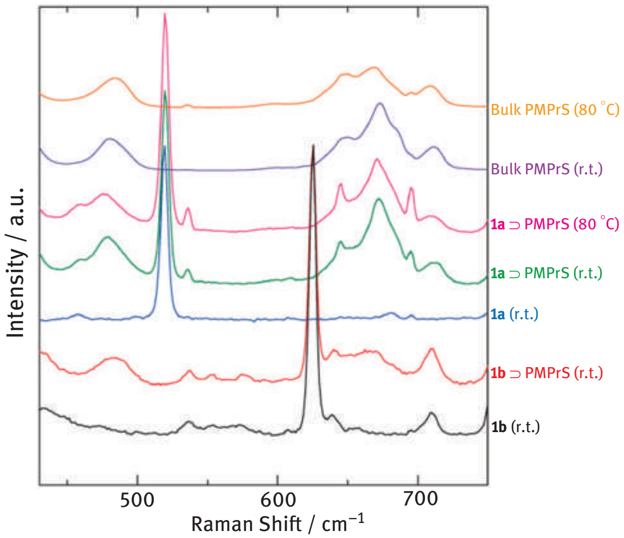

Figure 14.21: Varible temperature Raman spectra of 1, 1⊃PMPrS, and bulk PMPrS. Adapted with permission from J. Am. Chem. Soc. 137 (2015) 5231-5238. Copyright (2015) American Chemical Society [50].

1a⊃PMPrS was higher than that of 1b⊃PMPrS, indicating that PMPrS chains preferred to form a linear structure with increasing s-trans conformation in the smaller channels of 1a. At room temperature, the intensity of the ν(Si–C) peak of bulk PMPrS is similar to that of 1a⊃PMPrS. This is because bulk PMPrS includes chains of s-trans conformation. On heating the bulk PMPrS from room temperature to 80 °C, the intensity of the peak underwent a large change, which showed the transformation from solid to liquid states accompanied by a large conformational change in the PMPrS chains. However, it was striking that the intensity of PMPrS in 1a was almost unchanged at the same temperature of 80 °C (Figure 14.21). A stretched conformation of PMPrS resulted from the confinement effect of 1a, in which the PMPrS chains were forced to form an extended linear structure in the narrow 1D channels [50].

14.2 Summary

Vibrational spectroscopy can be a very useful tool for characterization of different types of materials. Although infrared absorption spectroscopy is a method complementary to Raman spectroscopy, however, it is not as versatile, useful, and informative as Raman spectroscopy. For many composite materials, especially those containing carbon allotropes, Raman spectroscopy can be a basic and widely used characterization technique. Moreover, polymers and other compounds used in composite materials possess their own vibrational fingerprints, so the vibrational spectroscopy methods can appear as essential characterization techniques. However, it is obvious that in the case of some complex hybrid materials, vibrational spectroscopy methods are not the only characterization methods but they are often useful, informative, and quite easy to apply.

References

[1] Lu W, Ruan G, Genorio B, Zhu Y, Novosel B, Peng Z, et al. Functionalized graphene nanoribbons via anionic polymerization initiated by alkali metal-intercalated carbon nanotubes. ACS Nano. 2013;7:2669–2675.
[2] Steenackers M, Gigler AM, Zhang N, Deubel F, Seifert M, Hess LH, et al. Polymer brushes on graphene. J Am Chem Soc. 2011;133:10490–10498.
[3] Viskadouros GM, Stylianakis MM, Kymakis M, Stratakis E. Enhanced field emission from reduced graphene oxide polymer composites. ACS Appl Mater Interfaces. 2014;6:388–393.
[4] Engelsen DE. The temptation of the field emission displays. Phys Proc. 2008;1:355–365.
[5] Stratakis E, Giorgi R, Barberoglou M, Dikonimos T, Salemitano E, Lisi N, et al. Three-dimensional carbon nanowall field emission arrays. Appl Phys Lett. 2010;96:043110.
[6] Jha A, Ghorai UK, Banerjee D, Mukherjee S, Chattopadhyay KK. Surface modification of amorphous carbon nanotubes with copper phthalocyanine leading to enhanced field emission. RSC Adv. 2013;3:1227–1234.
[7] Abdou JP, Braggin GA, Luo Y, Stevenson AR, Chun D, Zhang S. Graphene-induced oriented interfacial microstructures in single fiber polymer composites. ACS Appl Mater Interfaces. 2015;7:13620–13626.
[8] Kumar S, Raj S, Kolanthai E, Sood AK, Sampath S, Chatterjee K. Chemical functionalization of graphene to augment stem cell osteogenesis and inhibit biofilm formation on polymer composites for orthopedic applications. ACS Appl Mater Interfaces. 2015;7:3237–3252.
[9] Viswanathan G, Chakrapani N, Yang H, Wei B, Chung H, Cho K, et al. Single-step in situ synthesis of polymer–grafted single-wall nanotube composites. J Am Chem Soc. 2003;125:9258–9259.
[10] Dai HJ. Carbon nanotubes: opportunities and challenges. Surf Sci. 2002;500:218–241.
[11] Huang Y, Duan XF, Wei QQ, Lieber CM. Directed assembly of one-dimensional nanostructures into functional networks. Science. 2001;291:630–633.
[12] Hirsch A. Functionalization of single-walled carbon nanotubes. Angew Chem Int Ed. 2002;41: 1853–1859.
[13] Yao Z, Braidy N, Botton GA, Adronov A. Polymerization from the surface of single-walled carbon nanotubes - preparation and characterization of nanocomposites. J Am Chem Soc. 2003;125: 16015–16024.
[14] Ding W, Eitan A, Fisher FT, Chen X, Dikin DA, Andrews R, et al. Direct observation of polymer sheathing in carbon nanotube–polycarbonate composites. Nano Lett. 2003;3:1593–1597.
[15] Xu H, Wang X, Zhang Y, Liu S. Single-step in situ preparation of polymer–grafted multi-walled carbon nanotube composites under ^{60}Co γ-ray irradiation. Chem Mater. 2006;18:2929–2934.
[16] Hwang J-Y, Nish A, Doig J, Douven S, Chen C-W, Chen L-C, et al. Polymer structure and solvent effects on the selective dispersion of single-walled carbon nanotubes. J Am Chem Soc. 2008;130:3543–3553.
[17] Peng H. Aligned carbon nanotube/polymer composite films with robust flexibility, high transparency, and excellent conductivity. J Am Chem Soc. 2008;130:42–43.
[18] De S, Lyons PE, Sorel S, Doherty EM, King PJ, Blau WJ, et al. Transparent, flexible, and highly conductive thin films based on polymer–nanotube composites. ACS Nano. 2009;3:714–720.

[19] Hobbie EK, Fagan JA, Obrzut J, Hudson SD. Microscale polymer–nanotube composites. ACS Appl Mater Interfaces. 2009;1:1561–1566.

[20] Yao Q, Chen L, Zhang W, Liufu S, Chen X. Enhanced theromelectric performance of single-walled carbon nanotubes/polyaniline hybrid nanocomposites. ACS Nano. 2010;4:2445–2451.

[21] Yang PD, Wirnsberger G, Huang HC, Cordero SR, McGehee MD, Scott B, et al. Mirrorles lasing from mesostructured waveguides patterned by soft lithography. Science. 2000;287:465–467.

[22] Alberius PCA, Frindell KL, Hayward RC, Kramer EJ, Stucky GD, Chmelka BF. General predictive syntheses of cubic, hexagonal, and lamellar silica and titania mesostructured thin films. Chem Mater. 2002;14:3284–3294.

[23] Bartl MH, Boettcher SW, Hu EL, Stucky GD. Dye-activated hybrid organic/inorganic mesostructured titania waveguides. J Am Chem Soc. 2004;126:10826–10827.

[24] Boettcher SW, Bartl MH, Hu JG, Stucky GD. Structural analysis of hybrid titania-based mesostructured composites. J Am Chem Soc. 2005;127:9721–9730.

[25] Morin SA, Amos FF, Jin S. Biomimetic assembly of zinc oxide nanorods onto flexible polymers. J Am Chem Soc. 2007;129:13776–13777.

[26] Zhang Y, Wang Y, Deng Y, Li M, Bai J. Enhanced dielectric properties of ferroelectric polymer composites induced by metal-semiconductor Zn-ZnO Core–shell structure. ACS Appl Mater Interfaces. 2012;4:65–68.

[27] Yuan C, Duan B, Li L, Xie B, Huang M, Luo X. Thermal conductivity of polymer-based composites with magnetic aligned hexagonal boron nitride platelets. ACS Appl Mater Interfaces. 2015;7: 13000–13006.

[28] Roy D, Chhowalla M, Wang H, Sano N, Alexandrou I, Clyne TW, et al. Characterisation of carbon nano-onions using Raman spectroscopy. Chem Phys Lett. 2003;373:52–56.

[29] Gouadec G, Colomban P. Raman spectroscopy of nanomaterials: How spectra relate to disorder, particle size and mechanical properties. Prog Cryst Growth Charact. 2007;53:1–56.

[30] Ferrari AC, Robertson J. Interpretation of Raman spectra of disordered and amorphous carbon. Phys Rev B. 2000;61:14095–14107.

[31] Dienig T, Hollricher O, Toporski J. Confocal Raman microscopy. Berlin Heidelberg: Springer-Verlag, 2010.

[32] Frank O, Tsoukleri G, Riaz I, Papagelis K, Parthenios J, Ferrari AC, et al. Development of a universal stress sensor for graphene and carbon fibres. Nat Commun. 2011;2:1–6.

[33] Gong L, Young RJ, Kinloch IA, Riaz I, Jalil R, Novoselov KS. Optimizing the reinforcement of polymer–based nanocomposites by graphene. ACS Nano. 2012;6:2086–2095.

[34] Ni ZH, Yu T, Lu YH, Wang YY, Feng YP, Shen ZX. Uniaxial strain on graphene: Raman spectroscopy study and band-gap opening. ACS Nano. 2008;2:2301–2305.

[35] Tsoukleri G, Parthenios J, Papagelis K, Jalil R, Ferrari AC, Geim AK, et al. Subjecting a graphene monolayer to tension and compression. Small. 2009;5:2397–2402.

[36] Young RJ, Gong L, Kinloch IA, Riaz I, Jalil R, Novoselov KS. Strain mapping in a graphene monolayer nanocomposite. ACS Nano. 2011;5:3079–3084.

[37] Goh KL, Meakin JR, Hukins DWL. Influence of fiber taper on the interfacial shear stress i fiber-reinforced composites materials during elastic stress transfer. Compos. Interfaces. 2010;17: 75–81.

[38] Zengin H, Zhou W, Jin J, Czerw R, Smith DW. Carbon nanotube doped polyaniline. Adv Mater. 2002;14:1480–1483.

[39] Holzinger M, Vostrowsky O, Hirsch A, Hennrich F, Kappes M, Weiss R, et al. Sidewall functionalization of carbon nanotubes. Angew Chem Int Ed. 2001;40:4002–4005.

[40] Li H, Cheng F, Duft AM, Adronov A. Functionalization of single-walled carbon nanotubes with well-defined polystyrene by “click” coupling. J Am Chem Soc. 2005;127:14518–14524.

[41] Socrates G. Infrared characteristic group frequencies. New York: Wiley, 1980.

[42] Venz PA, Kloprogge JT, Frost RL. Chemically modified titania hydrolysates: Physical properties. Langmuir. 2000;16:4962–4968.

[43] Felske A, Plieth WJ. Raman spectroscopy of titanium dioxide layers. Electrochim Acta. 1989;34: 75–77.

[44] Grozema FC, Siebbeles LDA, Warman JM, Seki S, Tagawa S, Scherf U. Hole conduction along molecular wires: σ-bonded silicone versus π-bond-conjugated carbon. Adv Mater. 2002;14: 228–231.

[45] Okawa Y, Aono M. Materials science: Nanoscale control of chain polymerization. Nature. 2001;409:683–684.

[46] Sozzani P, Comotti A, Bracco S, Simonutti R. A family of supramolecular frameworks of polyconjugated molecules hosted in aromatic nanochannels. Angew Chem Int Ed. 2004;43: 2792–2797.

[47] Nguyen TQ, Wu JJ, Doan V, Schwartz BJ, Tolbert SH. Control of energy transfer in oriented conjugated polymer-mesoporous silica composites. Science. 2000;288:652–656.

[48] Uemura T, Horike S, Kitagawa K, Mizuno M, Endo K, Bracco S, et al. Conformation and molecular dynamics of single polystyrene chain confined in coordination nanospace. J Am Chem Soc. 2008;130:6781–6788.

[49] Cucinotta F, Carniato F, Paul G, Bracco S, Bisio C, Caldarelli S, et al. Incorporation of a semiconductive polymer into mesoporous SBA-15 platelets: Toward new luminescent hybrid materials. Chem Mater. 2011;23:2803–2809.

[50] Kitao T, Bracco S, Comotti A, Sozzani P, Naito M, Seki S, et al. Confinement of single polysilane chains in coordination nanospaces. J Am Chem Soc. 2015;137:5231–5238.

[51] Fujiki M. A correlation between global conformation of polysilane and UV absorption characteristics. J Am Chem Soc. 1996;118:7424–7425.

[52] Harrah LA, Zeigler JM. Electronic spectra of polysilanes. Macromolecules. 1987;20:601–608.

[53] Kamata N, Terunuma D, Ishii R, Satoh H, Aihara S, Yaoita Y, et al. Efficient energy transfer from polysilane molecules and its application to electroluminescence. J Organomet Chem. 2003;685:235–242.

Lorenc Gavilà, Edgar J Güell, Biniam T Maru, Francesc Medina and Magda Constantí

15 Combining catalytical and biological processes to transform cellulose into high value-added products

Abstract: Cellulose, the most abundant polymer of biomass, has an enormous potential as a source of chemicals and energy. However, its nature does not facilitate its exploitation in industry. As an entry point, here, two different strategies to hydrolyse cellulose are proposed. A solid and a liquid acid catalysts are tested. As a solid acid catalyst, zirconia and different zirconia-doped materials are proved, meanwhile liquid acid catalyst is carried out by sulfuric acid. Sulfuric acid proved to hydrolyse 78 % of cellulose, while zirconia doped with sulfur converted 22 % of cellulose. Both hydrolysates were used for fermentation with different microbial strains depending on the desired product: Citrobacter freundii H3 and Lactobacillus delbrueckii, for H_2 or lactic acid production respectively. A measure of 2 mol H_2/mol of glucose was obtained from the hydrolysate using zirconia with Citrobacter freundii; and Lactobacillus delbrueckii transformed all glucose into optically pure D-lactic acid.

Keywords: cellulose, fermentation, hydrolysis

15.1 Introduction

Currently, the source of about 85 % of all the energy used on the planet is fossil fuel [1]. As a result, pollution is a concerning problem all over the world; in addition petroleum reserves are depleting so rapidly that soon its demand will surpass its production. The development of clean and sustainable alternative sources of energy is, therefore, a global priority.

Biomass is an organic material that stores sunlight in the form of chemical energy. The rate of energy capture by photosynthesis around the globe is approximately 100 TW per day [2], about six times the world's energy consumption. This makes organic biomass a clear source of renewable energy.

Lignocellulosic biomass is a particular low-impact source of carbohydrates that can be used to produce fuels, chemicals, power and heat, since, unlike other sources such as corn, it does not interfere with the food industry [3]. Lignocellulose is composed of cellulose, hemicellulose and lignin. Cellulose is a linear polymer formed by units of glucose linked to each other through β-(1,4)-glycosidic bonds. These polymers are packed together forming microfibrils; among them intramolecular

https://doi.org/10.1515/9783110469745-015

and intermolecular hydrogen bonds strengthen its structure [4]. Consequently, cellulose is a robust polymer difficult to hydrolyse. The supramolecular structure of cellulose is divided into areas of high order (crystalline) and low order (amorphous) [5]. The presence of one or another is claimed to deeply have an impact on cellulose robustness [6]. While amorphous cellulose is more accessible and simpler to hydrolyse, taking profit of crystalline cellulose is more challenging.

Diverse approaches have been proposed for cellulose hydrolysis [7], the most popular one among them being the enzymatic treatment [8]. However, high enzyme cost and strict control of temperature and pH are a burden when scaling-up these processes [9].

As an alternative, this review presents two different catalytic approaches for cellulose hydrolysis, liquid acid hydrolysis and solid acid hydrolysis. As solid acid catalyst, zirconia and different zirconia-doped materials are tested; meanwhile liquid acid catalyst is carried out by sulfuric acid. Afterwards, the suitability of these methods to produce fermentable sugars is confirmed by two different bacterial strains, *Citrobacter freundii* H3 and *Lactobacillus delbrueckii*, for H_2 or lactic acid production respectively (Figure 15.1).

H_2 is a biofuel that is believed to have considerable potential for using with future technologies. Biological H_2 can be produced from a wide spectrum of carbohydrates. Of all known gaseous fuels, molecular hydrogen has the highest calorific value per unit mass (143 GJ/ton) [10]. The maximum H_2 yields obtained from these pure carbohydrates vary from 2.40 mol H_2/mol hexose for cellulose [11] to 3.33 mol H_2/mol hexose for starch [12] and glucose [11], indicating that these carbohydrates are indeed suitable as feedstocks for dark fermentation [13].

Lactic acid is a natural carboxylic acid with extended usages in industry. Recently, lactic acid has gained more importance in industry because of its usage as a precursor for polylactic acid (PLA) production. PLA, a thermoplastic aliphatic

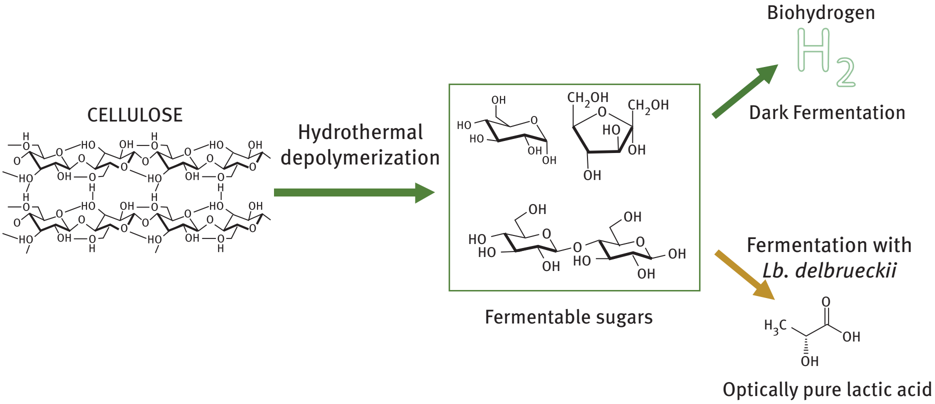

Figure 15.1: Scheme of a general hydrolysis-fermentation process.

polyester, is becoming a highly consumed bioplastic. European demand for PLA in 2008 was 25,000 tons per year and could potentially reach 650,000 tons per year in 2025 [14]. Lactic acid is produced either by chemical synthesis or by fermentative processes. Chemical-based synthesis involves the use of petrochemical resources, requires the use of aggressive chemical compounds and leads to a racemic mixture of lactic acid. However, high isomeric purity of the obtained lactic acid is required in order to obtain good physical properties of the further PLA [15]. Rather, using fermentative processes, glucose can be transformed into almost isomerically pure lactic acid [16, 17]. Furthermore, the energy consumption in fermentative process is lower than that in the chemical synthesis process.

15.2 Materials and methods

15.2.1 Preparation of the supports and catalysts

Zirconium dioxide (ZrO_2) (commercial sample from Degussa) was prepared for using as a catalyst for cellulose hydrolysis with three different promoters: sulphate, phosphate and fluoride. Calcined ZrO_2 at 673 K was impregnated with 5 % (w/w) of aqueous solutions of H_2SO_4, H_3PO_4 and HF, respectively. The resulting solids were dried at 373 K for 12 h and calcined at 673 K for 4 h in a muffle. The catalysts obtained were then labelled ZrO_2-S, ZrO_2-P and ZrO_2-F.

15.2.2 X-ray diffraction (XRD)

XRD was recorded using a Siemens D5000 diffractometer (Bragg Brentano focusing geometry and vertical θ–θ goniometer) with an angular 2θ – diffraction range from 9.5 to 70°. The samples were placed in a Si (510) support with a cavity that was 0.1 mm deep. The cavity was filled with the same amount of sample to ensure the sample packaging and the same baseline for all analyses. The diffraction data were collected with an angular step of 0.03° at 5 s per step and sample rotation. Cu Kα radiation (λ = 1.54056 Å) was obtained from a Cu X-ray tube operating at 40 kV and 30 mA. The crystalline phases were identified using the ICDD files (International Centre for Diffraction Data, release 2007). The crystallinity index (*CrI*) of cellulose was calculated using a modified Segal's method (Eq. 15.1)):

$$CrI = [(I_{cel} - I_{am})]/I_{cel} \tag{1}$$

where I_{cel} is the sum of intensities of peaks from cellulose that appear in the range 10–27° 2θ and I_{am} is the intensity of the amorphous peak (18° 2θ). It should be noted that this CrI refers only to a ratio between diffracted intensities not to a mass ratio.

The background was considered to be a straight line with constant slope. The amorphous part of the sample was assigned to a pseudo-Voigt peak at $2\theta = 18°$ with refinable peak width.

15.2.3 Cellulose characterization

Before and after the catalytic treatment, the surface morphology of the cellulose was imaged with scanning electron microscopy (SEM-JEOL JSM-35C), operating at 15 kV. The sample was gold-coated to facilitate SEM analysis.

15.2.4 Cellulose hydrolysis

15.2.4.1 ZrO_2-catalysed cellulose hydrolysis

The bulk cellulose hydrolysis (molecular biology, ≥99 %) was performed in an autoclave reactor (Parker Autoclave Engineers, UK, 100 mL), using 0.2 g of catalyst at 453 K and 30 bar for 15 h. The solution was continuously stirred at 400 rpm while the reactions were carried out. Prior to the reactions, the autoclave reactor was fed with 50 mL of water, 0.8 g of cellulose and 0.2 g of catalyst and then purged with Argon gas (Ar). The reactor was then heated to 453 K and pressurized to 30 bar with Ar.

15.2.4.2 H_2SO_4-catalysed cellulose hydrolysis

Cellulose was impregnated with 3 % w/w sulfuric acid and dried overnight at 373 K. The hydrolysis experiments were carried out in a PFTE (polytetrafluoroethylene) reactor loading 1 g of impregnated cellulose and 20 mL of deionized water. The samples were irradiated with a microwave system (Milestone ethos-touch control) at 393 K for 2 h.

15.2.5 Fermentation

15.2.5.1 Fermentable substrates

Pure cellulose (molecular biology, ≥99 %) and glucose (D-glucose, anhydrous) were obtained from Sigma Chemical Co. (Madrid, Spain). The water-soluble fractions (WSFs) derived from the hydrolysis reactions were used for fermentation without filtration or any further treatment.

15.2.5.2 Hydrogen production

Citrobacter freundii H3 was tested for their ability to produce H_2 from the liquid product derived from cellulose hydrolysis. *Citrobacter freundii* H3 was aerobically pre-cultured in a synthetic medium at 310 K in an incubator-shaker overnight at 200 rpm. Per liter, the synthetic medium used contained 7.0 g of K_2HPO_4, 5.5 g of KH_2PO_4, 1.0 g of $(NH_4)_2SO_4$, 0.25 g of $MgSO_4 \cdot 7H_2O$, 0.021 g of $CaCl_2 \cdot 2H_2O$, 0.12 g of $Na_2MoO_4 \cdot 2H_2O$, 2.0 mg of nicotinic acid, 0.172 mg of Na_2SeO_3, 0.02 mg of $NiCl_2$ and

10 mL of trace element solution containing, per liter, 0.5 g of $MnCl_2 \cdot 4H_2O$, 0.1 g of H_3BO_4, 0.01 g of $AlK(SO_4)_2 \cdot H_2O$, 0.001 g of $CuCl_2 \cdot 2H_2O$ and 0.5 g of Na_2EDTA. A complex medium was prepared by adding 0.5 g/L of yeast extract to the synthetic medium. To study the batch dark fermentation, the reaction medium was prepared by adding different carbon sources, at around 5 g/L. The pH of the synthetic medium was adjusted to 6.8 before autoclaving. Inoculation was performed under strictly anaerobic conditions, using Ar to purge. The cells were harvested at the end of the exponential growth phase and 10 % (v/v) were used as the inoculum for the main batch experiments.

H_2 production by dark fermentation was investigated in a batch system during 120 h, using 100 mL bioreactors sealed with rubber butyl stoppers and aluminium caps with a working volume of 50 mL. They were continuously agitated in a shaker at 200 rpm and a constant temperature of 310 K. Initially, an anaerobic atmosphere was created in each bottle by purging with 30 mL/min of Ar (99.99 %) for 15 min. Before inoculation, all reactors were autoclaved (for 20 min, 393 K and 1.5 Kg/cm^2 of pressure). Each experiment was performed in duplicate. The carbon source used in the experiments was WSF generated from the catalytic hydrolysis of the cellulose.

15.2.5.3 Lactic acid production

Lactobacillus delbrueckii delbrueckii, CECT 286, was grown on an impoverished MRS broth (5.0 g/L peptone, 5.0 g/L beef extract, 2.5 g/L yeast extract, 2.0 g/L ammonium citrate, 5.0 g/L sodium acetate, 0.2 g/L $MgSO_4 \cdot 7H_2O$, 0.05 g/L $MnSO_4 \cdot H_2O$, 2.0 g/L K_2HPO_4, 1.0 g/L cysteine hydrochloride, 11 g/L HEPES and 10 mg/L resazurin). This medium was selected after different optimization tests and used instead of MRS broth in order to decrease the nutrients, hence reducing media cost. After the pH adjustment at 6.2, the WSF obtained in the hydrolysis experiments was used as a source of carbohydrates for fermentation experiments without any purification step. The fermentative processes were carried out in batch reactors of 50 mL with 25 mL of aqueous media, sealed with rubber cap and aluminum seal and afterwards deoxygenated with 30 mL/min argon flow. Resazurin was used as indicator of oxygen presence. The inoculum consisted of 2.5 mL of previously grown *L. delbrueckii*.

15.2.6 Analytical methods

The WSFs remaining in the autoclave reactor were filtered and analysed by total organic carbon analyzer (TOC). TOC determined the total concentration of soluble carbon directly related to cellulose solubilization from the hydrolysis. The composition of glucose and other by-products of the liquid phase after the hydrolysis and dark fermentation steps was analysed with a high-performance liquid chromatograph (HPLC) (Agilent Technologies, Spain 1100 series), equipped with an ICSep ICE-COREGEL 87H3 Column, serial no. 12525124, a diode-array detector (DAD) and refractive index detectors (RIDs). A mobile phase of H_2SO_4 (2.2 %) was used at a constant flow of 0.6 mL/min, the temperature of the column was maintained at 323 K and each sample was analysed for 40 min. The total soluble carbon after the hydrolysis of cellulose was then compared to the initial carbon present in the cellulose to determine the extent to which it had dissolved or converted into a soluble chemical. With this information, the cellulose conversion capacity of each catalyst was calculated. Calculations were made analytically from TOC results as follows:

$$\text{Reactedcellulose} = 100 \times \frac{\text{mg}C_{\text{liquid phase}}}{\text{mg}C_{\text{initial cellulose}}} \tag{2}$$

$$\text{Glucose selectivity} = \frac{\text{Carbon moles in glucose}}{\text{Reacted carbon moles from cellulose}} \tag{3}$$

This formula describes the carbon moles of cellulose transformed into carbon moles of glucose.

The composition of the gas was measured using a GC-14B gas chromatograph equipped with a thermal conductivity detector (TCD) and a 80/100 Porapak-Q column. Argon was used as the carrier gas at a flow of 30 mL/min. The hydrogen from the fermentation was calculated by comparison with standard pure gas. Hydrogen was measured using a gas chromatograph GC-14B. The operational temperatures of the GC for the injection port, oven and detector were 423 K, 353 K and 473 K, respectively. The chromatogram was developed and analysed using the Turbochrome Navigator (version 4.1) software from Perkin Elmer, Spain.

A modified Gompertz equation Eq. 15.4 was used to estimate the maximum H_2 production rates.

$$H_2(t) = H_{\text{max, H2}}.\exp\left\{-\exp\left[\frac{R_{\text{max, H2}}.e}{\text{H}_{\text{max, H2}}}(\lambda_{\text{H2}} - t) + 1\right]\right\} \tag{4}$$

where $H_2(t)$ is the cumulative H_2 production (mmol/L), λ the lag-phase time (h), H_{max},H_2 the maximum H_2 production (mmol/L), R_{max},H_2 the maximum H_2 rate (mmol/L h) and t the incubation time (h). This equation was found to be suitable for modelling the experimental data on H_2 production [18].

15.3 Results and discussion

15.3.1 Cellulose hydrolysis

Structural characterization of cellulose surface was performed by SEM; pure cellulose (Figure 15.2a) shows a smooth surface. Figure 15.2(b)–(e) shows the images of

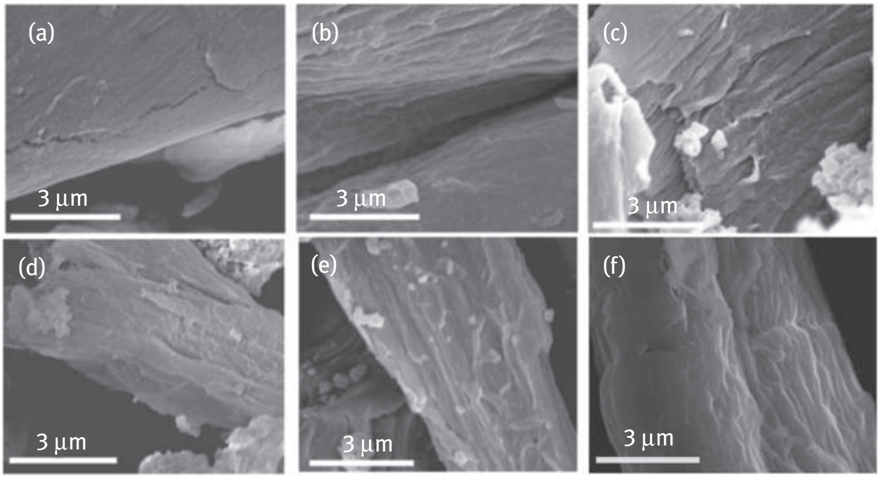

Figure 15.2: Images of cellulose fibers' wall before (a) and after hydrolysis with ZrO_2 (b), ZrO_2-P (c), ZrO_2-S (d), ZrO_2-F (e) and H_2SO_4- (f).

cellulose after catalytic hydrolysis with ZrO_2 materials, while Figure 15.2(f) shows the cellulose surface after hydrolysis with sulfuric acid.

Cracking of cellulosic fibres occurs alongside with hydrolysis as can be seen in Figure 15.2(b)–(f). As the images show, the fibres of the cellulose surface have become markedly more exposed. This change in morphology is equally observed independently of the acid catalyst, being patent for all the different promoted zirconia as well as sulfuric acid.

Despite a similar physical aspect, XRD (Table 15.1) proved that sulfuric acid combined with microwaves is a better method for hydrolysing the crystalline phase of cellulose (Table 15.1, entry 6). Pure ZrO_2 had a slight effect on depolymerization of crystalline cellulose. Instead, promoted ZrO_2 showed better ability to degrade crystalline cellulose, yet sulfuric acid had greater potential for depolymerizing the crystalline phase.

Figure 15.3 shows the conversion of cellulose after the treatment with different catalysts and the selectivity towards different products. For all promoted ZrO_2

Table 15.1: Crystalline index calculated by modified Segal's equation.

Entry	Sample	CI (%)
1	Cellulose	74
2	ZrO_2	73
3	ZrO_2-P	65
4	ZrO_2-S	70
5	ZrO_2-F	72
6	mw-H_2SO_4	57

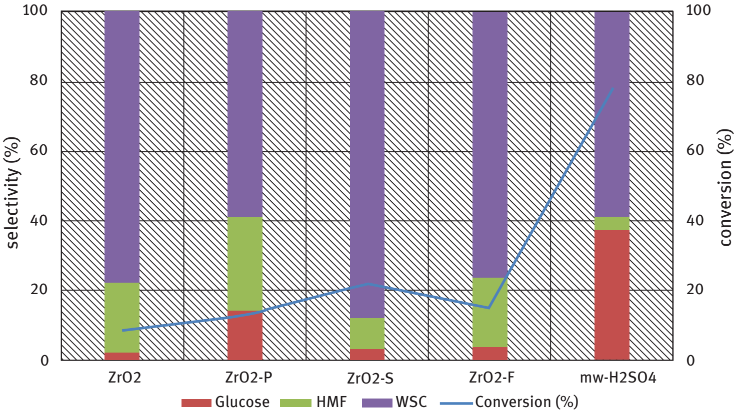

Figure 15.3: Conversion of cellulose with different catalysts and selectivity towards different products.

materials, cellulose conversion was greater than for pure ZrO_2. In fact, pure ZrO_2 showed the lowest cellulose conversion (only 9.3 %). Selectivity to glucose (14.6 %) was highest for the ZrO_2-P sample, for which cellulose conversion was 12.8 %. Selectivity to HMF (hydroxymethylfurfural) (26.9 %) was also highest for the ZrO2-P sample, which may stem from glucose dehydration [19]. On the other hand, cellulose conversion (22.0 %) was highest and selective to glucose and HMF lowest for ZrO_2-S (3.2 % and 8.9 %, respectively). ZrO_2 promotion by sulfate species conferred higher acidity, which may lead to a greater capacity for hydrolyzation and, in turn, other by-products. Thus, the hydrolysis product to be obtained will determine which promoted catalyst is selected.

However, it is clear that a liquid acid catalyst, sulfuric acid, combined with microwaves is much more efficient for depolymerizing cellulose. Not just reducing the treatment times, a liquid acid catalyst can as well increase cellulose conversion from 22 % (ZrO_2) to 78 % when sulfuric acid was used. It also has to be noted that the conditions of both hydrolysis are not the same: 453 K, 30 bars of Ar and 15 h of treatment time for solid acid catalysis as against 393 K and 2 h for liquid acid catalysis. Even though solid acid catalysts could theoretically be reused, liquid acid catalysis assisted by microwave proved to be a more cost-effective process. In addition, when using H_2SO_4 as catalyst, glucose was the most abundant identified product, hence presenting a more suitable process for production of fermentable sugars.

15.3.2 Fermentation of the water-soluble fractions (WSFs)

If WSFs are to be used in dark fermentation, monosaccharide yields must be higher, carbohydrate losses minimized and levels of inhibitory substances lower [20]. Glucose is the compound that is most easily fermented by most microorganisms.

Such by-products as furfural, HMF, phenols, aromatic substances and some organic acids can also inhibit bacterial growth [21].

Fermentation of the sugars obtained after hydrolysis catalysed by ZrO_2-P and ZrO_2-S by *Citrobacter freundii* H3 yielded 1.19 and 0.99 mol H_2/mol hexose, respectively, as can be seen in Figure 15.4. The maximum theoretical production is 4 mol of H_2 per mol of glucose consumed [22]. However, thermodynamically, this yield cannot be achieved by mesophilic organisms. The maximum possible yield that can be achieved without such additional adjustments such as lowering the partial pressure by purging inert gases is about 2 mol H_2/mol of glucose [11].

As shown in Figure 15.5, when fermenting the liquid phase obtained by dilute acid treatment of cellulose with 3 % of sulfuric acid for 2 h by *L. delbrueckii*, lactic acid

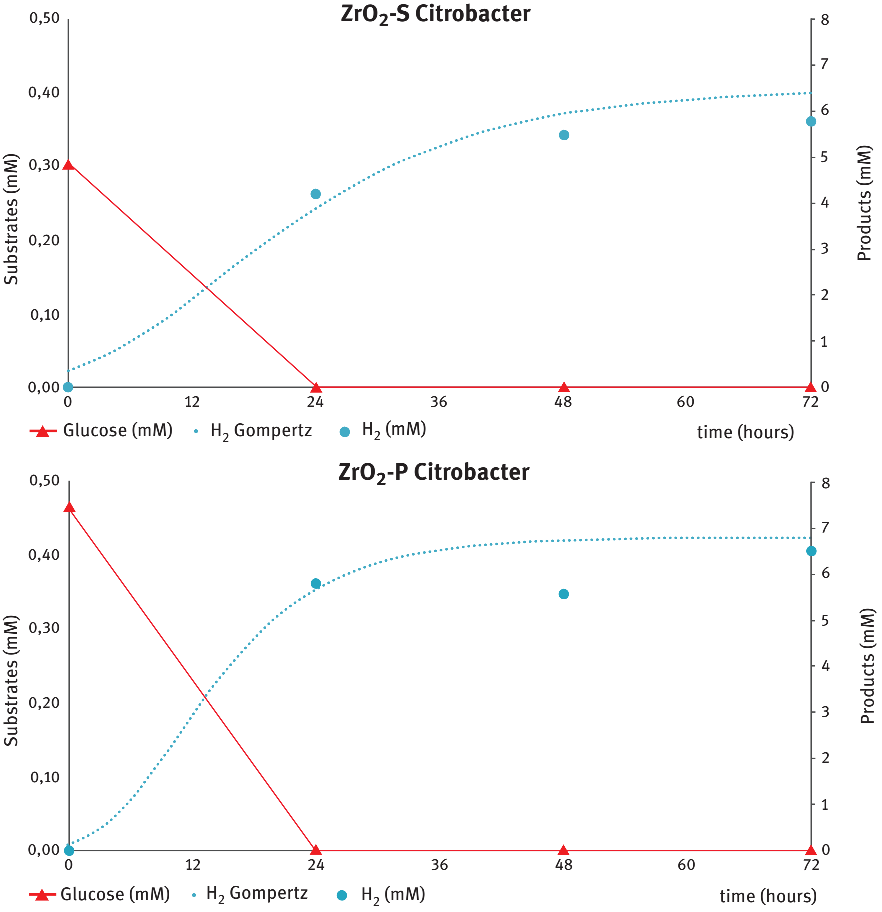

Figure 15.4: Dark fermentation profile using *Citrobacter freundii* H3 in the WSF resulting from the hydrolysis tests with (a) ZrO_2–P and (b) ZrO_2–S.

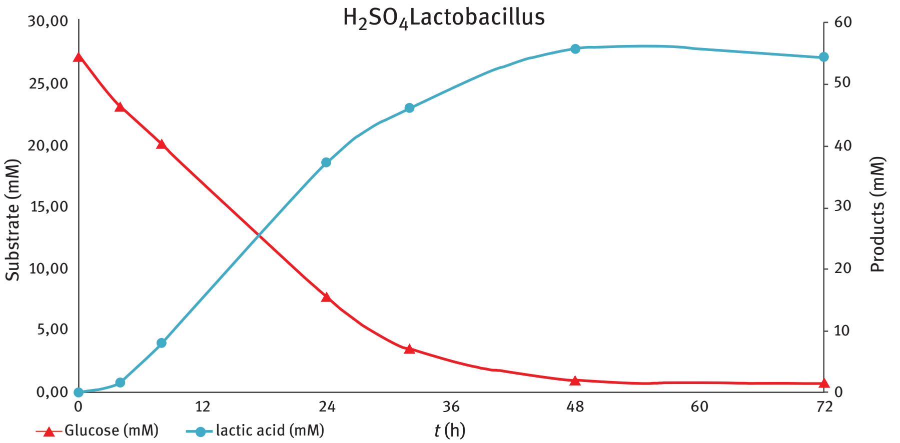

Figure 15.5: Lactic acid production by *L. delbrueckii* from the WSF obtained after cellulose treatment with 3 % H_2SO_4 at 2 h.

production was directly proportional to the amount of glucose. The rest of monitored compounds (levulinic acid, formic acid and HMF) remained constant during the fermentation. Therefore, there was no interference of the rest of generated compounds during cellulose hydrolysis in the metabolic pathway of *L. delbrueckii*. This fact is important because no separation step is needed. Thus, after the hydrolysis, the microbial fermentation can be performed directly. Furthermore, highly pure, 99 %, D-Lactic acid was formed by *L. delbrueckii*. TOC measurements revealed no major loss of organic dissolved carbon, meaning that no CO_2 was produced, consequently and only homolactic fermentation occurred. Therefore, the maximum yield of lactic acid per glucose molecule was achieved.

Consequently, by electing the appropriate strain, different compounds can be targeted. *Citrobacter freundii* H3 and *L. delbrueckii* were able to grow with the different compounds generated by solid or liquid acid catalysis, respectively, as well as transform glucose in the desired compound.

15.4 Conclusions

In this chapter, two different strategies for cellulose hydrolysis were presented. In one hand, solid acid catalysis presents the advantage of catalyst reuse and easier downstream processing. While, microwave-assisted liquid acid catalysis has shorter reaction times and greater conversions.

Here as well, two different microbial strains were presented for the production of biohydrogen or optically pure lactic acid. Demonstrating that both strains were appropriate for fermenting the obtained sugars after hydrothermal depolymerization of cellulose. Consequently, a full strategy from biomass to biofuels or green chemicals has proved to be feasible.

References

[1] Liu L, Cheng SY, Li JB, Huang YF. Mitigating environmental pollution and impacts from fossil fuels: the role of alternative fuels. Energy Sources Part A. 2007;29(12):1069–1080 .

[2] Stokes AR, Wilson AJC. A method of calculating the integral breadths of Debye-Scherrer lines. Proc Cambridge Philos Soc. 1942;38:313–322.

[3] Naik SN, Goud VV, Rout PK, Dalai AK. Production of first and second generation biofuels: a comprehensive review. Renew Sustain Energy Rev. 2010;14(2):578–597.

[4] Loerbroks C, Rinaldi R, Thiel W. The electronic nature of the 1,4-β-glycosidic bond and its chemical environment: DFT insights into cellulose chemistry. Chemistry. 2013;19(48): 16282–16294.

[5] Klemm D, Heublein B, Fink H, Bohn A. Fascinating biopolymer and sustainable row material. Angewandte. 2005;44:3358–3393.

[6] Haghighi S, Hossein Golfeshan A, Tabatabaei M, Salehi Jouzani G, Najafi GH, Gholami M, et al. Lignocellulosic biomass to bioethanol: a comprehensive review with a focus on pretreatment. Renew Sustain Energy Rev. 2013;27:77–93.

[7] Corma A, Iborra S, Velty A. Chemical routes for the transformation of biomass into chemicals. Chem Rev. 2007;107(6):2411–2502.

[8] Zhang Y-HP, Lynd LR. Toward an aggregated understanding of enzymatic hydrolysis of cellulose: noncomplexed cellulase systems. Biotechnol Bioeng. 2004;88(7):797–824.

[9] Zhou C-H, Xia X, Lin C-X, Tong D-S, Beltramini J. Catalytic conversion of lignocellulosic biomass to fine chemicals and fuels. Chem Soc Rev. 2011;40(11):5588–5617.

[10] Boyle D. Bioenergy: Technology, thermodynamics and costs. 1984. Ellis Horwood series in energy and fuel science. Halsted Press, N.Y.

[11] Van Niel EWJ, Budde MAW, De Haas G, Van Der Wal FJ, Claassen PAM, Stams AJM. Distinctive properties of high hydrogen producing extreme thermophiles, *Caldicellulosiruptor saccharalyticus* and *Thermotoga elfi*. Int J Hydrogen Energy. 2002;27(11–12):1391–1398.

[12] Kanai T, Imanaka H, Nakajima A, Uwamori K, Omori Y, Fukui T, et al. Continuous hydrogen production by the hyperthermophilic archean, *Thermococcus kodakaraensis* KOD1. J Biotechnol. 2005;116(3):271–282.

[13] Güell EJ, Maru BT, Chimentão RJ, Gispert-Guirado F, Constantí M, Medina F. Combined heterogeneous catalysis and dark fermentation systems for the conversion of cellulose into biohydrogen. Biochem Eng J. 2015;101:209–219.

[14] Nattrass L. D. A. H. NNFCC Renewable chemicals factsheet: lactic acid. http://www.nnfcc.co.uk/publications/nnfcc-renewable-chemicals-factsheet-lactic-acid.

[15] Lasprilla AJR, Martinez GAR, Lunelli BH, Jardini AL, Filho RM. Polylactic acid synthesis for application in biomedical devices: a review. Biotechnol Adv. 2012;30(1):321–328.

[16] Madhavan K, Nair NR, John RP. An overview of the recent developments in polylactide (PLA) research. Bioresour Technol. 2010;101(22):8493–8501.

[17] Gavilà L, Constantı M, Medina F. D-lactic acid production from cellulose: dilute acid treatment of cellulose assisted by microwave followed by microbial fermentation. Cellulose. 2015;22(5): 3089–3098.

[18] Maru BT, Bielen AAM, Constantí M, Medina F, Kengen SWM. Glycerol fermentation to hydrogen by *Thermotoga maritima*: proposed pathway and bioenergetic considerations. Int J Hydrogen Energy. 2013;38(14):5563–5572.

[19] Lanzafame P, Temi DM, Perathoner S, Spadaro AN, Centi G. Direct conversion of cellulose to glucose and valuable intermediates in mild conditions over solid acid catalysts. Catal. Today. 2012;179(1):178–184.

[20] Bhattarai S, Bottenus D, Ivory CF, Gao AH, Bule M, Garcia-Perez M, et al. Simulation of the ozone pretreatment of wheat straw. Bioresour Technol. 2015;196:78–87.

[21] Mussatto SI, Roberto IC. Alternatives for detoxification of diluted-acid lignocellulosic hydrolyzates for use in fermentative processes: a review. Bioresour Technol. 2004;93(1):1–10.

[22] Iannotti EL, Kafkewit D, Wolin MJ, Bryant MP. Glucose fermentation products of *Ruminococcus albus* grown in continuous culture with *Vibrio succinogenes*: changes caused by interspecies transfer of H2. J Bacteriol. 1973;114(3):1231–1240.

Index

https://doi.org/10.1515/9783110469745-016